# Ionic Liquids and Their Double Salts for Dissolution and Modification of Cellulose

**September 2023**

# Ionic Liquids and Their Double Salts for Dissolution and Modification of Cellulose

A Dissertation Submitted to University of Dhaka for the Partial Fulfillment of the Requirements of the Degree of Doctor of Philosophy in Chemistry

**Submitted by**
Registration No. 22
Session: 2017-2018


Physical Chemistry Research Laboratory
Department of Chemistry
University of Dhaka
Dhaka-1000, Bangladesh

**September 2023**

# Dedication

*This thesis is dedicated to my parents, wife, son and daughter, without whom I would be unable to complete this journey.*

# Acknowledgements

I am profoundly indebted to my supervisor, **Dr. Md. Abu Bin Hasan Susan**, a distinguished Professor in the Department of Chemistry at the University of Dhaka, Dhaka-1000, Bangladesh. He has been the guiding force behind my academic and research journey. His role in my development as a researcher has been truly remarkable. His unwavering dedication to the pursuit of knowledge, along with his profound insights into the field, has not only shaped the direction of my research but has also transformed me into a more inquisitive and rigorous researcher. His commitment to fostering a culture of intellectual curiosity within our research group has been instrumental in my growth as a researcher. His encouragement to questions, explorations, and innovations has been a constant source of inspiration.

I extend my deepest appreciation to my co-supervisors, **Dr. Md. Mominul Islam**, a renowned Professor in the Department of Chemistry at the University of Dhaka, Dhaka-1000, Bangladesh and **Dr. Md. Sarwar Jahan**, Director, BCSIR Dhaka Laboratories, Bangladesh Council of Scientific and Industrial Research, Dhaka-1205, Bangladesh. Their exceptional expertise in the field of chemistry has played a pivotal role in shaping the direction and depth of my research. Their mentorships have been instrumental in expanding my understanding of complex chemical phenomena and research methodologies. Their willingness to invest time and effort in guiding my academic pursuits, especially during challenging moments, has been invaluable in my academic development. Their support has not only enriched my research but has also inspired me to explore new horizons in the field of chemistry.

I am profoundly grateful for the invaluable contributions and mentorships of **Dr. Muhibur Rahman**, former Professor, Department of Chemistry, University of Dhaka, Dhaka-1000, Bangladesh and **Prof. Dr. M. Yousuf Ali Mollah**, former Professor, Department of Chemistry, University of Dhaka, Dhaka-1000, Bangladesh throughout my Ph.D. journey. Their extensive knowledge and expertise in the field of chemistry have been a beacon of guidance for me. I consider myself fortunate to have had the privilege of learning from scholars of their caliber.

I also extend my deepest appreciation to **Dr. Omar Ahmed**, Professor, Department of Chemistry, University of Dhaka, Dhaka-1000, Bangladesh and **Dr. Muhammed Shah Miran**, Professor, Department of Chemistry, University of Dhaka, Dhaka-1000, Bangladesh. Their role in my research journey has been transformative. Their expertise in the field of study and their

commitment to pushing the boundaries of scientific knowledge have been a constant source of inspiration.

I also acknowledge the **authority of Bangladesh Council of Scientific and Industrial Research**, Dhaka-1205, Bangladesh, for granting me permission to complete my doctoral degree.

I would like to extend my heartfelt appreciation and acknowledgment to my fellow lab mates at **Material Chemistry Research Lab**, University of Dhaka, Dhaka and **Fiber and Polymer Research Division**, BCSIR Dhaka Laboratories, BCSIR, Dhaka. Our shared research journey has been a collaborative and enriching experience that has significantly contributed to my academic growth and the overall success of my research endeavors. I am deeply grateful for their support, both academic and personal, that I have received from my lab mates. I also want to extend my gratitude to **my colleagues at BCSIR** for their immense supports during the analysis of materials.

Finally, my heartfelt appreciation goes out to my family. Their sacrifices and belief in my abilities have sustained me through the challenges of doctoral research. In conclusion, my Ph.D. thesis would not have been possible without the exceptional contributions, mentorship, and support of all these individuals. They have played an integral role in shaping my academic and research path, and I am sincerely grateful for their presence in my life and academic journey.

# Declaration

Experiments described in this thesis were carried out by the author of this thesis in the Department of Chemistry, University of Dhaka, Dhaka-1000, Bangladesh. This work has not been presented and will not be presented for any other degree.

**Dr. Md. Abu Bin Hasan Susan**
Professor
Department of Chemistry
University of Dhaka,
Dhaka-1000, Bangladesh
*Supervisor*

**Dr. Md. Mominul Islam**
Professor
Department of Chemistry
University of Dhaka,
Dhaka-1000, Bangladesh
*Co-Supervisor*

**Dr. Md. Sarwar Jahan**
Director, BCSIR Dhaka
Laboratories, Bangladesh
Council of Scientific and
Industrial Research
Dhaka-1205, Bangladesh
*Co-Supervisor*

**Mohammad Mahbubur Rahman**
Department of Chemistry
University of Dhaka, Dhaka-1000, Bangladesh
Ph.D. Student

# Abstract

Ionic liquids (ILs) are highly regarded in the scientific community due to their unique characteristics, including low vapor pressure, non-volatility, wide electrochemical potential window, and relatively low melting points below 100 ℃. Their diverse applications in physics, chemistry, and engineering, make them a prominent research focus in recent decades. Currently, double salts ionic liquids (DSILs), which are mixtures of ILs with varying cations, anions, or both, are gaining increasing attention among researchers. DSILs offer the ability to tailor their physicochemical properties and provide diverse molecular interactions, guiding the synthesis of task-specific ILs for specific applications. These properties result from various interactions, including hydrogen bonding, dipole-dipole interactions, coulombic interactions, and electron pair donor-acceptor interactions. Understanding the structural and physicochemical properties of DSILs is crucial for their potential use as solvents. In this study, 1-butyl-3-methyl imidazolium chloride ($[C_4mim]Cl$) and 1-butyl-3-methyl imidazolium acetate ($[C_4mim]CH_3CO_2$), were used for the preparation of DSILs, while maintaining a constant cation $[C_4mim]^+$ and varying the anion composition of $[C_4mim](CH_3CO_2)_{1-x}Cl_x$ (where x is the mole fraction of ILs). The structure of DSILs was investigated by utilizing ATR-FTIR, Raman, and NMR spectroscopic techniques. Furthermore, the study assesses the impact of ionic interactions on the liquid structure of DSILs through FTIR and Raman spectroscopy. To understand the adjustable characteristics of DSILs and differentiate them from conventional ILs, an investigation into their physicochemical properties is essential. In this study, temperature-dependent assessments of density, viscosity, refractive index, and conductivity were conducted from entire composition range, spanning from 30 to 70 ℃. Excess properties, including excess molar volume, excess viscosity, and excess refractive index, using appropriate models and equations were also evaluated. These analyses provide a deeper understanding of the interactions among the constituent ions $[C_4mim]^+$, $Cl^-$, and $CH_3CO_2^-$ within the DSILs. For the evaluation of DSILs as material, ILs and DSILs were subjected to UV-visible absorption spectroscopy, fluorescence spectroscopy, thermogravimetric analysis (TGA) and differential scanning calorimetry for investigating the optical and thermal properties of the DSILs and ILs. UV-Visible absorption spectroscopy reveals that DSILs showed UV-shielding behavior.

Thermal stabilities of the DSILs are in the range of 220 to 280 ℃ and isotherm TGA reveals the enhanced stability regarding the DSILs compared to ILs at 120 ℃. Heat capacities of the DSILs increase linearly with the operation temperature and DSILs have slightly lower heat capacities compared to ILs. Finally, the glass transition temperature ($T_g$) of the DSILs exhibits similar behavior as the single ILs. However, $T_g$ decreased in case of DSILs compared to ILs. In this research, for the first time DSILs was used over the whole mole fractions for the dissolution of cellulose. Due to the synergistic effect of the $Cl^-$, and $CH_3CO_2^-$ ions in DSILs, the dissolution enhanced upto 32.8 wt% in $[C_4mim](CH_3CO_2)_{0.6}Cl_{0.4}$ at 100 ℃. Cellulose was isolated from jute using kraft pulping process. It was found that $[C_4mim](CH_3CO_2)_{0.6}Cl_{0.4}$ is able dissolve 30.5 wt % of pre-hydrolysed kraft pulp (PHKP). Cellulose was regenerated from cellulose –DSILs solution using anti-solvent water. Effect of pre-hydrolysis pulping of jute fiber was investigated for the dissolution of cellulose. PHKP showed better solubility than KP due to higher purity of PHKP. As ILs are much more expensive than other common solvents involved in the cellulose dissolution and derivatization process, recovery operations of ILs must be highly efficient to make it economically viable and sustainable. In this study, the attempts that were taken for recycling a DSIL of $[C_4mim](CH_3CO_2)_{0.6}Cl_{0.4}$ after the dissolution of PHKP are discussed. The recycled DSIL was repeatedly use for the dissolution of fresh PHKP and regeneration of PHKP up to five times. A novel process was also developed to produce cellulose acetated (CA) from PHKP using $[C_4mim](CH_3CO_2)_{0.6}Cl_{0.4.}$ The successful acetylation was confirmed by FTIR and NMR spectroscopy. A strong band for stretching vibration of –OH of cellulose was absent and a strong band for carbonyl (C=O) group was observed in FTIR spectra suggesting successful esterification of PHKP. All cellulose, regenerated cellulose and synthesized cellulose acetate were characterized by FTIR, XRD, TGA, and SEM analysis. Finally, correlations were established with the obtained physicochemical properties of ILs and DSILs with the dissolution of cellulose.

## Title of the Thesis

# Ionic Liquids and Their Double Salts for Dissolution and Modification of Cellulose

**Submitted by**
**Mohammad Mahbubur Rahman**, Ph.D. Student, Department of Chemistry, University of Dhaka, Dhaka-1000, Bangladesh

**The general description and outline of this thesis are given below.**

### Chapter 1. General Introduction

In Chapter 1, the background, necessity, and objectives of the current research are discussed extensively.

### Chapter 2. Structure of Imidazolium-Based Double Salt Ionic Liquids at Molecular Level

Chapter 2 describes structural information of the Double Salt Ionic Liquids (DSILs) through spectroscopic investigations. DSILs exist as distinct material compared to mixture of ILs. Moreover, the structure of the DSILs vary depending on the composition of the individual component which creates different electronic environment around the IL constituents. A deeper understanding of the composition and arrangement of DSILs made of two ILs, namely 1-butyl-3-methyl imidazolium chloride ($[C_4mim]Cl$) and 1-butyl-3-methyl imidazolium acetate ($[C_4mim]CH_3CO_2$) while maintaining a cation constant of $[C_4mim](CH_3CO_2)_{1-x}Cl_x$ (where x represents the mole fraction of ILs) was attemted. This has been achieved through the utilization of ATR-FTIR, Raman, and NMR spectroscopy techniques. The application of ATR-FTIR spectroscopy provides valuable information regarding the interactions and functional groups that are present in DSILs. The C(2)-H stretching absorption peaks in FTIR spectra of DSILs have been significantly affected by the mixturing of $[C_4mim]Cl$ and $[C_4mim]CH_3CO_2$ at varying mole fractions. These particular peaks exhibit greater susceptibility to external factors. Significant blue shifts are found in the case of DSILs as compared to the $[C_4mim]CH_3CO_2$. The observed notable blue shifts seen with the addition of $[C_4mim]Cl$ in $[C_4mim]CH_3CO_2$ suggest that the $Cl^-$ and $CH_3CO_2^-$ ions synergistically participate in the creation of hydrogen bonds with the C(2)-H protons in DSILs, resulting in a weakening of the C(2)-H bond. The utilization of Raman spectroscopy enabled the identification of ring deformation within the $[C_4mim]^+$ cation. The

chemical shifts of C(2)-H, C(4,5)-H, and alkyl chain hydrogen in the imidazolium have been determined using $^{1}H$ NMR and $^{13}C$ NMR spectroscopy. These findings have contributed to the understanding of cation-anion interactions on the imidazolium cations. This study provides significant observations regarding the chemical changes shown by different nuclei in DSILs, including both proton and carbon nuclei. Chemical changes demonstrate a significant degree of responsiveness to the electronic environment in their immediate proximity, hence aiding the exploration of molecular structure.

**Chapter 3. Physicochemical Properties of Imidazolium-Based Double Salt Ionic Liquids**

In chapter 3, important features and properties of the both imidazolium based ILs and prepared DSILs is discussed extensively. More specifically the discussion revolves around the physicochemical properties such as density, viscosity, refractive index, and conductivity of both ILs, $[C_4mim]CH_3CO_2$ and $[C_4mim]Cl$, and their DSILs with different component mole fractions. All of the properties have been measured under varying temperature from 30 to 70 ℃. The changes following the different temperature environment have been further analyzed. The excess properties, namely excess molar volume, excess viscosity, and excess refractive index, were determined in order to gain a deeper understanding of the interactions between the constituent ions $[C_4mim]^+$, $Cl^-$, and $CH_3CO_2^-$. This was achieved by employing suitable models and equations. Redlich-Kister (R-K) polynomial equation was employed to establish a fitting model for the determination of excess molar volume, excess viscosity, and excess refractive index. The measurement of excess viscosity allows for a qualitative evaluation of the degree of intermolecular contacts, as viscosity is influenced by molecular-level phenomena such as electrostatic forces, hydrogen bonding, and van der Waals interactions. The departure from the conventional Arrhenius behavior was elucidated by the utilization of the Mauro-Yue-Ellison-Gupta-Allan (MYEGA) equation and the modified Vogel-Fulcher-Tammann (mVFT) equation. By applying these two equations to the data, the glass transition temperature ($T_g$) and fragility index (m) were determined. The investigation focused on examining the thermodynamic characteristics associated with the viscous flow of DSILs. Specifically, the changes in activation free energy ($\Delta G$), activation entropy ($\Delta S$), and activation enthalpy ($\Delta H$) were analyzed. The measurement of the ionicity of the prepared DSILs was conducted using the Walden plot. The excess molar volume of DSILs was determined to be of negative value suggesting a decrease in volume upon mixing the two ILs, indicating a volume contraction phenomenon. The presence of significant intermolecular interactions between

$[C_4mim]^+$, $CH_3CO_2^-$, and $Cl^-$ in DSILs is shown by the negative values of excess molar volume. The excess viscosity is found to be of positive value for most of the DSIL samples indicating the significant interactions between the $[C_4mim]CH_3CO_2$ and $[C_4mim]Cl$. $\Delta G$ and $\Delta s$ were found to be positive indicating the favorable mixing behavior of constituent ILs. The activation enthalpy $\Delta H$ increased with increase in the number of the $Cl^-$ ions restricting the movement of ions. The positive excess refractive index values of IL and DSIL increased with temperature, indicating stronger polarization at higher temperatures. DSILs have higher ionic conductivity due to triple ions disrupting inter-ionic interactions, exhibiting good IL behavior with temperature and amount.

**Chapter 4. Evaluation of Double Salt Ionic Liquids as Materials**

Chapter 4 discusses about the various important features necessary for the utilization of DSILs as materials in various field of applications. These important properties of materials include the optical and thermal properties for large scale application. Optical properties were analyzed with the UV-visible absorption spectroscopy and fluorescence spectroscopy. UV-visible absorption spectroscopy reveals that DSILs showed UV-shielding behavior. On the other hand, the thermal properties were determined using TGA and differential scanning calorimetry (DSC) technique. Fluorescence spectroscopy was used to investigate the optical properties of ILs and DSILs, with a particular DSIL sample demonstrating superior cellulose dissolution capability. Fluorescence spectra revealed self-association behavior of ILs and DSILs moieties, with the presence of the imidazolium ring contributing to emission spectra. Recycled DSIL from cellulose solution showed different properties compared to DSIL, with increased formation of associative species. Thermal analysis was conducted in three stages, determining thermal stabilities and heat capacity. ILs and DSILs showed good thermal stability at 220-250 ℃, with mixtures showing increased thermal conductivity ($T_d$) compared to ILs. DSILs showed increased heat capacities with increasing temperature, with $CH_3CO_2$ species increasing their heat capacity. Glass transition temperature ($T_g$) exhibits similar behavior as ILs, however decreases in DSILs. The aforementioned characteristics of ILs and DSILs have the potential to create novel opportunities for various applications, including but not limited to cellulose dissolving, enhanced reaction environments, optoelectronics, photoelectrochemical applications, sustainable fuel cell materials, and more.

**Chapter 5. Enhanced Dissolution of Cellulose in Imidazolium-Based Double Salt Ionic Liquids**

In chapter 5, dissolution characteristics of cellulose in ILs and prepared DSILs have been investigated. As mentioned in the previous chapter, the DSILs have been prepared using two ILs namely $[C_4mim]CH_3CO_2$ and $[C_4mim]Cl$ with varying mole fraction. The cellulose sources selected for this study are commercial cellulose powder, kraft pulp, and prehydrolysis kraft pulp. The solubility of cellulose was shown to be positively correlated with temperature and the concentration of $[C_4mim]Cl$ in DSILs, such as $[C_4mim](CH_3CO_2)_{0.6}Cl_{0.4}$. At a temperature of 100 °C, the highest solubility observed for commercial cellulose powder was 32.8 wt% when dissolved in a solution of $[C_4mim](CH_3CO_2)_{0.6}Cl_{0.4}$. In comparison, both kraft pulp and prehydrolysis kraft pulp exhibited solubilities of 30.1 and 30.5 wt% respectively under the same experimental conditions. DSILs that incorporate both chloride, $Cl^-$ and acetate, $CH_3CO_2^-$ anions have the potential to have a synergistic impact, leading to increased solubility of cellulose. Cellulose was successfully regenerated from DSILs through the utilization of water as an anti-solvent. The characterization of the regenerated cellulosic materials involved the analysis of their structure and morphology using various techniques, including ATR-FTIR, XRD, TGA, and SEM. The regenerated cellulose displayed a reduced level of crystallinity and a decreased degradation temperature. The expected advantage of a reduced crystallinity content in cellulose lies in its potential to facilitate future chemical processing initiatives involving various chemicals, hence enabling the production of diverse cellulosic products.

**Chapter 6. Effect of Pre-Hydrolysis on the Hardwood Pulp Dissolution in Ionic Liquids**

Chapter 6 describes the pre-hydrolysis process of the hardwood pulp prior to dissolution and expounds on the methods efficiency. Cellulose, a renewable biomass, is solubilized by the viscose method, predominantly derived from the pre-hydrolysis kraft process. The extraction of hemicellulose from the lignocellulosic matrix is a selective method for separating the hemicellulose. Hemicellulose inhibits the subsequent viscose processing step. Hence, ILs have been proposed as a potential solvent for the dissolution of cellulose, thereby necessitating a comprehensive understanding of the impact of hemicellulose on the dissolution of pulp in ILs and the subsequent regeneration process. The production of hardwood pulps was carried out using the kraft (KP) and pre-hydrolysis kraft (PHKP) processes in this study. The α-cellulose and residual pentosan levels in PHKP were found to be 95.6% and 4.2%, respectively. In comparison, KP had

α-cellulose and residual pentosan amounts of 84.3% and 9.9%, respectively. Both pulps were dissolved in DSILs of $[C_4mim](CH_3CO_2)_{0.6}Cl_{0.4}$ at 90°C due to its initial efficiency in dissolving higher amount of cellulose. Water was used to regenerate the dissolved pulps, which were then characterized by FTIR, TGA, X-ray diffraction, and viscosity measurements. The pre-hydrolysis procedure significantly improved α-cellulose content and reduced residual pentosan in pulp, increasing cellulose solubility in both ILs and DSIL. The regenerated cellulose exhibited a more pronounced absorption peak at 1647 $cm^{-1}$, which corresponds to the C–O stretching vibration of C–O–H. A homogeneous and smooth cellulose film was formed during regeneration of KP and PHKP in DSIL, suggesting complete dissolution and plasticization after treatment with $[C_4mim](CH_3CO_2)_{0.6}Cl_{0.4}$. The crystallinity index and crystalline structure of regenerated PHKP in both ILs $[C_4mim]CH_3CO_2$ and $[C_4mim]Cl$ were similar, indicating the pre-hydrolysis process helped maintain the original structure of cellulose I. The regenerated PHKP films showed good mechanical properties.

**Chapter 7. Recycling and Reuse of Double Salt Ionic Liquids**

This chapter focuses on the efforts made to recycle a DSIL of $[C_4mim](CH_3CO_2)_{0.6}Cl_{0.4}$ subsequent to the dissolving of pre-hydrolyzed kraft pulp (PHKP). A DSIL of $[C_4mim](CH_3CO_2)_{0.6}Cl_{0.4}$ has been prepared for the dissolution of PHKP. The pulp was coagulated using anti-solvent for cellulose water, and the regenerated (R) PHKP was obtained from the precipitate. DSIL was recycled from the filtrate by evaporation of water, and after the fifth recycling, 99.4% of DSIL was recovered and 96% of RPHKP was obtained. The structure of DSIL and recycled DSIL was investigated using FTIR and $^1H$ NMR spectroscopy. The FTIR spectra showed similar C-H stretching vibrations for DSIL and recycled DSIL. The $^1H$ NMR investigation revealed no obvious difference between the synthesized DSILs and the recycled DSIL. The δ values for DSIL being 10.65, 7.56, 7.31, and 10.51, 7.55,7.40 for the fifth times recycled DSIL, respectively. The thermal stability of DSIL and recycled DSILs was 197.9 and 227.6 °C, respectively. The structure of PHKP converted from cellulose I to cellulose II and the crystallinity index of the regenerated cellulose (RC) decreased significantly. SEM images showed a relatively homogeneous macrostructure of RC fibers, with lower thermal stability observed by TGA analysis. However, the high cost of ILs limits their large-scale industrial application, necessitating efficient recovery operations to make them economically viable and sustainable.

**Chapter 8. Functionalization of Jute-Based Cellulose in Double Salts Ionic Liquids**

In chapter 8, the possible industrial application of the DSIL in functionalization of the cellulose is demonstrated by synthesizing acetylated cellulose from jute fiber in DSIL medium. As previously discussed in previous chapter, $[C_4mim](CH_3CO_2)_{0.6}Cl_{0.4}$ exhibited better dissolution of cellulose compared to other DSILs. Hence, the $[C_4mim](CH_3CO_2)_{0.6}Cl_{0.4}$ was used as the solvent for the functionalization of cellulose derived from jute fibers. The characterization of the selected DSIL has been conducted using two spectroscopic techniques, FTIR and NMR spectroscopy. Furthermore, the prepared cellulose acetate is characterized using FTIR, $^1$H NMR, XRD, TGA-DSC, and SEM. The degree of substitution (DS) of the CA samples were calculated using $^1$H NMR technique. Maximum value of DS was found to be about 2.85 for CA4. The CA was synthesized successfully confirmed from the presence of strong band for carbonyl (C=O) group and absence of a strong band for stretching vibration of –OH of cellulose in the FTIR spectra of CA samples. XRD patterns were analyzed to find the crystallinity of the cellulose and CA samples. The crystallinity index of PHKP was found to be at 51.1% that was lowered upon acetylation. Finally, the TGA and DSC were conducted to assess the thermal stability and changes occurring during thermal treatment.

**Chapter 9. Correlation of the Properties of Imidazolium-Based Ionic Liquids and Their Double Salts with the Dissolution of Cellulose**

In this chapter, the dissolution performance of the DSILs has been correlated with the physicochemical properties of the DSILs. As the physicochemical properties dictate the behavior of the solvent and its dissolution performance. Physicochemical properties that affect the dissolution of cellulose includes, density, viscosity, and conductivity of the ILs. This study investigated the correlation between the density, viscosity, and conductivity of ILs and DSILs and their ability to dissolve cellulose. Cellulose dissolution can be impeded by increased densities and viscosities, as solvents with higher viscosities can limit mobility and hence lower the effectiveness of the dissolution process. The achievement of a suitable balance between penetration and solubility can be facilitated by the utilization of a viscosity level that is considered moderate. ILs and DSILs possessing enhanced electrical conductivities exhibit improved efficacy in the process of cellulose dissolving. The process of cellulose regeneration from a cellulose-ILs solution was conducted by employing water as an anti-solvent. Subsequently, an investigation was carried out to analyze the crystallinity and thermal stability of both cellulose and the regenerated cellulose.

**Chapter 10. General Conclusions and Future Prospects**

In Chapter 10, the general conclusions are presented in a comprehensive manner, encompassing overall findings and prospects for future research on DSILs. Specifically, the chapter focuses on their potential as effective solvents for cellulose dissolution for cellulose modification.

# Contents

## Chapter 1. General Introduction



## Chapter 2. Structure of Imidazolium-Based Double Salt Ionic Liquids

## Chapter 3. Studies on the Physicochemical Properties of Imidazolium-Based Double Salt Ionic Liquids

## Chapter 4. Double Salt Ionic Liquids as Materials



## Chapter 5. Enhanced Dissolution of Cellulose in Imidazolium-Based Double Salt Ionic Liquids

## Chapter 6. Effect of Pre-Hydrolysis on the Hardwood Pulp Dissolution in Ionic Liquids



## Chapter 7. Recycling and Reuse of Double Salt Ionic Liquids

## Chapter 8. Functionalization of Jute-Based Cellulose in Double Salts Ionic Liquids



## Chapter 9. Correlation of the Properties of Imidazolium-Based Ionic Liquids and their Double Salts with the Dissolution of Cellulose

## Chapter 10. General Conclusions and Future Prospects

# List of Figures

# List of Schemes

# List of Tables

# List of Symbols

| Name | Symbol |
|---|---|
| Absolute Temperature | $T$ |
| Avogadro Number | $N_A$ |
| Coefficients of Determination | $R^2$ |
| Density | $d$ |
| Enthalpy | $H$ |
| Entropy | $S$ |
| Excess Molar Volume | $V_m{}^E$ |
| Excess Viscosity | $\eta^E$ |
| Gibbs Free Energy | $G$ |
| Molar Gas Constant | $R$ |
| Molar Mass | $M$ |
| Mole Fraction | $x$ |
| Refractive Index | $n_D$ |
| Speed of Light | $c$ |
| Thermal Expansion Coefficient | $\alpha_p$ |
| Viscosity at Infinite Temperature | $\eta_o$ |
| Vogel Temperature | $T_o$ |
| Glass transition temperature | $T_g$ |

# List of Abbreviations

| Abbreviation | Elaborated Form |
|---|---|
| $[C_2mim]CH_3CO_2$ | 1-ethyl-3-methylimidazolium acetate |
| $[C_4eim]Br$ | 1-butyl-3-ethylimidazolium bromide |
| $[C_4mim]CH_3CO_2$ | 1-butyl-3-methylimidazolium acetate |
| $[C_4mim]Cl$ | 1-butyl-3-methyl imidazolium chloride |
| $[C_4mim]I$ | 1-butyl-3-methyl imidazolium iodide |
| $[C_4mpyr]^+$ | N-butyl-N-methylpyrrolidinium cation |
| $[C_4py]^+$ | Butylpyridinium |
| $[NTf_2]$ | Bis(trifluoromethanesulfonyl)amide |
| ATR-FTIR | Attenuated Total Reflectance Fourier-Transform Infrared |
| CA | Cellulose Acetate |
| DBU | 1,8-Diazabicyclo-[5,4,0]-undec-7-ene |
| DFT | Density Functional Theory |
| DMAc | Dimethylacetamide |
| DMF | Dimethylformamide |
| DMSO | Dimethyl Sulfoxide |
| DP | Degree of Polymerization |
| DS | Degree of Substitution |
| DSC | Differential Scanning Calorimetry |
| DSILs | Double Salts Ionic Liquids |
| EIS | Electrochemical Impedance Spectroscopy |
| GC | Gas Chromatography |
| GPC | Gel Permeation Chromatography |
| HER | Hydrogen Evolution Reaction |
| ILs | Ionic Liquids |
| KP | Kraft Pulp |
| mVFT | Modified Vogel-Fulcher-Tammann |
| MYEGA | Mauro-Yue-Ellison-Gupta-Allan |

| | |
|---|---|
| NMR | Nuclear Magnetic Resonance |
| OER | Oxygen Evolution Reaction |
| PHKP | Prehydrolysis Kraft Pulp |
| REE | Red Edge Effect |
| R-K | Redlich-Kister |
| RTILs | Room Temperature Ionic Liquids |
| SDTA | Simultaneous Differential Thermal Analysis |
| SEM | Scanning Electron Microscopy |
| TEM | Transmission Electron Microscopy |
| TGA | Thermogravimetric Analysis |
| UV | Ultraviolet |
| VFT | Vogel-Fulcher-Tammann |
| VOCs | Volatile Organic Compounds |
| XRD | X-Ray Diffraction |

# Chapter 1

# General Introduction

## 1.1. Introduction

Cellulose, a polysaccharide composed of interlinked D-glucose molecules via 1,4-β-glycosidic bonds, present abundantly within cellular walls of plants and serves as a fundamental structural element in the plant kingdom. As an abundant biopolymer, cellulose has garnered significant attention as a viable and sustainable raw resource for the prospective chemical industry [1,2]. Additionally, cellulose has a number of desirable qualities, including outstanding biocompatibility, complete biodegradability, high mechanical property, and structural designability. In several areas of human society, cellulose, and its derivatives are being exploited in our daily life, such as textiles, paper, food, pharmaceutical, engineering materials, composites and biofuels, etc. This natural polymer is environmentally benign and may play an alternate role in our over-dependence on fossil resources [1, 3-6]. Cellulose holds significance from an additional standpoint. The escalating demand for fibers with superior physiological performance, particularly in terms of moisture management and absorbance, is more effectively fulfilled by natural fibers like cellulose. In contrast, synthetic fibers made of petroleum i.e., polyamide, polyester, polyacrylonitrile, and polypropylene, lack these attributes and also exhibit a lower brightness and a variable molecular-weight distribution [6]. Cellulose is a linear biopolymer characterized by its elongated and rigid rod-like structure, which is facilitated by the equatorial conformations of the glucose units. The glucose molecules in a chain possess several hydroxyl groups (–OH) that engage in hydrogen bonding with oxygen atoms on either the same or adjacent chains. This intermolecular interaction results in the solid cohesion of the chains, leading to the formation of microfibrils characterized by exceptional tensile strength [1, 6]. The presence of strong hydrogen bonding inside natural cellulose results in its inherent crystalline structure. Cellulose, with its highly ordered structure and strong H-bonding network, exhibits a lack of meltable and soluble properties in commonly used solvents [1]. In recent decades, a range of derivatizing and non-derivatizing techniques have been devised for the dissolution of cellulose. These methods involve the process of viscose preparation [7], the N-methylmorpholine-N-oxide (NMMO) process [8], the cuprammonium rayon method [9], and the CarbaCell process [10], among others. Several solvent systems, i.e., molten salt hydrates, $[Cu(NH_3)_4](OH)_2$, $ZnCl_2$, and others, have been developed for

the purpose of dissolving cellulose. Notable examples include N, N-dimethylacetamide/lithium chloride (DMAc/LiCl), N,N-dimethylformamide/dinitrogen tetroxide (DMF/$N_2O_4$), and dimethyl sulfoxide/tetrabutylam [11-13]. All of these solvent systems exhibit significant limitations, including the requirement for pre-treatment procedures, instability, toxicity, high expenses, limited dissolving capacity, stringent processing conditions, challenges in solvent recyclability, and other related issues. These facts ultimately limit the utilization of mentioned methods in cellulose processing chemistry and hampers its application industrially. Hence, designing of an efficient solvent system cellulose – which will be stable, inexpensive, non-toxic, recyclable, biodegradable and yield high amount of desired product - for the dissolution and catalysis of cellulose is very crucial.

Ionic liquids (ILs), due to its attractive properties as solvents, could exhibit immense potential in the industrial cellulose processing. ILs are defined as a type of molten salts that melts and exist as liquid below 100 ℃ [14-16]. These materials in its entirety consists of ions. Their exceptional low vapor pressure is one of their significant characteristics. Hence, solvents like these are referred as "green" solvents, as opposed to conventional volatile organic compounds (VOCs). Ionic liquids (ILs) provide numerous appealing characteristics, including an excellent solvation capacity, the ability to adjust their structures, minimal vapor pressure, non-flammability, excellent thermal and chemical resistance, nontoxicity, recyclability, and a broad electrochemical potential window [14,15,17]. The ability to design task-specific ILs for different applications is enabled by the vast and easily accessible variety of ILs which have different physical properties, created by straightforward modification to the cations or anions - hence frequently referred to as “designer solvents” [14,16,18]. Therefore, one key interest may lie in the modification and manipulation of IL media, which has recently been addressed using the concept of mixtures of two or more ILs – which Rogers and their group have termed as Double Salt Ionic Liquids (DSILs) [19].

A DSIL is a new type of IL which is a combination of at least two different cations or anions; the combination is such that fixing one particular cation, one can vary the anions - and vice versa – to prepare a DSIL; combination of more than two different cations or anions has also been reported however. The concept lies in the fact that a single IL can be tuned to getting desirable electric and rheological properties without the use of volatile molecular solvents. Two possibilities arise when two ILs are mixed together- formulation of properties outside the range of the individual ILs or mixing being close to ideal; either outcome is considered as promising from the perspective of scientific understanding as well as applications. Having been a relatively new field

of research, the focus has been principally on the physicochemical and theoretical understanding through rheological, spectroscopic, and computational studies of DSILs- albeit scattered reports of their applications in gas sensing, organic reaction media and electrodeposition have been observed [20-22]. Some DSILs exhibit positive molar properties, when others show the opposite- which has its origin at the molecular environment and variation of ionic counterparts. Through the estimation of excess properties, DSILs have been claimed to behave similar to the mixtures of linear alcohols. One interesting feature of DSILs is that formation and manipulation of nano-structures are possible. A qualitative molecular model, the pseudo-lattice model, proposes that the ionic constituents are fixed and constricted but rather are fleeting and constantly changing their configurations [19]. As a result, the ionic contacts are random throughout the whole mixture. More flexible ionic placements in DSILs may contribute towards its increased conductivity and diffusion coefficient values. Based on optical Kerr effect spectroscopy, it was suggested that depending on the variation of anionic constituents, DSILs may even exhibit structural properties similar to the block- or random co-polymers [23]. Moreover, DSILs with one cation but two different anions exhibited unique thermal properties that are influenced solely by the anomaly in electronic environment imposed by the presence of different anions. Multiple local ionic combinations with each local arrangement having their unique electron density distribution is assumed to be the key to the exquisite physicochemical properties of DSILs – albeit more profound understanding on the topic requires cover a wide range ionic species to be combined to one another as well as more experimental data. Meanwhile, DSILs have garnered much interest in the field of chemical and industrial applications; fields include catalysts and solvents for organic synthesis, extraction and separation, solvent in gas-liquid chromatography, biomass processing and so on [19].

Long *et al.* reported complete dissolution of cellulose into industrially useful chemicals using DSILs- in which the ratios of various cations were manipulated in order to achieve both cellulose dissolution and low molecular weight organic products achieved by cellulose conversion through catalysis [24]. Moreover, DSILs were used to solubilize Pd(0) nanoparticles and lignin in DSILs. Enhanced transport of O to the active metal centers and the higher extent of oxidation of lignin have been observed in case of DSILs [25]. Notably, DSILs gained advantage over single ILs for by increasing the solubility of cellulose and provided with a route to one-pot robust and recyclable process with high product selectivity. Therefore, DSILs shows much promise – not only as a catalyst/solvent for dissolution of cellulose but also for gaining fundamental insight into the

effects of variation of cation and/or anion on the physicochemical aspects of DSILs; the understanding would prove to be pivotal for designing task-specific DSILs for ensuring highest efficiency and greener ionic media for performing cellulose processing chemistry.

This chapter basically describes the fundamentals and review of previous studies involving the dissolution of cellulose in ILs and DSILs. The physicochemical properties of ILs and DSILs that influence the dissolution of cellulose in ILs, ILs, and mixture of ILs, regeneration of cellulose from cellulose-ILs solution, derivatization of cellulose in ILs and mixture of ILs, recycling of ILs, purification of ILs, and reuse of ILs have been discussed.

### 1.2. Ionic liquids (ILs)

ILs are classified as type of molten salts with the presence of asymmetric organic cations and organic or inorganic anions. These compounds possess the unique property of being able to undergo melting at temperatures below 100 °C. These substances possess several distinctive attributes, such as exceptional solvency, non-volatility, elevated thermal stability, increased chemical stability, and easy recyclability. Walden for the first time introduced molten salts of ethyl ammonium nitrate ($[EtNH_3][NO_3]$) which melts at 12 °C and therefore referred as room temperature ILs (RTILs) [26]. These liquids started to draw significant attention after binary ILs consisting of aluminum(III) chloride and 1,3-dialkylimidazolium chloride or N-alkyl pyridinium has been discovered [27,28]. The moisture sensitivity was the major drawback of all chloroaluminate(III) ILs. In 1992, Wilkes and Zaworotko successfully synthesized 1-ethyl-3-methylimidazolium ($C_2$mim) based ILs that exhibited stability in the presence of water and moisture. These ILs were produced with various anions [29]. After that different types of cation and anions containing ILs have been developed for task-specific applications. Structures of some common types of cation and anions containing ILs are presented below.

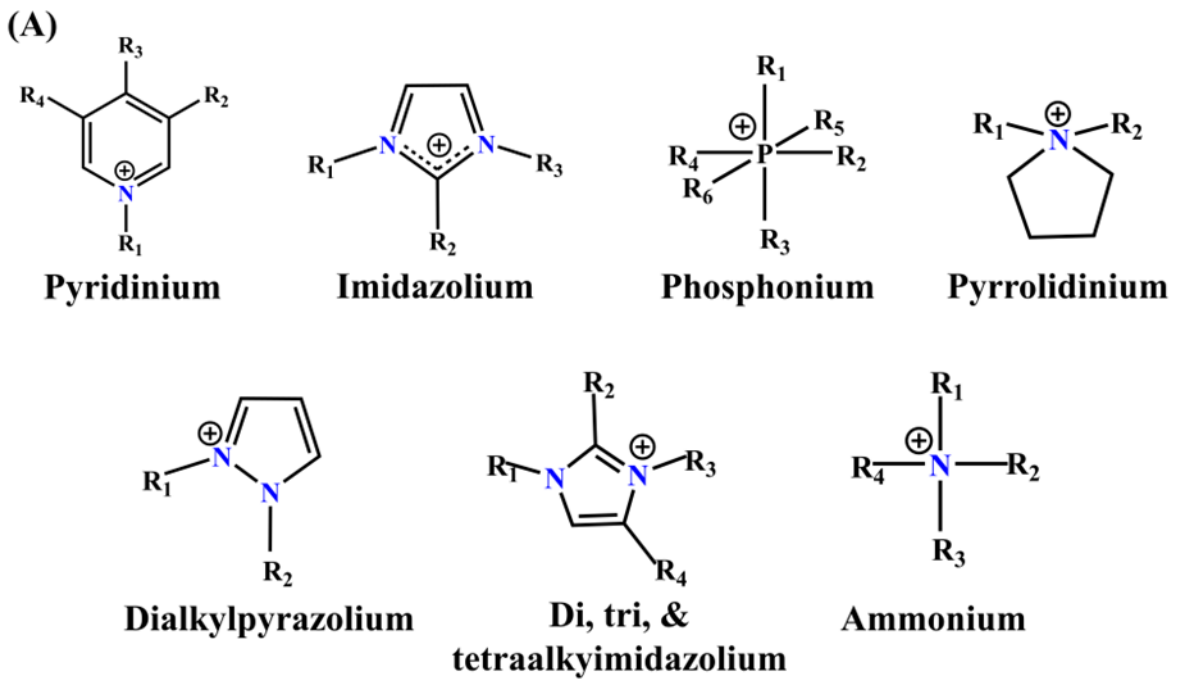


**Scheme 1.1.** Structures of some common (A) cations and (B) anions of ILs

In 1934, Graenacher proposed the utilization of molten N-ethylpyridinium chloride, along with nitrogen-containing bases, as a potential solvent for cellulose dissolution [30]. Rogers and his group in 2002 successfully introduced ILs having imidazolium cations with varying alkyl group i.e., $[C_4mim]^+$, $[C_6mim]^+$ and $[C_8mim]^+$ and anions of $Cl^-$, $Br^-$, $SCN^-$, $BF_4^-$ and $PF_6^-$ for the dissolution of cellulose. As ILs are nonderivatized in nature these materials are excellent as solvents for the dissolution of cellulose. They also investigated that some of the ILs are nonsolvent for the dissolution of cellulose such as noncoordinating anions of $BF_4^-$ and $PF_6^-$. Following to this, numerous research efforts have been undertaken to synthesize novel ILs with the purpose of facilitating the dissolution of cellulose [31]. Moreover, ILs have the numerous applications as new, sustainably acceptable solvents in organic synthesis [32,33], catalysis [32-34], electrochemistry [34], liquid-phase extraction [35], and analytical chemistry [36, 37] has increased significantly over the past 20 years.

### 1.2.1. Properties of ILs for the dissolution of cellulose

Paul Walden in 1914 first reported IL of ethylammonium nitrate [38]. ILs can be made in an unlimited combination of irregularly sized cations and anions. Consequently, ILs have significantly lower melting points and lattice energies than conventional crystalline structures [39]. Most ILs have a variety of cations, including imidazolium, pyridinium, and pyrrolidium as well as tetra-alkyl phosphonium and tetra-alkyl ammonium. [40]. Anions range from smaller anions such as halides, hydrogen sulphate, nitrate, and acetate to larger complex anions like acesufamate [41]. Hence, it is possible to create ionic liquids (ILs) with precise characteristics such as density, conductivity, viscosity, melting point, and other relevant properties. The potential of ILs was highlighted by Abushammala and Mao, who emphasized on the utilization of 1-alkyl-3-methylimidazolium ($[C_nmim]^+$) as an IL cation for the purpose of dissolving and fractionating wood and cellulose. The goal of this $[C_nmim]^+$ was to dissolute wood and cellulose and subsequently increase their susceptibility towards enzymatic hydrolysis for the generation of biofuels, fractionation of the components of wood, and extraction of cellulose nanoparticles from wood and cellulose, etc. [42]. Moreover, the characterization of its component ions and their physicochemical characteristics of ILs are crucial factors for the purpose of dissolving and fractionating wood and cellulose. The most important physicochemical properties i.e., density, viscosity, melting point, conductivity etc. of few imidazolium-based ILs are presented in Table

1.1. For example, at room temperature $[C_4mim]Cl$ and $[C_2mim]Cl$ exist as solid whereas $[C_4mim]CH_3CO_2$ and $[C_2mim]CH_3CO_2$ exist as liquids. On the other hand, at room temperature $[C_4mim]BF_4$ and $[C_2mim]BF_4$ exist as liquid however $[Bnmim]BF_4$ remain as solid. The viscosity of $[C_4mim]HSO_4$ and $[C_2mim]HSO_4$ are 31.0 and 15.0 P, respectively. The enhanced van der Waal force of alkyl chain length is the reason for the elevated viscosity of $[C_4mim]HSO_4$ [43,44]. Their viscosity is significantly more compared to the viscosities of $[C_4mim]BF_4$ and $[C_2mim]BF_4$ and $[C_4mim]PF_4$ and $[C_2mim]PF_4$, respectively. It was found that viscosities of the ILs change as the alkyl chain length of the carboxylate anions (formate, acetate, propionate, and butyrate) is varied with $[C_4mim]^+$ cation. The viscosities of ILs having carboxylate anions show a positive correlation with the length of the alkyl chain [45]. It is crucial to note that the presence of water and contaminants has noticeable impact on the values of melting temperature and viscosity. This is the cause of the literature's inconsistent reporting of melting point and viscosity value. Imidazolium-based ILs have a significantly higher density (1.0 to 1.4 $g/cm^3$) than typical organic solvents (0.7-1.0 $g/cm^3$) [46]. The cation and anion's molecular masses have a significant impact. For instance, $[C_4mim]PF_6$ has a higher density than $[C_4mim]BF_4$. Compared to $[C_4mim]Cl$, $[C_4mim]Br$, and $[C_4mim]CH_3CO_2$, they are both higher [47].

**Table 1.1.** Properties of imidazolium-based ILs for the purpose of dissolving and fractionating wood and cellulose [42]

| ILs | Melting point (K) | Density ($g/cm^3$) at 298 K | Viscosity (P) at 293-303K | Conductivity (mS/cm) at 298K | References |
|---|---|---|---|---|---|
| $[C_4mim]CH_3CO_2$ | -293 | 1.1 | 2.08 | 1.4 | [48,49] |
| $[C_4mim]Cl$ | 314-343 | 1.1 | Solid | - | [16,17] |
| $[C_4mim]Br$ | 333-354 | 1.1 | Solid | - | [48-50] |
| $[C_4mim]I$ | -345 | 1.4-1.5 | 11.10-11.83 | 0.5 | [48,49] |
| $[C_4mim]HSO_4$ | - | 1.3 | 30.88 | - | [48,49] |
| $[C_4mim]BF_4$ | -356-347 | 1.1-1.3 | 0.72-2.33 | 3.2 | [48,49] |
| $[C_4mim]PF_6$ | 284 | 1.3-1.4 | 2.07-4.50 | 1.5-4.8 | [48,49] |
| $[C_4mim]ACC$ | 303 | 1.2 | 8.00 | 0.5 | [51] |
| $[C_2mim]CH_3CO_2$ | -318-287 | 1.0-1.1 | 0.91-1.62 | 2.5-2.8 | [48,49] |
| $[C_2mim]Cl$ | 353-362 | 1.1-1.2 | Solid | - | [48,49] |
| $[C_2mim]Br$ | 338-364 | - | Solid | - | [48,49] |
| $[C_2mim]I$ | 352-358 | - | Solid | - | [48,49] |
| $[C_2mim]HSO_4$ | - | 1.4 | 15.10 | 0.5 | [49] |
| $[C_2mim]BF_4$ | 279-288 | 1.2-1.4 | 0.34-0.66 | 13.0-14.1 | [48,49] |
| $[C_2mim]PF_6$ | 331-337 | 1.4 | 4.50 | 5.2 | [48-50] |
| $[C_2mim]ACC$ | 307 | 1.3 | 5.56 | 0.6 | [51] |
| [Amim]Cl | 320 | - | - | - | [48] |
| [Amim]I | 330 | - | - | - | [48] |
| [Bnmim]Cl | 348 | - | Solid | - | [48] |
| $[Bnmim]BF_4$ | 351 | - | Solid | - | [48] |
| $[Bnmim]PF_6$ | 403-408 | - | Solid | - | [48,49] |

Thermophysical properties, i.e., melting point ($T_m$), degradation temperature ($T_d$), glass transition temperature ($T_g$), freezing point ($T_f$), cold crystallization temperature ($T_{cc}$) and heat capacities are very important for the designing of an industrial process. These properties depend on the constituents of ILs. Fredlake *et al.*, [52] investigated the thermophysical properties of 13 imidazolium based ILs with different cations and anions. They found that features of ILs varies

with the variation of cations and anions. Thermal stability has positive correlation with the size of the anions and heat capacities show positive correlation with the temperature and population of ions in ILs. In their study, Ngo *et al.* examined the thermal characteristics of imidazolium-based ILs through the utilization of DSC and TGA coupled with simultaneous differential thermal analysis (TGA/SDTA). The findings of their investigation revealed that a significant number of ILs exhibit a liquid state at temperatures below ambient conditions, transitioning into a glassy state at lower temperatures. They also found that these ILs have very low vapour pressure up to their degradation temperature (>400 °C). The decomposition of ILs with inorganic anions and organic anions possess endothermic and exothermic processes respectively. Halide ions drastically reduce the decomposition temperature (<300 °C) (53). Chancelier *et al.*, reported that anions are mainly responsible for the thermal stability of imidazolium-based ILs. The degradation temperature changes between 473 to 773K and increases according to $[PF_6] > [BF_4] > [Cl] = [Br] = [I]$ [54]. But, in $[C_2mim]$ and $[C_4mim]$ based ILs, minor changes in the degradation temperature occur [55]. The presence of cellulose in ILs could alter the degradation process. For example, the endothermic degradation of $[C_2mim]CH_3CO_2$ turned to exothermic process of degradation [56]. Erdmenger *et al.*, reported that branches of alkyl side chain in the imidazolium-based ILs influences the thermophysical properties of ILs such as $T_m$, $T_g$, $T_f$, and $T_{cc}$. They investigated that branching to the side chain in the alkyl constituents in the ILs can utilized to synthesize tailor made ILs for fine tuning of its thermophysical properties [57]. The acid/base properties of imidazolium-based ILs play an important role in their task-specific application. For example, $[C_4mim]HSO_4$ is an acidic ILs, whereas $[C_4mim]CH_3CO_2$ is basic due to the acidic nature of $HSO_4^-$ and basic nature of $CH_3CO_2^-$ ions. Anion's acidity and basicity significantly affects acidity and basicity of imidazolium ILs. For example, $[C_4mim]CH_3CO_2$ is significantly more basic than $[C_4mim]Cl$ because of higher basic nature of $CH_3CO_2^-$ ion, whereas $[C_2mim]CH_3CO_2$ shows slightly more basic than $[C_4mim]CH_3CO_2$ due to longer alkyl chain length [58].

### 1.3. Double salt ionic liquids (DSILs)

DSILs, defined as the combination of more than two types of ions, can be formed by the combination of two ILs of similar cations (a), two ILs of similar anions (b), or two ILs with both different cations and anions (c) are presented below where x is the mole fraction of single ILs.

(a) $[C_4mim](CH_3CO_2)_xCl_{1-x}$

(b) $[C_4mim]_x [C_2mim]_{1-x}Cl$

(c) $[C_4mim]_x [C_2mim]_{1-x}(CH_3CO_2)_xCl_{1-x}$

Thus, DSILs can be defined as the combination of more than two types of ions and adjusted physicochemical properties different from component ILs that can overcome the limitations of ILs, resulting in a new liquid phase consisting of both sets of ions and exhibit different properties than their individual components. The ions that make up a DSIL are thought of as one substance rather than as mixture of different salts when they crystallize together to form a DSIL, even though DSILs could be melted and the ion combinations categorized into more straightforward salts. DSILs is the combination of two ILs rather than a simple mixture of two different ILs, and behave as a unique compound, which is liquid (<100 ℃) and new intermolecular interactions and properties have been developed [59-64].

### 1.3.1. Selective properties of DSILs

To understand the new intermolecular interactions and properties that have been developed in DSILs to expand their application, it is imperative to study the physicochemical properties i.e., density, viscosity, conductivity, thermal stability, etc. These properties of DSILs mainly provide ideas relating to the association, dispersion and interactions existing in the DSILs.

#### 1.3.1.1. Density

To understand the volumetric properties of DSIL, the measurement of densities is crucial. From the density data of DSILs or a mixture of ILs, the excess molar volume ($V_m^E$) of DSILs can be measured. The value of $V_m^E$ helps to understand the types of interaction occurred in DSILs. The positive $V_m^E$ value indicates volume expansion, whereas the negative $V_m^E$ value indicates volume contraction. $V_m^E$ can explain the deviational behavior from the ideal additivity behavior of DSILs. $V_m^E$ can be determined using eq. 1 [65]

$$V_m^E = \left(\frac{X_1 M_1 + X_2 M_2}{d_{mix}}\right) - \left(\frac{X_1 M_1}{d_1} + \frac{X_2 M_2}{d_2}\right) \quad (1)$$

where, $d_1$, $d_2$ are the densities and $M_1$, $M_2$ are the molar masses of the ILs.

In recent years, a fair amount of research has been carried out on the physicochemical properties of pure ILs and their interactions with molecular solvents [66-72]. But, at present mixture of ILs or DSILs has become more attentive to the researchers. They found that the mixing of ILs exhibits closer to linear behavior. Seddon *et al.* investigated the $V_m^E$ of mixture of two ILs with identical cation of [$C_4$mim] combined with different anions of bis(trifluoromethylsulfonyl)amide, hexafluoro phosphate ($PF_6$) and tetra fluoro borate ($BF_4$). The density of DSIL of [$C_4$mim]$(NTf_2)_x(BF_4)_{1-x}$, [$C_4$mim]$(NTf_2)_x(PF_6)_{1-x}$ and [$C_4$mim]$(PF_6)_x(BF_4)_{1-x}$ (where x is the mole fraction of each ILs) were measured at temperature from 298 to 333 K and calculated the $V_m^E$. It was observed that all systems exhibit $V_m^E$ values that are significantly low and positive, demonstrating minimal dependence on pressure and temperature. These values are typically on the order of a few tenths of $cm^3\ mol^{-1}$. They also found that, the result showed additive trend and $V_m^E$ value become more positive if the chain length of the alkyl side in the cation increased. These results can be considered as nearly ideal [73]. Navia *et al.* also examined comparable findings [74]. The studied for the DSILs of common anion of [$C_2$mim]$_x$[$C_6$mim]$_{1-x}(BF_4)$, and [$C_4$mim]$_x$[$C_6$mim]$_{1-x}(BF_4)$, and common cation with different of [$C_4$mim]$(BF_4)_x(PF_6)_{1-x}$, and [$C_4$mim]$(BF_4)_x(MeSO_4)_{1-x}$ (where x is the mole fraction of each ILs) [74]. Densities were measured over the whole molar compositions at the temperature range from 298.15 to 303.15 K. Song *et al.* investigated the DSILs of [$C_2$mim]$_x$[$C_3$mim]$_{1-x}$[$BF_4$], [$C_3$mim]$_x$[$C_6$mim]$_{1-x}$[$BF_4$], and [$C_2$mim]$_x$[$C_6$mim]$_{1-x}$[$BF_4$] with common anion over the whole mole fraction range in atmospheric pressure and the temperature range from 293.15 to 343.15 K and found that a small negative $V_m^E$. They also fitted their experimental data with Redlich-Kister polynomial equation. They investigated that their experimental results follow Grunberg and Nissan's mixing law and only a small deviated from ideality [75].

### 1.3.1.2. Viscosity

Viscosities have a vital role as fundamental data in the design of equipment, solution theory, process modeling, and molecular dynamics [76,77]. A comprehensive understanding of viscosity is essential for the development of computational models pertaining to heat transfer, mass transfer, and fluid dynamics, and holds significant physicochemical significance. The control of viscosity influences the production and processing of various products across a wide range of industrial applications [78]. Viscosity for binary mixes provides information about the mixtures'

fluidity as well as the presence of molecular interactions in the system [79]. Recent years have seen a significant studies on the viscosity of binary mixes involving a range of constituents, and the results have been mainly explained using molecular interactions model between the constituents [80-82]. The viscosity of ILs can be manipulated by changing chain length of alkyl side of the cations and constituent ions [83-85]. The excess viscosity ($\eta^E$) of ILs mixture is the viscosity which is determined by the extent deviation from the ideal behavior of experimental viscosity. $\eta^E$ variation provides a qualitative assessment of the strength of intermolecular contacts because viscosity is connected with molecular interactions for example electrostatic forces, hydrogen bonds, and van der Waals interactions. The $\eta^E$ of the DSILs can be calculated from the data obtained from experiments involving ILs and DSILs by using eq. 2 [86]

$$\eta^E = \eta_{experimental} - \eta_{ideal} \quad (2)$$

Bingham's eq. 3 has been used to calculate ideal viscosity based on the principle of additivity [87].

$$\eta_{deal} = X_1\eta_1 + X_2\eta_2 \quad (3)$$

Simple Arrhenius relaxation is not applicable to glass formers or supercooled liquids. The viscosities of ILs at their $T_g$ increase quickly and sharply, exhibiting super Arrhenius behavior. This rise in viscosity cannot be predicted by Eyring's equation which assumes ideality. To model this behavior, phenomenological equations such as the VFT eq. 4 [88] are used

$$\log \eta = \log \eta_o + \frac{B}{T - T_o} \quad (4)$$

where, $\eta_o$ is the viscosity at infinite temperature, B is a constant related to fragility, and $T_o$ is the Vogel temperature which can be taken as $T_g$. The most widely used method for simulating and forecasting non-Arrhenius viscous flow is the VFT equation. While it works well above working temperatures, it approximates poorly at lower temperatures. Mauro *et al.* modified the VFT equation to a form having both $T_g$ and m [89]

$$\log \eta(T) = \log \eta_o + \frac{(12 - \log \eta_o)^2}{m\left(\frac{T}{T_g} - 1\right) + (12 - \log \eta_o)} \quad (5)$$

where $T$ and $\eta$ are the variables and $\eta_o$, m, and $T_g$ are the fitting parameters. They also proposed a new equation, now known as the MYEGA equation based on the temperature dependence of configurational entropy ($S_C$) which performs well at lower temperatures.

$$\log \eta(T) = \log \eta_o + (12 - \log \eta_o)\frac{T_g}{T} exp\left[\left(\frac{m}{12 - \log \eta_o} - 1\right)\left(\frac{T_g}{T} - 1\right)\right] \quad (6)$$

**1.3.1.3. Conductivity**

ILs consist of cations and anions as opposed to conventional liquids like water or organic solvents, which are composed of neutral molecules [90]. These ions are often big and asymmetric, which helps explain why ILs have special features. ILs have drawn a lot of attention as electrolyte materials for a variety of electrochemical technologies, such as batteries, supercapacitors, fuel cells, organic dye-sensitized solar cells, actuators, smart windows, and more [91]. This is because many ILs show attractive features, including superior electrochemical/thermal resistivity, a wide range of liquidity, reduced flammability, non-volatility at standard pressure, and conductivity [90, 91]. The ionic conductivity [92], which measures the quantity of ionic carriers and their mobility, is a critical factor in determining whether ILs may be used in electrochemical devices. Conductivity of room temperatures ILs, is typically too low to allow for their employment in industrial products [93]. Their room temperature conductivities can be improved with the addition of different solvents. Fox *et al.* investigated the effect of aprotic solvents on the physicochemical properties of ILs composed of bis(trifluoromethane sulfonyl)imide ($TFSI^-$) salts with *N*-methyl-*N*-pentylpyrrolidinium ($PY_{15}^+$), piperidinium ($PI_{15}^+$), or morpholinium ($MO_{15}^+$) cations. The viscosity of the mixed system greatly reduces increasing the overall conductivities [92]. The addition of organic solvents might also accelerate the ionic mobilities of ILs. Saba *et al.* (2014) studied the behavior of binary mixtures composed of 1-butyl-3-methyl imidazolium chloride ($[C_4mim]Cl$) and different organic solvents at 25 ℃. The added organic solvents break up the bond connections existing between $[C_4mim]^+$ and $Cl^-$, allowing ions to move around freely. This free mobility of ions increases conductivity and reduces viscosity to variable degrees in all the analyzed mixtures [93]. Ionic conductivity can be boost significantly when two or more ILs are mixed together to form DSILs. Transport properties of DSILs based on protic and aprotic ILs have been analyzed by Thawarkar *et al.* at 298.15 K. When DSILs are compared to their individual pure IL-constituents, a considerable improvement in ionic conductivity has been shown, and also

this improvement varies depending on the composition of the ILs. The increased conductivity is attributable to availability of more ions in the DSILs [94]. The ionic conductivities of 1,8-Diazabicyclo-[5,4,0]-undec-7-ene (DBU), an organic super-strong base, were examined in a different work by Miran *et al.* using a variety of anions. The [DBU]-based ILs displayed ionic conductivity in the range of $10^{-2}$ S $cm^{-1}$ at 150 °C [95]. Sometimes, it is found that the resultant conductivities of the DSILs are even higher than that of the linear additions of the conductivities of the constituents ILs. Zhang *et al.* generated triple ion based DSILs to investigate the conductive nature of the system. It has been seen that the DSILs exhibited more ionic conductivities than the linear averages of the conductivities of the ILs demonstrating a positive deviation [96]. The Walden rule is a measure of the ionicity of ILs. Under Walden's rule, the solid line denotes favorable ionic behavior. A Walden plot is utilized to estimate the ionicity approximately, with an aqueous solution of KCl as the reference line. The ideal line has a slope of one and symbolizes full ion dissociation. The variation from this ideal line approximates ionicity. The Walden plot depicts the categorization of ILs into superionic, good, and poor liquids, as well as the relationship between low equivalent conductivity and low ionicity (ion pairing) [94, 97]. The existence of ionic couples or aggregation can be inferred from any deviation from the ideal Walden solid line [98,99]. The Walden rule can be expressed as

$$\Lambda.\eta = constant \quad (7)$$

where, Λ is molar conductivity at infinite dilution and η is viscosity at infinite dilution [97].

**1.3.1.4. Thermal stability**

The interest in ILs has developed quite significantly in accredited to its tunable properties depending on the composition of the ILs [100]. These tunable properties enable ILs to be utilized as superior alternative to conventional solvent. One of the intriguing characteristics of ionic liquids (ILs) is their exceptionally low vapor pressure, rendering them highly desirable as solvents [101,102]. Moreover, it is non-flammable and mostly non-toxic. These properties of ILs open new possibilities for construction of specific solvents to dissolute certain compounds which are insoluble or difficult to dissolute in conventional solvents [103]. Depending on the composition of ILs their properties vary. Recent studies have focused on the application of single ILs for the dissolution of certain compounds, in this case, cellulose [104,105]. Single ILs are limited in their

ability to dissolve cellulose, hence studies have been conducted using mixture of different solvents and ILs as potential solvents. Although these mixtures provide somewhat of enhanced dissolution characteristics compared to single ILs, there are still room for improvement [106-108].

DSILs exhibit promising potential to cover the lacking of single ILs by introducing properties unique to single ILs. DSILs are commonly described as mixture of two single ILs involving more than two different types of ions. Each DSIL is unique in terms of combination of types of ions, ratio of ions, their characteristics compared to single ILs [62]. Currently, DSILs are considered to be mixture of molecular solvents rather than distinct ILs, which is not ideal for a deep analysis of the physicochemical properties of the DSILs. The studies regarding the physicochemical properties of DSILs have been very sparse hence, these materials need to be characterized to investigate their physicochemical properties. Understanding the physicochemical properties of DSILs is very important for designing solute specific solvents. The thermal properties of deep eutectic solvents with ionic liquids (DSILs) necessitate investigation in order to assess their thermal behavior. For applications in industrial level, thermal properties of DSILs are very important finding their operational temperature range.

$T_m$, $T_g$, $T_d$ etc. are various thermal properties that need to be determined to optimize the operational temperature range for the DSILs. Moreover, heat capacities provide insight into the heat storage capacity of the materials as well as can estimate the heating and cooling requirements of the material. Imidazolium based ILs are interesting as these ILs are mostly used in dissolution of cellulose [109]. There exists a substantial body of literature pertaining to the thermal properties of ILs that are based on imidazolium cations [52,110-112]. DSILs of imidazolium based ILs could be formed by combining different ions resulting in a vast combination of DSILs. This large field has been left little investigated or unexamined. Thus, thermal behavior of DSILs need to be evaluated for further applications for the purpose of dissolving the cellulose. Researches regarding the thermal behavior of imidazolium based DSILs have been conducted to a very few extent [113]. These researches mainly focused on the heat capacities, thermal stability, thermal storage density etc. of the DSIL. Most of the works varied only the anion keeping one common cation. Other works included the effect of variation of the alkyl side chain length of the imidazolium group on the thermal properties of the ILs and DSILs have also been investigated [52].

#### 1.3.1.5. Thermodynamic properties

The process of cellulose dissolving in ILs exhibits an exothermic nature, suggesting that the cellulose-ILs interaction is thermodynamically favorable [13, 114-118]. Andanson *et al.* [119] investigated the thermodynamic parameters of dissolution of cellulose in $[C_2mim]CH_3CO_2$. The enthalpy of cellulose dissolution in $[C_2mim]CH_3CO_2$ was exothermic in nature releasing about $-132 \pm 8$ J/g of energy. The negative value of enthalpy of dissolution indicates a highly favorable interaction occurred between cellulose and ILs. Hence, temperature do not affect the dissolution of cellulose in either positively or negatively, at least not in the thermodynamic aspect. With the increase in temperature, the fluidity of ILs increased which facilitated the transport properties of ILs. As a result, solubility of cellulose in ILs enhanced [120]. By breaking the H-bonds in cellulose, ILs may dissociate with cations and anions as the temperature rose. This assisted in the dissolution of cellulose. [118,121,122]. Andanson *et al.* also reported that mixing of co-solvent dimethyl sulfoxide (DMSO) with $[C_2mim]CH_3CO_2$ does not influence the enthalpy of dissolution significantly indicating co-solvent does not take part significantly with the ions of $[C_2mim]CH_3CO_2$ and dissolved cellulose chains [119].

### 1.4. Excellence of ILs for the dissolution of cellulose

Currently, bulk cellulose is isolated in the industry from wood by employing Kraft pulping, which is an environmentally detrimental process. To overcome the environmental problem, Fort *et al.* approached this issue with simplicity and novelty by solubilizing cellulose in $[C_4mim]Cl$ [123]. The duration of dissolution and temperature had been reduced significantly at high pressure which was reported by Ibrahim *et al*. They also observed that ILs directly dissolves cellulose without any modification and it is regenerated by anti-solvent and can be shaped into fibers, films, beads, or other types [124]. Swatloski *et al.* [6] for the first time reported that $[C_4mim]Cl$ could achieve efficient dissolution of cellulose. The formation of H-bonds between the –OH proton of cellulose and the $Cl^-$ of the IL has been proposed as the cause of high solubility of cellulose in $[C_4mim]Cl$ [125]. The dissolving process involves active interactions between the $[C_4mim]Cl$ anions, cellulose sites, and water molecules, as demonstrated by molecular dynamics simulations. Kosan *et al*. investigated cellulose dissolution in different ILs, namely $[C_4mim]Cl$, $[C_4mim]CH_3CO_2$, $[C_2mim]CH_3CO_2$ and $[C_2mim]CH_3CO_2$ and the results regarding dissolution were contrasted with cellulose solutions in monohydrate N-methyl-morpholine-N-oxide. Ionic

solutions with an acetate anion are more likely to contain the dopes than those that contain chloride at larger concentrations of cellulose [126]. To overcome the viscosity problem of cellulose solution in ILs an experiment was conducted by Yamamoto and Miyake [127]. They combined $[C_4mim]CH_3CO_2$ with the co-solvents DMSO, DMAc, and DMF. Depending on the process temperature, $[C_4mim]CH_3CO_2$/DMSO could undergo a violent exothermic reaction. Viron et al (2021) [128] observed that the IL, 1-butyl-3- ethylimidazolium bromide $[C_4eim]Br$ solution did not dissolve α-cellulose immediately, rather IL just absorbed on α-cellulose. The cellulose began to dissolve after the mixture reached 60 °C, and the mixture subsequently crystallized into a clear, viscous solution. According to Cao *et al.* the IL in this instance, $[C_4eim]Br$, disrupts the H-bonding between the –OH groups of cellulose. The interaction between the $[C_4eim]Br$ and the O and H atoms of the –OH occurs through the electron donor-acceptor mechanism (EDA) [129]. The O atom functions as an electron donor and engages in an interaction with the $[C_4eim]^+$ of the $[C_4eim]Br$ compound. The $Br^-$ of the $[C_4eim]Br$ compound engages in hydrogen bonding with the H atom of the –OH group. The H-bonding disruption both between and within the α-cellulose molecules caused the unfolding of the chains of cellulose, consequently dissolving cellulose in the ILs [6,129].

Although many ILs have been used to dissolved cellulose, but, $[C_4mim]Cl$ and $[C_4mim]CH_3CO_2$ are the most widely used. Many studies have made the tendency of anions of ILs to form H-bonds responsible for the enhanced solubility of cellulose [130]. Xia *et al.* was synthesized N-vinylimidazole and 2-chlorthanol and applied them to cellulose dissolution [131]. The experimental findings indicate that the prepared IL could readily dissolve cellulose without the need for derivatization or degradation, hence preserving the inherent properties of cellulose intact. In their study, Raut *et al.* [132] observed the dissolution of cellulose samples with varying weight percentages (30, 28 , and 25 wt%) and different degrees of polymerization (789, 1644, and 2082) in N-allyl-N-methylmorpholinium acetate ($[AMMorph][CH_3CO_2]$) at a temperature of 120 °C during a duration of 20 mins. In a study conducted by Ibrahim *et al.* [124], it was demonstrated that 1-ethyl-3-methylimidazolium acetate ($[C_2mim][CH_3CO_2]$) dissolved 5 wt.% cellulose solutions in 40% DMSO within 1 h at 80 °C under pressure of 20 bar. This was achieved utilizing a high pressure solubility measuring equipment. Regenerated cellulose from IL/DMSO exhibit below par thermal stability and crystallinity compared to the original microcrystalline cellulose. Reyes *et al.* [133] used five different ILs: $[C_4mim]Cl$ , $[C_4mim]CH_3CO_2$, $[C_4mim][HSO_4]$,

[$C_2$mim]Cl, [$C_2$mim]$CH_3CO_2$ to dissolved Bleached Hardwood Kraft Pulp. All of these ILs are capable to dissolve cellulose at different levels.

**Table 1.2.** Dissolution of cellulose in imidazolium ILs

| ILs | Cellulose source | Method | Temperature (°C) | Solubility (g/100g) | Ref. |
|---|---|---|---|---|---|
| [$C_4$mim]Cl | Dissolving pulp | Heating | 100 | 10 | [6] |
| [$C_4$mim]Cl | Dissolving pulp | Microwave heating | - | 25 | [6] |
| AmimCl | Dissolved pulp | Heating | 80 | 14.5 | [114] |
| AmimCl | Cotton liter | Heating | 80 | 8.0 | [114] |
| Amim[HCOO] | MCC(DP250) | Heating | 60-85 | 10-20 | [115] |
| AmimCl | MCC(DP250) | Heating | 100 | 10 | [115] |
| AmimCl | MCC | Sonication | - | 27 | [134] |
| AmimCl | Cotton linter | Sonication | - | 13 | [134] |
| AmimCl | Kraft pulp | Sonication | - | 8 | [134] |
| [AMMorph][$CH_3CO_2$] | MCC(DP789) | Heating | 80 | 17 | [135] |
| [AMMorph][$CH_3CO_2$] | MCC(DP789 | Heating | 100 | 28 | [132] |
| [AMMorph][$CH_3CO_2$] | MCC(DP789 | Heating | 120 | 30 | [132] |
| [$C_8$mim]$CH_3CO_2$ | Avicel | Heating | 110 | <1 | |
| [$C_4$mim]$CH_3CO_2$ | Avicel | Heating | 100 | 12 | |

### 1.4.1 Mechanism of the dissolution of cellulose in ILs

Scheme 1.2 illustrates the plausible interactions between ILs and functional sites of cellulose. In their key study, Swatloski *et al.* [6] were the first to employ ILs in the process of dissolving cellulose. The researchers demonstrated that cellulose is capable of undergoing dissolution in imidazolium-based ILs containing $Cl^-$ anions, at concentrations reaching up to 25% (w/w), opening new opportunity for the processing of cellulose for various industrial applications. Since then, various ILs have been synthesized and applied for numerous industrial applications [136-141]. ILs are organic or inorganic anions that can melt at temperatures lower than 100 °C when combined with asymmetric organic cations [142,143]. The cations could be imidazolium, pyridinium and pyrrolidinium cores, which can consist of different allyl-, ethyl-, or butyl-side chains. The anions of ILs could be chloride, acetate, formate, and alkyl phosphate and so on [143-146].

Donor-acceptor interactions have been used as explanation to understand the dissolution of cellulose in ILs, which involves the cellulose O atom serving as the electron pair donor and the cellulose H atom serving as the electron pair acceptor [146,147]. The solubility of cellulose in ILs

is mainly influenced by the nature of constituents of ILs. Many studies reveal that anions of ILs play the major role for the dissolution of cellulose. The more the electronegativity of anions can dissolve the more amount of cellulose. For example, [$C_4$mim]Cl have higher dissolving ability than[$C_4$mim]Br, and [$C_4$mim]I [148,149]. Solubility of cellulose in ILs is highly dependent on the viscosity of ILs. Chain length of the alkyl side in imidazolium cation had positive correlation with the viscosity of ILs. Lower viscosity of ILs have a higher capability to dissolve more amount of cellulose [148]. Another important can be mentioned that, the capacity of the ILs that have the ability to break down the supramolecular structure of cellulose by the cleavage of inter and intramolecular H-bonds of the cellulose sheets resulting in the dissolution of cellulose [150]. The basic process by which ILs dissolve cellulose is by the formation of H-bonds between the anions of ILs and the cellulose $H^+$ of the –OH group in cellulose [151].

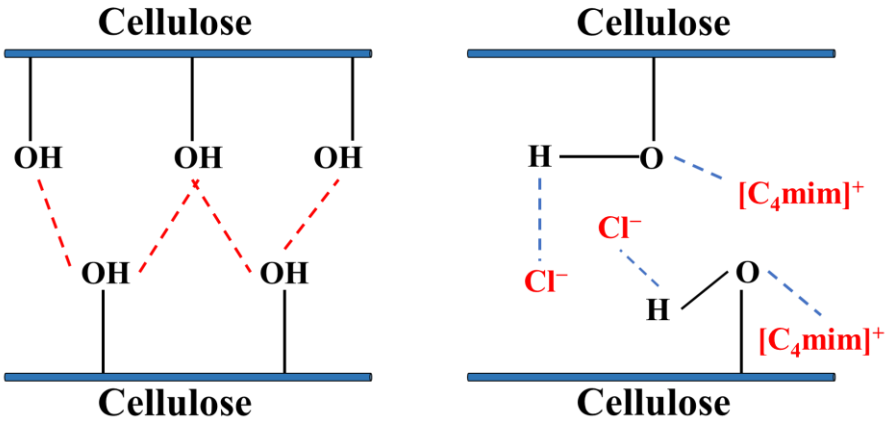


**Scheme 1.2.** Schematic representation of the mechanism of cellulose dissolution in [$C_4$mim]Cl [14]

Several studies have been conducted utilizing a combination of ILs that had a capacity to dissolve a greater amount of cellulose. The mixture of ILs with co-solvent such as DMSO, DMAC, DMF, etc., increases the solubility of cellulose in the mixture of ILs. The cations of ILs are solvated by the co-solvents and produced a greater number of free anions that is involved in the process of dissolution. Xu, *et al.* investigated the solubility of cellulose in [$C_4$mim]$CH_3CO_2$ + DMSO system and observed that this system can dissolve more amount of cellulose compared to ILs. They, suggested that, DMSO solvated the $[C_4mim]^+$ and more amount of free $CH_3CO_2^-$ produced which enhanced the dissolution process [152]. Another crucial element is that co-solvents can make ILs

less viscous, which is vital for the dissolving of more cellulose [153]. Research also showed that mixture of ILs enhanced the solubility of cellulose. Stolarska *et al.* investigated the solubility of cellulose in DSILs of $[C_2mim](CH_3CO_2)_{0.7}Cl_{0.3}$, and their eutectic of mixture $[C_2mim](CH_3CO_2)_{0.49}Cl_{0.51}$ and found that about 43 wt% of cellulose is dissolved in the mixture of of $[C_2mim](CH_3CO_2)_{0.7}Cl_{0.3}$ +DMSO system. They claimed that the synergistic effect of anions for breaking of the intra and intermolecular H-bonds of cellulose molecules is responsible for the dissolution of higher amounts of cellulose [154]. Zhao and coworkers [155] investigated the effect of co-solvents such as DMSO, DMF, $CH_3OH$ and $H_2O$ with $[C_4mim]CH_3CO_2$ for the dissolution of cellulose using molecular simulation and density functional theory (DFT) calculation. It was also reported by them that solubility of cellulose in ILs is influenced by both electrostatic interaction and H-bonding of cellulose-$CH_3CO_2^-$, and addition of co-solvents i.e., DMF and DMSO further enhanced the solubility. The role of co-solvent is to solvate the $[C_4mim]^+$ and break apart the $[C_4mim]^+$ and $CH_3CO_2^-$ ion pair. Thus, free $CH_3CO_2^-$ ions are produced which take part in H-bonding with cellulose consequently enhancing the solubility of cellulose in IL-solvent system. The schematic diagram of the mechanism of cellulose dissolution in the $[C_4mim]CH_3CO_2$+DMSO mixture have been presented in the following scheme.

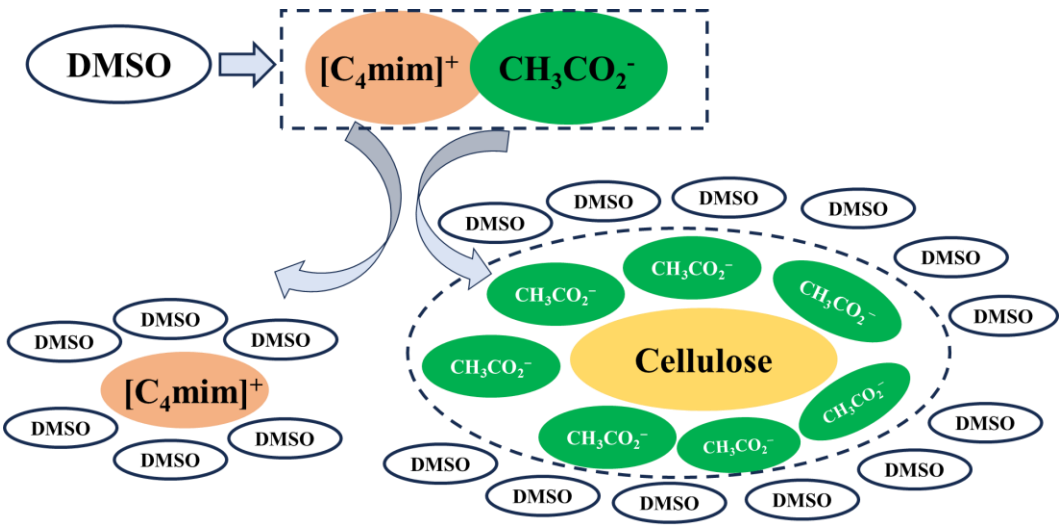


**Scheme 1.3.** Mechanism of the dissolution of cellulose in the $[C_4mim]CH_3CO_2$+DMSO mixture

### 1.4.2 Limitation of ILs for the dissolution of cellulose

Many researchers were motivated to develop a green alternative solvent due to the limitations of ILs, which include issues with toxicity, low biodegradability, and high cost [156]. It is true that large-scale industrial application of ILs is hindered by its high cost. Hence, recovery operations of ILs must be highly efficient to make them economically viable and sustainable. So far, various researches have been carried out to make the recycling of ILs economically sustainable [157-159]. In fact, efficient recycling and reuses can make ILs industrially feasible. Several studies have been conducted utilizing a combination of ILs that had a capacity to dissolve a greater amount of cellulose i.e., food, pharmaceutics, cosmetic, green energy storage materials, and polymer-based nanocomposites for sensor, energy storage, biomedicine, etc. [160-165]

## 1.5. Prospects of binary mixed ILs for the dissolution of cellulose

One of the important factors of ILs is their viscosity which heavily influences the solubility of cellulose in ILs. The viscosity of ILs is negatively correlated with the dissolution ability of the ILs. Hence, the viscosity of the ILs need to be reduced in order to efficiently solubilize cellulose. Individual ILs exhibit poor dissolution ability of cellulose due to its high viscosity. Thus, modification of the ILs system is required for enhanced dissolution of cellulose. Several studies have been conducted to reduce the viscosity of ILs and most preferred way is to add solvents in the ILs system. Table 1.3 presents the mixture of ILs and solvent system utilized to dissolve cellulose efficiently. In mixed solvent system, viscosity of the ILs is reduced and the mobility of the ions in the ILs increases. Consequently, this mobility of the ions is responsible for the increased solubility of cellulose in the IL system. Moreover, the conductivity of the system positively correlates with the addition of solvent and subsequent reduction of viscosity.

**Table 1.3.** Dissolution of cellulose in a mixture of ILs

| ILs medium | Cellulose source | Method | Temp. (°C) | Solubility (g/100g) | Ref. |
|---|---|---|---|---|---|
| $C_2$mim]Cl+[$C_2$mim]$CH_3CO_2$ (30:70 mol/mol) | MCC Sigma–Aldrich | Heating | 100 | 40 | [166] |
| [$C_2$mim]Cl | - | Heating | 100 | 12 | [166] |
| [$C_2$mim]$CH_3CO_2$ | - | Heating | 100 | 23 | [166] |
| [$C_4$mim]$CH_3CO_2$+DMSO ($R_{DMSO}$=2.54:1) | MCC (DP-229) | Immersed in an oil bath | 25 | 15.0 | [152] |
| [$C_4$mim]$CH_3CO_2$+DMF ($R_{DMF}$=2.71:1) | MCC (DP-229) | Immersed in an oil bath | 25 | 13.0 | [167] |
| [$C_4$mim]$CH_3CO_2$+DMAc ($R_{DMA}$=1.14:1) | MCC (DP-270) | Immersed in an oil bath | 25 | 9.0 | [168] |
| [$A_2$im]($CH_3OCH_2CO_2$)+MIM ($R_{MIM}$=0.50 | MCC Sigma–Aldrich | Immersed in an oil bath | 25 | 25.2 | [169] |
| [$A_2$im]($CH_3OCH_2CO_2$)+DMSO ($R_{DMSO}$=1.01) | MCC (DP-270) | Immersed in an oil bath | 25 | 26.1 | [170] |
| [$A_2$im]($CH_3OCH_2CO_2$)+DMAc ($R_{DMAc}$=1.01) | MCC (DP-270) | Immersed in an oil bath | 25 | 21.8 | [170] |
| [$C_4$mim]$CH_3CO_2$+LiAc | - | - | | 20.0 | [171] |
| [$C_4$mim]$CH_3CO_2$+LiCl | - | - | | 20 | [171] |
| [$C_4$mim]$CH_3CO_2$+$LiClO_4$ | - | - | | 21 | [171] |

$R_{DMSO}$ $R_{DMA}$, $R_{DMF}$, $R_{NMP}$ is the molar ratio of DMSO, DMAc, DMF and NMP to respective ILs.

### 1.6. Regeneration of cellulose from cellulose-ILs solution

Cellulose has the potential to undergo regeneration from a solution of cellulose-ILs by the addition of anti-solvents, including but not limited to water, acetone, ethanol, methanol, and acetonitrile [6,114,117, 134, 193, 194]. In theory, any solvent that dissolves IL can also be used as an anti-solvent. Cellulose-IL interaction is hampered because IL is dissolved in an anti-solvent, and cellulose precipitates out of the cellulose/IL solution as a result. The addition of anti-solvent to the solution is crucial for the cellulose regeneration process as it controls the morphology of the cellulose. The rapid addition of water with cellulose-IL solution results in the precipitation of cellulose in powder form [6]. The extrusion of the cellulose solution enables the formation of thin

fibers and rods [6, 126, 195]. Casting cellulose-ILs solution onto a glass plate leads to formation of cellulose thin films [114, 115, 196]. Cellulose aerogels can be prepared if the regenerated cellulose (RC) is washed with liquid $CO_2$ followed by drying under supercritical conditions [197]. The properties of RC changed from the native cellulose. The crystallinity of RC decreased [198], thermal stability decreased [199], and cellulose I (native cellulose) converted to cellulose II [200], degree of polymerization (DP) and weight average molecular weight decreased [6,132] and changed their surface morphology [133]. However, the majority of studies have consistently shown that the chemical composition of all research chemicals (RC) stays unaltered. The variety of structural forms of RC is the advantage for cellulose modification for various applications.

### 1.7. Functionalization of cellulose in ILs

Cellulose can be derivatized in homogeneous or heterogeneous synthesis methods. Heterogeneous synthesis method is applied for industrial production, but the method has some limitations for cellulose derivatives such as sluggish rate of reaction and lack of regioselectivity. The ability to overcome these restrictions is dependent upon the accessibility of -OH inside cellulose, which serves as the primary determinant for selectivity and the degree of substitution (DS). But when the derivatization of cellulose is conducted in a homogeneous phase system, the regioselectivity depends on the -OH groups but not the accessibility of -OH [172]. Due to their function as non-derivatizing solvents for cellulose, researchers have recently emphasized on the potential of ILs as innovative, environmental-friendly, homogenous reaction media for the production of derivatives of cellulose. Since –OH groups are widely dispersed in cellulose, it has an excellent capacity for chemical modification. The ILs are novel classes of aprotic and protic polar solvents that are extremely polar, chemically inert, and thermally stable, making them excellent media for the homogenous modification of cellulose. Nearly all typical cellulose derivatives were carefully and controllably created over the last two decades by homogenous reactions in the ILs. The recent introduction of numerous novel and functional groups onto cellulose chains through the process of modularization modification has given cellulose materials a number of new properties, including, melt processing capability, excellent solubility and processability, super-hydrophobicity, optical performance, flame-retardant capability, stimuli responsiveness, and adsorption and separation capabilities.

Cellulose derivatization is a process commonly employed for the synthesis of cellulose-based products, with heterogeneous methods traditionally being the preferred approach. However, researchers are recently motivated by the utilization of homogeneous methods for this purpose [173,174]. The homogeneous reaction has the following benefits: expanding the possibilities for the introduction of novel functional groups, providing fresh opportunities for product design, and providing a means of controlling the overall degree of replacement [175]. However, cellulose is very challenging to dissolve due to its rigid nature and close chain packing caused by multiple inter and intramolecular H-bonding. Appropriate solvents that can dissolve cellulose and create an environment that is conducive to the homogenous reaction are urgently required. Only a few solvent systems, namely DMAc/LiCl, DMF/$N_2O_4$, NMNO, and DMSO/TBAF, as well as some molten s/alt hydrates, including $LiClO_4.3H_2O$ and $LiSCN.2H_2O$, have been discovered so far. It has also been reported that homogeneous cellulose derivatizations, such as esterification, etherification, and other processes, can produce new compounds in these solvents [173,176-178]. Furthermore, these approaches may give rise to significant environmental challenges due to their inability to effectively recycle and reuse materials [114]. According to Zhang and his coworkers, homogeneous acetylation of cellulose in AMIMCl without requirement of any catalysts could be achieved. In addition, cellulose acetates with a variety of degrees of substitution could be produced [8]. Heinze and Barthel investigated the acetylation and carbonylation reaction of cellulose with [$C_4$mim]Cl without using any catalyst in mild conditions such as short reaction time and low amount of reagent.[115]. Heinze *et al.*, carried out carboxymethylation and acetylation of cellulose with [$C_4$mim]Cl without using any catalyst to produce highly substituted cellulose derivatives.[179]. Erdmenger *et al.* investigated the homogeneous tritylation of cellulose in [$C_4$mim]Cl using pyridine as base and observed the effect of duration of reaction and amount of trityl chloride. At about 3 h and a six times excess of trityl chloride were required to get DS of ~ 1[180]. Yang *et al.*, [181] carried out an esterification reaction of cellulose using switchable ILs of [DBUH][$O_2COCH_3$] composed of 1,8-diazabicyclo[5.4.0]undec-7-ene (DBU), methanol and $CO_2$ mixing with DMSO. This [DBUH][$O_2COCH_3$]-DMSO system could dissolve 8 wt% of cellulose. This solution was undergone a homogeneous esterification reaction to produced different esters such as cellulose acetate (CA), cellulose propionate (CP), and cellulose butyrate (CB) without using another catalyst. They observed that the DS of the product was maintained by optimizing the reaction condition and DMSO can facilitate the esterification reaction [182].

Similar to this research cellulose solution was used for homogeneous derivatization to produce CA, cellulose methyl carbonate, and cellulose levulinate [183-185]. Liu *et al.*, carried out homogeneous modification of cellulose succinilation with the mixture [$C_4$mim]Cl and DMSO and succinic anhydride in the presence of N-bromosuccinimide (NBS) as a catalyst. They found that the catalyst showed a significant effect on DS of succinylated cellulosic samples were 0.24-2.31 [186]. Barthel and coworkers (2006) carried out homogeneous acetylation and carbonylation of cellulose with the aprotic ILs of [$C_4$mim]Cl, [$C_2$mim]Cl, 1-butyl-2,3-dimethylimidazolium bromide ([$C_4$dmim]Br and 1-allyl-2,3-dimethylimidazolium bromide ([Admim]Br) for 2h at 80 °C under mild conditions, small excess reagent, and short period of reaction. They found that DS of CA in the range from 2.5 to 3.0 [187]. Huang *et al.*, prepared cellulose stearates with the DS value of 2.15, 2.19 and 2.57 from a homogeneous solution of cellulose and [$C_4$mim]Cl [188]. Liu *et al.* prepared cellulose acetoacetate (CAA) with the reaction of *tert*-butyl acetoacetate and AmimCl. Self-healing polysaccharide hydrogel was prepared by mixing this CAA with aqueous solution of chitosan through a Schiff-base reaction. The DS of CAA depends on the molar ratio of *tert*-butyl acetoacetate and AmimCl and the reaction time [189]. Polysaccharide hydrogels exhibiting redox/pH dual sensitive behavior were successfully synthesized, hence enabling self-healing capabilities [190]. Granström *et al.* carried out a green homogeneous esterification reaction of cellulose to produce highly water-repellent cellulose-stearoyl ester in AmimCl. This aerogel can spontaneously form from cellulose stearoyl esters with low DS, and the long stearoyl tails in combination with the porous aerogel structure cause a considerable rise in hydrophobicity from an aqueous contact angle of 0 to 124º [191]. Water soluble ionic cellulose can be formed from cellulose-dimethyl imidazolium methylphosphite solution at over 120 °C by phosphorylation reaction. Depending on the temperature and length of the reaction, the DS of phosphorylated cellulose varied between 0.4 and 1.3. With the DS value, this ionic cellulose became easier to dissolve [192].

### 1.8. Recycling of ILs

ILs are gaining popularity as promising solvents for a wide range of applications in academia and business. Due to ILs' inexpensive and effective utilization, there are currently few industrial processes that utilize them. Recycling and reusing ILs can increase their economic efficiency. Researchers have attempted various attempts to recover and recycle ILs throughout the

course of the previous few decades. For example, recycling ILs after cellulose processing offers a significant value proposition by reducing the IL preprocesses cost and making it more environmentally friendly [159]. However, thorough investigation is needed to optimize the economic aspect of the recycle process on a large scale. IL extraction techniques that have been researched include liquid-liquid extraction, distillation, induced phase separation, adsorption, and membrane-based procedures [158]. Because of restrictions related to hydrophobicity, all techniques are not equally applicable to all ILs. The known techniques for removing ILs from aqueous solution generally require a lot of money, require a lot of chemicals, or demand a lot of energy since ILs that solubilize cellulose are naturally water soluble. The biomass residues left in the aqueous coagulation and wash baths must be taken into consideration when using biomasses with higher levels of natural contaminants, such as fruit wastes. As a result, distillation—one of the most popular recapture techniques for hydrophilic ILs—is certainly unsuitable. Two procedures would likely be required to remove ILs from recycling streams using the most effective approaches, the first of which involves the removal of biomass residues and the second of which involves the removal of water [201,202]. As ILs are not susceptible to evaporation in typical drying process, it can be recycled from wood solution through evaporation of existing co-solvent and anti-solvent after the constituents of wood have been separated from the solution [203]. Due to their exceptional thermal stability and minimal vapor pressure, it has been suggested that ILs possess a high degree of recyclability with negligible losses. ILs, however, deteriorate because of the high temperatures utilized for the dissolution of wood and cellulose, according to numerous research. [204]. The wood moieties produced during dissolution may potentially act as a catalyst to accelerate their degradation [205]. The previously listed side reactions are another possible cause of losses [206,207].

In addition to mass loss, the performance of the recycled IL is also used to determine its recyclability of it. Wood could degrade and form oligomers at high dissolving temperatures rendering it impossible to regenerate from IL. These oligomers form aggregation in the IL resulting in reduction in its effectiveness [208,209]. The visual observation of darkening in ILs can be attributed to the presence of wood oligomers and heat degradants [210]. It is crucial to mention that that ILs may be evaporated in order to remove these oligomers. The successful execution of this process necessitates a significant heat and vacuum energy [211,212]. To solve this problem,

some methods have been developed, such as the creation of distillable carbenes and the back-alkylation of the anion [212]. In a range of applications, ILs have proven to be a potential alternative to traditional solvents. However, because ILs are somewhat expensive, very few methods are really commercialized. As a result, the commercialization of IL-using processes depends greatly on the recovery and reuse of ILs. The knowledge of the recyclability of ILs based on the literature that is now available in a variety of application domains is still in its early years, and this is acknowledged by ILs research communities.

### 1.9. Purification of ILs

The hygroscopic property of ILs facilitates their absorption of water during synthesis and utilization in diverse academic research or industrial applications. When ILs are exposed to atmospheric conditions, it becomes imperative to ascertain the water content inside ILs. Several techniques have been utilized to ascertain the water or moisture content in ionic liquids (ILs). The determination of small amounts water in ILs can be efficiently carried out using Karl-Fischer titration, which is a frequently employed method [213]. This technique allows for rapid measurement of water in ILs. Another method that can be employed for the determination of small quantities of water from ILs is gas chromatography (GC). This technique utilizes a single, clearly defined peak of $H_2O$, which does not have any impact on other components [214]. However, the process of water evaporation from ion ILs poses significant challenges due to its strong interaction with water molecules. Nevertheless, considering the little vapor pressure exhibited by ILs, the elimination of water from ILs can be achieved by means of controlled evaporation. The hydrophobic ILs can be purified by a series of steps involving washing with deionized water followed by evaporation. However, the purification of ILs can be achieved by the evaporation technique, which involves the measurement of electrical conductivity and the electrolysis of water molecules inside the ILs [215-220]. Momin *et al.* [221] have devised an electrochemical approach utilizing a platinum cathode and glassy carbon anode system to effectively eliminate water from ILs where water is broken down into $H_2$ and $O_2$ via the hydrogen evolution reaction (HER) and oxygen evolution reaction (OER), respectively, as described in eqs. 8 and 9.

Anodic reaction: $2\ H_2O = O_2 + 4\ H^+ + 4\ e^-$ (8)

Cathodic reaction: $4\ H_2O + 4\ e\text{-} = 2\ H_2 + 4\ OH^-$ (9)

Finally, a custom designed electrochemical cell with two compartments was used to remove water from an ILs system by employing a potentiostatic bulk electrolysis approach. The cell was composed of a cathode constructed from a graphite carbon plate, an anode composed of a platinum mesh in one compartment and an ionic liquid-based silver/silver ion reference electrode positioned in another compartment. They were successful to remove of water that has been studied using the $O_2/O_2^-$ couple redox reaction, the surface oxidation-reduction reactions of Au electrode, conductivity testing by using Karl Fisher titration.

**1.10. Reuse of ILs**

As ILs are highly cost, reuse of it several times may be a possible way to make ILs economically viable and sustainable at industrial scale. These applications include producing regenerated cellulose for textile industries, the yield of RC and the amount of recycled ILs is very important [158, 159, 223, 224]. In fact, efficient recycling and reuse can make ILs industrially feasible. So far, ILs have demonstrated promising features in various industrial applications such as food, pharmaceutics, cosmetics, green energy storage materials, and polymer-based nanocomposites for sensors, energy storage, biomedicine, etc. [160-165]. The recycling and reuse of ILs is crucial for implementing environmentally sustainable processes in several sectors. Numerous research has been conducted to investigate the recycling of ILs using various methodologies. The retrieval of the IL from the cellulose-IL solution was accomplished by introducing deionized water, which serves as an anti-solvent for the cellulose. The cellulose was subsequently isolated from the solution through the process of filtration. The filtrate obtained was subsequently subjected to evaporation and subsequent drying processes to get a purified IL. When subjected to significant biomass loadings, it is common for a gel phase to be generated, resulting in challenges in separating cellulose. However, this issue can be mitigated by employing a solution consisting of water and acetone in a 1:1 volume-to-volume ratio, as suggested by Sun *et al.* (2009). The IL recovery rate attained in a study done by Raut *et al.* was 97 wt%. Consequently, the investigators proceeded with further examination of the retrieved IL through the utilization of $^1$H NMR spectroscopy. Remarkably, there was no observed deterioration of the IL throughout the process of cellulose dissolution and subsequent regeneration. In the investigation conducted by Raut *et al.* it was observed that the IL exhibited successful utilization in the dissolution of cellulose

for three consecutive cycles, while consistently retaining its performance, even when exposed to roughly 3 wt% water. This way the reutilization of ILs could provide successive implementation of the ILs for the purpose of dissolving cellulose. These methods are not only economic but also environment-friendly making it feasible for the industrial application.

### 1.11. The complexity of DSILs for the dissolution of cellulose

The complexity due to DSILs for the dissolution of cellulose may arise from the multiple ions coexisting in DSILs. These DSILs typically consist of more than two complex organic cations and organic or inorganic anions, and their unique interactions with cellulose contribute to their distinctive properties. As DSILs are composed of multiple ions, complexity increases in their understanding of their interactions with cellulose and how these interactions affect the dissolution process. The properties of DSILs and interactions with cellulose can be tuned by varying the exact ion combination in them making it difficult to gain a deeper understanding. These combinations of ions in DSILs may cause high viscosity which influences the solubility of cellulose. The choice of anions in DSILs which play a major role in the dissolution can significantly impact their solvating ability and selectivity for cellulose. Theoretical studies could valuable insight into the complexity raised due to the use of DSILs during the dissolution of cellulose. This deep understanding could help in engineering ways to minimize this complexity.

### 1.12. Theoretical studies on ILs for the dissolution of cellulose

Computer simulation provides clear understanding of the microscopic interactions of cellulose-ILs solution and the reason of the enhancement of the dissolution of cellulose. Often confusion arises from the experimental studies of the dissolution of cellulose with ILs. For instance, the solubility of cellulose in ILs was found to be highly dependent on the anions of ILs interaction via H-bonding [219,220]. While some experiments revealed that interactions with anions are the major factor controlling cellulose dissolving [221,222] others revealed that cations significantly contribute in the cellulose dissolution process [223]. Hence, the underlying process of cellulose dissolution remains unclear. To understand the actual mechanism of the dissolution of cellulose in ILs or a mixture of ILs, Gupta *et al.* [224] have reviewed a number of computational studies. Simulations would give a better and thorough understanding of the enhancement of the dissolution of cellulose in DSILs. In recent years, several studies have explored the properties and

behavior of ILs through the utilization of molecular simulations. It is established experimentally and theoretically that mixtures of ILs with protic or aprotic co-solvents or DSILs tune their physicochemical properties for task-specific applications. Phadagi *et al.* [225] investigated experimentally and theoretically the role of co-solvent DMF with ILs of 1-butyl-3-methylimidazolium chloride ([$C_4$mim]Cl), 1-allyl-3-methylimidazolium chloride ([Amim]Cl) and 1-butyl-3-methylpyridinium chloride ([bmpy][Cl) for the dissolution of cellulose. Using the COSMO-RS theory and conceptual density functional theory (CDFT), they proved that DMF enhanced the dissolution of cellulose. In their study, Trenzado *et al.* [226] employed molecular dynamics techniques to explore the characteristics of the diffusion of $[BF_4]^-$ and $[TFSI]^-$ anions within the $[C_2mim][BF_4]_{0.5}[TFSI]_{0.5}$ liquid interface, as well as the underlying process of interface crossing. The findings provide a comprehensive analysis of the investigated DSIL. Therefore, the inclusion of multiple ions in ILs can be regarded as a potential approach to modulate physicochemical properties. This strategy enables the enhancement and alteration of the fluid's properties, thereby expanding its applicability across several domains. Dhakal *et al.*, [227] reviewed a number of articles based on molecular simulation analyses of the bulk properties and structure of ILs mixture. They mentioned that the mixing of ILs is a powerful technique for synthesizing DSILs of two cations or anions with tailor-made properties.

### 1.13. Objectives of the study

The main aim of this study is to develop a green and sustainable DSILs system for the efficient dissolution of cellulose through the following specific objectives.

1. Developing method for dissolution of cellulose using green solvents, ILs and their DSILs
2. Designing and computational modeling of the ILs and DSILs used for the dissolution of cellulose
3. Purification of dissolved cellulose via the concept of fractional precipitation and
4. Modification of cellulose via both physical and chemical means

### 1.14. Strategic plan of this study

The following strategies will be followed in order to accomplish the objectives of the proposed work-

- Utilizing various ILs – including protic and aprotic ILs – to develop an integrated processing route that would cover the efficient pulp extraction from natural sources and dissolution of cellulose from the pulp
- Studying the underlying physical chemistry of the dissolution process using spectroscopic, rheological and electrochemical methods
- Designing various combinations of DSILs – using a variety of cations and anions for the purpose- and preparation of the DSILs at various IL-to-IL mole fraction ratio
- Investigating the solution dynamics, rheology and nano-structure formation mechanism within the DSILs
- Applying density functional computational modeling to design and understand the nature of hydrophilic and hydrophobic regions in the DSILs and non-covalent interactions within the ions for ensuring the most efficient design of task-specific DSIL-based solvent media
- Applying the DSILs in the dissolution of cellulose and comparing their physical chemistry and efficiency with those of ILs
- Controlling the morphology of cellulose through physical means as well as perform chemical modification on cellulose using ILs and DSILs
- Gaining a deeper view of the structure of the cellulose IL systems from physical and chemical standpoint with an aim of industrial application

### 1.15. Experimental initiatives of this study

The cellulose used for the research will be obtained mainly from commercially available sources or by pulping any of the important common sources such as cotton, jute, wood, etc. Large batch will be prepared and the quality, average molecular weight, polydispersity etc. will be determined using solvent extraction, liquid chromatography, gel permeation chromatography, zeta potential measurement, and so on.

A range of DSILs using ILs with difference in structure of the cation and anion to give different hydrophilicity, in other words, hydrophobicity will be prepared at different compositions

and their physicochemical properties will be investigated in detail by studying density, viscosity, refractive index, solvatochromic behavior, conductivity, thermal stability, etc. The molecular environment in the DSIL systems will be studied by spectroscopic, computational and light scattering measurements.

Solutions of cellulose in ILs and DSILs will be prepared at different compositions. The solubility will be tested at different temperatures solubility limit determination. Correlation between IL structure, cellulose characteristics and solubility behavior will be developed.

Measurements of density, refractive index, and electrical conductivity will be performed on the cellulose solutions in ILs and DSILs. Density and refractive index data will provide information on volume change upon dissolution of cellulose in solvent and the molecular volumes. Electrical conductivity measurements will provide an understanding of the ionic environment of the polymer solutions. In order to gain insight into structure and nature of the solutions, a comparative analysis will be conducted between the empirical data and several theoretical models.

The variation of physicochemical properties of ILS and DSILs at different compositions will be exploited to purify/grade dissolved cellulose by varying the composition of the constituent ILs in the DSILs via the concept of fractional precipitation. The morphology of the cellulose will be analyzed by standard means using electron microscopy and x-ray diffraction, and differential scanning calorimetry. The dissolution of cellulose will be carried out in ILs and DSILs and it will be functionalized by oxidation to modify cellulose structure. The structural details of the modified cellulose will be elucidated.

**References**


[1] Klemm, D., Heublein, B., Fink, H. P., and Bohn, A. (2005). Cellulose: fascinating biopolymer and sustainable raw material. *Angewandte Chemie International Edition*, *44*(22), 3358-3393.

[2] Xia, Z., Li, J., Zhang, J., Zhang, X., Zheng, X., and Zhang, J. (2020). Processing and valorization of cellulose, lignin and lignocellulose using ionic liquids. *Journal of Bioresources and Bioproducts*, *5*(2), 79-95.

[3] Kumar, P., Barrett, D. M., Delwiche, M. J., and Stroeve, P. (2009). Methods for pretreatment of lignocellulosic biomass for efficient hydrolysis and biofuel production. *Industrial and Engineering Chemistry Research*, *48*(8), 3713-3729.

[4] Satari, B., Karimi, K., and Kumar, R. (2019). Cellulose solvent-based pretreatment for enhanced second-generation biofuel production: a review. *Sustainable Energy and Fuels*, *3*(1), 11-62.

[5] Yang, X., Xu, M., and Yang, S. T. (2015). Metabolic and process engineering of Clostridium cellulovorans for biofuel production from cellulose. *Metabolic Engineering*, *32*, 39-48.

[6] Biermann, C. J. (1996). *Handbook of Pulping and Papermaking*, Elsevier.

[7] Cross, C. F., Bevan, E. J., Beadle, C. (1892). Viscose Syndicate, British patent, 8700

[8] Johnson, D. L. (1969). *U.S. Patent No. 3,447,956*. Washington, DC: U.S. Patent and Trademark Office.

[9] Despeissis L. H. (1890). France Patent 203,741.

[10] Ekman, K., Eklund, V., Fors, J., Huttunen, J. I., Selin, J. F., and Turunen, O. T. (1986). In R. A. Young, and R. M. Rowell (Eds.), Cellulose structure, modification and hydrolysis, New York: Wiley, 131–148.

[11] Feng L, Chen Z-L (2008) Research progress on dissolution and functional modification of cellulose in ILss. *Journal of Molecular Liquids*, 142, 1–5.

[12] Klemm D, Philipp B, Heinze T, Heinze U (2004) Comprehensive cellulose chemistry. In: Wagenknecht W (ed) Fundamental and analytical methods, vol 1. Wiley-VCH publication, Weinheim.

[13] Zhang, J., Wu, J., Yu, J., Zhang, X., He, J., and Zhang, J. (2017). Application of ionic liquids for dissolving cellulose and fabricating cellulose-based materials: state of the art and future trends. *Materials Chemistry Frontiers*, *1*(7), 1273-1290.

[14] Holbrey, J. D., and Seddon, K. R. (1999). Ionic liquids. *Clean Products and Processes*, *1*(4), 223-236.

[15] Gordon, C. M., Holbrey, J. D., Kennedy, A. R., and Seddon, K. R. (1998). Ionic liquid crystals: hexafluorophosphate salts. *Journal of Materials Chemistry*, *8*(12), 2627-2636.

[16] Holbrey, J. D., and Seddon, K. R. (1999). The phase behaviour of 1-alkyl-3-methylimidazolium tetrafluoroborates; ionic liquids and ionic liquid crystals. *Journal of the Chemical Society, Dalton Transactions*, (13), 2133-2140.

[17] Plechkova, N. V., and Seddon, K. R. (2007). Ionic liquids: “designer” solvents for green chemistry. *Methods and Reagents for Green Chemistry: An Introduction*, 103-130.

[18] Wilkes, J. S., and Zaworotko, M. J. (1992). Air and water stable 1-ethyl-3-methylimidazolium based ionic liquids. *Journal of the Chemical Society, Chemical Communications*, (13), 965-967.

[19] Chatel, G., Pereira, J. F., Debbeti, V., Wang, H., and Rogers, R. D. (2014). Mixing ionic liquids–"simple mixtures" or "double salts"?. *Green Chemistry*, *16*(4), 2051-2083.

[20] Niedermeyer, H., Hallett, J. P., Villar-Garcia, I. J., Hunt, P. A., and Welton, T. (2012). Mixtures of ionic liquids. *Chemical Society Reviews*, *41*(23), 7780-7802.

[21] Annat, G., Forsyth, M., and MacFarlane, D. R. (2012). Ionic Liquid Mixtures-Variations in Physical Properties and Their Origins in Molecular Structure. *The Journal of Physical Chemistry B*, *116*(28), 8251-8258.

[22] Clough, M. T., Crick, C. R., Gräsvik, J., Hunt, P. A., Niedermeyer, H., Welton, T., and Whitaker, O. P. (2015). A physicochemical investigation of ionic liquid mixtures. *Chemical Science*, *6*(2), 1101-1114.

[23] Xiao, D., Rajian, J. R., Li, S., Bartsch, R. A., and Quitevis, E. L. (2006). Additivity in the optical Kerr effect spectra of binary ionic liquid mixtures: Implications for nanostructural organization. *The Journal of Physical Chemistry B*, *110*(33), 16174-16178.

[24] Long, J., Guo, B., Li, X., Jiang, Y., Wang, F., Tsang, S.C., Wang, L. and Yu, K.M.K. (2011). One step catalytic conversion of cellulose to sustainable chemicals utilizing cooperative ionic liquid pairs. *Green Chemistry*, *13*(9), 2334-2338.

[25] Zhu, Y., Chuanzhao, L., Sudarmadji, M., Hui Min, N., Biying, A. O., Maguire, J. A., and Hosmane, N. S. (2012). An efficient and recyclable catalytic system comprising nanopalladium (0) and a pyridinium salt of iron bis (dicarbollide) for oxidation of substituted benzyl alcohol and lignin. *ChemistryOpen*, *1*(2), 67-70.

[26] Al-Dahhan, W., Al-Zuhairi, A., Yousif, E., Rasool, H., and Hussein, F. (2017). Bad filling ionic liquid sample in split tube furnace. *Interdisciplinary Journal of Chemistry*, 2(2), 1-3.

[27] Chum, H. L., Koch, V. R., Miller, L. L., and Osteryoung, R. A. (1975). Electrochemical scrutiny of organometallic iron complexes and hexamethylbenzene in a room temperature molten salt. *Journal of the American Chemical Society*, *97*(11), 3264-3265.

[28] Wilkes, J.S., Levisky, J.A., Wilson, R.A., Hussey, C.L. Electron transfer. (1982). Reactions of dihydroriboflavin with metal-center oxidants. *Inorganic Chemistry*, 21, 1236-1264

[29] Wilkes, J. S., and Zaworotko, M. J. (1992). Air and water stable 1-ethyl-3-methylimidazolium based ionic liquids. *Journal of the Chemical Society, Chemical Communications*, (13), 965-967.

[30] Swatloski, R. P., Spear, S. K., Holbrey, J. D., and Rogers, R. D. (2002). Dissolution of cellose with ionic liquids. *Journal of the American Chemical Society*, *124*(18), 4974-4975.

[31] Welton, T. (1999). Room-temperature ionic liquids. Solvents for synthesis and catalysis. *Chemical Reviews*, *99*(8), 2071-2084.

[32] Hallett, J. P., and Welton, T. (2011). Room-temperature ionic liquids: solvents for synthesis and catalysis. 2. *Chemical Reviews*, *111*(5), 3508-3576.

[33] Mehnert, C. P., Cook, R. A., Dispenziere, N. C., and Afeworki, M. (2002). Supported ionic liquid catalysis− A new concept for homogeneous hydroformylation catalysis. *Journal of the American Chemical Society*, *124*(44), 12932-12933.

[34] Su, Y. Z., Fu, Y. C., Wei, Y. M., Yan, J. W., and Mao, B. W. (2010). The electrode/ionic liquid interface: electric double layer and metal electrodeposition. *ChemPhysChem*, *11*(13), 2764-2778.

[35] Poole, C. F., and Poole, S. K. (2010). Extraction of organic compounds with room temperature ionic liquids. *Journal of Chromatography A*, *1217*(16), 2268-2286.

[36] Sun, P., and Armstrong, D. W. (2010). Ionic liquids in analytical chemistry. *Analytica Chimica Acta*, *661*(1), 1-16.

[37] Anderson, J. L., Armstrong, D. W., and Wei, G. T. (2006). Ionic liquids in analytical chemistry. *Analytical Chemistry*, *78*(9), 2892-2902.

[38] Angell, C. A., Ansari, Y., and Zhao, Z. (2012). Ionic Liquids: Past, present and future. *Faraday Discussions*, *154*, 9-27.

[39] Seddon, K.R. (1997). Ionic liquids for clean technology. *Journal of Chemical Technology and Biotechnology: International Research in Process, Environmental and Clean Technology*, 68, 351–356.

[40] Pinkert, A., Marsh, K.N., Pang, S., and Staiger, M.P. (2009). Ionic liquids and their interaction with cellulose. *Chemical Reviews*, 109, 6712–6728.

[41] Wasserscheid, P., and Welton, T. (2008). Ionic liquids in synthesis, John Wiley and Sons: Hoboken, NJ, USA.

[42] Abushammala, H., and Mao, J. (2020). A review on the partial and complete dissolution and fractionation of wood and lignocelluloses using imidazolium ionic liquids. *Polymers*, *12*(1), 195.

[43] Rooney, D., Jacquemin, J., and Gardas, R. (2010). Thermophysical properties of ionic liquids. *Ionic Liquids*, 185-212.

[44] Handy, S. T. (2005). Room temperature ionic liquids: Different classes and physical properties. *Current Organic Chemistry*, *9*(10), 959-988.

[45] Xu, A., Zhang, Y., Li, Z., and Wang, J. (2012). Viscosities and conductivities of 1-butyl-3-methylimidazolium carboxylates ionic liquids at different temperatures. *Journal of Chemical and Engineering Data*, *57*(11), 3102-3108.

[46] Meindersma, G.W., Maase, M., and De Haan, A.B. (2000) Ionic liquids. In *Ullmann's Encyclopedia of IndustrialChemistry*, Wiley: Hoboken, NJ, USA.

[47] Othman, Z. S., Hassan, N. H., and Zubairi, S. I. (2017). Imidazolium-Based Ionic Liquid Binary Solvent System as an Extraction Medium in Enhancing the Rotenone Yield Extracted from Derris elliptica Roots. In *Progress and Developments in Ionic Liquids*. IntechOpen.

[48] Zhang, S., Lu, X., Zhou, Q., Li, X., Zhang, X., and Li, S. (2009). *Ionic liquids: physicochemical properties*. Elsevier.

[49] Iolitec Website. Available online: www.iolitec.de (accessed on 20 November 2019)

[50] Han, D., and Row, K. H. (2010). Recent applications of ionic liquids in separation technology. *Molecules*, *15*(4), 2405-2426.

[51] Pinkert, A., Goeke, D. F., Marsh, K. N., and Pang, S. (2011). Extracting wood lignin without dissolving or degrading cellulose: investigations on the use of food additive-derived ionic liquids. *Green Chemistry*, *13*(11), 3124-3136.

[52] Fredlake, C. P., Crosthwaite, J. M., Hert, D. G., Aki, S. N., and Brennecke, J. F. (2004). Thermophysical properties of imidazolium-based ionic liquids. *Journal of Chemical and Engineering Data*, *49*(4), 954-964.

[53] Ngo, H. L., LeCompte, K., Hargens, L., and McEwen, A. B. (2000). Thermal properties of imidazolium ionic liquids. *Thermochimica Acta*, *357*, 97-102.

[54] Chancelier, L., Boyron, O., Gutel, T., and Santini, C. (2016). Thermal stability of imidazolium-based ionic liquids. *French-Ukrainian Journal of Chemistry*, *4*(1), 51-64.

[55] Feng, W. Q., Lu, Y. H., Chen, Y., Lu, Y. W., and Yang, T. (2016). Thermal stability of imidazolium-based ionic liquids investigated by TG and FTIR techniques. *Journal of Thermal Analysis and Calorimetry*, *125*, 143-154.

[56] Wendler, F., Todi, L. N., and Meister, F. (2012). Thermostability of imidazolium ionic liquids as direct solvents for cellulose. *Thermochimica Acta*, *528*, 76-84.

[57] Erdmenger, T., Vitz, J., Wiesbrock, F., and Schubert, U. S. (2008). Influence of different branched alkyl side chains on the properties of imidazolium-based ionic liquids. *Journal of Materials Chemistry*, *18*(43), 5267-5273.

[58] Liu, C., Li, Y., and Hou, Y. (2018). Basicity characterization of imidazolyl ionic liquids and their application for biomass dissolution. *International Journal of Chemical Engineering*, *2018*, 1-8

[59] Peck, R. L., Brink, N. G., Kuehl Jr, F. A., Flynn, E. H., Walti, A., and Folkers, K. (1945). Streptomyces antibiotics.II. crystalline streptomycin trihydro chloride – calcium chloride double salt. *Journal of the American Chemical Society*, *67*(10), 1866-1867.

[60] Christov, C., and Balarew, C. (1995). Effect of temperature on the solubility of carnallite type double salts. *Journal of solution chemistry*, *24*, 1171-1182.

[61] Balarew, C., and Tepavitcharova, S. (2003). Double Salts Formation in the Systems MX–MeX 2–H 2 O (M= K, NH 4, Rb, Cs, Me= Mg, Mn, Fe, Co, Ni, Cu, X= Cl, Br). *Monatshefte für Chemie/Chemical Monthly*, *134*, 721-734.

[62] Chatel, G., Pereira, J. F., Debbeti, V., Wang, H., and Rogers, R. D. (2014). Mixing ionic liquids–"simple mixtures" or "double salts"?. *Green Chemistry*, *16*(4), 2051-2083.

[63] Rahman, A., Rahman, M. M., Mollah, M. Y. A., and Susan, M. A. B. H. (2019). Ultraslow Relaxation in Aprotic Double Salt Ionic Liquids. *The Journal of Physical Chemistry B*, *123*(26), 5577-5587.

[64] MacFarlane, D. R., Forsyth, M., Izgorodina, E. I., Abbott, A. P., Annat, G., and Fraser, K. (2009). On the concept of ionicity in ionic liquids. *Physical Chemistry Chemical Physics*, *11*(25), 4962-4967.

[65] Lehmann, J., Rausch, M. H., Leipertz, A., and Fröba, A. P. (2010). Densities and excess molar volumes for binary mixtures of ionic liquid 1-ethyl-3-methylimidazolium ethylsulfate with solvents. *Journal of Chemical and Engineering Data*, *55*(9), 4068-4074.

[66] Rodriguez, H., and Brennecke, J. F. (2006). Temperature and composition dependence of the density and viscosity of binary mixtures of water+ ionic liquid. *Journal of Chemical and Engineering Data*, *51*(6), 2145-2155.

[67] Liu, Q. S., Yang, M., Yan, P. F., Liu, X. M., Tan, Z. C., and Welz-Biermann, U. (2010). Density and surface tension of ionic liquids [C n py][NTf2](n= 2, 4, 5). *Journal of Chemical and Engineering Data*, *55*(11), 4928-4930.

[68] Zhang, S., Li, X., Chen, H., Wang, J., Zhang, J., and Zhang, M. (2004). Determination of physical properties for the binary system of 1-ethyl-3-methylimidazolium tetrafluoroborate+ $H_2O$. *Journal of Chemical and Engineering Data*, *49*(4), 760-764.

[69] Gonzalez, E. J., Alonso, L., and Domínguez, Á. (2006). Physical properties of binary mixtures of the ionic liquid 1-methyl-3-octylimidazolium chloride with methanol, ethanol, and 1-propanol at T=(298.15, 313.15, and 328.15) K and at P= 0.1 MPa. *Journal of Chemical and Engineering Data*, *51*(4), 1446-1452.

[70] Klomfar, J., Součková, M., and Pátek, J. (2011). Experimental p− ρ− T Data for 1-Butyl-3-methylimidazolium Tetrafluoroborate at Temperatures from (240 to 353) K and at Pressures up to 60 MPa. *Journal of Chemical and Engineering Data*, *56*(3), 426-436.

[71] Ali, M. A., and Susan, M. A. B. H. (2022). Volumetric and Spectroscopic Studies of 1-ethyl-3-methylimidazolium Ethylsulfate/Propane-1-ol Binary Mixtures at Different Temperatures. *Spectrum of Emerging Sciences*, *2*(2), 17-28.

[72] Marium, M., Auni, A., Rahman, M. M., Mollah, M. Y. A., and Susan, M. A. B. H. (2017). Molecular level interactions between 1-ethyl-3-methylimidazolium methanesulphonate and water: Study of physicochemical properties with variation of temperature. *Journal of Molecular Liquids*, *225*, 621-630. 14. Canongia Lopes, J. N., Cordeiro, T. C., Esperança, J. M., Guedes, H.

[73] J., Huq, S., Rebelo, L. P., and Seddon, K. R. (2005). Deviations from ideality in mixtures of two ionic liquids containing a common ion. *The Journal of Physical Chemistry B*, *109*(8), 3519-3525.

[74] Navia, P., Troncoso, J., and Romaní, L. (2007). Excess magnitudes for ionic liquid binary mixtures with a common ion. *Journal of Chemical and Engineering Data*, *52*(4), 1369-1374.

[75] Song, D., and Chen, J. (2014). Density and viscosity data for mixtures of ionic liquids with a common anion. *Journal of Chemical and Engineering Data*, *59*(2), 257-262.

[76] Wang, L. C., Xu, H. S., Zhao, J. H., Song, C. Y., and Wang, F. A. (2005). Density and viscosity of (3-picoline+ water) binary mixtures from T=(293.15 to 343.15) K. *The Journal of Chemical Thermodynamics*, *37*(5), 477-483.

[77] Mchaweh, A., Alsaygh, A., Nasrifar, K., and Moshfeghian, M. (2004). A simplified method for calculating saturated liquid densities. *Fluid phase equilibria*, *224*(2), 157-167.

[78] Bauer, K., Garbe, D., and Surburg, H. (2008). *Common fragrance and flavor materials: preparation, properties and uses*. John Wiley and Sons

[79] Rowlinson JS, Swinton FL. Liquids and liquid mixtures. London: Butterworth and Co. Ltd, 1982.

[80] Oswal, S. L., and Patel, N. B. (2000). Viscosities of nonelectrolyte liquid mixtures containing acrylonitrile. *International journal of thermophysics*, *21*, 999-1010.

[81] Cruz, R. D. C., Martins, R. J., Cardoso, M. J. D. M., and Barcia, O. E. (2002). Measurement of the viscosity of binary and ternary systems containing benzaldehyde, toluene, and benzyl alcohol at 293.15 K and 0.1 MPa. *Journal of Chemical and Engineering Data*, *47*(4), 927-931.

[82] Kumar Naidu, B. V., Rao, K. C., and Subha, M. C. S. (2002). Densities and viscosities of mixtures of some glycols and polyglycols in dimethyl sulfoxide at 308.15 K. *Journal of Chemical and Engineering Data*, *47*(3), 379-382.

[83] Tokuda, H., Hayamizu, K., Ishii, K., Susan, M. A. B. H., and Watanabe, M. (2004). Physicochemical properties and structures of room temperature ionic liquids. 1. Variation of anionic species. *The Journal of Physical Chemistry B*, *108*(42), 16593-16600.

[84] Tokuda, H., Hayamizu, K., Ishii, K., Susan, M. A. B. H., and Watanabe, M. (2005). Physicochemical properties and structures of room temperature ionic liquids. 2. Variation of alkyl chain length in imidazolium cation. *The Journal of Physical Chemistry B*, *109*(13), 6103-6110.

[85] Tokuda, H., Ishii, K., Susan, M. A. B. H., Tsuzuki, S., Hayamizu, K., and Watanabe, M. (2006). Physicochemical properties and structures of room-temperature ionic liquids. 3. Variation of cationic structures. *The Journal of Physical Chemistry B*, *110*(6), 2833-2839.

[86] Fan, W., Zhou, Q., Sun, J., and Zhang, S. (2009). Density, excess molar volume, and viscosity for the methyl methacrylate+ 1-butyl-3-methylimidazolium hexafluorophosphate ionic liquid binary system at atmospheric pressure. *Journal of Chemical and Engineering Data*, *54*(8), 2307-2311.

[87] Bingham, E. C. (1922). *Fluidity and plasticity*. McGraw-Hill.

[88] Tammann, G., Hesse, W. Die Abhängigkeit Der Viscosität von Der Temperatur Bie Unterkühlten Flüssigkeiten. Zeitschrift für Anorg. und Allg. Chemie 1926, 156 (1), 245–257.

[89] Mauro, J. C., Yue, Y., Ellison, A. J., Gupta, P. K., Allan, D. C. Viscosity of Glass-Forming Liquids. Proc. Natl. Acad. Sci. U. S. A. 2009, 106 (47), 19780–19784.

[90] Forsyth, S. A., Pringle, J. M., and MacFarlane, D. R. (2004). Ionic liquids—an overview. *Australian Journal of Chemistry*, *57*(2), 113-119.

[91] Plechkova, N. V., and Seddon, K. R. (2008). Applications of ionic liquids in the chemical industry. *Chemical Society Reviews*, *37*(1), 123-150.

[92] Fox, E. T., Paillard, E., Borodin, O., and Henderson, W. A. (2013). Physicochemical properties of binary ionic liquid–aprotic solvent electrolyte mixtures. *The Journal of Physical Chemistry C*, *117*(1), 78-84.

[93] Saba, H., Zhu, X., Chen, Y., and Zhang, Y. (2015). Determination of physical properties for the mixtures of [BMIM] Cl with different organic solvents. *Chinese Journal of Chemical Engineering*, *23*(5), 804-811.

[94] Khupse, N. D., Shinde, D. R., and Kumar, A. (2019). Understanding the behavior of mixtures of protic-aprotic and protic-protic ionic liquids: Conductivity, viscosity, diffusion coefficient and ionicity. *Journal of Molecular Liquids*, *276*, 986-994.

[95] Miran, M. S., Kinoshita, H., Yasuda, T., Susan, M. A. B. H., and Watanabe, M. (2012). Physicochemical properties determined by Δp K a for protic ionic liquids based on an organic super-strong base with various Brønsted acids. *Physical Chemistry Chemical Physics*, *14*(15), 5178-5186.

[96] Zhang, H., Cui, X., Li, P., Feng, T., and Feng, H. (2022). Measurement and correlation for the electrical conductivity of double salt ionic liquids with triple ions. *Journal of Molecular Liquids*, *365*, 120193.

[97] Schreiner, C., Zugmann, S., Hartl, R., and Gores, H. J. (2010). Fractional Walden rule for ionic liquids: examples from recent measurements and a critique of the so-called ideal KCl line for the Walden plot. *Journal of Chemical and Engineering Data, 55*(5), 1784-1788.

[98] Yoshida, Y., Baba, O., and Saito, G. (2007). Ionic liquids based on dicyanamide anion: influence of structural variations in cationic structures on ionic conductivity. *The Journal of Physical Chemistry B, 111*(18), 4742-4749.

[99] Gomez, E., Gonzalez, B., Domínguez, Á., Tojo, E., and Tojo, J. (2006). Dynamic viscosities of a series of 1-alkyl-3-methylimidazolium chloride ionic liquids and their binary mixtures with water at several temperatures. *Journal of Chemical and Engineering Data*, *51*(2), 696-701.

[100] Seddon, K. (2002). Ionic liquids: designer solvents for green synthesis. *Chemical Engineer*, 730, 33-35.

[101] Mallakpour, S., and Dinari, M. (2012). Ionic liquids as green solvents: progress and prospects. *Green solvents II: Properties and Applications of Ionic Liquids*, 1-32.

[102] Dai, Y., Van Spronsen, J., Witkamp, G. J., Verpoorte, R., and Choi, Y. H. (2013). Ionic liquids and deep eutectic solvents in natural products research: mixtures of solids as extraction solvents. *Journal of Natural Products*, *76*(11), 2162-2173.

[103] Marsh, K. N., Deev, A., Wu, A. C., Tran, E., and Klamt, A. (2002). Room temperature ionic liquids as replacements for conventional solvents–A review. *Korean Journal of Chemical Engineering*, 19(3), 357-362.

[104] Feng, L., and Chen, Z. L. (2008). Research progress on dissolution and functional modification of cellulose in ionic liquids. *Journal of Molecular Liquids*, *142*(1-3), 1-5.

[105] Vitz, J., Erdmenger, T., and Schubert, U. S. (2010). Imidazolium based ionic liquids as solvents for cellulose chemistry. In Cellulose Solvents: For analysis, shaping and chemical modification. *American Chemical Society*, 299-317.

[106] Verma, C., Mishra, A., Chauhan, S., Verma, P., Srivastava, V., Quraishi, M. A., and Ebenso, E. E. (2019). Dissolution of cellulose in ionic liquids and their mixed cosolvents: A review. *Sustainable Chemistry and Pharmacy*, *13*, 100162.

[107] Chhotaray, P. K., Biswal, S. K., and Pandey, S. (2020). Development of novel hybrid ionic fluids for efficient CO2 capture and cellulose dissolution. *Journal of Molecular Liquids*, *312*, 113477.

[108] Kasprzak, D., Krystkowiak, E., Stępniak, I., and Galiński, M. (2019). Dissolution of cellulose in novel carboxylate-based ionic liquids and dimethyl sulfoxide mixed solvents. *European Polymer Journal*, *113*, 89-97.

[109] Andanson, J. M., Bordes, E., Devémy, J., Leroux, F., Pádua, A. A., and Gomes, M. F. C. (2014). Understanding the role of co-solvents in the dissolution of cellulose in ionic liquids. *Green Chemistry*, *16*(5), 2528-2538.

[110] Erdmenger, T., Vitz, J., Wiesbrock, F., and Schubert, U. S. (2008). Influence of different branched alkyl side chains on the properties of imidazolium-based ionic liquids. *Journal of Materials Chemistry*, *18*(43), 5267-5273.

[111] Gómez, E., Calvar, N., Domínguez, Á., and A. Macedo, E. (2013). Thermal analysis and heat capacities of 1-Alkyl-3-methylimidazolium ionic liquids with $NTf^{2-}$, $TFO^{-}$, and $DCA^{-}$ anions. *Industrial and Engineering Chemistry Research*, *52*(5), 2103-2110.

[112] Kuhn, B.L., Osmari, B.F., Heinen, T.M., Bonacorso, H.G., Zanatta, N., Nielsen, S.O., Ranathunga, D.T., Villetti, M.A. and Frizzo, C.P. (2020). Dicationic imidazolium-based dicarboxylate ionic liquids: Thermophysical properties and solubility. *Journal of Molecular Liquids*, *308*, 112983.

[113] Kuhn, B.L., Osmari, B.F., Heinen, T.M., Bonacorso, H.G., Zanatta, N., Nielsen, S.O., Ranathunga, D.T., Villetti, M.A. and Frizzo, C.P. (2020). Dicationic imidazolium-based dicarboxylate ionic liquids: Thermophysical properties and solubility. *Journal of Molecular Liquids*, *308*, 112983.

[114] Zhang, H., Wu, J., Zhang, J., and He, J. (2005). 1-Allyl-3-methylimidazolium chloride room temperature ionic liquid: a new and powerful nonderivatizing solvent for cellulose. *Macromolecules*, *38*(20), 8272-8277.

[115] Fukaya, Y., Sugimoto, A., and Ohno, H. (2006). Superior solubility of polysaccharides in low viscosity, polar, and halogen-free 1, 3-dialkylimidazolium formates. *Biomacromolecules*, *7*(12), 3295-3297.

[116] Fukaya, Y., Hayashi, K., Wada, M., and Ohno, H. (2008). Cellulose dissolution with polar ionic liquids under mild conditions: required factors for anions. *Green Chemistry*, *10*(1), 44-46.

[117] Xu, A., Wang, J., and Wang, H. (2010). Effects of anionic structure and lithium salts addition on the dissolution of cellulose in 1-butyl-3-methylimidazolium-based ionic liquid solvent systems. *Green chemistry*, *12*(2), 268-275.

[118] Xu, A., Chen, L., and Wang, J. (2018). Functionalized imidazalium carboxylates for enhancing practical applicability in cellulose processing. *Macromolecules*, *51*(11), 4158-4166.

[119] Andanson, J. M., Padua, A. A. H., and Gomes, M. C. (2015). Thermodynamics of cellulose dissolution in an imidazolium acetate ionic liquid. *Chemical Communications*, *51*(21), 4485-4487.

[120] Andanson, J. M., Bordes, E., Devémy, J., Leroux, F., Pádua, A. A., and Gomes, M. F. C. (2014). Understanding the role of co-solvents in the dissolution of cellulose in ionic liquids. *Green Chemistry*, *16*(5), 2528-2538.

[121] Xu, A., Zhang, Y., Lu, W., Yao, K., and Wang, J. (2015). Transport properties of some 1-butyl-3-methylimidazolium carboxylate ionic liquids. *Journal of Chemical and Engineering Data*, *60*(3), 580-585.

[122] Xu, A., Zhang, Y., Li, Z., and Wang, J. (2012). Viscosities and conductivities of 1-butyl-3-methylimidazolium carboxylates ionic liquids at different temperatures. *Journal of Chemical and Engineering Data*, *57*(11), 3102-3108.

[123] Fort, D. A., Remsing, R. C., Swatloski, R. P., Moyna, P., Moyna, G., and Rogers, R. D. (2007). Can ionic liquids dissolve wood? Processing and analysis of lignocellulosic materials with 1-n-butyl-3-methylimidazolium chloride. *Green Chemistry*, *9*(1), 63-69.

[124] Ibrahim, F., Moniruzzaman, M., Yusup, S., and Uemura, Y. (2015). Dissolution of cellulose with ionic liquid in pressurized cell. *Journal of Molecular Liquids*, *211*, 370-372.

[125] Moulthrop, J. S., Swatloski, R. P., Moyna, G., and Rogers, R. D. (2005). High-resolution 13C NMR studies of cellulose and cellulose oligomers in ionic liquid solutions. *Chemical Communications*, (12), 1557-1559.

[126] Kosan, B., Michels, C., and Meister, F. (2008). Dissolution and forming of cellulose with ionic liquids. *Cellulose*, *15*, 59-66.

[127] Yamamoto, Y. K., and Miyake, A. (2017). Influence of a mixed solvent containing ionic liquids on the thermal hazard of the cellulose dissolution process. *Journal of Thermal Analysis and Calorimetry*, *127*(1), 743-748.

[128] Viron, K. P., Falcatan, A. M., and Leano Jr, J. L. (2021). Ionic liquid-mediated synthesis of cellulose/montmorillonite nanocomposite. *Cellulose Chemistry and Technology*, *55*(1-2), 169-175.

[129] Cao, Y., Wu, J., Zhang, J., Li, H., Zhang, Y., and He, J. (2009). Room temperature ionic liquids (RTILs): A new and versatile platform for cellulose processing and derivatization. *Chemical Engineering Journal*, *147*(1), 13-21.

[130] Sun, N., Parthasarathi, R., Socha, A.M., Shi, J., Zhang, S., Stavila, V., Sale, K.L., Simmons, B.A. and Singh, S. (2014). Understanding pretreatment efficacy of four cholinium and imidazolium ionic liquids by chemistry and computation. *Green Chemistry*, *16*(5), 2546-2557.

[131] Xia, Y., Ren, Q., Zhang, H., Zhong, Y., Guo, J., and Zhang, S. (2018). Ionic liquid based on alkyl imidazolium cation: Synthesis and application. *Cellulose Chemistry and Technology*, *52*, 1-7.

[132] Raut, D. G., Sundman, O., Su, W., Virtanen, P., Sugano, Y., Kordas, K., and Mikkola, J. P. (2015). A morpholinium ionic liquid for cellulose dissolution. *Carbohydrate Polymers*, *130*, 18-25.

[133] Reyes, G., Aguayo, M. G., Fernández Pérez, A., Pääkkönen, T., Gacitúa, W., and Rojas, O. J. (2019). Dissolution and hydrolysis of bleached kraft pulp using ionic liquids. *Polymers*, *11*(4), 673.

[134] Mikkola, J.P., Kirilin, A., Tuuf, J.C., Pranovich, A., Holmbom, B., Kustov, L.M., Murzin, D.Y. and Salmi, T. (2007). Ultrasound enhancement of cellulose processing in ionic liquids: from dissolution towards functionalization. *Green Chemistry*, *9*(11), 1229-1237.

[135] Heinze, T., and Koschella, A. (2005). Solvents applied in the field of cellulose chemistry: a mini review. *Polímeros*, *15*, 84-90.

[136] Azimi, B., Maleki, H., Gigante, V., Bagherzadeh, R., Mezzetta, A., Milazzo, M., Guazzelli, L., Cinelli, P., Lazzeri, A. and Danti, S. (2022). Cellulose-based fiber spinning processes using ionic liquids. *Cellulose*, *29*(6), 3079-3129.

[137] Wang, H., Gurau, G., and Rogers, R. D. (2012). Ionic liquid processing of cellulose. *Chemical Society Reviews*, *41*(4), 1519-1537.

[138] Greer, A. J., Jacquemin, J., and Hardacre, C. (2020). Industrial applications of ionic liquids. *Molecules*, *25*(21), 5207.

[139] Plechkova, N. V., and Seddon, K. R. (2008). Applications of ionic liquids in the chemical industry. *Chemical Society Reviews*, *37*(1), 123-150.

[140] Shiflett, M. B. (Ed.). (2020). *Commercial applications of ionic liquids* (Vol. 605). Cham, Switzerland: Springer.

[141] Toledo Hijo, A. A., Maximo, G. J., Costa, M. C., Batista, E. A., and Meirelles, A. J. (2016). Applications of ionic liquids in the food and bioproducts industries. *ACS Sustainable Chemistry and Engineering*, *4*(10), 5347-5369.

[142] Trujillo-Rodríguez, M. J., Nan, H., Varona, M., Emaus, M. N., Souza, I. D., and Anderson, J. L. (2018). Advances of ionic liquids in analytical chemistry. *Analytical Chemistry*, *91*(1), 505-531.

[143] Zhang, Q., and Shreeve, J. N. M. (2014). Energetic ionic liquids as explosives and propellant fuels: a new journey of ionic liquid chemistry. *Chemical Reviews*, *114*(20), 10527-10574.

[144] Tadesse, H., and Luque, R. (2011). Advances on biomass pretreatment using ionic liquids: an overview. *Energy and Environmental Science*, *4*(10), 3913-3929.

[145] Lopes, J. M., Bermejo, M. D., Martín, Á., and Cocero, M. J. (2017). Ionic liquid as reaction media for the production of cellulose-derived polymers from cellulosic biomass. *ChemEngineering*, *1*(2), 10.

[146] Beil, S., Markiewicz, M., Pereira, C. S., Stepnowski, P., Thöming, J., and Stolte, S. (2021). Toward the proactive design of sustainable chemicals: Ionic liquids as a prime example. *Chemical Reviews*, *121*(21), 13132-13173.

[147] Lindman, B., Karlström, G., and Stigsson, L. (2010). On the mechanism of dissolution of cellulose. *Journal of Molecular Liquids*, *156*(1), 76-81.

[148] Dadi, A. P., Varanasi, S., and Schall, C. A. (2006). Enhancement of cellulose saccharification kinetics using an ionic liquid pretreatment step. *Biotechnology and Bioengineering*, *95*(5), 904-910.

[149] Holm, J., and Lassi, U. (2011). Ionic liquids in the pretreatment of lignocellulosic biomass. In Ionic liquids: applications and perspectives. *IntechOpen*.

[150] Medronho, B., and Lindman, B. (2015). Brief overview on cellulose dissolution/regeneration interactions and mechanisms. *Advances in Colloid and Interface Science*, *222*, 502-508.

[151] Tian, Q., Liu, S., Sun, X., Sun, H., Xue, Z., and Mu, T. (2015). Theoretical studies on the dissolution of chitosan in 1-butyl-3-methylimidazolium acetate ionic liquid. *Carbohydrate Research*, *408*, 107-113.

[152] Xu, A., Zhang, Y., Zhao, Y., and Wang, J. (2013). Cellulose dissolution at ambient temperature: Role of preferential solvation of cations of ionic liquids by a cosolvent. *Carbohydrate Polymers*, *92*(1), 540-544.

[153] Dissanayake, N., Thalangamaarachchige, V. D., Thakurathi, M., Knight, M., Quitevis, E. L., and Abidi, N. (2019). Dissolution of cotton cellulose in 1: 1 mixtures of 1-butyl-3-methylimidazolium methylphosphonate and 1-alkylimidazole co-solvents. *Carbohydrate Polymers*, *221*, 63-72.

[154] Stolarska, O., Pawlowska-Zygarowicz, A., Soto, A., Rodríguez, H., and Smiglak, M. (2017). Mixtures of ionic liquids as more efficient media for cellulose dissolution. *Carbohydrate Polymers*, *178*, 277-285.

[155] Zhao, Y., Liu, X., Wang, J., and Zhang, S. (2013). Insight into the cosolvent effect of cellulose dissolution in imidazolium-based ionic liquid systems. *The Journal of Physical Chemistry B*, *117*(30), 9042-9049.

[156] Mohd, N., Draman, S. F. S., Salleh, M. S. N., and Yusof, N. B. (2017). Dissolution of cellulose in ionic liquid: A review. *AIP conference proceedings*, 1809 (1).

[157] Karadaghi, L. R., Malmstadt, N., Van Allsburg, K. M., and Brutchey, R. L. (2020). Techno-Economic Analysis of Recycled Ionic Liquid Solvent Used in a Model Colloidal Platinum Nanoparticle Synthesis. *ACS Sustainable Chemistry and Engineering*, *9*(1), 246-253.

[158] Mai, N. L., Ahn, K., and Koo, Y. M. (2014). Methods for recovery of ionic liquids—A review. *Process Biochemistry*, *49*(5), 872-881.

[159] Kuzmina, O. (2016). Economical aspects of ionic liquid application. In Application, Purification, and Recovery of Ionic Liquids, *Elsevier*, 249-263.

[160] Mesquita, L. M., Murador, D. C., and de Rosso, V. V. (2023). Application of ionic liquid solvents in the food industry. In Encyclopedia of ionic liquids, *Springer Nature Singapore*, 72-87.

[161] Zhuang, W., Hachem, K., Bokov, D., Ansari, M. J., and Nakhjiri, A. T. (2022). Ionic liquids in pharmaceutical industry: A systematic review on applications and future perspectives. *Journal of Molecular Liquids*, *349*, 118145.

[162] Toledo Hijo, A.A., Meirelles, A.A., Maximo, G.J., Cunha, R.L., Cristianini, M., Leite, T.S., Pereira, J.F. and Meirelles, A.J. (2022). Synergetic Application of Ionic Liquids as New Naturally based Antimicrobial Preservatives and Emulsifiers. *ACS Sustainable Chemistry and Engineering*, *10*(46), 15017-15024

[163] Vilas-Boas, S. M., Coelho, A. Z., Martins, M. A., Coutinho, J. A., Ferreira, O., and Pinho, S. P. (2023). Evaluation of Ionic Liquids for the Sustainable Fractionation of Essential Oils. *Industrial and Engineering Chemistry Research*, *62*(17), 6749-6758.

[164] Marfavi, Y., AliAkbari, R., Kowsari, E., Sadeghi, B., and Ramakrishna, S. (2022). Application of ionic liquids in green energy-storage materials. In Ionic Liquid-Based Technologies for Environmental Sustainability, *Elsevier*, 155-166.

[165] Mishra, K., Devi, N., Siwal, S. S., Zhang, Q., Alsanie, W. F., Scarpa, F., and Thakur, V. K. (2022). Ionic Liquid-Based Polymer Nanocomposites for Sensors, Energy, Biomedicine, and Environmental Applications: Roadmap to the Future. *Advanced Science*, *9*(26), 2202187.

[166] Stolarska, O., Pawlowska-Zygarowicz, A., Soto, A., Rodríguez, H., and Smiglak, M. (2017). Mixtures of ionic liquids as more efficient media for cellulose dissolution. *Carbohydrate Polymers*, *178*, 277-285.

[167] Xu, A., Cao, L., and Wang, B. (2015). Facile cellulose dissolution without heating in [C4mim][CH3COO]/DMF solvent. *Carbohydrate Polymers*, *125*, 249-254.

[168] Xu, A., Guo, X., and Xu, R. (2015). Understanding the dissolution of cellulose in 1-butyl-3-methylimidazolium acetate+ DMAc solvent. *International Journal of Biological Macromolecules*, *81*, 1000-1004.

[169] Xu, A., Wang, Y., Li, C., Xiao, Z., and Liu, R. (2019). Dissolution performance of cellulose in [A 2 im][MOA]/MIM solvents. *RSC Advances*, *9*(36), 20976-20981.

[170] Xu, A., Chen, L., Wang, Y., Liu, R., and Niu, W. (2019). Development of diallylimidazolium methoxyacetate/DMSO (DMF/DMA) solvents for improving cellulose dissolution and fabricating porous material. *Polymers*, *11*(5), 845.

[171] Xu, A., Wang, J., and Wang, H. (2010). Effects of anionic structure and lithium salts addition on the dissolution of cellulose in 1-butyl-3-methylimidazolium-based ionic liquid solvent systems. *Green Chemistry*, *12*(2), 268-275.

[172] Gürdağ, G., and Sarmad, S. (2013). Cellulose graft copolymers: synthesis, properties, and applications. *Polysaccharide Based Graft Copolymers*, 15-57.

[173] Edgar, K. J., Buchanan, C. M., Debenham, J. S., Rundquist, P. A., Seiler, B. D., Shelton, M. C., and Tindall, D. (2001). Advances in cellulose ester performance and application. *Progress in Polymer Science*, *26*(9), 1605-1688.

[174] Fischer, S., Thümmler, K., Pfeiffer, K., Liebert, T., and Heinze, T. (2002). Evaluation of molten inorganic salt hydrates as reaction medium for the derivatization of cellulose. *Cellulose*, *9*, 293-300.

[175] Wu, J., Zhang, J., Zhang, H., He, J., Ren, Q., and Guo, M. (2004). Homogeneous acetylation of cellulose in a new ionic liquid. *Biomacromolecules*, *5*(2), 266-268.

[176] Liebert, T. F., and Heinze, T. J. (2001). Exploitation of reactivity and selectivity in cellulose functionalization using unconventional media for the design of products showing new superstructures. *Biomacromolecules*, *2*(4), 1124-1132.

[177] Edgar, K. J., Arnold, K. M., Blount, W. W., Lawniczak, J. E., and Lowman, D. W. (1995). Synthesis and properties of cellulose acetoacetates. *Macromolecules*, *28*(12), 4122-4128.

[178] Fischer, S., Voigt, W., and Fischer, K. (1999). The behaviour of cellulose in hydrated melts of the composition LiXċn H2O (X= I−, NO3−, CH3COO−, ClO4−). *Cellulose*, *6*, 213-219.

[179] Barthel, S., and Heinze, T. (2006). Acylation and carbanilation of cellulose in ionic liquids. *Green Chemistry*, *8*(3), 301-306.

[180] Heinze, T., Schwikal, K., and Barthel, S. (2005). Ionic liquids as reaction medium in cellulose functionalization. *Macromolecular Bioscience*, *5*(6), 520-525.

[181] Erdmenger, T., Haensch, C., Hoogenboom, R., and Schubert, U. S. (2007). Homogeneous tritylation of cellulose in 1-butyl-3-methylimidazolium chloride. *Macromolecular Bioscience*, *7*(4), 440-445.

[182] Yang, Y., Xie, H., and Liu, E. (2014). Acylation of cellulose in reversible ionic liquids. *Green Chemistry*, *16*(6), 3018-3023.

[183] Yang, Y., Song, L., Peng, C., Liu, E., and Xie, H. (2015). Activating cellulose via its reversible reaction with CO 2 in the presence of 1, 8-diazabicyclo [5.4. 0] undec-7-ene for the efficient synthesis of cellulose acetate. *Green Chemistry*, *17*(5), 2758-2763.

[184] Onwukamike, K. N., Tassaing, T., Grelier, S., Grau, E., Cramail, H., and Meier, M. A. (2018). Detailed understanding of the DBU/$CO_2$ switchable solvent system for cellulose

solubilization and derivatization. *ACS Sustainable Chemistry and Engineering*, *6*(1), 1496-1503.

[185] Pei, M., Peng, X., Shen, Y., Yang, Y., Guo, Y., Zheng, Q., Xie, H. and Sun, H. (2020). Synthesis of water-soluble, fully biobased cellulose levulinate esters through the reaction of cellulose and alpha-angelica lactone in a DBU/CO 2/DMSO solvent system. *Green Chemistry*, *22*(3), 707-717.

[186] Liu, C. F., Zhang, A. P., Li, W. Y., Yue, F. X., and Sun, R. C. (2009). Homogeneous modification of cellulose in ionic liquid with succinic anhydride using N-bromosuccinimide as a catalyst. *Journal of Agricultural and Food Chemistry*, *57*(5), 1814-1820.

[187] Huang, K., Xia, J., Li, M., Lian, J., Yang, X., and Lin, G. (2011). Homogeneous synthesis of cellulose stearates with different degrees of substitution in ionic liquid 1-butyl-3-methylimidazolium chloride. *Carbohydrate Polymers*, *83*(4), 1631-1635.

[188] Liu, H., Sui, X., Xu, H., Zhang, L., Zhong, Y., and Mao, Z. (2016). Self-healing polysaccharide hydrogel based on dynamic covalent enamine bonds. *Macromolecular Materials and Engineering*, *301*(6), 725-732.

[189] Liu, H., Rong, L., Wang, B., Mao, Z., Xie, R., Xu, H., and Sui, X. (2017). Facile synthesis of cellulose derivatives based on cellulose acetoacetate. *Carbohydrate Polymers*, *170*, 117-123.

[190] Liu, H., Rong, L., Wang, B., Xie, R., Sui, X., Xu, H., and Mao, Z. (2017). Facile fabrication of redox/pH dual stimuli responsive cellulose hydrogel. *Carbohydrate Polymers*, *176*, 299-306.

[191] Granström, M., née Pääkkö, M. K., Jin, H., Kolehmainen, E., Kilpeläinen, I., and Ikkala, O. (2011). Highly water repellent aerogels based on cellulose stearoyl esters. *Polymer Chemistry*, *2*(8), 1789-1796.

[192] Vo, H. T., Kim, Y. J., Jeon, E. H., Kim, C. S., Kim, H. S., and Lee, H. (2012). Ionic-liquid-derived, water-soluble ionic cellulose. *Chemistry–A European Journal*, *18*(29), 9019-9023.

[193] Vitz, J., Erdmenger, T., Haensch, C., and Schubert, U. S. (2009). Extended dissolution studies of cellulose in imidazolium based ionic liquids. *Green Chemistry*, *11*(3), 417-424.

[194] Mäki-Arvela, P., Anugwom, I., Virtanen, P., Sjöholm, R., and Mikkola, J. P. (2010). Dissolution of lignocellulosic materials and its constituents using ionic liquids—a review. *Industrial Crops and Products*, *32*(3), 175-201.

[195] Quan, S. L., Kang, S. G., and Chin, I. J. (2010). Characterization of cellulose fibers electrospun using ionic liquid. *Cellulose*, *17*, 223-230.

[196] Bagheri, M., Rodríguez, H., Swatloski, R. P., Spear, S. K., Daly, D. T., and Rogers, R. D. (2008). Ionic liquid-based preparation of cellulose− dendrimer films as solid supports for enzyme immobilization. *Biomacromolecules*, *9*(1), 381-387.

[197] Aaltonen, O., and Jauhiainen, O. (2009). The preparation of lignocellulosic aerogels from ionic liquid solutions. *Carbohydrate Polymers*, *75*(1), 125-129.

[198] Ibrahim, F., Moniruzzaman, M., Yusup, S., and Uemura, Y. (2015). Dissolution of cellulose with ionic liquid in pressurized cell. *Journal of Molecular Liquids*, *211*, 370-372.

[199] Liu, Z., Sun, X., Hao, M., Huang, C., Xue, Z., and Mu, T. (2015). Preparation and characterization of regenerated cellulose from ionic liquid using different methods. *Carbohydrate Polymers*, *117*, 99-105.

[200] Cao, Y., Li, H., Zhang, Y., Zhang, J., and He, J. (2009). Structure and properties of novel regenerated cellulose films prepared from cornhusk cellulose in room temperature ionic liquids. *Journal of Applied Polymer Science*, *116*(1), 547-554.

[201] Halder, P., Kundu, S., Patel, S., Setiawan, A., Atkin, R., Parthasarthy, R., and Shah, K. (2019). Progress on the pre-treatment of lignocellulosic biomass employing ionic liquids. *Renewable and Sustainable Energy Reviews*, *105*, 268-292.Mai, N. L., Ahn, K.,

[202] solvents for the synthesis of sugar fatty acid ester. *Biotechnology Journal*, *9*(12), 1565-1572

[203] Liu, C. Z., Wang, F., Stiles, A. R., and Guo, C. (2012). Ionic liquids for biofuel production: opportunities and challenges. *Applied Energy*, *92*, 406-414.

[204] Kimon, K. S., Alan, E. L., and Sinclair, D. W. O. (2011). Enhanced saccharification kinetics of sugarcane bagasse pretreated in 1-butyl-3-methylimidazolium chloride at high temperature and without complete dissolution. *Bioresource Technology*, *102*(19), 9325-9329.

[205] Abushammala, H., Winter, H., Krossing, I., and Laborie, M. P. (2014). On the prevalence of side reactions during ionosolv pulping of Norway spruce with 1-butyl-3-methylimidazolium acesulfamate. *Cellulose*, *21*, 4607-4619.

[206] Abushammala, H., Krossing, I., and Laborie, M. P. (2015). Ionic liquid-mediated technology to produce cellulose nanocrystals directly from wood. *Carbohydrate Polymers*, *134*, 609-616.

[207] Köhler, S., Liebert, T., Schöbitz, M., Schaller, J., Meister, F., Günther, W., and Heinze, T. (2007). Interactions of Ionic Liquids with Polysaccharides 1. Unexpected Acetylation of Cellulose with 1-Ethyl-3-methylimidazolium Acetate. *Macromolecular Rapid Communications*, *28*(24), 2311-2317.

[208] Rigual, V., Santos, T. M., Domínguez, J. C., Alonso, M. V., Oliet, M., and Rodriguez, F. (2017). Recovery and Reuse of 1-Allyl-3-methylimidazolium Chloride in the Fractionation of Pinus radiata Wood. *ACS Sustainable Chemistry and Engineering*, *5*(3), 2384-2392.

[209] Ohno, E., and Miyafuji, H. (2014). Decomposition of cellulose in an ionic liquid, 1-ethyl-3-methylimidazolium chloride. *Journal of Wood Science, 60*, 428-437.

[210] Mao, J., Osorio-Madrazo, A., and Laborie, M. P. (2013). Preparation of cellulose I nanowhiskers with a mildly acidic aqueous ionic liquid: Reaction efficiency and whiskers attributes. *Cellulose*, *20*, 1829-1840.

[211] Brennan, T. C., Datta, S., Blanch, H. W., Simmons, B. A., and Holmes, B. M. (2010). Recovery of sugars from ionic liquid biomass liquor by solvent extraction. *BioEnergy Research*, *3*, 123-133.

[212] Lipscomb, G., Varanasi, S., Paripati, P., and Dadi, A. P. (2013). *U.S. Patent Application, 13, 884,460*.

[213] Bonhote, P., Dias, A. P., Papageorgiou, N., Kalyanasundaram, K., and Grätzel, M. (1996). Hydrophobic, highly conductive ambient-temperature molten salts. *Inorganic Chemistry*, *35*(5), 1168-1178.

[214] Stark, A., Behrend, P., Braun, O., Müller, A., Ranke, J., Ondruschka, B., and Jastorff, B. (2008). Purity specification methods for ionic liquids. *Green Chemistry*, *10*(11), 1152-1161.

[215] Islam, M. M., Okajima, T., Kojima, S., and Ohsaka, T. (2008). Water electrolysis: an excellent approach for the removal of water from ionic liquids. *Chemical Communications*, (42), 5330-5332.

[216] Řehák, K., Morávek, P., and Strejc, M. (2012). Determination of mutual solubilities of ionic liquids and water. *Fluid Phase Equilibria*, *316*, 17-25.

[217] Abu-Eishah, S. I. (2011). Ionic liquids recycling for reuse. *Ionic Liquids-Classes and Properties*, 239-272.

[218] Dibble, D. C., Li, C., Sun, L., George, A., Cheng, A., Çetinkol, Ö. P., and Simmons, B. A. (2011). A facile method for the recovery of ionic liquid and lignin from biomass pretreatment. *Green Chemistry*, *13*(11), 3255-3264.

[219] Vitz, J., Erdmenger, T., Haensch, C., Schubert, U.S., 2009. Extended dissolution studies of cellulose in imidazolium based ionic liquids. *Green Chemistry*, 11, 417–424.

[220] Zhao, H., Baker, G. A., Song, Z., Olubajo, O., Crittle, T., and Peters, D. (2008). Designing enzyme-compatible ionic liquids that can dissolve carbohydrates. *Green Chemistry*, *10*(6), 696-705.

[221] Remsing, R. C., Swatloski, R. P., Rogers, R. D., and Moyna, G. (2006). Mechanism of cellulose dissolution in the ionic liquid 1-n-butyl-3-methylimidazolium chloride: a 13 C and 35/37 Cl NMR relaxation study on model systems. *Chemical Communications*, 12, 1271-1273.

[222] Remsing, R. C., Hernandez, G., Swatloski, R. P., Massefski, W. W., Rogers, R. D., and Moyna, G. (2008). Solvation of carbohydrates in N, N′-dialkylimidazolium ionic liquids: a multinuclear NMR spectroscopy study. *The Journal of Physical Chemistry B*, *112*(35), 11071-11078

[223] Remsing, R.C., Petrik, I.D., Liu, Z., Moyna, G., 2010. Comment on "NMR spectroscopic studies of cellobiose solvation in emimac aimed to understand the dissolution mechanism of cellulose in ionic liquids". *Physical Chemistry Chemical Physics*, 12, 14827–14828.

[224] Gupta, K.M., Jiang, J., (2014), Cellulose dissolution and regeneration in ionic liquids: A computational perspective. *Chemical Engineering Science.*

[225] Phadagi, R., Singh, S., Hashemi, H., Kaya, S., Venkatesu, P., Ramjugernath, D., and Bahadur, I. (2021). Understanding the role of dimethylformamide as co-solvents in the dissolution of cellulose in ionic liquids: Experimental and theoretical approach. *Journal of Molecular Liquids*, *328*, 115392.

[226] Trenzado, J. L., Rodríguez, Y., Gutiérrez, A., Cincotti, A., and Aparicio, S. (2021). Experimental and molecular modeling study on the binary mixtures of [EMIM][BF4] and [EMIM][TFSI] ionic liquids. *Journal of Molecular Liquids*, *334*, 116049.

[227] Dhakal, P., and Shah, J. K. (2019). Recent advances in molecular simulations of ionic liquid–ionic liquid mixtures. *Current Opinion in Green and Sustainable Chemistry*, *18*, 90-97.

# Chapter 2

## Structure of Imidazolium-Based Double Salt Ionic Liquids at Molecular Level


### Abstract

Ionic liquids (ILs) have attracted significant attention in the scientific community owing to their distinctive qualities. These features include minimal vapor pressure, non-volatility, wide electrochemical potential window, and relatively low melting point. ILs have a widespread application in the field of physics, chemistry, and engineering and have been an emerging topic in the field of research in the last few decades. But at present, mixture of ionic liquids such as double salts ionic liquids (DSILs) varying cations, anions or both gain more attention to the researcher over single ILs, because DSILs can tune their physicochemical properties, and provide different types of molecular interactions and guidelines for the synthesis of task-specific ionic liquids (TSILs) for desired applications. Their properties are imposed by various types of interactions, such as H-bonding, dipole-dipole interactions, coulombic interactions and electron pair donor-acceptor interactions, etc. For the potential application of DSILs as a solvent, understanding of their structural and physiochemical properties is crucial. The objective of this study is to gain insight into structure of DSILs, 1-butyl-3-methyl imidazolium chloride ($[C_4mim]Cl$) and 1-butyl-3-methyl imidazolium acetate ($[C_4mim]CH_3CO_2$), and their DSILs keeping cation constant of $[C_4mim](CH_3CO_2)_{1-x}Cl_x$ (where x is the mole fraction of ILs) by using ATR-FTIR, Raman and NMR spectroscopy. The effect of ionic interactions on the liquid structure of DSILs have been analyzed using FTIR and Raman spectroscopy. The sharp blue shifts observed in ATR-FTIR spectra for C-H stretching vibrations for DSILs with the addition of $[C_4mim]Cl$ in $[C_4mim]CH_3CO_2$ indicated the disruption of the hydrogen bonds in DSILs due to the synergistic effect of of $Cl^-$ and $CH_3CO_2^-$ ions which weakens the C(2)-H bond, but it is less significant in C(4)-H and C(5)-H bonds. $^1H$ and $^{13}C$ NMR spectroscopy have been used to understand the insights of the interactions between ionic species in DSILs. It can reveal information about ion pairing, hydrogen bonding, and other intermolecular interactions that influence the DSIL's properties. $^1H$ NMR chemical shifts of C(2)-H, C(4)-H and C(4)-H and alkyl chain of imidazolium ring proton provided useful information about the cation-anions interaction in DSILs.

**Keywords:** Double salts ionic liquids, FTIR, Raman and NMR spectroscopy

## 2.1. Introduction

Ionic liquids (ILs) are a unique class of liquids consisting entirely of ions, which are charged particles [1-4]. They typically exhibit melting points often below 100 ℃, and exhibit variety of physical and chemical properties [1]. Due to their fascinating characteristics, ILs have drawn substantial interest in various fields, including materials science, engineering, and chemistry. The constituents of ILs include bulky, asymmetric organic cations in combination with either inorganic or organic anions. The combination of different cations and anions allows for a wide variety of ILs with different properties [2]. One of the most notable features of ILs is their low volatility, which makes them non-volatile or low-volatile compared to traditional molecular solvents. This property contributes to their potential as ecofriendly and sustainable replacements for volatile organic solvents. Several studies have been focused on ILs owing to their interesting solvent properties [3]. Due to their ionic nature, they can dissolve a wide range of polar and non-polar compounds, making them versatile solvents for numerous applications. Furthermore, ILs, with their excellent ionic conductivity and thermal stability, is considered be promising candidates for various electrochemical applications [3, 4].

Double salt ionic liquids (DSILs) are a subclass of ILs that contain at least three different types of ions, typically derived from two distinct salts [5-10]. These unique liquids offer synergistic properties and functionalities providing superior efficiency in various applications [5]. DSILs are the homogeneous mixture of two different ILs, resulting in a more complex ILs structure [6,7]. In addition, DSILs are formed by the results of strong interactions among multi-ions systems where all the interactions affecting the physicochemical properties considerably. The multi-ionic environment in DSILs does not behaves as a simple mixture of ions rather acts as distinct material. The presence of multi-ions in DSILs can lead to enhanced properties, such as increased solubility, improved conductivity, and tunable physicochemical characteristics [6, 9]. These features of DSILs make them attractive for a variety of applications, i.e., electrochemistry, separation processes, catalysis, and biological activity [10-15]. To understand the enhanced properties of DSILs the investigation of its physicochemical properties and structural elucidation is crucial.

Attenuated Total Reflectance-Fourier Transform Infrared (ATR-FTIR) analysis is a valuable characterizing technique for analyzing DSILs [8, 16]. ATR-FTIR provides information about the functional groups present in DSILs, their molecular structure, and the ionic interactions

within the liquid [9, 17]. ATR-FTIR spectroscopy allows for the analysis of both the cation and anion components, providing insights into their chemical environments and bonding characteristics. By measuring the absorption of infrared light, ATR-FTIR analysis can identify specific functional groups and their variations within the DSILs [10,18]. One of the key applications of ATR-FTIR analysis in the characterization of DSILs is the investigation of ion pairing and interactions. DSILs often exhibit unique ion-ion interactions due to the presence of two different salts. FTIR-ATR spectroscopy can provide information about the formation and stability of ion pairs within the DSILs. A study by Cha *et al.* [11, 19] utilized ATR-FTIR spectroscopic analysis to investigate the ion pairing behavior in the mixture imidazolium ILs with nonpolar solvent. They observed that, C(2)-H and $Cl^-$ ion pair include higher frequency of H-bonding in high concentration and lower frequency of H-bonding in low concentration. FTIR spectra indicated presence of ion pairs and allowed them to investigate the influence of different cation-anion combinations on ion pairing. This technique can detect shifts in vibrational bands and peak intensities, providing information about the molecular arrangement and ordering of the ions within the liquid. They found an absorption band at 3020 $cm^{-1}$ for the stretching vibration of C(2)-H…..$Cl^-$ H-bond. Jaganathan *et al*. [12, 20] investigated the structural changes due to changing oxidative anions of [$C_4$mim] based ILs. They observed changes in the FTIR spectra upon heating, indicating phase transitions and changes in the molecular arrangement of the ILs. Moreover, ATR-FTIR analysis [16-18] can provide insights into the solvation behavior of DSILs. It can help to determine the interactions between the ILs and other molecules or surfaces. By measuring the shifts in vibrational bands or the appearance of new peaks, ATR-FTIR spectroscopic analysis can identify specific interactions, i.e., H-bonding or ion-surface interactions. Bonomo *et al.* [13, 21] utilized ATR-FTIR spectroscopy to investigate ILs and silica surfaces interaction. They observed shifts of peaks in FTIR spectra, indicating the formation of hydrogen bonds between the ILs and the silica surface. In summary, ATR-FTIR spectroscopic analysis is a valuable technique for the characterization of DSILs. It provides information about the functional groups, ion pairing behavior, structural changes, and solvation behavior within ILs [16-18]. The application of ATR-FTIR spectroscopy enhances the understanding of the molecular properties and interactions among the ions in DSILs, contributing to their further development and utilization in various applications [19-21].

Raman spectroscopy is a powerful technique for the characterization of DSILs. Raman analysis provides valuable information about the vibrational modes, molecular structure, and interactions within DSILs. Raman spectroscopy allows for the identification and structural elucidation of DSILs [22, 23]. It provides information about the molecular vibrations and chemical bonds present in DSILs, enabling the determination of the structures of cation and anion [16]. The Raman spectrum of DSILs can exhibit characteristic peaks corresponding to the stretching, bending, and rotational vibrations of the ions. By comparing the Raman spectra with reference compounds or using spectral deconvolution techniques, the constituents and structures of DSILs can be determined. For example, a study by Fujii *et al*. [25] utilized the Raman spectroscopic technique to understand influence of anions on the structure of room temperature ILs. They investigated that the characteristic Raman peaks corresponding to specific vibrational modes, allowing for the determination of the ILs structures and confirming the presence of specific anions. In addition to structural characterization, Raman spectroscopy provides insights into the interactions and phase behavior of DSILs [18, 26]. The Raman spectrum can exhibit shifts or changes in peak intensities due to ion-ion interactions, hydrogen bonding, or solvation effects. These spectral changes can be used to investigate the solvation behavior of DSILs, the formation of ion pairs, or the presence of specific intermolecular interactions [24,25]. A study by Zhu *et al.* [18, 26] employed Raman spectroscopy to investigate the solvation behavior of DSILs with different cations and anions. The researchers observed shifts and changes in the Raman peaks, providing information about the solvation structures and interactions within the DSILs. Furthermore, Raman spectroscopy can be used to study the dynamic behavior and phase transitions of DSILs. The Raman spectrum can exhibit changes in peak positions or intensities upon variations in temperature, pressure, or composition, indicating phase transitions or changes in molecular arrangements. This allows for the characterization of phase behavior, crystal formation, and phase transitions in DSILs. Zhu *et al.* [18, 26] investigated the structure of DSIL by the experimental together with the theoretically vibrational structure. Raman spectroscopy enables the determination of chemical structures, investigation of intermolecular interactions, and study of phase behavior and dynamic processes within DSILs [24]. The application of Raman spectroscopy provides valuable insight into the properties and behavior of DSILs, facilitating their further development and utilization in various fields [25,26].

Nuclear Magnetic Resonance (NMR) spectroscopy is an important technique for the characterization of DSILs. NMR analysis provides valuable information about the chemical structure, dynamics, and interactions within DSILs [27,28]. NMR spectroscopy allows for the identification and structural elucidation of DSILs. It can provide information about the connectivity and arrangement of atoms within the DSIL molecules, as well as the presence of impurities or side products [20,28]. The chemical shifts observed in NMR spectra can be correlated to specific functional groups, allowing for the determination of the cation and anion structures in DSILs. Recently, Damodaran *et al.* [21,29] reviewed the development of NMR spectroscopic techniques for understanding the structure of ILs and their dynamics. They found that ILs have a large number of NMR active nuclei, allowing for the broad utilization of multinuclear NMR investigations. ILs and the products created by their covalent interactions with other materials are frequently studied using chemical shifts and multinuclear coupling constants. In addition to structural characterization, NMR analysis can provide insights into the dynamics and mobility of ions within DSILs. NMR relaxation measurements can determine the rotational or translational motions of the ions, which are related to the viscosity and diffusion properties of the DSILs [30]. By analyzing the relaxation times, one can obtain information about the molecular dynamics and the influence of temperature and composition on the mobility of DSIL ions. A study by Tokuda *et al.* [31-33] employed the NMR technique to investigate the structure of RTILs with the variation of cations, anions, and the alkyl chain length of cation. Furthermore, NMR spectroscopy can be used to probe the interactions and solvation behavior of ILs with other molecules or surfaces Through the observation of chemical shift changes, NMR can provide information about ion-solvent or ion-solute interactions. This is particularly useful for understanding the solvation properties and interactions in DSIL-based electrolytes. A study by Pauric *et al*. [23] utilized NMR spectroscopy to investigate the solvation behavior of binary system electrolytes with lithium ions.

## 2.2. Materials and Methods

The materials and methodologies employed in this chapter for the purpose of conducting this study have been described in the subsequent sections.

### 2.2.1. Materials

1-butyl-3-methylimidazolium chloride (purity ≥98%) and 1-butyl-3-methylimidazolium acetate (purity ≥95%,) used in this study were purchased from Sigma -Aldrich and used without further purification.

### 2.2.2. Preparation of DSILs

The IL, $[C_4mim](CH_3CO_2)$ was added to the IL, $[C_4mim]Cl$ at varying mole fractions to prepare $[C_4mim](CH_3CO_2)_xCl_{1-x}$, ( where $x$ is 0.1, 0.2, 0.3, 0.4, 0.5, 0.6, 0.7, 0.8, and 0.9 mole fraction of single ILs). The mass of the individual IL needed for the mixture was calculated and measured using a METTLER TOLEDO electrical balance, model no. MS105, EMC with a precision level of ±0.00001 g. About 2 g of the mixtures for each mole fraction of DSILs were prepared, taken into vials, sealed to restrict moisture, and then heated at 75 ℃ above the melting point of $[C_4mim]Cl$ with continuous stirring in an oil bath for proper mixing until a clear homogeneous phase was obtained. To DSILs were stored in an electric desiccator. Since the physicochemical properties of ILs is negatively affected by the water content resulting in poor rate of dissolution of cellulose, maximum precaution was made to avoid moisture. The ILs and synthesized DSILs were stored in an electrical desiccator to protect them from moisture.

### 2.2.3. Characterizations

The structure of synthesized DSILs have been characterized using different spectroscopic techniques. The methods and instrumental descriptions have been presented below.

#### 2.2.3.1. ATR-FTIR spectroscopy

The structural identification of the cellulose samples and ILs were carried out by attenuated total reflectance-Fourier transform-infrared (ATR-FT-IR) spectroscopy (Frontier, Perkin-Elmer, UK; Software: Spectrum version 10.4.4). The FT-IR spectra were recorded in ATR mode equipped with a diamond crystal. For every measurement, the crystal of the diamond was polished with acetone, and a background scan was taken before every measurement. The spectra were recorded between 650 to 4000 $cm^{-1}$ range at 4 $cm^{-1}$ spectral resolution and with 16 scans per spectrum.

### 2.2.3.2. Raman spectroscopy

Raman spectroscopic measurements of ILs and DSILs were carried out by Horiba T64000 Raman spectrometer with He-Ne laser as source of light. All measurements were conducted with He-Ne laser with wavelength at 632.8 nm and 10 mW of power. The laser beam was focused on the sample, and the resulting Raman-scattered radiation was collected using an oblique collecting geometry at (70 to 90°) a large-aperture convex lens with an aperture of 0.98. This radiation was then focused to the entrance window of the optical fiber. The unnecessary Rayleigh Scattering was attenuated using a Weuseda 632.8 nm notch filter (COHERENT) located in front of the optical fiber entrance. The entrance slit of Czerny Turner configured spectrograph Acton Spectra Pro-2758 was attached with the outlet of the optical fiber. CCD camera (Princeton PIMAX with unigene II coating) with imaging array of 1024×1024 pixels cooled to –200 ℃ by a Peltier cooler is utilized as detector to record the spectrum. The resolution was 2 $cm^{-1}$. Raman spectra were acquired using a backscattering geometry across various spectral bands ranging from 200 to 3500 $cm^{-1}$.

### 2.2.3.2. NMR spectroscopy

For the measurement of $^{1}H$ and $^{13}C$ NMR of the prepared ILs and DSILs used in this investigation were dried individually to eliminate the moisture absorbed during preparation under a high vacuum at 70 ℃ for 24 h. All $^{1}H$ and $^{13}C$ NMR spectra were recorded by BRUKER 400 UltraShield$^{TM}$.

## 2.3. Results and Discussion

The structure and characteristics of ILs and DSILs can be studied using spectroscopic methods such as FTIR, Raman, and NMR spectroscopy. These spectroscopic methods each offer distinctive perceptions of ILs and their DSILs, advancing knowledge of their molecular and structural characteristics. Scheme 2.1 represents possible structure of DSILs.

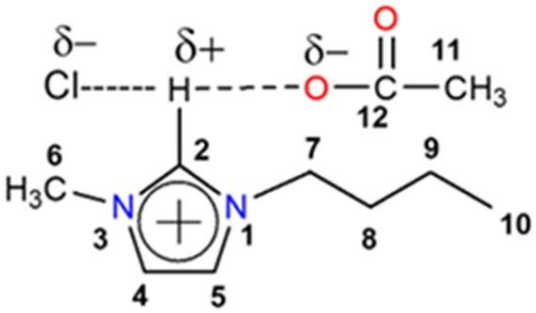


**Scheme 2.1.** Possible structure of DSIL

### 2.3.1. ATR-FTIR spectroscopy

FTIR spectroscopy provides valuable information about the functional groups and the interactions at a molecular level in DSILs. The ATR-FTIR spectra of ILs synthesized DSILs of $[C_4mim](CH_3CO_2)_{1-x}Cl_x$ (x is the mole fraction of ILs) over the whole mole fraction range have been plotted in Fig. 2.1. Extensive information regarding the structure and interaction characteristics of ILs and DSILs can be found in the C-H stretching vibrational regions, particularly those present in the aromatic ring of the cation [35]. Fig. 2.1(a) and (k) represent the spectra regarding $[C_4mim]Cl$ and $[C_4mim]CH_3CO_2$, respectively. The rest of the spectra, from Fig. 2.1(b) to (j), are for DSILs prepared by mixing $[C_4mim]Cl$ and $[C_4mim]CH_3CO_2$ in different mole ratios.

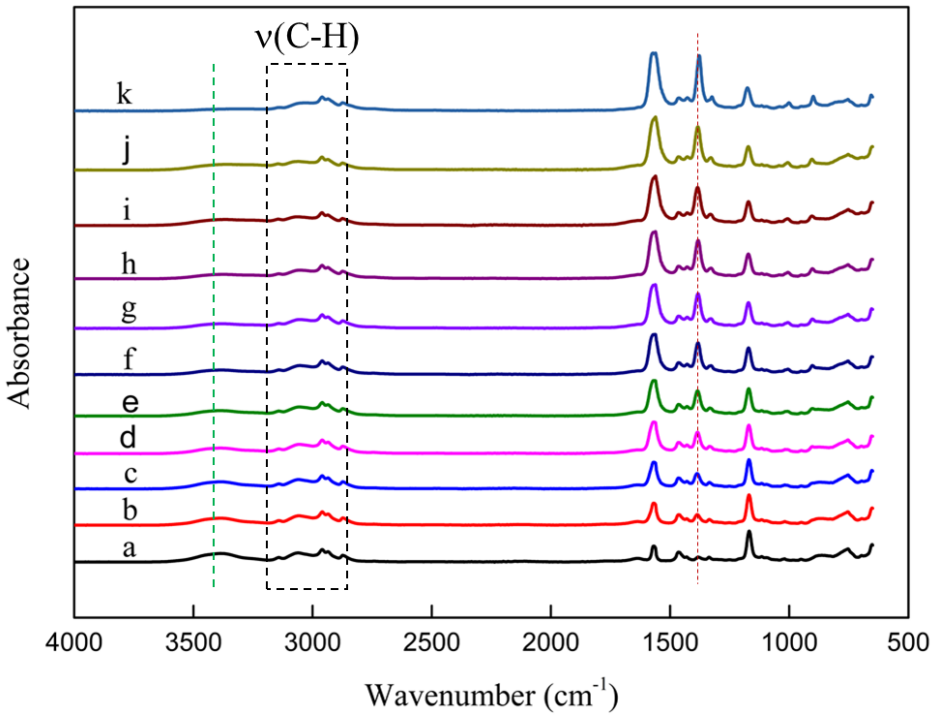


**Figure 2.1.** ATR-FTIR spectra of (a) $[C_4mim]Cl$, (b) $[C_4mim](CH_3CO_2)_{0.1}Cl_{0.9}$, (c) $[C_4mim](CH_3CO_2)_{0.2}Cl_{0.8}$ (d) $[C_4mim](CH_3CO_2)_{0.3}Cl_{0.7}$ (e) $[C_4mim](CH_3CO_2)_{0.4}Cl_{0.6}$ (f) $[C_4mim](CH_3CO_2)_{0.5}Cl_{0.5}$ (g) $[C_4mim](CH_3CO_2)_{0.6}Cl_{0.4}$ (h) $[C_4mim](CH_3CO_2)_{0.7}Cl_{0.3}$ (i) $[C_4mim](CH_3CO_2)_{0.8}Cl_{0.2}$ (j) $[C_4mim](CH_3CO_2)_{0.9}Cl_{0.1}$ (k) $[C_4mim]CH_3CO_2$

In Fig. 2.1, the wavenumber range 3190–2800 $cm^{-1}$ represents the C-H stretching vibrations in $[C_2mim]^+$ cation. Fig. 2.2 depicts the deconvoluted ATR-FTIR spectra for (A-B)$[C_4mim]Cl$, (C-D) $[C_4mim]CH_3CO_2$, and (E-F) $[C_4mim](CH_3CO_2)_{0.9}Cl_{0.1}$. In this study, the bands at 2873, 2936, and 2956 $cm^{-1}$ represent several C-H stretching vibrations of the alkyl group and 3059 and 3141 $cm^{-1}$ indicates C(2)-H and C(4, 5)-H stretching vibrations, respectively for $[C_4mim]Cl$ (Fig. 2.2, A). The bands at 2874,2936,2960 $cm^{-1}$ for C-H stretching vibration for alkyl side chain and 3006 and 3028 $cm^{-1}$ for C(2)-H and C(4,5)-H, respectively for $[C_4mim]CH_3CO_2$ (Fig. 2.2,C). Again for $[C_4mim](CH_3CO_2)_{0.9}Cl_{0.1}$, C-H stretching vibration for alkyl group in imidazolium cation was found to be 2873,2935,2959 $cm^{-1}$ and 3057, 3140 $cm^{-1}$ for C(2)-H and C(4,5)-H, respectively (Fig. 2.2,E). A similar observation was made by many researchers. Umebayashi *et al*. [36] have found bands 2951, 2970, and 2992 $cm^{-1}$ for C-H stretching vibrations of alkyl group. They also found C(2)-H and C(4, 5)-H stretching vibrations at 3124 and 3162 $cm^{-1}$, respectively. Cha *et al.* [37] found C(2)-H and C(4,5)-H stretching vibrations at 3114 and 3163

$cm^{-1}$, respectively. Bands at 2877, 2938, and 2965 $cm^{-1}$ are attributable to several C-H stretching vibrations of alkyl group. In all the spectra, for both ILs and DSILs, the C-H stretching region marked with a rectangle in Fig. 2.1 remains somewhat unaltered with very little or minute alterations. This behavior suggests that the simultaneous presence of both ILs has slightly perturbed local structures [36]. Fig. 2.2 (A), (C), and (E) depicts this slight perturbation effectively in the deconvoluted spectra. The bands approximately at 3141 and 3059 $cm^{-1}$ are ascribed to coupled C-H stretching modes of C(4, 5)-H and C(2)-H of the imidazolium cation. The rest are for C-H stretching vibrations of the aliphatic part. These slight variations may have resulted from the extent of the H-bond in ILs and DSILs. The geometric nature of H-bonds also gets modified in the DSILs. This may occur due to the presence of $Cl^-$ and $CH_3CO_2^-$ simultaneously [35,36]. The band near 1375 $cm^{-1}$ (marked with redline) is absent in Fig. 2.1(a). It becomes much more prominent as the mole fraction of $[C_4mim]CH_3CO_2$ is increased, eventually becomes maximum for $[C_4mim]CH_3CO_2$.

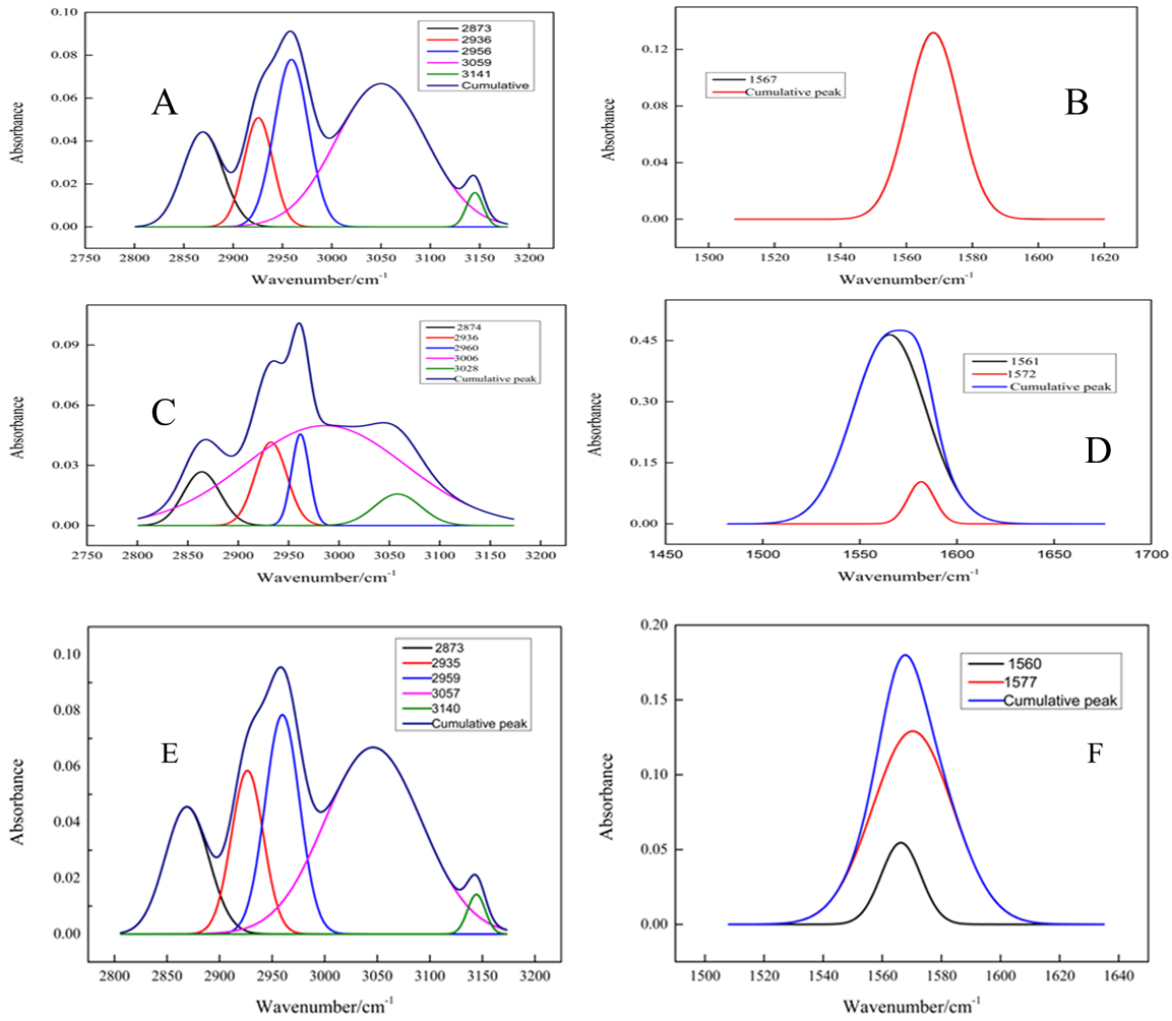


**Figure 2.2.** Deconvoluted ATR-FTIR spectra of (A-B)[$C_4$mim]Cl, (C-D) [$C_4$mim]$CH_3CO_2$, and (E-F) [$C_4$mim]$(CH_3CO_2)_{0.9}Cl_{0.1}$

The band at 1570-1560 $cm^{-1}$ can be seen for both of the ILs and for all the DSILs. The deconvoluted spectrum in Fig. 2.2(B) reveals the presence of only a peak. So, it can be concluded that this band may be attributed to ring C=C for [$C_4$mim]Cl. Again, the deconvoluted spectra of both DSILs and [$C_4$mim]$CH_3CO_2$ (Fig. 2.2, D and F) near 1570-1560 $cm^{-1}$ demonstrate the presence of two bands. They may have originated because of the vibration of C=O of the $CH_3CO_2^-$ ion and C=C of the imidazolium ring [36, 38].

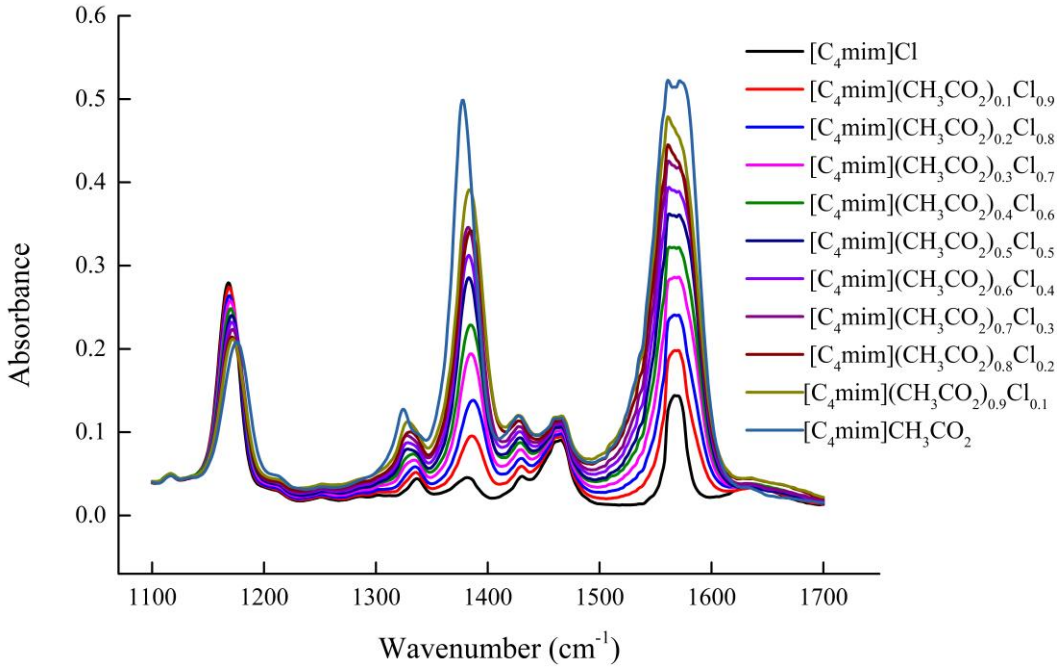


**Figure 2.3.** ATR-FTIR spectra of the ILs and DSILs in the region of 1700-1100 $cm^{-1}$

The range at 1700-1100 $cm^{-1}$ has been shown in Fig. 2.3. This region holds significant and valuable information regarding the characterization of ILs and DSILs. All the bands of both ILs and the corresponding DSILs are similar. This signifies that the mixing of ILs have not generated any new functional groups. There is no chemical interaction here, the interaction is physical in nature. With the increase in the amount of $[C_4mim]CH_3CO_2$ in the DSILs then the absorbance of all the functional groups is boosted and eventually becomes maximum for $[C_4mim]CH_3CO_2$. This means that the population of different functional groups increases. In $[C_4mim]Cl$, 1567 $cm^{-1}$ indicates C=C bond. Shiflett *et al*. [38] identified new peaks at 1666, 1508, 1323 $cm^{-1}$ in the ATR-FTIR spectra. These peaks are consistent with spectra of Fig. 2.3 with slight shift in the wavenumbers. At 1578 and 1379 $cm^{-1}$, the acetate carboxylate (C=O and C-O combined) band appears. In DSILs, both C=O and C=C groups are present simultaneously. The bands at 1561 and 1571 $cm^{-1}$ represent C=C and C=O, respectively.

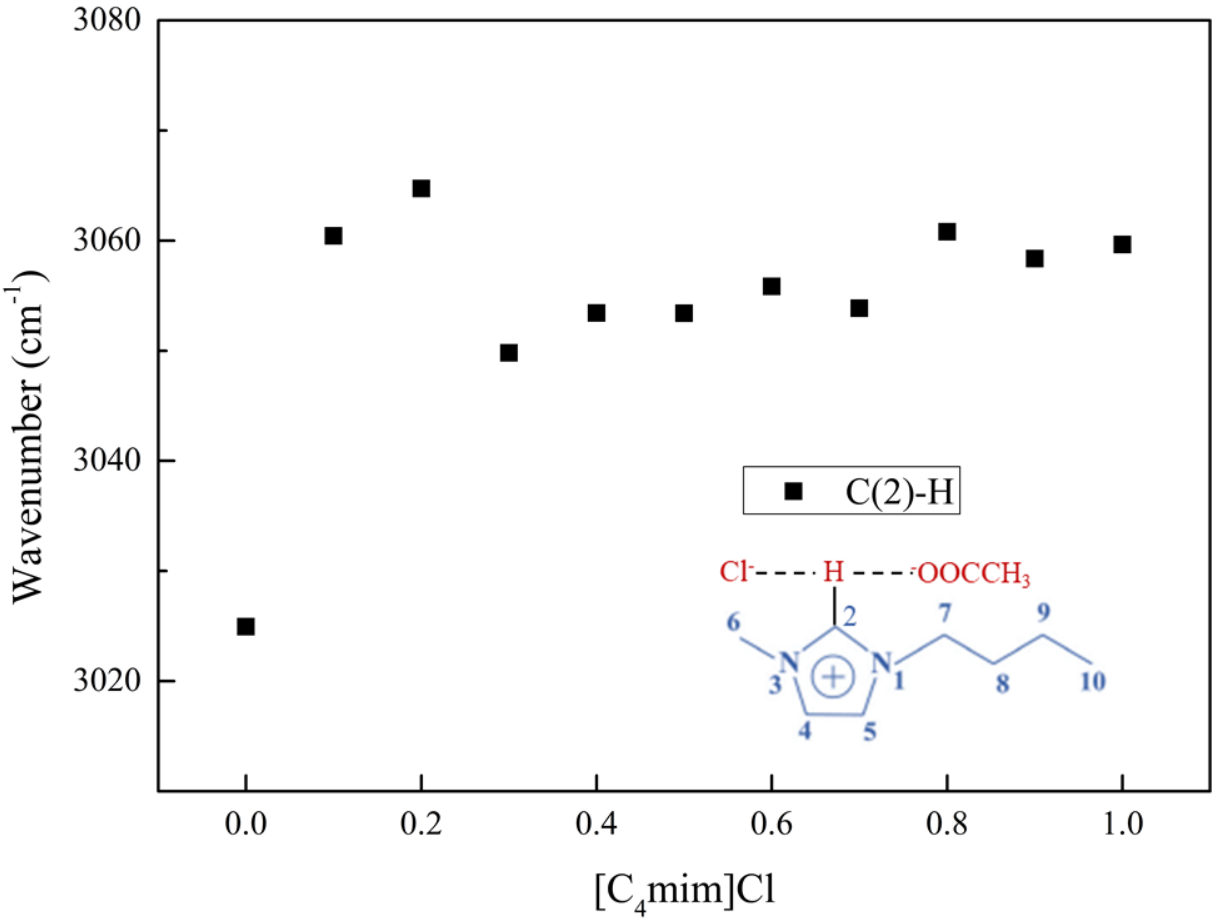


**Figure 2.4.** Variation of stretching frequency of C(2)-H in imidazolium ion in $[C_4mim](CH_3CO_2)_xCl_{1-x}$ with the mole fraction of $[C_4mim]Cl$

The C(2)–H proton, owing to the electron deficit nature of the C=N bond, is highly acidic in nature. In Fig. 2.4, all the stretching frequencies of C(2)-H in $[C_4mim]^+$ ion in DSILs with the mole fraction of $[C_4mim]Cl$ have been plotted. The C(2)–H stretching absorption band for $[C_4mim]CH_3CO_2$ occurs near 3025 $cm^{-1}$. All the other bands occur higher than 3025 $cm^{-1}$. The stretching band for $[C_4mim]Cl$ occurs near 3060 $nm^{-1}$. All the C(2)-H bands for DSILs occur in between these two values except for $[C_4mim](CH_3CO_2)_{0.8}Cl_{0.2}$. The blue shift in DSILs is quite reasonable with increasing $[C_4mim]Cl$ mole fraction as its C(2)-H band lies at 3060 $cm^{-1}$. These changes in wavenumber for DSILs suggest an alteration of interaction strengths. The $Cl^-$ and $CH_3COO^-$ anions now can simultaneously form H-bonds with the C(2)-H. As a result, the C(2)-H bond gets weakened hence peaks of C(2)-H can be observed blue shift in the DSILs. The H-bond

strength between C(2)-H is stronger for $Cl^-$ than that for $CH_3COO^-$ hence it can be seen a higher wavenumber for $[C_4mim]Cl$ than $[C_4mim]CH_3CO_2$ [37, 38].

### 2.3.2. Raman spectroscopic analysis

Raman spectroscopy offers a unique and characteristic identification method for ILs due to its capacity to detect and analyze alterations in polarizability that occur during molecular vibrations. This property renders it very suitable for the identification and characterization of DSILs. Comparative examinations of the structures of ILs and DSILs have been conducted with the Raman spectroscopy. Fig. 2.6 displays the Raman spectra of $[C_4mim]Cl$, $[C_4mim]CH_3CO_2$ and their DSILs.

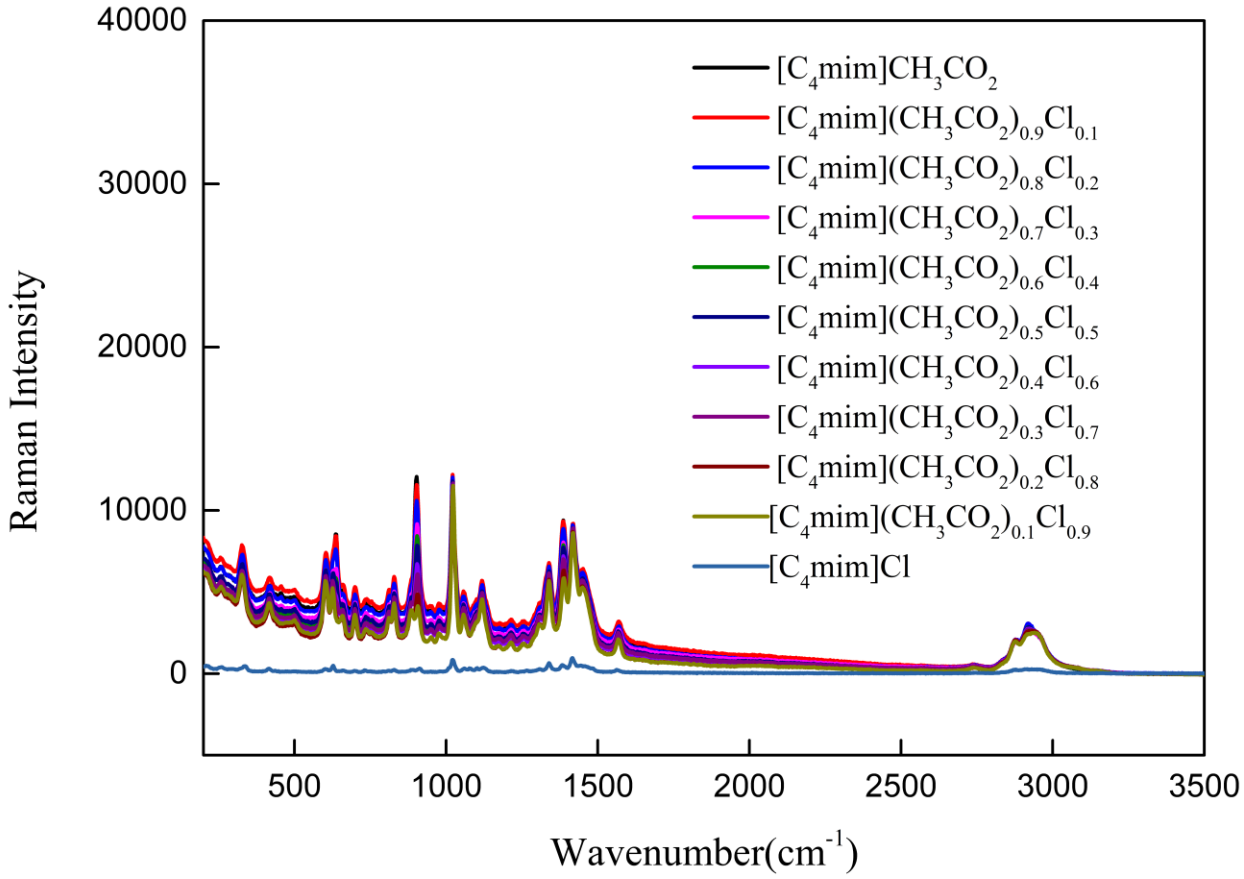


**Figure 2.5.** Raman spectra of $[C_4mim](CH_3CO_2)_xCl_{1-x}$

The halogen anions, in this case, $Cl^-$, exhibit inactivity in Raman scattering. But lattice vibrations are still present located below 200 $cm^{-1}$ [39, 40]. Hence, all existing Raman bands in Fig. 2.5 is

attributable to the $[C_4mim]^+$ cation and $CH_3CO_2^-$ anion. As a result, $[C_4mim]^+$ cation exhibits two distinct conformations in those salts according to Fig. 2.5. At least one cation in $[C_4mim]Cl$ must assume the same molecular shape. The variations in the Raman spectra arises because of the rotational isomerism of butyl chain of the $[C_4mim]^+$ cation specifically around C7-C8 [39, 40].

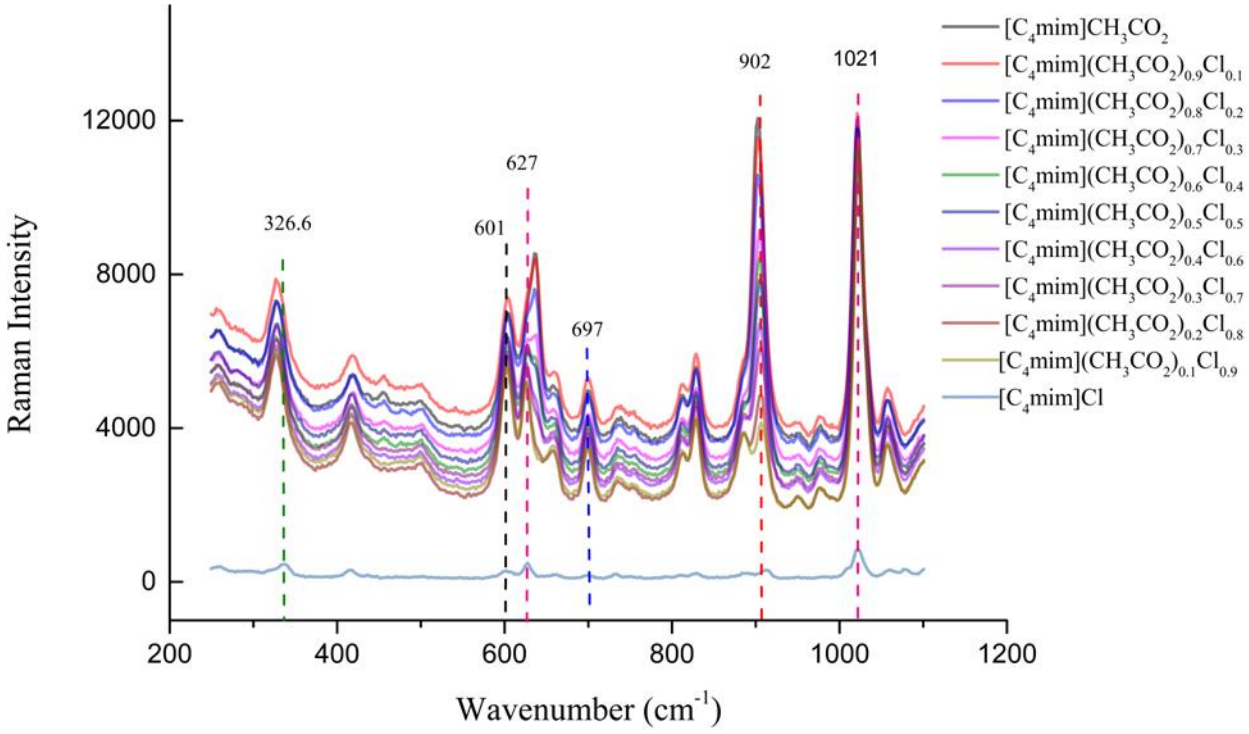


**Figure 2.6.** Raman spectra of $[C_4mim](CH_3CO_2)_xCl_{1-x}$ in the region of 200-1100 $cm^{-1}$

Fig. 2.6 showcases the Raman spectra of all the ILs and DSILs in the region of 200-1100 $cm^{-1}$. All the bands are common here and prevail in all the studied systems. The bands at 697 and 627 $cm^{-1}$ corresponds to ring deformation of $[C_4mim]^+$ cation. Rest of the bands also result from some extent of ring and chain distortion. Relative intensity of the bands is very much pronounced in all the DSILs and $[C_4mim]CH_3CO_2$ compared to $[C_4mim]Cl$. This pronounced absorption intensity is due to the presence of acetate anion [20, 41]. In Fig. 2.6, some significant bands with high intensity are 326.6, 601, 627, 902 and 1021 $cm^{-1}$. Rolf W. Berg [42] found similar bands with slight alterations. They found absorption at 327.1, 619.6, 636.2, 945.3, and 1043.6 $cm^{-1}$. All of these bands are associated with ring and chain vibrations. The symmetric (1383 $cm^{-1}$) and asymmetric modes of $CH_3COO^-$ is highly Raman active hence give strong absorption. In Fig. 2.7 it is seen that with increasing the content of $[C_4mim]CH_3CO_2$, the absorption intensity increases except $[C_4mim](CH_3CO_2)_{0.9}Cl_{0.1}$. From this, it can be inferred that $CH_3COO^-$ anion imparts a strong

influence on the intensity of the absorption of Raman intensity of the DSILs [43]. With the mixed spectroscopic analysis with FTIR (Fig. 2.9) and Raman spectroscopy (Fig. 2.7), we can conclude that the strong band near 1572 $cm^{-1}$ results corresponds to C=C of the ring rather than the $CH_3COO^-$ anion [43].

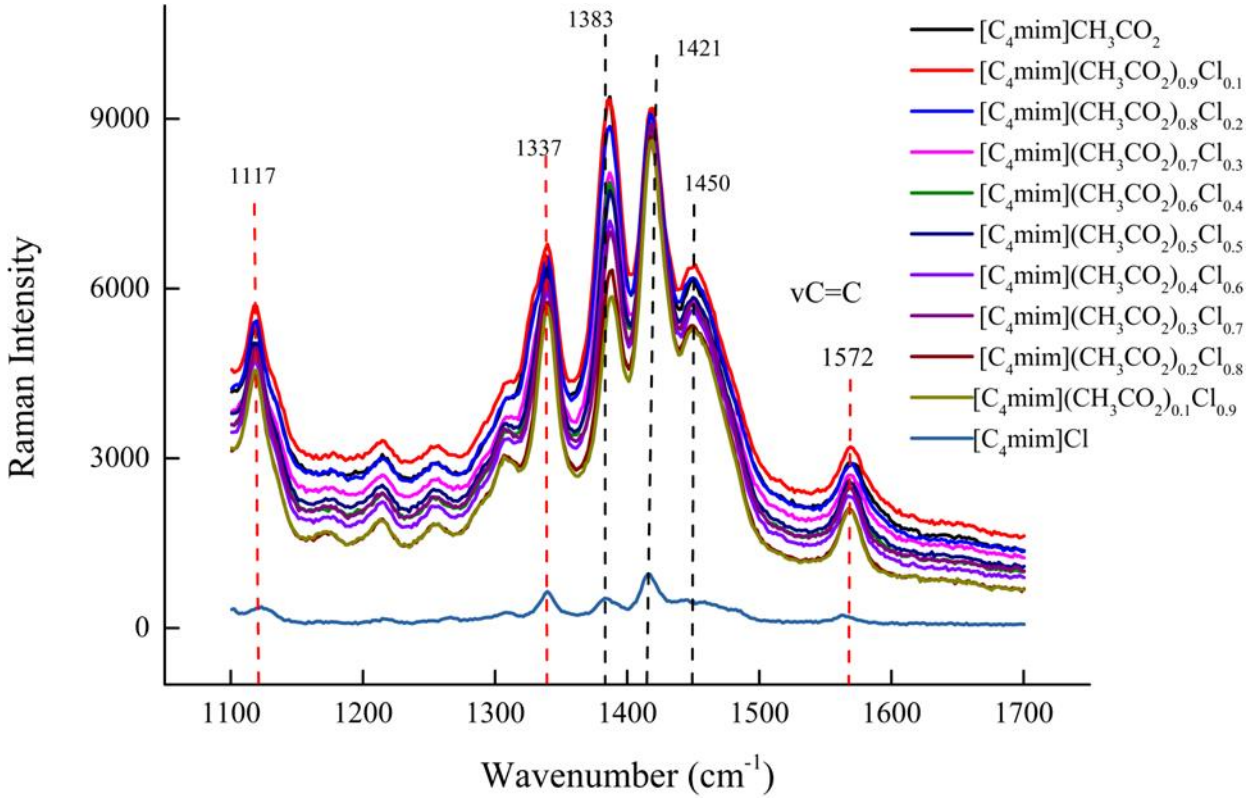


**Figure 2.7.** Raman spectra of $[C_4mim](CH_3CO_2)_xCl_{1-x}$ in the region of 1100-1700 $cm^{-1}$

In Fig. 2.7, it is seen that there have been some shifts in wavenumber for DSILs. Significant bands in this figure are 1117, 1337, 1383, 1421, 1450 and 1572 $cm^{-1}$. These are associated with ring, chain deformations. Similar results were found by Rolf W. Berg [42] having bands 1106.6, 1324.3, 1388.9, 1413.6, 1443.7, and 1450.6 $cm^{-1}$

### 2.3.3. NMR spectroscopic analysis

NMR spectroscopy is imperative in elucidating the intricate molecular structure of DSILs, encompassing the precise positioning of atoms and the spatial alignment of functional groups. It offers valuable insights into the chemical changes shown by various nuclei within DSILs, encompassing both proton and carbon nuclei. Chemical changes exhibit a remarkable degree of

sensitivity towards the electronic surroundings in their immediate vicinity, hence facilitating the process of structural investigation.

### 2.3.3.1. $^{1}$H NMR

The $^{1}$H NMR chemical shifts ($\delta$) of DSILs of $[C_4mim](CH_3CO_2)_{1-x}Cl_x$ for whole mole fractions range have been presented in Fig. 2.8 and 2.9. The $\delta$ values extracted from Fig. 2.8 and 2.9 for all protons of imidazole ring with different substituents and counter anions of ILs and DSILs are tabulated in Table 2.1. There are two important factors that have strongly influenced the $\delta$ values. The protons are forming hydrogen bonds with the anion, while the presence of the anion is inducing an effect on the imidazolium ring [37, 44]. The imidazole cation's C(2)-H proton is closest to the two neighboring electron-withdrawing groups of nitrogen atoms from the structure itself, which caused the NMR signals to be slightly in downfield. To understand the structure of DSILs, three important chemical shifts for the proton of C(2)-H, C(4)-H, and C(5)-H in $[C_4mim]^+$ ion are crucial. The chemical shifts for the proton of C(2)-H, C(4)-H, and C(5)-H in $[C_4mim]CH_3CO_2$ are 10.60, 7.35, and 7.22 ppm, respectively whereas $\delta$ values regarding the proton of C(2)-H, C(4)-H, and C(5)-H in $[C_4mim]Cl$ are 10.24, 7.64, and 7.35 ppm, respectively. Hesse-Ertelt *et al.* [45] investigated chemical shifts values for $[C_4mim]CH_3CO_2$ were found 10.03, 7.85, and 7.78ppm for C(2)-H, C(4)-H, and C(5)-H, respectively and 9.50, 7.86 and 7.78 for C(2)-H, C(4)-H, and C(5)-H, respectively for $[C_4mim]Cl$. Zaoui *et al.* [46] reported that the 3-octyl-1-vinylimidazolium bromide imidazolium ring structure also had $\delta$ values at 7.32, 7.68, and 9.69 ppm, which corresponds to C(5)-H, C(4)-H, and C(2)-H, respectively. The $\delta$ values of C(2)-H protons of all mole fractions showed the highest value in the more downfield region. The anions of $Cl^-$ and $CH_3CO^-$ form H-bonding with the C(2)-H proton due to the more acidic nature as its respective carbon is attached to two electron-withdrawing N atoms. The ions of imidazolium-based ILs have a significant role in the variation of $\delta$ values of protons. Bystrov *et al.* [47] investigated the local mobility of $[C_4mim]^+$ in response to changes in reaction temperature and counter anion type such as $BF_4^-$, $Cl^-$, $Br^-$, $I^-$, $NO_3^-$, and $TfO^-$ utilizing the NMR relaxation technique. The results revealed that the reaction temperature and nature of counter anions had a substantial impact on the $\delta$ values of $^{1}$H NMR spectra pattern. Cha, *et al.* investigated $^{1}$H NMR of $[C_4mim]Cl$, $[C_4mim]Br$, and $[C_4mim]I$ keeping cation fixed and with the varying of anions of $Cl^-$, $Br^-$, and $I^-$ and found that with increasing H-bond strength increased the $\delta$ values of C-H protons are 10.22, 9.78, and

9.28 ppm, respectively. The H-bonds strength of C(2)-H protons are increased with the following order C(2)–H…..Cl > C(2)–H……Br > C(2)–H……I. These results were also supported by Shukla *et al.*, [47] (2010) that the $\delta$ values of C(2)-H protons with halide by DFT calculation suggested possibly responsible for the material's structures. The strength of H-bonding depends on the halide ions especially on its electronegativity. Electronegativity positively affects the H-bond formation. Computer investigations utilizing the cluster and polarizable continuum models show that hydrogen bonding interaction is mostly responsible for the chemical downfield shift of the acidic protons of the aromatic ring [44, 48]. Another research was carried out by Pillai *et al.* [49] with the variation of cations of $[C_8mim]^+$, $[C_{10}mim]^+$, and $[C_{12}mim]^+$ keeping $[BF_4]^-$ constant investigated the structure of ILs and observed that $\delta$ values of C(2)-H, C(4)-H, and C(5)-H have been affected. The $\delta$ values of C(2)-H, C(4)-H, and C(5)-H for $[C_8mim][BF_4]^-$ are 8.849, 7.45, and 7.388, for $[C_{10}mim][BF_4]^-$ are 8.843, 7.429 and 7.356 and 8.884, 7.446, and 7.371 ppm for $[C_{12}mim][BF_4]^-$, respectively. The C(2)-H protons in DSILs showed more downfield with higher $\delta$ values for all most all mole fractions exhibited 10.87, 10.74, 10.65, 10.64, 10.61, 10.63 ppm of $[C_4mim](CH_3CO_2)_{0.9}Cl_{0.1}$, $[C_4mim](CH_3CO_2)_{0.7}Cl_{0.3}$, $[C_4mim](CH_3CO_2)_{0.6}Cl_{0.4}$, $[C_4mim](CH_3CO_2)_{0.4}Cl_{0.6}$, $[C_4mim](CH_3CO_2)_{0.3}Cl_{0.7}$, respectively due to the synergistic effect of $Cl^-$ and $CH_3CO^-$ ions forming in strong H-bonds with the C(2)-H protons compared to $[C_4mim]Cl$ and $[C_4mim]CH_3CO_2$ due to less proton around the nucleus of H. The strength of H-bonds forming by anions of DSILs is possibly higher than H-bonds strength forming by anions of ILs. The $\delta$ values of C(2)-H, C(4)-H, and C(5)-H protons are shown in Fig. 2.10. The $\delta$ value C(2)-H showed more downfield region compared to C(4)-H and C(5)-H protons and C(4)-H protons of all mole fractions showed a slightly higher $\delta$ value than C(5)-H. The $\delta$ values of C(4)-H is almost close to all DSILs except for $[C_4mim](CH_3CO_2)_{0.8}Cl_{0.2}$, $[C_4mim](CH_3CO_2)_{0.6}Cl_{0.4}$, $[C_4mim](CH_3CO_2)_{0.4}Cl_{0.6}$, $[C_4mim](CH_3CO_2)_{0.2}Cl_{0.8}$, and $[C_4mim](CH_3CO_2)_{0.1}Cl_{0.9}$ showed slightly higher $\delta$ values of 7.37, 7.56, 7.55, 7.54, and 7.57 ppm, respectively. The higher $\delta$ values of C(4)-H and C(5)-H compared to substituents protons due to the formation of H-bonds by $Cl^-$ and $CH_3CO^-$ ions result in more downfield shifts.

For the butyl chain of $[C_4mim]^+$, the $\delta$ values rapidly decreased starting from the C(7)-H protons, and then it decreased monotonically as a function of the studied protons of C(7)-H, C(8)-H, C(9)-H and C(10)-H numbered according to their distance from the imidazolium ring. The $\delta$ values of C(7)-H, C(8)-H, C(9)-H and C(10)-H protons of $[C_4mim]CH_3CO_2$ are 4.22, 1.75, 1.25,

0.85, and 4.05, 1.80, 1.29, 0.88 ppm for $[C_4mim]Cl$, respectively. DSILs, e.g., $[C_4mim](CH_3CO_2)_{0.6}Cl_{0.4,}$ $[C_4mim](CH_3CO_2)_{0.4}Cl_{0.6,}$ and $[C_4mim](CH_3CO_2)_{0.2}Cl_{0.8}$ of C(7)-H, C(8)-H, C(9)-H and C(10) protons showed $\delta$ values of 4.66, 1.35,1.17, 0.93, 4.30, 1.88, 1.35, 0.98, and 4.20, 1.77, 1.24, 0.82 ppm, respectively. The $\delta$ values of C-11 protons of DSILs showed in the downfield region comparative to C(8)-H, C(9)-H, and C(10)-H protons due to the -C=O groups attached to it [45].

**Table 2.1.** $^{1}H$ and $^{13}C$ NMR chemical shifts for all protons and carbons of the ILs and DSILs

| DSILs | Chemical shifts (ppm) |
|---|---|
| $[C_4mim]CH_3CO_2$ | $^{1}H$: 10.60 (H2), 7.35(H4), 7.22(H5), 4.45(H7), 4.22(H6), 1.75(H8), 1.25(H9), 0.85(H10)<br>$^{13}C$: 177.32(C12), 139.82(C2), 123.11(C4),121.22(C5), 49.91(C7), 36.41(C6), 32.31(C8), 19.8(C9), 13.51(C10) |
| $[C_4mim](CH_3CO_2)_{0.9}Cl_{0.1}$ | $^{1}H$:10.87(H2), 7.54(H4), 7.24(H5), 4.76(H7), 4.26(H6), 1.93(H-11), 1.86(H8), 1.80(9), 0.92(10)<br>$^{13}C$:177.95 (C12), 139.93(C2), 122.82(C4), 121.19(C5), 49.67(C7), 36.36(C6), 32.15(C8), 24.97 (C-11), 19.47(C9), 13.42(C10) |
| $[C_4mim](CH_3CO_2)_{0.8}Cl_{0.2}$ | $^{71}H$: 10.46(H2), 7.37(H4), 7.26(H5), 4.11(H7), 3.87(6), 1.69(H8), 1.18(H9), 0.77(H10)<br>$^{13}C$: 177.5(C12), 138.5(C2), 123.6(C4), 121.7(C5), 49.4(C7), 36.2(C6), 32.0(C8), 25.1(C11),19.4(C9), 13.7(10) |
| $[C_4mim](CH_3CO_2)_{0.7}Cl_{0.3}$ | $^{1}H$: 10.74(H2), 7.30(H4), 7.22(H5), 4.27(H7), 4.04(H6), 1.94(H-11), 1.86(H8), 1.80(H9), 0.95(H10)<br>$^{13}C$: 177.82(C12), 139.42(C2), 122.96(C4), 121.32(C5), 49.73(C7), 36.44(C6), 32.15(C11), 24.80(C8), 19.47(C9), 13.42(C10) |
| $[C_4mim](CH_3CO_2)_{0.6}Cl_{0.4}$ | $^{1}H$: 10.65(H2), 7.56(H4),7.23(H5), 4.66(H7), 4.28(6), 1.35(H8),1.17(H9), 0.93(H10)<br>$^{13}C$: 178(C12), 139.1(C2), 136.8(C4), 123.9(C5), 49.6(C7), 36.4(C6), 31.9(C11), 24.6(C8), 19.4(C9), 13.7(C10) |

| | |
|---|---|
| $[C_4mim](CH_3CO_2)_{0.5}Cl_{0.5}$ | $^{1}H$: 10.64(H2), 7.34(H4), 7.24(H5), 4.65(H7), 4.30(H6), 1.95 (H-11), 1.89(H8), 1.46(H9), 0.94(H10)<br>$^{13}C$: 177.61(C12), 139.0(C2),123.07(C4), 121.42(C5), 49.79(C7), 36.53(C6), 32.15(C11), 24.49(C8), 19.48(C9), 13.42(C10) |
| $[C_4mim](CH_3CO_2)_{0.4}Cl_{0.6}$ | $^{1}H$: 10.61(H2), 7.55(H4), 7.35(H5), 4.30(H7), 4.09(H6), 1.95(H11), 1.88(H8), 1.35(H9), 0.98(H10)<br>$^{13}C$: 138.7(C2), 123.1(C4), 121.6(C5), 49.9(C7), 36.4(C6), 32.3(C8), 19.7(C9), 13.6(C10) |
| $[C_4mim](CH_3CO_2)_{0.3}Cl_{0.7}$ | $^{1}H$: 10.63(H2), 7.34(H4), 7.26(H5), 4.32(H7), 4.09(H6), 1.99 (H11), 1 .87(H8), 1.42(H9), 0.97(H10)<br>$^{13}C$: 138.71(C2), 123.07(C4), 121.46(C5), 49.90(C7), 36.64(C6), 32.16(C8), 19.49(C9), 13.43(C10) |
| $[C_4mim](CH_3CO_2)_{0.2}Cl_{0.8}$ | $^{1}H$: 10.23(H2), 7.54(H4), 7.26(H5), 4.20(H7), 3.97(H6), 1.77(H8), 1.24(H9), 0.82(H10)<br>$^{13}C$: 177.3(C12), 139.8(C2), 50.0(C7), 36.5(C7), 32.4(C7), 25.0(C), 19.8, 13.7 |
| $[C_4mim](CH_3CO_2)_{0.1}Cl_{0.9}$ | $^{1}H$: 10.30(H2), 7.53(H4), 7.39(H5), 4.30(H7), 4.27(6), 1.93(H11), 1.91(H8), 1.34(H9), 0.91(H10)<br>$^{13}C$: 137.84(C2), 123.95(C4), 121.85(C5), 49.75(C7), 36.58(C6), 32.14(C8), 19.44(C9), 13.42(C10) |
| $[C_4mim]Cl$ | $^{1}H$: 10.24(H2), 7.64(H4), 7.35(H5), 4.25(H7), 4.05(H6), 1.80(H8), 1.29(H9), 0.88(H10)<br>$^{13}C$: 137.68(C2), 123.75(C4), 121.98(C5), 49.68(C7), 36.61(C6), 32.14(C8), 19.49(C9), 13.38(C10) |

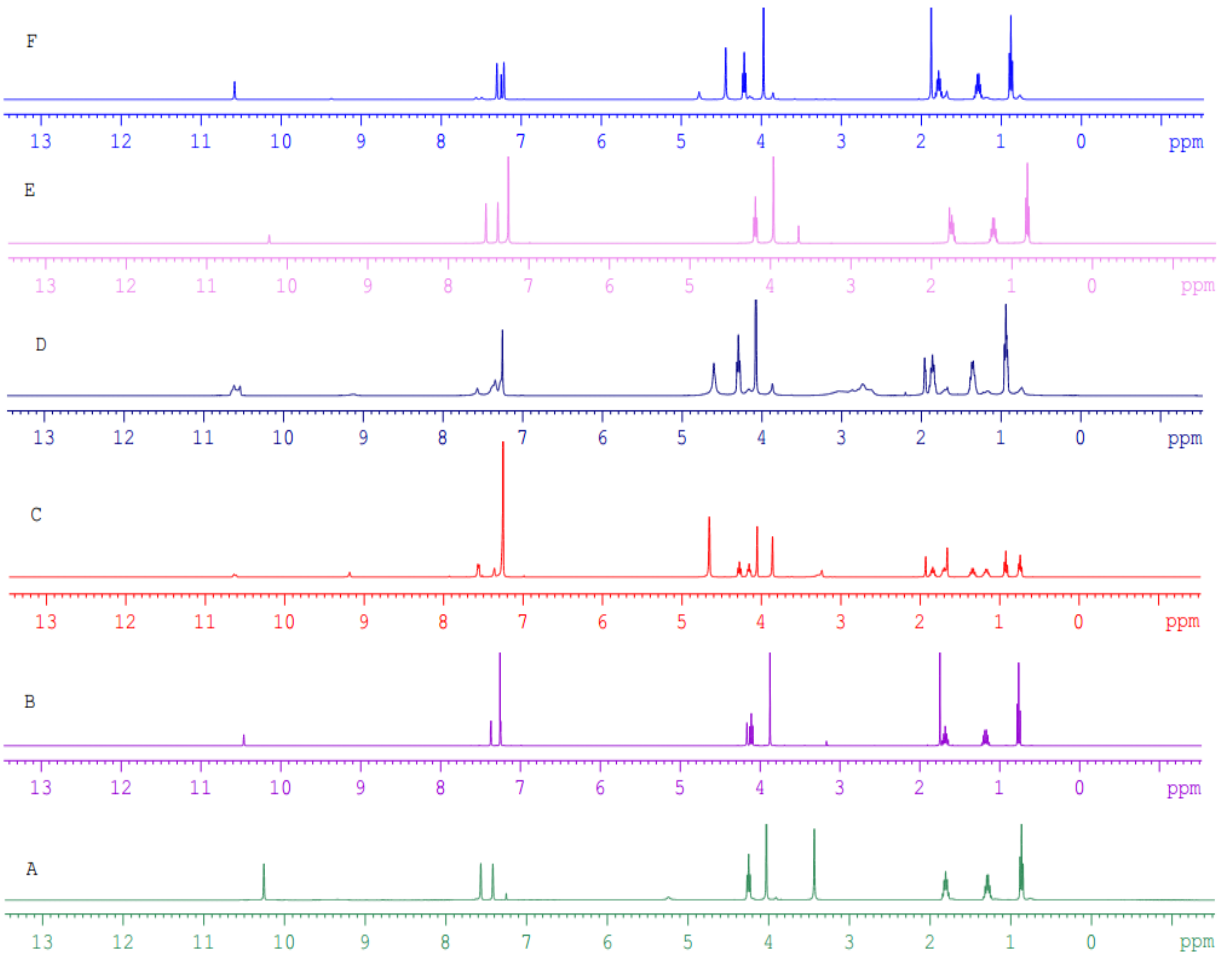


**Figure 2.8.** $^{1}H$ NMR spectra of (A)[$C_4$mim]Cl (B) [$C_4$mim]$(CH_3CO_2)_{0.8}Cl_{0.2}$ (C) [$C_4$mim]$(CH_3CO_2)_{0.6}Cl_{0.4}$ (D) [$C_4$mim]$(CH_3CO_2)_{0.4}Cl_{0.6}$ (E) [$C_4$mim]$(CH_3CO_2)_{0.2}Cl_{0.8}$ (F) [$C_4$mim]$CH_3CO_2$

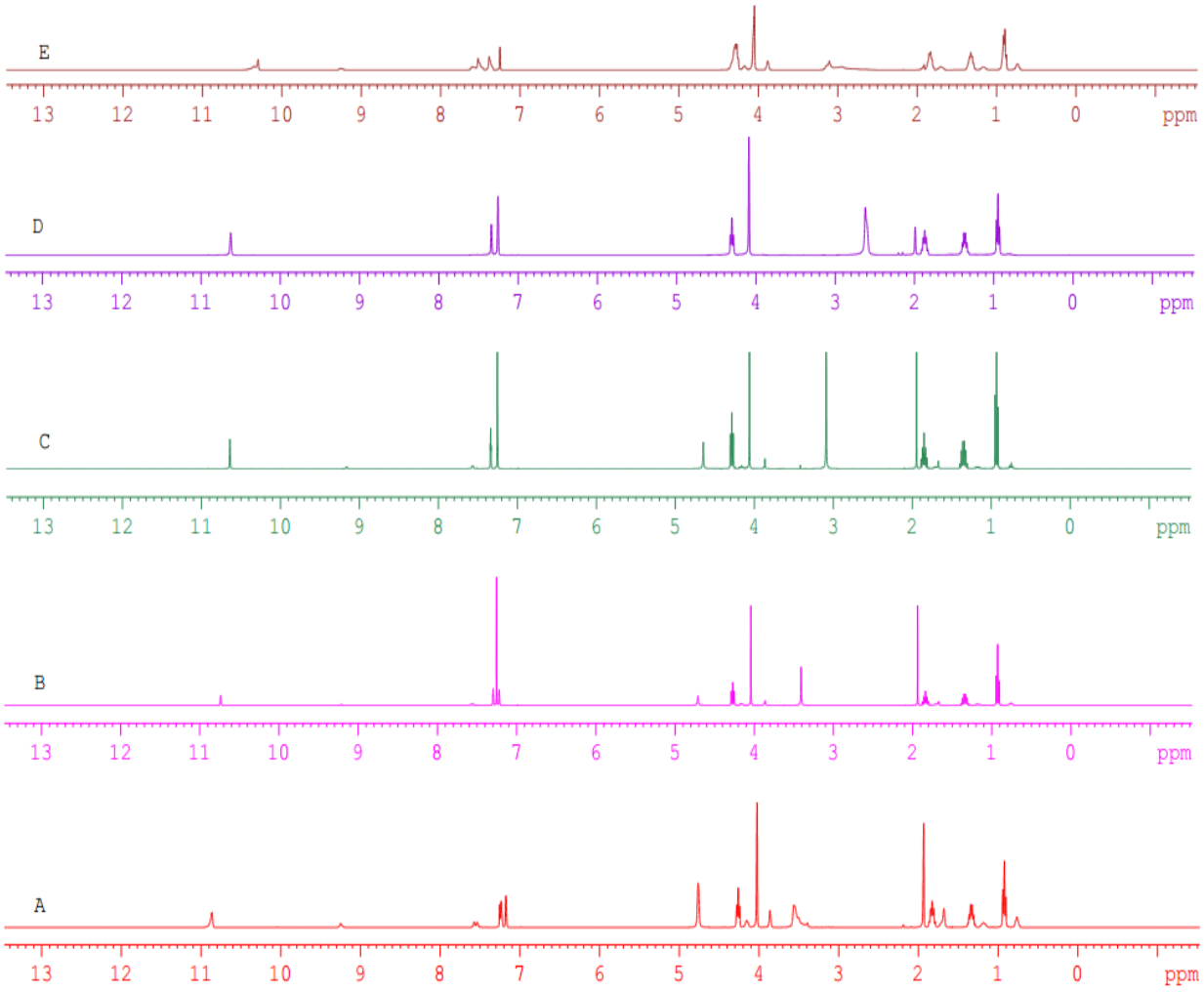


**Figure 2.9.** $^{1}$H NMR spectra of (A) $[C_4mim](CH_3CO_2)_{0.9}Cl_{0.1}$ (B) $[C_4mim](CH_3CO_2)_{0.7}Cl_{0.3}$ (C) $[C_4mim](CH_3CO_2)_{0.5}Cl_{0.5}$ (D) $[C_4mim](CH_3CO_2)_{0.3}Cl_{0.7}$ (E) $[C_4mim](CH_3CO_2)_{0.1}Cl_{0.9}$

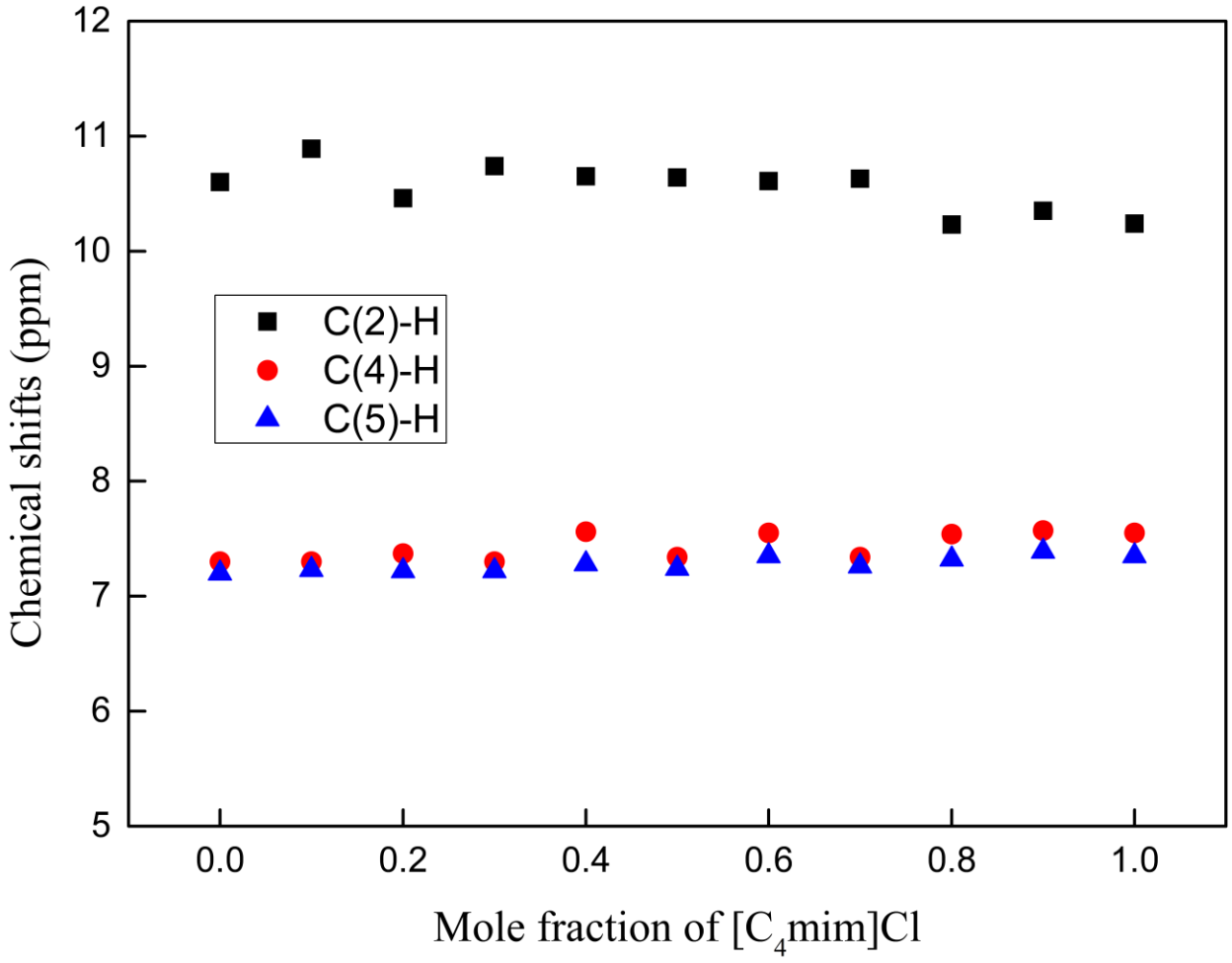


**Figure 2.10.** Variation of $^{1}H$ NMR chemical shifts of C(2)-H, C(4)-H and C(5)-H in imidazolium ion of $[C_4mim](CH_3CO_2)_xCl_{1-x}$ with the mole fraction of $[C_4mim]Cl$

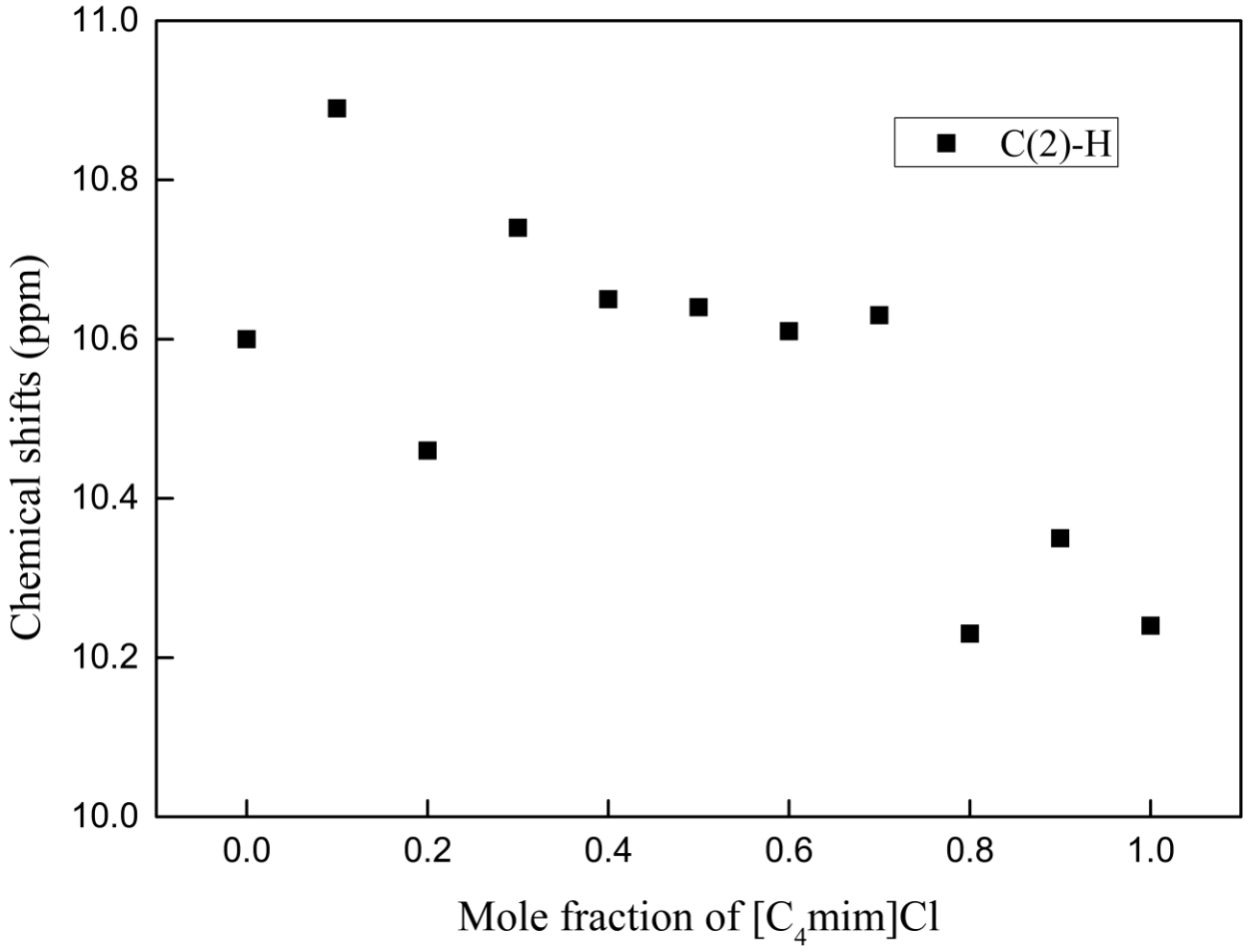


**Figure 2.11.** Variation of $^{1}$H NMR chemical shifts of C(2)-H in imidazolium ion of $[C_4mim](CH_3CO_2)_xCl_{1-x}$ with the mole fraction of $[C_4mim]Cl$

**2.3.3.2. $^{13}$C NMR**

Similarly, $^{13}$C NMR spectroscopy is used to characterize and determine the structure of imidazolium-based ILs [47, 50, 51]. The $^{13}$C NMR chemical shifts ($\delta$) of DSILs of $[C_4mim](CH_3CO_2)_{1-x}Cl_x$ for the whole mole fractions range have been presented in Fig. 2.12, Fig. 2.13 and Fig. 2.14. The $\delta$ values extracted from Fig. 2.12, Fig. 2.13, and Fig. 2.14 for all carbons present in ILs and DSILs are tabulated in Table 2.1. Three important signals namely C2, C4 and C5 have been used to determine the structure of imidazolium-based ILs. Two significant aspects that have exerted a substantial influence on the δ values are the H-bonding within the anion and the imidazolium ring, as well as the inductive effect resulting from the presence of the anion. [37, 44, 51]. In their study, Cha *et al.* [37] further examined the factors contributing to the δ values,

identifying the same two main influences as formerly explained. The proximity of the C(2)-H proton of the imidazole cation to the adjacent nitrogen atoms, which possess electron-withdrawing properties, is responsible for the minor downfield shift observed in the NMR signals. In this investigation, signals of C2, C4 and C5 for $[C_4mim]CH_3CO_2$ were found at the position of 138.5, 123.6, and 121.7 ppm, respectively. The $\delta$ values for $[C_4mim]Cl$ for the same carbons were found at 137.68, 123.75, and 121.98, respectively. Hesse-Ertelt *et al.* [45] investigated chemical shift values C2, C4 and C5 using different solvents for $[C_4mim]CH_3CO_2$ and found that the position at 138.3, 122.7, 124.0, and 137.2 122.7 124.0 ppm shows respectively for $[C_4mim]Cl$. These results are very close to the experimental results. Fig. 2.15 shows the $\delta$ position of C2, C4 and C5 for ILs and DSILs with the varying of composition of $[C_4mim]CH_3CO_2$ and $[C_4mim]Cl$. It was investigated that; no regular trend was observed for $\delta$ values. Fig. 2.16 represents the of $\delta$ values C2 of DSILs with the mole fraction of $[C_4mim]Cl$, it can be seen that as the mole fraction of $[C_4mim]Cl$ increased in DSILs the of $\delta$ values of C2 moved towards in the downfield region. Many research works have been conducted to investigate the structure of imidazolium-based ILs with the variation of cationic and anionic species. Ameta *et al.* [51] investigated the structure of 1,3-dibutylimidazolium $[C_4mim]^+$-based ILs with the change in anionic species such as $Br^-$, $[SO_4]^-$, $[Tos]^-$, and $[TfO]^-$ and found that no discernable change in $\delta$ value for C4 and C5 carbons, but significant change was observed for C2 signal position. The $\delta$ values shifted more downfield region following the increase in the strength of H-bonds of anions with C(2)-H. They found the $\delta$ values in downfield region according to the following order of strength C(2)-H···Br > C (2)-H···$[SO_4]$>C (2)-H···[TfO] > C (2)-H···[Tos] which affects $\delta$. Similar results were found by Kavya *et al.* [42]. The C2 of 1-octyl-3- methylimidazolium underwent a greater $\delta$ value in the presence of $Br^-$ anion than with $PF_6^-$ anion as a result of a larger H bonding effect from the interaction of $Br^-$ counter anions with the hydrogen atom that joined the carbon atom. The $\delta$ value of C2 for $[C_4mim]CH_3CO_2$ is higher than $[C_4mim]Cl$ that are 139.82(C2),and 137.68(C2), respectively owing to the formation of strong H-bonds by $CH_3CO_2^-$ than $Cl^-$ ion attached to the H atoms of that carbon. A similar observation was made by the group of Hesse-Ertelt, *et al.* [45] and found that $\delta$ value of $[C_4mim]CH_3CO_2$ and $[C_4mim]Cl$ were 138.3 and 137.2 ppm, respectively whereas 137.9 and 137.0 ppm for $[C_2mim]CH_3CO_2$ and $[C_2mim]Cl$, respectively. In DSILs, as the $[C_4mim]Cl$ was mixed with $[C_4mim]CH_3CO_2$ showed an adjustable *d* shifting in between ILs except for $[C_4mim](CH_3CO_2)_{0.9}Cl_{0.1}$ with higher d value was observed for C2 carbon 139.93 ppm, due to

synergistic behavior of the anions of $CH_3CO_2^-$ than $Cl^-$ ions. For the butyl chain of $[C_4mim]^+$, the $\delta$ values rapidly decreased starting from the C7 and then it decreases monotonically as a function of the examined carbons of C7, C8, C9 and C10 numbered according to their distance from the imidazolium ring. The $\delta$ values for alkyl chain of $[C_4mim]CH_3CO_2$ were observed 49.91(C7), 36.41(C6), 32.31(C8), 19.8(C9), 13.51(C10) and 49.68(C7), 36.61(C6), 32.14(C8), 19.49(C9), 13.38(C10) ppm for $[C_4mim]Cl$, respectively. DSILs, e.g., $[C_4mim](CH_3CO_2)_{0.9}Cl_{0.1}$ showed 49.67(C7), 36.36(C6), 32.15(C8), 19.47(C9), 13.42(C10). The $\delta$ values of C11 carbons of DSILs showed in the downfield region comparative to C8, C9, and C10 protons due to the -C=O groups attached to it. The carbons of C=O groups denoted with C12 showed more downfield shifting with maximum values of 177.95, 177.5, 177.82, 178, 177.61, 177.3 ppm for $[C_4mim](CH_3CO_2)_{0.9}Cl_{0.1}$, $[C_4mim](CH_3CO_2)_{0.8}Cl_{0.2}$, $[C_4mim](CH_3CO_2)_{0.7}Cl_{0.3}$, $[C_4mim](CH_3CO_2)_{0.6}Cl_{0.4}$, $[C_4mim](CH_3CO_2)_{0.5}Cl_{0.5}$, respectively due to the attachment of electro negative O atom to the carbon atoms [45].

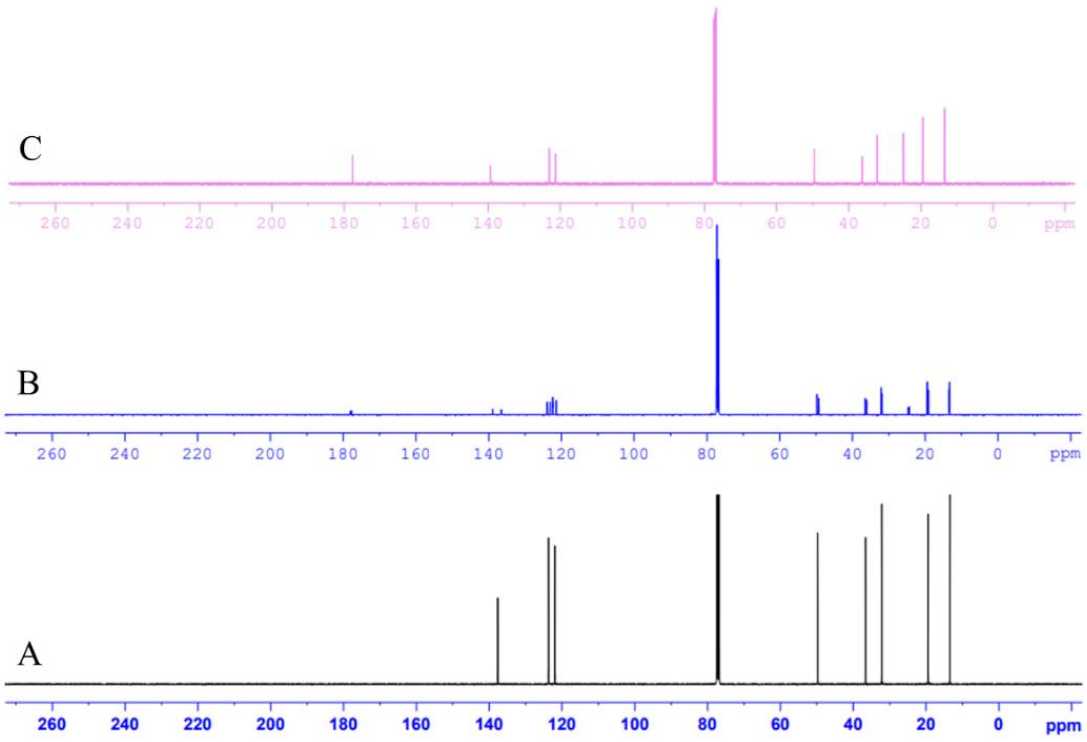


**Figure 2.12.** $^{13}C$ NMR spectra of (A)$[C_4mim]Cl$ (B) $[C_4mim](CH_3CO_2)_{0.6}Cl_{0.4}$ (C) $[C_4mim]CH_3CO_2$

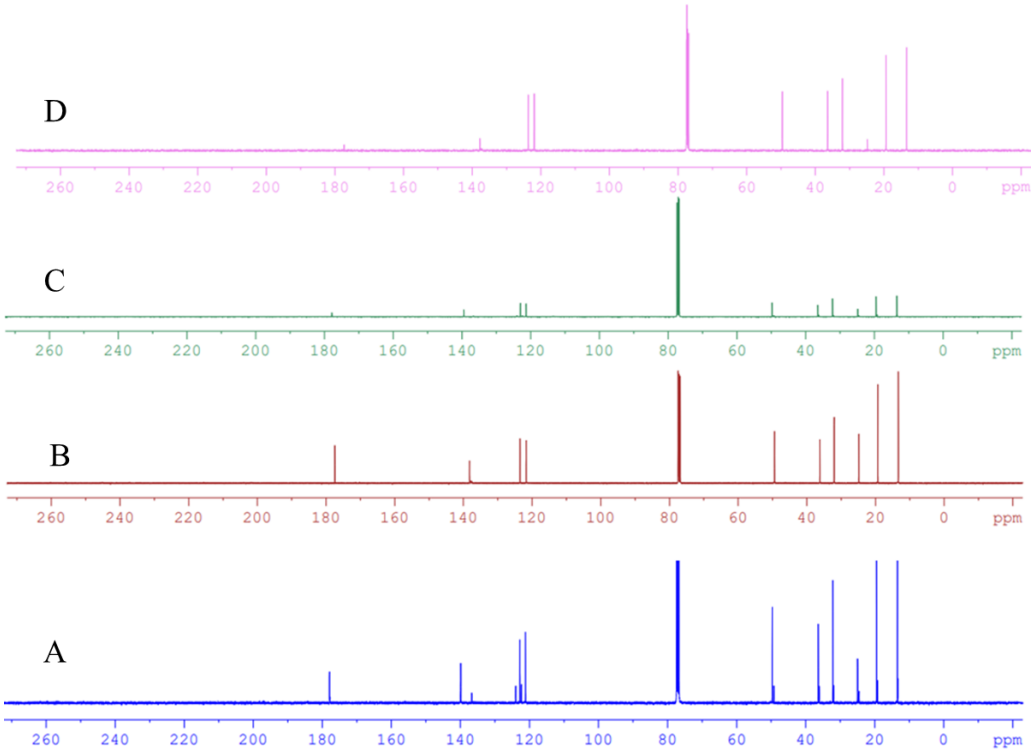


**Figure 2.13.** $^{13}C$ NMR spectra of (A) $[C_4mim](CH_3CO_2)_{0.9}Cl_{0.1}$ (B) $[C_4mim](CH_3CO_2)_{0.8}Cl_{0.2}$ (C) $[C_4mim](CH_3CO_2)_{0.7}Cl_{0.3}$ (D) $[C_4mim](CH_3CO_2)_{0.3}Cl_{0.7}$ (E) $[C_4mim](CH_3CO_2)_{0.1}Cl_{0.9}$

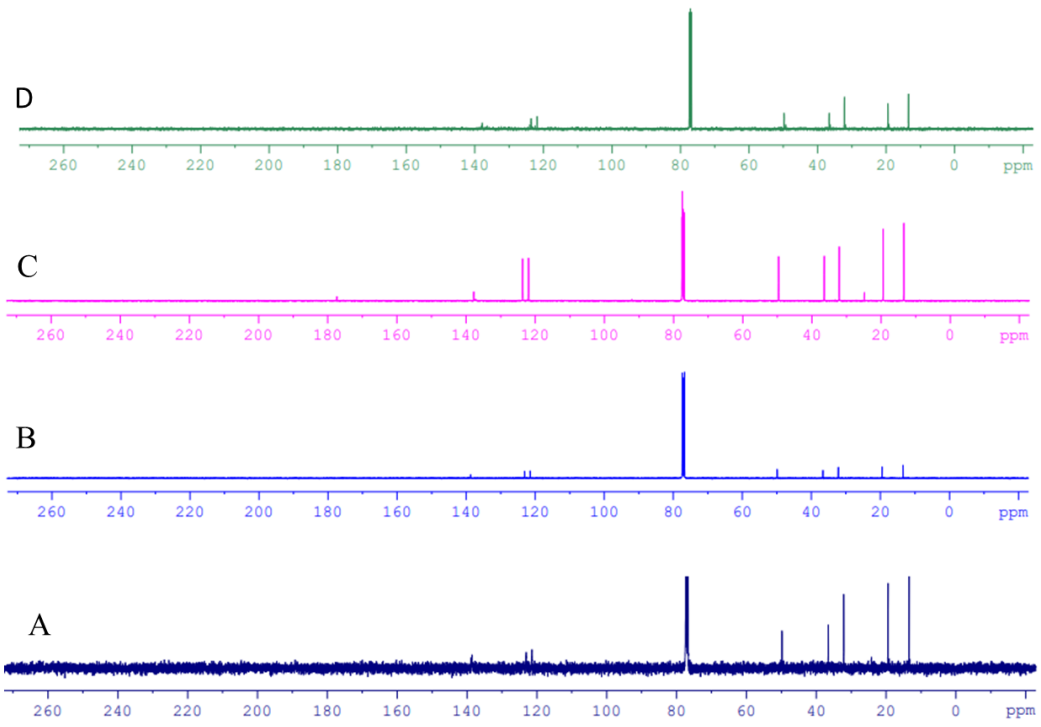


**Figure 2.14.** $^{13}C$ NMR spectra of (A)$[C_4mim](CH_3CO_2)_{0.4}Cl_{0.6}$ (B) $[C_4mim](CH_3CO_2)_{0.3}Cl_{0.7}$ (C) $[C_4mim](CH_3CO_2)_{0.2}Cl_{0.8}$ (D) $[C_4mim](CH_3CO_2)_{0.1}Cl_{0.9}$

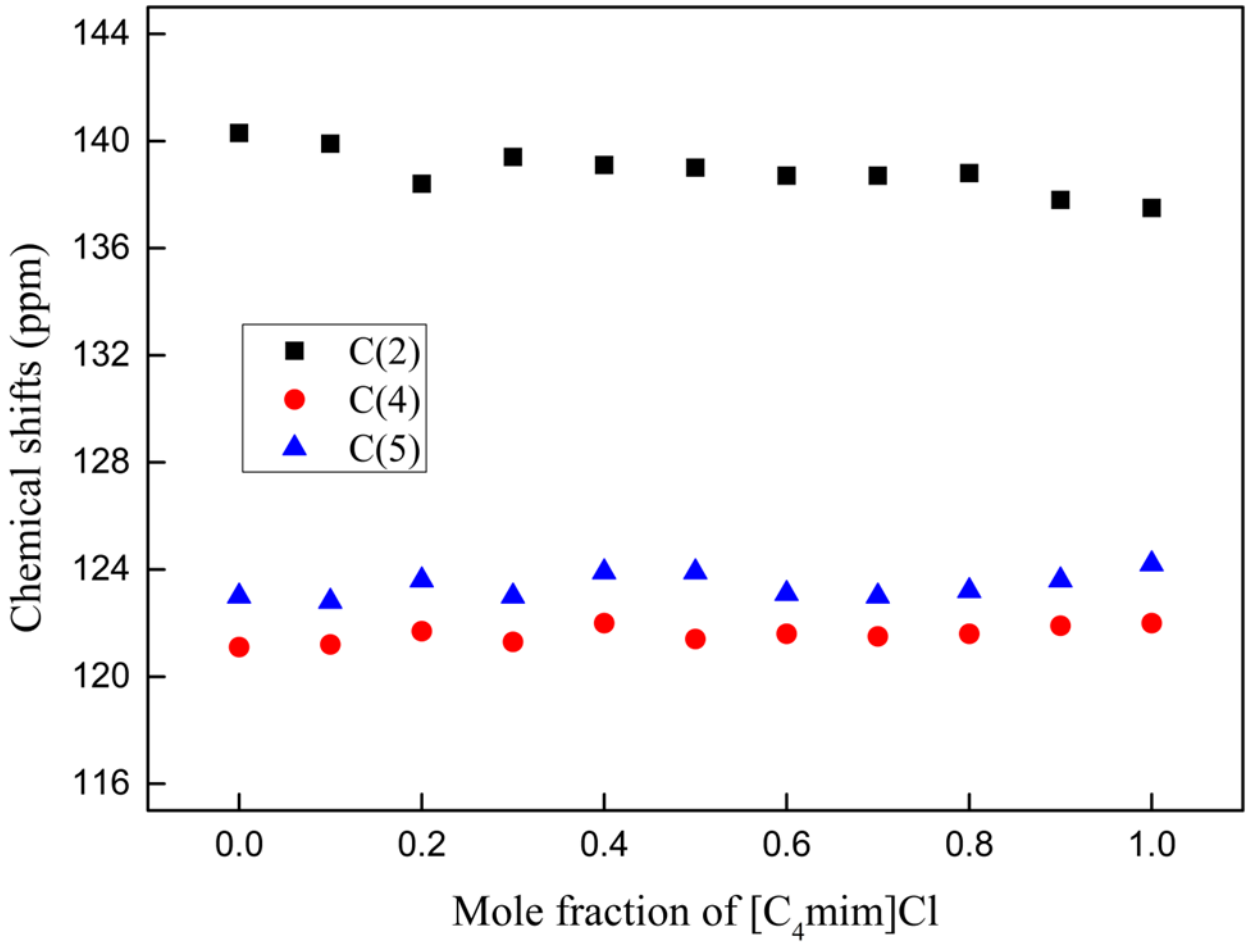


**Figure 2.15.** Variation of $^{13}C$ NMR chemical shifts of C(2)-H, C(4)-H and C(5)-H in imidazolium ion of $[C_4mim](CH_3CO_2)_xCl_{1-x}$ with the mole fraction of $[C_4mim]Cl$

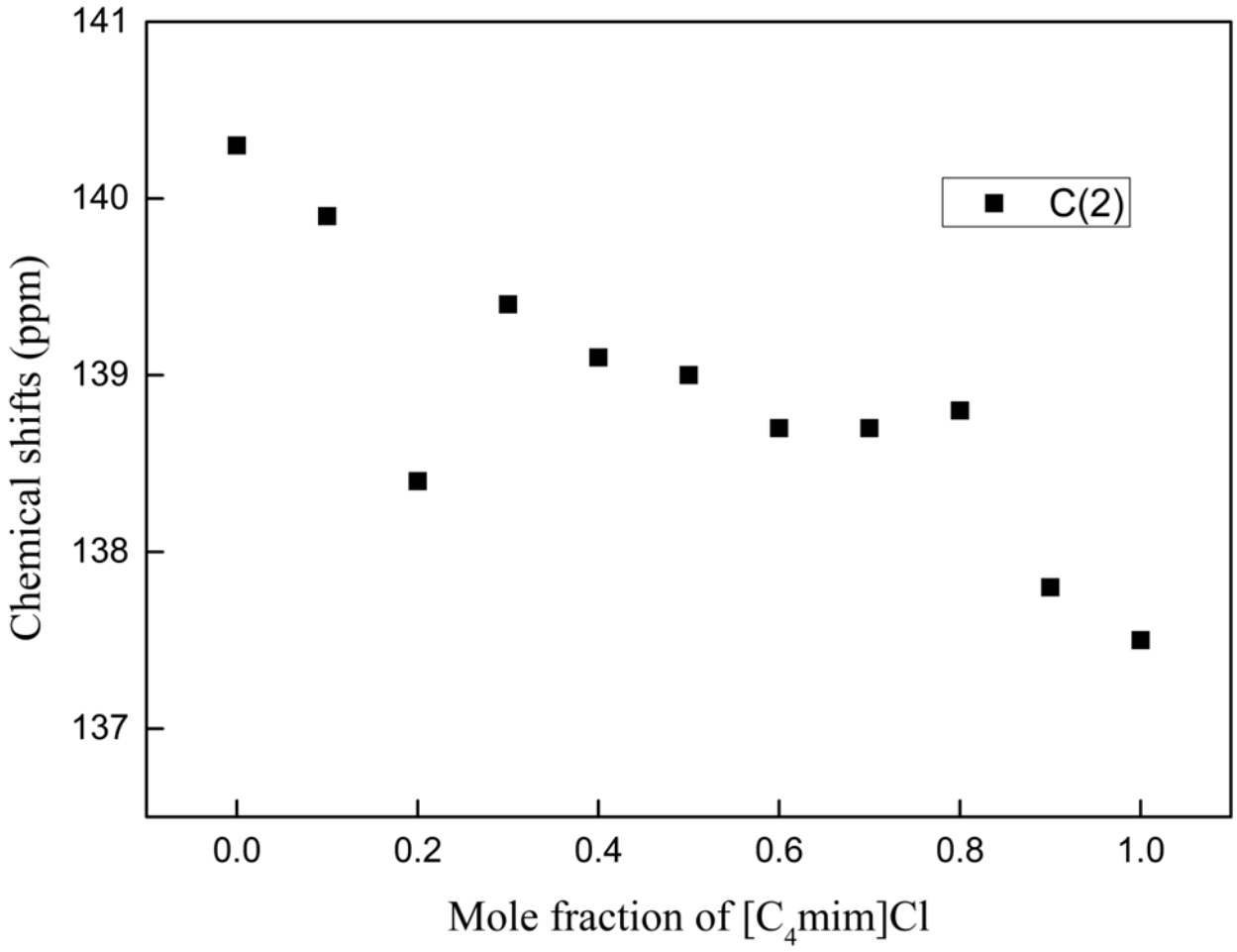


**Figure 2.16.** Variation of $^{13}C$ NMR chemical shifts of C(2)-H in imidazolium ion of $[C_4mim](CH_3CO_2)_xCl_{1-x}$ with the mole fraction of $[C_4mim]Cl$

## 2.4. Conclusions

Double salts ionic liquids have been prepared by the homogeneous mixing of 1-butyl-3-methyl imidazolium chloride ([$C_4$mim]Cl) and 1-butyl-3-methyl imidazolium acetate ([$C_4$mim]$CH_3CO_2$) over the whole mole fraction range. The structure of the prepared DSILs have been investigated at a molecular level by the help of ATR-FTIR, Raman and NMR spectroscopy. ATR-FTIR spectroscopy reveals the insights of interactions and functional groups present in DSILs. The most vulnerable C(2)-H stretching absorption peaks for DSILs in FTIR spectra have been strongly influenced by the mixing of [$C_4$mim]Cl and [$C_4$mim]$CH_3CO_2$ with different mole fractions. The stretching absorption peaks at 3025, 3060, 3065, 3050, 3053, 3054, 3056, 3054, 3061, 3059, and 3060 $cm^{-1}$ for [$C_4$mim]$CH_3CO_2$, [$C_4$mim]$(CH_3CO_2)_{0.9}Cl_{0.1}$ [$C_4$mim]$(CH_3CO_2)_{0.8}Cl_{0.2}$ [$C_4$mim]$(CH_3CO_2)_{0.7}Cl_{0.3}$ [$C_4$mim]$(CH_3CO_2)_{0.6}Cl_{0.4}$ [$C_4$mim]$(CH_3CO_2)_{0.5}Cl_{0.5}$ [$C_4$mim]$(CH_3CO_2)_{0.4}Cl_{0.6}$ [$C_4$mim]$(CH_3CO_2)_{0.3}Cl_{0.7}$ [$C_4$mim]$(CH_3CO_2)_{0.2}Cl_{0.1}$, [$C_4$mim]$(CH_3CO_2)_{0.1}Cl_{0.9}$, and [$C_4$mim]Cl respectively. These sharp blue shifts for the addition [$C_4$mim]Cl in [$C_4$mim]$CH_3CO_2$ indicated the synergistic participation of $Cl^-$ and $CH_3CO_2^-$ ions in the H-bonds formation with the C(2)-H protons in DSILs which weakens the C(2)-H bond. Raman spectroscopy offers a unique and characteristic identification of DSILs due to its capacity to detect and analyze alterations in polarizability that occur during molecular vibrations. The bands at 697 and 627 $cm^{-1}$ correspond to ring deformation of $[C_4mim]^+$ cation. Rest of the bands also result from some extent of ring and chain distortion. Relative intensity of the bands is very much pronounced in all the DSILs and [$C_4$mim]$CH_3CO_2$ compared to [$C_4$mim]Cl. This pronounced absorption intensity is due to the presence of acetate anion. NMR spectroscopy is imperative in elucidating the intricate molecular structure of DSILs. It offers valuable insights into the chemical changes shown by various nuclei within DSILs, encompassing both proton and carbon nuclei. Chemical changes exhibit a remarkable degree of sensitivity towards the electronic surroundings in their immediate vicinity, hence facilitating the process of structural investigation. The C(2)-H protons in DSILs showed more downfield with higher chemical shifts ($\delta$) values for all most all mole fractions exhibited 10.87, 10.74, 10.65, 10.64, 10.61, 10.63 ppm of [$C_4$mim]$(CH_3CO_2)_{0.9}Cl_{0.1}$, [$C_4$mim]$(CH_3CO_2)_{0.7}Cl_{0.3}$, [$C_4$mim]$(CH_3CO_2)_{0.6}Cl_{0.4}$, [$C_4$mim]$(CH_3CO_2)_{0.4}Cl_{0.6}$, [$C_4$mim]$(CH_3CO_2)_{0.3}Cl_{0.7}$ , respectively due to the synergistic effect of $Cl^-$ and $CH_3CO^-$ ions forming in strong H-bonds with the C(2)-H protons compared to [$C_4$mim]Cl and [$C_4$mim]$CH_3CO_2$ due to less electron around the nucleus of H. The strength of H-bonds

forming by anions of DSILs is possibly higher than H-bonds strength forming by anions of $[C_4mim]Cl$ and $[C_4mim]CH_3CO_2$. The $\delta$ value C(2)-H showed more downfield region compared to C(4)-H and C(5)-H protons. Similar to 1H NMR, the of $\delta$ values C2 of DSILs shifted to the more downfield region with the increase of the amount of $[C_4mim]Cl$ in DSILs.

**References**


[1] Holbrey, J. D., and Seddon, K. R. (1999). Ionic liquids. *Clean Products and Processes*, *1*(4), 223-236.

[2] Ghandi, K. (2014). A review of ionic liquids, their limits and applications. *Green and Sustainable Chemistry*, *2014*.

[3] Hajipour, A. R., and Rafiee, F. (2009). Basic ionic liquids. A short review. *Journal of the Iranian Chemical Society*, *6*, 647-678.

[4] Welton, T. (2018). Ionic liquids: a brief history. *Biophysical Reviews*, *10*(3), 691-706.

[5] Chatel, G., Pereira, J. F., Debbeti, V., Wang, H., and Rogers, R. D. (2014). Mixing ionic liquids–"simple mixtures" or "double salts"?. *Green Chemistry*, *16*(4), 2051-2083.

[6] Ijardar, S. P., Saparov, A., and Shah, D. (2019). Insights into Non-Ideal Behavior of Double Salt Ionic Liquids with Common Cation: Volumetric Behaviour, Molecular Dynamics Simulations and NMR Experiments. *ChemistrySelect*, *4*(44), 12861-12870.

[7] Rahman, A., Rahman, M. M., Mollah, M. Y. A., and Susan, M. A. B. H. (2019). Ultraslow Relaxation in Aprotic Double Salt Ionic Liquids. *The Journal of Physical Chemistry B*, *123*(26), 5577-5587.

[8] Pereira, J. F., Barber, P. S., Kelley, S. P., Berton, P., and Rogers, R. D. (2017). Double salt ionic liquids based on 1-ethyl-3-methylimidazolium acetate and hydroxyl-functionalized ammonium acetates: Strong effects of weak interactions. *Physical Chemistry Chemical Physics*, *19*(39), 26934-26943.

[9] Garcia, G., Atilhan, M., and Aparicio, S. (2015). Interfacial properties of double salt ionic liquids: A molecular dynamics study. *The Journal of Physical Chemistry C*, *119*(51), 28405-28416.

[10] Atilhan, M., Anaya, B., Ullah, R., Costa, L. T., and Aparicio, S. (2016). Double salt ionic liquids based on ammonium cations and their application for CO2 capture. *The Journal of Physical Chemistry C*, *120*(31), 17829-17844.

[11] Stolarska, O., Pawlowska-Zygarowicz, A., Soto, A., Rodríguez, H., and Smiglak, M. (2017). Mixtures of ionic liquids as more efficient media for cellulose dissolution. *Carbohydrate Polymers*, *178*, 277-285.

[12] Kore, R., Kelley, S. P., Aduri, P., and Rogers, R. D. (2018). Mixed metal double salt ionic liquids comprised of [HN 222] 2 [$ZnCl_4$] and $AlCl_3$ provide tunable Lewis acid catalysts related to the ionic environment. *Dalton Transactions*, *47*(23), 7795-7803.

[13] Song, Z., Hu, X., Zhou, Y., Zhou, T., Qi, Z., and Sundmacher, K. (2019). Rational design of double salt ionic liquids as extraction solvents: separation of thiophene/n-octane as example. *AIChE Journal*, *65*(8), e16625.

[14] Rzemieniecki, T., Wojcieszak, M., Materna, K., Praczyk, T., and Pernak, J. (2021). Synthetic auxin-based double salt ionic liquids as herbicides with improved physicochemical properties and biological activity. *Journal of Molecular Liquids*, *334*, 116452.

[15] Xu, M., Jiang, B., Dou, H., Yang, N., Xiao, X., Tantai, X., and Zhang, L. (2021). Double-salt ionic liquid derived facilitated transport membranes for ethylene/ethane separation. *Journal of Membrane Science*, *639*, 119773.

[16] Hind, A. R., Bhargava, S. K., and McKinnon, A. (2001). At the solid/liquid interface: FTIR/ATR—the tool of choice. *Advances in Colloid and Interface Science*, *93*(1-3), 91-114.

[17] Glassford, S. E., Byrne, B., and Kazarian, S. G. (2013). Recent applications of ATR FTIR spectroscopy and imaging to proteins. *Biochimica et Biophysica Acta (BBA)-Proteins and Proteomics*, 1834(12), 2849-2858.

[18] Kadari, M., Belarbi, E. H., Moumene, T., Bresson, S., Haddad, B., Abbas, O., and Khelifa, B. (2017). Comparative study between 1-Propyl-3-methylimidazolium bromide and trimethylene bis-methylimidazolium bromide ionic liquids by FTIR/ATR and FT-RAMAN spectroscopies. *Journal of Molecular Structure*, *1143*, 91-99.

[19] Cha, S., Lee, M., and Kim, D. (2019). Concentration Dependence of Ion Pairing in Imidazolium-Based Ionic Liquid Solutions. *ChemPhysChem*, *20*(3), 482-488.

[20] Jaganathan, J. R., Sivapragasam, M., and Wilfred, C. D. (2016). Thermal characteristics of 1-butyl-3-methylimimidazolium based oxidant ionic liquids. *J. Chem. Eng. Process Technol*, *7*, 1-6.

[21] Maier, F., Cremer, T., Kolbeck, C., Lovelock, K.R.J., Paape, N., Schulz, P.S., Wasserscheid, P., and Steinrück, H.P. (2010). Insights into the surface composition and enrichment effects of ionic liquids and ionic liquid mixtures. *Physical Chemistry Chemical Physics, 12*(8), 1905-1915.

[22] Iwata, K., Okajima, H., Saha, S., and Hamaguchi, H. O. (2007). Local structure formation in alkyl-imidazolium-based ionic liquids as revealed by linear and nonlinear Raman spectroscopy. *Accounts of Chemical Research*, *40*(11), 1174-1181.

[23] Berg, R. W. (2007). Raman spectroscopy and ab-initio model calculations on ionic liquids. *Monatshefte für Chemie-Chemical Monthly*, *138*, 1045-1075.

[24] Kiefer, J., Fries, J., and Leipertz, A. (2007). Experimental vibrational study of imidazolium-based ionic liquids: Raman and infrared spectra of 1-ethyl-3-methylimidazolium bis (trifluoromethylsulfonyl) imide and 1-ethyl-3-methylimidazolium ethylsulfate. *Applied Spectroscopy*, *61*(12), 1306-1311.

[25] Fujii, K., Fujimori, T., Takamuku, T., Kanzaki, R., Umebayashi, Y., and Ishiguro, S. I. (2006). Conformational equilibrium of bis (trifluoromethanesulfonyl) imide anion of a room-temperature ionic liquid: Raman spectroscopic study and DFT calculations. *The Journal of Physical Chemistry B*, *110*(16), 8179-8183.

[26] Zhu, S., Li, H., Zhu, W., Jiang, W., Wang, C., Wu, P., Zhang, Q., and Li, H. (2016). Vibrational analysis and formation mechanism of typical deep eutectic solvents: An experimental and theoretical study. *Journal of Molecular Graphics and Modelling*, *68*, 158-175.27.

[27] Damodaran, K. (2016). Recent NMR studies of ionic liquids. *Annual Reports on NMR Spectroscopy*, *88*, 215-244.

[28] Giernoth, R., Bankmann, D., and Schlörer, N. (2005). High performance NMR in ionic liquids. *Green Chemistry*, *7*(5), 279-282.

[29] Damodaran, K. (2022). Recent advances in NMR spectroscopy of ionic liquids. *Progress in Nuclear Magnetic Resonance Spectroscopy*, *129*, 1-27.22.

[30] Wang, Y., Chen, W., Zhao, Q., Jin, G., Xue, Z., Wang, Y., and Mu, T. (2020). Ionicity of deep eutectic solvents by Walden plot and pulsed field gradient nuclear magnetic resonance (PFG-NMR). *Physical Chemistry Chemical Physics*, *22*(44), 25760-25768.

[31] Tokuda, H., Hayamizu, K., Ishii, K., Susan, M. A. B. H., and Watanabe, M. (2004). Physicochemical properties and structures of room temperature ionic liquids. 1. Variation of anionic species. *The Journal of Physical Chemistry B*, *108*(42), 16593-16600.

[32] Tokuda, H., Hayamizu, K., Ishii, K., Susan, M. A. B. H., and Watanabe, M. (2005). Physicochemical properties and structures of room temperature ionic liquids. 2. Variation of alkyl chain length in imidazolium cation. *The Journal of Physical Chemistry B*, *109*(13), 6103-6110.

[33] Tokuda, H., Ishii, K., Susan, M. A. B. H., Tsuzuki, S., Hayamizu, K., and Watanabe, M. (2006). Physicochemical properties and structures of room-temperature ionic liquids. 3. Variation of cationic structures. *The Journal of Physical Chemistry B*, *110*(6), 2833-2839.

[34] Pauric, A. D., Halalay, I. C., and Goward, G. R. (2016). Combined NMR and molecular dynamics modeling study of transport properties in sulfonamide based deep eutectic lithium electrolytes: LiTFSI based binary systems. *Physical Chemistry Chemical Physics*, *18*(9), 6657-6667.

[35] Zheng, Y. Z., Zhou, Y., Deng, G., Guo, R., and Chen, D. F. (2020). The structure and interaction properties of two task-specific ionic liquids and acetonitrile mixtures: A combined FTIR and DFT study. *Spectrochimica Acta Part A: Molecular and Biomolecular Spectroscopy*, *226*, 117641.

[36] Umebayashi, Y., Jiang, J. C., Shan, Y. L., Lin, K. H., Fujii, K., Seki, S., and Chang, H. C. (2009). Structural change of ionic association in ionic liquid/water mixtures: A high-pressure infrared spectroscopic study. *The Journal of Chemical Physics*, *130*(12), 124503.

[37] Cha, S., Ao, M., Sung, W., Moon, B., Ahlström, B., Johansson, P., and Kim, D. (2014). Structures of ionic liquid–water mixtures investigated by IR and NMR spectroscopy. *Physical Chemistry Chemical Physics*, *16*(20), 9591-9601.

[38] Shiflett, M. B., Drew, D. W., Cantini, R. A., and Yokozeki, A. (2010). Carbon dioxide capture using ionic liquid 1-butyl-3-methylimidazolium acetate. *Energy and Fuels*, *24*(10), 5781-5789.

[39] Hayashi, S., Ozawa, R., and Hamaguchi, H. O. (2003). Raman spectra, crystal polymorphism, and structure of a prototype ionic-liquid [bmim] Cl. *Chemistry Letters*, *32*(6), 498-499.

[40] Ozawa, R., Hayashi, S., Saha, S., Kobayashi, A., and Hamaguchi, H. O. (2003). Rotational isomerism and structure of the 1-butyl-3-methylimidazolium cation in the ionic liquid state. *Chemistry Letters*, *32*(10), 948-949.

[41] Cabaço, M. I., Besnard, M., Danten, Y., and Coutinho, J. A. P. (2011). Solubility of CO2 in 1-butyl-3-methyl-imidazolium-trifluoro acetate ionic liquid studied by Raman spectroscopy and DFT investigations. *The Journal of Physical Chemistry B*, *115*(13), 3538-3550.

[42] Berg, R. W. (2007). Raman spectroscopy and ab-initio model calculations on ionic liquids. *Monatshefte für Chemie-Chemical Monthly*, *138*, 1045-1075.

[43] Ribeiro, M. C. (2012). High viscosity of imidazolium ionic liquids with the hydrogen sulfate anion: a Raman spectroscopy study. *The Journal of Physical Chemistry B*, *116*(24), 7281-7290.22.

[44] Becker, E. D. (1999). *High resolution NMR: theory and chemical applications*. *Elsevier.*

[45] Hesse-Ertelt, S., Heinze, T., Kosan, B., Schwikal, K., and Meister, F. (2010). Solvent effects on the NMR chemical shifts of imidazolium-based ionic liquids and cellulose therein. In Macromolecular Symposia. *Weinheim: WILEY-VCH Verlag*, 294(2), 75-89.

[46] Zaoui, A., Cherifi, Z., and Belbachir, M. (2019). Ultrasound-induced synthesis of an imidazolium based poly (ionic liquid) in an aqueous media: A structural, thermal and morphological study. *Ultrasonics Sonochemistry*, *55*, 149-156.

[47] Bystrov, S. S., Matveev, V. V., Chernyshev, Y. S., Balevičius, V., and Chizhik, V. I. (2019). Molecular mobility in a set of imidazolium-based ionic liquids $[bmim]^+$ A–by the NMR-relaxation method. *The Journal of Physical Chemistry B*, *123*(10), 2362-2372.

[48] Ebenso, E. E. (2003). Synergistic effect of halide ions on the corrosion inhibition of aluminium in $H_2SO_4$ using 2-acetylphenothiazine. *Materials Chemistry and Physics*, *79*(1), 58-70.

[49] Pillai, P., Pal, N., and Mandal, A. (2017). Synthesis, characterization, surface properties and micellization behaviour of imidazolium-based ionic liquids. *Journal of Surfactants and Detergents*, *20*, 1321-1335.

[50] Matveev, V. V., Markelov, D. A., Ievlev, A. V., Brui, E. A., Tyutyukin, K. V., and Lähderanta, E. (2018). Molecular mobility in several imidazolium-based ionic liquids according to data of $^{1}H$ and $^{13}C$ NMR relaxation. *Magnetic Resonance in Chemistry*, *56*(2), 140-143.

[51] Ameta, G., Pathak, A. K., Ameta, C., Ameta, R., and Punjabi, P. B. (2015). Sonochemical synthesis and characterization of imidazolium based ionic liquids: A green pathway. *Journal of Molecular Liquids*, *211*, 934-937.

[52] Kavya, S. H., Vijaya Kumar, V., and Kumar, C. R. (2020). Synthesis and characterization of stable ZnO nanoparticles using imidazolium-based ionic liquids and their applications in esterification reaction. *Indian Journal of Chemistry-Section A, 57*(8-9), 1112-1120

# Chapter 3

## Physicochemical Properties of Imidazolium-Based Double Salt Ionic Liquids


### Abstract

A new type of ionic liquid (IL) with different properties from ILs is created by mixing two ILs with a common cation, anion, or four different ions. These mixtures are termed double salt ILs (DSILs). To get an insight into tunable properties of DSILs and to gather the knowledge on how these properties are different from the ILs, the physicochemical properties are need to be investigated. In this chapter, temperature-dependent measurements of the density, viscosity, refractive index, and conductivity of imidazolium-based ILs and their DSILs were made for the entire composition range between 30 and 70 °C. The studied ILs were 1-butyl-3-methyl imidazolium chloride ($[C_4mim]Cl$) and 1-butyl-3-methyl imidazolium acetate ($[C_4mim]CH_3CO_2$) and their DSILs $[C_4mim](CH_3CO_2)_{1-x}Cl_x$ (x is the mole fraction of ILs). The excess properties such as excess molar volume, excess viscosity, and excess refractive index were calculated for a improved comprehension of interactions between constituent ion interactions of $[C_4mim]^+$, $Cl^-$ and $CH_3CO_2^-$ using appropriate models and equations. The Redlich-Kister (R-K) polynomial equation was used to fit the excess molar volume, excess viscosity, and excess refractive index. The variation of excess viscosity provides a qualitative assessment of the extent of intermolecular interactions because viscosity is connected with molecular-level interactions such as electrostatic force, hydrogen bond, and van der Waals interaction. The deviation from straightforward Arrhenius behavior was explained by the Mauro-Yue-Ellison-Gupta-Allan (MYEGA) equation and the modified Vogel-Fulcher-Tammann (mVFT) equation. Fitting the data into these two equations yielded the glass transition temperature ($T_g$) and fragility index ($m$). For the viscous flow of DSILs, the thermodynamic parameters of change in activation free energy ($\Delta G$), change in activation entropy ($\Delta S$), and change in activation enthalpy ($\Delta H$) were investigated. The ionicity of the prepared DSILs was measured using the Walden plot.



**Keywords:** Double salt ionic liquids, conductivity, viscosity, density, and refractive index

## 3.1. Introduction

Ionic liquids (ILs) are a distinct class of solvents with melting points below 100 °C that are entirely made up of ions of large organic cations and relatively small organic or inorganic anions. The asymmetric combination and strong electrostatic attraction between cations and anions of ILs form a stable liquid phase at room temperature. The numerous physicochemical features of ILs, namely their insignificant vapor pressure, nonflammability, high ionic conductivity, superior thermal stability, wide electrochemical windows, chemical, and electrochemical stability, ability to dissolve solutes, and ability to recycle, have contributed to the gradually increasing interest in them [1-5]. Because of their special qualities in fields like chemistry, materials science, engineering, and pharmaceuticals, ILs have a wide range of industrial applications. They are used as solvents, electrolytes, catalysts, and more, offering advantages over traditional solvents and materials in terms of performance, safety, and environmental impact [5-16]. The IL designer idea has given flexibility in selecting various combinations of cations and anions as well as manipulating physicochemical attributes for the anticipated applications. Theoretically, the combination of two, three, or four pure ILs are expected to prepare about $10^{18}$ various kinds of ILs [13]. Tokuda *et al.*, looked into how different anionic species can change the physicochemical characteristics of pure ILs [17] in addition to the variation in alkyl chain length [18], and the cationic structures [19]. [$C_4$mim]-based ILs were studied with the change of several anionic species such as bis-(trifluoromethyl sulfonyl) imide $(CF_3SO_2)_2N$, trifluoroacetate ($CF_3CO_2$), trifluoromethane sulfonate ($CF_3SO_3$), etc. Similarly, keeping the anion constant as $(CF_3SO_2)_2N$, the effect of variations in cationic species such as [$C_4$mim], butylpyridinium, [$C_4$py], *N*-butyl-*N*-methylpyrrolidinium, ([$C_4$mpyr]) etc., on the physicochemical property directing parameters, i.e., ionic conductivity, density, viscosity, and thermal behavior of the system were studied. They discovered that the combined impact of the inductive interactions between the ions, aggregates, and clusters and the supramolecular interactions among the ionic species determines the features of ILs. As the alkyl chain length varies, so do the forces that interact among the ILs. There has been a lot of investigation into the physicochemical properties of ILs and their binaries with molecular solvents in recent years [20-26].

Recently, double salt ionic liquids (DSILs) have gained more attention from researchers for their fine-tuning ability of the physical and chemical traits of ILs by the variation of ionic constituents. The combination of ILs offers a potential method for adjusting their characteristics.

DSILs are formed by joining two identical ILs that share a common anion or cation, or by using entirely different cations and anions which results in a new type of IL that has different properties than individual ILs. Each DSIL is thus considered to have distinct unique properties [27]. During the formation of DSILs, the ion association in individual ILs was disrupted, and several molecular interactions were established. DSIL solvent properties can be fine-tuned by varying the composition and abundance of ions involved in the supramolecular interactions like hydrogen bonds and electrostatic interactions between the ions [28]. In addition to adjusting physicochemical properties, DSILs provide instructions for synthesizing task-specific ILs (TSILs) and aid in facilitating the development of thermodynamic models that may be used in selecting the optimal DSIL for applications with set physicochemical features [29]. DSILs have been potentially used in several field of applications such as gas solubilities [30], dye-sensitized solar cells [31-33]. A few theoretical investigations of DSILs have also been conducted [34-36]. The physical characteristics of DSILs have been measured only sometimes such as transport and volumetric properties [37, 38], molecular association [39], dielectric measurements [40], and nanostructures [41]. There are have been some instances of improved characteristics than the pure ILs [30, 37]

It is necessary to understand, how changing the ions can affect the physicochemical properties of DSILs and their possible application. Physicochemical properties, thermal behavior, and structures of DSILs are investigated by theoretical studies like MD simulations, and their applications in absorptions are only a few of the topics covered in recent studies [27, 42, 43]. Niedermeyer *et al.* examined the existing research on these IL mixtures to determine the way their properties change and whether they might be used [42]. For the majority of DSILs, near-ideal behavior is reported [44-49]. However, certain DSILs exhibit non-ideal behavior because of unanticipated modifications to their physicochemical characteristics and molecular rearrangements that are absent from pure ILs [27]. Canongia Lopez *et al.* [44] investigated that DSILs with a common cation or anion showed ideal behavior: $[C_nmim]_x[C_mmim]_{1-x}[NTf_2]$, $[C_4mim][NTf_2]_{1-x}[PF_6]_x$, $[C_4mim][NTf_2]_x[BF_4]_{1-x}$, $[C_4mim][BF_4]_x[PF_6]_{1-x}$, found that the excess molar volume ($V_m^E$) of DSILs is -0.06 to -0.18 which was 1.5 % less than total volume difference of pure ILs. Navia *et al.* [45,46] also investigated the negative value of $V_m^E$ of DSILs with common $[C_4mim]^+$ and varying anions of $[BF_4]$ and $[PF_6]$. Recently, Stoppa *et al.* [47] investigated the nearly ideal behavior of $[C_2mim][BF_4]_{1-x}[SCN]_x$. However, Larriba *et al.* have looked into the volumetric properties of DSILs based on pyridinium [48]. Navia *et al.* [46] also investigated the viscosities of the DSILs

with a common ion $[C_6mim]_x[C_2mim]_{1-x}[BF_4]$, $[C_6mim]_x[C_4mim]_{1-x}[BF_4]$, $[C_4mim][BF_4]_x[MeSO_4]_{1-x}$ and $[C_4mim][PF_6]_x[BF_4]_{1-x}$ considering the temperature from 298.15 to 308.15 K. The effect of temperature on viscosity for ILs is evaluated using the Vogel-Tammann-Fulcher (VFT) equation, and various mixing rules are applied to the DSILs. They discovered that, if the "ideal" Grunberg and Nissan and Katti mixing laws are assumed to apply to the viscosity of an ideal mixture, the systems show almost ideal behavior. Experimental and theoretical investigation on the structure of DSILs of ($[b_3mpy][BF_4]_x[N(CN)_2]_{1-x}$ and $[b_3mpy]_x[o_3mpy]_{1-x}[BF_4]$) at molecular level was carried out by Aparicio and Atilhan. These findings demonstrate that the mixture properties of the analyzed mixed systems are influenced by the dilution effects of the corresponding ions, and their parameters almost linearly change over time. [49]. Song *et al.* [50] investigated the density and viscosity of DSILs of ($[C_2mim]_x[C_3mim]_{1-x}$ $[BF_4]$, $[C_3mim]_x[C_6mim]_{1-x}[BF_4]$, and $[C_2mim]_x[C_6mim]_{1-x}[BF_4]$ over the range of temperature from 298.15 K to 343.15 K. Redlich−Kister type polynomial equation was used to calculate and correlate the excess molar volume. The viscosity of the ILs was analyzed using the VFT equation and the mixture was treated with ideal mixture principles.

On the contrary, the refractive indices have a close relation with particular chemical characteristics such as polarity and relative ability to give and receive hydrogen bonds, which helps in calculating reaction rates, partition constants, and solubility [51]. In order to confirm materials, ensure their purity, or determine the concentration of a mixture, it is typically crucial to know the refractive index of a compound. Additionally, it has to do with how molecules interact with one another or behave in solutions [52], and can be easily connected using thermodynamic equations with particular material characteristics like the dielectric constant and density [53]. The addition of co-solvent with ILs allows for fine-tuning of material density and refractive index. Saba *et al.*, (2014) measured the density and refractive index of $[C_4mim]Cl$ with organic molecular solvent and found that refractive index values depend on the concentration of $[C_4mim]Cl$ [54]. However, the refractive index not only gives insight into the purity of the ILs but also correlates with the density and refractive index of the ILs. The relationship between the density and refractive index of ILs made of imidazolium was inspected by A.N. Soriano *et al.* They discovered that the results reported by various literature for the density and refractive indices of imidazolium-based ILs are comparable. Moreover, the refractive indices vary with temperature linearly [55]. Iglesias-Otero *et al.* also conducted a study to predict the density from the refractive indices of ILs containing

imidazolium and the binary mixtures of them with organic solvents such as ethanol, nitromethane, 1, 3-Dichloropropane, etc. [56]. In contrast, studies involving the refractive index of DSILs is scarce and need to be addressed with in-depth analysis. As the combinations of DSILs changes, their physicochemical properties changes. This is the reason the density of these different combinations of DSILs will have different values.

Similar to viscosity measurement, it has been conducted many experiments for the determination of conductivities of ILs with molecular solvents [57-59]. Only a few research are available for the measurements of conductivities of the mixture of ILs. In their investigation of the conductivity of DSILs made of $[C_2mim][NTf_2]_x[OTf]_{1-x}$, MacFarlane *et al.* [60] discovered that, for all compositions examined, the molar conductivity deviated positively from a simple linear mixing rule and exceeded the value of the higher conducting simple liquid**.** This behavior was explained on the basis of more charge carrier ions or enhanced movement of the ions. They claimed that the enhanced conductivity can be explained by decreased ion clustering, which results in less coupled ion movement and more independent charge carriers. This is due to the fact that the self-diffusion constants of the ions remained relatively constant across the range of compositions. Additionally, DSILs of $[C_2mim][BF_4]_x[N(CN)_2]_{1-x}$ were found to deviate positively from linear mixing, however, the values for the mixtures were inferior to that of the pure component with the highest conductivity [47]. It is necessary to conduct additional systematic investigations on volumetric behavior to promote applications of new combinations of DSILs.

It is thus clear from the above discussion that the proper choice of ions of participating ILs in DSILs and their compositions are crucial for achieving the desired physicochemical properties as a solvent. In this study, measurements of density, viscosity, refractive index, and conductivity of $[C_4mim]CH_3CO_2$, $[C_4mim]Cl$, and their DSILs have been carried out. The detailed investigation of DSILs of whole mole fractions is limited. So, the systematic investigation of the physicochemical properties of DSILs at various temperatures over the whole mole fractions range has been discussed. This study will help to reveal the underlying features of DSIL media used for enhanced solubility of cellulose studied in the following chapters.

### 3.2. Materials and Methods

The materials and methods applied in this chapter for the purpose of conducting this study have been described in the subsequent sections.

#### 3.2.1. Materials

ILs, $[C_4mim]Cl$ and $[C_4mim]CH_3CO_2$, were purchased from Sigma-Aldrich with purities of $\geq$98% and $\geq$95%, respectively.

#### 3.2.2. Preparation of DSILs

The preparation DSILs have been carried out by mixing of $[C_4mim]Cl$ and $[C_4mim](CH_3CO_2)$ at varying mole fractions to prepare $[C_4mim](CH_3CO_2)_xCl_{1-x}$, ( where *x* is 0.1, 0.2, 0.3, 0.4, 0.5, 0.6, 0.7, 0.8, and 0.9 mole fraction of single ILs). The details of the preparation procedure have been described in chapter 2 (sub-section 2.2.2).

#### 3.2.3. Characterizations

The physicochemical properties of DSILs have been studied by measuring density, viscosity, refractive index and conductivity. The details procedure of these techniques have described in the following sub-sections.

##### 3.2.3.1. Measurement of Density

The densities of the ILs, and their DSILs were measured with the density meter (Model: DMA 4500 M, Anton Paar, UK) that works on the basis of the oscillating U-tube method. Prior to measurement, the density meter was calibrated with ultra-pure water and then ethanol. It was allowed to dry at atmospheric pressure. The repeatability of density measurement was 0.00001 $g/cm^3$ and the accuracy of measurement was 0.000005 $g/cm^3$. As the density is highly temperature-dependent, the measuring cell was highly thermostated. Densities were measured by injecting a small amount of sample (less than 2 mL) into a U-shaped borosilicate glass tube and setting the temperatures from 30 to 70°C at 10 °C intervals. Air and water checks were performed before measuring the density of samples. For each measurement, deionized water and ethanol were used to clean and dry the glass tube.

##### 3.2.3.2. Measurement of Viscosity

An Anton Paar micro-viscometer (Model: Lovis 2000 ME, UK) was used to measure the viscosity of the ILs and their DSILs following the rolling ball principle having an accuracy of $\pm10^{-6}$ mPa.s. Glass capillaries with diameters of 1.59 mm and 2.50 mm and corresponding gold balls with a maximum deviation of 0.2% were used for the measurements. The rolling ball

principle, which this device uses, involves rolling a ball through a closed, liquid-filled capillary that is angled at a particular angle. Three inductive sensors calculate the rolling time of the ball between the designated markings**.** The viscosity of the sample is directly proportional to the rolling time. The micro viscometer records the time of rolling. Measurement of opaque liquids is made possible by inductive sensors. To control the temperature, the temperature was controlled by a built-in thermostat with a precision level of ±0.01 K. Using a syringe and a temperature-controlled capillary block, a tiny amount of sample (nearly 1 mL) was injected into a glass capillary. This block was angled in various predetermined ways. Measurements were carried out from 30 to 70 ℃ at 10 ℃ intervals.

#### 3.2.3.3. Measurement of Refractive Index

An automated refractometer (Abbemat 300, Anton Paar) with a high-resolution optical sensor was used to measure the refractive index of ILs and DSILs. To control the temperature, a built-in temperature controller with an accuracy level of 0.01 K was used. The refractive index was determined using reflected light. To regulate the temperature, a built-in temperature controller with an accuracy level of 0.01 K was used. The reflected beam was detected by a sensor array. This led to the calculation of the critical angle for total reflection, which was then used to ascertain the refractive index of the sample.

#### 3.2.3.4. Measurement of Conductivity

Electrochemical impedance spectroscopic (EIS) measurements of ILs and DSILs were performed using a high-performance Autolab PGSTAT302N impedance analyzer with the FRAN32M module over a large frequency range of 10 μHz to 32 MHz. In order to measure the ionic conductivity, stainless steel electrodes were used. Before measuring the impedance, the ILs and DSILs were filled between two mirror-finished stainless-steel electrodes using a teflon ring spacer.

### 3.3. Results and Discussion

The physicochemical properties of ILs and their DSILs have been characterized by measuring density, viscosity, refractive index, and conductivity of the ILs and DSILs. The details have been provided in below subsections.

#### 3.3.1. Density of pure ILs and DSILs

The densities ($\rho$) of $[C_4mim]CH_3CO_2$ and $[C_4mim]Cl$ and their DSILs of $[C_4mim](CH_3CO_2)_xCl_{1-x}$ (x is the mole fraction of ILs) were measured between 30-70 °C at 10 °C intervals in the whole mole fraction range are listed in Table 3.1 and plotted in Fig. 3.1 and 3.2. The $\rho$ of $[C_4mim]CH_3CO_2$ are found to be 1.04896, 1.04294, 1.03692, 1.03097, 1.02506 g/cm$^3$ at 30, 40, 50, 60, 70 °C, respectively. The $\rho$ of $[C_4mim]Cl$ was measured only at 70 °C was 1.06001 g/cm$^3$, due to the sampling restriction of $[C_4mim]Cl$ as it is solid at room temperature. It was found that the $\rho$ of $[C_4mim]CH_3CO_2$ and $[C_4mim]Cl$ were 1.02506 and 1.06001 g/cm$^3$ at 70 °C, respectively. All DSILs showed values of $\rho$ in between the ILs at all temperatures. Fig. 3.1 shows that $\rho$ decreases with increasing temperature and increases with increasing mole fraction of $[C_4mim]Cl$ in DSILs because of the dominance of the $\rho$ of $[C_4mim]Cl$. A provable reason for the decrease in $\rho$ of DSILs with temperature is that the raise in temperature increases the thermal motion of the constituent ions in the systems that causes the expansion of volume which lowers the $\rho$. Ijardar *et al.* [61] carried out a similar to this experiment between $[C_2mim][Ntf_2]$, $[C_2mim][EtSO_4]$ and their DSILs and investigated the change in densities for $[C_2mim][Ntf_2]$, $[C_2mim][EtSO_4]$ and their DSILs in the whole mole fraction range from 25-50 °C at 5 °C intervals. They found that densities decrease with the temperature and the amount of $[C_2mim][EtSO_4]$. They observed that the density of $[C_2mim][Ntf_2]$, $[C_2mim][EtSO_4]$ were 1.51301 and 1.23378 g/cm$^3$ were, respectively, at 30 °C and increased with the mole fraction of $[C_2mim][Ntf_2]$ for DSILs. In this analysis, all the measured densities of ILs and DSILs were correlated with the Levenberg-Marquardt method of linear expression of the equation, $\rho$ = a - b($T$), where a and b denote the adjustable parameters, and $T$ is the temperature [19]. The slope and intercept of the plot were used to calculate the correlation parameters a and b, respectively. It was investigated that $\rho$ of ILs and DSILs were linearly dependent on temperature are plotted in Fig. 3.2. The equation parameters of a and b and coefficients of determination ($R^2$) values of ILs and DSILs are tabulated in Table 3.2. It was discovered that $R^2$ values for all measurements are ~1.00, demonstrating the linearity of the relationship and indicating there is no requirement to use polynomial equations of higher degrees at the experimental temperature.

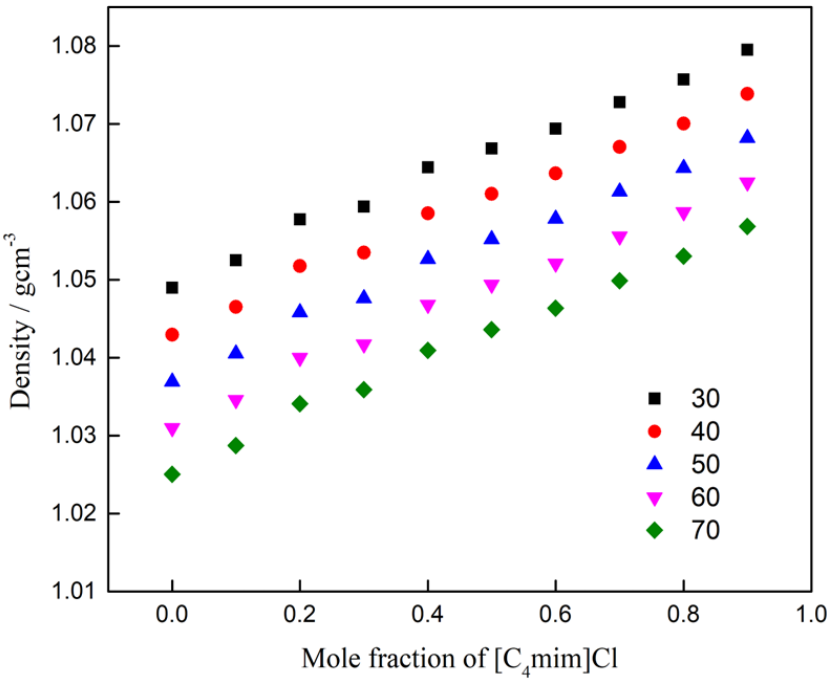


**Figure 3.1.** Densities of $[C_4mim](CH_3CO_2)_xCl_{1-x}$ at $T$ = 30 - 70 °C

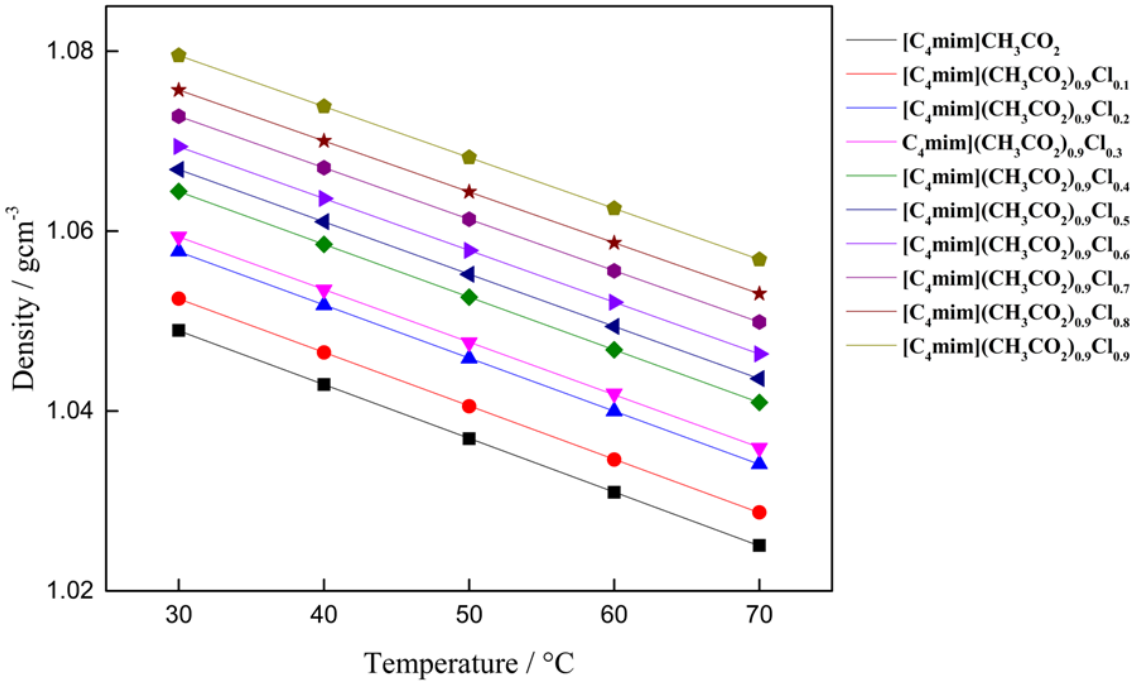


**Figure 3.2.** Densities of $[C_4mim](CH_3CO_2)_xCl_{1-x}$ as a function of temperature

**Table 3.1.** Density (g/cm$^3$) of $[C_4mim](CH_3CO_2)_xCl_{1-x}$ at different temperatures

| DSILs | 30 °C | 40 °C | 50 °C | 60 °C | 70 °C |
|---|---|---|---|---|---|
| $[C_4mim]CH_3CO_2$ | 1.04896 | 1.04294 | 1.03692 | 1.03097 | 1.02506 |
| $[C_4mim](CH_3CO_2)_{0.9}Cl_{0.1}$ | 1.0525 | 1.04652 | 1.04054 | 1.03461 | 1.02874 |
| $[C_4mim](CH_3CO_2)_{0.8}Cl_{0.2}$ | 1.05775 | 1.05178 | 1.04584 | 1.03998 | 1.03411 |
| $[C_4mim](CH_3CO_2)_{0.7}Cl_{0.3}$ | 1.05938 | 1.05348 | 1.04761 | 1.04173 | 1.0359 |
| $[C_4mim](CH_3CO_2)_{0.6}Cl_{0.4}$ | 1.06441 | 1.05852 | 1.05265 | 1.0468 | 1.04096 |
| $[C_4mim](CH_3CO_2)_{0.5}Cl_{0.5}$ | 1.06685 | 1.06104 | 1.0552 | 1.0494 | 1.0436 |
| $[C_4mim](CH_3CO_2)_{0.4}Cl_{0.6}$ | 1.06939 | 1.06363 | 1.05784 | 1.05209 | 1.04635 |
| $[C_4mim](CH_3CO_2)_{0.3}Cl_{0.7}$ | 1.07277 | 1.06705 | 1.06132 | 1.05558 | 1.04989 |
| $[C_4mim](CH_3CO_2)_{0.2}Cl_{0.8}$ | 1.07568 | 1.07003 | 1.06436 | 1.05869 | 1.05304 |
| $[C_4mim](CH_3CO_2)_{0.1}Cl_{0.9}$ | 1.07951 | 1.07386 | 1.06818 | 1.06252 | 1.05684 |
| $[C_4mim]Cl$ | - | - | - | - | 1.06001 |

**Table 3.2.** Different parameters extracted from density measurement data of $[C_4mim](CH_3CO_2)_xCl_{1-x}$

| | $\rho = a - b(T)$ | | |
|---|---|---|---|
| **DSILs** | b/$10^{-4}$ gcm$^{-3}$ °C$^{-1}$ | a/gcm$^{-3}$ | $R^2$ / $10^{-1}$ |
| $[C_4mim]CH_3CO_2$ | 5.98 | 1.07 | 9.99 |
| $[C_4mim](CH_3CO_2)_{0.9}Cl_{0.1}$ | 5.94 | 1.07 | 9.99 |
| $[C_4mim](CH_3CO_2)_{0.8}Cl_{0.2}$ | 5.91 | 1.08 | 9.99 |
| $[C_4mim](CH_3CO_2)_{0.7}Cl_{0.3}$ | 5.85 | 1.08 | 9.99 |
| $[C_4mim](CH_3CO_2)_{0.6}Cl_{0.4}$ | 5.86 | 1.08 | 1.00 |
| $[C_4mim](CH_3CO_2)_{0.5}Cl_{0.5}$ | 5.81 | 1.08 | 1.00 |
| $[C_4mim](CH_3CO_2)_{0.4}Cl_{0.6}$ | 5.76 | 1.09 | 1.00 |
| $[C_4mim](CH_3CO_2)_{0.3}Cl_{0.7}$ | 5.72 | 1.09 | 1.00 |
| $[C_4mim](CH_3CO_2)_{0.2}Cl_{0.8}$ | 5.66 | 1.09 | 1.00 |
| $[C_4mim](CH_3CO_2)_{0.1}Cl_{0.9}$ | 5.67 | 1.10 | 1.00 |

### 3.3.1.1. Isobaric Thermal Expansion Coefficient

The coefficient of thermal expansion ($\alpha_p$) of ILs and DSILs was calculated from the experimental $\rho$ values using eq. (1) [62]

$$\alpha(\mathrm{K}^{-1}) = \frac{1}{V_m}\left(\frac{\delta V_m}{\delta T}\right)_p = -\left(\frac{\delta \rho}{\delta T}\right)_p \quad (1)$$

The $\alpha_p$ values of $[C_4mim]CH_3CO_2$ and DSILs were determined and listed in Table 3.3. It was investigated that $[C_4mim]CH_3CO_2$ showed the highest of 5.75 whereas it is slightly decreased with the addition of [C4mim]Cl with DSILs. The $\alpha_p$ values of DSILs do not change significantly in the temperature range of 30-70 ℃ and 0.1MPa. Almeida *et al.* also reported similar findings [62].

**Table 3.3.** Thermal expansion coefficients, α for the studied $[C_4mim](CH_3CO_2)_xCl_{1-x}$

| ILs and DSILs | Thermal expansion coefficient $10^4$ ($\alpha_p$) |
|---|---|
| $[C_4mim]CH_3CO_2$ | 5.75 ± 0.01 |
| $[C_4mim](CH_3CO_2)_{0.9}Cl_{0.1}$ | 5.70 ± 0.02 |
| $[C_4mim](CH_3CO_2)_{0.8}Cl_{0.2}$ | 5.65 ± 0.03 |
| $[C_4mim](CH_3CO_2)_{0.7}Cl_{0.3}$ | 5.58 ± 0.02 |
| $[C_4mim](CH_3CO_2)_{0.6}Cl_{0.4}$ | 5.58 ± 0.01 |
| $[C_4mim](CH_3CO_2)_{0.5}Cl_{0.5}$ | 5.57 ± 0.05 |
| $[C_4mim](CH_3CO_2)_{0.4}Cl_{0.6}$ | 5.45 ± 0.02 |
| $[C_4mim](CH_3CO_2)_{0.3}Cl_{0.7}$ | 5.38 ± 0.05 |
| $[C_4mim](CH_3CO_2)_{0.2}Cl_{0.8}$ | 5.35 ± 0.04 |
| $[C_4mim](CH_3CO_2)_{0.1}Cl_{0.9}$ | 5.30 ± 0.05 |

### 3.3.1.2. Excess molar volume of DSILs

To study the volumetric behavior of DSILs, excess molar volume ($V_m^E$) represents the interactions between the constituent ions in DSILs, The $V_m^E$ can be calculated by eq. (2)

$$\boldsymbol{V_m^E = \frac{x_1 M_1 + x_2 M_2}{\rho} - \left[\frac{x_1 M_1}{\rho_1} + \frac{x_2 M_2}{\rho_2}\right]} \quad (2)$$

where, $\rho$ denotes the density of the DSILs, $\rho_1$ and $\rho_2$ denote the densities of ILs, $x_1$ and $x_2$ represent the mole fractions, $M_1$ and $M_2$ represent the molar masses of $[C_4mim]CH_3CO_2$ and [C4mim]Cl, respectively. The experimental densities were used to calculate $V_m^E$ volume for the system of

$[C_4mim](CH_3CO_2)_xCl_{1-x}$ (where x = 0.1-0.9).The calculated $V_m^E$ are plotted in Fig. 3.3 and listed in Table 3.4.

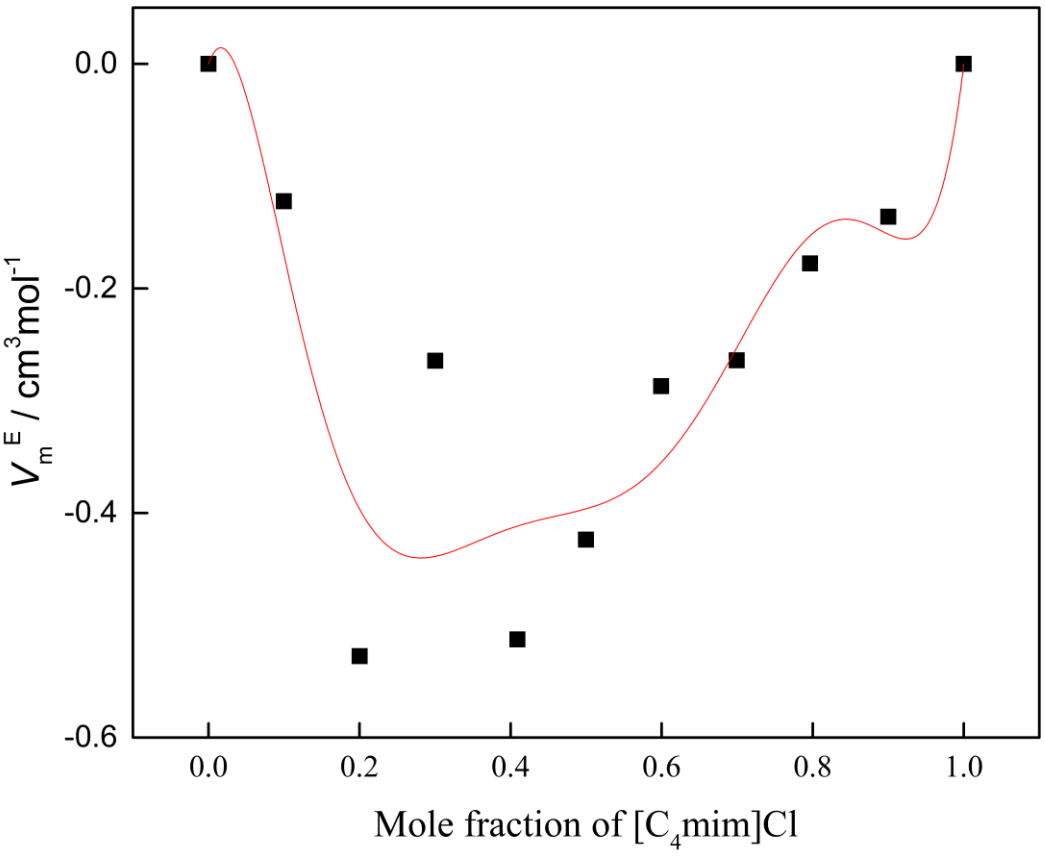


**Figure 3.3.** Excess molar volume of $[C_4mim](CH_3CO_2)_xCl_{1-x}$ with the variation of mole fraction of $[C_4mim]Cl$ fitted with Redlich-Kister (R-K) polynomial equation

The $V_m^E$ signifies the volume expansion or volume contraction by mixing of two or more ILs. The main factors that cause volume expansion in mixed systems include weak London dispersion forces, disruption of stronger and more specific interactions between the dissimilar components, and an unfavorable packing effect between the mixed components. On the other hand, the contraction of volume in mixtures may be caused by ion-dipole, dipole-dipole, hydrogen bonding, donor-acceptor (D-A) complexes, n-π and π-π interactions present in the various components of the mixture, and geometrical fitting of smaller molecules into other interstices [63, 64]. Fig. 3.4 depicts that all the calculated $V_m^E$ of DSILs at 70 ℃ are negative indicating volume contraction. This indicates that strong intermolecular interactions between $[C_4mim]^+$, $CH_3CO_2^-$

and $Cl^-$ are present in DSILs. It was investigated that with the increase in $[C_4mim]Cl$ in DSILs the value reaches a minimal value and then increases. In the minimal value where the maximum interaction occurred [64, 65]. This kind of trend is typically seen as a result of a significant discrepancy between the molar volume and molar mass of the constituting components in DSILs [66].

**Table 3.4.** Summary of different parameters of $[C_4mim](CH_3CO_2)_xCl_{1-x}$

| DSILs | Excess molar volume | Excess viscosity | Excess Gibbs free energy of activation |
|---|---|---|---|
| $[C_4mim]CH_3CO_2$ | 0 | 0 | 0 |
| $[C_4mim](CH_3CO_2)_{0.9}Cl_{0.1}$ | -0.12238 | 1.97574 | -5386.85824 |
| $[C_4mim](CH_3CO_2)_{0.8}Cl_{0.2}$ | -0.52754 | -0.51147 | -2971.00811 |
| $[C_4mim](CH_3CO_2)_{0.7}Cl_{0.3}$ | -0.26444 | 3.1028 | -1546.16405 |
| $[C_4mim](CH_3CO_2)_{0.6}Cl_{0.4}$ | -0.5126 | 0.63385 | -517.84189 |
| $[C_4mim](CH_3CO_2)_{0.5}Cl_{0.5}$ | -0.42369 | 1.28647 | 74.52509 |
| $[C_4mim](CH_3CO_2)_{0.4}Cl_{0.6}$ | -0.28707 | 8.90441 | 511.15529 |
| $[C_4mim](CH_3CO_2)_{0.3}Cl_{0.7}$ | -0.26413 | 8.03941 | 753.9697 |
| $[C_4mim](CH_3CO_2)_{0.2}Cl_{0.8}$ | -0.17771 | 17.36646 | 805.89775 |
| $[C_4mim](CH_3CO_2)_{0.1}Cl_{0.9}$ | -0.13614 | 2.96427 | 628.0893 |
| $[C_4mim]Cl$ | 0 | 0 | 0 |

### 3.3.2. Viscosity of ILs and DSILs

Viscosity serves as a crucial parameter regarding the ILs that are taken into account for prospective industrial applications. It assists other properties of the ILs such as flow resistance, mixing, and electrical conductivities. The viscosities of ILs are generally higher than those of conventional solvents. The viscosities of ILs and DSILs were measured at a temperature range of 30 to 70 °C at 10 °C intervals in the whole mole fraction range and are listed in Table 3.5. The viscosities are plotted in Fig. 3.4 and 3.5. The viscosities of $[C_4mim](CH_3CO_2)$ are 235.3, 124.1, 72.15, 45.56, 30.74 mPa.s at 30, 40, 50, 60, and 70 °C, respectively. $[C_4mim]Cl$ is solid, so due to the instrumental restriction viscosity at 70 °C was measured only is 38.09 mPa.s. Fig. 3.4 shows the viscosity of DSILs is higher with various compositions of $[C_4mim]Cl$ and $[C_4mim]CH_3CO_2$

compared to ILs. The viscosity of DSILs not have been following a regular order. The order of viscosity of DSILs was found to be $[C_4mim](CH_3CO_2)_{0.2}Cl_{0.8}$ > $[C_4mim](CH_3CO_2)_{0.3}Cl_{0.7}$ > $[C_4mim](CH_3CO_2)_{0.4}Cl_{0.6}$ > $[C_4mim](CH_3CO_2)_{0.1}Cl_{0.9}$ > $[C_4mim](CH_3CO_2)_{0.7}Cl_{0.3}$ > $[C_4mim](CH_3CO_2)_{0.5}Cl_{0.5}$ > $[C_4mim](CH_3CO_2)_{0.6}Cl_{0.4}$ > $[C_4mim](CH_3CO_2)_{0.9}Cl_{0.1}$ > $[C_4mim](CH_3CO_2)_{0.8}Cl_{0.2}$ at 30 ℃. Two factors may play a vital role in the variation of viscosity among the DSILs. These include the ion size or entanglement and the development of strong interactions between various ions. The most vicious $[C_4mim](CH_3CO_2)_{0.2}Cl_{0.8}$ might have strong interaction among the ions of $[C_4mim]^+$ $CH_3CO_2^-$ and $Cl^-$ and the capability to the formation of strong H-bonding of C(2)-H of the common cation $[C_4mim]^+$ and the different anions $CH_3CO_2^-$ and $Cl^-$ [67]. Fig. 3.5 shows the decrease in the viscosity with the temperature for ILs and DSILs. With the increase in temperature, the ions in ILs and DSILs get energy to move freely. Song *et al.*, (2014) [68] investigated the viscosities of DSILs with the variation of cationic species $[C_2mim]_x[C_3mim]_{1-x}[BF_4]$, $[C_3mim]_x[C_6mim]_{1-x}[BF_4]$, and $[C_2mim]_1[C_6mim]_{1-x}[BF_4]$ at atmospheric pressure and a temperature range of 20 ℃ to 70 ℃. They discovered that the experimental outcomes were not significantly different from the ideal mixture.

**Table 3.5.** Dynamic viscosity (mPa.s) of $[C_4mim](CH_3CO_2)_xCl_{1-x}$ at different temperatures

| DSILs | **30 °C** | **40 °C** | **50 °C** | **60 °C** | **70 °C** |
|---|---|---|---|---|---|
| $[C_4mim]CH_3CO_2$ | 235.3 | 124.1 | 72.15 | 45.56 | 30.74 |
| $[C_4mim](CH_3CO_2)_{0.9}Cl_{0.1}$ | 268.5 | 140.1 | 80.57 | 50.14 | 33.45 |
| $[C_4mim](CH_3CO_2)_{0.8}Cl_{0.2}$ | 245.5 | 129.6 | 75.26 | 47.22 | 31.7 |
| $[C_4mim](CH_3CO_2)_{0.7}Cl_{0.3}$ | 304.1 | 156.7 | 88.91 | 54.69 | 36.05 |
| $[C_4mim](CH_3CO_2)_{0.6}Cl_{0.4}$ | 290.2 | 145.1 | 83.33 | 51.78 | 34.38 |
| $[C_4mim](CH_3CO_2)_{0.5}Cl_{0.5}$ | 293.5 | 153 | 87.47 | 54.04 | 35.7 |
| $[C_4mim](CH_3CO_2)_{0.4}Cl_{0.6}$ | 407.5 | 204.5 | 113.4 | 68.29 | 44.05 |
| $[C_4mim](CH_3CO_2)_{0.3}Cl_{0.7}$ | 407.9 | 205 | 113.4 | 68.17 | 43.92 |
| $[C_4mim](CH_3CO_2)_{0.2}Cl_{0.8}$ | 563.3 | 273 | 146.3 | 85.67 | 53.96 |
| $[C_4mim](CH_3CO_2)_{0.1}Cl_{0.9}$ | 340.5 | 176.9 | 100.5 | 61.56 | 40.32 |
| $[C_4mim]Cl$ | - | - | - | - | 38.09 |

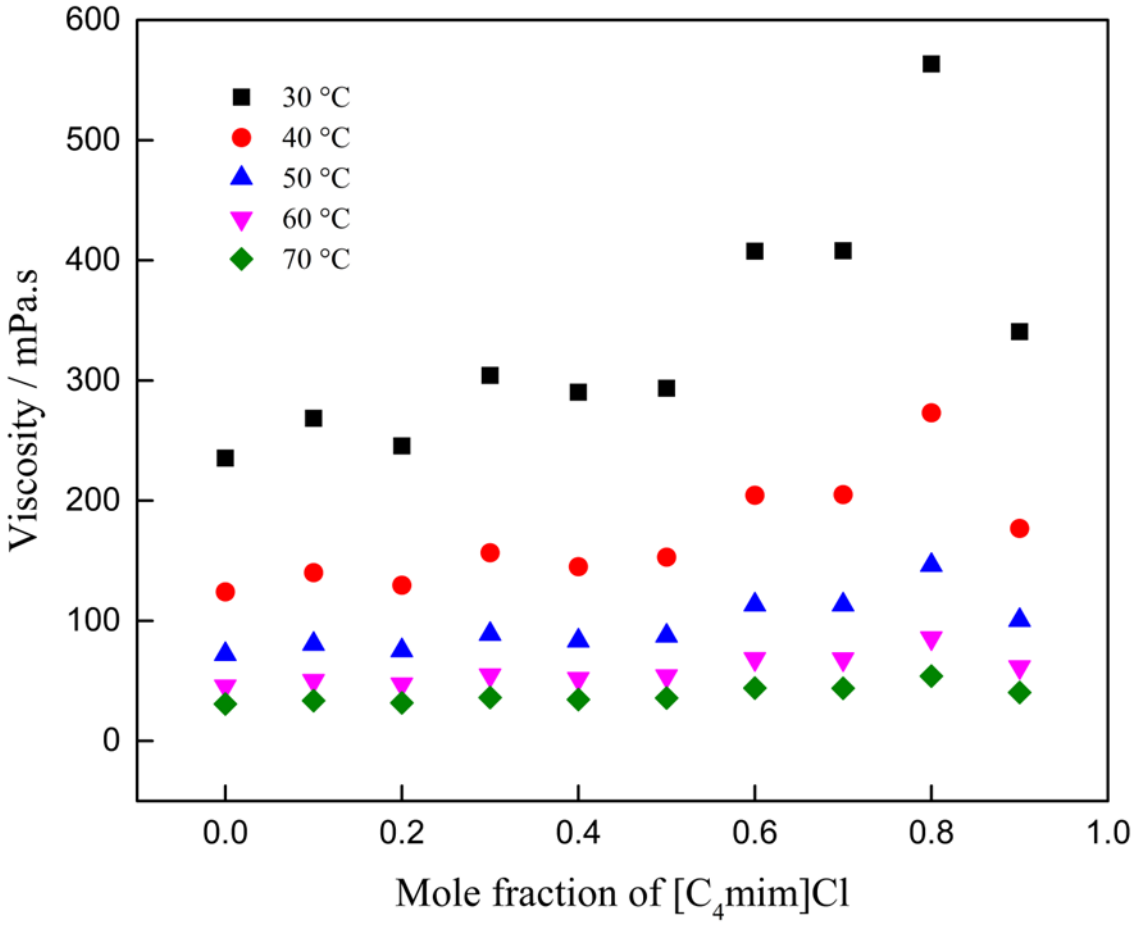


**Figure 3.4.** Viscosity of $[C_4mim](CH_3CO_2)_xCl_{1-x}$ at T=30-70 °C

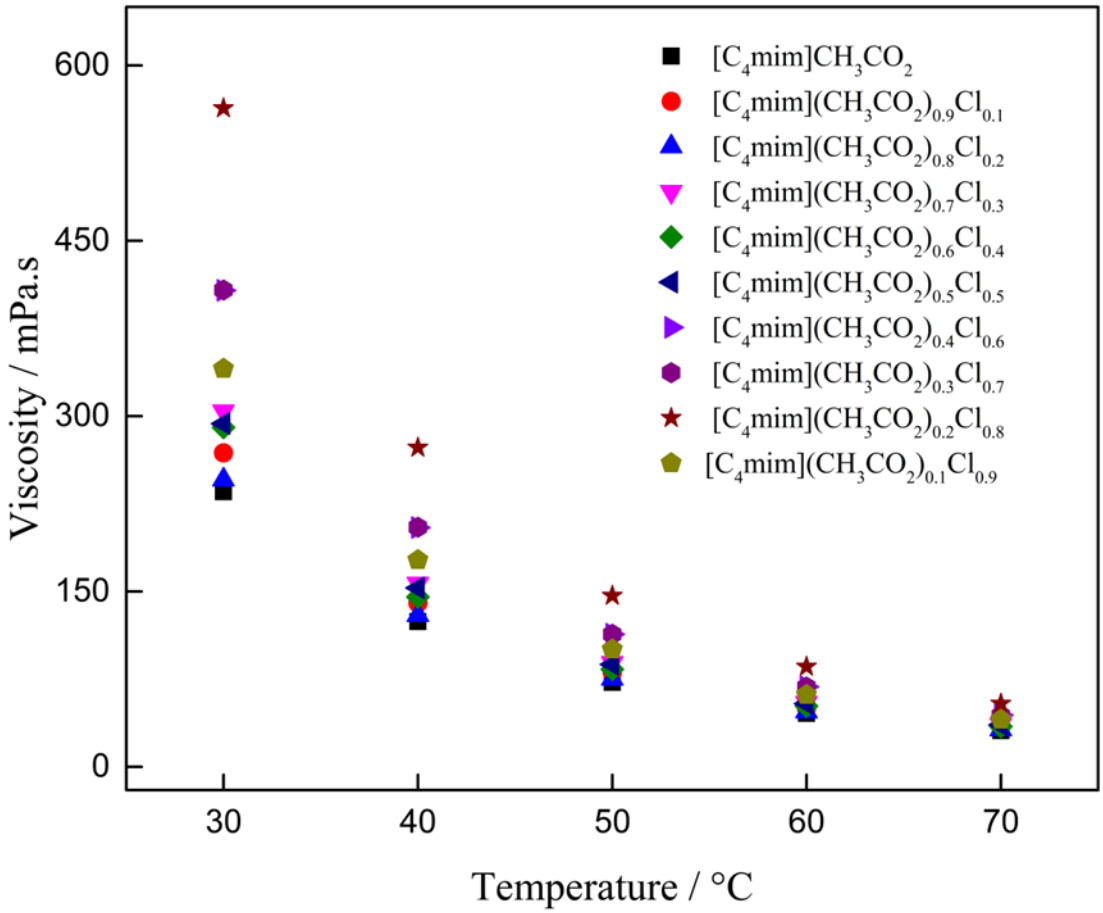


**Figure 3.5.** Variation of the viscosity of ILs and DSILs with the variation of temperature

### 3.3.2.1. Excess viscosity

Excess viscosity ($\eta^E$) refers to the deviation of experimental viscosities from the ideal behavior. The variation of excess viscosity provides a qualitative assessment of the extent of intermolecular contacts because viscosity is connected with molecular interactions, i.e., electrostatic forces, hydrogen bonds, and van der Waals interactions. The $\eta^E$ of the prepared DSILs was calculated using the eq. 3.

$$\eta^E = \eta_{experimental} - \eta_{ideal} \quad (3)$$

Bingham's equation was used to calculate ideal viscosity based on the principle of additivity, $\eta_{deal} = X_1\eta_1 + X_2\eta_2$. The $\eta^E$ of DSILs over the whole mole fractions range was calculated at 70 °C and are tabulated in Table 3.4. The $\eta^E$ has been plotted against mole fractions [C4mim]Cl and the data were fitted with Redlich-Kister (R-K) polynomial equation that is presented in Fig. 3.6. The $\eta^E$ of $[C_4mim](CH_3CO_2)_{0.9}Cl_{0.1}$, $[C_4mim](CH_3CO_2)_{0.8}Cl_{0.2}$, $[C_4mim](CH_3CO_2)_{0.7}Cl_{0.3}$,

$[C_4mim](CH_3CO_2)_{0.6}Cl_{0.4}$, $[C_4mim](CH_3CO_2)_{0.5}Cl_{0.5}$, $[C_4mim](CH_3CO_2)_{0.4}Cl_{0.6}$, $[C_4mim](CH_3CO_2)_{0.3}Cl_{0.7}$, $[C_4mim](CH_3CO_2)_{0.2}Cl_{0.8}$, and $[C_4mim](CH_3CO_2)_{0.1}Cl_{0.9}$ are found to be 1.97574, -0.51147, 3.1028, 0.63385, 1.28647, 8.90441, 8.03941, 17.36646, and 2.96427, respectively. $\eta^E$ values of all DSILs are found to be positive except $[C_4mim](CH_3CO_2)_{0.8}Cl_{0.2}$. The positive $\eta^E$ values of DSILs indicate that the interactions between $[C_4mim]Cl$ and $[C_4mim]CH_3CO_2$ or its complexes in the liquid state are greater than those of the individual $C_4mim]Cl$ and $[C_4mim]CH_3CO_2$. This strong association can occur by the formation of hydrogen bonds among, unlike ILs. The negative $\eta^E$ i.e., lower viscosities than the ideal values can arise from the trapping of smaller molecules into the matrices of larger species [69, 70].

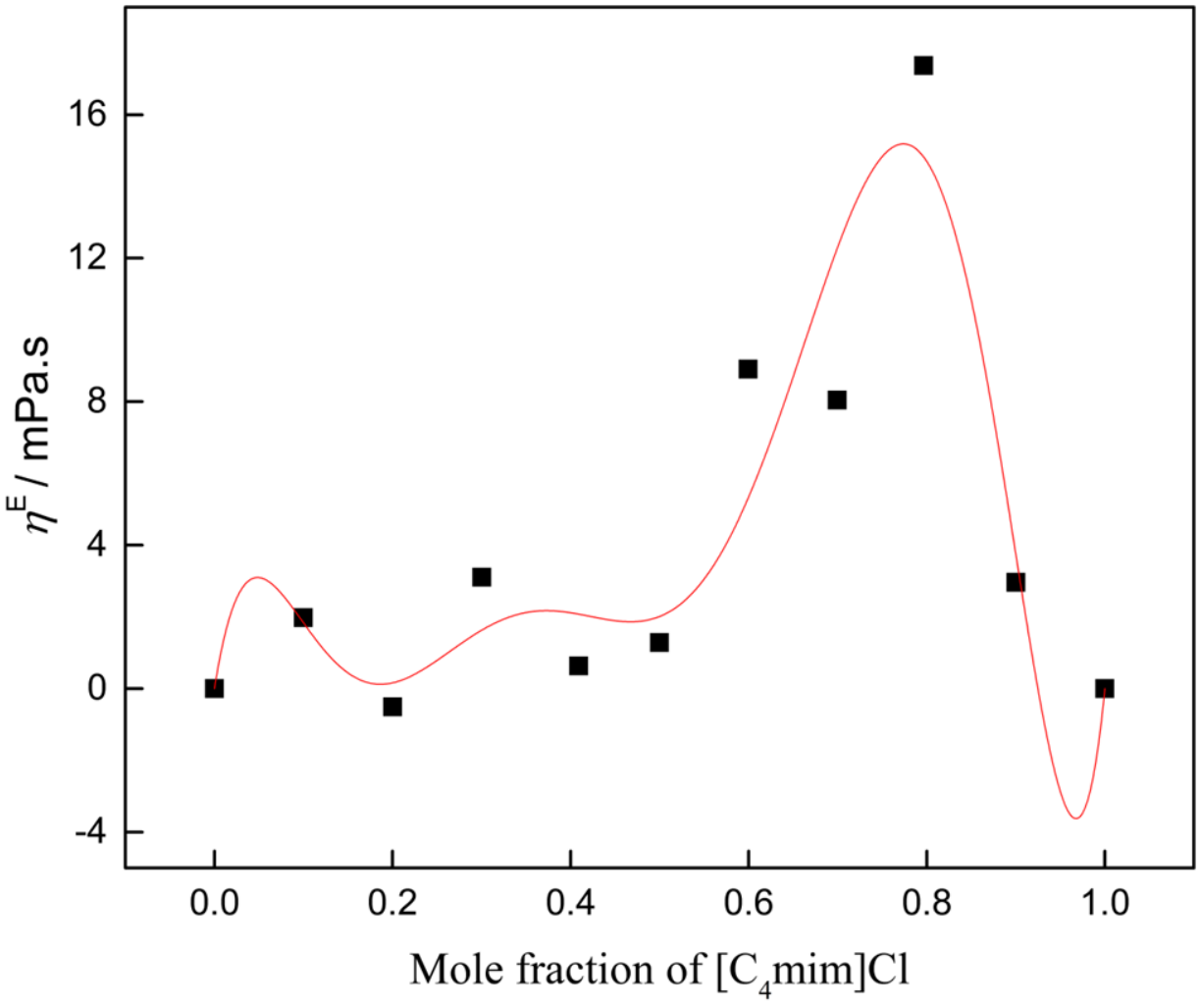


**Figure 3.6.** Variation of excess viscosity of DSILs with the variation of mole fraction of $[C_4mim]Cl$

### 3.3.2.2. Dynamic viscosity

Simple Arrhenius relaxation is not applicable to glass formers or supercooled liquids. As the temperature falls to the $T_g$, their viscosities increase quickly and sharply, exhibiting super Arrhenius behavior. This rise in viscosity cannot be predicted by Eyring equation (eq. 4) which assumes ideality. To model this behavior, phenomenological equations such as the VFT equation, eq. (4) [71] are used

$$\log \eta = .\log \eta_o + \frac{B}{T - T_o} \quad \textbf{(4)}$$

where, $T_o$ is the Vogel temperature, which can be thought of as $T_g$, and $\eta_o$ is the viscosity at infinite temperature. $B$ is a constant related to fragility.

The VFT equation is the most popular choice for modeling and predicting non-Arrhenius viscous flow. While it performs excellently at working temperatures and above, it shows poor approximation at lower temperatures. Mauro *et al.* modified the VFT equation to a form having both $T_g$ and m in the form of eq.5 [72]

$$\log \eta(T) = \log \eta_o + \frac{(12 - \log \eta_o)^2}{m\left(\frac{T}{T_g} - 1\right) + (12 - \log \eta_o)} \quad \textbf{(5)}$$

where $T$ and $\eta$ are the variables and $\eta_o$, m, and $T_g$ are the fitting parameters.

They also proposed a new equation, now known as the MYEGA equation (eq.6) on the basis of temperature-dependent configurational entropy ($S_C$) which performs well at lower temperatures.

$$\log \eta(T) = \log \eta_o + (12 - \log \eta_o)\frac{T_g}{T} exp\left[\left(\frac{m}{12 - \log \eta_o} - 1\right)\left(\frac{T_g}{T} - 1\right)\right] \quad \textbf{(6)}$$

The change in logarithmic dynamic viscosity of $[C_4mim]CH_3CO_2$, $[C_4mim](CH_3CO_2)_{0.9}Cl_{0.1}$, $[C_4mim](CH_3CO_2)_{0.8}Cl_{0.2}$, $[C_4mim](CH_3CO_2)_{0.7}Cl_{0.3}$, $[C_4mim](CH_3CO_2)_{0.6}Cl_{0.4}$, $[C_4mim](CH_3CO_2)_{0.5}Cl_{0.5}$, $[C_4mim](CH_3CO_2)_{0.4}Cl_{0.6}$, $[C_4mim](CH_3CO_2)_{0.3}Cl_{0.7}$, $[C_4mim](CH_3CO_2)_{0.2}Cl_{0.8}$, and $[C_4mim](CH_3CO_2)_{0.1}Cl_{0.9}$ are plotted with temperature and fitted with mVFT (Fig. 3.7) and MYEGA equation (Fig. 3.8). Fig. 3.7 and 3.8 show that the viscosity decreases with the raise in

temperature. The highest viscosity observed in $[C_4mim](CH_3CO_2)_{0.2}Cl_{0.8}$ followed by $[C_4mim](CH_3CO_2)_{0.3}Cl_{0.7}$, $[C_4mim](CH_3CO_2)_{0.4}Cl_{0.6}$, $[C_4mim](CH_3CO_2)_{0.1}Cl_{0.9}$, $[C_4mim](CH_3CO_2)_{0.7}Cl_{0.3}$, $[C_4mim](CH_3CO_2)_{0.5}Cl_{0.5}$, $[C_4mim](CH_3CO_2)_{0.6}Cl_{0.4}$, $[C_4mim](CH_3CO_2)_{0.9}Cl_{0.1}$, $[C_4mim](CH_3CO_2)_{0.8}Cl_{0.2}$ and $[C_4mim]CH_3CO_2$. As the increase in the amount of $[C_4mim]Cl$ in DSILs, the viscosity increases, but does not follow the regular trend. The increase in viscosity is due to the interactions and H-bonding between ions of $[C_4mim]^+$, $Cl^-$ and $CH_3CO_2^-$. Chatel *et al*. [73] investigated that viscosity can be correlated with various types of intermolecular interactions. These include electrostatic interactions, van der Waals interactions, and hydrogen bonding interactions. The degree of hydrogen bonding capacity displayed by the anions in the investigated ILs and DSILs can be correlated with the order of viscosity of those substances. The type and ratio of the anions could be the reason for the higher viscosity of $[C_4mim](CH_3CO_2)_{0.2}Cl_{0.8}$. Hunt *et al.* [74] looked into how different anions affected the viscosity of ILs. They found the following order of $[C_2mim]^+$ based ILs with various anions $[MeSO_3]^- > [CH_3CO_2]^- > [ESO_4]^- > [OTf]^- > [NTf_2]^- > BF_4^-$. The fitting parameters obtained from them are the $T_g$, the fragility index (m) and viscosity at infinite temperature (log $\eta_o$). All the parameters have been compiled in Table 3.6. In nearly all the ILs and DSILs studied, the mVFT equation seems to higher values of $T_g$ and m than eq. (6).

**Table 3.6.** mVFT and MYEGA equation-fitted $T_g$, m and log $\eta_o$ for the $[C_4mim](CH_3CO_2)_xCl_{1-x}$

| DSILs | $T_g$ / K | | m | | Log $\eta_o$ | |
|---|---|---|---|---|---|---|
| | mVFT | MYEGA | mVFT | MYEGA | mVFT | MYEGA |
| $[C_4mim]CH_3CO_2$ | 220 | 200 | 164 | 77 | -3.8 | -3.1 |
| $[C_4mim](CH_3CO_2)_{0.9}Cl_{0.1}$ | 217 | 199 | 151 | 74 | -3.9 | -3.2 |
| $[C_4mim](CH_3CO_2)_{0.8}Cl_{0.2}$ | 217 | 198 | 152 | 73 | -3.9 | -3.2 |
| $[C_4mim](CH_3CO_2)_{0.7}Cl_{0.3}$ | 216 | 198 | 143 | 72 | -4.0 | -3.3 |
| $[C_4mim](CH_3CO_2)_{0.6}Cl_{0.4}$ | 227 | 207 | 188 | 83 | -3.6 | -2.9 |
| $[C_4mim](CH_3CO_2)_{0.5}Cl_{0.5}$ | 214 | 196 | 136 | 70 | -4.0 | -3.4 |
| $[C_4mim](CH_3CO_2)_{0.4}Cl_{0.6}$ | 216 | 199 | 132 | 70 | -4.1 | -3.4 |
| $[C_4mim](CH_3CO_2)_{0.3}Cl_{0.7}$ | 215 | 198 | 129 | 69 | -4.1 | -3.4 |
| $[C_4mim](CH_3CO_2)_{0.2}Cl_{0.8}$ | 216 | 200 | 125 | 69 | -4.2 | -3.4 |
| $[C_4mim](CH_3CO_2)_{0.1}Cl_{0.9}$ | 211 | 194 | 125 | 67 | -4.2 | -3.5 |
| $[C_4mim]Cl$ | - | - | - | - | - | - |

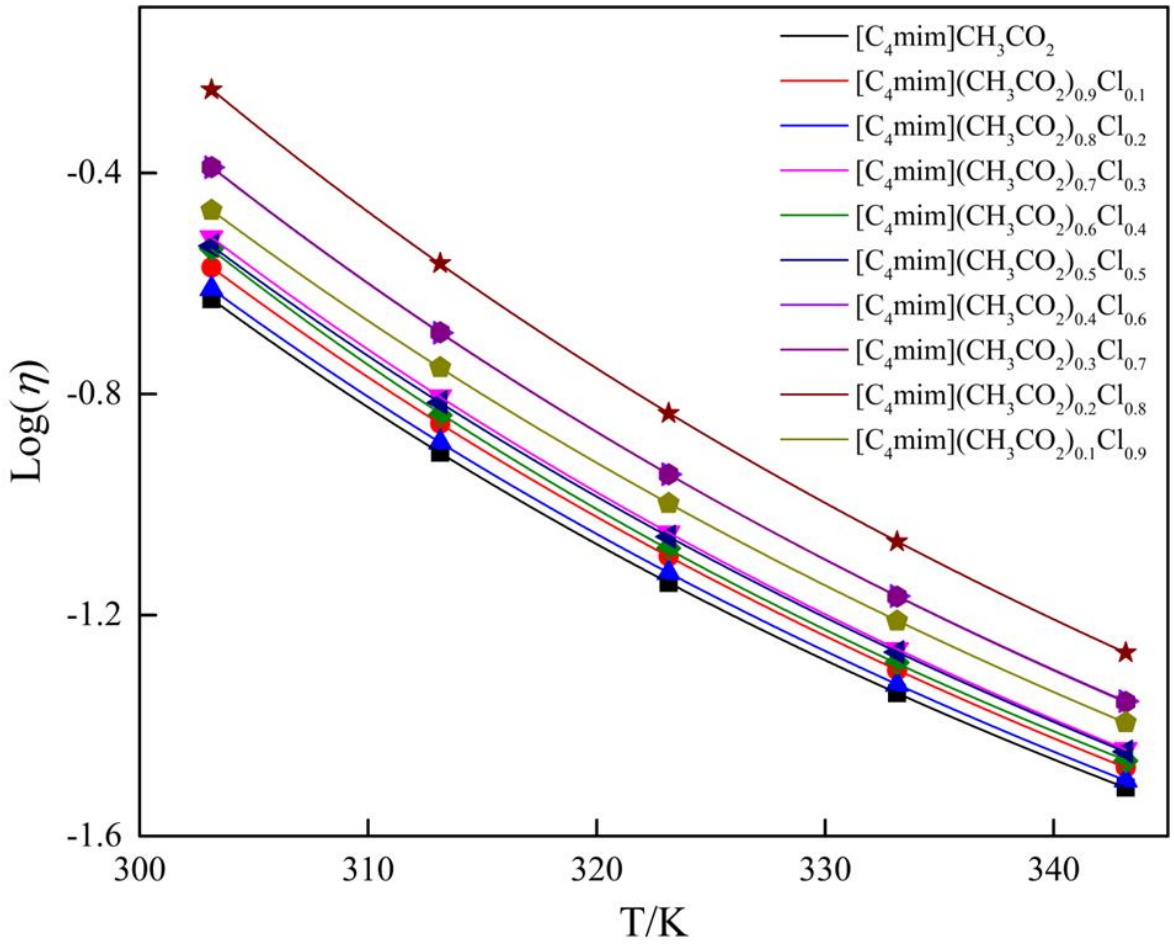


**Figure 3.7.** Log(η) of $[C_4mim](CH_3CO_2)_xCl_{1-x}$ against temperature, fitted with mVFT equation

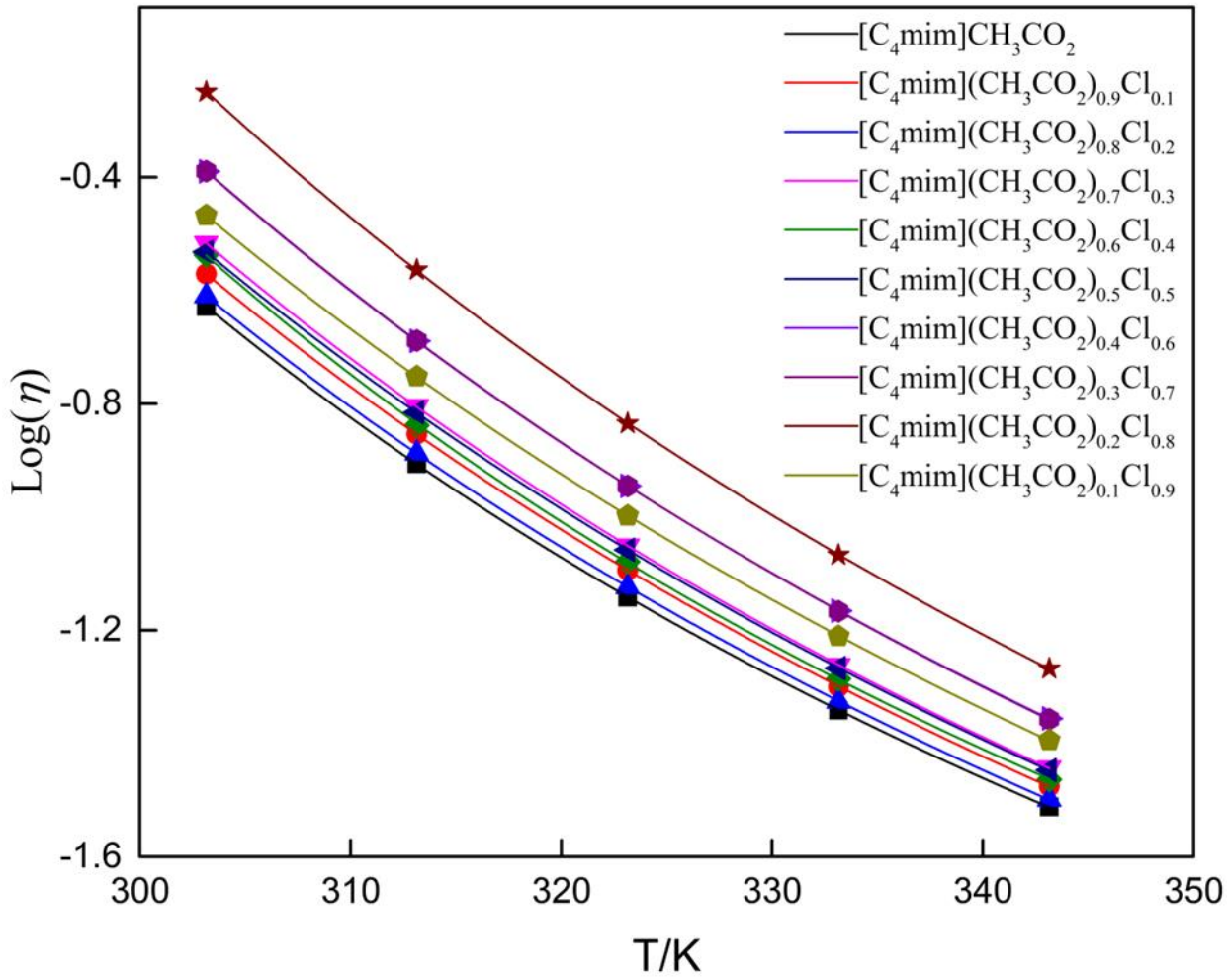


**Figure 3.8.** Log(η) of $[C_4mim](CH_3CO_2)_xCl_{1-x}$ as a function of temperature, fitted with MYEGA equation

### 3.3.3. Thermodynamic parameters

#### 3.3.3.1. Energy of activation for viscous flow

Changes in the activation free energy of viscous flow of $[C_4mim]CH_3CO_2$ and DSILs has been calculated from 303.15 K to 343.15 K by using the Eyring eq. (7),

$$\Delta G = RT \ln \frac{\eta V}{hN} \qquad (7)$$

The work required to create a hole in the liquid for the viscous flow is related to the change in Gibbs free energy of activation, $\Delta G$. Due to the dense packing of each ion inside a "cage" created by its closest neighbors, each ion's motion is primarily restricted to vibration. An energy barrier of

height $G/N_A$, where $N_A$ represents the Avogadro number, serves as a visual representation of this "cage". A molar free energy of activation $\Delta G$ is required for the stationary fluid to "escape" the cage into the nearest hole or unoccupied site. The calculated $\Delta G$ of $[C_4mim]CH_3CO_2$ and DSILs from temperature 303.15-343.15K are tabulated in Table 3.7. Fig. 3.9 shows how the temperature affects the $\Delta G$ of ILs and DSILs. From Table 3.7, it has been noted that the highest $\Delta G$ was found for $[C_4mim](CH_3CO_2)_{0.2}Cl_{0.8}$ followed by $[C_4mim](CH_3CO_2)_{0.4}Cl_{0.6}$, $[C_4mim](CH_3CO_2)_{0.3}Cl_{0.7}$, $[C_4mim](CH_3CO_2)_{0.1}Cl_{0.9}$, $[C_4mim](CH_3CO_2)_{0.7}Cl_{0.3}$, $[C_4mim](CH_3CO_2)_{0.6}Cl_{0.4}$, $[C_4mim](CH_3CO_2)_{0.5}Cl_{0.5}$, $[C_4mim](CH_3CO_2)_{0.9}Cl_{0.1}$, $[C_4mim](CH_3CO_2)_{0.8}Cl_{0.2}$ $[C_4mim]CH_3CO_2$ are 31.18, 30.44, 30.40, 29.87, 29.43, 29.67, 29.51, 29.58, 29.32, 29.29 kJ/mol at 303.15 K, respectively. Fig. 3.9 shows that the positive values of $\Delta G$ of ILs and DSILs decrease as the temperature increases. This indicates the favorable mixing of constituent ILs efficiently forming the DSILs [75]. This phenomenon is further supported by the changing trends in entropy presented in Fig. 3.10 and Table 3.8. The value of the energy barrier to cross is lowered when thermal energy increases because it makes it easier for ions to move around.

**Table 3.7.** Changes in the activation-free energy of viscous flow, $\Delta G$ of $[C_4mim](CH_3CO_2)_xCl_{1-x}$ determined at different temperatures

| DSILs | 303.15 K | 313.15 K | 323.15 K | 333.15 K | 343.15 K |
|---|---|---|---|---|---|
| $[C_4mim]CH_3CO_2$ | 29.29 | 28.61 | 28.08 | 27.69 | 27.41 |
| $[C_4mim](CH_3CO_2)_{0.9}Cl_{0.1}$ | 29.58 | 28.88 | 28.33 | 27.91 | 27.61 |
| $[C_4mim](CH_3CO_2)_{0.8}Cl_{0.2}$ | 29.32 | 28.63 | 28.11 | 27.70 | 27.41 |
| $[C_4mim](CH_3CO_2)_{0.7}Cl_{0.3}$ | 29.84 | 29.11 | 28.53 | 28.08 | 27.75 |
| $[C_4mim](CH_3CO_2)_{0.6}Cl_{0.4}$ | 29.67 | 28.86 | 28.30 | 27.88 | 27.56 |
| $[C_4mim](CH_3CO_2)_{0.5}Cl_{0.5}$ | 29.51 | 28.95 | 28.38 | 27.94 | 27.61 |
| $[C_4mim](CH_3CO_2)_{0.4}Cl_{0.6}$ | 30.44 | 29.66 | 29.04 | 28.55 | 28.17 |
| $[C_4mim](CH_3CO_2)_{0.3}Cl_{0.7}$ | 30.40 | 29.63 | 29.00 | 28.50 | 28.12 |
| $[C_4mim](CH_3CO_2)_{0.2}Cl_{0.8}$ | 31.18 | 30.33 | 29.64 | 29.09 | 28.66 |
| $[C_4mim](CH_3CO_2)_{0.1}Cl_{0.9}$ | 29.86 | 29.16 | 28.58 | 28.13 | 27.78 |
| $[C_4mim]Cl$ | - | - | - | - | - |

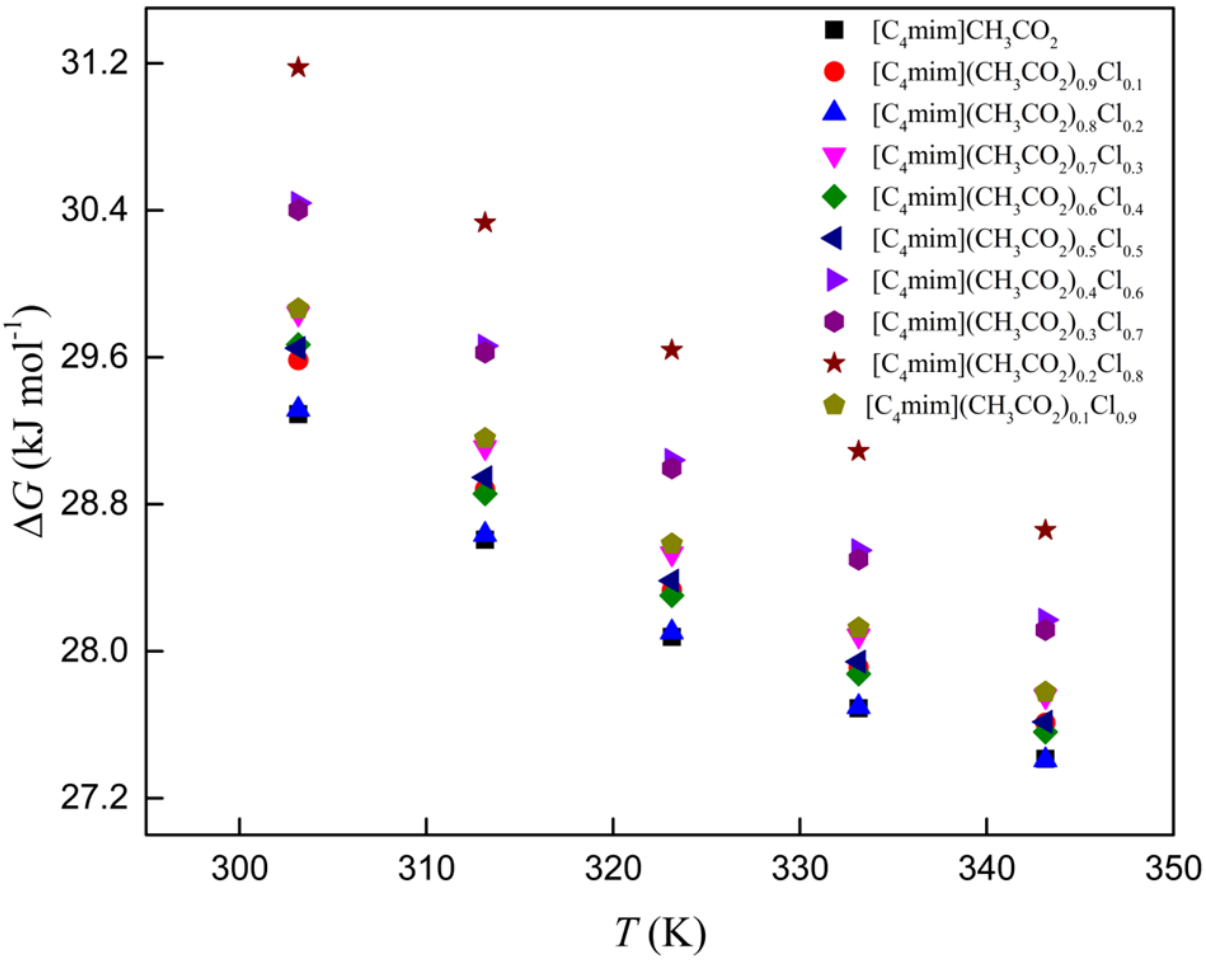


**Figure 3.9.** Change in ΔG of activation for $[C_4mim](CH_3CO_2)_xCl_{1-x}$ as a function of temperature.

### 3.3.3.2. Entropy of activation for viscous flow

The change in activation entropy for the viscous flow, (Δ*S*) of ILs and DSILs was calculated by using the equation of −d(Δ*G*)/dT. Table 3.8 lists the calculated Δ*S* values for DSILs and $[C_4mim]CH_3CO_2$. The change in Δ*S* with respect to temperature is presented in Fig. 3.10. Fig. 3.10 shows that Δ*S* decreases with increases in temperature despite some discontinuity. From table 3.8 it has been noted that the highest Δ*G* was found for $[C_4mim](CH_3CO_2)_{0.2}Cl_{0.8}$ followed by $[C_4mim](CH_3CO_2)_{0.6}Cl_{0.4}$, $[C_4mim](CH_3CO_2)_{0.4}Cl_{0.6}$, $[C_4mim](CH_3CO_2)_{0.3}Cl_{0.7}$, $[C_4mim](CH_3CO_2)_{0.7}Cl_{0.3}$, $[C_4mim](CH_3CO_2)_{0.1}Cl_{0.9}$, $[C_4mim](CH_3CO_2)_{0.5}Cl_{0.5}$, $[C_4mim](CH_3CO_2)_{0.9}Cl_{0.1}$, $[C_4mim]CH_3CO_2$, and $[C_4mim](CH_3CO_2)_{0.8}Cl_{0.2}$ are 84.37, 81.14, 77.69, 77.45, 72.72, 70.61, 70.38, 70.29, 68.45, and 68.15 at 303.15 K. The positive values of ΔS denote that the system becomes less organized relating to its starting states [76]. The decrease in Δ*S* with an increase in temperature shown in Fig. 3.10 suggests that at higher temperatures ordered

structure of ILs and DSILs became more random and have a high value of entropy. So, the required change in entropy of activation for viscous flow lowers. As the increase in highly viscous $[C_4mim]Cl$ in DSILs the $\Delta S$ of activation increased.

**Table 3.8.** Summary of entropy of activation, $\Delta S$ in kJ/mol for viscous flow of $[C_4mim](CH_3CO_2)_xCl_{1-x}$ determined at different temperatures

| DSILs | 303.15 K | 313.15 K | 323.15 K | 333.15 K | 343.15 K |
|---|---|---|---|---|---|
| $[C_4mim]CH_3CO_2$ | 68.45 | 60.63 | 45.83 | 33.18 | 27.50 |
| $[C_4mim](CH_3CO_2)_{0.9}Cl_{0.1}$ | 70.29 | 62.58 | 48.49 | 36.09 | 30.07 |
| $[C_4mim](CH_3CO_2)_{0.8}Cl_{0.2}$ | 68.15 | 60.61 | 46.82 | 34.76 | 28.94 |
| $[C_4mim](CH_3CO_2)_{0.7}Cl_{0.3}$ | 72.72 | 65.24 | 51.24 | 38.85 | 32.98 |
| $[C_4mim](CH_3CO_2)_{0.6}Cl_{0.4}$ | 81.14 | 68.25 | 49.00 | 37.10 | 31.56 |
| $[C_4mim](CH_3CO_2)_{0.5}Cl_{0.5}$ | 70.38 | 63.34 | 50.17 | 38.42 | 32.82 |
| $[C_4mim](CH_3CO_2)_{0.4}Cl_{0.6}$ | 77.69 | 69.96 | 55.66 | 43.46 | 37.83 |
| $[C_4mim](CH_3CO_2)_{0.3}Cl_{0.7}$ | 77.45 | 70.23 | 56.37 | 44.03 | 38.34 |
| $[C_4mim](CH_3CO_2)_{0.2}Cl_{0.8}$ | 84.37 | 76.84 | 62.17 | 49.03 | 43.04 |
| $[C_4mim](CH_3CO_2)_{0.1}Cl_{0.9}$ | 70.61 | 63.99 | 51.61 | 40.31 | 34.78 |
| $[C_4mim]Cl$ | - | - | - | - | - |

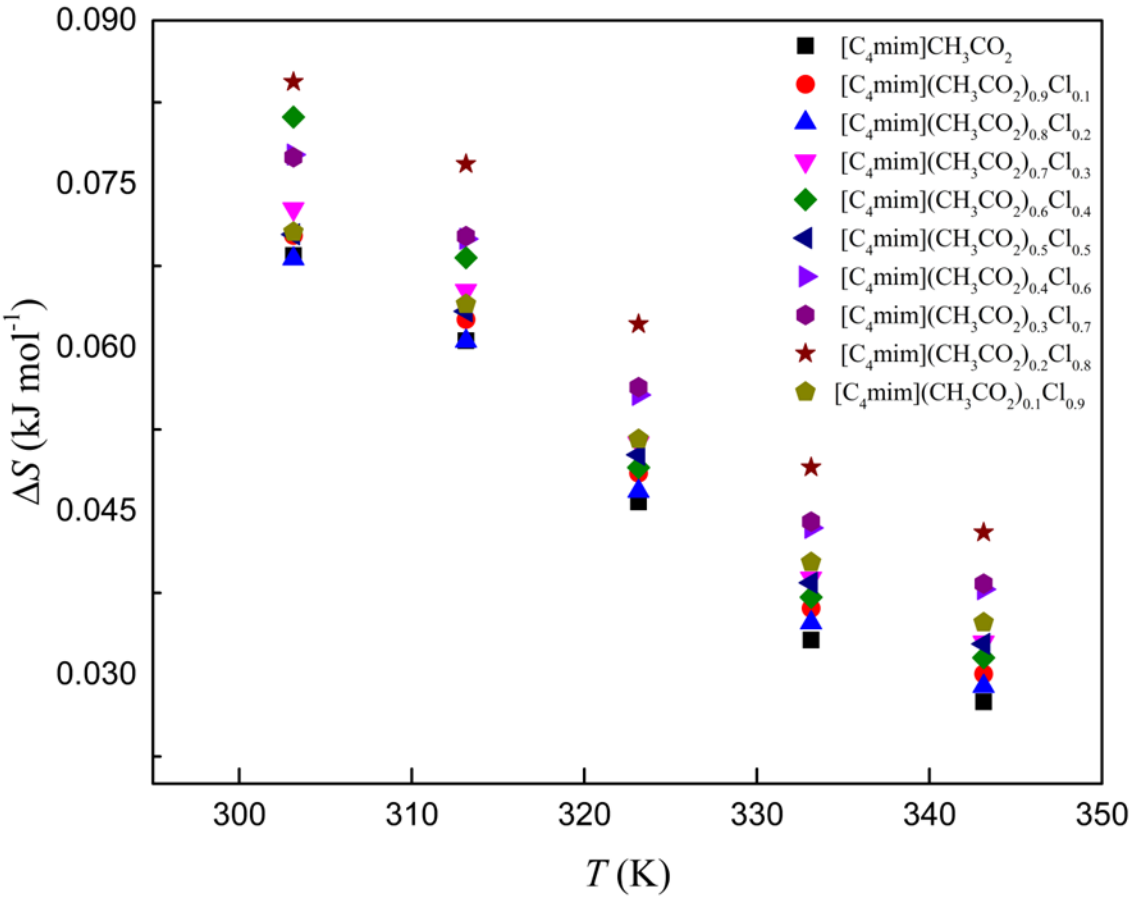


**Figure 3.10.** Change in $\Delta S$ of activation for $[C_4mim](CH_3CO_2)_xCl_{1-x}$ as a function of temperature

### 3.3.3.3. Enthalpy of activation for viscous flow

The change in activation enthalpy for the viscous flow, ($\Delta H$) of ILs and DSILs was calculated using the following thermodynamic relation by eq. (8).

$$\Delta H = \Delta G + T\Delta S \qquad (8)$$

The values of $\Delta H$ of DSILs and $[C_4mim]CH_3CO_2$ for the temperatures of 303.15 to 343.15K are tabulated in Table 3.9. The change in $\Delta H$ with the temperature have been presented in Fig. 3.11. Similar to $\Delta H$ and $\Delta S$ the $\Delta H$ value of $[C_4mim](CH_3CO_2)_{0.2}Cl_{0.8}$, $[C_4mim](CH_3CO_2)_{0.6}Cl_{0.4}$, $[C_4mim](CH_3CO_2)_{0.4}Cl_{0.6}$, $[C_4mim](CH_3CO_2)_{0.3}Cl_{0.7}$, $[C_4mim](CH_3CO_2)_{0.7}Cl_{0.3}$, $[C_4mim](CH_3CO_2)_{0.1}Cl_{0.9}$, $[C_4mim](CH_3CO_2)_{0.5}Cl_{0.5}$, $[C_4mim](CH_3CO_2)_{0.9}Cl_{0.1}$, $[C_4mim]CH_3CO_2$, are found to be 56.76, 54.27, 53.99, 53.88, 51.88, 51.27, 50.98, 50.89, 50.04, and 49.97at

303.15K, respectively. Positive values for Δ*H* suggest that the synthesis procedure of DSILs is an endothermic process. Fig. 3.11 shows that Δ*H* decreases with the increase in temperature. This figure also indicates that Δ*H* increased with the increase in $Cl^-$ ion concentration in DSILs to restrict the movement of ions. This indicates the increase of activation energy for viscous flow. This is based on the idea that holes are necessary for solvents to flow, according to the hole theory [77, 78].

**Table 3.9.** Calculation of the activation enthalpy for viscous flow (Δ*H*, kJ/mol) of $[C_4mim](CH_3CO_2)_xCl_{1-x}$ at various temperatures

| DSILs | 303.15 K | 313.15 K | 323.15 K | 333.15 K | 343.15 K |
|---|---|---|---|---|---|
| $[C_4mim]CH_3CO_2$ | 50.04 | 47.59 | 42.89 | 38.74 | 36.85 |
| $[C_4mim](CH_3CO_2)_{0.9}Cl_{0.1}$ | 50.89 | 48.48 | 44.00 | 39.94 | 37.93 |
| $[C_4mim](CH_3CO_2)_{0.8}Cl_{0.2}$ | 49.97 | 47.61 | 43.23 | 39.28 | 37.34 |
| $[C_4mim](CH_3CO_2)_{0.7}Cl_{0.3}$ | 51.88 | 49.54 | 45.09 | 41.03 | 39.07 |
| $[C_4mim](CH_3CO_2)_{0.6}Cl_{0.4}$ | 54.27 | 50.23 | 44.14 | 40.24 | 38.39 |
| $[C_4mim](CH_3CO_2)_{0.5}Cl_{0.5}$ | 50.98 | 48.78 | 44.59 | 40.74 | 38.88 |
| $[C_4mim](CH_3CO_2)_{0.4}Cl_{0.6}$ | 53.99 | 51.57 | 47.03 | 43.03 | 41.15 |
| $[C_4mim](CH_3CO_2)_{0.3}Cl_{0.7}$ | 53.88 | 51.62 | 47.21 | 43.17 | 41.27 |
| $[C_4mim](CH_3CO_2)_{0.2}Cl_{0.8}$ | 56.75 | 54.39 | 49.73 | 45.42 | 43.44 |
| $[C_4mim](CH_3CO_2)_{0.1}Cl_{0.9}$ | 51.27 | 49.20 | 45.26 | 41.55 | 39.71 |
| $[C_4mim]Cl$ | - | - | - | - | - |

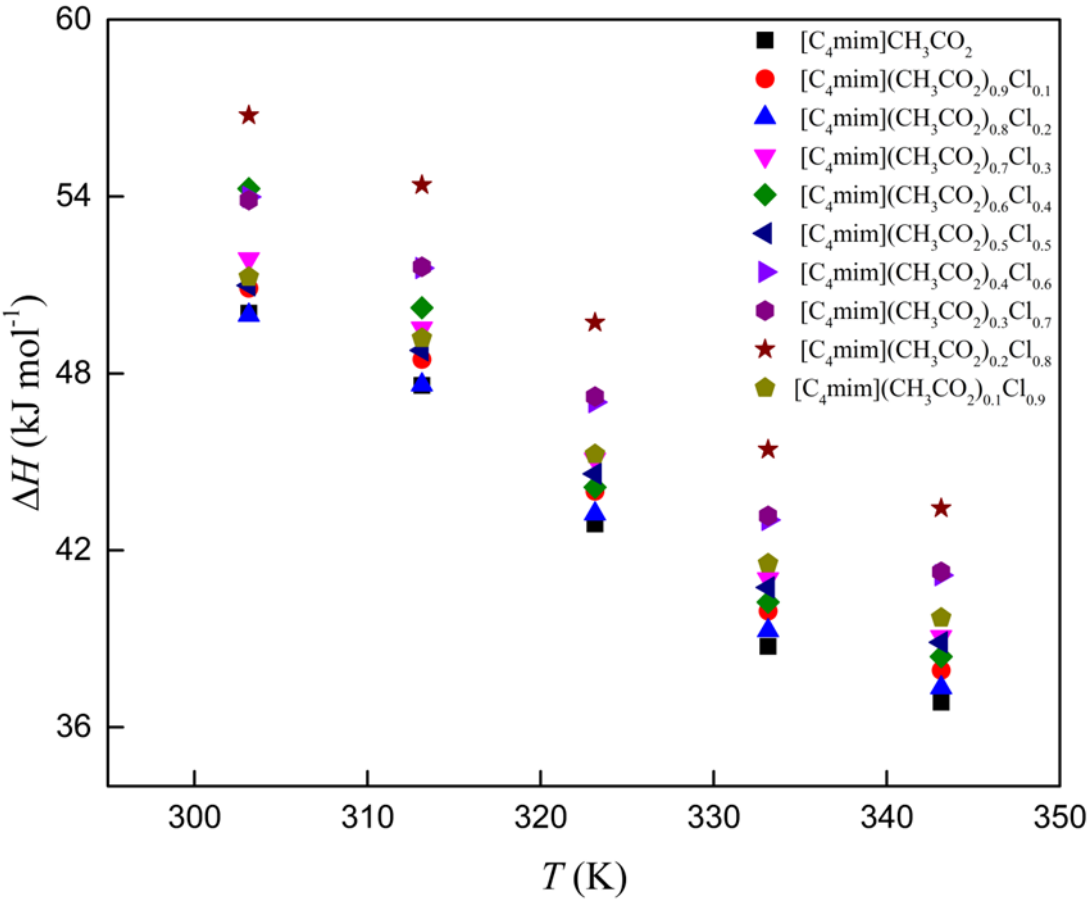


**Figure 3.11.** Change in $\Delta H$ of activation for $[C_4mim](CH_3CO_2)_xCl_{1-x}$ as a function of temperature

### 3.3.4. Refractive index of ILs and DSILs

The refractive index ($n_D$), which can reflect electronic polarizability and provide crucial details about interactions in the solution, is an effective tool for understanding the optical characteristics of a mixture of ILs. The dimensionless intensive property of a phase known as the index of refraction, or n, can be described by the eq. (9)

$$n = \frac{c_0}{c} \tag{9}$$

where the speed of light in a vacuum, $c_0$, is equal to the speed of light in a phase difference, $c$. In temperature intervals of 10 °C, the refractive indices of ILs and the synthesized DSILs were measured in the temperature range of 30 to 70 °C. All the measured refractive index values of ILs and DSILs are enlisted in Table 3.10. The experimental refractive index has been plotted against the mole fraction of $[C_4mim]Cl$ (Fig. 3.12) and temperature (Fig. 3.13). With an increase in

[$C_4$mim]Cl concentration, the refractive index of DSILs rises and decreases with increasing temperature. The range of refractive index measurement is narrow (1.49877 to 1.51631). The order of refractive index of the DSILs are [$C_4$mim]$(CH_3CO_2)_{0.1}Cl_{0.9}$ > [$C_4$mim]$(CH_3CO_2)_{0.2}Cl_{0.8}$ > [$C_4$mim]$(CH_3CO_2)_{0.3}Cl_{0.7}$ > [$C_4$mim]$(CH_3CO_2)_{0.4}Cl_{0.6}$ > [$C_4$mim]$(CH_3CO_2)_{0.5}Cl_{0.5}$ > [$C_4$mim]$(CH_3CO_2)_{0.6}Cl_{0.4}$ > [$C_4$mim]$(CH_3CO_2)_{0.7}Cl_{0.3}$ > [$C_4$mim]$(CH_3CO_2)_{0.8}Cl_{0.2}$ > [$C_4$mim]$(CH_3CO_2)_{0.9}Cl_{0.1.}$ This indicates that the refractive index of DSILs clearly depends on the amount of $Cl^-$ ion concentration. As $Cl^-$ ion concentration rises, *n* rises as well, indicating maximum light interaction in the solution and consequently less free space within the molecule. As a result, it is quite obvious that intermolecular interactions and aggregate formation occur. The formation of aggregates that would raise the refractive index may be predicted as a result of the numerous inter- and intramolecular interactions between/within the molecules of DSILs [79]. The variation of *n* is very much in agreement with the results of the density of DSILs shown in Table 3.1. As the density of DSILs increased the refractive index also increased. Fig. 3.13 shows the temperature dependence refractive index of ILs and DSILs. It is observed that a highly linear temperature dependence refractive index of ILs and DSILs were observed, as in the case of temperature dependences of density (Fig. 3.2).

### 3.3.4.1. Excess refractive index of DSILs

The excess refractive index gives the clear understanding about the interaction among the ions in DSILs. The excess refractive of DSILs can be calculated using eq. (11) [80]

$$\Delta n_D = n_D - (\chi_1 n_{D1} + \chi_2 n_{D2}) \qquad (11)$$

where $\chi_1$ and $\chi_2$ are the refractive indices of [$C_4$mim]Cl and [$C_4$mim]$CH_3CO_2$, respectively, and $n_1$ and $n_2$ are the mole fractions of the substances. The excess refractive index of the synthesized DSILs is tabulated in Table 3.11. The excess refractive was plotted against mole fraction of [$C_4$mim]Cl in Fig. 3.14 and R-K polynomial equation was used to fit the data. Most of the values of excess refractive index of DSILs were found to be negative except [$C_4$mim]$(CH_3CO_2)_{0.8}Cl_{0.2,}$ [$C_4$mim]$(CH_3CO_2)_{0.7}Cl_{0.3}$ and [$C_4$mim]$(CH_3CO_2)_{0.2}Cl_{0.8.}$ Strong specific molecular forces, like hydrogen bonds between constituent molecules, result in positive refractive index deviations. [81-83]. Excess molar refraction varies with the degree of intermolecular interactions. The magnitude

and sign of any variation in excess molar refraction between identical molecules serve as a measure of their size. When two different molecules with different molar volumes are combined, the intestinal position of one molecule may fit into another [84]. The positive excess refractive index values of DSILs and increased with temperature suggest that at low temperatures, the experimental *n* was closer to the ideal *n* and that polarization was stronger at high temperatures [85].

**Table 3.10.** Refractive index of $[C_4mim](CH_3CO_2)_xCl_{1-x}$ at different temperatures

| DSILs | 30 °C | 40 °C | 50 °C | 60 °C | 70 °C |
|---|---|---|---|---|---|
| $[C_4mim]CH_3CO_2$ | 1.49383 | 1.48446 | 1.47862 | 1.47454 | 1.47099 |
| $[C_4mim](CH_3CO_2)_{0.9}Cl_{0.1}$ | 1.49877 | 1.48719 | 1.47902 | 1.47116 | 1.46622 |
| $[C_4mim](CH_3CO_2)_{0.8}Cl_{0.2}$ | 1.49945 | 1.49192 | 1.48616 | 1.48142 | 1.47744 |
| $[C_4mim](CH_3CO_2)_{0.7}Cl_{0.3}$ | 1.50321 | 1.49447 | 1.48887 | 1.4831 | 1.47878 |
| $[C_4mim](CH_3CO_2)_{0.6}Cl_{0.4}$ | 1.49995 | 1.49139 | 1.48599 | 1.48123 | 1.47733 |
| $[C_4mim](CH_3CO_2)_{0.5}Cl_{0.5}$ | 1.50186 | 1.49289 | 1.48775 | 1.48335 | 1.47885 |
| $[C_4mim](CH_3CO_2)_{0.4}Cl_{0.6}$ | 1.50381 | 1.49457 | 1.48988 | 1.48575 | 1.48054 |
| $[C_4mim](CH_3CO_2)_{0.3}Cl_{0.7}$ | 1.51027 | 1.49824 | 1.49391 | 1.49068 | 1.48815 |
| $[C_4mim](CH_3CO_2)_{0.2}Cl_{0.8}$ | 1.51503 | 1.50847 | 1.50517 | 1.50139 | 1.49718 |
| $[C_4mim](CH_3CO_2)_{0.1}Cl_{0.9}$ | 1.51631 | 1.50975 | 1.50292 | 1.49488 | 1.48999 |
| $[C_4mim]Cl$ | 1.52035 | 1.51419 | 1.50612 | 1.49929 | 1.49428 |

**Table 3.11.** Excess refractive index of $[C_4mim](CH_3CO_2)_xCl_{1-x}$ at different temperatures

| DSILs | 30 °C | 40 °C | 50 °C | 60 °C | 70 °C |
|---|---|---|---|---|---|
| $[C_4mim]CH_3CO_2$ | 0 | 0 | 0 | 0 | 0 |
| $[C_4mim](CH_3CO_2)_{0.9}Cl_{0.1}$ | 0.002291 | -0.00045 | -0.00235 | -0.00585 | -0.0071 |
| $[C_4mim](CH_3CO_2)_{0.8}Cl_{0.2}$ | 0.000311 | 0.001084 | 0.002034 | 0.001925 | 0.001787 |
| $[C_4mim](CH_3CO_2)_{0.7}Cl_{0.3}$ | 0.001416 | 0.000445 | 0.001992 | 0.001128 | 0.000796 |
| $[C_4mim](CH_3CO_2)_{0.6}Cl_{0.4}$ | -0.00473 | -0.0061 | -0.00388 | -0.00343 | -0.00319 |
| $[C_4mim](CH_3CO_2)_{0.5}Cl_{0.5}$ | -0.00522 | -0.00749 | -0.00461 | -0.00356 | -0.00378 |
| $[C_4mim](CH_3CO_2)_{0.4}Cl_{0.6}$ | -0.00592 | -0.00898 | -0.00522 | -0.00363 | -0.00441 |
| $[C_4mim](CH_3CO_2)_{0.3}Cl_{0.7}$ | -0.00211 | -0.0085 | -0.00394 | -0.00117 | 0.000871 |
| $[C_4mim](CH_3CO_2)_{0.2}Cl_{0.8}$ | 7.95E-05 | -0.00136 | 0.004649 | 0.007139 | 0.007642 |
| $[C_4mim](CH_3CO_2)_{0.1}Cl_{0.9}$ | -0.00139 | -0.00338 | -0.00045 | -0.00194 | -0.00196 |
| $[C_4mim]Cl$ | 0 | 0 | 0 | 0 | 0 |

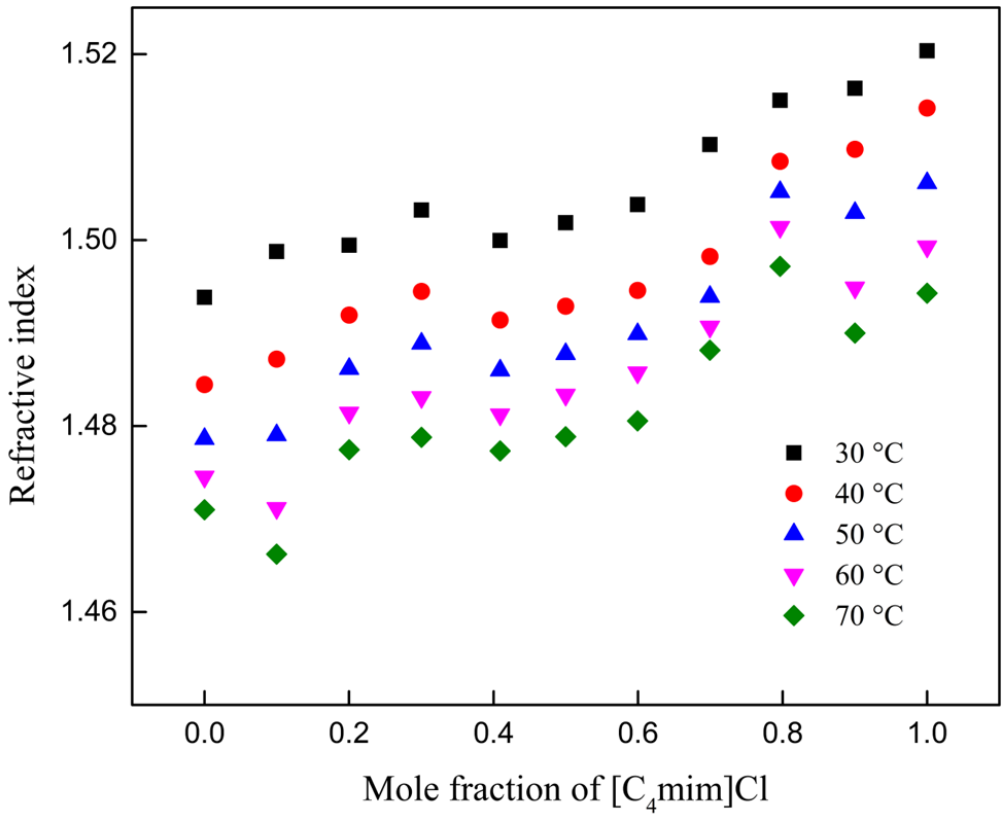


**Figure 3.12.** Variation of the refractive index of DSILs with the variation of mole fraction of [C4mim]Cl at temperature of 30 to 70 ℃.

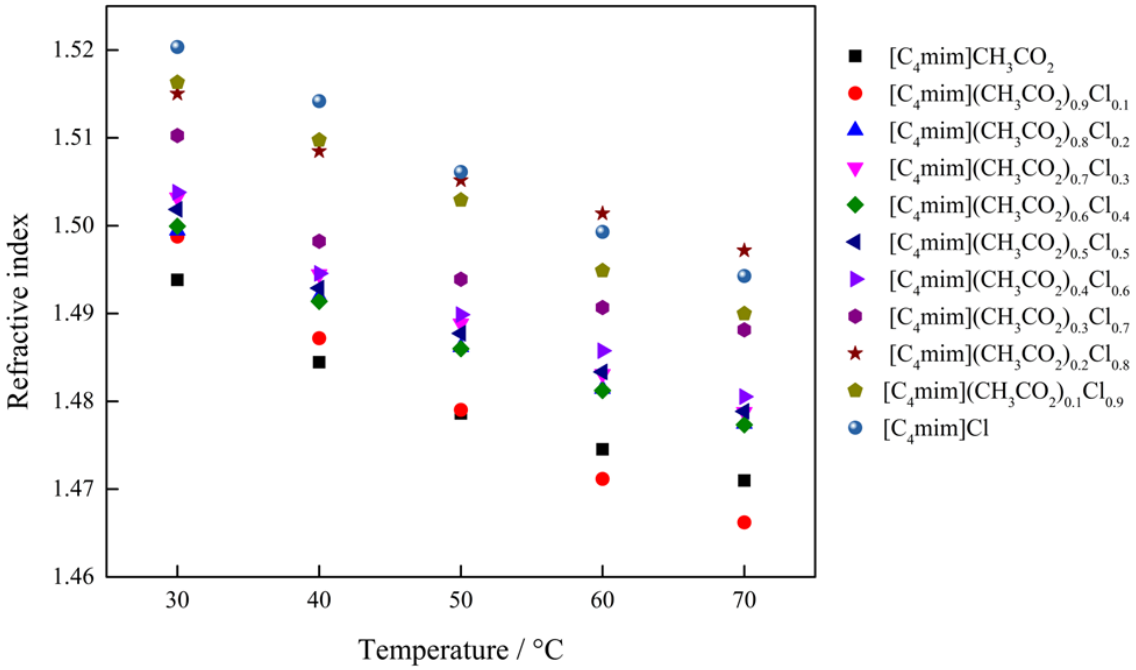


**Figure 3.13.** Change in the refractive index of DSILs with the temperature of 30 to 70 ℃ of different mole fractions of [C4mim]Cl

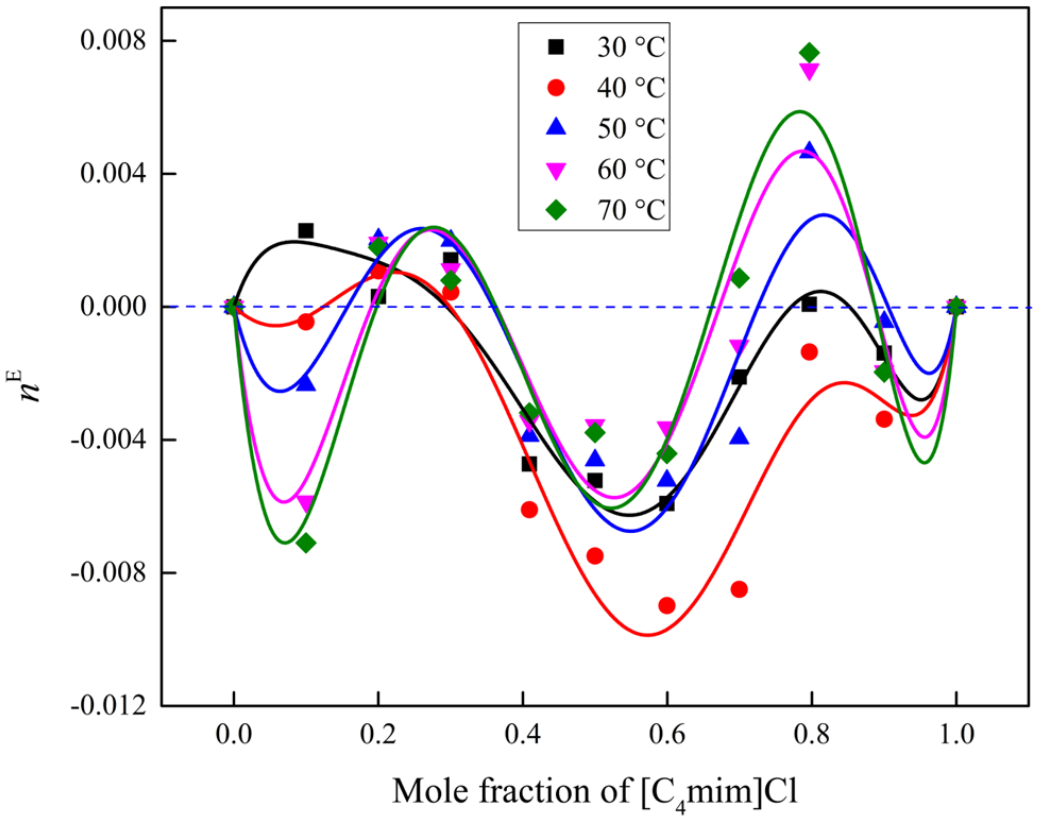


**Figure 3.14.** Variation of the excess refractive index of DSILs with mole fraction of [C4mim]Cl at the temperature of 30 to 70 ℃ and fitted with R-K equation

### 3.3.5. The conductivity of ILs and DSILs

The investigated conductivities of DSILs and their ionic conductivities have been measured at various temperatures from 30 to 70 ℃ with 10 ℃ intervals (Table 3.12). The variation of conductivities with the variation of mole fractions of [C4mim]Cl have been presented in Fig. 3.15 and with temperature in Fig. 3.16.

#### 3.3.5.1. Effect of mole fraction

As introducing [C4mim]Cl with [C4mim]$CH_3CO_2$ then the number of available overall ionic species such as $[C_4mim]^+$, $Cl^-$, and $CH_3CO_2^-$ increases in DSILs thus conductivity of DSILs increased with some exceptions shown in Table 3.12 and Fig. 3.15. The order of conductivities of DSILs are found to be $[C_4mim](CH_3CO_2)_{0.1}Cl_{0.9}$ > $[C_4mim](CH_3CO_2)_{0.3}Cl_{0.7}$ > $[C_4mim](CH_3CO_2)_{0.6}Cl_{0.4}$ > $[C_4mim](CH_3CO_2)_{0.5}Cl_{0.5}$ > $[C_4mim](CH_3CO_2)_{0.4}Cl_{0.6}$ >

$[C_4mim](CH_3CO_2)_{0.8}Cl_{0.2}$ > $[C_4mim](CH_3CO_2)_{0.7}Cl_{0.3}$ > $[C_4mim](CH_3CO_2)_{0.2}Cl_{0.8}$ > $[C_4mim](CH_3CO_2)_{0.9}Cl_{0.1.}$ and found to be 3.34892, 2.53857, 2.51569, 2.49981, 2.47309, 2.30413, 1.86679, 1.78434, 1.77763 mS/cm at 30 ℃ respectively. The mobility of $Cl^-$ ion is much greater than compared to $CH_3CO_2^-$ ions [86, 87]. Hence, with the addition of $Cl^-$ ion in DSILs, the overall conductivity boosts. Moreover, the presence of triple ions $[C_4mim]^+$, $Cl^-$, and $CH_3CO_2^-$ in DSILs disrupts the prevailing inter-ionic interactions and H-bonds making the ionic species more mobile and freer [88]. Therefore, DSILs have a higher ionic conductivity than ILs.

### 3.3.5.2. Effect of temperature

The conductivities in each case increase with increasing temperature as shown in Fig. 3.16, attributable to the linear decrease in density values and viscosities of each DSILs. The density and viscosity have been presented in Table 3.1 and Table 3.5. Two crucial macroscopic attributes, density and viscosity of ILs and DSILs represent the microscopic qualities dictated by a number of interconnected factors, including molar mass, ionic shape and size, intermolecular and interionic interacting forces like as hydrogen bonding, Coulombic interactions, and van der Waals [89-91].

**Table 3.12.** Conductivity (mS/cm) of $[C_4mim](CH_3CO_2)_xCl_{1-x}$ at different temperatures

| DSILs | 30 °C | 40 °C | 50 °C | 60 °C | 70 °C |
|---|---|---|---|---|---|
| $[C_4mim]CH_3CO_2$ | 1.8608 | 2.63628 | 3.71189 | 5.43254 | 8.77794 |
| $[C_4mim](CH_3CO_2)_{0.9}Cl_{0.1}$ | 1.77763 | 2.50308 | 3.58708 | 5.40511 | 8.52143 |
| $[C_4mim](CH_3CO_2)_{0.8}Cl_{0.2}$ | 2.30413 | 3.20975 | 4.82345 | 7.73568 | 9.96012 |
| $[C_4mim](CH_3CO_2)_{0.7}Cl_{0.3}$ | 1.86679 | 2.69076 | 4.65094 | 6.84614 | 8.78506 |
| $[C_4mim](CH_3CO_2)_{0.6}Cl_{0.4}$ | 2.51569 | 3.51599 | 6.06438 | 8.46957 | 11.07548 |
| $[C_4mim](CH_3CO_2)_{0.5}Cl_{0.5}$ | 2.49981 | 4.37438 | 6.28387 | 8.86744 | 11.97649 |
| $[C_4mim](CH_3CO_2)_{0.4}Cl_{0.6}$ | 2.47309 | 3.71175 | 6.09321 | 8.74013 | 11.98813 |
| $[C_4mim](CH_3CO_2)_{0.3}Cl_{0.7}$ | 2.53857 | 3.6054 | 5.39284 | 8.60956 | 11.8125 |
| $[C_4mim](CH_3CO_2)_{0.2}Cl_{0.8}$ | 1.78434 | 2.58273 | 3.56124 | 6.40116 | 9.14211 |
| $[C_4mim](CH_3CO_2)_{0.1}Cl_{0.9}$ | 3.34892 | 5.60963 | 8.7042 | 11.43139 | 15.62249 |
| $[C_4mim]Cl$ | - | - | - | - | - |

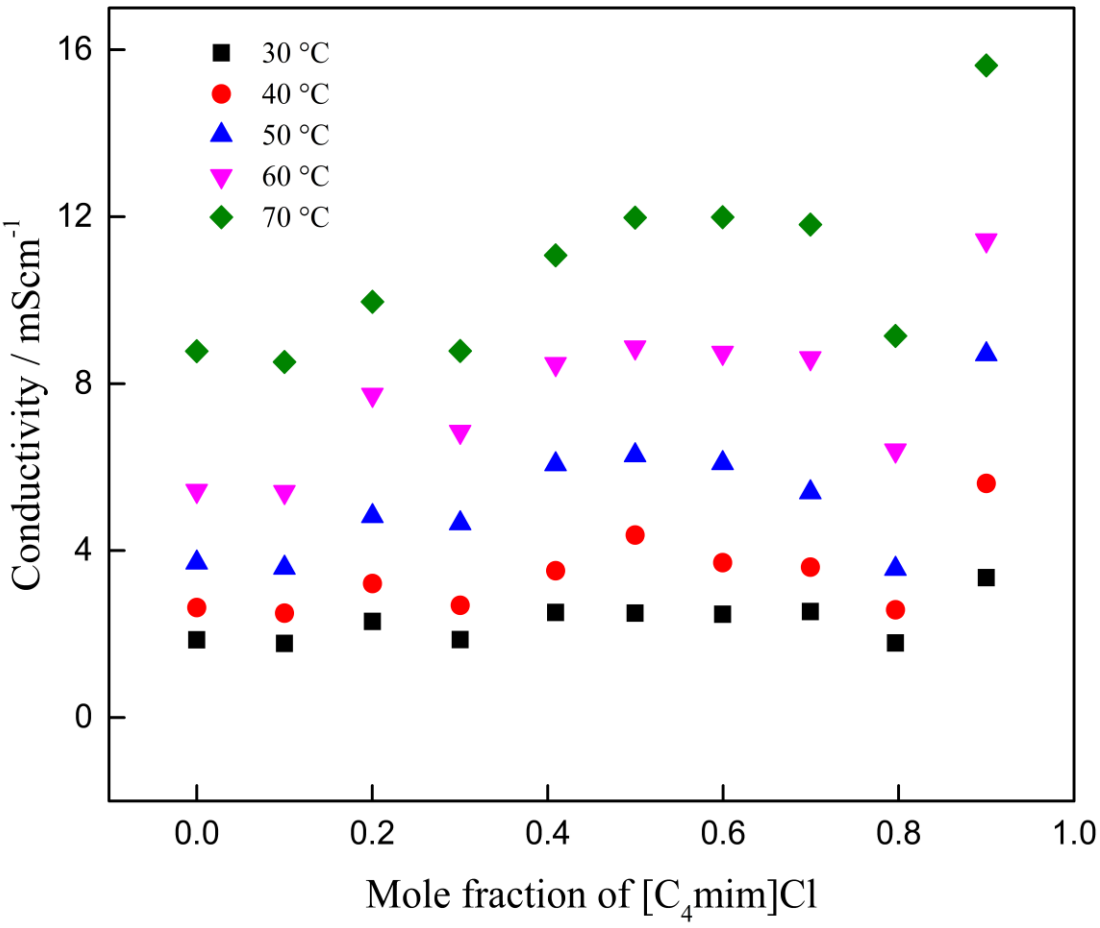


**Figure 3.15.** Variation of conductivities of $[C_4mim](CH_3CO_2)_xCl_{1-x}$ at T=30-70 °C

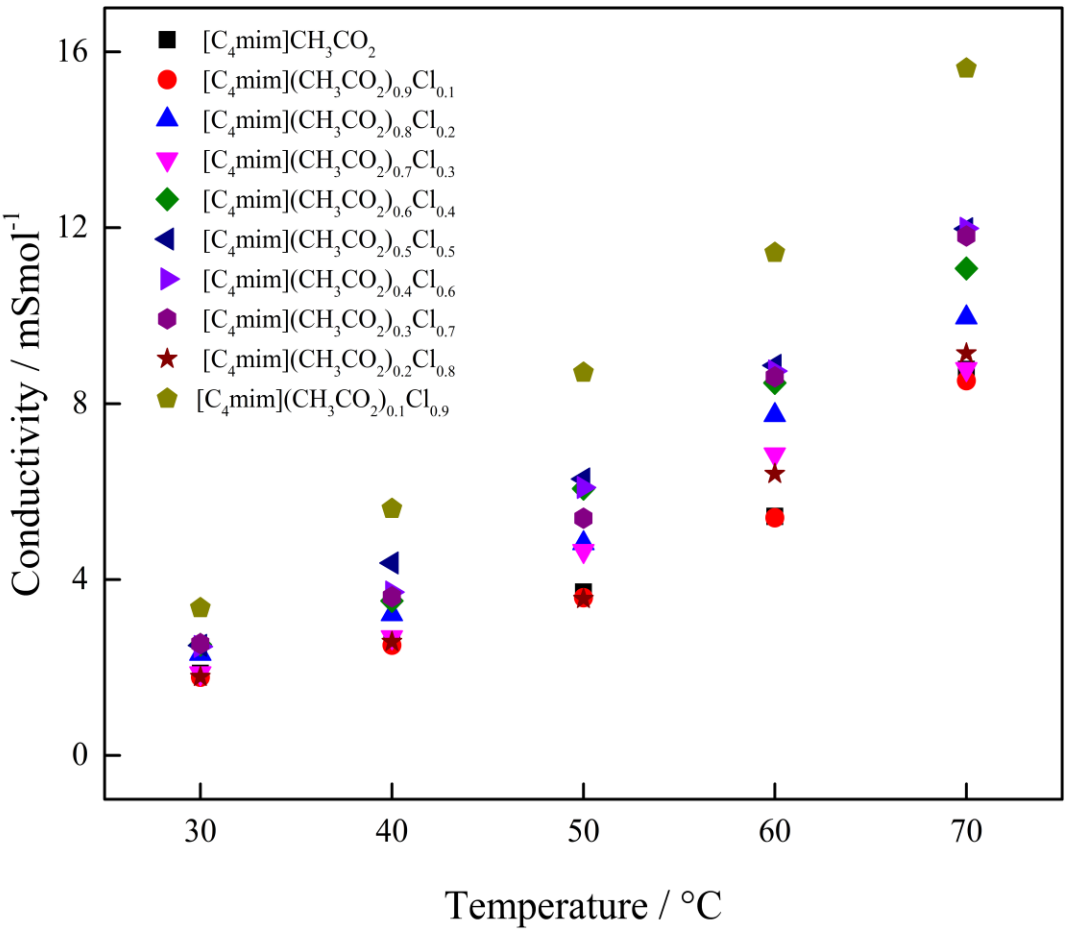


**Figure 3.16.** Variation of conductivities of $[C_4mim](CH_3CO_2)_xCl_{1-x}$ as a function of temperature.

### 3.3.5.3. Ionicity of DSILs

In the context of electrolytes, estimating and comprehending ionicity are critical. The ionicity is roughly estimated using a Walden plot, with a KCl aqueous solution serving as the reference line. The ideal line, which represents complete ion dissociation, has a slope of 1. The variation from this ideal line approximates ionicity. The Walden plot depicts the categorization of ILs into superionic, good, and poor liquids, as well as the relationship between low equivalent conductivity and low ionicity (ion pairing) [92, 93]. Fig. 3.17 represents the Walden plot for the studied DSILs system. As the temperature increases and fraction of $[C_4mim]Cl$, then in both cases, the ionic conductivity of DSILs seem to improve exhibiting good ILs behavior. In some compositions, superionic behavior is also seen. These kinds of trends seen in Walden plot, demonstrate superior ionic conductivity of the synthesized DSILs.

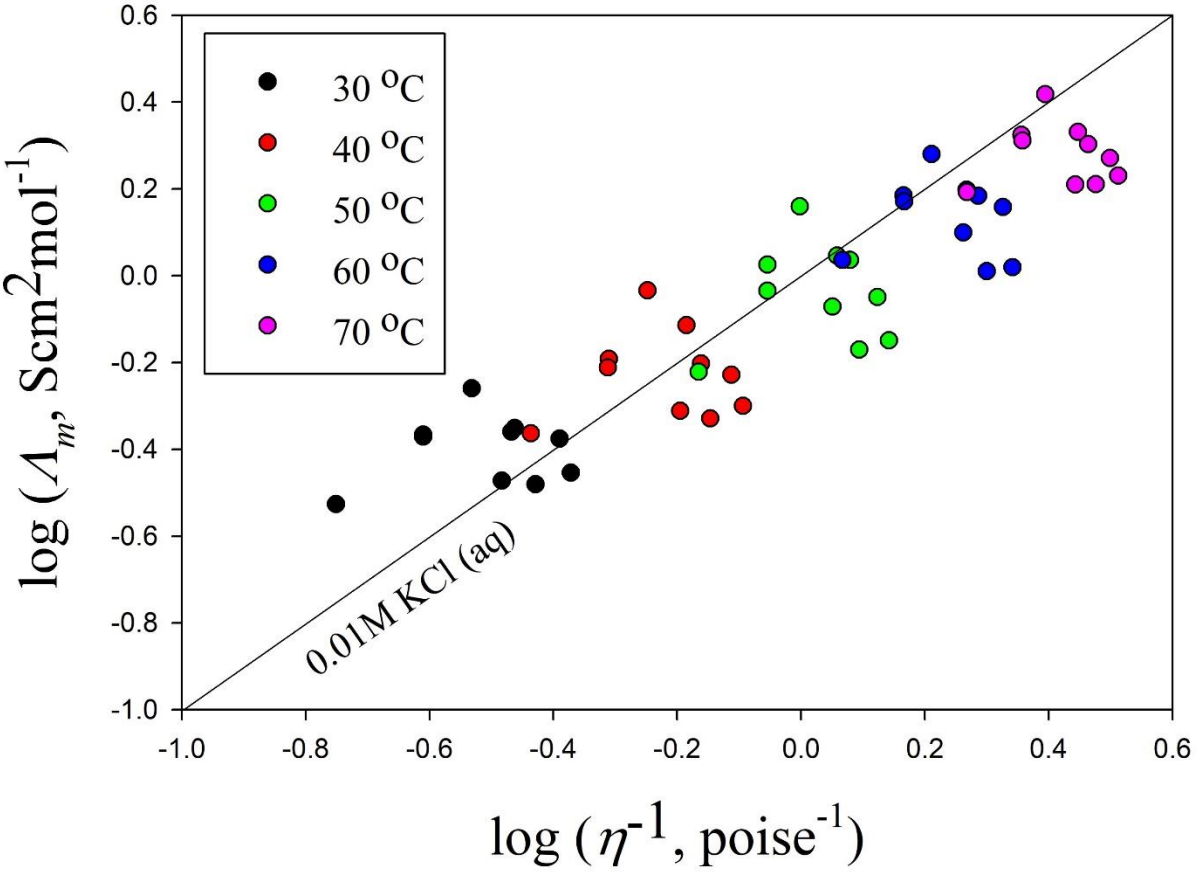


**Figure 3.17.** Walden plot for $[C_4mim](CH_3CO_2)_xCl_{1-x}$. A 0.01 M KCl aqueous solution with perfect dissociation represented by the solid line

### 3.4. Conclusions

At atmospheric pressure and over the entire mole fraction range, the density, viscosity, refractive index, and conductivity of $[C_4mim]Cl$ and $[C_4mim]CH_3CO_2$ and their DSILs have been measured at various temperatures (from 30 to 70 ℃). The excess molar volume and isothermal expansion coefficient have been determined from the density data. The excess molar volume of DSILs were measured at 70 ºC only as $[C_4mim]Cl$ is solid at room temperature found to be negative that indicates the volume construction occurred when two ILs are mixed together. The negative vales of excess molar volume also indicate that strong intermolecular interactions between $[C_4mim]^+$, $CH_3CO_2^-$ and $Cl^-$ are present in DSILs. The excess viscosity was also calculated at 70 ºC for the same reason. All excess viscosity found to be positive except $[C_4mim](CH_3CO_2)_{0.8}Cl_{0.2.}$ The positive excess viscosity values of DSILs indicate that the interactions between $[C_4mim]Cl$ and $[C_4mim]CH_3CO_2$ or its complexes in the liquid state are greater than those of the individual $[C_4mim]Cl$ and $[C_4mim]CH_3CO_2$. This strong association can be occurred by the formation of hydrogen bonds among, unlike ILs. As the increase in the amount of $[C_4mim]Cl$ in DSILs, the viscosity increases, with a few exceptions. The increase in viscosity is due to the interactions and H-bonding between ions of $[C_4mim]^+$, $Cl^-$ and $CH_3CO_2^-$. The viscosity data were used to estimate the thermodynamic characteristics of DSILs. $\Delta G$ of $[C_4mim]CH_3CO_2$ and DSILs were found to be positive and decreased with the temperature indicating favorable mixing of constituent ILs efficiently forming of the DSILs. The positive $\Delta S$ values of DSILs denote that the system becomes less organized relating to its starting states and decreases with increasing temperature suggesting at higher temperatures ordered structure of ILs and DSILs became more random and have a high value of entropy. Consequently, the required change in activation entropy for viscous flow decreases. $\Delta H$ decreases with the increase in temperature indicates that $\Delta H$ increased with the increase in $Cl^-$ ion concentration in DSILs to restrict the movement of ions increasing the activation energy. This is based on the idea that holes are necessary for solvents to flow, according to the hole theory. Excess refractive index are found to be negative except $[C_4mim](CH_3CO_2)_{0.8}Cl_{0.2,}$ $[C_4mim](CH_3CO_2)_{0.7}Cl_{0.3}$ and $[C_4mim](CH_3CO_2)_{0.2}Cl_{0.8.}$ The fact that the positive excess refractive index values of IL and DSIL rose with temperature suggests that polarization was stronger at higher temperatures and that the experimental refractive index was closer to the ideal at lower temperatures. DSILs have a higher ionic conductivity than ILs. The presence of triple ions $[C_4mim]^+$, $Cl^-$, and $CH_3CO_2^-$ in DSILs disrupts the prevailing inter-ionic interactions and H-bonds

making the ionic species more mobile and free. The Walden plot depicts with the temperature and amount of [$C_4$mim]Cl, the ionic conductivity of DSILs seem to be improve exhibiting good ILs behavior.

**References**


[1] Welton, T. (1999). Room-temperature ionic liquids. Solvents for synthesis and catalysis. *Chemical Reviews*, *99*(8), 2071-2084.

[2] Earle, M. J., and Seddon, K. R. (2000). Ionic liquids. Green solvents for the future. *Pure and Applied Chemistry*, *72*(7), 1391-1398.

[3] Pârvulescu, V. I., and Hardacre, C. (2007). Catalysis in ionic liquids. *Chemical Reviews*, *107*(6), 2615-2665.

[4] Greaves, T. L., and Drummond, C. J. (2008). Protic ionic liquids: properties and applications. *Chemical Reviews*, *108*(1), 206-237.

[5] Brenneck, J. F., and Maginn, E. J. (2001). Ionic liquids: innovative fluids for chemical processing. *American Institute of Chemical Engineers. AIChE Journal*, *47*(11), 2384.

[6] Lu, J., Yan, F., and Texter, J. (2009). Advanced applications of ionic liquids in polymer science. *Progress in Polymer Science*, *34*(5), 431-448.

[7] Keskin, S., Kayrak-Talay, D., Akman, U., and Hortaçsu, Ö. (2007). A review of ionic liquids towards supercritical fluid applications. *The Journal of Supercritical Fluids*, *43*(1), 150-180.

[8] 7.Sakaebe, H., and Matsumoto, H. (2003). N-Methyl-N-propylpiperidinium bis (trifluoromethanesulfonyl) imide (PP13–TFSI)–novel electrolyte base for Li battery. *Electrochemistry Communications*, *5*(7), 594-598.

[9] Liu, S., Liu, W., Liu, Y., Lin, J. H., Zhou, X., Janik, M. J., and Zhang, Q. (2010). Influence of imidazolium-based ionic liquids on the performance of ionic polymer conductor network composite actuators. *Polymer International*, *59*(3), 321-328.

[10] Sato, T., Masuda, G., and Tkagi, K. (2004). Electrochemical properties of novel ionic liquids for electric double layer capacitor applications. *Electrochimica Acta*, *49*(21), 3603-3611.

[11] Singh, S. K., and Savoy, A. W. (2020). Ionic liquids synthesis and applications: An overview. *Journal of Molecular Liquids*, *297*, 112038.

[12] Arumugam, V., Redhi, G., and Gengan, R. M. (2018). The application of ionic liquids in nanotechnology. In *Fundamentals of Nanoparticles* (pp. 371-400). Elsevier.

[13] Plechkova, N. V., and Seddon, K. R. (2008). Applications of ionic liquids in the chemical industry. *Chemical Society Reviews*, *37*(1), 123-150.

[14] Susan, M. A., Noda, A., Mitsushima, S., and Watanabe, M. (2003). Brønsted acid–base ionic liquids and their use as new materials for anhydrous proton conductors. *Chemical Communications*, (8), 938-939.

[15] Noda, A., Susan, M. A. B. H., Kudo, K., Mitsushima, S., Hayamizu, K., and Watanabe, M. (2003). Brønsted acid− base ionic liquids as proton-conducting nonaqueous electrolytes. *The Journal of Physical Chemistry B*, *107*(17), 4024-4033.

[16] Chakraborty, R., Asthana, A., Singh, A. K., Jain, B., and Susan, A. B. H. (2022). Adsorption of heavy metal ions by various low-cost adsorbents: a review. *International Journal of Environmental Analytical Chemistry*, *102*(2), 342-379.

[17] Tokuda, H., Hayamizu, K., Ishii, K., Susan, M. A. B. H., and Watanabe, M. (2004). Physicochemical properties and structures of room temperature ionic liquids. 1. Variation of anionic species. *The Journal of Physical Chemistry B*, *108*(42), 16593-16600.

[18] Tokuda, H., Hayamizu, K., Ishii, K., Susan, M. A. B. H., and Watanabe, M. (2005). Physicochemical properties and structures of room temperature ionic liquids. 2. Variation of alkyl chain length in imidazolium cation. *The Journal of Physical Chemistry B*, *109*(13), 6103-6110.

[19] Tokuda, H., Ishii, K., Susan, M. A. B. H., Tsuzuki, S., Hayamizu, K., and Watanabe, M. (2006). Physicochemical properties and structures of room-temperature ionic liquids. 3. Variation of cationic structures. *The Journal of Physical Chemistry B*, *110*(6), 2833-2839.

[20] Marium, M., Rahman, M. M., Mollah, M. Y. A., and Susan, M. A. B. H. (2015). Molecular level interactions in binary mixtures of 1-ethyl 3-methylimidazolium tetrafluoroborate and water. *RSC Advances*, *5*(26), 19907-19913.

[21] Seddon, K. R., Stark, A., and Torres, M. J. (2000). Influence of chloride, water, and organic solvents on the physical properties of ionic liquids. *Pure and Applied Chemistry*, *72*(12), 2275-2287.

[22] Gutiérrez, A., Atilhan, M., Alcalde, R., Trenzado, J. L., and Aparicio, S. (2018). Insights on the mixtures of imidazolium based ionic liquids with molecular solvents. *Journal of Molecular Liquids*, *255*, 199-207.

[23] Marsh, K. N., Boxall, J. A., and Lichtenthaler, R. (2004). Room temperature ionic liquids and their mixtures—a review. *Fluid Phase Equilibria*, *219*(1), 93-98.

[24] Ali, M. A., and Susan, M. A. B. H. (2022). Volumetric and Spectroscopic Studies of 1-ethyl-3-methylimidazolium Ethylsulfate/Propane-1-ol Binary Mixtures at Different Temperatures. *Spectrum of Emerging Sciences*, *2*(2), 17-28.

[25] Rodriguez, H., and Brennecke, J. F. (2006). Temperature and composition dependence of the density and viscosity of binary mixtures of water+ ionic liquid. *Journal of Chemical and Engineering Data*, *51*(6), 2145-2155.

[26] Gonzalez, E. J., Alonso, L., and Domínguez, Á. (2006). Physical properties of binary mixtures of the ionic liquid 1-methyl-3-octylimidazolium chloride with methanol, ethanol, and 1-propanol at T=(298.15, 313.15, and 328.15) K and at P= 0.1 MPa. *Journal of Chemical and Engineering Data*, *51*(4), 1446-1452.

[27] Clough, M. T., Crick, C. R., Gräsvik, J., Hunt, P. A., Niedermeyer, H., Welton, T., and Whitaker, O. P. (2015). A physicochemical investigation of ionic liquid mixtures. *Chemical Science*, *6*(2), 1101-1114.

[28] Wang, H., Kelley, S. P., Brantley III, J. W., Chatel, G., Shamshina, J., Pereira, J. F., and Rogers, R. D. (2015). Ionic fluids containing both strongly and weakly interacting ions of the same charge have unique ionic and chemical environments as a function of ion concentration. *ChemPhysChem*, *16*(5), 993-1002.

[29] Ijardar, S. P., Saparov, A., and Shah, D. (2019). Insights into Non-Ideal Behavior of Double Salt Ionic Liquids with Common Cation: Volumetric Behaviour, Molecular Dynamics Simulations and NMR Experiments. *ChemistrySelect*, *4*(44), 12861-12870.

[30] Finotello, A., Bara, J. E., Narayan, S., Camper, D., and Noble, R. D. (2008). Ideal gas solubilities and solubility selectivities in a binary mixture of room-temperature ionic liquids. *The Journal of Physical Chemistry B*, *112*(8), 2335-2339.

[31] Zistler, M., Wachter, P., Schreiner, C., Fleischmann, M., Gerhard, D., Wasserscheid, P., and Gores, H. J. (2007). Temperature dependent impedance analysis of binary ionic liquid electrolytes for dye-sensitized solar cells. *Journal of the Electrochemical Society*, *154*(9), B925.

[32] Wang, P., Zakeeruddin, S. M., Humphry-Baker, R., and Grätzel, M. (2004). A binary ionic liquid electrolyte to achieve≥ 7% power conversion efficiencies in dye-sensitized solar cells. *Chemistry of Materials*, *16*(14), 2694-2696.

[33] Hao, F., Lin, H., Liu, Y., and Li, J. (2011). Anionic structure-dependent photoelectrochemical responses of dye-sensitized solar cells based on a binary ionic liquid electrolyte. *Physical Chemistry Chemical Physics*, *13*(14), 6416-6422.

[34] Shimizu, K., Tariq, M., Rebelo, L. P., and Lopes, J. N. C. (2010). Binary mixtures of ionic liquids with a common ion revisited: a molecular dynamics simulation study. *Journal of Molecular Liquids*, *153*(1), 52-56.

[35] Canongia Lopes, J. N., and Pádua, A. A. (2006). Nanostructural organization in ionic liquids. *The Journal of Physical Chemistry B*, *110*(7), 3330-3335.

[36] Bruessel, M., Brehm, M., Voigt, T., and Kirchner, B. (2011). Ab initio molecular dynamics simulations of a binary system of ionic liquids. *Physical Chemistry Chemical Physics*, *13*(30), 13617-13620.

[37] Every, H., Bishop, A. G., Forsyth, M., and Macfarlane, D. R. (2000). Ion diffusion in molten salt mixtures. *Electrochimica Acta*, *45*(8-9), 1279-1284.

[38] Annat, G., MacFarlane, D. R., and Forsyth, M. (2007). Transport properties in ionic liquids and ionic liquid mixtures: the challenges of NMR pulsed field gradient diffusion measurements. *The Journal of Physical Chemistry B*, *111*(30), 9018-9024.

[39] Llovell, F., Valente, E., Vilaseca, O., and Vega, L. F. (2011). Modeling complex associating mixtures with [C n-mim][Tf2N] ionic liquids: predictions from the soft-SAFT equation. *The Journal of Physical Chemistry B*, *115*(15), 4387-4398.

[40] Stoppa, A., Buchner, R., and Hefter, G. (2010). How ideal are binary mixtures of room-temperature ionic liquids?. *Journal of Molecular Liquids*, *153*(1), 46-51.

[41] Greaves, T. L., Kennedy, D. F., Kirby, N., and Drummond, C. J. (2011). Nanostructure changes in protic ionic liquids (PILs) through adding solutes and mixing PILs. *Physical Chemistry Chemical Physics*, *13*(30), 13501-13509.

[42] Niedermeyer, H., Hallett, J. P., Villar-Garcia, I. J., Hunt, P. A., and Welton, T. (2012). Mixtures of ionic liquids. *Chemical Society Reviews*, *41*(23), 7780-7802.

[43] Chatel, G., Pereira, J. F., Debbeti, V., Wang, H., and Rogers, R. D. (2014). Mixing ionic liquids–"simple mixtures" or "double salts"?. *Green Chemistry*, *16*(4), 2051-2083.

[44] Canongia Lopes, J. N., Cordeiro, T. C., Esperança, J. M., Guedes, H. J., Huq, S., Rebelo, L. P., and Seddon, K. R. (2005). Deviations from ideality in mixtures of two ionic liquids containing a common ion. *The Journal of Physical Chemistry B*, *109*(8), 3519-3525.

[45] Navia, P., Troncoso, J., and Romaní, L. (2007). Excess magnitudes for ionic liquid binary mixtures with a common ion. *Journal of Chemical and Engineering Data*, *52*(4), 1369-1374.

[46] Navia, P., Troncoso, J., and Romaní, L. (2008). Viscosities for ionic liquid binary mixtures with a common ion. *Journal of Solution Chemistry*, *37*, 677-688.

[47] Stoppa, A., Buchner, R., and Hefter, G. (2010). How ideal are binary mixtures of room-temperature ionic liquids?. *Journal of Molecular Liquids*, *153*(1), 46-51.

[48] Larriba, M., Garcia, S., Navarro, P., Garcia, J., and Rodriguez, F. (2012). Physical properties of N-butylpyridinium tetrafluoroborate and N-butylpyridinium bis (trifluoromethylsulfonyl) imide binary ionic liquid mixtures. *Journal of Chemical and Engineering Data*, *57*(4), 1318-1325.

[49] Aparicio, S., and Atilhan, M. (2012). Mixed ionic liquids: the case of pyridinium-based fluids. *The Journal of Physical Chemistry B*, *116*(8), 2526-2537.

[50] Song, D., and Chen, J. (2014). Density and viscosity data for mixtures of ionic liquids with a common anion. *Journal of Chemical and Engineering Data*, *59*(2), 257-262.

[51] Huddleston, J. G., Visser, A. E., Reichert, W. M., Willauer, H. D., Broker, G. A., and Rogers, R. D. (2001). Characterization and comparison of hydrophilic and hydrophobic room temperature ionic liquids incorporating the imidazolium cation. *Green Chemistry*, *3*(4), 156-164.

[52] Sattari, M., Kamari, A., Mohammadi, A. H., and Ramjugernath, D. (2015). Prediction of refractive indices of ionic liquids–A quantitative structure-property relationship based model. *Journal of the Taiwan Institute of Chemical Engineers*, *52*, 165-180.

[53] Gardas, R. L., and Coutinho, J. A. (2009). Group contribution methods for the prediction of thermophysical and transport properties of ionic liquids. *AIChE Journal*, *55*(5), 1274-1290.

[54] Saba, H., Zhu, X., Chen, Y., and Zhang, Y. (2015). Determination of physical properties for the mixtures of [BMIM] Cl with different organic solvents. *Chinese Journal of Chemical Engineering*, *23*(5), 804-811.

[55] Soriano, A. N., Doma Jr, B. T., and Li, M. H. (2009). Measurements of the density and refractive index for 1-n-butyl-3-methylimidazolium-based ionic liquids. *The Journal of Chemical Thermodynamics*, *41*(3), 301-307.

[56] Iglesias-Otero, M. A., Troncoso, J., Carballo, E., and Romani, L. (2008). Density and refractive index in mixtures of ionic liquids and organic solvents: Correlations and predictions. *The Journal of Chemical Thermodynamics*, *40*(6), 949-956.

[57] Stoppa, A., Hunger, J., and Buchner, R. (2009). Conductivities of binary mixtures of ionic liquids with polar solvents. *Journal of Chemical and Engineering Data*, *54*(2), 472-479.

[58] Jarosik, A., Krajewski, S. R., Lewandowski, A., and Radzimski, P. (2006). Conductivity of ionic liquids in mixtures. *Journal of Molecular Liquids*, *123*(1), 43-50.

[59] Wang, X., Chi, Y., and Mu, T. (2014). A review on the transport properties of ionic liquids. *Journal of Molecular Liquids*, *193*, 262-266.

[60] MacFarlane, Douglas R., Maria Forsyth, Ekaterina I. Izgorodina, Andrew P. Abbott, Gary Annat, and Kevin Fraser. "On the concept of ionicity in ionic liquids." *Physical Chemistry Chemical Physics* 11, no. 25 (2009): 4962-4967.

[61] Ijardar, S. P., Saparov, A., and Shah, D. (2019). Insights into Non-Ideal Behavior of Double Salt Ionic Liquids with Common Cation: Volumetric Behaviour, Molecular Dynamics Simulations and NMR Experiments. *ChemistrySelect*, *4*(44), 12861-12870.

[62] Almeida, H. F., Canongia Lopes, J. N., Rebelo, L. P., Coutinho, J. A., Freire, M. G., and Marrucho, I. M. (2016). Densities and viscosities of mixtures of two ionic liquids containing a common cation. *Journal of Chemical and Engineering Data*, *61*(8), 2828-2843.

[63] Musiał, M., Zorębski, E., and Geppert-Rybczyńska, M. (2015). Is there any sense to investigate volumetric and acoustic properties of more binary mixtures containing Ionic Liquids?. *The Journal of Chemical Thermodynamics*, *87*, 147-161.

[64] Bhanuprakash, P., Rao, C. N., and Sivakumar, K. (2016). Evaluation of molecular interactions by volumetric and acoustic studies in binary mixtures of the ionic liquid [EMIM][$MeSO_4$] with ethanoic and propanoic acid at different temperatures. *Journal of Molecular Liquids*, *219*, 79-87.

[65] Rao, P. R., Krishna, T. S., Bharath, P., Dey, R., and Ramachandran, D. (2021). Understanding of molecular interactions between ethyl acetate and 1-butyl-3-methyl-imidazolium bis (trifluoromethylsulfonyl) imide: A thermophysical study. *The Journal of Chemical Thermodynamics*, *156*, 106383.

[66] Bhanuprakash, P., Prathibha, R., Gardas, R. L., Sivakumar, K., and Jyothi, N. V. V. (2020). Effect of temperature, nature of anion, and alkyl chain length on the volumetric and acoustic properties of ionic liquid [$C_4C_1$im][$MeSO_4$] with alkyl nitriles. *Journal of Molecular Liquids*, *302*, 112507.

[67] Cláudio, A. F. M., Swift, L., Hallett, J. P., Welton, T., Coutinho, J. A., and Freire, M. G. (2014). Extended scale for the hydrogen-bond basicity of ionic liquids. *Physical Chemistry Chemical Physics*, *16*(14), 6593-6601.

[68] Song, D., and Chen, J. (2014). Density and viscosity data for mixtures of ionic liquids with a common anion. *Journal of Chemical and Engineering Data*, *59*(2), 257-262.

[69] Liu, Q., Ma, L., Wang, S., Ni, Z., Fu, X., Wang, J., and Zheng, Q. (2021). Study on the properties of density, viscosity, excess molar volume, and viscosity deviation of [$C_2$mim][$NTf_2$],[$C_2$mmim][$NTf_2$],[$C_4$mim][$NTf_2$], and [$C_4$mmim][$NTf_2$] with PC binary mixtures. *Journal of Molecular Liquids*, *325*, 114573.

[70] Steltenpohl, P., and Graczová, E. (2022). Binary mixtures containing imidazolium ionic liquids: properties measurement. *Acta Chimica Slovaca*, *15*(1), 18-28.

[71] Tammann, G., Hesse, W. Die Abhängigkeit Der Viscosität von Der Temperatur Bie Unterkühlten Flüssigkeiten. Zeitschrift für Anorg. und Allg. Chemie 1926, 156 (1), 245–257.

[72] Mauro, J. C., Yue, Y., Ellison, A. J., Gupta, P. K., Allan, D. C. Viscosity of Glass-Forming Liquids. Proc. Natl. Acad. Sci. U. S. A. 2009, 106 (47), 19780–19784.

[73] Chatel, G., Pereira, J. F. B., Debbeti, V., Wang, H., and Rogers, R. D. (2014). Mixing Ionic Liquids- "simple Mixtures" or “Double Salts”? *Green Chemistry*, 16 (4), 2051–2083.

[74] Hunt, P. A., Ashworth, C. R., Matthews, R. P. Hydrogen Bonding in Ionic Liquids. Chem. Soc. Rev. 2015, 44 (5), 1257–1288.

[75] Mullen, J. W., Li, H., Atkin, R., and Silvester, D. S. (2022). Mixing Ionic Liquids Affects the Kinetics and Thermodynamics of the Oxygen/Superoxide Redox Couple in the Context of Oxygen Sensing. *ACS Physical Chemistry Au*, *2*(6), 515-526.

[76] Das, S., Patra, N., Banerjee, A., Das, B., and Ghosh, S. (2020). Studies on the self-aggregation, interfacial and thermodynamic properties of a surface active imidazolium-based ionic liquid in aqueous solution: effects of salt and temperature. *Journal of Molecular Liquids*, *320*, 114497.

[77] Afrin, T., Mafy, N. N., Rahman, M. M., Mollah, M. Y. A., and Susan, M. A. B. H. (2014). Temperature perturbed water structure modification by d (−)-fructose at different concentrations. *RSC Advances*, *4*(92), 50906-50913.

[78] Jones, G., and Colvin, J. H. (1940). The viscosity of solutions of electrolytes as a function of the concentration. VII. Silver nitrate, potassium sulfate and potassium chromate. *Journal of the American Chemical Society*, *62*(2), 338-340.

[79] Saba, H., Zhu, X., Chen, Y., and Zhang, Y. (2015). Determination of physical properties for the mixtures of [BMIM] Cl with different organic solvents. *Chinese Journal of Chemical Engineering*, *23*(5), 804-811.

[80] Xu, Y., Yao, J., Wang, C., and Li, H. (2012). Density, viscosity, and refractive index properties for the binary mixtures of n-butylammonium acetate ionic liquid+ alkanols at several temperatures. *Journal of Chemical and Engineering Data*, *57*(2), 298-308.

[81] Rathnam, M. V., Mohite, S., and Kumar, M. S. S. (2011). Thermophysical properties of binary mixtures (dimethyl carbonate+ ketones) at T=(303.15, 308.15 and 313.15) K. *Journal of Molecular Liquids*, *163*(3), 170-177.

[82] Dey, R., Singh, A. K., and Pandey, J. D. (2008). A temperature dependent viscometric study of binary liquid mixtures. *Journal of Molecular Liquids*, *137*(1-3), 88-91.

[83] Kumar, H., Gulati, N., and Kundi, V. (2012). Viscometric studies of binary liquid mixtures of cyclopentane (1)+ branched alkanols (2) at T=(298.15 and 308.15) K. *Journal of Molecular Liquids*, *174*, 63-69.

[84] Bhanupriya, Rajwade, R. P., and Pande, R. (2009). Densities, Refractive Indices and Excess Properties of N-p-Tolylbenzohydroxamic Acid in Dimethyl Sulfoxide at 298.15 to 313.15 K. *Journal of Solution Chemistry*, *38*, 1173-1181.

[85] Larriba, M., Navarro, P., Beigbeder, J. B., García, J., and Rodríguez, F. (2015). Mixing and decomposition behavior of {[4bmpy][Tf2N]+[emim][EtSO4]} and {[4bmpy][Tf2N]+[emim][TFES]} ionic liquid mixtures. *The Journal of Chemical Thermodynamics*, *82*, 58-75.

[86] Gunning, H. E., and Gordon, A. R. (1942). The conductance and ionic mobilities for aqueous solutions of potassium and sodium chloride at temperatures from 15° to 45° C. *The Journal of Chemical Physics*, *10*(2), 126-131.

[87] Koval, D., Kašička, V., and Zusková, I. (2005). Investigation of the effect of ionic strength of Tris-acetate background electrolyte on electrophoretic mobilities of mono-, di-, and trivalent organic anions by capillary electrophoresis. *Electrophoresis*, *26*(17), 3221-3231.

[88] Zhang, H., Cui, X., Li, P., Feng, T., and Feng, H. (2022). Measurement and correlation for the electrical conductivity of double salt ionic liquids with triple ions. *Journal of Molecular Liquids*, *365*, 120193.

[89] Fox, E. T., Paillard, E., Borodin, O., and Henderson, W. A. (2013). Physicochemical properties of binary ionic liquid–aprotic solvent electrolyte mixtures. *The Journal of Physical Chemistry C*, *117*(1), 78-84.

[90] Saba, H., Zhu, X., Chen, Y., and Zhang, Y. (2015). Determination of physical properties for the mixtures of [BMIM] Cl with different organic solvents. *Chinese Journal of Chemical Engineering*, *23*(5), 804-811.

[91] Thawarkar, S., Khupse, N. D., Shinde, D. R., and Kumar, A. (2019). Understanding the behavior of mixtures of protic-aprotic and protic-protic ionic liquids: Conductivity, viscosity, diffusion coefficient and ionicity. *Journal of Molecular Liquids*, *276*, 986-994.

[92] Thawarkar, S., Khupse, N. D., Shinde, D. R., and Kumar, A. (2019). Understanding the behavior of mixtures of protic-aprotic and protic-protic ionic liquids: Conductivity, viscosity, diffusion coefficient and ionicity. *Journal of Molecular Liquids*, *276*, 986-994.

[93] Schreiner, C., Zugmann, S., Hartl, R., and Gores, H. J. (2010). Fractional Walden rule for ionic liquids: examples from recent measurements and a critique of the so-called ideal KCl line for the Walden plot. *Journal of Chemical and Engineering Data*, *55*(5), 1784-1788.

# Chapter 4

## Evaluation of Double Salt Ionic Liquids as Materials


### Abstract

Ionic liquids (ILs) have been recently used as solvent material for dissolution of cellulose however, it has certain limitations. ILs mixture such as double salt ionic liquids (DSILs) can serve as wonderful alternative to ILs. Although researches regarding physicochemical properties of the ILs are available, physicochemical properties of DSILs are scarce in literature due to huge number of possible combinations of DSILs. In this study, two ILs namely, [$C_4$mim] $CH_3CO_2$ and [$C_4$mim]Cl have been taken as precursor for the preparation of DSILs with formula, [$C_4$mim] $(CH_3CO_2)_xCl_{1-x}$. Nine composition of DSILs have been prepared with mole fraction of x = 0.1, 0.2, 0.3, 0.4, 0.5, 0.6, 0.7, 0.8, and 0.9. ILs and DSILs have been subjected to UV-Visible absorption spectroscopy, fluorescence spectroscopy, thermogravimetric analysis and differential scanning calorimetry for investigating the optical and thermal properties of the DSILs and ILs. Optical spectroscopy reveals the possible presence of imidazolium associative species in the DSILs. Moreover, the recycled DSIL shows an increase in the association of imidazolium ring moieties due to interruption from cellulose molecules. Hence, the associative species plays an important role in the dissolution of cellulose. Thermal stabilities of the DSILs are in the range of 220 to 280 ℃ and isotherm TGA reveals the enhanced stability regarding the DSILs compared to ILs at 120 ℃. Heat capacities of the DSILs increase linearly with the operation temperature and DSILs have slightly lower heat capacities compared to single ILs. Finally, the glass transition temperature ($T_g$) of the DSILs exhibits similar behavior as the single ILs. However, $T_g$ decreased in case of DSILs compared to ILs.



**Keywords:** Double salts ionic liquids, UV-visible spectroscopy, UV-fluorescence, Thermal properties


### 4.1 Introduction

Ionic liquids (ILs) are widely used in a wide range of industries [1–6] due to the freedom with which their properties can be changed by altering their ionic component. Salts known as ILs have a low melting point of approximately 100 °C or less. It has been referred to as "designer solvents" [7] because of the flexibility of altering the characteristics with various ionic components in ILs. Numerous studies have been done to describe different aspects of the ILs. These research

studies have brought insight into a number of inherent characteristics of ILs, such as their high volatility, high thermal stability, high viscosity, high electrical conductivity, etc. The most appealing feature of ILs as a solvent is their low vapor pressure. Subsequently, ILs are more environmentally friendly than traditional solvents because of this characteristic and their capacity to be recycled. Therefore, the majority of research is done on present-day environmental and energy-related challenges. However, despite having distinct advantages over traditional solvents, ILs exhibit a variety of issues, including poor biodegradability [8, 9], high cost [10], and possible toxicity [11], which hinders their use in industry [12, 13]. Despite these possible drawbacks, there are a number of IL studies that include both an anion and a cation. IL combinations, as it turns out, can offer a wide range of alternatives for various fields of study [5, 14]. This is ideal for the development of task-specific ILs.

These IL mixtures are referred to as Double Salt Ionic Liquids (DSILs), which include more than two different types of ions. Each DSIL is distinct in terms of the combination of ion types, ion ratios, and their attributes [14]. The features of each combination are distinct from those of two ion ILs because each combination of ion types forms a unique DSIL. These DSILs respond differently than diverse mixtures of ILs for each distinct combination of ion types [14]. In recent research, these ions have been considered a mixture of molecular solvents rather than distinct ILs, which is less than ideal for an in-depth investigation of the physicochemical characteristics of DSILs [15, 16]. These studies investigate the most important physicochemical parameters that deviate from ideal behavior. Depending on the property being measured, the combination may behave optimally or not. As a result, it is important to research DSILs in order to identify new ion combinations that have distinctive and different characteristics from pure ILs [17].

The ILs have been the subject of several spectroscopic research in recent works. Characterizations regarding NMR, Raman, and IR spectroscopic characteristics have been made [18–20]. There are, however, very few publications that discuss the optical characteristics of ILs. Therefore, there are several information gaps in this area. UV-visible spectroscopy and fluorescence spectroscopy are used to examine the optical characteristics of ILs based on imidazolium. Although the majority of research focuses on the optical behavior of the dissolved solutes in these ILs, there are not many studies that address the optical behavior of the IL solvent [21–24].

Optical properties of the ILs in the available literature includes UV-visible absorption spectroscopy, fluorescence spectroscopy, and refractive index. UV-visible absorption spectra of the ILs reveal the possible electronic activity of the cationic moiety present in the ILs. In general, the cationic moiety contributes towards the UV-visible activity of the ILs. This is due to the fact that the possible electronic transition states depend on the structure of the cations as most of these cations are unsaturated or aromatic organic cations. As a result, transitions like $\pi \rightarrow \pi^*$ or $n \rightarrow \pi^*$ occurs revealing the photoactivity of the ILs. However, most of the studies related to the UV-visible absorption spectra of ILs indicate that ILs are transparent in the visible range of the electromagnetic spectrum whereas it shows distinct UV absorption due to the presence of unsaturated or aromatic cation moiety. Zhu *et al.* investigated the interaction between the pyrene in the pyridinium ILs as solvent. They concluded that there is red shift in the absorption peak of the pyrene dissolved in pyridinium ILs. However, the red shift is not because of the concentration of pyrene but the fraction of ILs present in the solution. This is due to formation of different reasons such as change in polarity of the solvents, microstructure formation, and different chemical and physical interaction of the ILs [25]. In case of imidazolium based ILs, most of the works are conducted using the ILs as solvent. It is observed that imidazolium based ILs show little absorption in the visible range and is deemed as transparent in under visible light. Furthermore, these ILs show absorption in the UV range due to the presence of ring structure and unsaturated species and are termed as semi-transparent in the UV range of the electromagnetic spectrum. Studies related to UV-visible spectra of solutes dissolved in imidazolium based ILs have been conducted. The purpose of these studies was to evaluate the coordination and ligand sphere of the cations of Lanthanide series and Actinide series [26, 27]. Other applications include investigating the progress of the oxidation of olefins in ILs solvent systems [28]. Thus, identifying the solvent polarity through the solvatochromic shift of dissolved dyes has by far been the focus of the majority of UV-visible spectroscopic measurements in ILs.

The purpose of conducting fluorescence spectra of ILs is generally divided into two parts. The most common reason for this approach is to measure the solvent polarity of the ILs through dissolving dye molecules in these systems. On the other hand, determination of solvation dynamics of different dye molecules in the ILs by time resolved fluorescence spectroscopy is also done extensively. However, very few studies are conducted to evaluate the luminescence properties of the ILs as they are transparent in visible light region. López *et al.* discussed the optical properties

of symmetric ILs i.e., cations with symmetric structure [29]. Samanta *et al.* studied the optical characteristics of imidazolium-based ILs, such as UV-visible absorption and emission spectra [23–24, 30]. They discovered that the fluorescence spectra of imidazolium-based ILs exhibit the "red edge effect" [31]. The maximum emission wavelength of REE is said to have shifted toward the red edge of the absorption band as a result of a change in the excitation wavelength. The microheterogeneity of the ILs and the existence of different related species are responsible for this behavior [32]. Due to the absence of excited state events such as solvation energy or energy transfer, imidazolium ILs have uneven fluorescence lifetimes [32]. Additionally, unlike the traditional solvents, the ILs feature complicated interactions like coulombic, dipolar, van der Waals, or H-bonding, among others [32]. Most of the fluorescence spectral studies include complex of lanthanide series elements with the ILs. These complex exhibit significant luminescence properties and do not need any stabilization of the liquid states with co-ligands. Hence, there is a need of in-depth study to be focused on the inherent fluorescence properties of the ILs itself.

Although studies concerning the optical characteristics of pure imidazolium-based ILs have recently been reported, the new focus should be on DSILs of imidazolium-based ILs. DSILs containing imidazolium moiety are anticipated to exhibit distinctive optical features since the imidazolium moiety of ILs is responsible for the optical behavior in the UV region of the electromagnetic spectrum [23]. DSILs with imidazolium moiety are expected to have distinctive optical characteristics. There are not many studies on the optical characteristics of DSILs, and the ones that are available are novel work.

Among the physicochemical properties, thermal properties of the DSILs need to be investigated to find the thermal behavior of the DSIL. For applications in the industrial level, the thermal properties of DSILs are very important in finding their operational temperature range. Melting points ($T_m$), glass transition temperature ($T_g$), thermal decomposition temperature ($T_d$) etc. are various thermal properties that need to be determined to optimize the operational temperature range for the DSILs. Moreover, heat capacities provide insight into the heat storage capacity of the materials as well as estimate the heating and cooling requirements of the material. Imidazolium-based ILs are interesting as these ILs are mostly used in the dissolution of cellulose [33]. There are numerous reports on the thermal properties of imidazolium based ILs [34–37]. DSILs of imidazolium based ILs could be formed by combining different ions resulting in a vast

combination of DSILs. This large field has been left little investigated or unexamined. Thus, thermal behavior of DSILs need to be evaluated for further applications into the dissolution of cellulose. Researches regarding the thermal behavior of imidazolium based DSILs have been conducted to a very few extent [38]. These researches mainly focused on the heat capacities, thermal stability, thermal storage density etc. of the DSIL. Most of the works varied only the anion keeping one common cation. Other works included the effect of variation of the alkyl side chain length of the imidazolium group on the thermal properties of the ILs and DSILs have also been investigated [34].

This research aims to investigate the optical characteristics of $[C_4mim]Cl$ and $[C_4mim]CH_3CO_2$ and their DSILs in various ratios. Both of the solvents are examined using UV-visible absorption spectroscopy, and fluorescence spectroscopy. This research analyzes the optical properties of both the ILs and their DSILs in great detail. Moreover, several different compositions of DSILs have been subjected to thermal treatment to find important thermal properties such as thermal stability, heat capacity, and heat storage ability of the DSILs. Thermal analysis of the single ILs also have been conducted. The various processes occurring during the thermal treatment have been characterized by the differential scanning calorimetry (DSC). In addition to that, the results obtained has been compared with the existing literature.

## 4.2 Materials and Methods

The materials and methods applied in this chapter to conduct this study have been described in the following sub-sections.

### 4.2.1 Materials

ILs, $[C_4mim]Cl$ and $[C_4mim]CH_3CO_2$, were purchased from Sigma-Aldrich with purities of $\geq$98% and $\geq$95%, respectively. Acetone is purchased from Sigma-Aldrich with purity of $\geq$ 99.5.

### 4.2.2 Preparation of DSILs of $[C_4mim]Cl$ and $[C_4mim]CH_3CO_2$

The preparation DSILs have been carried out by mixing of $[C_4mim]Cl$ and $[C_4mim](CH_3CO_2)$ at varying mole fractions to prepare $[C_4mim](CH_3CO_2)_xCl_{1-x}$, ( where $x$ is 0.1, 0.2, 0.3, 0.4, 0.5, 0.6, 0.7, 0.8, and 0.9 mole fraction of single ILs). The details of the preparation procedure have been described in chapter 2 (sub-section 2.2.2).

### 4.2.3. Spectroscopic analysis

The optical properties and associative behaviors of DSILs have been examined using UV-visible spectroscopy and fluorescence spectroscopy.

#### 4.2.3.1. UV-Visible

Spectroscopic characterization of the IL and DSIL samples were performed in a quartz cuvette with an optical pathway of 1 cm. UV-visible absorption spectroscopy were conducted by using Perkin-Elmer Lambda 35 spectrophotometer.

#### 4.2.3.2. UV-fluorescence

Photoluminescence properties of the DSIL and IL were recorded using a Perkin-Elmer FL 6500 spectrofluorimeter equipped with pulse Xe lamp with user defined power settings with peak power varying from 20 kW to 120 kW, maximum resolution of 1 nm, wavelength scan speed of 24000 nm/min and with a fast response of 0.002 seconds. The samples were excited at the wavelength 200 nm, their respective $\lambda_{max}$, and at 375 nm. DSIL with superior cellulose dissolution capability were selected prior to dissolution and for excitation wavelength dependent fluorescence spectra with wavelength ranging from 280 nm to 440 nm. Similarly, recycled DSIL from the dissolution solution were also subjected to excitation wavelength dependent fluorescence spectroscopy applying the same range of excitation wavelength.

### 4.2.4. Thermal analysis

The thermal properties of the ILs and DSILs need to be investigated to find the thermal behavior of the ILs and DSIL. For applications in the industrial level, the thermal properties of DSILs are very important in finding their operational temperature range. Melting points ($T_m$), glass transition temperature ($T_g$), thermal decomposition temperature ($T_d$), heat capacity ($C_{p)}$ etc. have been measured by the using following techniques.

#### 4.2.4.1. Thermogravimetric analysis (TGA)

Thermogravimetric measurements and differential thermal analysis of the DSILs were performed by using a Hitachi TG/DTA 7200 under a $N_2$ atmosphere. Aluminum pans served as sample holders and reference pans. The measurement sensitivity for DTA was 0.06 V and for TG analysis it was 0.2 g. TGA of DSILs was performed with a gas flow rate of 60 mL $min^{-1}$ in a $N_2$ environment. A programmed heating from 300 to 550 ℃ with a heating rate of 100 ℃ $min^{-1}$ was carried out for each measurement. From the TG analysis, the onset temperature ($T_{onset}$) was calculated. The thermal decomposition temperatures have an uncertainty of ±2 ℃ due to the manual determination of the tangent point for the onset temperature, which is the source of the highest uncertainty.

#### 4.2.4.2 Differential Scanning Calorimetry (DSC)

Differential scanning calorimetric measurements carried out using Hitachi DSC 7020 under $N_2$ atmosphere. Sealed aluminum pans were used as sample holder and reference pans. The range of DSC instrument is ±350 mW and sensitivity is 0.2 μW. DSC measurements were carried out by cooling the samples from 100 °C to -150 °C, followed by heating from -150 ℃ to 100 ℃ under $N_2$ atmosphere. $T_m$ and $T_g$ were determined from the heating curve in the DSC thermograms. Both cooling and heating scans were performed at a rate of 5.0 ℃ $min^{-1}$. A cooling system using liquid $N_2$ was installed in the system.

### 4.3. Results and Discussion

#### 4.3.1. UV shielding property

UV-shielding, also known as ultraviolet (UV) protection or UV-blocking, refers to the ability of a material or substance to block or reduce the penetration of harmful ultraviolet radiation from the sun or artificial UV sources. The prepared DSILs shows UV-sheilding phenomenon which is explain by the study of UV-visible spectroscopy.

**Table 4.1.** $\lambda_{max}$ and absorbance of ILs and DSILs

| DSILs | $\lambda_{max,}$ nm | Absorbance |
|---|---|---|
| $[C_4mim]CH_3CO_2$ | 352 | 0.34 |
| $[C_4mim](CH_3CO_2)_{0.9}Cl_{0.1}$ | 303 | 5.51 |
| $[C_4mim](CH_3CO_2)_{0.8}Cl_{0.2}$ | 311 | 1.73 |
| $[C_4mim](CH_3CO_2)_{0.7}Cl_{0.3}$ | 306 | 1.64 |
| $[C_4mim](CH_3CO_2)_{0.6}Cl_{0.4}$ | 304 | 0.97 |
| $[C_4mim](CH_3CO_2)_{0.5}Cl_{0.5}$ | 303 | 0.82 |
| $[C_4mim](CH_3CO_2)_{0.4}Cl_{0.6}$ | 295 | 1.04 |
| $[C_4mim](CH_3CO_2)_{0.3}Cl_{0.7}$ | 238 | 2.56 |
| $[C_4mim](CH_3CO_2)_{0.2}Cl_{0.8}$ | 229 | 2.76 |
| $[C_4mim](CH_3CO_2)_{0.1}Cl_{0.9}$ | 267 | 1.23 |
| $[C_4mim]Cl$ | 220 | 10.00 |

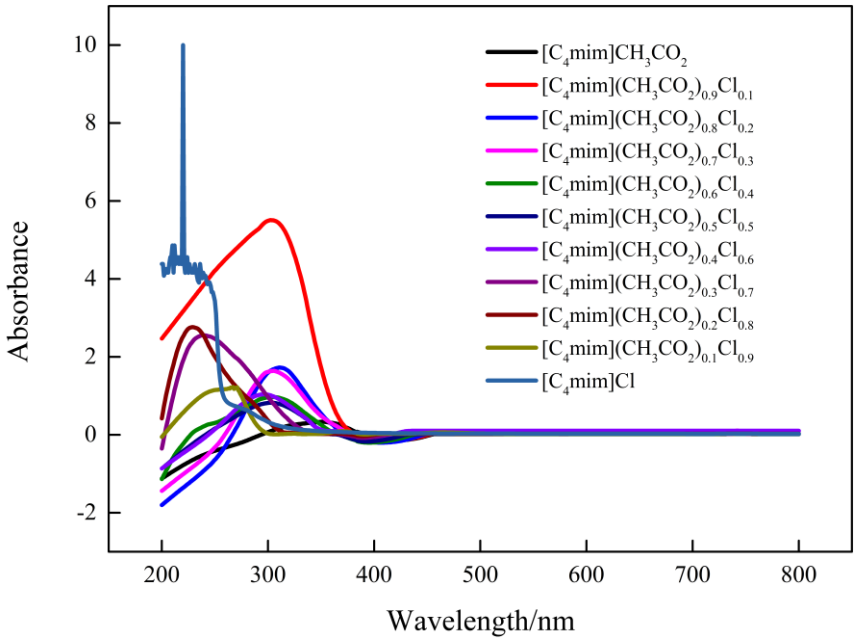


**Figure 4.1.** UV-visible absorption spectra of $[C_4mim]CH_3CO_2$, $[C_4mim]Cl$, and their DSILs

Fig. 4.1 depicts the absorption spectra of $[C_4mim]CH_3CO_2$ and $[C_4mim]Cl$ and their DSILs as measured with 1 cm path length cuvette without adding any solvent into the system. Almost in all cases, the absorption peak is located at around the UV region. The absorbance for each system is significant indicating strong interaction with UV light. Another important observation is the presence of long absorption tail for all the systems. In case of pure ILs, absorption bands are located at different wavelengths even though the cationic moiety is the same in both cases. Moreover, $[C_4mim]CH_3CO_2$ exhibits absorption peak of lower intensity compared to $[C_4mim]Cl$. In contrast, DSILs consisting of $[C_4mim]CH_3CO_2$ show significant increase in the intensity which is absent in case of pure $[C_4mim]CH_3CO_2$. Furthermore, absorption peaks of the DSILs are located at different wavelength depending on the composition of DSILs. The absorption band of pure ILs is due to the $\pi-\pi^*$ transition of the monomeric imidazolium molecule, and the extended absorption tail has been attributed to the presence of energetically different associated species. [23, 40]. This long absorption tail originates from the presence of imidazolium moiety and not because of impurities as it was thought before [21]. Fig. 4.2 depicts the variation of $\lambda_{max}$ with the increase in the amount of the $[C_4mim]Cl$. As the amount of $[C_4mim]Cl$ is increased, blue shift in $\lambda_{max}$ is observed which is closer to the $\lambda_{max}$ of the $[C_4mim]Cl$. The effect of anion on the absorption peak of the ILs and DSILs are noticeable. The anions contribute significantly towards the $\pi-\pi^*$ electronic transition of the imidazolium moiety. The blue shift towards shorter wavelengths with increasing $[C_4mim]Cl$ concentration suggests potential tuning of UV-shielding properties, while the role of anions highlights the importance of molecular structure in determining their UV-absorbing behavior. Table 4.1 lists the $\lambda_{max}$ and corresponding absorbance of the pure ILs and the DSILs. These wavelengths are utilized as excitation wavelength for the PL spectra. Samanta *et al.* have conducted study on the optical properties of imidazolium based ILs where UV-visible absorption spectra of $[C_4mim][PF_6]$ is reported. It has been noticed that the imidazolium based ILs generally show $\lambda_{max}$ at lower than 300 nm. This confirms the $\pi-\pi^*$ electronic transition of the imidazolium moiety of the ILs [39].

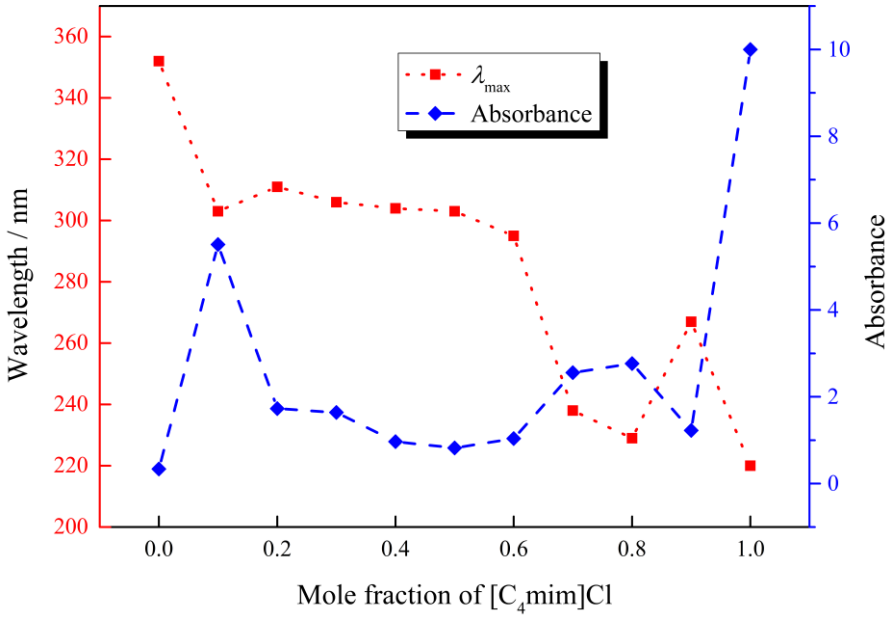


**Figure 4.2.** Variation of $\lambda_{max,}$ and absorbance of [$C_4$mim]Cl, [$C_4$mim]($CH_3CO_2$) and DSILs

### 4.3.2. Photoluminescence properties

Fig. 4.3 demonstrates the PL spectral behavior of both pure ILs and their DSILs. The fluorescence spectra of ILs and DSILs are obtained and two excitation wavelengths ($\lambda_{ex}$) were varied. Fig. 4.3 shows the PL spectra of the DSILs at $\lambda_{ex}$ of 200 nm. Significant number of emission bands are observed and most of these bands are located closer to the UV region of the spectra. Two intense bands are noticeable in this figure both of which is in the range of 220 to 270 nm wavelength. In case of [$C_4$mim]Cl 0.1, the most intense band is closer to the 220 nm and as the amount of [$C_4$mim]Cl increases the intensity of the band decreases. That is evident in case of [$C_4$mim]Cl 0.9 DSILs in which the second band has almost similar intensity compared to the first band. The high number of peaks present in the PL spectra with $\lambda_{ex}$ of 200 nm is due to the isolated imidazolium cation. Most of the single cation moiety is present in the DSILs in different energy states hence, more discrete peaks are observed. This indicates most of the single imidazolium cation population exist in the DSILs closer to the UV region of the of the PL spectra.

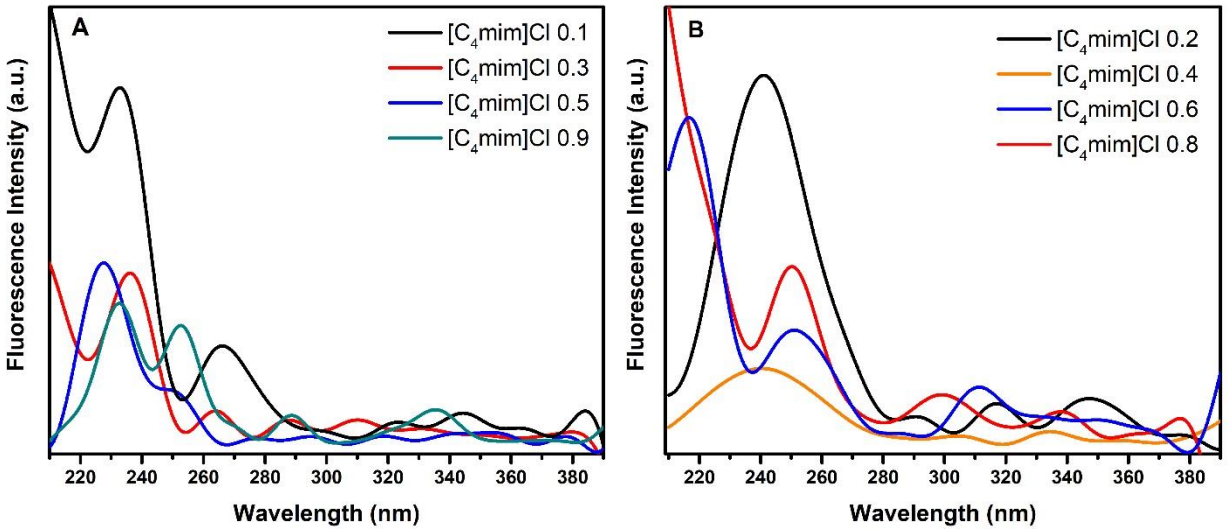


**Figure 4.3.** PL spectra of DSILs of [$C_4$mim]Cl and [$C_4$mim]($CH_3CO_2$) at $\lambda_{ex}$ = 200 nm

Fig. 4.4 depicts the PL spectra of the DSILs with $\lambda_{ex}$ optimized to the $\lambda_{max}$ of the corresponding DSILs obtained from the UV-visible absorption spectra. This was done to observe whether the DSILs exhibit emission spectra in visible region of the electromagnetic spectrum. This figure shows various broad bands of emission for different DSILs which gives peak at different wavelength than each other. This could be attributed towards the Red Edge Effect (REE), which results in photoluminescence dependent on the $\lambda_{ex}$ of the light irradiated. Due to irradiating the DSILs at different $\lambda_{ex}$, the position of the emission band varied for different DSILs. Intensity of the emission bands also varied for different DSILs. The lowest intensity is observed for the [$C_4$mim]Cl 0.1 whereas the highest intensity is exhibited by the [$C_4$mim]Cl 0.9. Emission of broad band at longer wavelength for all of the DSILs is due to the associative nature of the imidazolium cation present in the both the ILs [40]. Even in the pure ILs this association exists which suggest that this interaction also exists in the prepared DSILs. Moreover, the different anions affect the associative behavior between the molecules. One of the studies is conducted by varying the anion of the pure ILs which resulted in change in fluorescence behavior with similar imidazolium cation. It was found that the larger the anion, the lesser the association occurred between the IL molecules resulting in a blue shift in the PL spectra. However, this is only observed for the imidazolium based ILs [39]. Majhi *et al.* studied the effect of size of anion on the associative behavior of the imidazolium based ILs by using time resolved fluorescence spectroscopy, NMR and fluorescence correlation spectroscopy. They found the more the size of the anion, the lesser the aggregation

between the imidazolium cation and the anion. Interestingly, the particle size of the IL with larger anion has been found smaller compared to the particle size of the IL with smaller size of anion. This further confirms that association between the imidazolium cation and anion increases with the decrease in the size of the anion [40]. In this case, both $[C_4mim]Cl$ and $[C_4mim]CH_3CO_2$ contains same imidazolium cation but $Cl^-$ is smaller in size compared to the $CH_3CO_2^-$. So, $[C_4mim]Cl$ should exhibit more associative behavior than $[C_4mim]CH_3CO_2$.

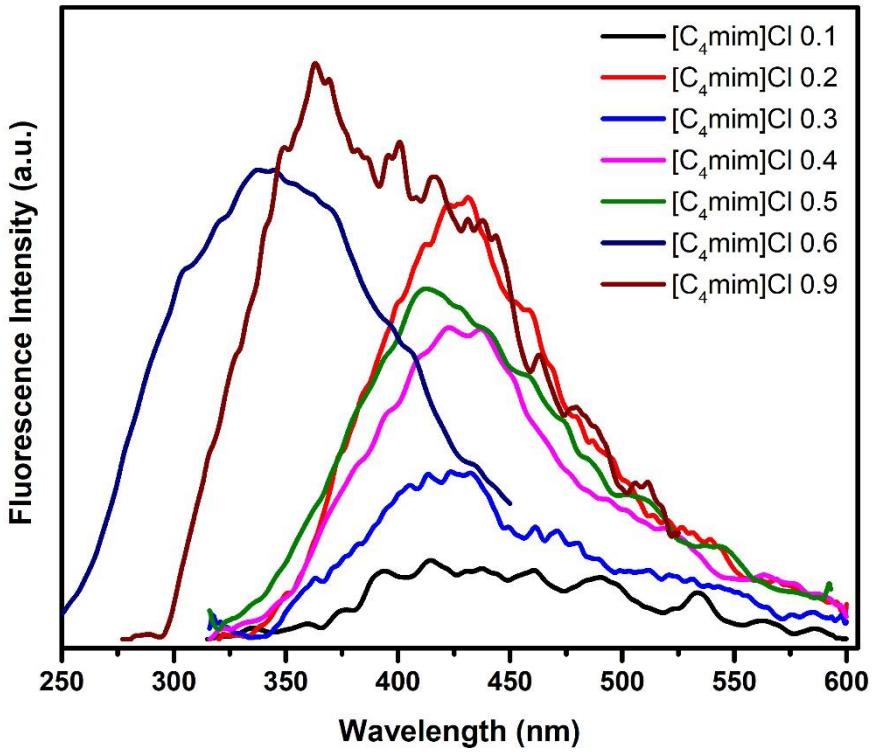


**Figure 4.4.** PL spectra of DSILs of $[C_4mim]Cl$ and $[C_4mim](CH_3CO_2)$ at $\lambda_{ex}$ optimized at $\lambda_{max}$ for corresponding DSILs

The PL spectra of the equimolar DSILs and ILs at 375 nm is given at Fig. 4.5. $[C_4mim](CH_3CO_2)$ exhibited intense emission band at ~450 nm whereas $[C_4mim]Cl$ showed a weak band at lower wavelengths than $[C_4mim](CH_3CO_2)$. As the DSILs are excited at wavelength 375 nm, the position of the emission band varied with the composition of DSILs. DSILs with higher composition of $[C_4mim](CH_3CO_2)$ showed intense emission band located around 450 nm. However, blue shift of the emission band is observed with increased composition of $[C_4mim]Cl$ in the DSILs. These PL spectra are expected to be convolution of individual bands arising from the distinct emission of associated structures in the ILs.

[$C_4$mim]Cl exhibited band at lower wavelength due to the anion effect. Both ILs used in this work are imidazolium based and have the same cation. Hence, any change in the optical properties of the DSILs is related to the effect of anion. Generally, the size of the anion affects the fluorescence behavior of the ILs [39]. The association within IL moieties increased with the decrease in the size of the anion, in this case $Cl^-$ has higher ionic radius compared to $CH_3CO_2^-$. As a result, [$C_4$mim]($CH_3CO_2$) exhibits red shifted and intense band compared to [$C_4$mim]Cl. Intensity of the PL spectra of the DSILs varied according to the composition of the ILs.

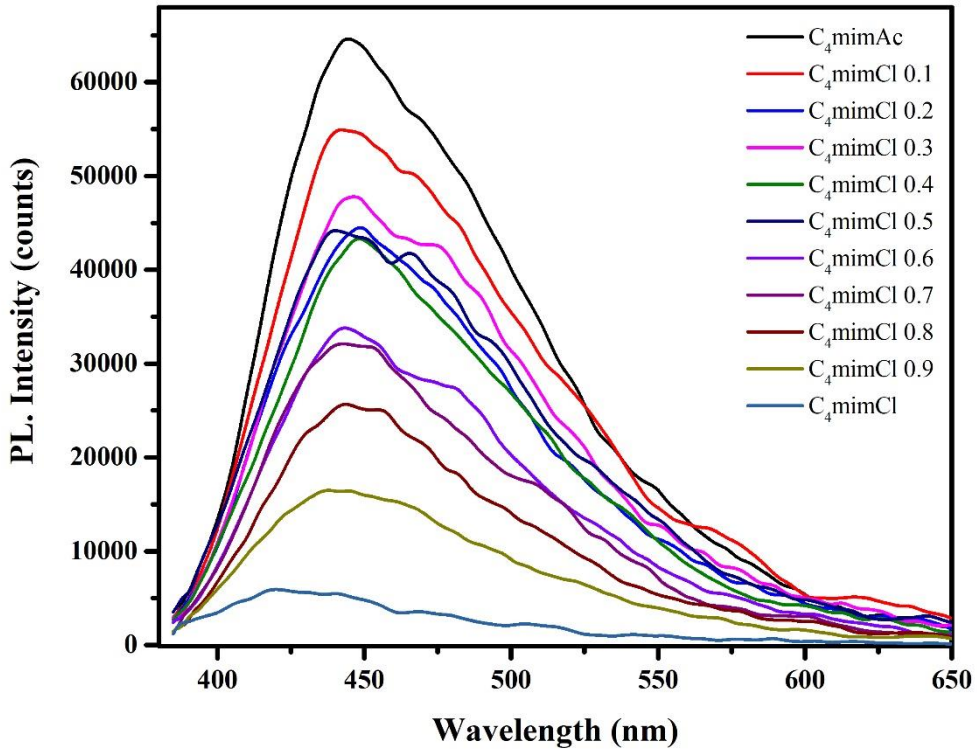


**Figure 4.5.** PL spectra of [$C_4$mim]Cl and [$C_4$mim]($CH_3CO_2$) and their DSILs at various composition ($\lambda_{ex}$ = 375 nm)

The intensity of the bands is dependent on the specific extinction co-efficient and the degree of association of the ILs. Interestingly, the intensity of the band for [$C_4$mim]$Cl_{0.2}(CH_3CO_2)_{0.8}$ lowered compared to [$C_4$mim]$Cl_{0.3}(CH_3CO_2)_{0.7}$. [$C_4$mim]$Cl_{0.4}(CH_3CO_2)_{0.6}$ and [$C_4$mim]$Cl_{0.5}(CH_3CO_2)_{0.5}$ exhibit peaks located at longer and shorter wavelength with similar intensity, respectively. PL Bands of [$C_4$mim]$Cl_{0.2}(CH_3CO_2)_{0.8}$ and [$C_4$mim]$Cl_{0.4}(CH_3CO_2)_{0.6}$ has identical peak shape and a presence of weak shoulder located around emission maxima. In contrast to, spectra of [$C_4$mim]$Cl_{0.3}(CH_3CO_2)_{0.7}$ and

$[C_4mim]Cl_{0.5}(CH_3CO_2)_{0.5}$ shows similar shape with a presence of shoulder with noticeable intensity. Other PL bands of the DSILs show significant decrease in the intensity due to the presence of higher composition of the $[C_4mim]Cl$.

Reduced intensity of the $[C_4mim]Cl_{0.2}(CH_3CO_2)_{0.8}$ indicates probable reduction of the associated structures in the DSILs whereas, increase in the intensity of the $[C_4mim]Cl_{0.3}(CH_3CO_2)_{0.7}$ suggests formation of new association. This association of the DSILs occurs as a consequence of microheterogeneities arising from two different anion groups existing in the same mixture at different compositions.

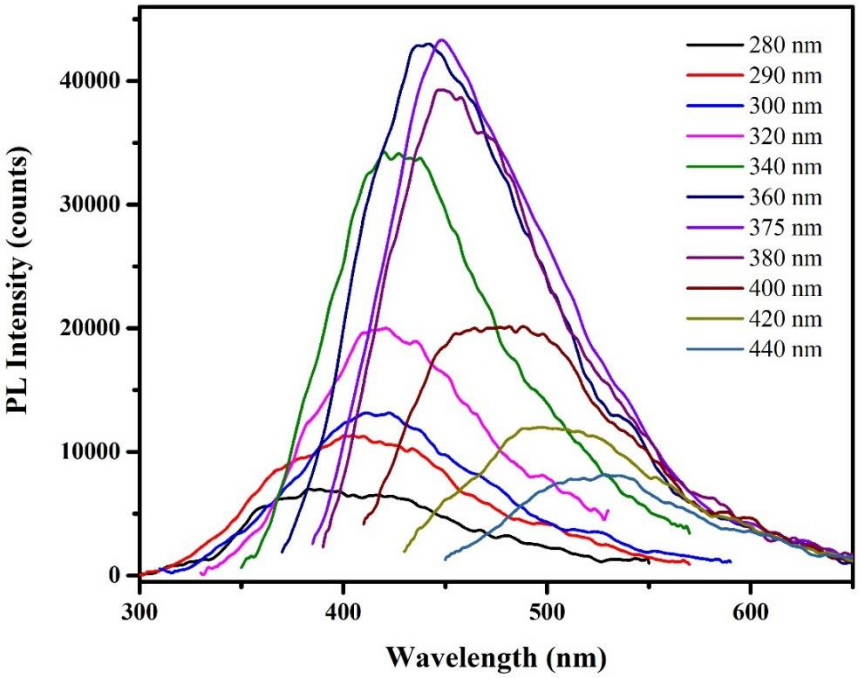


**Figure 4.6.** PL spectra of pure $[C_4mim]Cl_{0.4}(CH_3CO_2)_{0.6}$ DSIL with different $\lambda_{ex}$ ranging from 280 to 440 nm

The different association of IL moieties exist at different state of energies in the DSILs which exhibit emission at different wavelength depending on the $\lambda_{ex}$ of the light. $[C_4mim]Cl_{0.4}(CH_3CO_2)_{0.6}$ has been utilized to dissolve cellulose and then recycled from the solution. To differentiate between the fluorescence behavior of $[C_4mim]Cl_{0.4}(CH_3CO_2)_{0.6}$, $\lambda_{ex}$ dependent fluorescence has been conducted for both pure and recycled DSIL. $\lambda_{ex}$ has been varied from 280-440 nm to identify the presence of different interaction between both the ILs. Fig. 4.6 and 4.7 depicts the fluorescence spectra for pure and recycled $[C_4mim]Cl_{0.4}(CH_3CO_2)_{0.6}$,

respectively. It is observed from Fig. 4.6 as the $\lambda_{ex}$ increases the emission peak shifted towards longer wavelength exhibiting Red Edge Effect (REE). At $\lambda_{ex}$ = 280 and 290 nm, emission wavelength is located at ~400 nm with increasing intensity, respectively. Similarly, from $\lambda_{ex}$ = 300-340 nm, red shifting of the emission band is observed with increasing intensity. Emission spectra for $\lambda_{ex}$ = 360 nm exhibit significant band shift towards longer wavelength around ~450 nm with maximum intensity. In contrast to PL spectra at longer wavelengths (>360 nm), showed continuous red shifting with decreasing intensity.

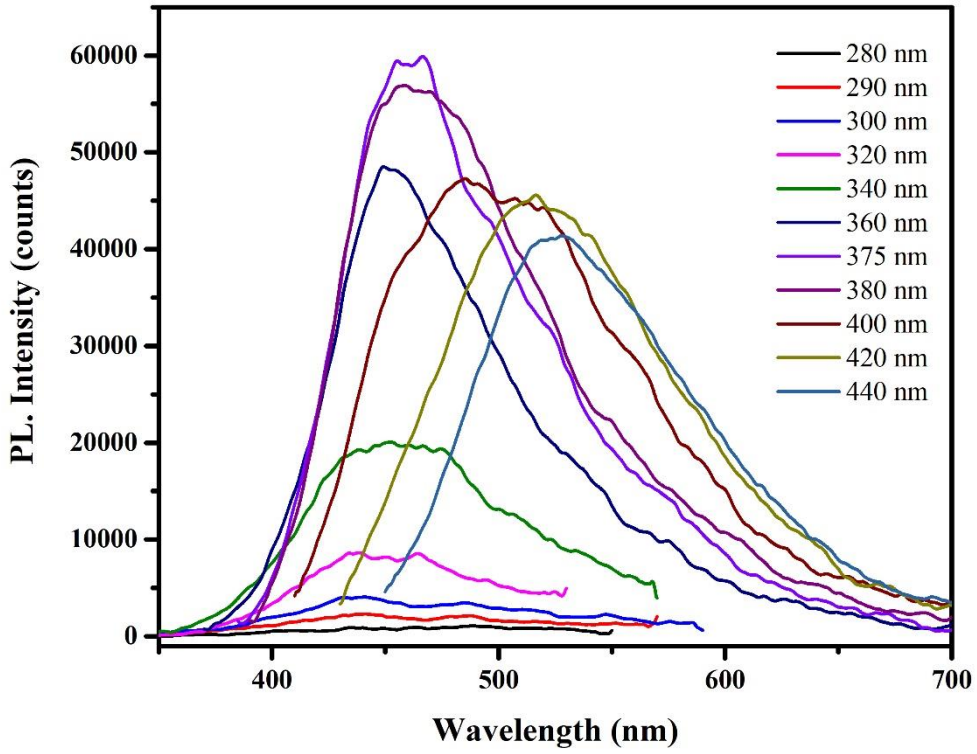


**Figure 4.7.** PL spectra of recycled $[C_4mim]Cl_{0.4}(CH_3CO_2)_{0.6}$ DSIL with different $\lambda_{ex}$ ranging from 280 to 440 nm

Emission spectra at $\lambda_{ex}$ = 375 nm, showed maximum emission intensity indicating the association species at this energy level is mostly present in the DSIL. Hence, other distinct association species are lower in population compared to the former one. In case of recycled $[C_4mim]Cl_{0.4}(CH_3CO_2)_{0.6}$, REE is observed and peak intensity for $\lambda_{ex}$ = 280-300 nm exhibits lower intensity compared to the synthesized DSILs which indicates depletion of associated species in that energy state. In contrast to DSILs, associated species with low energy states increased in population which may have been caused by interaction with cellulose molecules and existing associative moieties. This observation

suggests that during the dissolution of cellulose in the DSILs, certain association moieties broke down and other moieties started to build up. Even though ILs are highly recyclable, cellulose molecules persisted in the recycled IL.

### 4.3.3. Thermal properties of ILs and DSILs

Thermal properties of prepared ILs and DSILs have been investigated by TGA and DSC. The thermal stability has been determined by the TGA while the thermal parameters have been identified using the DSC technique. Table 4.2 lists the $T_g$ and $T_d$ of the single ILs and DSILs. $T_g$ has been determined using the DSC analysis whereas the $T_d$ has been evaluated from the thermograms of the samples. Thermograms of $[C_4mim]Cl$, $[C_4mim]\ CH_3CO_2$, and their DSILs have been depicted in Fig. 4.8.

**Table 4.2.** Determination of glass transition temperature ($T_g$ ) and decomposition temperature ($T_d$) of DSILs at different temperature

| **DSILs** | $T_g$ / °C | $T_d$ / °C | |
|---|---|---|---|
| | | 1st | 2nd |
| $[C_4mim]CH_3CO_2$ | -65.5 | 218.9 | - |
| $[C_4mim](CH_3CO_2)_{0.9}Cl_{0.1}$ | -68.3 | 224.6 | 268.8 |
| $[C_4mim](CH_3CO_2)_{0.8}Cl_{0.2}$ | -70.3 | 222.0 | 279.5 |
| $[C_4mim](CH_3CO_2)_{0.7}Cl_{0.3}$ | -69.0 | 221.7 | 280.0 |
| $[C_4mim](CH_3CO_2)_{0.6}Cl_{0.4}$ | -67.6 | 223.3 | 277.8 |
| $[C_4mim](CH_3CO_2)_{0.5}Cl_{0.5}$ | -61.6 | 224.3 | 278.2 |
| $[C_4mim](CH_3CO_2)_{0.4}Cl_{0.6}$ | -63.8 | 221.8 | 277.2 |
| $[C_4mim](CH_3CO_2)_{0.3}Cl_{0.7}$ | -65.9 | 223.8 | 279.0 |
| $[C_4mim](CH_3CO_2)_{0.2}Cl_{0.8}$ | -64.7 | 224.1 | 277.4 |
| $[C_4mim](CH_3CO_2)_{0.1}Cl_{0.9}$ | -65.4 | 218.8 | 274.5 |
| $[C_4mim]Cl$ | -61.0 | 263.1 | - |

ILs $[C_4mim]$ Cl and $[C_4mim]\ CH_3CO_2$ exhibits single $T_d$ in contrast to DSILs which consists of two distinct $T_d$ as observed from the thermogram. This observation is consistent with the fact that DSILs are mixture of two ILs having two different $T_d$. The first $T_d$ of the DSILs is

related to the [$C_4$mim] $CH_3CO_2$ component and the second $T_d$ at a higher temperature than the former corresponds to the [$C_4$mim] Cl component. One interesting observation is that, both $T_d$ in case of DSILs have increased from its respective pure components. This increase in $T_d$ suggests that DSILs have higher thermal stability than ILs. The first $T_d$ increased to a maximum of 224.6 ℃ which is ~6 ℃ from the $T_d$ of the [$C_4$mim]$CH_3CO_2$. Similarly, the second $T_d$ for the DSILs increased to a maximum of 280.0 ℃ which is ~17 ℃ more than the $T_d$ of [$C_4$mim] Cl. This enhancement of $T_d$ indicates that the DSILs exhibit a noticeable change in thermal behavior compared to the ILs. Fig. 4.9 shows the variation of first and second $T_d$ with increasing mole fraction of [$C_4$mim] Cl. $T_d$ values vary with the mole fraction of [$C_4$mim] Cl and the first and second $T_d$ values are confined within range of ~225 and ~280 ℃, respectively. DTG curves of the corresponding TGA curves gives insight into the thermal behavior of the prepared DSILs. Fig. 4.10 depicts the DTG curves for the corresponding TGA curves. As expected, pure ILs show only single significant loss of mass. DSILs exhibits two peaks which corresponds to the loss of mass corresponding to the components of the pure ILs in the DSILs mixtures. Moreover, the extent of loss of mass for each component in the DSILs depends on its mole fraction. As the mole fraction of any component increases, the loss of mass for that component in DSILs also increases which is expected.

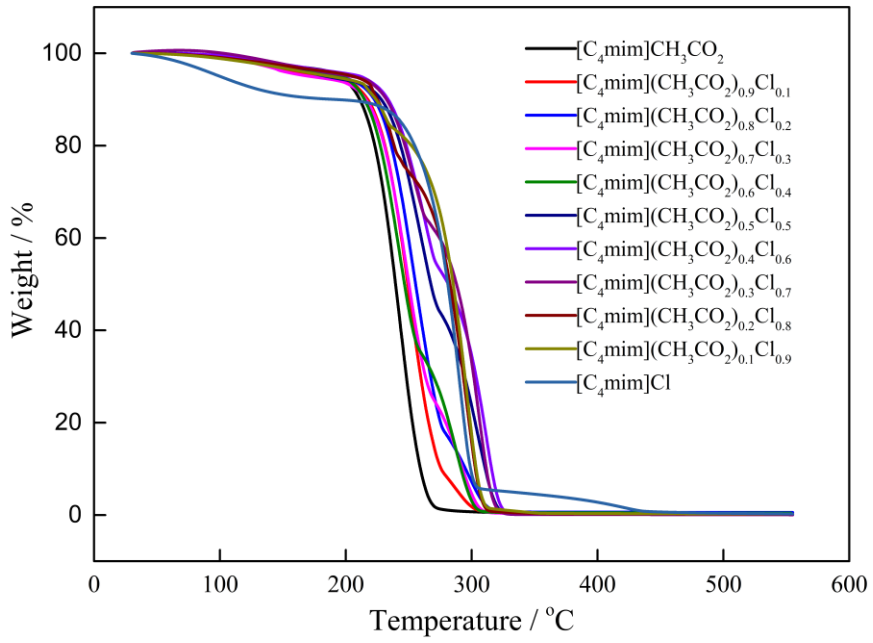


**Figure 4.8.** TGA curves of DSILs

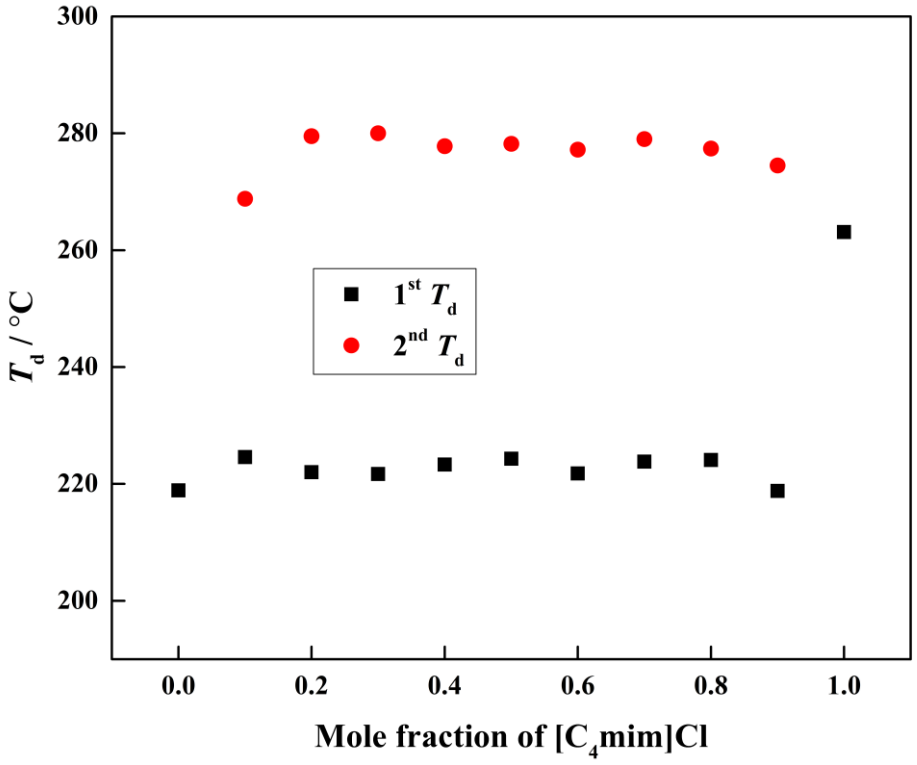


**Figure 4.9.** 1st and 2nd decomposition temperature of DSILs

The thermal decomposition of the ILs occurs by the complete structural degradation of the imidazolium ring. As both of the ILs and DSILs consists of $[C_4mim]^+$ cation and under thermal treatment at the range of 218-280 ℃ completely degrades the $[C_4mim]^+$ cation [41]. The variation in the thermal stability between the ILs and their DSILs arises from the anions. As expected, inorganic anion, $Cl^-$ is much more thermally stable compared to the organic $CH_3CO_2^-$ anion. Hence, $[C_4mim]Cl$ is slightly more stable compared to $[C_4mim]CH_3CO_2$. The higher thermal stability of the DSILs in comparison to ILs is interesting to observe. These DSILs consisting of various mole fractions of two different ILs behave as solutions to an extent. DSILs $[C_4mim](CH_3CO_2)_x Cl_{1-x}$, behave somewhat as solution. This solution exhibits higher thermal stability due to two reasons. One, the colligative properties of the solution can be responsible for the enhanced thermal stability and second, there is the presence of associative species in the DSILs, as suggested from its PL spectra, which contribute towards the higher thermal decomposition temperature of the DSILs. Fig. 4.11 illustrates the DTA curves of the prepared ILs and DSILs. Curves related to the single ILs exhibit a single endothermic peak indicating the decomposition of the ILs. In contrast

to, DSILs show two different endothermic peaks suggesting the decomposition of individual component of

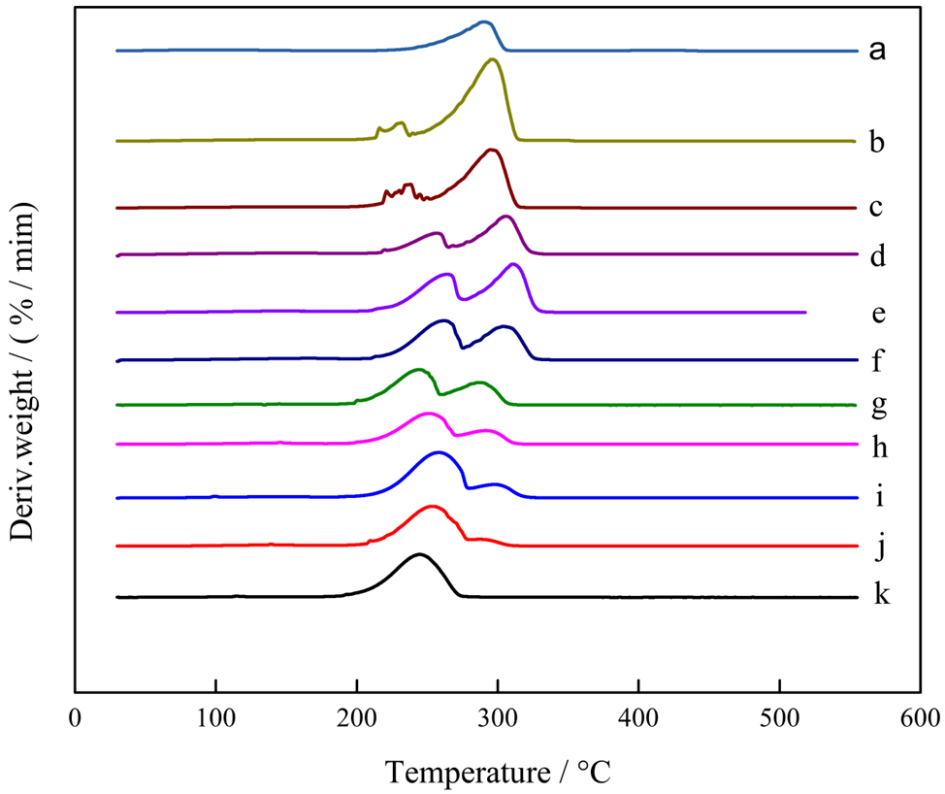


**Figure 4.10.** DTG thermographs of (a) $[C_4mim]Cl$, (b) $[C_4mim](CH_3CO_2)_{0.1}Cl_{0.9}$ (c) $[C_4mim](CH_3CO_2)_{0.2}Cl_{0.8}$ (d) $[C_4mim](CH_3CO_2)_{0.3}Cl_{0.7}$ (e) $[C_4mim](CH_3CO_2)_{0.4}Cl_{0.6}$ (f) $[C_4mim](CH_3CO_2)_{0.5}Cl_{0.5}$ (g) $[C_4mim](CH_3CO_2)_{0.6}Cl_{0.4}$ (h) $[C_4mim](CH_3CO_2)_{0.7}Cl_{0.3}$ (i) $[C_4mim](CH_3CO_2)_{0.8}Cl_{0.2}$ (j) $[C_4mim](CH_3CO_2)_{0.9}Cl_{0.1}$ (k) $[C_4mim]CH_3CO_2$. (b) (c) (d) (e) (f) (h) (i) under an $N_2$ atmosphere

the DSILs. This is an expected result which has been previously discussed in the results of TGA and DTG curves. As there are two different components in the DSILs, two different $T_d$ are observed and the generated heat is proportional to the mole fraction of each component in the DSILs. Decomposed gas of the corresponding ILs and DSILs may consist of 4 species, $NH_4^+$, $CH_3^+$, $CH_3Cl^+$, $C_3H_2N^+$, and $C_4H_4$ [41]. These species indicate the decomposition of the imidazolium ring. Moreover, the presence of inorganic ions such as $Cl^-$ increases the thermal stability of the $[C_4mim]Cl$ and also the DSILs in comparison to the $[C_4mim]CH_3CO_2$.

Fig. 4.12 illustrates ITG curves of ILs and DSILs at 120 ℃ for 120 min to determine whether any processes are propagating at this particular temperature. The curves of $[C_4mim]CH_3CO_2$ and DSILs gradually decreased at this temperature however, $[C_4mim]Cl$ shows a decrease in different steps. This change is responsible for the evaporation of trapped water in the IL structure. Single ILs and DSILs are thermally stable under 120 ℃ and can be used at solvent in this temperature window.

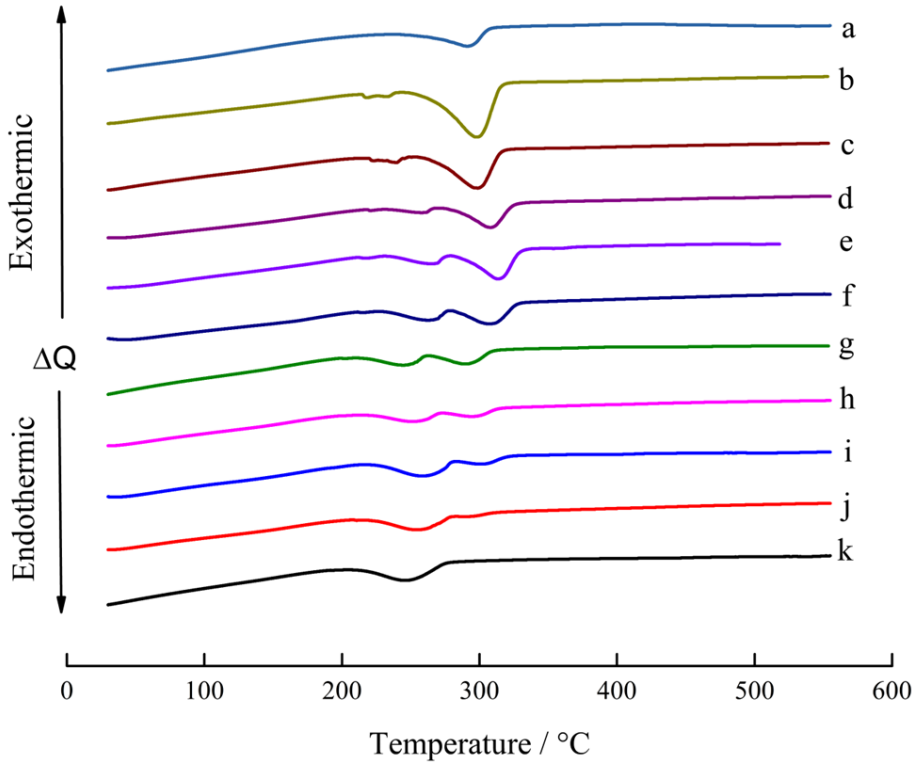


**Figure 4.11.** DTA thermographs of (a) $[C_4mim]Cl$, (b) $[C_4mim](CH_3CO_2)_{0.1}Cl_{0.9}$ (c) $[C_4mim](CH_3CO_2)_{0.2}Cl_{0.8}$ (d) $[C_4mim](CH_3CO_2)_{0.3}Cl_{0.7}$ (e) $[C_4mim](CH_3CO_2)_{0.4}Cl_{0.6}$ (f) $[C_4mim](CH_3CO_2)_{0.5}Cl_{0.5}$ (g) $[C_4mim](CH_3CO_2)_{0.6}Cl_{0.4}$ (h) $[C_4mim](CH_3CO_2)_{0.7}Cl_{0.3}$ (i) $[C_4mim](CH_3CO_2)_{0.8}Cl_{0.2}$ (j) $[C_4mim](CH_3CO_2)_{0.9}Cl_{0.1}$ (k) $[C_4mim]CH_3CO_2$

$T_g$ and heat capacities of ILs and prepared DSILs have been investigated with DSC technique. Table 4.3. enlists the various heat capacity of the prepared DSILs within –23 to 37 ℃ temperature. Fig. 4.13 shows the heating curve of the prepared DSILs from –100 to 10 ℃. This figure shows the presence of one endothermic peak which corresponds to the $T_g$ of the DSILs. This $T_g$ brings about changes in the properties of the DSILs. DSILs forms amorphous glass like phase during cooling and upon heating this amorphous glass transforms into liquid. One interesting observation is the absence of freezing or melting points in the DSC curves even though the DSILs are liquid at

room temperature. From literature, [$C_4$mim] Cl and [$C_4$mim] $CH_3CO_2$, show $T_g$ at –69 and –70 °C, respectively [42, 43]. In this study, [$C_4$mim] Cl and [$C_4$mim] $CH_3CO_2$ show different $T_g$ located at –61.0 and –65.3 °C, respectively. [$C_4$mim]$(CH_3CO_2)_{0.9}Cl_{0.1}$ exhibit significantly higher $T_g$ compared to their ILs components. As the mole fraction of [$C_4$mim]Cl increased the $T_g$ decreased. However, further increasing the mole fraction of [$C_4$mim] Cl increased the $T_g$ closer to the value of the ILs. [$C_4$mim] $(CH_3CO_2)_{0.5}$ $Cl_{0.5}$ again show larger value of $T_g$ similar to the [$C_4$mim] Cl. This fluctuation of $T_g$ highly depends on the arrangement of the ILs moieties in DSILs as well as the mole fraction of the ILs components.

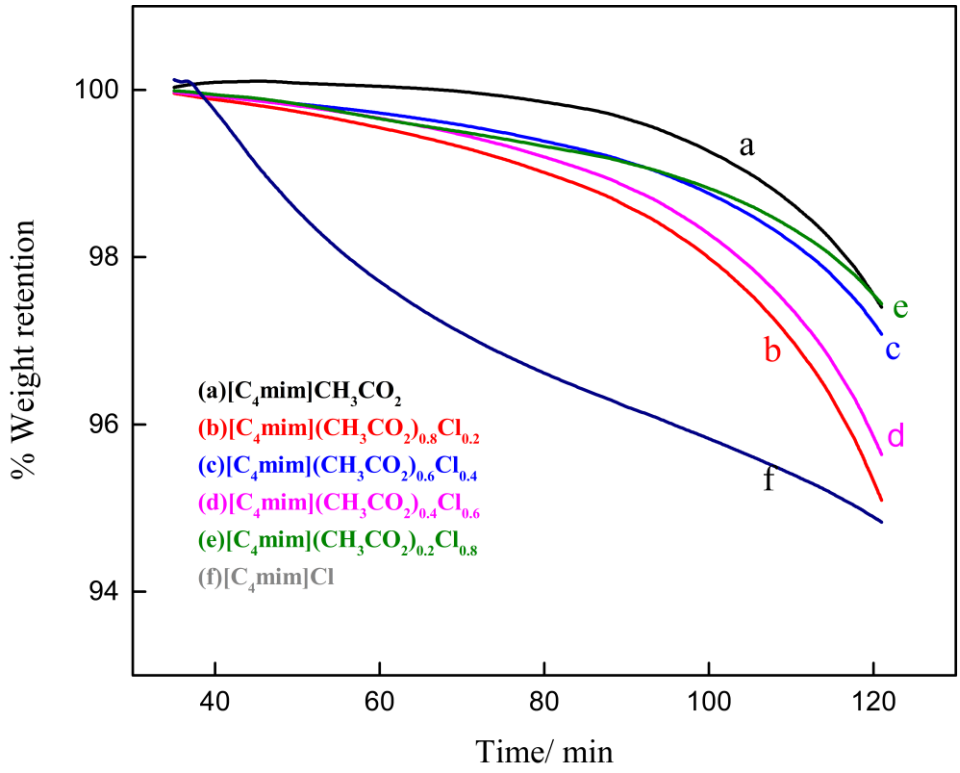


**Figure 4.12.** ITG curves of (a) [$C_4$mim]$CH_3CO_2$ (b) [$C_4$mim]$(CH_3CO_2)_{0.8}Cl_{0.2}$ (c) [$C_4$mim]$(CH_3CO_2)_{0.6}Cl_{0.4}$ (d) [$C_4$mim]$(CH_3CO_2)_{0.4}Cl_{0.6}$ (e) [$C_4$mim]$(CH_3CO_2)_{0.2}Cl_{0.8}$ (f) [$C_4$mim]Cl at 120 °C for 2 h under an $N_2$ atmosphere

Heat capacities of the prepared DSILs show various results depending on the combination of the ILs components. As expected, the $C_p$ values increase with the increase in the operation temperature. [$C_4$mim]$(CH_3CO_2)_{0.9}Cl_{0.1}$ and [$C_4$mim]$(CH_3CO_2)_{0.2}Cl_{0.8}$ shows more or less similar values of $C_p$ ranging from ~329 to 386 J $K^{-1}$ $mol^{-1}$ along in the range of –23 to 37 °C. [$C_4$mim]$(CH_3CO_2)_{0.8}Cl_{0.2}$ shows uniquely lower values of $C_p$ at the higher temperature compared

to other DSILs. $[C_4mim](CH_3CO_2)_{0.7}Cl_{0.3}$ and $[C_4mim](CH_3CO_2)_{0.3}Cl_{0.7}$ exhibits similar values of $C_p$ increasing up to ~307 J $K^{-1}$ $mol^{-1}$. $[C_4mim](CH_3CO_2)_{0.6}Cl_{0.4}$ is exhibits increased heat capacity at 37 °C. Finally, $[C_4mim](CH_3CO_2)_{0.5}Cl_{0.5}$ and $[C_4mim](CH_3CO_2)_{0.4}Cl_{0.6}$ shows similar values of $C_p$ starting initially from ~175-185 and ending up at 324-338 J $K^{-1}$ $mol^{-1}$. The variation of heat capacities depends on the presence of molecules and their degree of freedoms.

**Table 4.3.** Heat capacity of DSILs media at different temperatures

| **DSILs** | **Heat capacity ($C_p$, J $K^{-1}$ $mol^{-1}$)** | | | | | | |
|---|---|---|---|---|---|---|---|
| | 250 K | 260 K | 270 K | 280 K | 290 K | 300 K | 310 K |
| $[C_4mim](CH_3CO_2)_{0.9}Cl_{0.1}$ | 365.13 | 362.63 | 371.32 | 383.10 | 391.03 | 394.02 | 386.80 |
| $[C_4mim](CH_3CO_2)_{0.8}Cl_{0.2}$ | 258.64 | 281.21 | 252.62 | 248.77 | 256.20 | 210.63 | 150.41 |
| $[C_4mim](CH_3CO_2)_{0.7}Cl_{0.3}$ | 276.87 | 249.80 | 268.34 | 286.00 | 308.41 | 309.40 | 307.20 |
| $[C_4mim](CH_3CO_2)_{0.6}Cl_{0.4}$ | 241.95 | 181.67 | 238.90 | 216.02 | 294.84 | 260.72 | 324.15 |
| $[C_4mim](CH_3CO_2)_{0.5}Cl_{0.5}$ | 186.15 | 264.31 | 239.22 | 256.22 | 250.45 | 293.25 | 338.39 |
| $[C_4mim](CH_3CO_2)_{0.4}Cl_{0.6}$ | 175.91 | 176.92 | 135.72 | 211.62 | 273.21 | 291.96 | 314.64 |
| $[C_4mim](CH_3CO_2)_{0.3}Cl_{0.7}$ | 283.27 | 260.26 | 292.08 | 300.84 | 307.51 | 308.93 | 306.79 |
| $[C_4mim](CH_3CO_2)_{0.2}Cl_{0.8}$ | 340.79 | 329.74 | 343.31 | 353.78 | 360.10 | 362.20 | 342.00 |
| $[C_4mim](CH_3CO_2)_{0.1}Cl_{0.9}$ | 282.32 | 304.37 | 292.66 | 296.15 | 302.34 | 301.77 | 307.64 |

DSIL moieties contribute towards the storing heat through translational, vibrational, and rotational motions. Hence, the higher the degree of freedoms of the IL moieties, the higher the $C_p$. The DSILs show lowered $C_p$ compared to $[C_4mim]$ $CH_3CO_2$ whereas the $C_p$ of the increased in contrast to $[C_4mim]$ Cl. As the number of molecules in the DSILs increases, the energy storage modes also increase and thus, the overall heat capacity increases as well [42]. The effect of anion is another factor affecting the value of $C_p$. The higher the size of the anion, the higher the heat capacity hence, when the $Cl^-$ is added into the $[C_4mim]CH_3CO_2$, heat capacity increases.

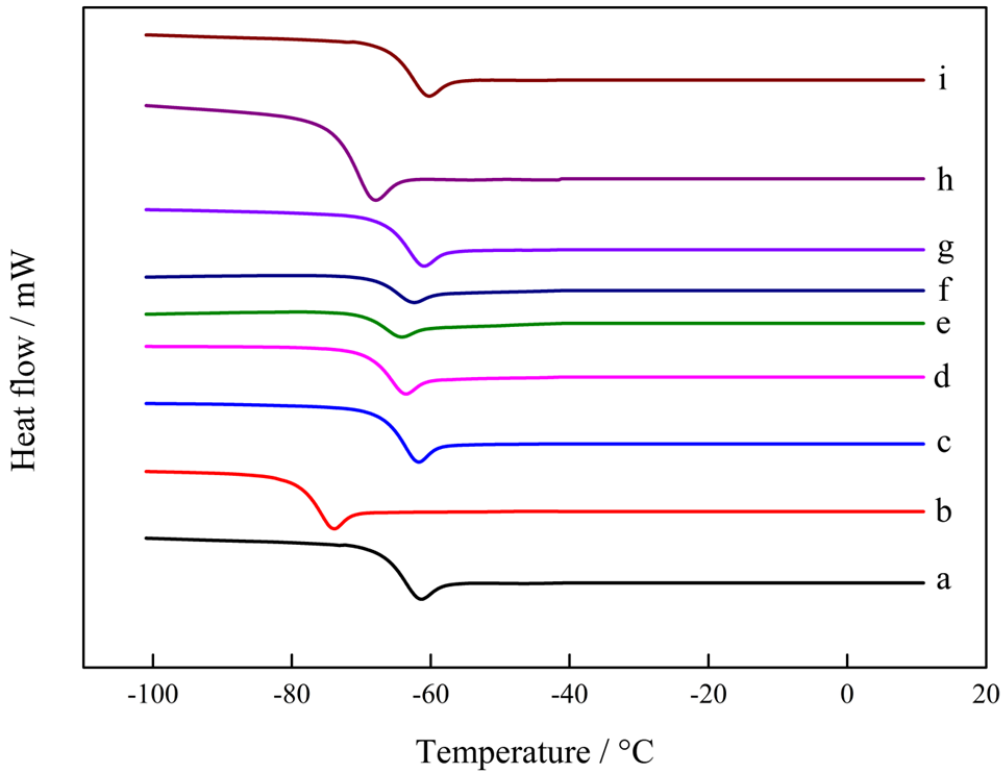


**Figure 4.13.** DSC thermographs of (a) $[C_4mim](CH_3CO_2)_{0.9}Cl_{0.1}$ (b) $[C_4mim](CH_3CO_2)_{0.8}Cl_{0.2}$ (c) $[C_4mim](CH_3CO_2)_{0.7}Cl_{0.3}$ (d) $[C_4mim](CH_3CO_2)_{0.6}Cl_{0.4}$ (e) $[C_4mim](CH_3CO_2)_{0.5}Cl_{0.5}$ (f) $[C_4mim](CH_3CO_2)_{0.4}Cl_{0.6}$ (g) $[C_4mim](CH_3CO_2)_{0.3}Cl_{0.7}$ (h) $[C_4mim](CH_3CO_2)_{0.2}Cl_{0.8}$ (i) $[C_4mim](CH_3CO_2)_{0.1}Cl_{0.9}$ under an $N_2$ atmosphere

## 4.4. Conclusions

In this work, the optical and the thermal analysis of single ILs and DSILs have been carried out to gain insight into the optical and thermal behavior of the subjected materials. The optical properties of ILs and DSILs have been investigated using fluorescence spectroscopy. One particular DSIL sample with superior cellulose dissolution capability has also been subjected to fluorescence spectroscopy to find any changes in the optical behavior of DSILs after recycling. On the other hand, the thermal stabilities and the identification of thermal processes have been studied using TGA and DSC techniques. Fluorescence spectra of the samples reveal the self-association behavior of the ILs and DSILs moieties. The presence of the imidazolium ring in both samples contribute towards the emission spectra. Interestingly, two different emission spectra are observed at higher and lower wavelengths which corresponds to the single and associative imidazolium ring. Moreover, the recycled DSIL from the cellulose solution exhibit different properties compared to only DSIL. Recycled DSIL shows increased formation of associative species than the DSIL prior to recycling. Cellulose molecules thus, modifies the association behavior of the DSILs. Thermal analysis has been carried out in three stages. First, thermal stabilities of the ILs and the DSILs have been determined from the TGA analysis. ILs and DSILs both exhibit good thermal stability at around 220-250 ℃. Interestingly, the mixtures of ILs show increased $T_d$ in comparison to single ILs which is a positive factor in case of industrial usage. DSC has been carried out to find the glass transition temperature ($T_g$) and determine the heat capacity ($C_p$) of the DSILs. $T_g$ of ILs are observed at higher temperature than other literature. The $T_g$ of the DSILs do not drastically deviate from the single ILs however, it slightly decreased. All of the values of $T_g$ for DSILs did not exceed the individual values of the ILs. $C_p$ of the DSILs increased proportionally with increasing temperature as expected. As the $CH_3CO_2$ species increased, $C_p$ of the DSILs also increased. Hence, the anion and their composition in the DSILs largely affects their $C_p$. The above-mentioned properties of ILs and DSILs will open new pathways for applications such as the dissolution of cellulose, efficient reaction medium, optoelectronics, photoelectrochemical applications, sustainable fuel cell materials, and so on.

**References**

[1] Roy, K., Kar, S., and Das, R. N. (2015). Chapter 12-Future Avenues. *Roy K, Kar S, Das RN, Book Title-Understanding the Basics of QSAR for Applications in Pharmaceutical Sciences and Risk Assessment (eds). Academic Press, Boston*, 455-462.

[2] Singh, S. K., and Dhepe, P. L. (2016). Ionic liquids catalyzed lignin liquefaction: mechanistic studies using TPO-MS, FT-IR, RAMAN and 1D, 2D-HSQC/NOSEY NMR. *Green Chemistry*, *18*(14), 4098-4108.

[3] Zhao, D., Wu, M., Kou, Y., and Min, E. (2002). Ionic liquids: applications in catalysis. *Catalysis Today*, *74*(1-2), 157-189.

[4] MacFarlane, D. R., Tachikawa, N., Forsyth, M., Pringle, J. M., Howlett, P. C., Elliott, G. D., Davis Jr., J. H., Watanabe, M., Simon, P. and Angell, C. A. (2014). Energy applications of ionic liquids. *Energy and Environmental Science*, *7*(1), 232-250.

[5] Plechkova, N. V., and Seddon, K. R. (2008). Applications of ionic liquids in the chemical industry. *Chemical Society Reviews*, *37*(1), 123-150.

[6] Liang, L., Gan, Q., and Nancarrow, P. (2014). Composite ionic liquid and polymer membranes for gas separation at elevated temperatures. *Journal of Membrane Science*, *450*, 407-417.

[7] Seddon, K. (2002). Ionic liquids: designer solvents for green synthesis. *Chemical Engineer*, 730, 33-35.

[8] Hospido, A., and Rodríguez, H. (2019). Life cycle assessment (LCA) of ionic liquids. In Encyclopedia of ionic liquids, *Springer Singapore*, 1-9.

[9] Jordan, A., Haiß, A., Spulak, M., Karpichev, Y., Kümmerer, K., and Gathergood, N. (2016). Synthesis of a series of amino acid derived ionic liquids and tertiary amines: green chemistry metrics including microbial toxicity and preliminary biodegradation data analysis. *Green Chemistry*, *18*(16), 4374-4392.

[10] Chen, L., Sharifzadeh, M., Mac Dowell, N., Welton, T., Shah, N., and Hallett, J. P. (2014). Inexpensive ionic liquids: $[HSO_4]^-$-based solvent production at bulk scale. *Green Chemistry*, *16*(6), 3098-3106.

[11] Egorova, K. S., and Ananikov, V. P. (2014). Toxicity of ionic liquids: eco (cyto) activity as complicated, but unavoidable parameter for task-specific optimization. *ChemSusChem*, *7*(2), 336-360.

[12] Diallo, A. O., Len, C., Morgan, A. B., and Marlair, G. (2012). Revisiting physico-chemical hazards of ionic liquids. *Separation and Purification Technology*, *97*, 228-234.

[13] Maculewicz, J., Świacka, K., Stepnowski, P., Dołżonek, J., and Białk-Bielińska, A. (2022). Ionic liquids as potentially hazardous pollutants: Evidences of their presence in the environment and recent analytical developments. *Journal of Hazardous Materials*, 129353.

[14] Chatel, G., Pereira, J. F., Debbeti, V., Wang, H., and Rogers, R. D. (2014). Mixing ionic liquids– "simple mixtures" or "double salts"?. *Green Chemistry*, *16*(4), 2051-2083.

[15] Clough, M. T., Crick, C. R., Gräsvik, J., Hunt, P. A., Niedermeyer, H., Welton, T., and Whitaker, O. P. (2015). A physicochemical investigation of ionic liquid mixtures. *Chemical Science*, *6*(2), 1101-1114.

[16] Canongia Lopes, J. N., Cordeiro, T. C., Esperança, J. M., Guedes, H. J., Huq, S., Rebelo, L. P., and Seddon, K. R. (2005). Deviations from ideality in mixtures of two ionic liquids containing a common ion. *The Journal of Physical Chemistry B*, *109*(8), 3519-3525.

[17] Atilhan, M., Anaya, B., Ullah, R., Costa, L. T., and Aparicio, S. (2016). Double salt ionic liquids based on ammonium cations and their application for CO2 capture. *The Journal of Physical Chemistry C*, *120*(31), 17829-17844.

[18] Talaty, E. R., Raja, S., Storhaug, V. J., Dölle, A., and Carper, W. R. (2004). Raman and infrared spectra and ab initio calculations of $C_{2\text{-}4}$MIM imidazolium hexafluorophosphate ionic liquids. *The Journal of Physical Chemistry B*, *108*(35), 13177-13184.

[19] Holbrey, J. D., and Seddon, K. R. (1999). The phase behaviour of 1-alkyl-3-methylimidazolium tetrafluoroborates, ionic liquids and ionic liquid crystals. *Journal of the Chemical Society, Dalton Transactions*, (13), 2133-2140.

[20] Suarez, P. A., Dullius, J. E., Einloft, S., De Souza, R. F., and Dupont, J. (1996). The use of new ionic liquids in two-phase catalytic hydrogenation reaction by rhodium complexes. *Polyhedron*, *15*(7), 1217-1219.

[21] Paul, A., Mandal, P. K., and Samanta, A. (2005). How transparent are the imidazolium ionic liquids? A case study with 1-methyl-3-butylimidazolium hexafluorophosphate, [bmim][$PF_6$]. *Chemical Physics Letters*, *402*(4-6), 375-379.

[22] Billard, I., Moutiers, G., Labet, A., El Azzi, A., Gaillard, C., Mariet, C., and Lützenkirchen, K. (2003). Stability of divalent europium in an ionic liquid: Spectroscopic investigations in 1-methyl-3-butylimidazolium hexafluorophosphate. *Inorganic Chemistry*, *42*(5), 1726-1733.

[23] Paul, A., Mandal, P. K., and Samanta, A. (2005). On the optical properties of the imidazolium ionic liquids. *The Journal of Physical Chemistry B*, *109*(18), 9148-9153.

[24] Mandal, P. K., Sarkar, M., and Samanta, A. (2004). Excitation-wavelength-dependent fluorescence behavior of some dipolar molecules in room-temperature ionic liquids. *The Journal of Physical Chemistry A*, *108*(42), 9048-9053.

[25] Zhu, G., Zhang, L., Wang, Y., Xu, X., and Peng, X. (2016). Interactions between pyrene and pyridinium ionic liquids studied by ultraviolet–visible spectroscopy. *Journal of Molecular Liquids*, *213*, 289-293.

[26] Nikitenko, S. I., and Moisy, P. (2006). Formation of higher chloride complexes of Np (IV) and Pu (IV) in water-stable room-temperature ionic liquid [BuMeIm][$Tf_2N$]. *Inorganic Chemistry*, *45*(3), 1235-1242.

[27] Nockemann, P., Servaes, K., Van Deun, R., Van Hecke, K., Van Meervelt, L., Binnemans, K., and Görller-Walrand, C. (2007). Speciation of uranyl complexes in ionic liquids by optical spectroscopy. *Inorganic Chemistry*, *46*(26), 11335-11344.

[28] Owens, G. S., Durazo, A., and Abu-Omar, M. M. (2002). Kinetics of MTO-Catalyzed Olefin Epoxidation in Ambient Temperature Ionic Liquids: UV/Vis and 2H NMR Study. *Chemistry–A European Journal*, *8*(13), 3053-3059.

[29] Rodríguez-Fernández, C. D., Montes-Campos, H., Lopez-Lago, E., de la Fuente, R., and Varela, L. M. (2020). Microstructure, dynamics and optical properties of metal-doped imidazolium-based ionic liquids. *Journal of Molecular Liquids*, *317*, 113866.

[30] Paul, A., and Samanta, A. (2006). Optical absorption and fluorescence studies on imidazolium ionic liquids comprising the bis (trifluoromethanesulphonyl) imide anion. *Journal of Chemical Sciences, 118*, 335-340.

[31] Guleria, A., Singh, A. K., and Adhikari, S. (2015). Optical properties of irradiated imidazolium- based room temperature ionic liquids: new microscopic insights into the radiation induced mutations. *Physical Chemistry Chemical Physics*, *17*(16), 11053-11061.

[32] Ghosh, A., Chatterjee, T., and Mandal, P. K. (2012). On the heterogeneity of fluorescence lifetime of room temperature ionic liquids: onset of a journey for exploring red emitting dyes. *Chemical Communications*, *48*(50), 6250-6252.

[33] Andanson, J. M., Bordes, E., Devémy, J., Leroux, F., Pádua, A. A., and Gomes, M. F. C. (2014). Understanding the role of co-solvents in the dissolution of cellulose in ionic liquids. *Green Chemistry*, *16*(5), 2528-2538.

[34] Fredlake, C. P., Crosthwaite, J. M., Hert, D. G., Aki, S. N., and Brennecke, J. F. (2004). Thermophysical properties of imidazolium-based ionic liquids. *Journal of Chemical and Engineering Data*, *49*(4), 954-964.

[35] Erdmenger, T., Vitz, J., Wiesbrock, F., and Schubert, U. S. (2008). Influence of different branched alkyl side chains on the properties of imidazolium-based ionic liquids. *Journal of Materials Chemistry*, *18*(43), 5267-5273.

[36] Gómez, E., Calvar, N., Domínguez, Á., and A. Macedo, E. (2013). Thermal analysis and heat capacities of 1-Alkyl-3-methylimidazolium ionic liquids with $NTf^{2-}$, $TFO^{-}$, and $DCA^{-}$ anions. *Industrial and Engineering Chemistry Research*, *52*(5), 2103-2110.

[37] Kuhn, B.L., Osmari, B.F., Heinen, T.M., Bonacorso, H.G., Zanatta, N., Nielsen, S.O., Ranathunga, D.T., Villetti, M.A. and Frizzo, C.P. (2020). Dicationic imidazolium-based dicarboxylate ionic liquids: Thermophysical properties and solubility. *Journal of Molecular Liquids*, *308*, 112983.

[38] Gindri, I. M., Siddiqui, D. A., Bhardwaj, P., Rodriguez, L. C., Palmer, K. L., Frizzo, C. P., and Rodrigues, D. C. (2014). Dicationic imidazolium-based ionic liquids: A new strategy for non-toxic and antimicrobial materials. *RSC Advances*, 4(107), 62594-62602.

[39] Binetti, E., Panniello, A., Triggiani, L., Tommasi, R., Agostiano, A., Curri, M. L., and Striccoli, M. (2012). Spectroscopic study on imidazolium-based ionic liquids: effect of alkyl chain length and anion. *The Journal of Physical Chemistry B*, *116*(11), 3512-3518.

[40] Majhi, D., Pabbathi, A., and Sarkar, M. (2016). Probing the aggregation behavior of neat imidazolium-based alkyl sulfate (alkyl= ethyl, butyl, hexyl, and octyl) ionic liquids through time resolved florescence anisotropy and NMR and fluorescence correlation spectroscopy study. *The Journal of Physical Chemistry B*, *120*(1), 193-205.

[41] Efimova, A., Hubrig, G., and Schmidt, P. (2013). Thermal stability and crystallization behavior of imidazolium halide ionic liquids. *Thermochimica Acta*, *573*, 162-169.

[42] Fredlake, C. P., Crosthwaite, J. M., Hert, D. G., Aki, S. N., and Brennecke, J. F. (2004). Thermophysical properties of imidazolium-based ionic liquids. *Journal of Chemical and Engineering Data*, *49*(4), 954-964.

[43] Strechan, A. A., Paulechka, Y. U., Blokhin, A. V., and Kabo, G. J. (2008). Low-temperature heat capacity of hydrophilic ionic liquids [BMIM][$CF_3COO$] and [BMIM][$CH_3COO$] and a correlation scheme for estimation of heat capacity of ionic liquids. *The Journal of Chemical Thermodynamics*, *40*(4), 632-639.

# Chapter 5

## Enhanced Dissolution of Cellulose in Imidazolium-Based Double Salt Ionic Liquids


### Abstract

The dissolution of cellulose has been investigated in double salt ionic liquids (DSILs). To address the issue, acetate, and chloride salts of 1-butyl-3-methylimidazolium were used to prepare DSILs, $[C_4mim](CH_3CO_2)_xCl_{1-x}$ ($x$ is the mole fraction of the single component ionic liquids) and for the first time used for a detailed investigation for the enhancement of solubility of cellulose. Commercial cellulose powder, kraft pulp, and prehydrolysis kraft pulp were chosen as cellulose sources. The solubility of cellulose increased with an increase in temperature and with increasing $[C_4mim]Cl$ in DSILs as in $[C_4mim](CH_3CO_2)_{0.6}Cl_{0.4}$. The maximum solubility of commercial cellulose powder was 32.8 wt% in $[C_4mim](CH_3CO_2)_{0.6}Cl_{0.4}$ at 100 $^oC$, while for kraft pulp and prehydrolysis kraft pulp solubilities were 30.1 and 30.5 wt% respectively at the same condition. The cellulose was regenerated from the DSILs using water as an anti-solvent. The structure and morphology of the regenerated cellulosic materials were characterized using ATR-FTIR, XRD, TGA, and SEM. The regenerated cellulose exhibited lower crystallinity and degradation temperature. Finally, the prospects of DSILs for enhanced dissolution and regenerated cellulose for further chemical processing to produce different cellulosic materials have been envisioned.



**Keywords**: Cellulose solubility, Double salt ionic liquids, Regenerated cellulose, Crystallinity, Cellulose II


### 5.1. Introduction

Cellulose is the most widely available, cheap, non-toxic, renewable, and abundant polymer on the earth based on forestry plants. However, the extensive hydrogen bonding network and organized structure of cellulose prevent the penetration of solvent molecules in the framework making it insoluble in common solvents such as water. Therefore, the application of cellulose in practical purposes necessitates its transformation into a soluble derivative [1]. Recently, cellulose has been dissolved and derivatized using ionic liquids (ILs), a neoteric solvent having chemical and thermal stability, non-flammability, and very low vapor pressures [2-4]. ILs can directly

dissolve cellulose without any modifications. Bodachivskyi *et al.* have presented a clear and concise discussion of the various features of ILs as solvents for dissolution of cellulose to foster new perspectives and encourage further research into exploiting the full potential of ILs as a new promising alternative in the realm of cellulose processing [5]. Interestingly, cellulose can be regenerated using an anti-solvent which can be reshaped into fibers, beads, or films, or other types. Swatloski *et al.* reported for the first time that cellulose samples are effectively dissolved in 1-butyl-3-methylimidazolium chloride ([$C_4$mim]Cl) [6]. The superb dissolution of cellulose in [$C_4$mim]Cl has been attributed to the generation of extensive hydrogen-bonds among the -OH protons of cellulose and the $Cl^-$ ions of the ILs [7]. Although several ILs have been used to dissolve cellulose [8-10], [$C_4$mim]Cl and [$C_4$mim]$CH_3CO_2$ are common. The hydrogen bond acceptor capability of anions of ILs is responsible for the solubility of cellulose [11]. Raut *et al.* reported that 30, 28, and 25 wt% of cellulose with degree of polymerization of 789, 1644, and 2082, respectively, could be solubilized in *N*-allyl-*N*-methylmorpholinium acetate ([AMMorp]$CH_3CO_2$) at 120 $^oC$ in 20 min [12]. Ibrahim *et al.* have showed that 1-ethyl-3-methylimidazolium acetate [$C_2$mim]$CH_3CO_2$ along with a 40% (v/v) load of dimethyl sulfoxide (DMSO) could generate 5 wt % cellulose solutions within a time span of 1 h at 80 $^oC$ under the influence of applied pressure of 20 bar [13]. The regenerated cellulose from ILs/DMSO exhibited lower thermal stability and crystallinity in comparison with the original microcrystalline cellulose. Reyes *et al.* have used five different ILs: [$C_4$mim]Cl, [$C_4$mim]$CH_3SO_2$,1-butyl-3-methylimidazolium hydrogen sulfate [$C_4$mim]$HSO_4$, 1-ethyl-3-methylimidazolium chloride [$C_2$mim]Cl, and [$C_2$mim]$CH_3CO_2$ to dissolve bleached hardwood kraft pulp [14]. All of these ILs have the capability to dissolve cellulose to different extents.

Furthermore, the properties of ILs may be modified with the variations of anionic species [15], the alkyl chain length [16] and the cationic structures [17]. [$C_4$mim]-based ILs were studied with the change of several anionic species such as bistrifluoromethylsulfonyl imide $(CF_3SO_2)_2N$, trifluoroacetate ($CF_3CO_2$), trifluoromethane sulfonate ($CF_3SO_3$). Similarly, keeping the anion constant as $(CF_3SO_2)_2N$, the effect of variations in cationic species such as [$C_4$mim], butylpyridinium, [$C_4$py], *N*-butyl-*N*-methylpyrrolidinium, ([$C_4$mpyr]) on the properties of the system were studied. The variations of anionic and cationic species demonstrated pronounced effects on the ion dynamics, especially on the "ionicity" of the room temperature ILs. Modification of ionicity directly influences the hydrogen bonding capabilities of the ILs. The interacting forces

among the ILs change as the length of the alkyl chain changes, and the characteristics of the ILs are then dictated by the cumulative impact of the electrostatic interactions between the ionic species and the induction interactions between the ions, aggregates, and clusters. The variation of alkyl change length of ILs can reduce the viscosity and thus enhance the rate of dissolution of cellulose [12].

According to molecular dynamics simulations, the anion of $[C_4mim]Cl$ tends to interact strongly to disrupt the hydrogen bonding network through displacement of the hydroxyl proton to water or cellulose oxygen during the dissolution process [14]. Kosan *et al.* have investigated cellulose dissolution in different ILs such as $[C_4mim]Cl$, $[C_4mim]CH_3SO_2$, $[C_2mim]Cl$ and $[C_2mim]CH_3CO_2$ and characterized them by means of light microscopy, rheometry and particle analysis [18]. The results have been compared with those of cellulose solutions in *N*-methyl-morpholine-*N*-oxide monohydrate. ILs containing $CH_3CO_2^-$ anion rather than $Cl^-$ enabled spinning dopes at higher cellulose concentrations. To overcome the viscosity problem of cellulose solution in ILs, Yamamoto and Miyake have used mixed solvents of $[C_4mim]CH_3CO_2$ with DMSO, dimethyl acetamide (DMAc), *N*, *N*-dimethylformamide (DMF), dimethyl disulfide (DMDS) and dimethyl sulfide (DMS) [19]. Depending on the process temperature, $[C_4mim]CH_3CO_2$/DMSO could undergo a violent exothermic reaction. The enthalpy of reaction for $[C_4mim]CH_3CO_2$/DMSO has been reported as 377 J $g^{-1}$ at 230°C, while it is 14.6 J $g^{-1}$ for $[C_4mim]CH_3CO_2$/DMF and 25.9 J $g^{-1}$ for $[C_4mim]CH_3CO_2$/DMAc. Sealed-cell differential scanning calorimetric (SC-DSC) mixtures were carried out on mixtures of $[C_4mim]CH_3CO_2$ and possible decomposition products of DMSO. Exothermic reactions occurred with $[C_4mim]CH_3CO_2$/DMDS and with $[C_4mim]CH_3CO_2$/DMS, although no exotherms were observed for the pure substances. These results indicate that abnormal reactions occurred between $[C_4mim]CH_3CO_2$ and DMDS, and between $[C_4mim]CH_3CO_2$ and DMS. This abnormal reaction probably caused the violent exothermic reaction of $[C_4mim]CH_3CO_2$/DMSO. To increase the cellulose dissolution efficiency, mixtures of ILs, $[C_4mim]CH_3CO_2$ and 1-butyl-3-methylimidazolium thiocyanate ($[C_4mim]SCN$) with a molar ratio of 4:1 has been studied [20]. The viscosity of cellulose solution has been found to decrease due to the addition of a co-solvent in each system and a system with $[C_4mim]CH_3CO_2$+DMF mixture has been found to exhibit an improved result on cellulose dissolution dissolving 22.3 wt%, which is about twice of the value for individual $[C_4mim]CH_3CO_2$.

Despite a plethora of positive outcomes, ILs also have seen their disadvantages in this particular field, for example, not all ILs are efficient as solvent media in cellulose dissolution – the most popular ILs comprising alkylimidazolium cations with anions such as tetrafluoroborate, ethylsulfate, hexafluorophosphate, methanesulfonate have been found to act as non-solvents for cellulose. Most of the processes involving ILs also require the presence of water- and water is one of the principal obstacles for dissolution of cellulose. In addition, cellulose dissolution in ILs is a tedious and time-consuming process. Furthermore, ILs are much more expensive than conventional solvents involved in the cellulose dissolution and derivatization process, recovery operations of ILs must be highly efficient to make it economically viable and sustainable. So far, various researches have been carried out to make the recycling of ILs economically sustainable [21-23]. One of the ways of making ILs industrially feasible is by efficiently recycling and reusing it. ILs have demonstrated incredible potential in various industrial applications such as food, pharmaceutics, cosmetic, green energy storage materials and polymer-based nanocomposites for sensor, energy storage, biomedicine, etc. [24-29]. As the ILs can only dissolve small amount of cellulose therefore, ensuring complete interfacial contacts between cellulose and the ILs media is often difficult – resulting in poor efficiency of the overall process. Therefore, one key interest may lie in the modification and manipulation of IL media to minimize the above-mentioned limitations, through the exploitation of the concept of double salt ionic liquids (DSILs).

DSILs are special types of ILs that are usually composed of a combination of organic cations with organic or inorganic anions. These liquids have unique properties compared to traditional ILs, including increased solubility and conductivity. DSILs are formed by combining two different ILs that can overcome the limitations of pure ILs, resulting in the formation of a new liquid phase that contains both sets of ions and does not retain their individual nature [30, 31]. This allows for the creation of liquids with specific properties, such as increased solubility for specific chemical compounds like cellulose or increased ionic conductivity for use in electrochemical devices like batteries [32] or fuel cells [33]. The binary mixtures of two protic ILs namely diethylmethylammonium hydrogensulfate ([dema]$HSO_4$) and diethylmethylammonium bis(trifluoromethanesulfonyl)amide ([dema][$NTf_2$] exhibited enhanced electrochemical properties originating from anion/$H^+$ exchange via hydrogen bonds that alter the N−H bond strengths. The anion/$H^+$ exchange results in average N−H bond strength making the system suitable for fuel cell

application. The change in the open circuit potential played an important role for the improved responses in fuel cells and batteries.

Long *et al.* have reported the complete dissolution of cellulose into industrially useful chemicals using DSILs- in which the ratios of various cations were manipulated in order to achieve both cellulose dissolution and catalytic conversion of cellulose into low molecular weight organic products [34]. Moreover, DSILs were used to solubilize Pd(0) nanoparticles and lignin in DSILs, which improved the transport of oxygen to the active metal centers and increased the oxidation of lignin [35]. DSILs thus have the potential to overcome the disadvantages of single ILs for dissolution of cellulose. They have promise – not only as a solvent for dissolution of cellulose but for fundamental insight into the effects of anion and/or cation variation on the physicochemical aspects of DSILs. In this study, mixtures of ILs, $[C_4mim]Cl$ and $[C_4mim]CH_3CO_2$ with a common cation in different mole ratios were used to prepare a series of DSILs and to dissolve commercial (CC) cellulose and jute pulp. The dissolved cellulose was regenerated with the controlled addition of an anti-solvent, water. The solubility profile was monitored with optical microscopy by monitoring cellulosic fiber in the mixture. The regenerated cellulose was characterized by state of the art techniques and the prospect for modification of cellulose for further applications was envisaged. The ultimate goal has been to design a DSIL for enhanced dissolution of cellulose followed by its efficient regeneration and cost-effective recycling of DSILs from the solution. Furthermore, this study explores the potential of task-specific DSILs as efficient components in cellulose processing chemistry.

## 5.2. Materials and Methods

The materials and methods used in this chapter to carry out this study have been described in the following sub-sections.

### 5.2.1. Materials

Commercial cellulose powder (CAS number 9004-34-6, white color, grain size for column chromatography, fiber size 0.01 to 0.10 mm) was purchased from Merck KGaA, Germany. Kraft pulp (KP) and prehydrolysis kraft pulp (PHKP) were prepared from jute by following the detailed conditions described elsewhere [36]. Acetone (Sigma-Aldrich, $\geq$ 99.5%) and distilled water (distilled by Laboratory Water Purification System, MRC) were used throughout the study. ILs, $[C_4mim]Cl$ and $[C_4mim]CH_3CO_2$, were purchased from Sigma-Aldrich with purities of $\geq$98% and $\geq$95%, respectively.

### 5.2.2. Preparation of DSILs

The preparation DSILs have been carried out by mixing of $[C_4mim]Cl$ and $[C_4mim](CH_3CO_2)$ at varying mole fractions to prepare $[C_4mim](CH_3CO_2)_xCl_{1-x}$, ( where $x$ is 0.1, 0.2, 0.3, 0.4, 0.5, 0.6, 0.7, 0.8, and 0.9 mole fraction of single ILs). The details of the preparation procedure have been described in chapter 2 (sub-section 2.2.2).

### 5.2.3. Dissolution of cellulose and regeneration

To minimize the water content and any traces of volatile compounds, the samples were always dried under vacuum at 90 $^oC$ for 2 h prior to dissolution of cellulose experiments. For each experiment, a known amount of DSILs (ca. 2 g) was placed in a vial containing a magnetic stirring bar. Initially, 2 wt% of cellulose was added to the vial and stirred for half an hour at room temperature. The cellulose-IL mixture was then heated in an oil bath with constant stirring at 80 $^oC$. Cellulose samples used in this study were dried for 24 h under vacuum before use. The dissolution of cellulose was carried out in a closed system. All the experiments were carried out very carefully to keep the moisture at a negligible amount to avoid adsorption by cellulose samples for consequent interference with the dissolution process. The dissolution of cellulose was followed by an optical microscope (Oxion, Euromax, Holland) as well as by visual monitoring. Initially, the dissolution of cellulose is relatively fast with 5 wt% cellulose dissolving in 40 min. The saturation of cellulose in solution was carried out by the subsequent addition of cellulose. The degree of

dissolution was monitored at 3 h intervals. The effect of temperature on the dissolution was monitored by increasing temperature in the presence of excess amount of cellulose in the system. When cellulose was swollen in ILs, fibers could be clearly observed, number of visible fibers reduced after partial dissolution, and finally no fiber was observed for the complete dissolution of cellulose in the microscopic image. All dissolution experiments were carried out in triplicate and the average reading was recorded. The protic anti-solvent, water, was added to the cellulose solution to precipitate out cellulose. The obtained precipitates were separated from the $H_2O$/ILs mixture by filtration with G-2 filter (Funnels, Buchner, with Sintered Disc, Glasscolabs) under vacuum. The precipitates were washed several times until complete removal of ILs from the precipitates. The obtained regenerated cellulose was dried under vacuum for 24 h at 75 °C and 0.1 MPa. ILs were recycled from the filtrate of $H_2O$/ILs by the evaporation of $H_2O$ and removing cellulose completely. The recycled ILs were mixed with acetone to precipitate the trace amount of cellulose remaining in the recycled ILs. Then it was filtered again to remove cellulose. This process was repeated several times to remove cellulose and trapped water completely from recycled ILs.

### 5.2.4. Thermogravimetric analysis

Thermogravimetric analysis (TGA) of cellulose samples was carried out in a Hitachi TGA analysis (TG- DTA 6200) operated from an initial temperature of 30 $^oC$ to a final temperature of 550 $^oC$ at 10 $^oC$ $min^{-1}$ under an inert nitrogen atmosphere (100 mL $min^{-1}$) in aluminum pans.

### 5.2.5. X-ray diffraction (XRD) analysis

The crystallinity and crystal structure of the jute pulp and the regenerated cellulose was studied by an X-ray diffractometer (ARL $^{TM}$ EQUINOX 1000 X-ray diffractometer, Thermo Fisher scientific, USA). The analyzer was operated at 40 kV and 15 mA with CuK α radiation of wavelength 0.156 nm with an acquisition time of 10 min.

### 5.2.6. FT-IR spectroscopic analysis

The structural identification of the cellulose samples and ILs were carried out by attenuated total reflectance-Fourier transform-infrared (ATR-FT-IR) spectroscopy (Frontier, Perkin-Elmer, UK, Software: Spectrum version 10.4.4). The FT-IR spectra were recorded in ATR mode equipped with a diamond crystal. For every measurement, the crystal of the diamond was polished with

acetone, and a background scan was taken before every measurement. The spectra were recorded between 650 to 4000 $cm^{-1}$ range at 4 $cm^{-1}$ spectral resolution and with 16 scans per spectrum.

### 5.2.7. Scanning electron microscopy analysis

Scanning electron microscopy (SEM) (EV018, Carl ZEISS AG, UK) was used to study the morphological structures of cellulose samples isolated from jute fiber and regenerated cellulose, under the condition of vacuum and accelerating voltage of 5.0 kV. The samples were dried and coated with gold on an aluminum stub. The SEM micrographs were taken at 5.0 KX magnifications.

### 5.2.8 Dynamic viscosity measurement

Dynamic viscosity of KP and ReKP were measured by a rotational rheometer (Brand: Anton-Paar, Model: RheolabQC) using a measuring cup (C-DG26.7/SS.QC-LTD) and cylinder (double gap; DG26.7) with a variable shear rate, 10-50 $s^{-1}$ at 30-80 °C in 5 °C intervals.

## 5.3. Results and Discussion

### 5.3.1. Dissolution of commercial cellulose in DSILs

Dissolution of CC in DSILs, $[C_4mim](CH_3CO_2)_xCl_{1-x}$ was investigated in different mole ratios at different temperatures. As presented in Fig. 5.1, the dissolution of C-C increased with an increase in temperature. Approximately, 2 wt% of CC was added each time. Initially, 5 wt% of cellulose required only 40 min for dissolution. After that, as the CC-DSIL solution became viscous, longer time was required for further dissolution. For example, $[C_4mim](CH_3CO_2)_{0.6}Cl_{0.4}$ solvent system required an overall 30 h for dissolution of 26.2 wt% of cellulose at 80 $^oC$. Then, the temperature was raised to dissolve more amount of CC. Approximately, 40 h was required to dissolve 32.8 wt% of CC at 100 $^oC$. Similar observations were noted in the case of KP and PHKP. Dissolution of CC in $[C_4mim]CH_3CO_2$ alone was 11.2 wt% at 80 °C, which increased to 18.0 wt% at 100 °C. Dissolution of CC increased with increasing mole fraction of $[C_4mim]Cl$ in DSILs up to $[C_4mim](CH_3CO_2)_{0.6}Cl_{0.4}$. CC of 26.2, 31.2, and 32.8 wt% was dissolved in $[C_4mim](CH_3CO_2)_{0.6}Cl_{0.4}$ at 80, 90 and 100 °C, respectively. The most important factor of the dissolution process is the disruption of hydrogen bonds inside the cellulose. The intermolecular hydrogen bonding in cellulose molecules is originated from the hydroxyl groups of cellulose. Mohd *et al.* have described that ILs having $Cl^-$ and $CH_3CO_2^-$ anions are used widely for the dissolution of cellulose [37]. The $Cl^-$ ion in ILs forms hydrogen bonds with the hydroxyl groups of cellulose which results in the solubilization of cellulose; on the other hand, ILs with $CH_3CO_2^-$ ion can dissolve cellulose through bonding associated with the conjugation of cellulose reducing ends [38, 39]. Although it is the intermolecular hydrogen bonding, mediated by entrapped water, that must be disrupted to affect dissolution; the reducing-end conjugation has also been reported to contribute to cellulose dissolution albeit the contribution from the end group would seem to be an extremely minor path to the full solvation of cellulose polymers of any even moderate sized chain length. DSILs containing both $Cl^-$ and $CH_3CO_2^-$ anion may have a synergistic effect, which results in higher dissolution of cellulose.

The computational studies could give a better idea and thorough understanding of enhancement of the dissolution of cellulose in DSILs. A number of research articles have appeared in the literature over the last few years investigating ILs by means of molecular simulations. It is established experimentally and theoretically that mixtures of ILs with protic or aprotic co-solvents or DSILs tune their physicochemical properties for task-specific applications. Phadagi *et al.*

investigated experimentally and theoretically the role of co-solvent DMF with ILs of 1-butyl-3-methylimidazolium chloride ([$C_4$mim]Cl), 1-allyl-3-methylimidazolium chloride ([Amim]Cl) and 1-butyl-3-methylpyridinium chloride ([bmpy][Cl) for the dissolution of cellulose [42]. Using the COSMO-RS theory and conceptual density functional theory (CDFT), they proved that DMF enhanced the dissolution of cellulose. Trenzado *et al.* investigated the insights of the DSIL of $[C_2mim][BF_4]_{0.5}[TFSI]_{0.5}$ using molecular dynamics methods to examine the diffusion of $[BF_4]^-$ and $[TFSI]^-$ anions in the $[C_2mim][BF_4]_{0.5}[TFSI]_{0.5}$ liquid interface, and the mechanism of interface crossing [43]. The results allow a multiscale characterization of the considered DSIL. Thus, ILs containing several types of ions can be considered for tuning their physicochemical properties, increasing and changing the nature of these fluids, and thus the suitability for different applications. Dhakal *et al.* reviewed a number of articles based on molecular simulation analyses of the bulk properties and structure of ILs mixture [44]. They mentioned that the mixing of ILs is a powerful technique for synthesizing DSILs of two cations or anions with tailor-made properties. Based on the observations in this study, theoretical calculations are in progress to understand the actual mechanism for the enhanced dissolution of cellulose in DSILs. The results will be presented elsewhere.

Furthermore, dissolution of cellulose in ILs became highly viscous up to the solubility level shown in Fig. 5.1, and stirring using the magnetic bar became increasingly difficult. As the temperature was increased, viscosity started to reduce and more cellulose was dissolved. An inverse relationship between the degree of polymerization (DP) and the content of dissolved cellulosic material was reported in the study of Raut *et al.* [12]. In fact, [AMMorp]$CH_3CO_2$ could dissolve 17.0 wt% microcrystalline cellulose (DP = 789), 13.0 wt% cellulose (DP = 1644) and 11.0 wt% cellulose (DP 2082), respectively, in 20 min at a temperature of 80 °C resulting in the formation of a transparent gel. The solubility of cellulose increased markedly at an elevated temperature. In fact, ILs containing halide, acetate, formate, and alkylphosphonate anions demonstrate positive impacts toward good solubility of cellulose [8, 45, 46].

In addition, complexity due to the use of DSILs for the dissolution of cellulose may arise from the multiple ions coexisting in DSILs. These DSILs typically consist of more than two complex organic cations and organic or inorganic anions, and their unique interactions with cellulose contribute to their distinctive properties. As DSILs are composed of multiple ions, complexity increases in their understanding of their interactions with cellulose and how these interactions

affect the dissolution process. The properties of DSILs and interactions with cellulose can be tuned by changing the exact ion combination in them, which makes it difficult to gain a deeper understanding. These combinations of ions in DSILs may cause high viscosity which can affect the dissolution of cellulose. The choice of anions in DSILs which play a major role in the dissolution can significantly impact their solvating ability and selectivity for cellulose. Further extensive work is underway through theoretical studies to resolve the issue.

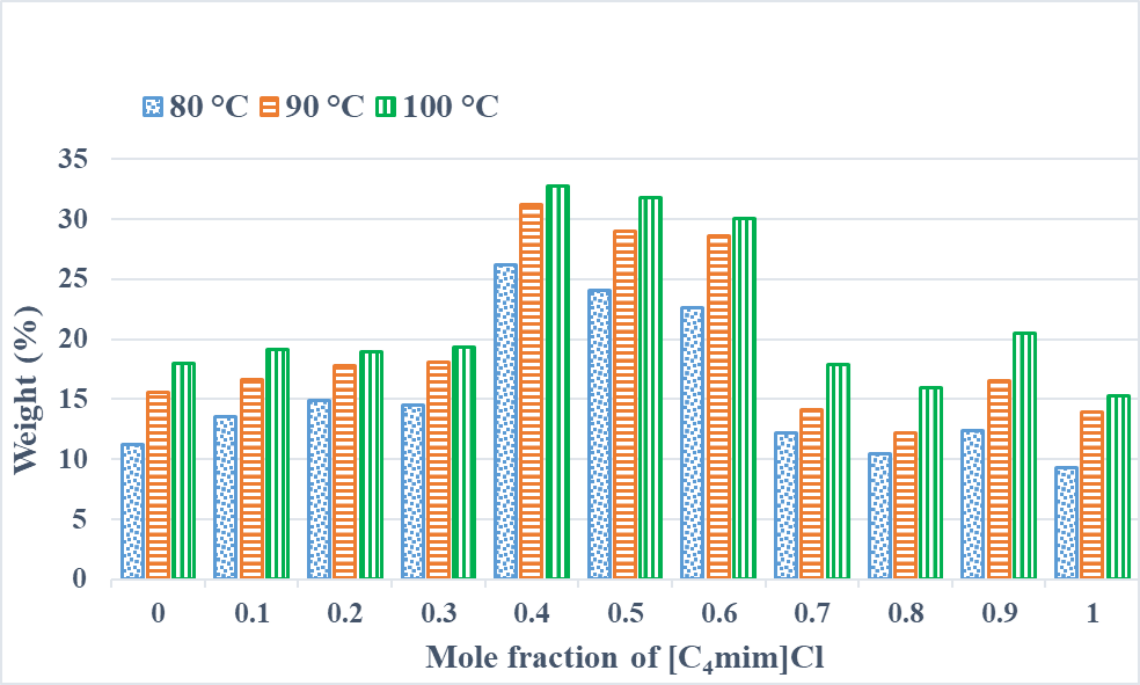


**Figure 5.1.** Dissolution of commercial cellulose in $[C_4mim]Cl$, $[C_4mim]CH_3CO_2$ and DSILs of $[C_4mim](CH_3CO_2)_xCl_{1-x}$ of different mole ratios (where, $x$ = 0.1, 0.2, 0.3, 0.4, 0.5, 0.6, 0.7, 0.8, and 0.9) at 80, 90, and 100 °C

Fig. 5.2 shows images of prepared DSIL ($[C_4mim](CH_3CO_2)_{0.6}Cl_{0.4}$), solution of PHKP in $[C_4mim](CH_3CO_2)_{0.6}Cl_{0.4}$ and recycled ILs, ($[C_4mim]Cl$ and $[C_4mim]CH_3CO_2$), DSIL of $[C_4mim](CH_3CO_2)_{0.6}Cl_{0.4}$. The prepared DSIL was a clear liquid while the dissolved cellulose in DSIL and recycled ILs and DSIL were darker. Raut *et al.* have also reported that the yellow color of cellulosic solution in $[AMMorp]CH_3CO_2$ darkened as the content of cellulose they progressively increased in the solvated state [12]. Raut *et al.* have also observed darkening upon heating of cellulose solution in $[C_4mim]HSO_4$ [12]. On the contrary, Reyes *et al.* have reported formation of highly viscous and transparent hydrogel upon dissolving pulp in $[C_4mim]Cl$ [14].

This strongly depends on the molar mass of cellulose and viscosity of the cellulose- [$C_4$mim]Cl solution [47].

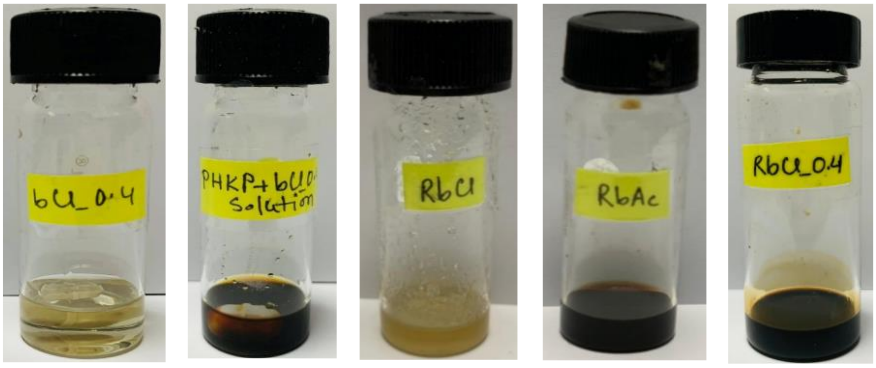


**Figure 5.2.** Photographs of (A) prepared [$C_4$mim]$(CH_3CO_2)_{0.6}Cl_{0.4}$, (B) solution of PHKP in [$C_4$mim]$(CH_3CO_2)_{0.6}Cl_{0.4}$, (C) recycled [$C_4$mim]Cl, (D) recycled [$C_4$mim]$CH_3CO_2$, and (E) recycled [$C_4$mim]$(CH_3CO_2)_{0.6}Cl_{0.4}$

Dissolution of cellulose in DSILs was also monitored by an optical microscope. As shown in Fig. 5.3, the cellulosic fibers can be visually observed in the snaps taken with the aid of a microscope after the soaking of cellulose in ILs at room temperature (A), a few fibers were observed when cellulose was partially dissolved, indicating the incomplete dissolution of cellulose (B), and after the total dissolution of cellulose in ILs and DSILs at other temperatures, no cellulosic strands were noticed in the microscopic images (C).

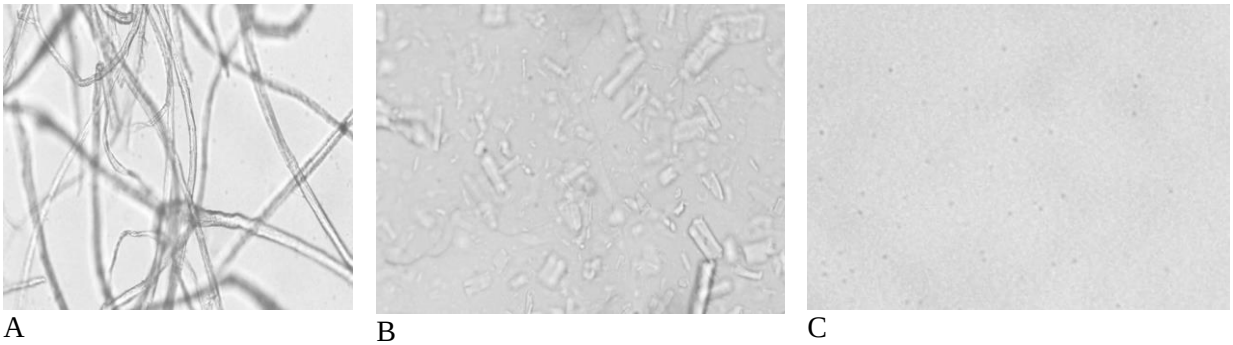


**Figure 5.3.** Optical microscopic images of various states of cellulose in ionic liquids at room temperature: (A) insoluble, (B) partially soluble, and (C) completely soluble. All images were taken at 10X magnification.

### 5.3.2. Dissolution of jute pulp in DSILs

Similar to CC, jute pulp from kraft and prehydrolysis kraft processes were dissolved in $[C_4mim]Cl$, $[C_4mim]CH_3CO_2$, and DSILs of $[C_4mim](CH_3CO_2)_xCl_{1-x}$ at different mole ratios at different temperatures as shown in Fig. 5.4. With increase in temperature, larger amount of pulp can be dissolved. The amount of ILs in DSILs also influenced the dissolution of cellulose. Liu *et al.* have also observed that solubility of cotton pulp in $[C_4mim]Cl$ increased to 24.0 wt% at 130 °C from 10.0 wt% at 80 °C [40]. The highest dissolution of pulp was observed in $[C_4mim](CH_3CO_2)_{0.6}Cl_{0.4}$ at 100 °C. For further increase of $[C_4mim]Cl$ in the DSILs, solubility of cellulose decreased. No significant difference could be observed between KP and PHKP. But the solubility of pulp was slightly lower than the CC due to impurities, like lignin, hemicellulose, and extractives present in the pulp.

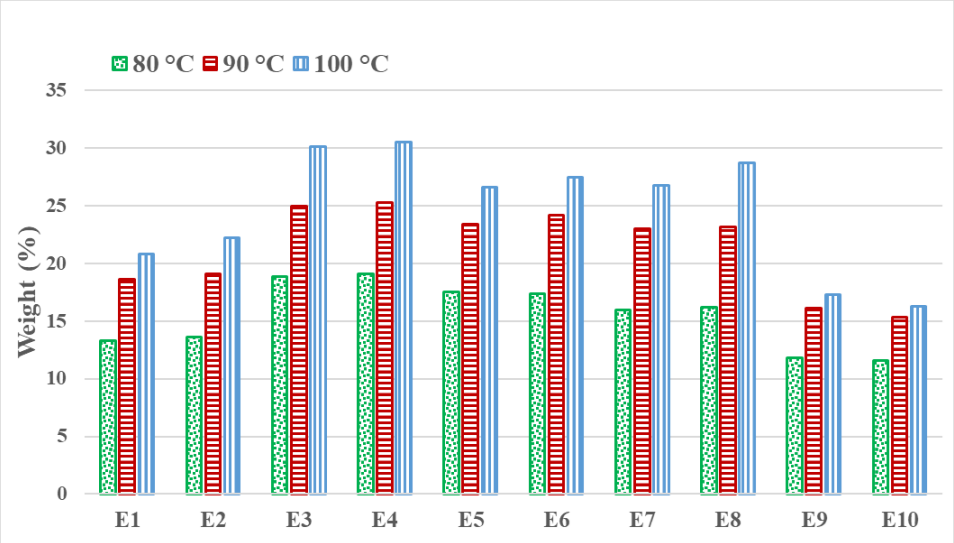


**Figure 5.4.** Dissolution of KP in $[C_4mim]CH_3CO_2$ (E1), PHKP in $[C_4mim]CH_3CO_2$(E2), KP in $[C_4mim](CH_3CO_2)_{0.6}Cl_{0.4}$ (E3), PHKP in $[C_4mim](CH_3CO_2)_{0.6}Cl_{0.4}$ (E4), KP in $[C_4mim](CH_3CO_2)_{0.5}Cl_{0.5}$ (E5), PHKP in $[C_4mim](CH_3CO_2)_{0.5}Cl_{0.5}$ (E6), KP in $[C_4mim](CH_3CO_2)_{0.4}Cl_{0.6}$ (E7), PHKP in $[C_4mim](CH_3CO_2)_{0.4}Cl_{0.6}$ (E8), KP in $[C_4mim]Cl$ (E9), and PHKP in $[C_4mim]Cl$ (E10) at 80, 90, and 100 °C

The solubility of cellulose in ILs also depends on the DP [5]. A high solubility of cellulose with microcrystalline morphology as high as 25.0 wt% was found in [Amim]Cl. But with increasing DP of cellulose samples to 516 and 726, the content of dissolved cellulose in ILs decreased to 15.0 and 6.0 wt% respectively. Liu et al. have dissolved 16.0 wt% and 14.0 wt% cotton pulp in

[$C_2$mim]$CH_3CO_2$ and [$C_2$mim]Cl respectively at 90 °C for 7 h [40]. The higher solubility of cellulose in DSILs in this investigation can be explained by the disruption of the cellulose hydrogen-bonded network through the hydrogen-bonding between anions of DSILs and moieties of the cellulose network.

### 5.3.3. Regeneration of cellulose

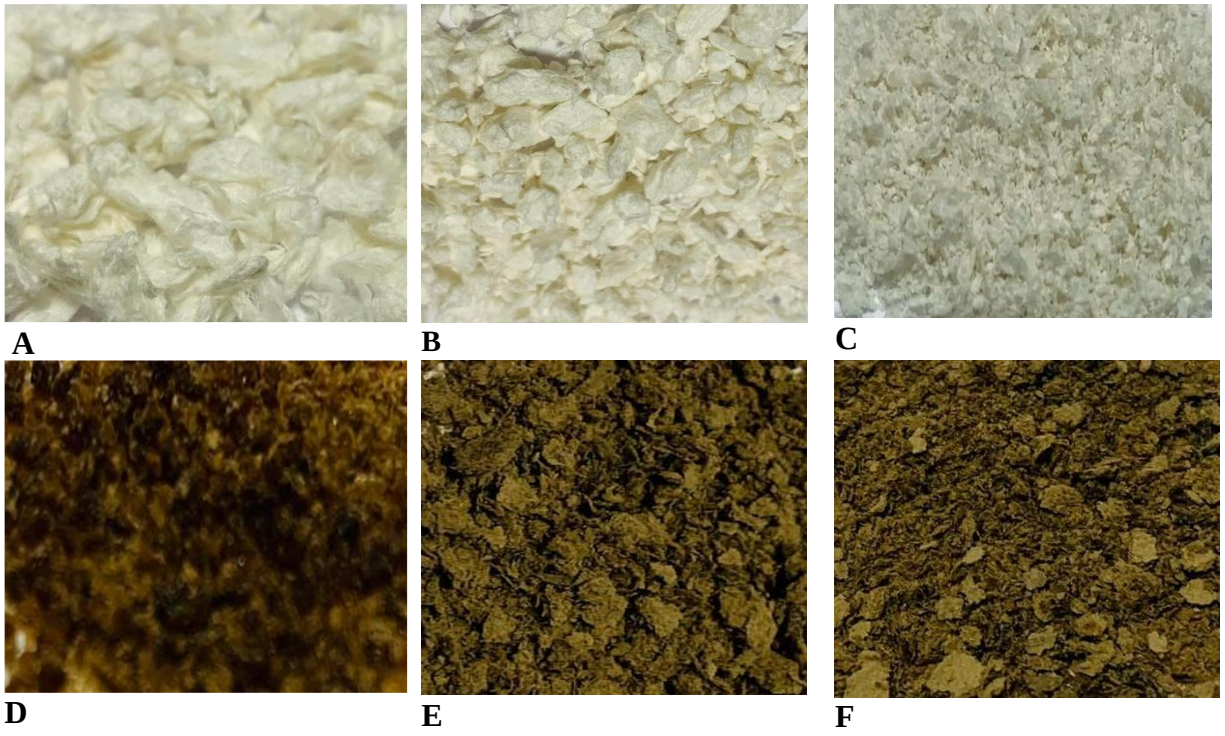


**Figure 5.5.** Optical photographs of (A) KP, (B) PHKP, (C) RePHKP from [$C_4$mim]Cl, (D) RePHKP from [$C_4$mim]$CH_3CO_2$, (E) RePHKP from [$C_4$mim]$(CH_3CO_2)_{0.6}Cl_{0.4}$, and (F) RePHKP from [$C_4$mim]$(CH_3CO_2)_{0.5}Cl_{0.5}$

Water was used as an anti-solvent to regenerate dissolved cellulose in ILs and DSILs. All cellulose regeneration was carried out from dissolved PHKP. The regenerated cellulose (RC) was characterized using wide-angle XRD, SEM, FT-IR spectroscopy, and TGA Fig. 5.5 shows the photograph of RC and isolated cellulose (pulp) obtained from jute. The appearance of the RC from [$C_4$mim]Cl solution was lighter in color, while the same from [$C_4$mim]$CH_3CO_2$ and DSIL solution was darker. This is consistent with the observations of Raut *et al.* [12], wherein they have reported that the regenerated pulp from [$C_4$mim]$CH_3CO_2$, [$C_4$mim]$HSO_4$ and [$C_4$mim]Cl was darker in color as compared to a whiter regenerated pulp in the case of [$C_4$mim]Cl and [$C_2$mim]$CH_3CO_2$.

The partial hydrolysis of cellulose into sugars, which is then broken down by oxidative processes to produce the distinctive brown hue, may be one cause of the dark color of the regenerated pulp [48], and the presence of residual ions and moisture is another reason for color changes [49].

As shown in Fig. 5.6, both the KP and PHKP became plasticized after treatment with $[C_4mim](CH_3CO_2)_{0.6}Cl_{0.4}$. The surface of the regenerated pulp (B and D) was found to be homogeneous, soft, smooth, and more densely packed compared to the rough, hard, and scattered outer layer surface of the isolated pulp samples (A and C) as observed in the SEM images presented in Fig. 5.6. Reyes *et al.* have observed whiter plasticized structures of regenerated pulp from $[C_4mim]CH_3CO_2$ compared to smooth gel-like structures from $[C_2mim]CH_3CO_2$ [14]. Partly broken fibers are obsrved on the surface of the regenerated pulp (B). Some H-bonds remained unbroken during the dissolution process. Similar observations were reported by many researchers [50, 51].

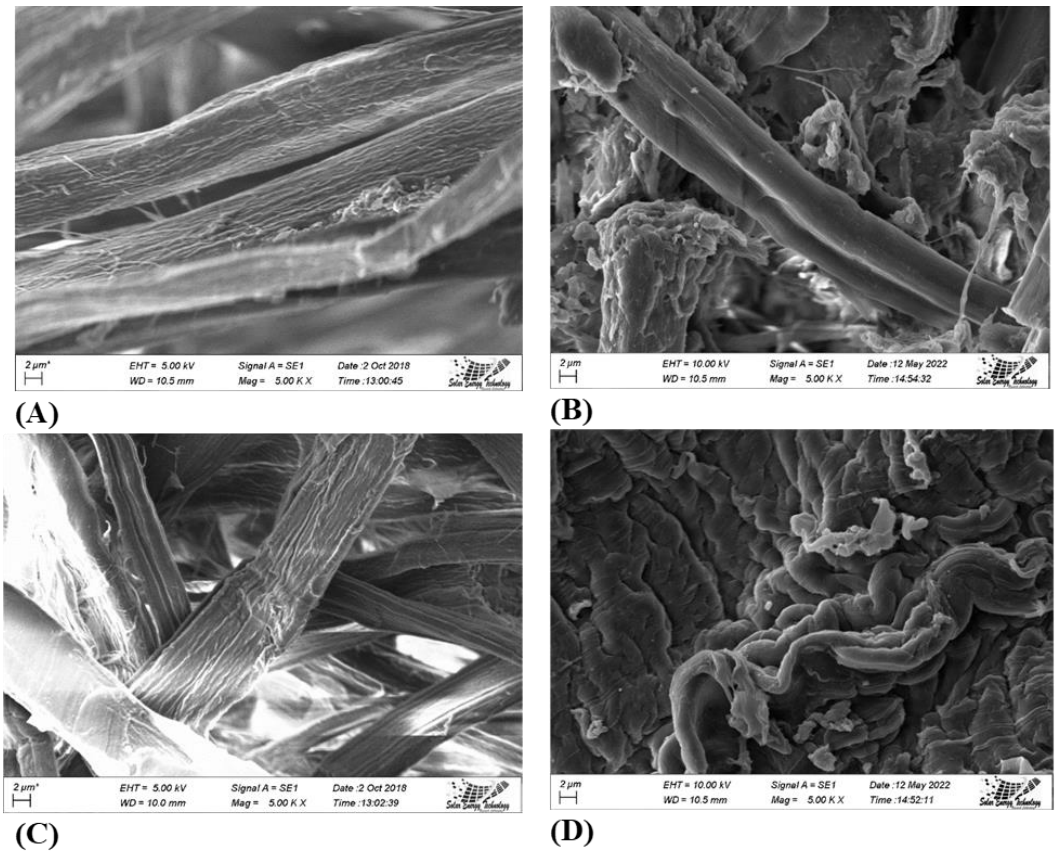


**Figure 5.6.** SEM micrographs of (A) KP, (B) ReKP from $[C_4mim](CH_3CO_2)_{0.6}Cl_{0.4}$, (C) PHKP, and (D) RePHKP from $[C_4mim](CH_3CO_2)_{0.6}Cl_{0.4}$

### 5.3.4. X-ray diffraction of cellulose and regenerated cellulose

To understand the changes in the crystallinity of the cellulose (KP and PHKP) on the dissolution in $[C_4mim]Cl$, $[C_4mim]CH_3CO_2$ and DSILs, a wide-angle XRD pattern was taken. Fig. 5.7, shows the XRD pattern of the cellulose (pulp) and RC. The peaks for native cellulose I ($I_\beta$) are located at $2\theta$ = 14°, 16°, 22.5°, and 35° corresponding to the (101), (10$\underline{1}$), (002) and (040) crystallographic plane reflections, respectively [52, 53]. All cellulose and RC showed these peaks except RC from the $[C_4mim]CH_3CO_2$ solution of KP and PHKP. These results clearly indicate that upon regeneration of the dissolved cellulose in $[C_4mim]CH_3CO_2$, the transformation from cellulose I into cellulose II occurred. Cao *et al.* also reported that the RC from corn husk dissolved in $[C_2mim]CH_3CO_2$ was cellulose II [54]. After the dissolution of cellulose in $[C_2mim]CH_3CO_2$/DMSO and its concomitant recovery with water, the regenerated cellulose demonstrated a diffraction pattern at $2\theta$ = 20.5°, originating from the cellulose II form [13]. Zhao *et al.* have also observed conversion of cellulose I to cellulose II from cellulose I in native cellulose during regeneration from phosphate based ILs [55].

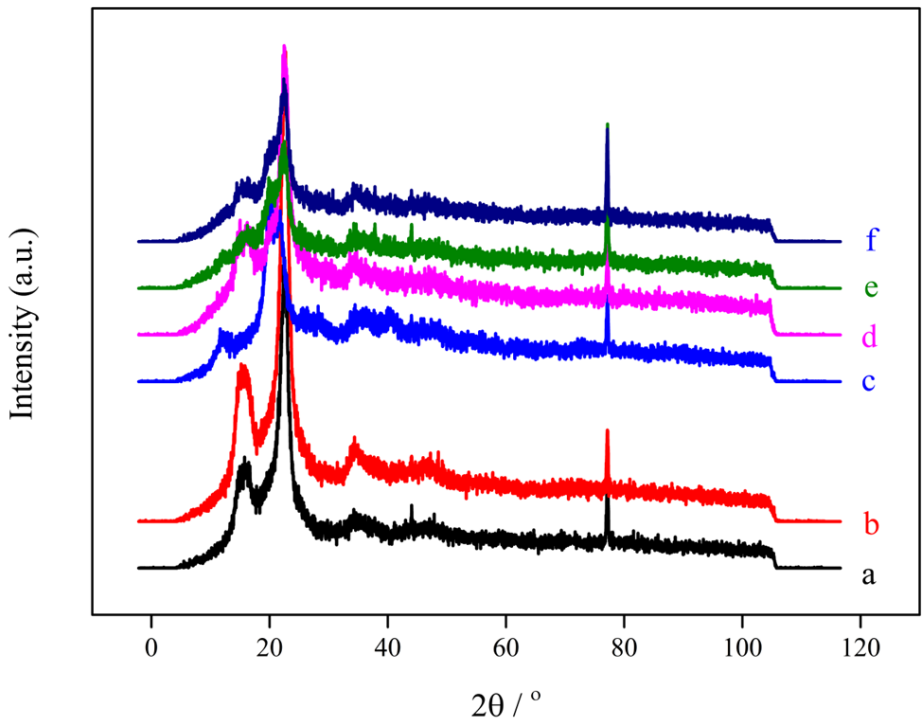


**Figure 5.7.** XRD patterns of (a) KP, (b) PHKP, (c) RePHKP from $[C_4mim]CH_3CO_2$, (d) RePHKP from $[C_4mim]Cl$, (e) RePHKP from $[C_4mim](CH_3CO_2)_{0.6}Cl_{0.4}$, and (f) RePHKP from $[C_4mim](CH_3CO_2)_{0.5}Cl_{0.5}$

As shown in Table 5.1, the crystallinity of KP increased from 48.5% to 55.1% on pre-hydrolysis resulting from the deletion of hemicellulose during pre-hydrolysis process. After dissolution of cellulose samples in $[C_4mim]Cl$, $[C_4mim]CH_3CO_2$ and DSILs, the RC showed similar diffraction patterns, which indicate no alteration of the original cellulose structure I.

**Table 5.1. Crystallinity of cellulose and regenerated samples**

| **Sample** | **2 $\theta$ / °** | **Crystallinity (%)** |
|---|---|---|
| KP | 22.7 | 48.5 |
| PHKP | 22.5 | 55.1 |
| ReKP from$[C_4mim]Cl$ | 22.5 | 26.5 |
| ReKP from $[C_4mim]CH_3CO_2$ | 20.6 | 25.2 |
| RePHKP from $[C_4mim]Cl$ | 22.3 | 25.2 |
| RePHKP from $[C_4mim]CH_3CO_2$ | 20.6 | 28.8 |
| RePHKP from $[C_4mim](CH_3CO_2)_{0.6}Cl_{0.4}$ | 22.5 | 26.6 |
| RePHKP_from $[C_4mim](CH_3CO_2)_{0.5}Cl_{0.5}$ | 22.4 | 27.7 |

A significant diminution of crystallinity was noticed for the RC. The crystallinity index of regenerated KP (ReKP) decreased to 26.5 and 25.2% from the $[C_4mim]Cl$ and $[C_4mim]CH_3CO_2$ solution respectively from the original crystallinity of 48.5%, and the crystallinity of regenerated PHKP (RePHKP) decreased to 25.1, 28.8, 26.6, and 27.7% from the $[C_4mim]Cl$, $[C_4mim]CH_3CO_2$, $C_4mim](CH_3CO_2)_{0.6}Cl_{0.4}$ and $C_4mim](CH_3CO_2)_{0.5}Cl_{0.5}$ respectively.

In general, the structure of regenerated cellulose possesses a cellulose II structure. For both dissolution and regeneration, H-bonding plays an important role. Dissolution in ILs is initiated by the disruption of H-bonds in cellulose, driven by the formation of H-bonds between cellulose and anions, as well as the hydrophobic interactions with cations. For regeneration, antisolvents possess a strong affinity for ILs, and disrupt the newly formed H-bonds between cellulose and ILs; consequently, cellulose–cellulose H-bonds get reformed and is precipitated. In this study, regenerated cellulose from $[C_4mim]Cl$, $[C_4mim](CH_3CO_2)_{0.6}Cl_{0.4}$ and $[C_4mim](CH_3CO_2)_{0.6}Cl_{0.4}$ remain in original form of cellulose I structure. This is the consequence of some intra and

intermolecular H-bonds in the supramolecular structure of cellulose that remained unbroken during the dissolution process. Therefore, when cellulose was regenerated from cellulose-ILs solution, the regenerated cellulose remained in its original form however, its crystallinity decreased. These results are supported by the FT-IR spectra (Fig. 5.9f) of the RC from the solution of $[C_4mim](CH_3CO_2)_{0.6}Cl_{0.4}$. The -OH stretching band of the cellulose structure was expected to shift towards a higher wavenumber as seen from FT-IR spectra of the cellulose II structure. This shifting to higher wavenumber for -OH stretching band indicates the change in the crystallinity of cellulose I to cellulose II due to the reduced H-bonding in RC [56]. However, the -OH stretching band remained at the same position indicating the presence of cellulose I structure. Hence, the RC regenerated from the $[C_4mim]Cl$, $[C_4mim](CH_3CO_2)_{0.6}Cl_{0.4}$ and $[C_4mim](CH_3CO_2)_{0.6}Cl_{0.6}$ consists of the cellulose I structure suggesting the lack of H-bond rearrangement during regeneration.

### 5.3.5. Thermogravimetric analysis

The thermal degradation of CC, KP, PHKP, and regenerated pulp from $[C_4mim]CH_3CO_2$ and $[C_4mim](CH_3CO_2)_{0.6}Cl_{0.4}$ is shown in Fig. 5.8. The initial mass loss was about 5% at 110 °C due to evaporation of retained moisture, followed by a slow mass loss for CC, KP, and PHKP up to around 275 °C, regenerated pulp from $[C_4mim]CH_3CO_2$ up to 185 °C, and regenerated pulp from $[C_4mim](CH_3CO_2)_{0.6}Cl_{0.4}$ up to 245 °C. Then each sample started to decompose and underwent an obvious mass loss because of the pyrolytic cleavage of the polysaccharide units. As summarized in Table 5.2, the degradation temperature of CC was 322 °C, which was close to the degradation temperature of KP and PHKP. The degradation temperature of ReKP and RePHKP from $[C_4mim]CH_3CO_2$ was 245 and 260 °C, while RePHKP from $[C_4mim](CH_3CO_2)_{0.6}Cl_{0.4}$ was 310 °C. This can be explained in terms of crystallinity (Fig. 5.7). The dissolution and subsequent regeneration processes disrupt the hydrogen bond networks and crystal structures of cellulose, consequently lowers the thermal stability of cellulose. A similar result was also observed by Liu *et al.* where cellulose was dissolved in $[C_4mim]CH_3CO_2$ and regenerated by compressed $CO_2$ [41].

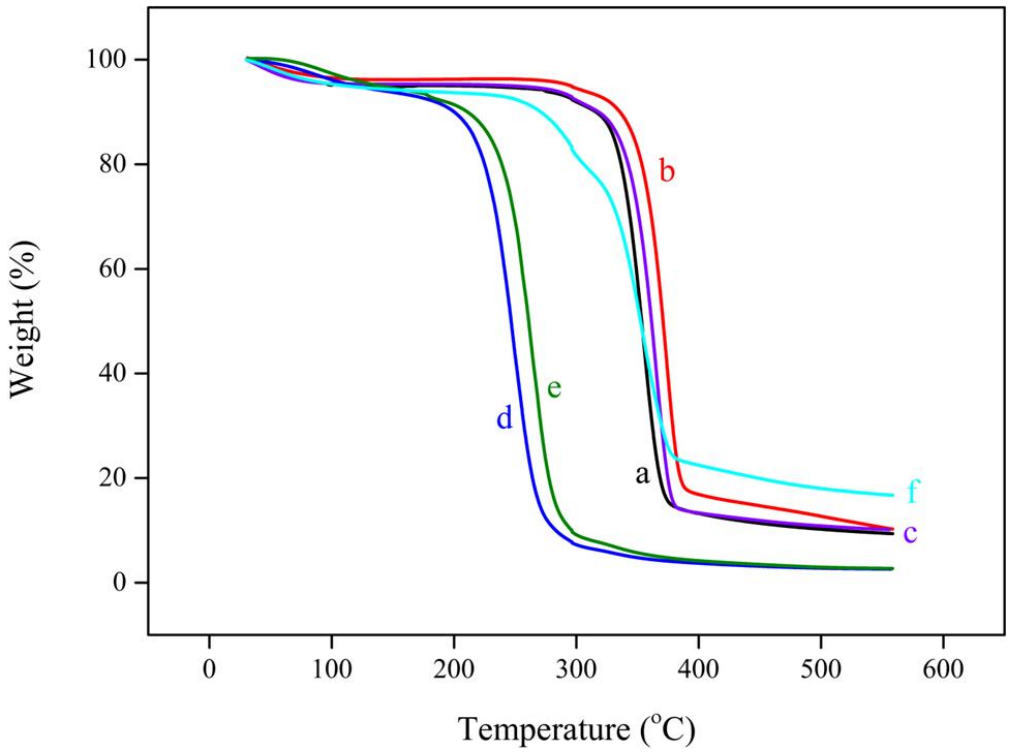


**Figure 5.8.** TGA thermograms of (a) CC, (b) KP, (c) PHKP, (d) REKP from $[C_4mim]CH_3CO_2$, (e) RePHKP from $[C_4mim]CH_3CO_2$, and (f) RePHKP from $[C_4mim](CH_3CO_2)_{0.6}Cl_{0.4}$

**Table 5.2.** The onset degradation temperature ($T_d$) of KP and PHKP, ReKP from $[C_4mim]CH_3CO_2$. RePHKP from $[C_4mim]CH_3CO_2$ and RePHKP from $[C_4mim](CH_3CO_2)_{0.6}Cl_{0.4}$

| Sample | $T_d$ / °C |
|---|---|
| CC | 322 |
| KP | 337 |
| PHKP | 340 |
| ReKP from$[C_4mim]CH_3CO_2$ | 245 |
| RePHKP from $[C_4mim]CH_3CO_2$ | 260 |
| RePHKP from $[C_4mim](CH_3CO_2)_{0.6}Cl_{0.4}$ | 310 |

### 5.3.6 FTIR spectra of cellulose and RC

As displayed in Fig. 5.9, ATR-FTIR spectra of the RC were very close to that of the original cellulose, suggesting that except for the breakage of hydrogen bonds no other changes on chemical structure occurred in the dissolution of cellulose and regeneration processes [57]. The broad absorption band originated due to the strong stretching vibration of OH groups occurring at 3300–

3500 $cm^{-1}$, the vibration for methylene ($CH_2$) groups at 2700–2900 $cm^{-1}$ were observed in all samples [58]. The RC demonstrated a strong absorption band at 1647 $cm^{-1}$ attributable to the C–O stretching vibration of the C–O–H bond, as reported in other studies [40]. Furthermore, a sharp band at 896 $cm^{-1}$ was observed for the RC corresponding to the glycosidic C–H deformation with ring vibration and O–H bending, which is characteristic of β-glycosidic linkages between glucose in cellulose [59]. The band at 896 $cm^{-1}$ is attributable to the amorphous part of cellulose and cellulose II absorption. This band is usually more prominent in RC. The band at around 1425 $cm^{-1}$ depicts the crystalline region absorption band and is usually more striking in cellulose I, which is the stronger band in original cellulose [60]. This is consistent with XRD data. Other studies also reported similar FT-IR results of RC [41].

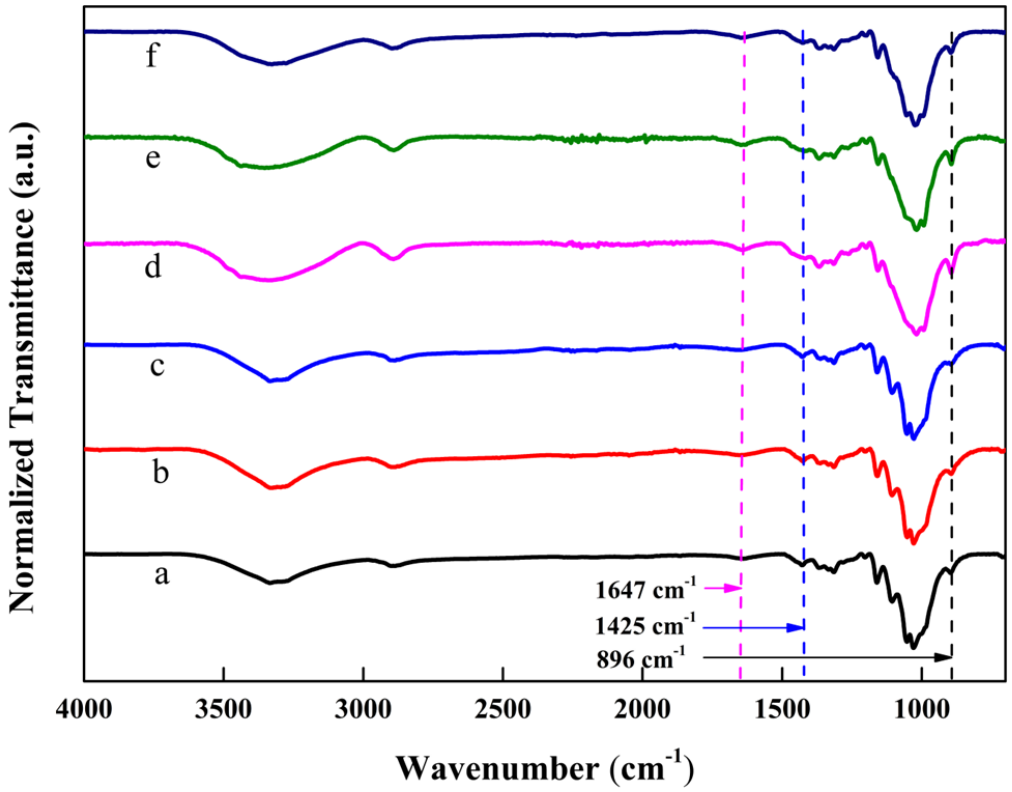


**Figure 5.9.** Normalized ATR-FTIR spectra of (a) CC, (b) KP, (c) PHKP, (d) ReKP from $[C_4mim]CH_3CO_2$, (e) RePHKP from $[C_4mim]CH_3CO_2$, and (f) RePHKP from $[C_4mim](CH_3CO_2)_{0.6}Cl_{0.4}$

### 5.3.7. Dynamic viscosity of KP and ReKP

The dynamic viscosity of KP and ReKP are presented in Fig. 5.10 and Fig. 5.11. The viscosity of KP and ReKP decreases with increasing temperature and shear rate. The viscosity of KP and ReKP at 30 °C is 32950, 20340, and 7760, 3314 mPa-s at 80 °C respectively. The lower viscosity for ReKP is due to the more amorphous regions of regenerated cellulose produced due to the disruption of hydrogen bonds. The decrease in viscosity with shear rate indicates the shear thinning properties of KP and ReKP solution in $[C_4mim](CH_3CO_2)_{0.6}Cl_{0.4}$. Similarly, increasing the temperature decreases viscosity and leads to highly homogeneous cellulose/DSIL solutions. These results confirmed the dispersal ability of $[C_4mim](CH_3CO_2)_{0.6}Cl_{0.4}$, resulting in increased local intermolecular interactions between polymer chains and $[C_4mim](CH_3CO_2)_{0.6}Cl_{0.4}$. The observed shear-thinning behavior was caused by an increase in the repulsion between the KP and ReKP and the anions $CH_3CO_2^-$ and $Cl^-$ in contact with them and less interaction between hydroxyl groups of cellulose and anions of DSILs [61]. Chen. et al. investigated the shear thinning behavior of 10 wt% cellulose/$[C_4mim]Cl$ solution resulting from both shear induced reduction in the number of entanglements and the dissolution of macromolecules by the high shear rate [62].

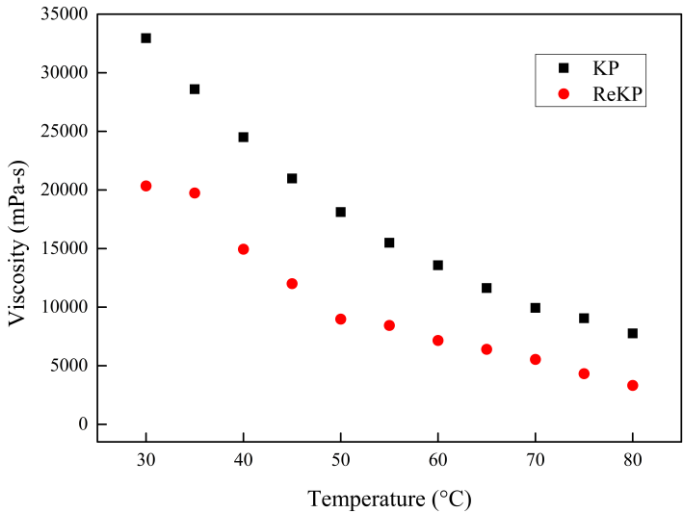


**Figure 5.10.** Variation of viscosity of 5 wt % solution of KP and ReKP in $[C_4mim](CH_3CO_2)_{0.6}Cl_{0.4}$ as a function of temperature

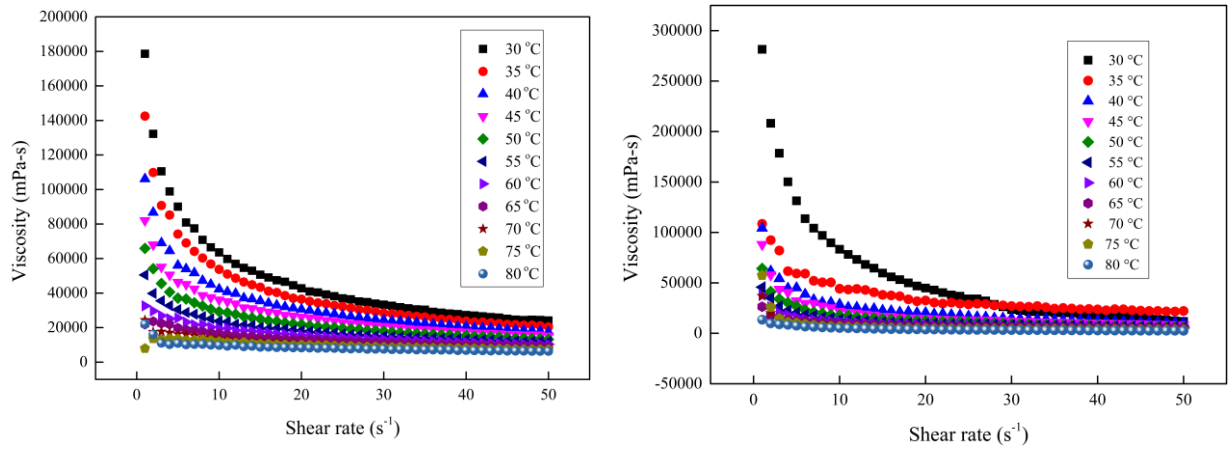


**Figure 5.11.** Variation of viscosity of (A) 5 wt % solution of KP in $[C_4mim](CH_3CO_2)_{0.6}Cl_{0.4}$ (B) Regenerated KP in $[C_4mim](CH_3CO_2)_{0.6}Cl_{0.4}$ at a different shear rate as a function of temperature

### 5.3.8. Recycling of ILs/DSIL

As ILs are usually more expensive compared to other solvents involved in the cellulose dissolution and derivatization process, recovery operations must be highly efficient to make the process economically viable and sustainable. The recycling should effectively eliminate solutes and demand use of the least amount of new or non-recycled reagents and avoidance of any significant degradation of the ILs/DSILs. The recycling and reuse of single ILs are reported in the literature [22, 23]. In this work, the recycling experiments of both ILs and DSILs were carried out to check whether the solvent system may be economically viable and sustainable for industrial applications, such as producing regenerated cellulose for textile industries. For example, the DSIL of $[C_4mim](CH_3CO_2)_{0.6}Cl_{0.4}$ has been used for the dissolution of cellulose and recycled and reused five times successively. More than 99% of $[C_4mim](CH_3CO_2)_{0.6}Cl_{0.4}$ has been recovered from each cycle and was characterized by FTIR, $^1$H NMR spectroscopy, and TGA. No change in the chemical structure was noticed and degradation did not occur during dissolution and regeneration process. This has been first instance of recycling and reuse of a DSIL, $[C_4mim](CH_3CO_2)_{0.6}Cl_{0.4}$. A detailed study is now underway for the recycling and reuse of ILs for the regeneration of cellulose from cellulose-ILs/DSIL solution. The dependence of the dissolution and yield recovery of regenerated cellulose on the particle size, DP, and the structure of the ILs and composition of the constituent DSIL will be communicated elsewhere.

## 5.4. Conclusions

The dissolution of CC, KP, and PHKP were studied in $[C_4mim]Cl$ and $[C_4mim]CH_3CO_2$ and their DSILs at three different temperatures 80, 90 and 100 °C. Dissolution of CC in $[C_4mim]CH_3CO_2$ and $[C_4mim]Cl$ alone was 11.2 and 9.3 wt% at 80 °C respectively, which increased to 18.0 and 15.3 wt% at 100 °C respectively. Dissolution of CC was further enhanced using DSILs increased with increasing mole fraction of $[C_4mim]Cl$ in DSILs up to $[C_4mim](CH_3CO_2)_{0.6}Cl_{0.4}$. CC of 26.2, 31.2, and 32.8 wt% was dissolved in $[C_4mim](CH_3CO_2)_{0.6}Cl_{0.4}$ at 80, 90 and 100 °C, respectively. The most important factor of the dissolution process has been the disruption of hydrogen bonds inside the cellulose, which enhanced through the hydrogen-bonding between anions of DSILs and moieties of the cellulose network. DSILs containing both $Cl^-$ and $CH_3CO_2^-$ anion may have a synergistic effect, which results in higher dissolution of cellulose. A similar trend was observed for KP and PHKP. The highest dissolution of KP and PHKP was observed in $[C_4mim](CH_3CO_2)_{0.6}Cl_{0.4}$ at 100 °C were 30.13 and 30.52 wt% respectively. But the solubility of pulp was slightly lower than the CC due to impurities, like lignin, hemicellulose, and extractives present in the pulp. The dissolved cellulose can be regenerated by adding water, and the crystallinity index of regenerated cellulose decreased. The crystallinity index of ReKP decreased to 26.5% and 25.2% from the $[C_4mim]Cl$ and $[C_4mim]CH_3CO_2$ solution respectively from the original crystallinity of 48.5%. The crystallinity of RePHKP decreased to 25.1, 28.8, 26.6 % from the $[C_4mim]Cl$, $[C_4mim]CH_3CO_2$, and $C_4mim](CH_3CO_2)_{0.6}Cl_{0.4}$ respectively from the original crystallinity of 55.1%. This is supported by the glycosidic C–H deformation with ring vibration and O–H bending vibration in FT-IR spectra. The TGA analysis showed a reduced degradation temperature of regenerated cellulose. The structure of the regenerated cellulose from $[C_4mim]CH_3CO_2$ system was converted to cellulose II. Weaker structural organization results from the lower crystallinity content of cellulose, which is projected to be beneficial for its future chemical processing with other chemicals to produce different cellulosic materials. Computational analyses of the cellulose-DSILs system are in progress. These analyses will give insights into the microscopic interactions between cellulose and DSILs, which will reveal the significant factors responsible for the enhanced dissolution of cellulose in DSILs. Computer simulation may also assist to reveal the underlying factors associating the use DSILs with asymmetric ions.

**References**


[1] Pinkert, A., Marsh, K. N., and Pang, S. (2010). Reflections on the solubility of cellulose. *Industrial and Engineering Chemistry Research*, *49*(22), 11121-11130.

[2] Dupont, J., de Souza, R. F., and Suarez, P. A. (2002). Ionic liquid (molten salt) phase organometallic catalysis. *Chemical Reviews*, *102*(10), 3667-3692.

[3] Wasserscheid, P., and Keim, W. (2000). Ionic liquids—new "solutions" for transition metal catalysis. *Angewandte Chemie International Edition*, *39*(21), 3772-3789.

[4] Welton, T. (1999). Room-temperature ionic liquids. Solvents for synthesis and catalysis. *Chemical Reviews*, *99*(8), 2071-2084.

[5] Bodachivskyi, I., Page, C. J., Kuzhiumparambil, U., Hinkley, S. F., Sims, I. M., and Williams, D. B. G. (2020). Dissolution of cellulose: are ionic liquids innocent or noninnocent solvents?. *ACS Sustainable Chemistry and Engineering*, *8*(27), 10142-10150.

[6] Swatloski, R. P., Spear, S. K., Holbrey, J. D., and Rogers, R. D. (2002). Dissolution of cellose with ionic liquids. *Journal of the American Chemical Society*, *124*(18), 4974-4975.

[7] Moulthrop, J. S., Swatloski, R. P., Moyna, G., and Rogers, R. D. (2005). High-resolution 13C NMR studies of cellulose and cellulose oligomers in ionic liquid solutions. *Chemical Communications*, (12), 1557-1559.

[8] Pinkert, A., Marsh, K. N., Pang, S., and Staiger, M. P. (2009). Ionic liquids and their interaction with cellulose. *Chemical Reviews*, *109*(12), 6712-6728.

[9] Verma, C., Mishra, A., Chauhan, S., Verma, P., Srivastava, V., Quraishi, M. A., and Ebenso, E. E. (2019). Dissolution of cellulose in ionic liquids and their mixed cosolvents: A review. *Sustainable Chemistry and Pharmacy*, *13*, 100162.

[10] Wang, H., Gurau, G., and Rogers, R. D. (2012). Ionic liquid processing of cellulose. *Chemical Society Reviews*, *41*(4), 1519-1537.

[11] Xu, A., Wang, J., and Wang, H. (2010). Effects of anionic structure and lithium salts addition on the dissolution of cellulose in 1-butyl-3-methylimidazolium-based ionic liquid solvent systems. *Green Chemistry*, *12*(2), 268-275.

[12] Raut, D. G., Sundman, O., Su, W., Virtanen, P., Sugano, Y., Kordas, K., and Mikkola, J. P. (2015). A morpholinium ionic liquid for cellulose dissolution. *Carbohydrate Polymers*, *130*, 18-25.

[13] Ibrahim, F., Moniruzzaman, M., Yusup, S., and Uemura, Y. (2015). Dissolution of cellulose with ionic liquid in pressurized cell. *Journal of Molecular Liquids*, *211*, 370-372.

[14] Reyes, G., Aguayo, M. G., Fernández Pérez, A., Pääkkönen, T., Gacitúa, W., and Rojas, O. J. (2019). Dissolution and hydrolysis of bleached kraft pulp using ionic liquids. *Polymers*, *11*(4), 673.

[15] Tokuda, H., Hayamizu, K., Ishii, K., Susan, M. A. B. H., and Watanabe, M. (2004). Physicochemical properties and structures of room temperature ionic liquids. 1. Variation of anionic species. *The Journal of Physical Chemistry B*, *108*(42), 16593-16600.

[16] Tokuda, H., Hayamizu, K., Ishii, K., Susan, M. A. B. H., and Watanabe, M. (2005). Physicochemical properties and structures of room temperature ionic liquids. 2. Variation of alkyl chain length in imidazolium cation. *The Journal of Physical Chemistry B*, *109*(13), 6103-6110.

[17] Tokuda, H., Ishii, K., Susan, M. A. B. H., Tsuzuki, S., Hayamizu, K., and Watanabe, M. (2006). Physicochemical properties and structures of room-temperature ionic liquids. 3. Variation of cationic structures. *The Journal of Physical Chemistry B*, *110*(6), 2833-2839.

[18] Kosan, B., Michels, C., and Meister, F. (2008). Dissolution and forming of cellulose with ionic liquids. *Cellulose*, *15*(1), 59-66.

[19] Yamamoto, Y. K., and Miyake, A. (2017). Influence of a mixed solvent containing ionic liquids on the thermal hazard of the cellulose dissolution process. *Journal of Thermal Analysis and Calorimetry*, *127*(1), 743-748.

[20] 20Mqoni, N., Singh, S., Bahadur, I., Hashemi, H., and Ramjugernath, D. (2022). Ionic liquids, the mixture of ionic liquids and their co-solvent with N, N-dimethylformamide as solvents for cellulose using experimental and COSMO study. *Results in Engineering*, 100484.

[21] Karadaghi, L. R., Malmstadt, N., Van Allsburg, K. M., and Brutchey, R. L. (2020). Techno-Economic Analysis of Recycled Ionic Liquid Solvent Used in a Model Colloidal Platinum Nanoparticle Synthesis. *ACS Sustainable Chemistry and Engineering*, *9*(1), 246-253.

[22] Mai, N. L., Ahn, K., and Koo, Y. M. (2014). Methods for recovery of ionic liquids-A review. *Process Biochemistry*, *49*(5), 872-881.

[23] Kuzmina, O. (2016). Economical aspects of ionic liquid application. In *Application, Purification, and Recovery of Ionic Liquids* (pp. 249-263). Elsevier.

[24] Mesquita, L. M., Murador, D. C., and de Rosso, V. V. (2023). Application of ionic liquid solvents in the food industry. In *Encyclopedia of ionic liquids* (pp. 72-87). Singapore: Springer Nature Singapore.

[25] Zhuang, W., Hachem, K., Bokov, D., Ansari, M. J., and Nakhjiri, A. T. (2022). Ionic liquids in pharmaceutical industry: A systematic review on applications and future perspectives. *Journal of Molecular Liquids*, *349*, 118145.

[26] Toledo Hijo, A. A., Meirelles, A. A., Maximo, G. J., Cunha, R. L., Cristianini, M., Leite, T. S., and Meirelles, A. J. (2022). Synergetic Application of Ionic Liquids as New Naturally based Antimicrobial Preservatives and Emulsifiers. *ACS Sustainable Chemistry and Engineering*, *10*(46), 15017-15024

[27] Vilas-Boas, S. M., Coelho, A. Z., Martins, M. A., Coutinho, J. A., Ferreira, O., and Pinho, S. P. (2023). Evaluation of Ionic Liquids for the Sustainable Fractionation of Essential Oils. *Industrial and Engineering Chemistry Research*, *62*(17), 6749-6758.

[28] Marfavi, Y., AliAkbari, R., Kowsari, E., Sadeghi, B., and Ramakrishna, S. (2022). Application of ionic liquids in green energy-storage materials. In *Ionic Liquid-Based Technologies for Environmental Sustainability* (pp. 155-166). Elsevier.

[29] Mishra, K., Devi, N., Siwal, S. S., Zhang, Q., Alsanie, W. F., Scarpa, F., and Thakur, V. K. (2022). Ionic Liquid-Based Polymer Nanocomposites for Sensors, Energy, Biomedicine, and Environmental Applications: Roadmap to the Future. *Advanced Science*, *9*(26), 2202187.

[30] Chatel, Gregory, Jorge FB Pereira, Varun Debbeti, Hui Wang, and Robin D. Rogers. "Mixing ionic liquids–"simple mixtures" or "double salts"?." *Green Chemistry* 16, no. 4 (2014): 2051-2083.

[31] Rahman, A., Rahman, M. M., Mollah, M. Y. A., and Susan, M. A. B. H. (2019). Ultraslow Relaxation in Aprotic Double Salt Ionic Liquids. *The Journal of Physical Chemistry B*, *123*(26), 5577-5587.

[32] Saikat, M. S. H., Islam, M. M., Mollah, M. Y. A., Susan, M. A. B. H., and Miran, M. S. (2019). Thermal and electrochemical properties of protic ionic liquids and their binary mixtures with water. *Materials Today: Proceedings*, *15*, 498-503.

[33] Miran, M. S., Yasuda, T., Susan, M. A. B. H., Dokko, K., and Watanabe, M. (2014). Binary protic ionic liquid mixtures as a proton conductor: high fuel cell reaction activity and facile proton transport. *The Journal of Physical Chemistry C*, *118*(48), 27631-27639.

[34] Long, J., Guo, B., Li, X., Jiang, Y., Wang, F., Tsang, S.C., Wang, L. and Yu, K.M.K. (2011). One step catalytic conversion of cellulose to sustainable chemicals utilizing cooperative ionic liquid pairs. *Green Chemistry*, *13*(9), 2334-2338.

[35] Zhu, Y., Chuanzhao, L., Sudarmadji, M., Hui Min, N., Biying, A. O., Maguire, J. A., and Hosmane, N. S. (2012). An efficient and recyclable catalytic system comprising nanopalladium (0) and a pyridinium salt of iron bis (dicarbollide) for oxidation of substituted benzyl alcohol and lignin. *ChemistryOpen*, *1*(2), 67-70.

[36] Jahan, M. S., Al-Maruf, A., and Quaiyyum, M. A. (2007) Comparative studies of pulping of jute fiber, jute cutting and jute caddis. *Bangladesh Journal of Scientific and Industrial Research*, 42(4):425-434.

[37] Mohd, N., Draman, S. F. S., Salleh, M. S. N., and Yusof, N. B. (2017). Dissolution of cellulose in ionic liquid: A review. *AIP Conference Proceedings*, 1809(1), 020035.

[38] King, A. W., Asikkala, J., Mutikainen, I., Järvi, P., and Kilpeläinen, I. (2011). Distillable acid–base conjugate ionic liquids for cellulose dissolution and processing. *Angewandte Chemie International Edition*, *50*(28), 6301-6305.

[39] Liu, H., Sale, K. L., Holmes, B. M., Simmons, B. A., and Singh, S. (2010). Understanding the interactions of cellulose with ionic liquids: a molecular dynamics study. *The Journal of Physical Chemistry B*, *114*(12), 4293-4301.

[40] Liu, Z., Wang, H., Li, Z., Lu, X., Zhang, X., Zhang, S., and Zhou, K. (2011). Characterization of the regenerated cellulose films in ionic liquids and rheological properties of the solutions. *Materials Chemistry and Physics*, *128*(1-2), 220-227.

[41] Liu, Z., Sun, X., Hao, M., Huang, C., Xue, Z., and Mu, T. (2015). Preparation and characterization of regenerated cellulose from ionic liquid using different methods. *Carbohydrate Polymers*, *117*, 99-105.

[42] Phadagi, R., Singh, S., Hashemi, H., Kaya, S., Venkatesu, P., Ramjugernath, D., Ebenso, E.E., and Bahadur, I. (2021). Understanding the role of dimethylformamide as co-solvents in the dissolution of cellulose in ionic liquids: Experimental and theoretical approach. *Journal of Molecular Liquids*, *328*, 115392.

[43] Trenzado, J. L., Rodríguez, Y., Gutiérrez, A., Cincotti, A., and Aparicio, S. (2021). Experimental and molecular modeling study on the binary mixtures of [EMIM][$BF_4$] and [EMIM][TFSI] ionic liquids. *Journal of Molecular Liquids*, *334*, 116049.

[44] Dhakal, P., and Shah, J. K. (2019). Recent advances in molecular simulations of ionic liquid–ionic liquid mixtures. *Current Opinion in Green and Sustainable Chemistry*, *18*, 90-97.

[45] Fukaya, Y., Hayashi, K., Wada, M., and Ohno, H. (2008). Cellulose dissolution with polar ionic liquids under mild conditions: required factors for anions. *Green Chemistry*, *10*(1), 44-46.

[46] Vitz, J., Erdmenger, T., Haensch, C., and Schubert, U. S. (2009). Extended dissolution studies of cellulose in imidazolium based ionic liquids. *Green Chemistry*, *11*(3), 417-424.

[47] Ahn, Y., Kwak, S. Y., Song, Y., and Kim, H. (2016). Physical state of cellulose in BmimCl: dependence of molar mass on viscoelasticity and sol-gel transition. *Physical Chemistry Chemical Physics*, *18*(3), 1460-1469.

[48] Zhou, L., Yang, X., Xu, J., Shi, M., Wang, F., Chen, C., and Xu, J. (2015). Depolymerization of cellulose to glucose by oxidation–hydrolysis. *Green Chemistry*, *17*(3), 1519-1524.

[49] Shen, Y., Zhang, Y., Han, D., Wang, Z., Kuehner, D., and Niu, L. (2009). Preparation of colorless ionic liquids “on water” for spectroscopy. *Talanta*, *78*(3), 805-808.

[50] Meenatchi, B., Renuga, V., and Manikandan, A. (2017). Cellulose dissolution and regeneration using various imidazolium based protic ionic liquids. *Journal of Molecular Liquids*, *238*, 582-588.

[51] Kasprzak, D., Krystkowiak, E., Stępniak, I., and Galiński, M. (2019). Dissolution of cellulose in novel carboxylate-based ionic liquids and dimethyl sulfoxide mixed solvents. *European Polymer Journal*, *113*, 89-97.

[52] Davidson, T. C., Newman, R. H., and Ryan, M. J. (2004). Variations in the fibre repeat between samples of cellulose I from different sources. *Carbohydrate Research*, *339*(18), 2889-2893

[53] Khalifa, B. A., Abdel-Zaher, N., and Shoukr, F. S. (1991). Crystalline character of native and chemically treated Saudi Arabian cotton fibers. *Textile Research Journal*, *61*(10), 602-608.

[54] Cao, Y., Li, H., Zhang, Y., Zhang, J., and He, J. (2009). Structure and properties of novel regenerated cellulose films prepared from cornhusk cellulose in room temperature ionic liquids. *Journal of Applied Polymer Science*, *116*(1), 547-554.

[55] Zhao, D., Li, H., Zhang, J., Fu, L., Liu, M., Fu, J., and Ren, P. (2012). Dissolution of cellulose in phosphate-based ionic liquids. *Carbohydrate Polymers*, *87*(2), 1490-1494.

[56] Huang, Z., Liu, C., Feng, X., Wu, M., Tang, Y., and Li, B. (2020). Effect of regeneration solvent on the characteristics of regenerated cellulose from lithium bromide trihydrate molten salt. *Cellulose*, *27*, 9243-9256.

[57] Zhang, H., Wu, J., Zhang, J., and He, J. (2005). 1-Allyl-3-methylimidazolium chloride room temperature ionic liquid: a new and powerful nonderivatizing solvent for cellulose. *Macromolecules*, *38*(20), 8272-8277.

[58] King, A. W., Asikkala, J., Mutikainen, I., Järvi, P., and Kilpeläinen, I. (2011). Distillable acid–base conjugate ionic liquids for cellulose dissolution and processing. *Angewandte Chemie International Edition*, *50*(28), 6301-6305.

[59] Jin, A. X., Ren, J. L., Peng, F., Xu, F., Zhou, G. Y., Sun, R. C., and Kennedy, J. F. (2009). Comparative characterization of degraded and non-degradative hemicelluloses from barley straw and maize stems: Composition, structure, and thermal properties. *Carbohydrate Polymers*, *78*(3), 609-619.

[60] Adsul, M., Soni, S. K., Bhargava, S. K., and Bansal, V. (2012). Facile approach for the dispersion of regenerated cellulose in aqueous system in the form of nanoparticles. *Biomacromolecules*, *13*(9), 2890-2895.

[61] Aghmih, K., Wakrim, H., Boukhriss, A., El Bouchti, M., Majid, S., and Gmouh, S. (2022). Rheological study of microcrystalline cellulose/pyridinium-based ionic liquids solutions. *Polymer Bulletin*, 1-13.

[62] Chen, X., Zhang, Y., Cheng, L., and Wang, H. (2009). Rheology of concentrated cellulose solutions in 1-butyl-3-methylimidazolium chloride. *Journal of Polymers and the Environment*, *17*, 273-279.

# Chapter 6

## Effect of Pre-Hydrolysis on the Dissolution of Hardwood Pulp in Ionic Liquid


### Abstract

Cellulose, an abundant and sustainable bio-resource, stands as the foremost constituent on earth. The cellulose is derivatized to dissolve it; such process is called viscose process. Viscose is produced from the dissolving pulp, which is produced predominantly by pre-hydrolysis kraft process. Pre-hydrolysis is conducted as a preliminary step preceding pulping in order to selectively extract hemicellulose from the lignocellulosic matrix. This deliberate extraction of hemicellulose poses challenges during the subsequent viscose processing stage. Ionic liquids (ILs) are potentially alternative solvent for the cellulose dissolution. It is an interest to gather knowledge on, how hemicellulose affects in pulp dissolution in ILs and the regeneration process. In this study, hardwood pulps were produced by kraft (KP) and pre-hydrolysis kraft (PHKP) processes. The α-cellulose and residual pentosan contents were 95.6% and 4.2% in PHKP and 84.3% and 9.9% in KP, respectively. Both pulps were dissolved in 1-butyl-3-methylimidazolium chloride $[C_4mim]Cl$, 1-butyl-3-methylimidazolium acetate $[C_4mim]CH_3CO_2$ and their double salt (DSILs) of $[C_4mim](CH_3CO_2)_{0.6}Cl_{0.4}$ at 90°C. It was observed that PHKP had slightly higher solubility in both ILs and DSILs. The dissolved pulps were regenerated by water and characterized by FTIR, TGA, X-ray diffraction, and viscosity. Regenerated pulp film formed smooth and homogenous surface. The viscosity of regenerated PHKP was higher than PHKP, which affected the strength of the produced cellulose film. As observed in FTIR, the regenerated cellulose showed a stronger absorption band at 1647 $cm^{-1}$ corresponding to the C–O stretching vibration of C–O–H. The crystalline structures of regenerated PHKP from $[C_4mim]CH_3CO_2$ and regenerated KP and PHKP from DSILs were found to change to form cellulose II. The crystallinity index of regenerated KP from $[C_4mim]Cl$ decreased, while the same from other regenerated pulps remained same or increased.



**Keywords:** Prehydrolysis, Double salt ionic liquid, Cellulose regeneration, Crystallinity, Viscosity

## 6.1. Introduction

Concerns with climate change have motivated scientist and policymaker to replace fossil fuel based materials and energy consuming processes by sustainable materials and energy efficient processes [1-3]. Lignocellulosic materials are promising alternative for replacing fossil fuel based polymers [4-7]. Cellulose is the most abundant biopolymer followed by lignin and hemicellulose on earth. In high-tech fields like biomedical products, bioenergy sources, and engineered structural reinforcing materials, cellulose is being used in a variety of applications [8-10]. Only a little percentage of cellulose is being used in these days since it is not soluble in common solvents due to the crystalline structure. Therefore, search for effective and green solvents for dissolution of cellulose has been the key task for scientist in past few decades. Recently, interest is growing on ionic liquids (ILs) for dissolution of cellulose. ILs are a distinct category of innovative organic salts that exhibit liquid states at temperatures lower than 100 °C. The extremely low vapor pressure of ILs is an important property. As a result, they are referred to as 'green' solvents, as opposed to typical volatile organic compounds. Chemical and thermal stability, nonflammability, strong ionic conductivity, and a broad electrochemical potential window are just a few of the appealing qualities of ILs [11]. DSILs are special types of ILs that are usually composed of a combination of organic cations with organic or inorganic anions. These liquids have unique properties compared to traditional ILs, including increased solubility and conductivity. DSILs are formed by combining two different ILs that can overcome the limitations of pure ILs, resulting in the formation of a new liquid phase that contains both sets of ions and does not retain their individual nature [11a,11b]. This allows for the creation of liquids with specific properties, such as increased solubility for specific chemical compounds like cellulose or increased ionic conductivity for use in electrochemical devices like batteries [11c] or fuel cells [11d].

Different ILs are being studied for dissolution of cellulose. For the first time, Swatloski *et al.* [12] reported that [$C_4$mim]Cl could successfully dissolve cellulose. The reason for the high solubility of cellulose in [$C_4$mim]Cl is due the formation of H-bonding within –OH of cellulose and $Cl^-$ of the IL as explained by the authors [13]. The 3-butyric acid-1-methyl imidazolium chloride and 3-N,N-diethyl-butyramide-1-methyl imidazolium chloride dissolved 5 wt% cotton fibers completely in 3 h at room temperature [14]. Wei *et al.* [15] showed that the deterioration of wood pulped cellulose in the order of 1-ethyl-3-methylimidazolium dimethyl phosphate followed by 1-butyl-3-ethylimidazolium diethyl phosphate) and 1-ethyl-3-methylimidazolium diethyl

phosphate. No reducing sugar was discovered in any recycled ILs, and the degree of polymerization of regenerated cellulose was reduced by 30.4%. Kosan *et al.* [16] investigated cellulose dissolution in different ILs, $[C_4mim]Cl$, $[C_4mim]CH_3CO_2$, $[C_2mim]Cl$, and $[C_2mim]CH_3CO_2$. The utilization of $[C_2mim]^+$ cation within an IL as opposed to a $[C_4mim]^+$ cation, while maintaining the identical anion, results in decreased zero shear viscosities of the spinning dopes. Using a dry-wet spinning process, cellulose solutions in ILs display good spinnability and produce fibers with comfortable textile physical characteristics. Fort *et al.* [17] studied a simple and novel alternative approach to soluble in the IL 1-n-butyl-3-methylimidazolium chloride ($[C_4mim]Cl$). Cellulose dissolution time and temperature were reduced significantly at pressurized condition [18]. Dissolution cellulose in ILs can be done directly without any modification and is regenerated by anti-solvent, and can be shaped into fibers, films, beads or other types. Molecular dynamics simulations revealed that throughout the dissolving process, the $[C_4mim]Cl$ anions interact strongly with cellulose sites and water molecules. Dopes containing ILs with an acetate anion are more likely to contain the higher cellulose percentage than the dopes that contain ILs with chloride ion. To overcome the viscosity problem of cellulose solution in IL, Yamamoto and Miyake [19] mixed $[C_4mim]CH_3CO_2$ with dimethyl sulfoxide (DMSO), dimethyl acetamide (DMAc), and N,N-dimethylformamide (DMF). Depending on the process temperature, $[C_4mim]Cl$/DMSO could experience a vigorous exothermic reaction.

Prehydrolysis is the key process step for purification of the dissolving pulp. The hemicellulose removal provides an indication about the efficiency of this prehydrolysis process. As a result, bleaching sequences often include at least one stage focused at hemicellulose removal, as it disrupts the viscose process [20]. The decrease in filterability of viscose is associated with the accumulation of byproducts resulting from the oxidative breakdown of hemicellulose [21]. As a result, a high hemicellulose percentage in pulps is detrimental to cellulose dissolution. The spinning properties and viscose fiber quality are extremely dependent on the origin of pulp, carbohydrate composition and molecular weight distribution. The lower contents of ß- and γ-celluloses, as well as a uniform molecular weight distribution are important for viscose strong fiber [22]. During cell wall production, hemicelluloses are deposited as an amorphous element which fill gaps within the fibrils in both primary and secondary walls [23]. Because H-bonding and van der Waals forces between hemicelluloses and cellulose restrict cellulose separation from the cell

wall matrix, removing hemicellulose may enhance cellulosic material breakdown [24,25]. Therefore, the presence of hemicellulose may also affect pulp dissolution in ILs. So far, no report has been presented on the effect of hydrolysis on the dissolution of pulp in ILs. In this investigation, kraft pulp (KP) and prehydrolysis kraft pulp (PHKP) were prepared from hardwood, *Trema orientalis* and the prepared pulps were dissolved in both ILs and their DSILs. The KP, PHKP, regenerated (R) KP and RPHKP were characterized by viscosity, FTIR, XRD, and SEM analysis.

## 6.2. Materials and Methods

The materials and methods applied in this chapter to conduct this study have been described in the following sub-sections.

### 6.2.1. Materials

KP and PHKP were prepared from *Trema orientalis* in the laboratory by following the detailed conditions described elsewhere [6]. The pulping process was carried out in an electrically heated stainless-steel digester of 5L capacity, rotating at 1 rpm. The prehydrolysis was done with water at 170 $^{o}$C for 30 min. The material to liquor ratio was 1:5 (g/mL). The time required to raise max temperature was 40 min. After completing pre-hydrolysis, pressure was released by venting the valve and the liquor was separated from the solid mass by filtration. Then the material was washed with water, disintegrated and kept for pulping.The kraft pulping process was done with the mention procedure. ILs, [$C_4$mim]Cl and [$C_4$mim]$CH_3CO_2$, were purchased from Sigma-Aldrich with purities of $\geq$98% and $\geq$95%, respectively. Acetone (Sigma-Aldrich, $\geq$99.5%) and distilled water (distilled by Laboratory Water Purification System, MRC) were used throughout the study.

### 6.2.2. Preparation of DSIL

To prepare DSIL of [$C_4$mim]$(CH_3CO_2)_{0.6}Cl_{0.}$4, 0.6 mole of [$C_4$mim]$CH_3CO_2$ and 0.4 mole of [$C_4$mim]Cl were mixed together to prepare 10 g of DSIL. The details of the preparation procedure have been described in chapter 2 (sub-section 2.2.2).

### 6.2.3. Characterization

The structure of cellulose and regenerated cellulose, and their morphology and thermal stabilities have been investigated by the following methods.

#### 6.2.3.1. Thermogravimetric analysis

Thermogravimetric analysis was employed to investigate the thermal characteristics of cellulose samples. A comprehensive account of the instrument specifications and operational parameters may be provided in Chapter 5 (Sub-section 5.2.4.1).

#### 6.2.3.2. X-ray diffraction (XRD) analysis

The X-ray diffractometer was utilized to investigate the crystallinity and crystal structure of the cellulose samples. A comprehensive account of the instrument specifications and operational parameters may be found in Chapter 5 (Sub-section 5.2.4.2).

#### 6.2.3.3. FT-IR spectroscopic analysis

The characterization of the structure of cellulose samples was conducted through the utilization of ATR-FTIR spectroscopy. A comprehensive account of the instrument specifications and operational parameters may be described in Chapter 2 (Sub-section 2.2.3.1).

#### 6.2.3.4. Scanning electron microscopic (SEM) analysis

The investigation of morphology of cellulose samples was conducted by the utilization of scanning electron microscopy (SEM). The instrument specifications and operating parameters have been thoroughly elucidated in Chapter 5 (Sub-section 5.2.4.4).

## 6.3. Results and Discussion

The properties of cellulose including degree of solubility in a particular solvent depends on the method of pulping. To reveal the role of modification of properties of cellulose on the degree of dissolution in ILs, the extents of solubility of KP and KHKP prepared were investigated using different ILs media. However, the properties of pulps prepared are discussed first.

### 6.3.1. Pulp properties

The cellulose pulp yield in pre-hydrolysis kraft process was 35.8%, while the same in the kraft process was 47.9%. During the prehydrolysis step, about 16% of wood biomass (mostly hemicellulose) was dissolved, consequently lowering the pulp yield. In another study, prehydrolysis of jute fiber at 170 ℃ lowered the yield to roughly 80%, resulting in a decrease in overall pulp yield and pulp viscosity [27]. After 60 minutes of prehydrolysis at 150 ℃, jute cutting produced 90% solid residue with a residual pentosan concentration of 9.88% [28]. In the present study, the purity of cellulose in prehydrolysis kraft process was 95.6% with residual pentosan content of 4.2% (Table 6.1). The kappa number of cellulose pulp obtained from the prehydrolysis-kraft process exhibited a reduction of 2.4 points in comparison to the pulp obtained from the kraft process (Table 6.1). In another investigation, the screened pulp yield of $Na_2CO_3$ pre-extracted *Trema orientalis* was almost similar to non-preextracted *T. orientalis* at a kappa number of 21-22, where 2% less alkali was required in cooking [29]. The process of prehydrolysis enhances the delignification of prehydrolyzed biomass through the augmentation of porosity of wood chips, partial degradation of lignin, and cleavage of carbohydrate-lignin linkages [26]. In 10% NaOH ($S_{10}$), both hemicellulose and degraded cellulose are dissolved, while in 18% NaOH ($S_{18}$) only hemicellulose is dissolved. Therefore, $S_{10}$-$S_{18}$ represents degraded cellulose. The degraded cellulose in prehydrolysis kraft process was 11.62% and in the kraft process was 2.66% only. The viscosity of the kraft was 13.61 mPa.s, while the same for pre-hydrolysis pulp was only 3.09 mPa.s. The high purity and controlled viscosity are prerequisite for viscose grade dissolving pulp. The low cellulose viscosity of dissolving pulp is considered a positive trait for the production of superior rayon fiber. In many applications, the viscosity of the dissolving pulp needs to be further decreased before processing the dissolving pulp [30]. In this investigation, the effect of pulp viscosity on the cellulose dissolution in DSIL will also be observed.

**Table 6.1.** Kraft pulp (KP) and pre-hydrolysis pulp (PHKP) properties

| Parameter | PHKP | KP |
|---|---|---|
| Yield, % | 35.8 | 47.9 |
| Kappa number | 16.3 | 18.7 |
| α-cellulose, % | 95.6 | 84.3 |
| Pentosan, % | 4.2 | 9.9 |
| $S_{18}$, % | 4.54 | 15.68 |
| $S_{10}$,% | 16.16 | 18.34 |
| Viscosity, mPa.s | 3.09 | 13.61 |
| Ash content, % | 0.24 | 0.32 |

### 6.3.2. Dissolution of pulp in ILs

The dissolution of KP and PHKP in $[C_4mim]Cl$, $[C_4mim](CH_3CO_2)$ and $C_4mim](CH_3CO_2)_{0.6}Cl_{0.4}$ at 90 ℃ are presented in Table 6.2. The pulp solubility in $[C_4mim]Cl$ and $[C_4mim]CH_3CO_2$ was 14.5% and 19.2% for KP and 15.2% and 20.3% for PHKP, respectively. The solubility increased to 28.7% and 31.3% for KP and PHKP, respectively, using their DSIL. In the previous investigation, solubility of cellulose enhanced with temperature, however the solution became darker in color (Chapter 5). Therefore, pulp solubility was carried out at 90 ℃ in this investigation.

It has been reported that the dissolution of cellulose can be improved by the inclusion of co-solvent, which consequently reduces the viscosity of the mixture of ILs. Olsson *et al.* [31] used N-methylimidazole as a promising co-solvent together with the IL 1-ethyl-3-methylimidazolium acetate and increased cellulose solubility through the reduction of solution viscosity. It was observed that PHKP had slightly higher solubility in both ILs and DSIL. This observation indicates lowered viscosity of PHKP pulp solution in IL (Table 6.1), which will be discussed later. The higher solubility in PHKP can also be explained by impurities, like lignin, hemicellulose, and extractives present in KP. Cao *et al.* [31a] showed that the solubility of cellulose in IL depends on the degree of polymerization (DP). Cao *et al.* discovered that the best dissolution of microcrystalline cellulose in AmimCl was up to 25%, however cellulose samples with increased DP from 516 to 726 reduced the quantity of dissolved product in ILs from 15% and 6%,

respectively [31a]. Liu *et al.* [32] dissolved 16 wt% and 14 wt% cotton pulp in $[C_2mim]CH_3CO_2$ and $[C_2mim]Cl$, respectively at 90 ℃ for 7 h. Ibrahim *et al.* [18] showed that the cellulose dissolution increased under pressurized conditions due to the greater penetration of IL into the cellulose network and breaking the intramolecular hydrogen bonding easily. The higher solubility in DSIL in this investigation is due to the formation of hydrogen bonds between hydroxyl groups cellulose and $Cl^-$ and $CH_3CO_2^-$ anions of DSIL. The anions played a vital role in cellulose solubility through the formation of H- bond. Liu *et al.* [32] showed that the change of anion $Cl^–$ by $Br^–$ keeping cation intact, the cellulose solubility decreased because $Br^–$ had more difficulty in forming hydrogen bonds with cellulose than $Cl^–$.

**Table 6.2.** Dissolution of KP and PHKP in ILs at 90 ℃

| **ILs** | **Dissolution (weight %)** | |
|---|---|---|
| | KP | PHKP |
| $[C_4mim]Cl$ | 14.5 | 15.2 |
| $[C_4mim]CH_3CO_2$ | 19.2 | 20.3 |
| $[C_4mim](CH_3CO_2)_{0.6}Cl_{0.4}$ | 28.7 | 31.3 |

### 6.3.3. Regeneration of KP and PHKP

The water was used as an anti-solvent to regenerate dissolved cellulose in IL. The regenerated cellulose was characterized by SEM, XRD, thermogravimetric analysis (TGA), and Fourier transform infrared (FTIR) spectroscopy. Fig. 6.1 shows that photograph of KP and PHKP solution and regenerated cellulose. The appearance of the KP solution and was slightly lighter in color, which can be explained by lower viscosity. Raut *et al.* [33] also showed that the regenerated pulp in ILs $[C_4mim]CH_3CO_2$, $[C_2mim]CH_3CO_2$ $[C_4mim][HSO_4]$ and $[C_2mim]Cl$ was darker color compared to a whiter regenerated pulp for $[C_4mim]Cl$ and $[C_2mim]CH_3CO_2$ ILs. The dark color in the regenerated pulp can be explained by several occurrences: first, the possible conversion of cellulose into sugars through partial hydrolysis, which is subsequently broken down by oxidative reactions giving the samples a characteristic brown color [34]. Furthermore, the presence of residual ions resulting from the synthesis process, condensed gaseous substances, or water vapor can potentially induce alterations in hue [35].

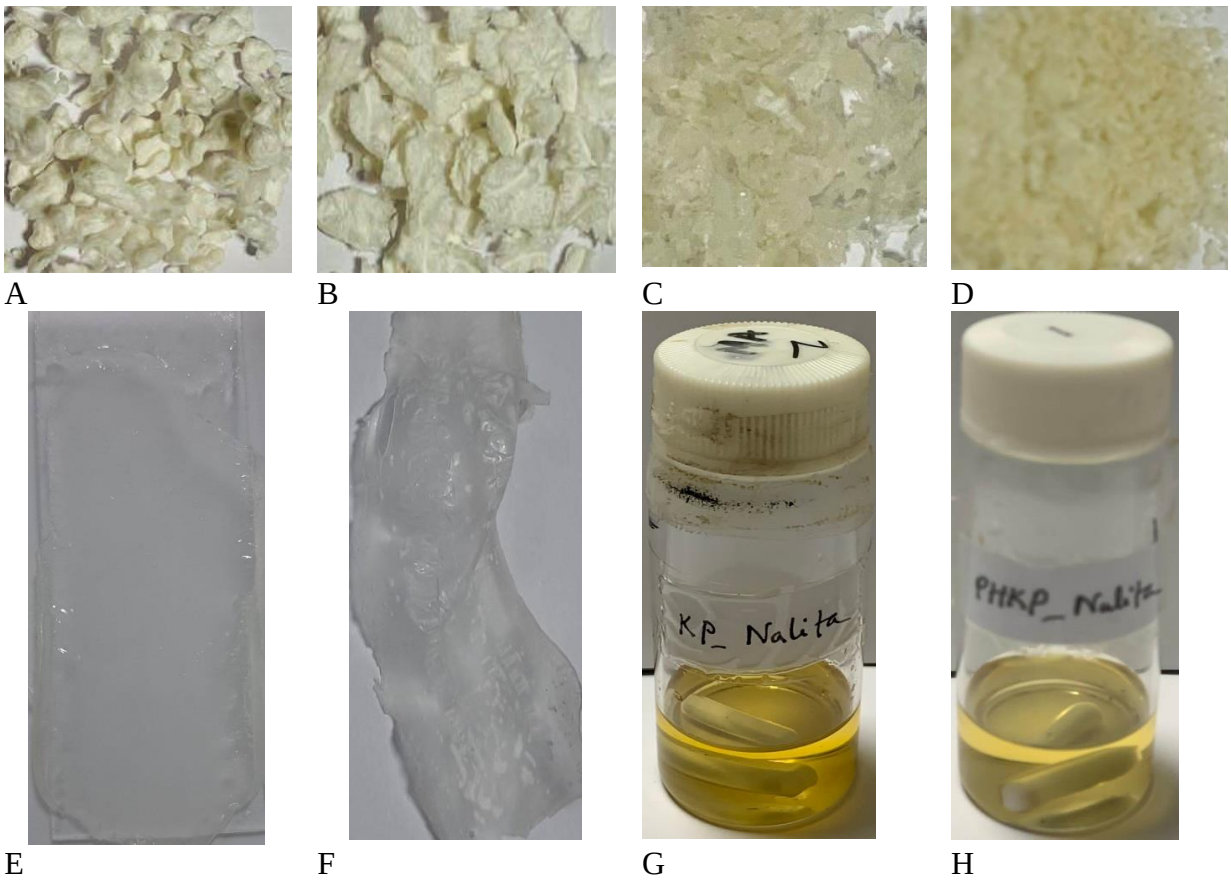


**Figure 6.1.** Photographs of (A) KP, (B) PHKP, (C) RKP, (D) RPHKP, (E) film before drying, (F) film after drying, (G) KP solution in $[C_4mim](CH_3CO_2)_{0.6}Cl_{0.4}$ and (H) PHKP solution in $[C_4mim](CH_3CO_2)_{0.6}Cl_{0.4}$

SEM analysis was performed on the samples to assess the morphology of the regenerated cellulose films KP and PHKP. As shown in SEM images in Fig. 6.2, homogeneous and smooth surface of cellulose film suggested that the dissolution of both KP and PHKP in DSIL was successful. Moreover, the film became plasticized after treatment with $[C_4mim](CH_3CO_2)_{0.6}Cl_{0.4}$. The regenerated cellulose film from PHKP was much smoother than KP. Reyes *et al.* [36] found plasticized forms resembling smooth gels in $[C_4mim]CH_3CO_2$ which was whiter in contrast to a less white in $[C_2mim]CH_3CO_2$ their studies also showed a smooth surface during the regeneration of cellulose film, but nodules and contours were found [37, 38]. Liu *et al.* also showed that nodules and contours in cellulose film when plasticized (sorbitol and carboxymethyl cellulose) was used, but a better homogeneous and smooth morphology of the cellulose film was observed when cellulose solution blended with glycerol.

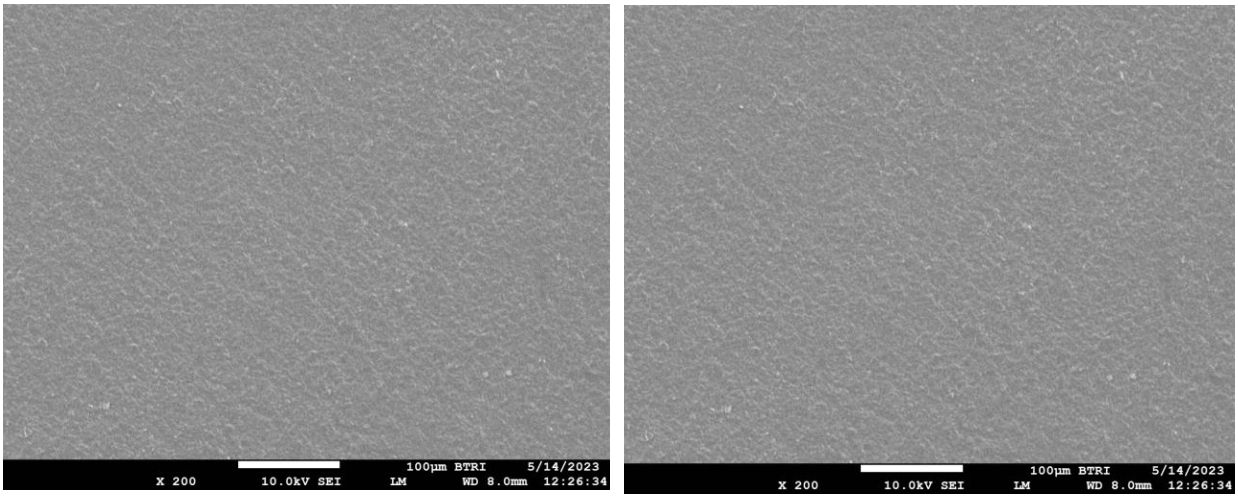


KP PHKP

**Figure 6.2.** SEM micrographs of KP and PHKP

### 6.3.4. Viscosity of regenerated KP, PHKP

After a steady state of homogeneous cellulose solution formation, the shear to the cellulose solution was applied by the rotation in rheometer cone. In general concept, viscosity increases with polymer concentration and decreases with temperature. In this experiment, cellulose concentration was constant. The viscosities of 5 wt% KP, PHKP, RKP, and RPHKP dissolved in $[C_4mim](CH_3CO_2)_{0.6}Cl_{0.4}$ and investigated as a function of temperature.

As is expected, the viscosity decreased with temperature (Fig. 6.3). The viscosity of KP was 32950 mPa.s at 30 ℃, which decreased to 20340 mPa.s on regeneration, while the viscosity of PHKP 27140 Pa.s, which increased 36380 mPa.s on regeneration. It means that a slight degradation of KP occurred during the dissolution process but in the PHKP new crystalline structure was formed during the regeneration process. Thus, the regenerated PHKP films are expected to have good mechanical properties.

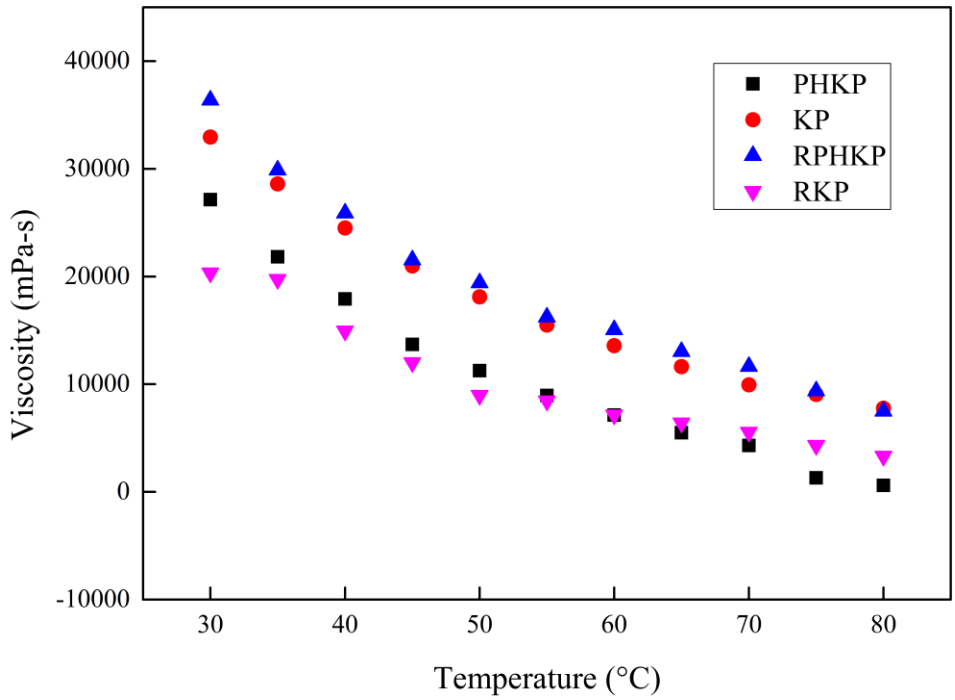


**Figure 6.3.** The variation of viscosity of 5 wt % KP, PHKP, RKP and RPHKP in $[C_4mim](CH_3CO_2)_{0.6}Cl_{0.4}$ solution at temperatures 30-80 ℃ with 5 ℃ intervals

### 6.3.5. XRD analysis

The X-ray diffraction patterns of original KP and PHKP and regenerated pulps are shown in Fig. 6.4. The diffraction pattern of original KP and PHKP exhibited typical cellulose I structure. Characteristic sharp diffraction peak was located at 22.6◦ and a wide peak between 15.5º, which correspond to (200) and (110) planes, respectively. The peak at 2θ = 22º is sharper for PHKP. The sharper detraction peak is an indication of higher crystallinity degree. The crystallinity index of KP was found to be 75.7 %, which increased to 79.7 % during hydrolysis due to the loss of amorphous hemicellulose.

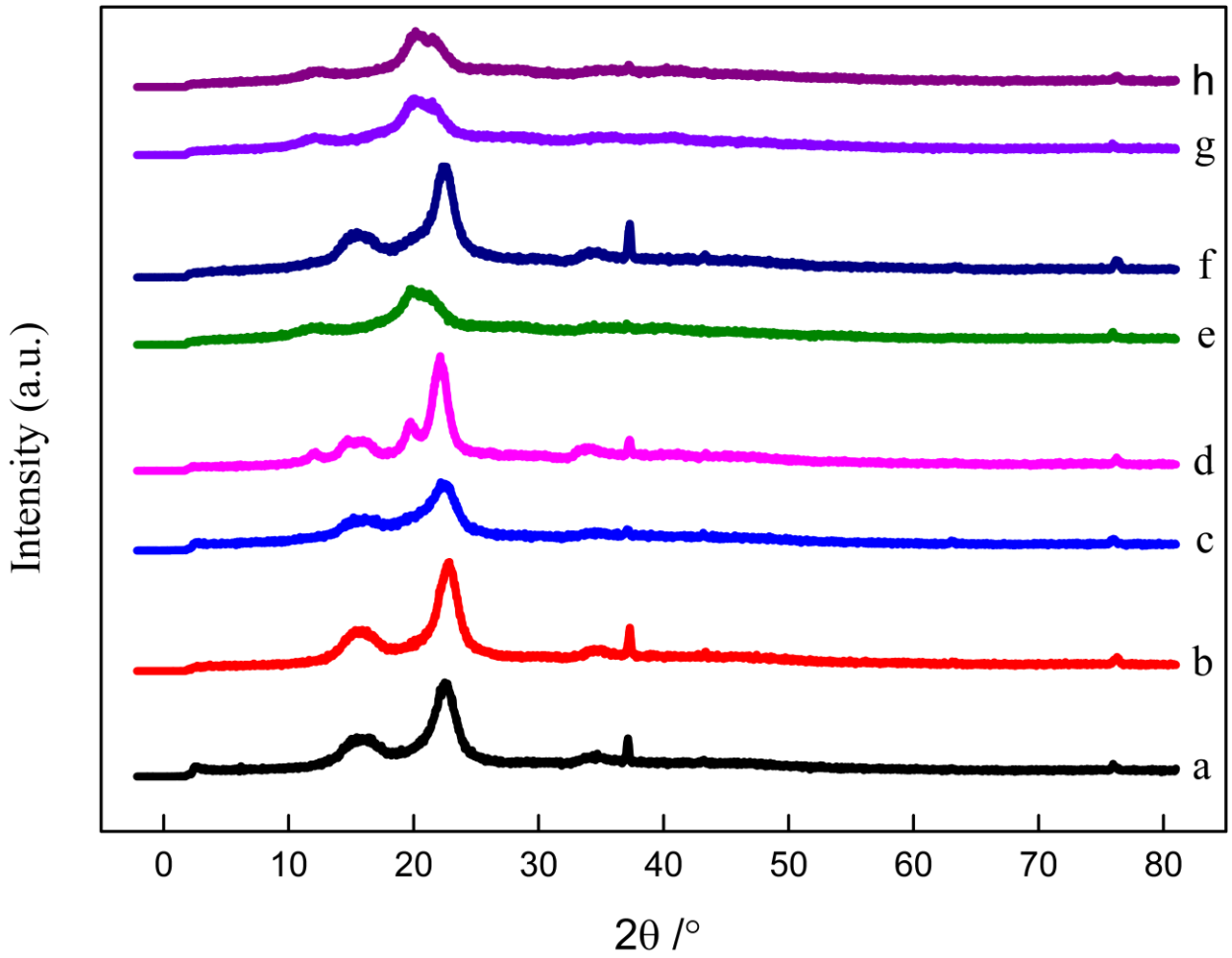


**Figure 6.4.** XRD patterns of (a) KP, (b) PHKP (c) RKP regenerated from $[C_4mim]Cl$, (d) RPHKP from $[C_4mim]Cl$, (e) RKP from $[C_4mim]CH_3CO_2$, (f) RPHKP from $[C_4mim]CH_3CO_2$,(g) RKP from $[C_4mim](CH_3CO_2)_{0.6}Cl_{0.4}$, (h) RPHKP from $[C_4mim](CH_3CO_2)_{0.6}Cl_{0.4}$

The regenerated KP and PHKP regenerated from cellulose and DSIL solution and regenerated KP from cellulose and $[C_4mim]CH_3CO_2$ solution demonstrated broad peak at approximately 12.8 and 20.5º with Miller indices of (110), (110) (direction c of the unit cell is along the chain axis of the polymer), which characterized for the crystalline form of cellulose II structure. The findings revealed that the cellulose I crystal structure shifted to cellulose II during pulp disintegration and regeneration [39]. This phenomenon was also reported in other studies for cellulose dissolution in ILs [18]. The simple association or aggregation of cellulose chains in ILs may have been what caused this change in the crystalline structure of the cellulose pulp. But the regenerated KP and PHKP from $[C_4mim]Cl$ and RPHKP from $[C_4mim]CH_3CO_2$ maintained their original cellulose I structure. There was no significant difference between the crystallinity index of original KP and

PHKP with RKP and RPHKP (Table 6.3) except regenerated KP from [$C_4$mim]Cl. The crystallinity index and crystalline structure of regenerated PHKP in both ILs [$C_4$mim]$CH_3CO_2$ [$C_4$mim]Cl were similar, which indicated that the pre-hydrolysis process help to get original structure of cellulose II. In most of the studies showed that the crystallinity index decreased during the regeneration process from the ILs solution due to the breaking down of hydrogen bonds in the dissolution process, thus destroying the original crystalline [32, 37].

**Table 6.3.** The crystallinity of KP, PHKP, RKP and RPHKP regenerated from different IL media

| **Pulp** | **Crystallinity degree (2 θ / º)** | **Crystallinity index (%)** |
|---|---|---|
| KP | 22.5 | 75.7 |
| PHKP | 22.7 | 79.7 |
| RKP from [$C_4$mim]Cl | 22.3 | 61.6 |
| RPHKP from [$C_4$mim]Cl | 22.1 | 85.5 |
| RKP from [$C_4$mim]$CH_3CO_2$ | 20.0 | 73.7 |
| RPHKP from [$C_4$mim]$CH_3CO_2$ | 22.3 | 75.7 |
| RKP from [$C_4$mim]$(CH_3CO_2)_{0.6}Cl_{0.4}$ | 20.3 | 74.4 |
| RPHKP from [$C_4$mim]$(CH_3CO_2)_{0.6}Cl_{0.4}$ | 20.1 | 76.7 |

### 6.3.6. FTIR spectroscopic analysis

Fig. 6.5 shows that the FTIR spectra of the regenerated pulps from dissolved KP and PHKP in [$C_4$mim]Cl, [$C_4$mim]$CH_3CO_2$ and their DS was similar to that of the original KP and PHKP. This observation indicates that the dissolution and regeneration processes solely included the breaking of H-bonds, without any other chemical reactions taking place. As shown in Fig. 6.5, the band at 3340-3420 $cm^{-1}$ related to stretching of H-bonded OH groups and around 2900 $cm^{-1}$ to the C-H stretching [40, 41] . The peak at around 1645 $cm^{-1}$ was observed in all samples, which is attributed to water associated with the amorphous region [42]. All samples showed a band at 1430 $cm^{-1}$, indicating that they all contained a mixture of amorphous cellulose and crystalline cellulose II. [39]. The bending vibration of O-H is giving rise to the band at 1372 $cm^{-1}$, whereas stretching vibration of the C-O bond is responsible for the characteristic band at 1215 $cm^{-1}$. All samples exhibited bands at 1375, 1315, and 1156 $cm^{-1}$ corresponding to CH-stretching, $CH_2$ wagging, and

C-O stretching in cellulose IL, respectively [43]. These results suggested that the all samples had mixture of cellulose I and II in different proportions.

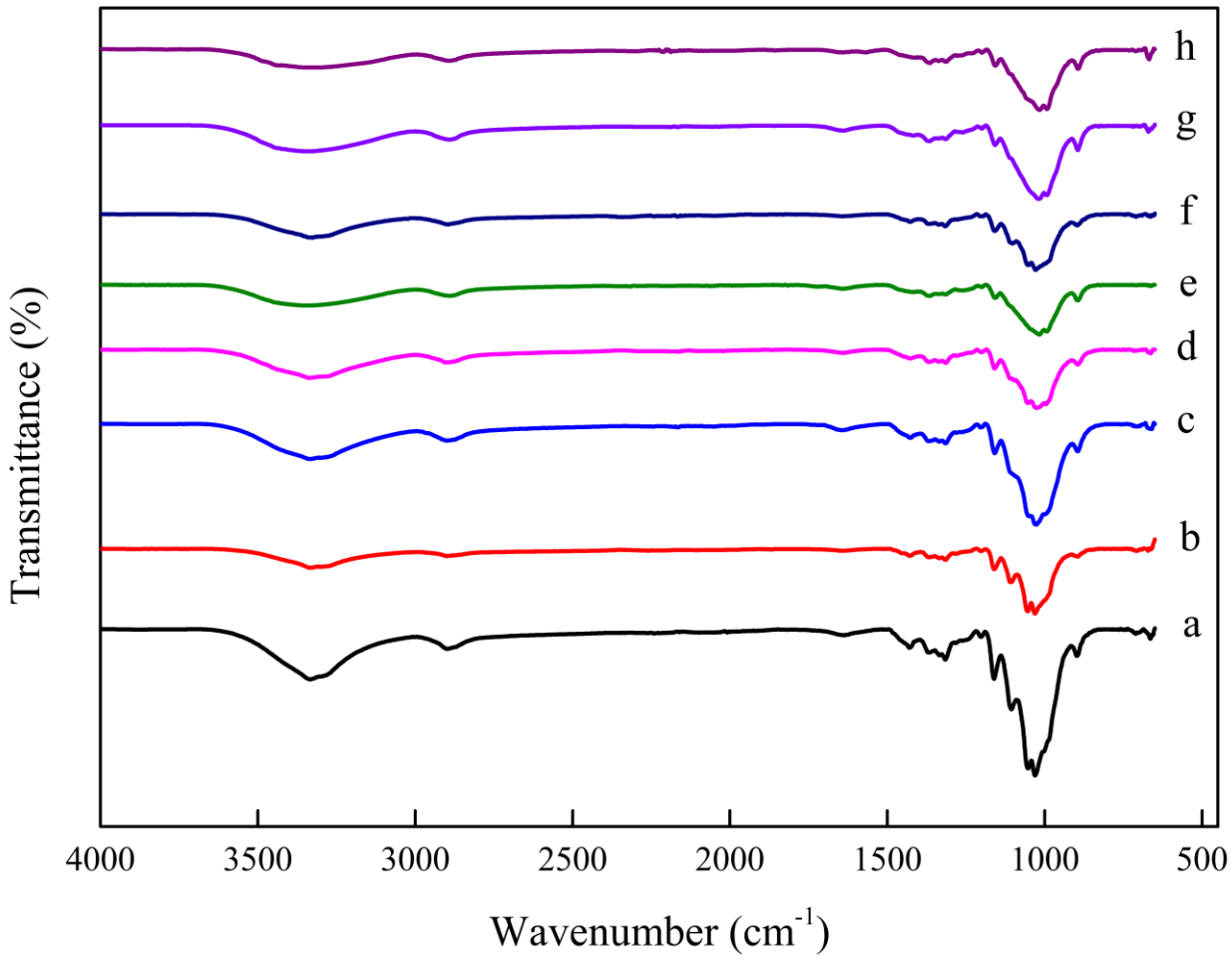


**Figure 6.5**. ATR-FTIR spectra of (a) KP of Nalita, (b) pre-hydrolyzed PHKP of Nalita, (c) Regenerated (R) KP from [$C_4$mim]Cl, (d) RPHKP from [$C_4$mim]Cl, (e) RKP from [$C_4$mim]$CH_3CO_2$, (f) RPHKP from [$C_4$mim]$CH_3CO_2$,(g) RKP from [$C_4$mim]$(CH_3CO_2)_{0.6}Cl_{0.4}$, (h) RPHKP from [$C_4$mim]$(CH_3CO_2)_{0.6}Cl_{0.4}$

A clear band at 894 $cm^{-1}$ was discovered, which corresponds to glycosidic C-H deformation with ring vibration and O-H bending of glycosidic linkages between glucose molecules in cellulose, that had higher intensity in the spectra of regenerated KP and PHKP from DSIL and KP from [$C_4$mim]$CH_3CO_2$ [44]. This observation is well consistent with XRD results (Table 6.3). It also noted that a similar FTIR result was found for regenerated cellulose films from ILs [37]. Carrillo *et al.* also showed that the intensity of this band was relatively higher in cellulose I as compared with cellulose II.

### 6.3.7. TG analysis

The TGA and DTG thermograms of KP, PHKP and regenerated pulps from different ILs are shown in Figs. 6.6 and 6.7 As shown in Fig. 6.6, the water desorption was observed at around 100-110 ℃, which accounts 5-6% for KP and PHKP, while regenerated KP and PHKP from [$C_4$mim]Cl lost 4-5% weight at around 85C then the weight loses remained constant up to 230 ℃. Initial weight loss for regenerated KP and PHKP was about 6-7% at around 150 ℃.

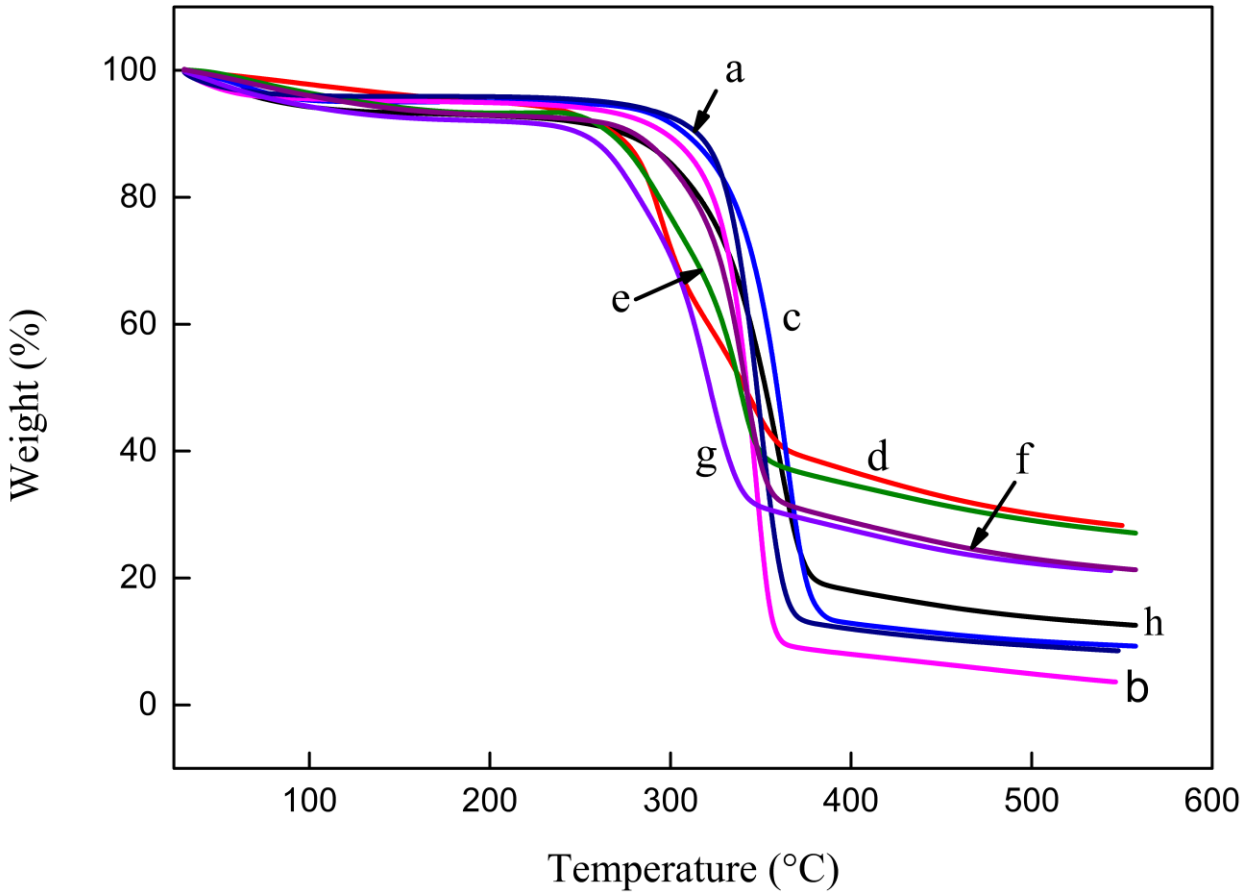


**Figure 6.6.** XRD pattern of (a) KP of Nalita, (b) PHKP of Nalita, (c) Regenerated (R) KP from [$C_4$mim]Cl, (d) RPHKP from [$C_4$mim]Cl, (e) RKP from [$C_4$mim]$CH_3CO_2$, (f) RPHKP from [$C_4$mim]$CH_3CO_2$,(g) RKP from [$C_4$mim]$(CH_3CO_2)_{0.6}Cl_{0.4}$, (h) RPHKP from [$C_4$mim]$(CH_3CO_2)_{0.6}Cl_{0.4}$

The rapid decomposition was observed between 240 and 390 ℃ depending on samples. Due to the higher onset temperature of decomposition of KP, it exhibited the highest thermal stability. But the degradation behavior of PHKP was different, the degradation temperature started at 230 ℃ and continued to 364 ℃, where 40% residues remained. Further rise of temperature, the

degradation continued up to 545 ℃ and residue remained 28%. The high degree of crystallinity of cellulose showed superior thermal stability. Cellulose with higher DP values had a greater resilience to thermal breakdown than the cellulose with lower DP values [44]. Pang *et al*. [37] investigated this relation between DP values and the thermal stability. It was observed that the enhanced thermal stability of regenerated cellulose had a positive correlation with the rise in the DP values. These results suggested that the thermal stability of cellulose is somewhat dependent on the DP values of the cellulose. As seen from the DTG curves in Fig. 6.7, pyrolysis of 200 PHKP revealed two degradation peaks, indicating that the PHKP contains some low molecular weight cellulose. This result is consistent with viscosity data (Fig. 6.7).

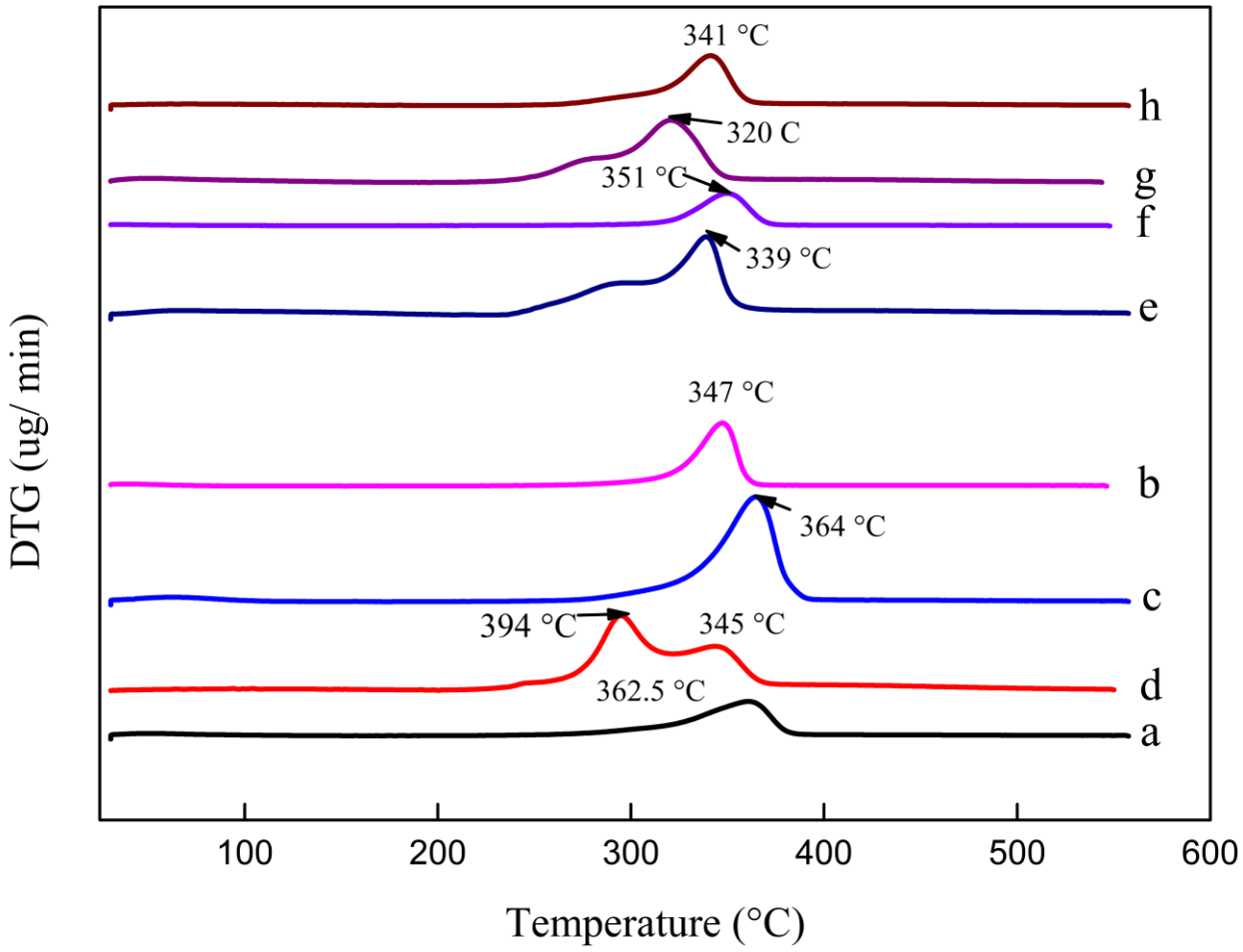


**Figure 6.7.** XRD patterns of (a) KP, (b) PHKP, (c) RKP from $[C_4mim]Cl$, (d) RPHKP from $[C_4mim]Cl$, (e) RKP from $[C_4mim]CH_3CO_2$, (f) RPHKP from $[C_4mim]CH_3CO_2$,(g) RKP from $[C_4mim](CH_3CO_2)_{0.6}Cl_{0.4}$, (h) RPHKP from $[C_4mim](CH_3CO_2)_{0.6}Cl_{0.4}$

## 6.4. Conclusions

The pre-hydrolysis procedure improved α-cellulose content (95.6%) and reduced residual pentosan (4.2%) in pulp. The pre-hydrolysis process also increased cellulose solubility in both ILs and DSIL. Cellulose film with a homogeneous and smooth surface was formed during the regeneration of both KP and PHKP in DSIL, which suggested a complete dissolution of both KP and PHKP occurred and became plasticized after treatment with $[C_4mim](CH_3CO_2)_{0.6}Cl_{0.4}$. The crystallinity index and crystalline structure of regenerated PHKP in both ILs $[C_4mim]CH_3CO_2$ $[C_4mim]Cl$ were similar, which indicated that the pre-hydrolysis process helped to get the original structure of cellulose II. The pre-hydrolysis process decreased pulp viscosity. The viscosity of PHKP was 27140 mPa.s, which increased by 36380 mPa.s on regeneration, which is expected to have good mechanical properties of the regenerated PHKP films.

**References**


[1] Fiorentino, G., Zucaro, A., and Ulgiati, S. (2019). Towards an energy efficient chemistry. Switching from fossil to bio-based products in a life cycle perspective. *Energy*, *170*, 720-729.

[2] Mikulčić, H., Klemeš, J. J., Vujanović, M., Urbaniec, K., and Duić, N. (2016). Reducing greenhouse gasses emissions by fostering the deployment of alternative raw materials and energy sources in the cleaner cement manufacturing process. *Journal of cleaner production*, *136*, 119-132.

[3] Rahimifard, S., Seow, Y., and Childs, T. (2010). Minimising Embodied Product Energy to support energy efficient manufacturing. *CIRP Annals*, *59*(1), 25-28.

[4] Ahsan, L., Jahan, M. S., and Ni, Y. (2014). Recovering/concentrating of hemicellulosic sugars and acetic acid by nanofiltration and reverse osmosis from prehydrolysis liquor of kraft based hardwood dissolving pulp process. *Bioresource Technology*, *155*, 111-115.

[5] Jahan, M. S., Uddin, M. N., and Akhtaruzzaman, A. F. M. (2016). An approach for the use of agricultural by-products through a biorefinery in Bangladesh. *The Forestry Chronicle*, *92*(4), 447-452.

[6] Jahan, M. S., Chowdhury, D. N., and Islam, M. K. (2007). Atmospheric formic acid pulping and TCF bleaching of dhaincha (Sesbania aculeata), kash (Saccharum spontaneum) and banana stem (Musa Cavendish). *Industrial Crops and Products*, *26*(3), 324-331.

[7] Sutradhar, S., Arafat, K. M. Y., Nayeem, J., and Jahan, M. S. (2020). Organic acid lignin from rice straw in phenol-formaldehyde resin preparation for plywood. *Cellul Chem Technol*, *54*(5-6), 463-471.

[8] Seddiqi, H., Oliaei, E., Honarkar, H., Jin, J., Geonzon, L. C., Bacabac, R. G., and Klein-Nulend, J. (2021). Cellulose and its derivatives: Towards biomedical applications. *Cellulose*, *28*(4), 1893-1931.

[9] Ong, V. Z., and Wu, T. Y. (2020). An application of ultrasonication in lignocellulosic biomass valorisation into bio-energy and bio-based products. *Renewable and Sustainable Energy Reviews*, *132*, 109924.

[10] Zhang, L., Guan, Y., and Rao, J. (2018). Preparation and characterization of hybrid film from cellulose and $Fe_3O_4$ nanoparticles. *Cellulose Chemistry and Technology*, *52*(3-4), 209-214.

[11] Seddon, K. (2002). Ionic liquids: designer solvents for green synthesis. *Chemical Engineer*, 730, 33-35.

[11a] Chatel, Gregory, Jorge FB Pereira, Varun Debbeti, Hui Wang, and Robin D. Rogers. "Mixing ionic liquids–"simple mixtures" or "double salts"?." *Green Chemistry* 16, no. 4 (2014): 2051-2083.

[11b] Rahman, A., Rahman, M. M., Mollah, M. Y. A., and Susan, M. A. B. H. (2019). Ultraslow Relaxation in Aprotic Double Salt Ionic Liquids. *The Journal of Physical Chemistry B*, *123*(26), 5577-5587.

[11c] Saikat, M. S. H., Islam, M. M., Mollah, M. Y. A., Susan, M. A. B. H., and Miran, M. S. (2019). Thermal and electrochemical properties of protic ionic liquids and their binary mixtures with water. *Materials Today: Proceedings*, *15*, 498-503.

[11d] Miran, M. S., Yasuda, T., Susan, M. A. B. H., Dokko, K., and Watanabe, M. (2014). Binary protic ionic liquid mixtures as a proton conductor: high fuel cell reaction activity and facile proton transport. *The Journal of Physical Chemistry C*, *118*(48), 27631-27639.

[12] Swatloski, R. P., Spear, S. K., Holbrey, J. D., and Rogers, R. D. (2002). Dissolution of cellose with ionic liquids. *Journal of the American Chemical Society*, *124*(18), 4974-4975.

[13] Moulthrop, J. S., Swatloski, R. P., Moyna, G., and Rogers, R. D. (2005). High-resolution 13C NMR studies of cellulose and cellulose oligomers in ionic liquid solutions. *Chemical Communications*, (12), 1557-1559.

[14] Aghmih, K., Bouftou, A., El Bouchti, M., Boukhriss, A., Gmouh, S., and Majid, S. (2023). Synthesis and application of functionalized ionic liquids-based imidazolium as solvent for cotton fibre cellulose dissolution. *Cellulose*, *30*(3), 1467-1481.

[15] Wei, J., Gao, H., Li, Y., and Nie, Y. (2022). Research on the degradation behaviors of wood pulp cellulose in ionic liquids. *Journal of Molecular Liquids*, *356*, 119071.

[16] Kosan, B., Michels, C., and Meister, F. (2008). Dissolution and forming of cellulose with ionic liquids. *Cellulose*, *15*(1), 59-66. Fort, D. A., Remsing, R. C., Swatloski, R. P.,

[17] Moyna, P., Moyna, G., and Rogers, R. D. (2007). Can ionic liquids dissolve wood? Processing and analysis of lignocellulosic materials with 1-n-butyl-3-methylimidazolium chloride. *Green Chemistry*, *9*(1), 63-69.

[18] Ibrahim, F., Moniruzzaman, M., Yusup, S., and Uemura, Y. (2015). Dissolution of cellulose with ionic liquid in pressurized cell. *Journal of Molecular Liquids*, *211*, 370-372.

[19] Yamamoto, Y. K., and Miyake, A. (2017). Influence of a mixed solvent containing ionic liquids on the thermal hazard of the cellulose dissolution process. *Journal of Thermal Analysis and Calorimetry*, *127*(1), 743-748.

[20] Schlesinger, R., Röder, T., Götzinger, G., Sixta, H., Harasek, M., Friedl, A. Influence of hemicellulose aggregate and gel layer formation on flux and retention during nanofiltration of alkaline solutions. *Desalination* 2005, *175*, 121–134.

[21] Serkov, A. A., Kuzicheva, N. A., Fedotova, V. K., and Kruglova, N. I. (1986). Effect of hemicellulose on the productivity of mercerizing units and viscose filterability. *Fibre Chemistry*, *17*(5), 364-366.

[22] Strunk, P., Lindgren, Å., Eliasson, B., and Agnemo, R. (2012). Chemical changes of cellulose pulps in the processing to viscose dope. *Cellulose Chemistry and Technol*ogy, *46*(9-10), 559-569.

[23] Wan J, Wang Y, Xiao Q (2010) Effects of hemicellulose removal on cellulose fiber structure and recycling characteristics of eucalyptus pulp. *Bioresources Technology*, 101, 4577–4583

[24] Moigne N, Navard P (2010) Dissolution mechanisms of wood cellulose fibres in NaOH–water. *Cellulose* 17:31–45.

[25] Shi Z, Yang Q, Cai J, Kuga S, Matsumoto Y (2014) Effects of lignin and hemicellulose contents on dissolution of wood pulp in aqueous NaOH/urea solution. *Cellulose* 21:1205–1215.

[26] Sixta H. (2006). Handbook of pulp. Herbert Sixta. Wiley-VCH, 325-365.

[27] Jahan, M. S., "Studies on the effect of prehydrolysis and amine in cooking liquor on producing dissolving pulp from jute (*Corchorus capsularis*)", *Wood Science and Technology*, 43(3-4): 213 (2009).

[28] Nayeem, J., Jahan, M. S., Popy, R. S., Uddin, M. N., and Quaiyyum, M. A. (2019). Prehydrolysis kraft pulping of jute cutting and caddis mixture for rayon production. *TAPPI Journal*, *18*(5), 287-293.

[29] Jahan, M. S., Sarkar, M., and Rahman, M. M. (2015). Sodium carbonate pre-extraction of Trema orientalis in the production of paper grade pulp. *Drewno. Prace Naukowe. Doniesienia. Komunikaty*, *58*(195).

[30] Liu, S., Wang, Q., Yang, G., Chen, J., Ni, Y., and Ji, X. (2015). Kinetics of viscosity decrease by cellulase treatment of bleached hardwood kraft-based dissolving Pulp. *BioResources*, *10*(2), 2418-2424.

[31] Olsson, C., Hedlund, A., Idström, A., and Westman, G. (2014). Effect of methylimidazole on cellulose/ionic liquid solutions and regenerated material therefrom. *Journal of Materials Science*, *49*, 3423-3433.

[31a] Cao, Y., Li, H., Zhang, Y., Zhang, J., and He, J. (2009). Structure and properties of novel regenerated cellulose films prepared from cornhusk cellulose in room temperature ionic liquids. *Journal of Applied Polymer Science*, *116*(1), 547-554.

[32] Liu, Z., Wang, H., Li, Z., Lu, X., Zhang, X., Zhang, S., and Zhou, K. (2011). Characterization of the regenerated cellulose films in ionic liquids and rheological properties of the solutions. *Materials Chemistry and Physics*, *128*(1-2), 220-227.

[33] Raut, D. G., Sundman, O., Su, W., Virtanen, P., Sugano, Y., Kordas, K., and Mikkola, J. P. (2015). A morpholinium ionic liquid for cellulose dissolution. *Carbohydrate Polymers*, *130*, 18-25.

[34] Zhou, L., Yang, X., Xu, J., Shi, M., Wang, F., Chen, C., and Xu, J. (2015). Depolymerization of cellulose to glucose by oxidation–hydrolysis. *Green Chemistry*, *17*(3), 1519-1524.

[35] Shen, Y., Zhang, Y., Han, D., Wang, Z., Kuehner, D., and Niu, L. (2009). Preparation of colorless ionic liquids “on water” for spectroscopy. *Talanta*, *78*(3), 805-808.

[36] Reyes, G., Aguayo, M. G., Fernández Pérez, A., Pääkkönen, T., Gacitúa, W., and Rojas, O. J. (2019). Dissolution and hydrolysis of bleached kraft pulp using ionic liquids. *Polymers*, *11*(4), 673.

[37] Pang, J. H., Liu, X., Wu, M., Wu, Y. Y., Zhang, X. M., and Sun, R. C. (2014). Fabrication and characterization of regenerated cellulose films using different ionic liquids. *Journal of Spectroscopy*, *2014*.

[38] Liu, X., Pang, J., Zhang, X., Wu, Y., and Sun, R. (2013). Regenerated cellulose film with enhanced tensile strength prepared with ionic liquid 1-ethyl-3-methylimidazolium acetate (EMIMAc). *Cellulose*, *20*, 1391-1399.

[39] Nelson, M. L., and O'Connor, R. T. (1964). Relation of certain infrared bands to cellulose crystallinity and crystal lattice type. Part II. A new infrared ratio for estimation of crystallinity in celluloses I and II. *Journal of Applied Polymer Science*, *8*(3), 1325-1341.

[40] Perera, P. N., Fega, K. R., Lawrence, C., Sundstrom, E. J., Tomlinson-Phillips, J., and Ben-Amotz, D. (2009). Observation of water dangling OH bonds around dissolved nonpolar groups. *Proceedings of the National Academy of Sciences*, *106*(30), 12230-12234.

[41] Parida, C., Dash, S. K., and Pradhan, C. (2014). FTIR and Raman studies of cellulose fibers of luffa cylindrica. *Open Journal of Composite Materials*, *5*(01), 5.

[42] Yin, J., Luo, K., Chen, X., and Khutoryanskiy, V. V. (2006). Miscibility studies of the blends of chitosan with some cellulose ethers. *Carbohydrate Polymers*, *63*(2), 238-244.

[43] Široký, J., Blackburn, R. S., Bechtold, T., Taylor, J., and White, P. (2010). Attenuated total reflectance Fourier-transform Infrared spectroscopy analysis of crystallinity changes in lyocell following continuous treatment with sodium hydroxide. *Cellulose*, *17*, 103-115.

[44] Carrillo, F., Colom, X., Sunol, J. J., and Saurina, J. (2004). Structural FTIR analysis and thermal characterization of lyocell and viscose-type fibers. *European Polymer Journal*, *40*(9), 2229-2234.

# Chapter 7

## Recycling and Reuse of Double Salt Ionic Liquid


### Abstract

Ionic liquids (ILs) are much more expensive than other common solvents involved in the cellulose dissolution and derivatization process, recovery operations of ILs must be highly efficient to make it economically viable and sustainable. Double salt ionic liquids (DSIL) is the combination of two single ILs with common ions or different ions where new intermolecular interactions occur producing tunable physicochemical properties. In this chapter, the attempts that were taken for recycling a DSIL of $[C_4mim](CH_3CO_2)_{0.6}Cl_{0.4}$ after the dissolution of pre-hydrolyzed kraft pulp (PHKP) are discussed. The recycled DSIL was used repeatedly use for the dissolution of fresh PHKP and regeneration of PHKP up to five times. The regenerated cellulose (RC) was obtained from cellulose-DSIL solution using water as an anti-solvent, which was then removed via filtration. The filtrate was subsequently evaporated and dried to obtain purified DSIL. The PHKP was completely dissolved in recycled DSIL, and RC was 94-98%. The recovery of DSIL was 99.4% after five consecutive cycles. The recycled DSIL and RC were characterized by $^1$H NMR, FT-IR, TGA, and SEM analysis. The $^1$H NMR analysis indicated that there was no noticeable difference observed between the synthesized DSILs and recycled DSIL. The FTIR spectra of recycled DSIL was superimposed on the synthesized DSIL, which confirms that the chemical structure remained unchanged during the dissolution. The crystallinity index of PHKP was found to be 55.69% previously, which was decreased to 20.53% on regeneration and converted from cellulose I to cellulose II structure. SEM images showed that the morphology of the RC fibers was fused into a relatively homogeneous macrostructure, and RC had lower thermal stability as observed by TGA analysis.



**Keywords:** Double salts ionic liquids, recycling, and reuse.


### 7.1. Introduction

Ionic liquids (ILs) have developed into a hopeful method for biomass fractionation and dissolving. These ILs consist of a combination of organic cations and organic or inorganic anions with a melting temperature below 100 °C. ILs have attracted considerable interest as potential

environmental-friendly solvents due to their advantageous properties such as low vapor pressure, excellent chemical and thermal stability, non-flammability, and convenient reusability and recyclability. Pretreatment in ILs often takes place under conditions of moderate temperatures and ambient pressure. Certain ILs completely dissolve wood and other lignocelluloses. A precipitating agent, commonly water or alcohol, is introduced to induce the precipitation of a cellulose fraction within the dissolved biomass. Subsequently, the cellulosic product that has been successfully recovered is subjected to a washing procedure in order to eliminate any remaining ILs. The resultant mixture of precipitation and wash liquids is then subjected to further treatment with the aim of recovering the ILs and any remaining solutes derived from the biomass. The high expense associated with ILs is an important challenge to its successful commercialization. One potential approach for addressing this issue involves the implementation of large-scale IL generation, a strategy that has already been successfully implemented.

Another way is to successfully recycle and reuse ILs, which is also vital for protecting the environment. Many studies were carried out regarding the recycling of ILs in different methods. The recovery of the ILs from the solution of cellulosic-ILs was achieved through the addition of deionized water, which acts as an anti-solvent for the cellulose. The cellulose was subsequently separated from the solution by the process of filtration. The resulting filtrate was then subjected to evaporation and subsequent drying in order to get ILs.

Sun *et al*. [1] investigated that at high biomass loadings, a gel phase is often formed, then cellulose separation becomes difficult, which can be avoided by using water: acetone (1:1, v/v) solution . In a study conducted by Raut *et al.* [2], a recovery rate of 97 wt% of the IL was achieved. The researchers therefore continued to investigate the recovered IL using $^{1}$H NMR spectroscopy. Interestingly, no degradation of the IL was seen during the cellulose dissolution-regeneration cycle. They also observed that the ILs, after recovery, was successfully employed in the dissolution of cellulose for three successive cycles, while maintaining a consistent performance, even in the presence of approximately 3 wt% water. In another study, Huang *et al.* [3] employed molecular distillation to extract the ILs of 1-allyl-3-methylimidazolium chloride (AmimCl) from a homogenous cellulose acetylation reaction media. The IL underwent a total of five cycles of recycling and reutilization under a homogenous cellulose acetylation system, following the application of ideal conditions. The level of purity achieved in the fifth iteration of recycled IL was measured to be 99.56%. Xiong *et al.* [4] introduced an innovative approach to retrieve ILs

through the utilization of carbon dioxide ($CO_2$)-induced creation of aqueous two-phase systems (ATPSs). This study revealed that the addition of amines to aqueous IL solutions at 25 ℃ and atmospheric pressure resulted in the creation of ATPSs upon introduction of $CO_2$. These ATPSs consisted of an upper phase rich in ammonium salts and a lower phase rich in ILs. Elsayed *et al.* [5] examined the spinnability and recyclability of $CH_3CO_2^-$ based ILs across five consecutive cycles. The ILs were retrieved from the coagulation bath through a series of successive heat treatments conducted under reduced pressure. Consequently, the ILs that were retrieved were employed in dissolving cellulose with a weight percentage of 13% in each cycle, without the need for additional IL, resulting in the formation of a uniform solution appropriate for the dry-jet wet spinning process. In their study, Mai *et al.* [6] conducted an investigation on the utilization of simulated moving bed (SMB) chromatography, which was equipped with an ion exclusion column holding the $[C_2mim]^+$ cation. The purpose of this investigation was to separate sugars, specifically glucose and xylose, as well as 1-ethyl-3-methylimidazolium acetate $[C_2mim]CH_3CO_2$. A four-zone SMB system, consisting of two ion exclusion columns in each zone, was employed to extract glucose, xylose, and $[C_2mim]CH_3CO_2$ from the aqueous mixture of biomass treated with IL. The system achieved yields of 71.38% for glucose, 99.37% for xylose, and 98.92% for $[C_2mim]$. A rotary evaporator was employed to achieve a recovery rate of 90% for $[C_2mim]CH_3CO_2$. Furthermore, according to Lazko *et al.* [7], the binary system is predominantly composed of $[C_4mim]Cl$, accounting for around 95% of its composition. Additionally, the study found that $[SBmim][HSO_4]$, specifically 1-(4-sulfobutyl)-3-methylimidazolium hydrogen sulfate, showed the ability to be recovered and reused up to three times without experiencing any loss in its activity.

In chapter 5, it was observed that is $[C_4mim](CH_3CO_2)_{0.6}Cl_{0.4}$ efficiently dissolved cellulose due to double anion $Cl^-$ and $CH_3CO_2^-$ effectively broke the extensive hydrogen bonding network and the ability to dissolve the higher amount of cellulose than the conventional solvent systems. In this study, 5 wt% PHKP was dissolved in the DSIL of $[C_4mim](CH_3CO_2)_{0.6}Cl_{0.4}$, and cellulose was regenerated by using anti-solvent. The DSIL was recovered by evaporation of anti-solvent, and the recovered DSIL was again used to dissolve pure 5 wt% of PHKP, and this process was repeated five times. The RC was characterized by means of XRD, FTIR, TGA, and SEM, and recovered DSILs were characterized by $^1$H-NMR, FTIR, and TGA.

## 7.2. Materials and Methods

The chemicals and methods applied in this chapter to conduct this study have been described in the following sub-sections.

### 7.2.1. Materials

PHKP were prepared from *Trema orientalis* in the laboratory by following the detailed conditions described elsewhere [6] and have been used as a source of cellulose throughout the study. ILs, $[C_4mim]Cl$ and $[C_4mim]CH_3CO_2$, were purchased from Sigma-Aldrich with purities of $\geq$98% and $\geq$95%, respectively. Acetone (Sigma-Aldrich, $\geq$99.5%) and distilled water (distilled by Laboratory Water Purification System, MRC) were used throughout the study.

### 7.2.2. Preparation of DSIL

To prepare DSIL of $[C_4mim](CH_3CO_2)_{0.6}Cl_{0.}4$, 0.6 mole of $[C_4mim]CH_3CO_2$ and 0.4 mole of $[C_4mim]Cl$ were mixed together to prepare 10 g of DSIL. The details of the preparation procedure have been described in chapter 2 (sub-section 2.2.2).

### 7.2.3. Methods for recycling and reuse of DSILs

The way of recycling, purification, and reuse of DSIL, and regeneration of cellulose from cellulose-DSIL solution are illustrated in Scheme 7.1. At first, 5 wt % cellulose was added with the synthesized DSIL. Dissolution of cellulose was carried out by heating at 80 ℃ with continuous stirring. The dissolution of cellulose was confirmed visually and using optical microscopy viewing the absence of cellulose fibers in images. Then, non-solvent for cellulose, water was added to the cellulose-DSILs solution to precipitate cellulose. It was then filtered. The solid phase was termed as regenerated cellulose (RC), which was washed with water several times to remove DSIL completely. The filtrate contained DSILs. Water was evaporated from the filtrate by heating. Acetone was added with the recycled DSIL and heated to evaporate water completely. The recycled DSIL was reused for the dissolution of cellulose.

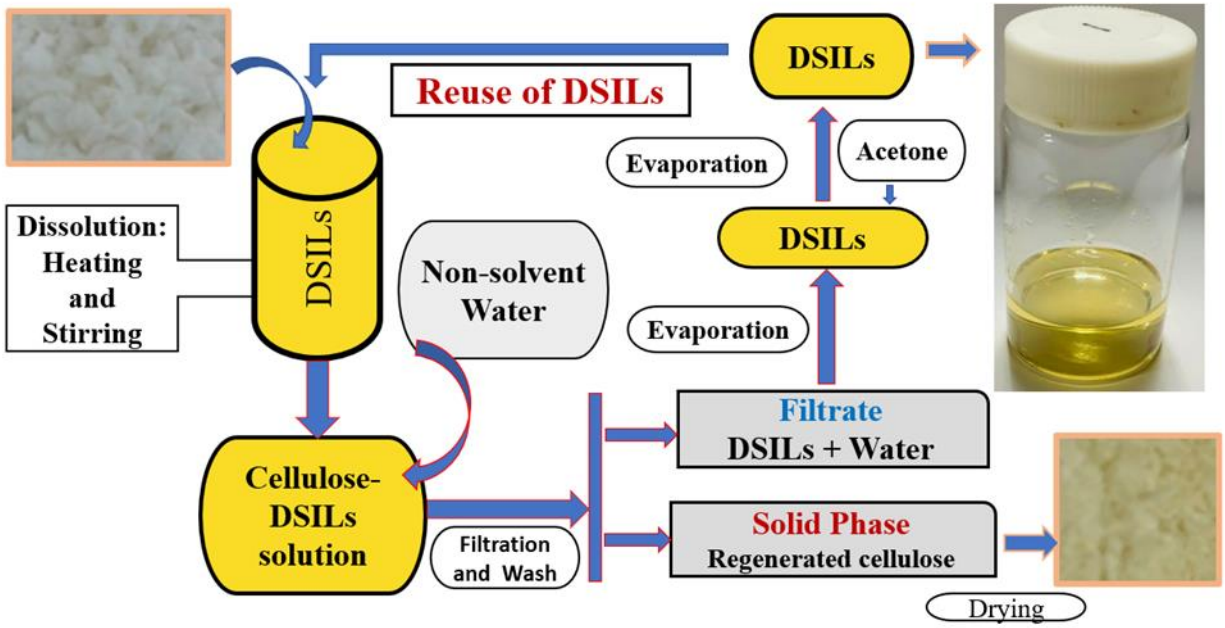


**Scheme 7.1.** Recycling of DSIL and regeneration of cellulose

### 7.2.4. Characterizations

The structure and thermal properties of DSIL, and crystallinity, morphology, and thermal properties of PHKP and regenerated PHKP, have been investigated by the following methods.

#### 7.2.4.1. ATR-FTIR spectroscopic analysis

The structure of ILs and DSIL, cellulose, and RC were characterized by using ATR-FTIR spectroscopy. The details of the instrument and operating conditions have been described in Chapter 2 (Sub-section 2.2.3.1)

#### 7.2.4.2. $^{1}$H NMR spectroscopic analysis

The structure of ILs and DSIL were characterized by using $^{1}$H NMR spectroscopy. The details of the instrument and operating conditions have been described in Chapter 2 (Sub-section 2.2.3.3)

#### 7.2.4.3. X-ray diffraction (XRD) analysis

The crystallinity and crystal structure of the cellulose and the RC were studied by an X-ray diffractometer. The details of the instrument and operating conditions have been described in Chapter 5 (Sub-section 5.2.4.2)

#### 7.2.4.4. Scanning electron microscopic analysis

The morphology of PHKP and regenerated PHKP were studied by using scanning electron microscopy (SEM). The details of the instrument and operating conditions have been described in Chapter 5 (Sub-section 5.2.4.4)

#### 7.2.4.5. Thermogravimetric analysis

The thermal properties ILs, DSIL, cellulose and RC have been studied by thermogravimetric analysis. The details of the instrument and operating conditions have been described in Chapter 5 (Sub-section 5.2.4.1)

## 7.3. Results and Discussion

The necessity of recycling of ILs are important, since the commercial utilization of ILs in biomass pretreatment, fractionation, and cellulose dissolving requires the implementation of recovery and recycling processes due to their high cost. In addition, recycling and successful repeated use of ILs media by keeping the desired quality of RC would be challenging task that are to be clarified.

### 7.3.1. Efficiency of DSIL recycled

The detailed recycling procedure is discussed above. The cellulose was dissolved in the synthesized DSIL. The dissolution of cellulose was carried out by breaking strong intra and inter-molecular H-bonding among the cellulose network. Water was used as an anti-solvent for cellulose as a coagulation solvent for the regeneration of cellulose from the cellulose-DSIL solution. The precipitation, filtration, and RC washing were done several times. The outcomes of these experiments are presented in Table 7.1. Subsequently, the cellulose was separated from the solution using the process of filtration. Finally, the filtrate underwent evaporation and subsequent drying in order to acquire DSIL.

As shown in Table 7.1, cellulose was completely dissolved in recycled DSIL, and regenerated cellulose was 94-98%. The recovery of DSIL was 99% after five cycles. Raut *et al.* [2] recovered 97% IL (N-allyl-N-methylmorpholinium acetate). There was no decomposition of IL occurred upon cellulose dissolution-regeneration cycle as evident by $^{1}$H NMR. Lan *et al.* [11] have used the molecular solvent acetonitrile for the recycling of concentrated [$C_4$mim]Cl solution. They obtained 95% of ILs by the evaporating the molecular solvent followed by drying. They also observed a change in the color of the recycled [$C_4$mim]Cl solution to an amber hue which is likely to be attributed to the presence of pollutants within the [$C_4$mim]Cl solution. The color of recycled DSIL in this experiment was increasingly darker with increased recycle numbers (data are not shown). In a study conducted by Li *et al.*, [12] wood was pretreated with [$C_4$mim]Cl and was recycled four times, and the yield of the recycled IL was found to be 96% when methanol was used as the anti-solvent solvent. On the other hand, when water was used as the anti-solvent, the regeneration yield of the IL was determined to be 91%. The following parts will discuss the attributes of DSIL that have been successfully restored.

The regeneration of cellulose occurred by the formation of H-bonds between water and the free anions in the system and then it removes free anions from the cellulose surface and hydrates the -OH groups of the cellulose network resulting in the formation of H-bonding between the cellulose chain and reformed it [7a]. The presence of cellulose components in the recycled DSIL will result in a decrease in the recovery efficiency of DSILs. The solid RC was washed and dried. The ILs have a strong interaction with water. Troshenkova *et al.* [8] reported that 11 kJ $mole^{-1}$ energy was required for the removal of water which was strongly bonded with ILs forming a complex of $[C_2mim][OAc]\cdot 12H_2O$. Dibble *et al.* [9] proposed the utilization of the strong interaction between water and other solvents that act as hydrogen bond donors with hydrophilic ILs.

Using this concept, in this study dry acetone (<0.1 wt% $H_2O$) has been used as shown in Scheme 7.1. When there is a substantial biomass loading, cellulose separation is challenging because the addition of water causes a gel phase to form. The gel formation was avoided with the addition of water: acetone (1:1, v/v) solution [1]. Gutowski *et al.*, [10] suggested an alternate method for the recycling of ILs, which involves the addition of an aqueous solution containing a kosmotropic anion, such as $PO_4^{3-}$, $CO_3^{2-}$ or $SO_4^{2-}$. This approach is based on the ability of the ILs to form a biphasic system. According to the report, an aqueous biphasic system was formed using $[C_4mim]Cl$, water, and $K_3PO_4$.

**Table 7.1.** Amount of recycled DSILs and regenerated cellulose (RC)

| Cycle No. | Cellulose | DSILs | Regenerated cellulose | | Recycled DSILs | |
|---|---|---|---|---|---|---|
| | g | g | g | % | (g) | % |
| Cycle-1 | 0.50 | 10.98 | 0.49 | 98 | 10.82 | 98.54 |
| Cycle-2 | | 10.82 | 0.47 | 94 | 10.79 | 99.72 |
| Cycle-3 | | 10.79 | 0.48 | 96 | 10.75 | 99.62 |
| Cycle-4 | | 10.75 | 0.47 | 94 | 10.70 | 99.53 |
| Cycle-5 | | 10.70 | 0.48 | 96 | 10.64 | 99.44 |

### 7.3.2. Quality of ILs and DSILs recycled

The recycled ILs media were characterized by following spectral analysis as described below.

#### 7.3.2.1. FTIR spectral analysis

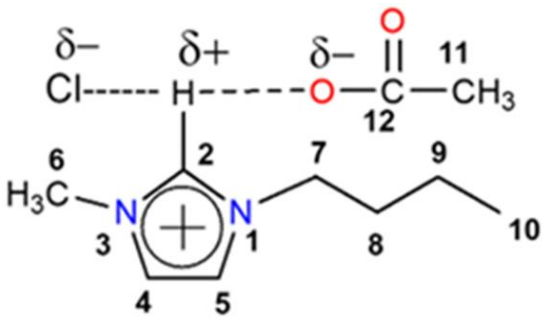


**Scheme 7.2.** Possible structure of DSIL

The FTIR spectra of ILs and recycled ILs have been presented in Fig. 7.1. The FT-IR spectra of synthesized DSIL and recycled DSIL are depicted in Fig. 7.2. As shown from the figures, the FTIR spectra of recycled IL and DSIL are identical to the FTIR spectra of IL and synthesized DSIL. In both spectra, the bands at 3200–2800 $cm^{-1}$ represents the C-H stretching vibrations of the aromatic ring and the alkyl chain length of common cation $[C_4mim]^+$ of $[C_4mim]Cl$ and $[C_4mim]CH_3CO_2$ and recycled $[C_4mim]Cl$ and $[C_4mim]CH_3CO_2$ . In Fig. 7.1, the absorption bands at 2869, 2933, and 2958 $cm^{-1}$ represent several C-H stretching vibrations of the alkyl group. The bands at 3058 and 3146 $cm^{-1}$ indicate the stretching vibration of C(2)-H and C(4, 5), respectively. Cha *et al.* [13] found absorption bands for C(2)-H and C(4, 5)-H stretching vibrations at 3114 and 3163 $cm^{-1}$, respectively. Bands at 2877, 2938, and 2965 $cm^{-1}$ represent several C-H stretching vibrations of the alkyl group. In Fig. 7.2, the C-H stretching vibrations of the alkyl chain and of C(2)-H and C(4, 5) stretching vibrations are found to be similar are 2870, 2935, 2955, and 3046, 3147 $cm^{-1}$, respectively. The peak intensity at 3400 $cm^{-1}$ was almost similar to recycled and corresponding IL. However, in the case of recycled DSIL, the peak intensity at 3397 $cm^{-1}$ was stronger than the synthesized DSIL due to the presence of water. A similar result was observed for the recycled IL, which was assigned to H-bonding due to the presence of water investigated by Haron *et al.* [14]. For $[C_4mim]Cl$ and $[C_4mim]CH_3CO_2$, peaks at 2856, 2877, 2913, 2938 and 2965 $cm^{-1}$ are attributed to the modes of $\nu_{ss}CH_2$, $\nu_{ss}CH_3$, $\nu_{as}CH_2$, $\nu_{FR}CH_3$ and $\nu_{as}CH_3$, respectively (ss, as, and FR represent the symmetric stretch, the antisymmetric stretch, and the Fermi resonance,

respectively)[15, 16]. The FTIR spectra of ILs and recycled ILs indicate that the structure remains unchanged which indicates the potential of the recycling of ILs. All of these results suggest the possible structure of IL used is conserved as illustrated in Scheme 7.2.

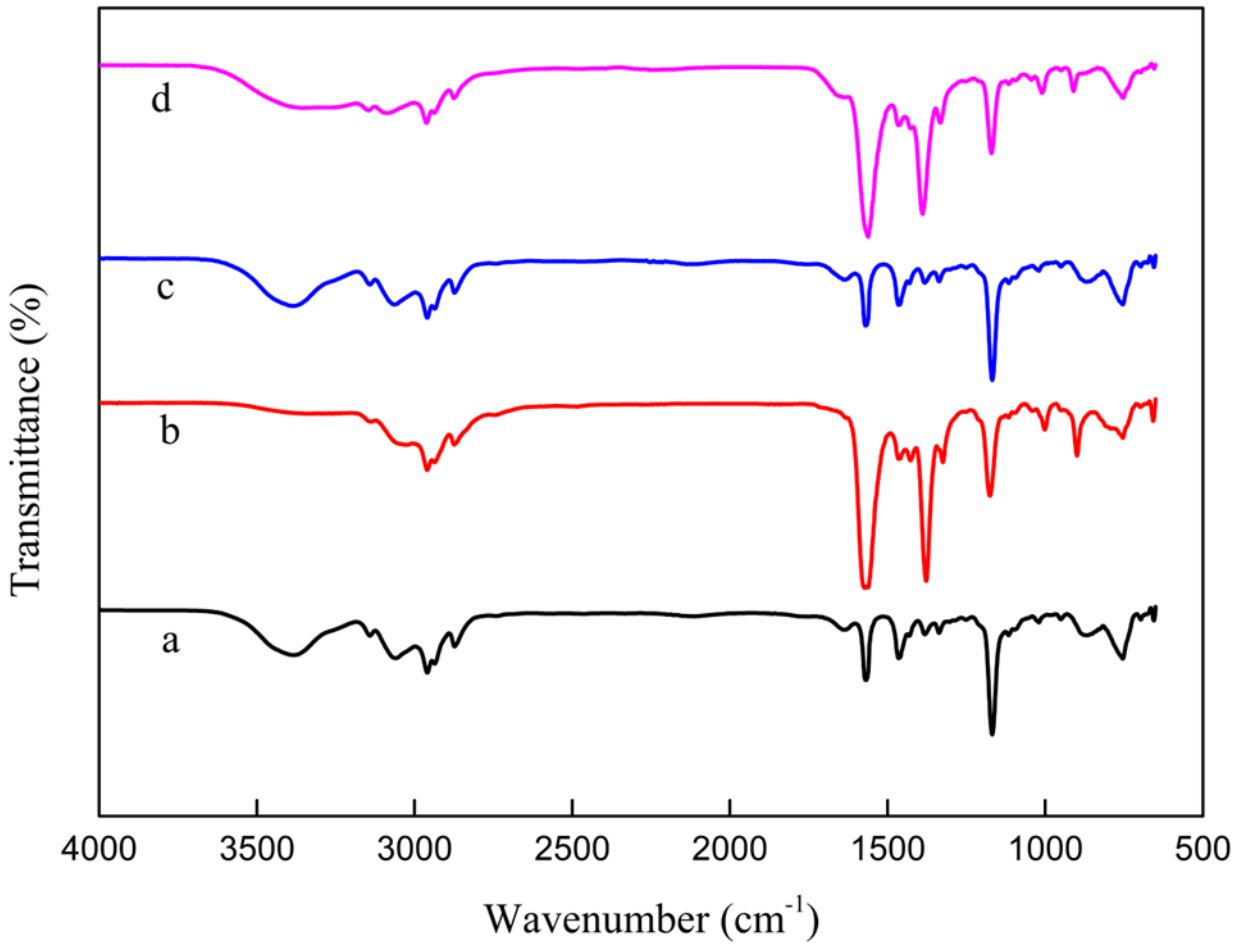


**Figure 7.1.** ATR-FTIR spectra of (a) $[C_4mim]Cl$, (b) $[C_4mim]CH_3CO_2$, (C) Recycled $[C_4mim]Cl$, and (d) Recycled $[C_4mim]CH_3CO_2$

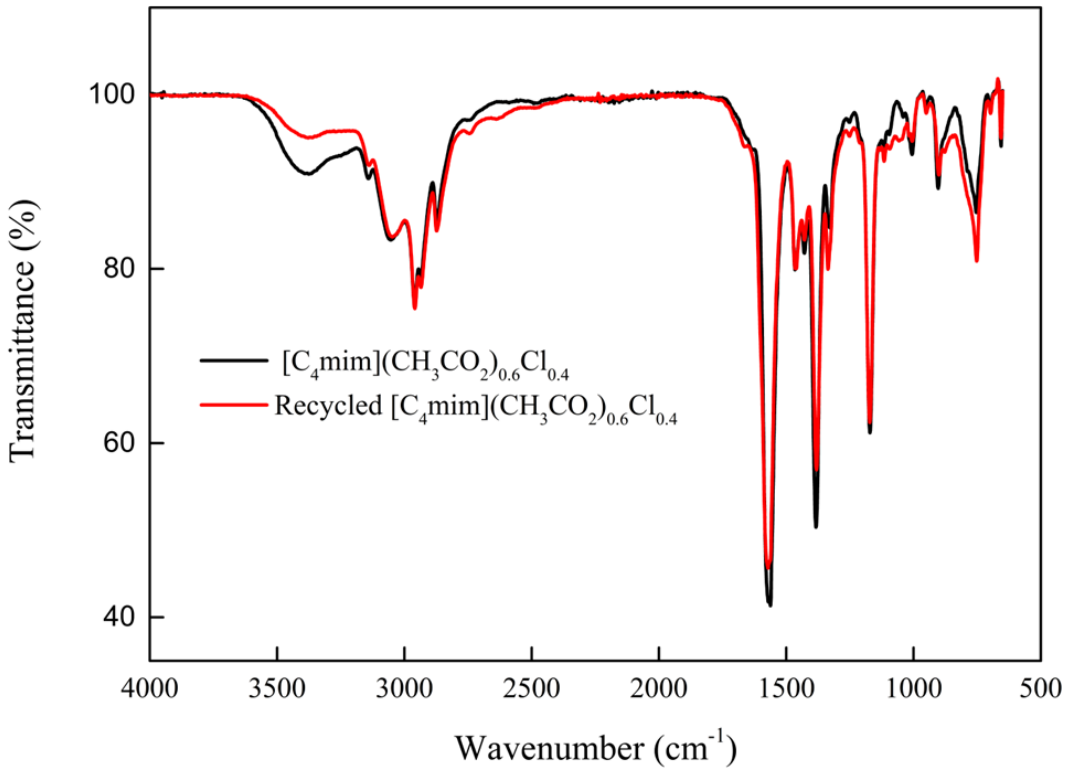


**Figure 7.2.** FTIR spectra of (a) $[C_4mim](CH_3CO_2)_{0.6}Cl_{0.4}$ and (b) Recycled $[C_4mim](CH_3CO_2)_{0.6}Cl_{0.4}$

### 7.3.2.2. $^1$H NMR spectroscopic analysis

$^1$H NMR is a powerful tool that has been used to determine the structure of imidazolium-based ILs and DSILs. The $^1$H NMR chemical shifts ($\delta$) of $[C_4mim]Cl$, $[C_4mim]CH_3CO_2$, $[C_4mim](CH_3CO_2)_{0.6}Cl_{0.4}$ and recycled $[C_4mim]Cl$, $[C_4mim]CH_3CO_2$, $[C_4mim](CH_3CO_2)_{0.6}Cl_{0.4}$ are presented in Fig.7.3 and Fig. 7.4. The $^1$H NMR $\delta$ values extracted from Fig. 7.3 and Fig. 7.4 have been tabulated in Table 7.2. The findings obtained from the $^1$HNMR analysis indicated that there was no discernible distinction between $[C_4mim]Cl$, $[C_4mim]CH_3CO_2$, $[C_4mim](CH_3CO_2)_{0.6}Cl_{0.4}$ and recycled $[C_4mim]Cl$, $[C_4mim]CH_3CO_2$, $[C_4mim](CH_3CO_2)_{0.6}Cl_{0.4}$ samples. In the imidazolium cation, $[C_4mim]^+$, acidic proton C(2)-H, which mainly participates in task-specific applications such as the dissolution of cellulose, is the most important proton. As two electron-withdrawing N atoms are attached to C-2 (Scheme 7.2) that makes the C(2)-H proton more acidic, which causes the NMR $\delta$ in a more downfield region. There are two factors such as inductive effect and hydrogen bonding that strongly influence the $\delta$ values of protons in the imidazolium cation and the alkyl chain [17].

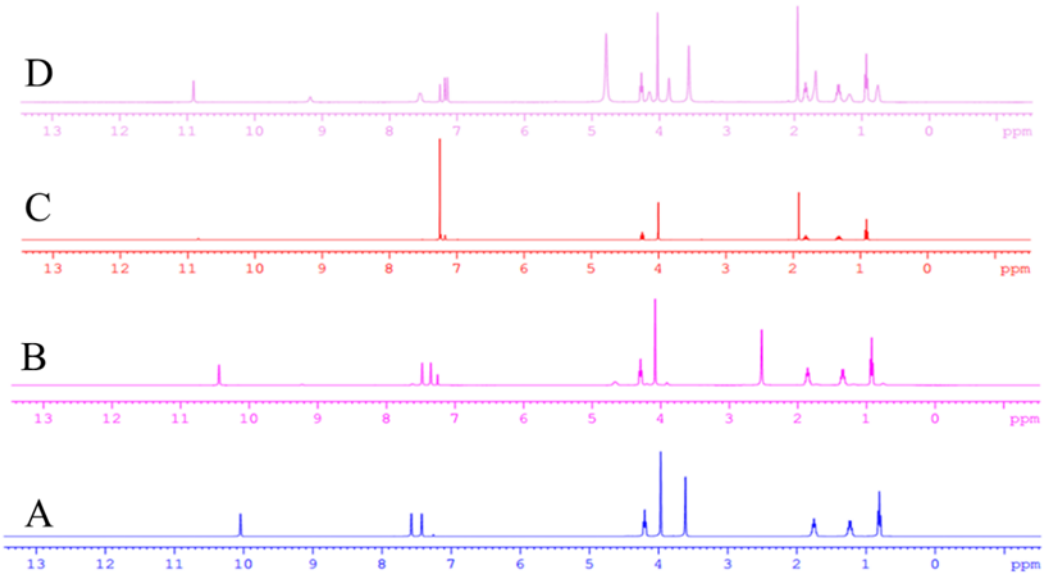


**Figure 7.3.** $^{1}$H NMR spectra of (A) [$C_4$mim]Cl, (B) Recycled [$C_4$mim]Cl, (C) [$C_4$mim]$CH_3CO_2$, (D) Recycled [$C_4$mim]$CH_3CO_2$

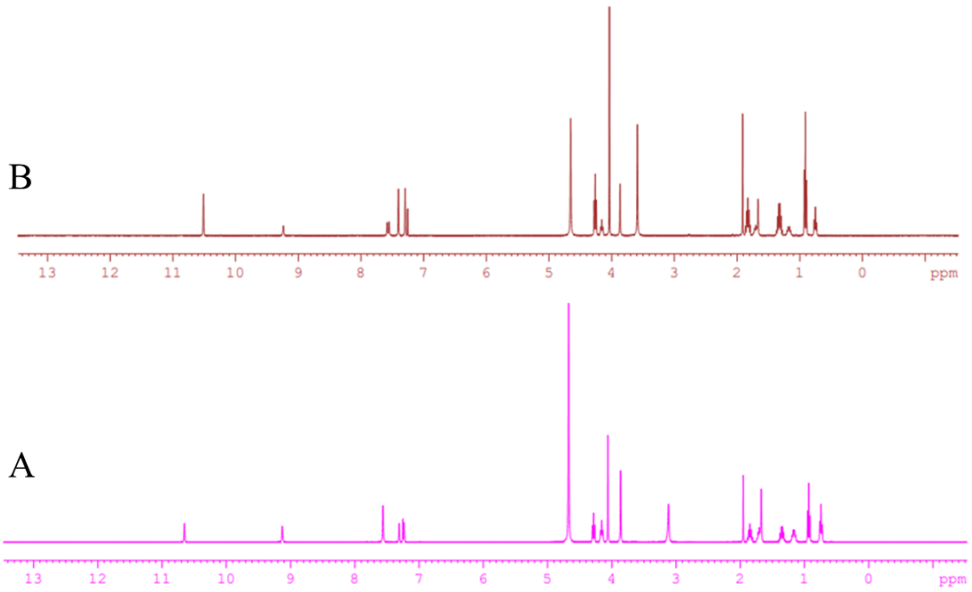


**Figure 7.4.** $^{1}$H NMR spectra of (A) [$C_4$mim]$(CH_3CO_2)_{0.6}Cl_{0.4}$ (B) Recycled [$C_4$mim]$(CH_3CO_2)_{0.6}Cl_{0.4}$ (Cycle-5)

To understand the structure of $[C_4mim](CH_3CO_2)_{0.6}Cl_{0.4}$ and , recycled $[C_4mim](CH_3CO_2)_{0.6}Cl_{0.4}$ three important $\delta$ values for the proton of C(2)-H, C(4)-H, and C(5)-H in $[C_4mim]^+$ ion is crucial. The $\delta$ values of C(2)-H, C(4)-H, and C(5)-H for $[C_4mim](CH_3CO_2)_{0.6}Cl_{0.4}$ are found to be 10.65, 7.56,7.31 and 10.51, 7.55,7.40 for fifth times recycled $[C_4mim](CH_3CO_2)_{0.6}Cl_{0.4}$ respectively. However, a slight disparity was observed in the $^1$HNMR spectrum recycled $[C_4mim]Cl$, $[C_4mim]CH_3CO_2$, $[C_4mim](CH_3CO_2)_{0.6}Cl_{0.4}$ compared to recycled $[C_4mim]Cl$, $[C_4mim]CH_3CO_2$, $[C_4mim](CH_3CO_2)_{0.6}Cl_{0.4}$, suggesting the presence of trace impurities in the recycled ILs. The presence of these pollutants can arise due to the presence of celluloses. A similar observation was evident in recycled $[C_4mim]Cl$ by Li *et al.* [18]. Cha *et al.* also examined the factors which contributed to the $\delta$ values, which were shown to be influenced by two main aspects: the hydrogen bonding between the anion and the imidazole ring, and the inductive effect of their interaction. FTIR and $^1$H-NMR analyses confirmed the recycling of DSIL after the fifth recycle does not alter the structure of DSIL, which helps for the potential application of the dissolution of cellulose.

**Table 7.2**. $^1$H NMR chemical shifts for all protons of the ILs and DSILs

| ILs and DSILs | Chemical shifts ($\delta$, ppm) |
|---|---|
| $[C_4mim]Cl$ | $^1$H: 10.32(H2), 7.68(H4), 7.32(H5), 4.44(H7), 4.21(H6), 1.75(H8), 1.25(H9), 0.81(H10) |
| Recycled $[C_4mim]Cl$ | $^1$H: 10.40 (H2), 7.65(H4), 7.35(H5), 4.30(H7), 4.10 (H6), 1.73(H8), 1.35(H9), 0.93(H10) |
| $[C_4mim]CH_3CO_2$ | $^1$H: 10.85 (H2), 7.24(H4), 7.18(H5), 4.23(H7), 4.00(H6), 1.81(H8), 1.33(H9), 0.88(H10) |
| Recycled$[C_4mim]CH_3CO_2$ | $^1$H: 10.90 (H2), 7.56(H4), 7.16(H5), 4.24(H7), 4.04(H6), 1.85(H8), 1.35(H9), 0.93(H10) |
| $[C_4mim](CH_3CO_2)_{0.6}Cl_{0.4}$ | $^1$H: 10.65(H2), 7.56(H4),7.31(H5), 4.67(H7), 4.30(H6),1.35(H8), 1.93 (H11), 1.17(H9), 0.94(H10) |
| Recycled $[C_4mim](CH_3CO_2)_{0.6}Cl_{0.4}$ | $^1$H: 10.51(H2), 7.55H4),7.40(H5), 4.66(H7), 4.26(H6), 1.34(H8), 1.91 (H11), 1.18(H9), 0.92(H10) |

### 7.3.3. Assessment of quality of cellulose regenerated by reusing ILs media

The assessment of the quality of cellulose regenerated by reusing ILs media can be measured by studying its structure, crystallinity, thermal stability, and morphology.

#### 7.3.3.1. FTIR spectral characterizations

Typically FTIR spectra of PHKP and regenerated PHKP (RPHKP) from cycle-1 to cycle -5 are displayed in Fig. 7.5. The FTIR analysis reveals that both PHKP and cellulose, which has undergone repeated regeneration up to five cycles from the PHKP-$[C_4mim](CH_3CO_2)_{0.6}Cl_{0.4}$ solution, have identical fundamental structures, as depicted in Fig. 7.5. Compared to the Fig 7.2, it is seen that the characteristic peaks for the $[C_4mim](CH_3CO_2)_{0.6}Cl_{0.4}$ were absence, which indicated the complete removal of DSIL after washing. The range between 3400 and 3300 $cm^{-1}$ was determined to be attributed to hydrogen bonding in both DSIL and RPHKP samples. Man *et al.* [19] reported a C–H stretching vibration at 2900 $cm^{-1}$, as well as a peak around 1426 $cm^{-1}$ due to the $–CH_2–$ (C6)– bending vibration in cellulose moiety. This showed that amorphous cellulose and crystalline cellulose II were present together in all samples. [20]. A weak shoulder at around 1650 $cm^{-1}$ for –OH bending of absorbed water in cellulose-water interaction was seen for PHKP, RPHKP-2 and RPHKP-3. A strong peak at around 1010 $cm^{-1}$ attributed to the CO of carbohydrates was seen in all samples. The presence of a distinct peak at 890 $cm^{-1}$ in the spectra indicates the occurrence of glycosidic C–H deformation accompanied by ring vibration and O–H bending in the $\beta$-glycosidic links between glucose molecules inside cellulose. This particular peak exhibited a greater intensity in the RC derived from DSIL [21]. All samples showed bands at 1366, 1310, and 1150 $cm^{-1}$, which is due to the stretching and wagging vibration of -CH, $-CH_2$, and C–O stretching in cellulose II, respectively [22]. These results suggested that all samples had a mixture of cellulose I and cellulose II structures in different proportions.

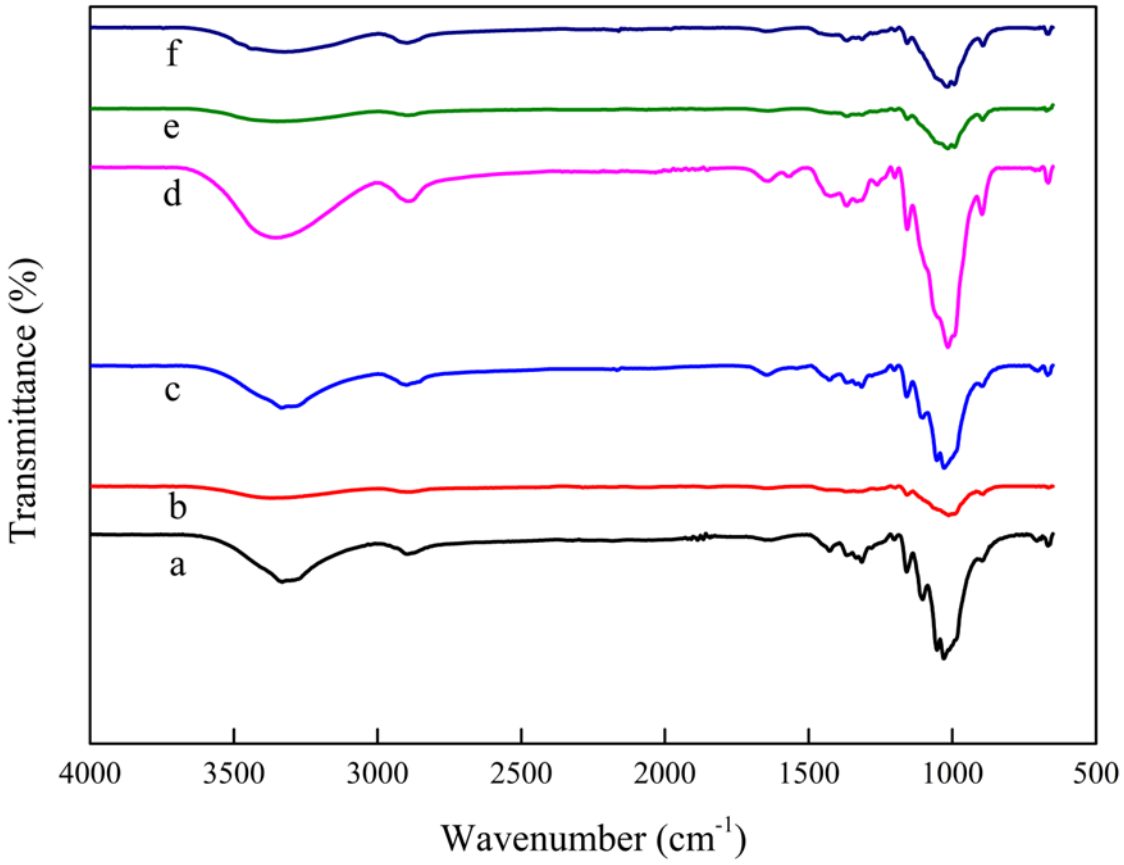


**Figure 7.5.** ATR-FTIR spectra of (a) PHKP, (b) RPHKP-1 (1st recycling), (c) RPHKP-2 (2nd recycling), (d) RPHKP-3 (3rd recycling), (e) RPHKP-4 (4th recycling), and (f) RPHKP-5 (5th recycling)

### 7.3.3.2. Microstate analysis

The XRD patterns of PHKP and RC from recycled DSIL are shown in Fig. 7.6 and their crystallinity index have been tabulated in Table 7.3. Cellulose I structure was identified from the XRD pattern of PHKP giving a sharp peak at 23.0° and a broad peak between 15.5°, which corresponds to (200) and (110) planes, respectively. However, RC showed cellulose II structure and broad peaks at around 20°. The peak at 2θ=23° was sharper for PHKP, while the peak intensity at around 20° for RC decreased drastically. This indicates that PHKP exhibits higher crystallinity compared to RC. The crystallinity index of PHKP was found to be 55.69 %, which was decreased to 20.53% after regeneration. Recycled DSIL dissolved fresh PHKP and showed similar results. The crystallinity index of RC from dissolved PHKP in fifth time recycled DSIL was 24.15%. Li *et al.* [12] showed that the degree of crystallinity decreased in RC from hardwood and softwood

pulps dissolved in $[C_4mim]CH_3CO_2$, and cellulose I was permanently converted to cellulose II. Dadi. [23] showed that the RC can easily hydrolysable to short glucose oligomers, making it easier to mass transfer in the overall reaction. In addition, the authors proposed that the RC contains a higher proportion of β-glucosidic linkages that are accessible to cellulose as a result of the pretreatment process's reduced crystallinity and a probable increase in the surface area. Therefore, regenerated cellulose from IL is more reactive to produce cellulose based products.

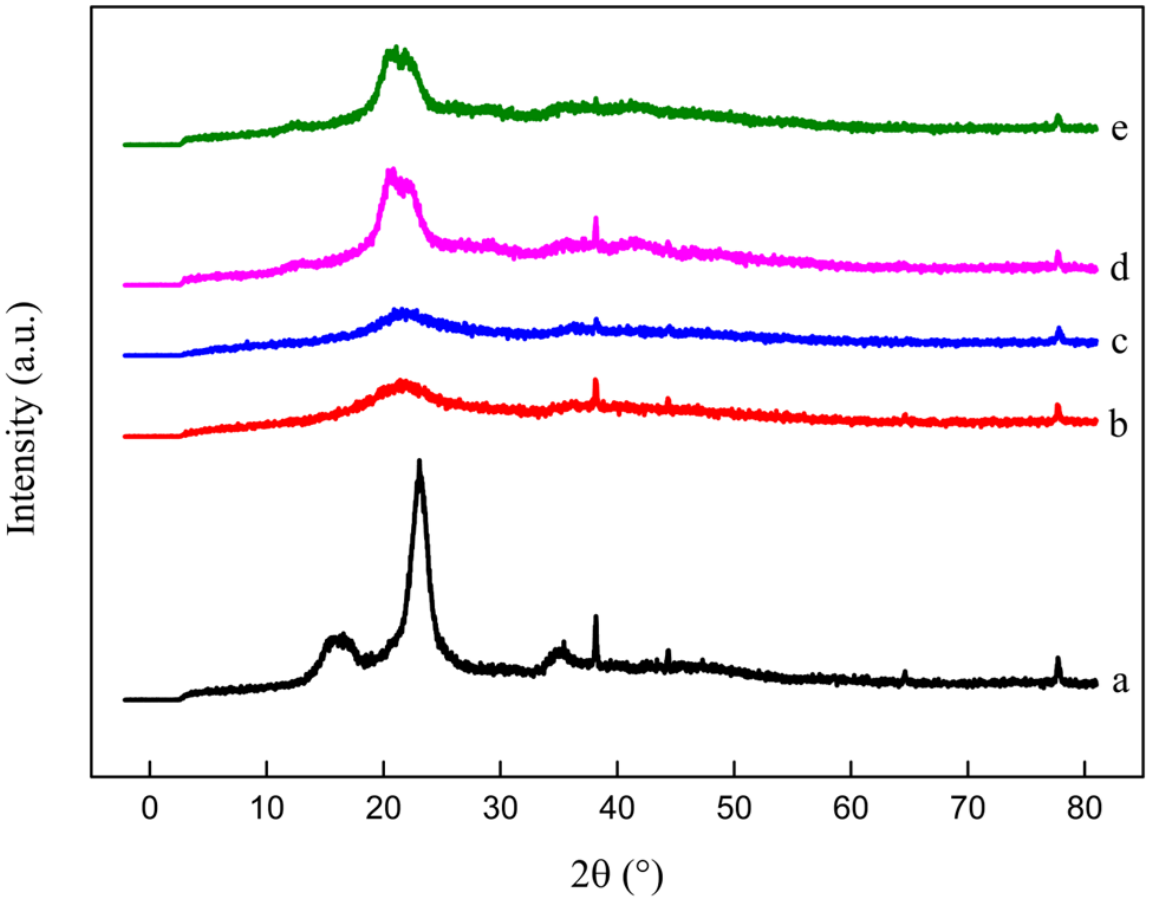


**Figure 7.6.** XRD pattern of a) PHKP, (b) RPHKP-1 (c) RPHKP-2 (d) RPHKP-3 (e) RPHKP-4, and (f) RPHKP-5

**Table 7.3.** The crystallinity index of PHKP and RPHKP (RC)

| Samples | Crystallinity (%) |
|---|---|
| (a) PHKP | 55.69 |
| (b) RPHKP-1 | 20.53 |
| (c) RPHKP-3 | 18.37 |
| (d) RPHKP-4 | 24.97 |
| (e) RPHKP-5 | 24.15 |

### 7.3.3.3. Evaluation of morphology

The SEM images of PHKP and RPHKP displayed in Fig. 7.7. The morphology of RPHKP significantly changed compared to PHKP. In the RPHKP, it is evident that the fibers are merged together, and homogenous microstructure has been developed, related observations have been made elsewhere [1, 24]. The macroscopic morphology of the RC varied depending on the IL solution and the recycled ILs. Powdery floc-type cellulose was formed by the rapid mixing of ILs with an aqueous system. Thin fibers and rods can be made by extruding the IL/cellulose solution into water.

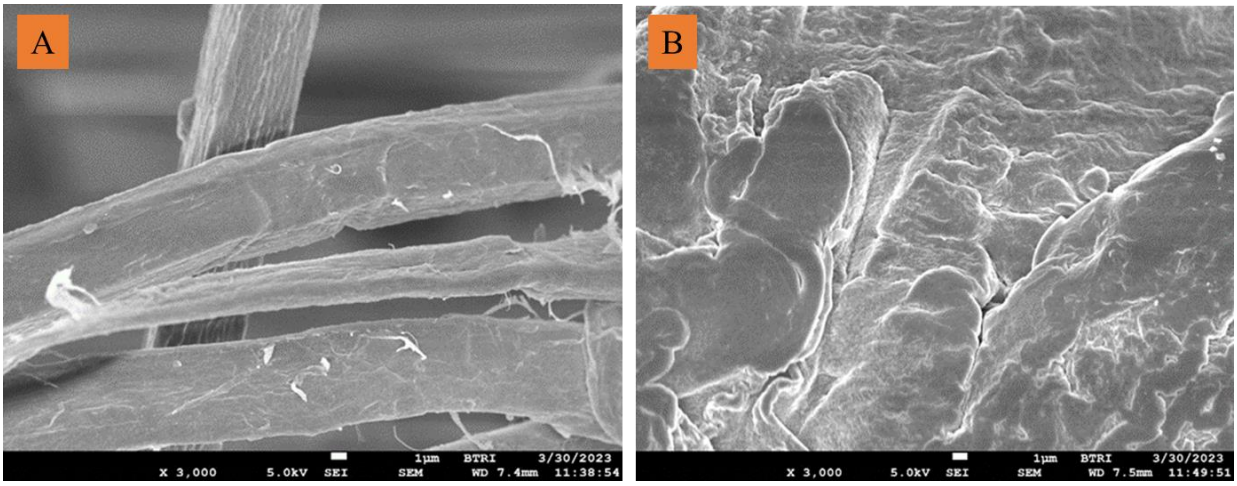


**Figure 7.7.** SEM images of (A) PHKP and (B) RPHKP-5

### 7.3.4. Thermal stability

Among the physicochemical properties, the thermal properties of the DSILs and cellulose need to be investigated to find the thermal behavior the DSIL and cellulose. For applications in industrial level, the thermal properties of DSILs and cellulose are very important in finding their operational temperature range such as melting points ($T_m$), glass transition temperature ($T_g$), thermal decomposition temperature ($T_d$) etc. and various thermal properties that need to be determined to optimize the operational temperature range for the DSILs and cellulose.

### 7.3.4.1. ILs and recycled ILs

The thermal properties of ILs and DSILs have been studied by TGA as it the most versatile technique to investigate the stability of ILs and DSILs. The thermograms of $[C_4mim]Cl$, $[C_4mim]CH_3CO_2$, $[C_4mim](CH_3CO_2)_{0.6}Cl_{0.4}$ and recycled $[C_4mim]Cl$, $[C_4mim]CH_3CO_2$, $[C_4mim](CH_3CO_2)_{0.6}Cl_{0.4}$ have been presented in Fig. 7.8. The degradation temperature $T_d$ of $[C_4mim]Cl$, $[C_4mim]CH_3CO_2$, $[C_4mim](CH_3CO_2)_{0.6}Cl_{0.4}$ and recycled $[C_4mim]Cl$, $[C_4mim]CH_3CO_2$, $[C_4mim](CH_3CO_2)_{0.6}Cl_{0.4}$ .4 have been tabulated in Table 7.4.

**Table 7.4.** Decomposition temperature ($T_d$) of ILs and DSIL at different temperature

| **DSILs** | $T_d$ / °C | |
|---|---|---|
| | 1st | 2nd |
| $[C_4mim]Cl$ | 238 | - |
| Recycled $[C_4mim]Cl$ | 252.3 | - |
| $[C_4mim](CH_3CO_2)_{0.6}Cl_{0.4}$ | 197.9 | 256.9 |
| Recycled $[C_4mim](CH_3CO_2)_{0.6}Cl_{0.4}$ | 227.6 | 266.3 |
| $[C_4mim]CH_3CO_2$ | 197.9 | - |
| Recycled $[C_4mim]CH_3CO_2$ | 201.3 | - |

In Table 7.4, it can be seen that $[C_4mim]Cl$, $[C_4mim]CH_3CO_2$ exhibits single ($T_d$) in contrast to $[C_4mim](CH_3CO_2)_{0.6}Cl_{0.4}$ and recycled $[C_4mim](CH_3CO_2)_{0.6}Cl_{0.4}$ displays two distinct $T_d$ as observed from the thermogram. This observation is consistent with the fact that $[C_4mim](CH_3CO_2)_{0.6}Cl_{0.4}$ is mixture of $[C_4mim]Cl$, $[C_4mim]CH_3CO_2$ having two different $T_d$. The first $T_d$ of the $[C_4mim](CH_3CO_2)_{0.6}Cl_{0.4}$ is related to the $[C_4mim]CH_3CO_2$ component and the second $T_d$ at a higher temperature than the former corresponds to the highly stable $[C_4mim]Cl$ component. One interesting observation is that both $T_d$ in the case of $[C_4mim](CH_3CO_2)_{0.6}Cl_{0.4}$ lies in between $[C_4mim]Cl$, $[C_4mim]CH_3CO_2$ . As shown in Fig. 7.7. The weight loss at 170 °C of $[C_4mim](CH_3CO_2)_{0.6}Cl_{0.4}$ was only 3.5% and 13.5% for recycled $[C_4mim](CH_3CO_2)_{0.6}Cl_{0.4}$. This was due to the presence of moisture in the recycled $[C_4mim](CH_3CO_2)_{0.6}Cl_{0.4}$. The first and second $T_d$ of $[C_4mim](CH_3CO_2)_{0.6}Cl_{0.4}$ are 197.9 and 256.9 °C, respectively. Similarly, the first and second $T_d$ of recycled $[C_4mim](CH_3CO_2)_{0.6}Cl_{0.4}$ are 198 and 265 °C, respectively. The slight increase in $T_d$ of recycled $[C_4mim](CH_3CO_2)_{0.6}Cl_{0.4}$ is due to the presence of impurities such as

cellulose. The $T_d$ of $[C_4mim](CH_3CO_2)_{0.6}Cl_{0.4}$ was started at 202 ℃ and continued up to 300 ℃ with 1.8 % residual mass. On the other hand, $T_d$ of recycled $[C_4mim](CH_3CO_2)_{0.6}Cl_{0.4}$ started at 198 ℃ and continued up to 318 ℃ with 5% residual mass. The above results indicated that recycled DSIL remained unchanged and remained thermally stable.

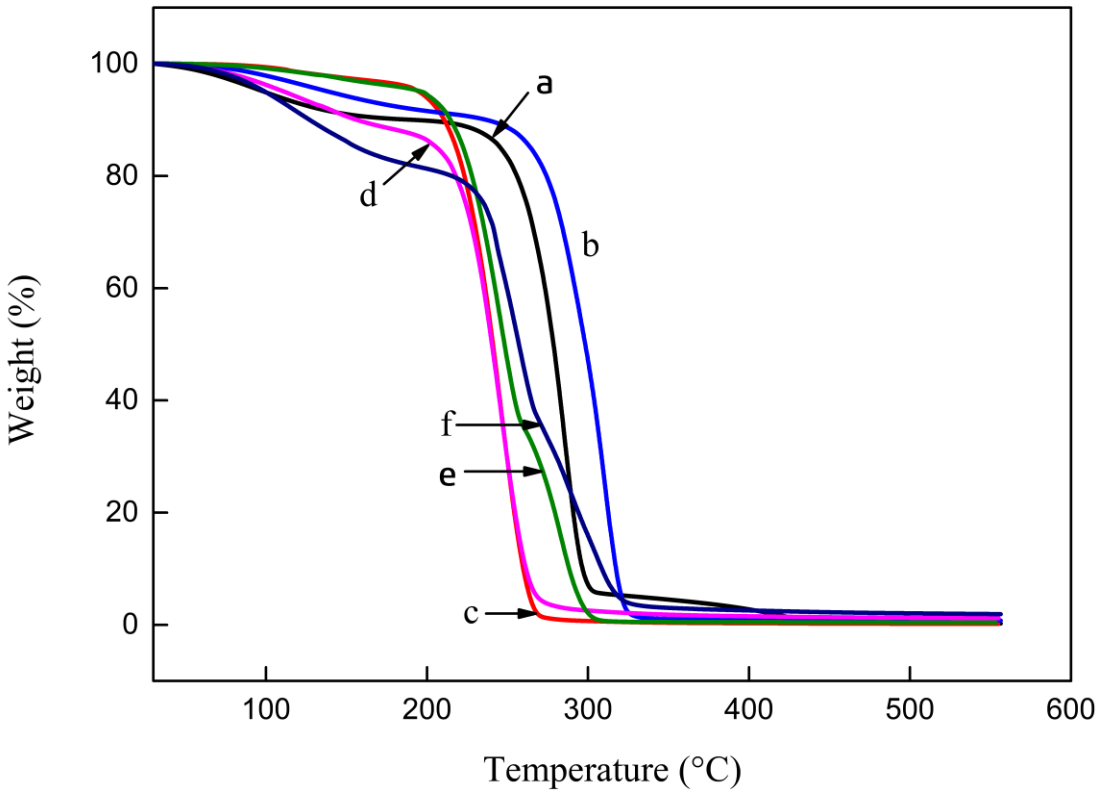


**Figure 7.8.** TGA thermograms of (a) $[C_4mim]Cl$, (b) Recycled $[C_4mim]Cl$ (c) $[C_4mim]CH_3CO_2$ (d) Recycled $[C_4mim]CH_3CO_2$ (e) $[C_4mim](CH_3CO_2)_{0.6}Cl_{0.4}$ and (f) recycled $[C_4mim](CH_3CO_2)_{0.6}Cl_{0.4}$

### 7.3.4.2. PHKP and regenerated PHKP

Fig. 7.9 represents TGA curves of PHKP and RPHKP. A small weight loss was observed for all samples at around 110 ℃, which was due to the evaporation of moisture. The RPHKP showed lower $T_d$ compared to PHKP indicating lower thermal stability of the RPHKP. The lower stability can be explained by the lower crystallinity index of the RPHKP (Table 7.3). As shown in Table 7.5, the $T_d$ of PHKP was 320 ℃, which decreased to 282.7 ℃ on RC from first recycling. The RC from the PHKP dissolved in the fifth time recycled DSIL was 253.7 ℃. Other studies also showed lower thermal stability compared to original cellulose [12, 25]. The $T_d$ of RPHKP is lower

than and regenerated PHKP from DSIL. The crystallinity of RPHKP is also lower than PHKP. The $T_d$ decreased with the decrease in crystallinity. This suggests that the hydrogen bond networks and crystal structure in cellulose may have been largely disrupted by the processes of dissolution and subsequent regeneration, which are responsible for the decrease in the thermal stability of regenerated PHKP. DTG curves of the corresponding TGA curves gives insight into the thermal behavior of the prepared PHKP and RPHKP. Fig. 7.10 depicts the DTG curves for the corresponding TGA curves. As expected, rate of maximum degradation for RPHKP should be occurred at lower temperature except for RC from 3$^{rd}$ cycle. Fig. 7.9 and Table 7.6 provide clear evidence that the thermal stability of PKHP is influenced by the crystallinity of PHKP. Specifically, the thermal stability of PKHP decreases as the crystallinity of PHKP decreases.

**Table 7.5.** Decomposition temperature ($T_d$) of ILs and PHKP and regenerated PHKP

| **Sample** | **Degradation temperature ($T_d$), °C** | **Derivatives of TG (µg/min) at temperature (°C)** |
|---|---|---|
| PHKP | 320 | 367.7 |
| RPHKP-1 | 282.7 | 343.2 |
| RPHKP-2 | 319.8 | 366.5 |
| RPHKP-3 | 243.4 | 319.1 |
| RPHKP-4 | 284.3 | 347.1 |
| RPHKP-5 | 253.7 | 332.5 |

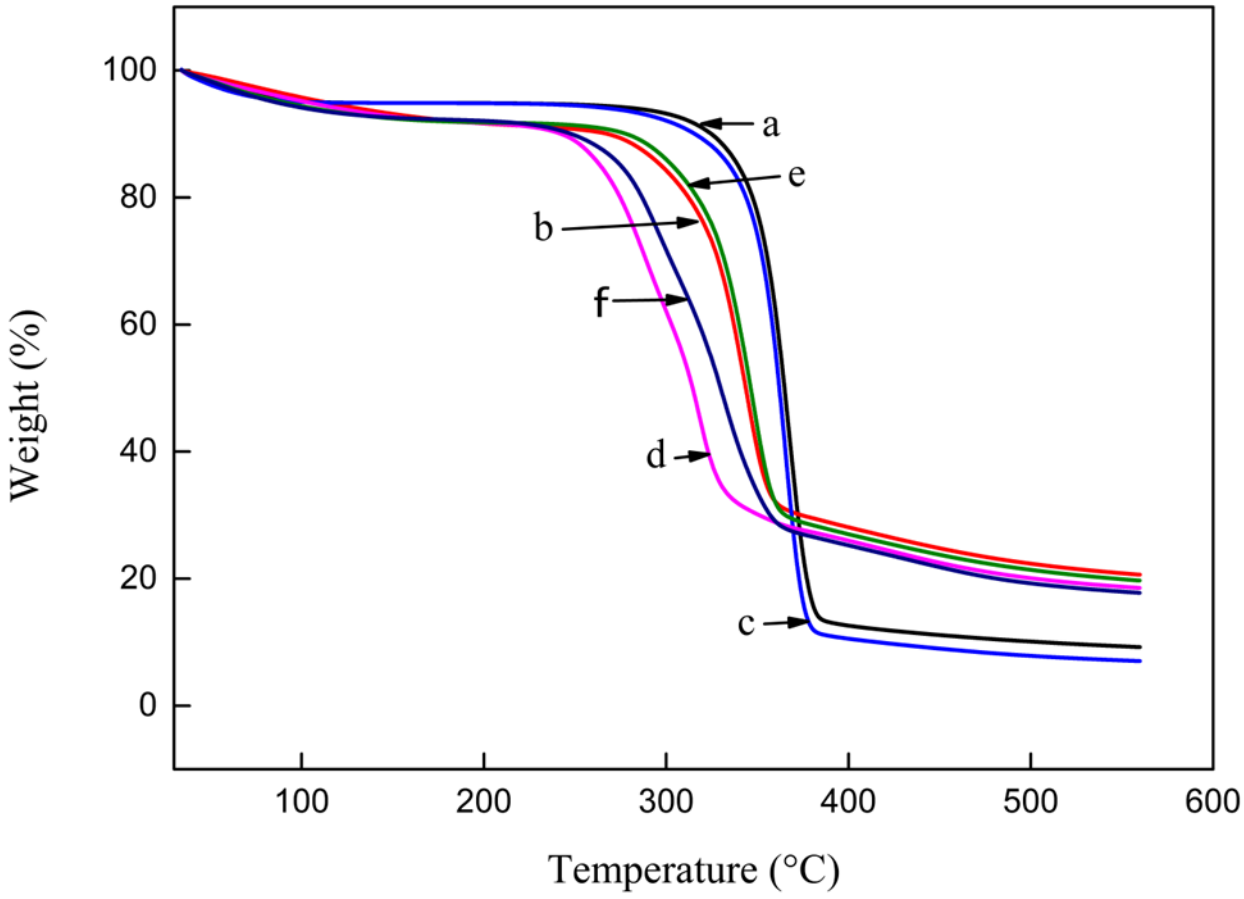


**Figure 7.9.** TGA thermograms of (a) PHKP, (b) RPHKP-1 (c) RPHKP-2 (d) RPHKP-3 (e) RPHKP-4, and (f) RPHKP-5

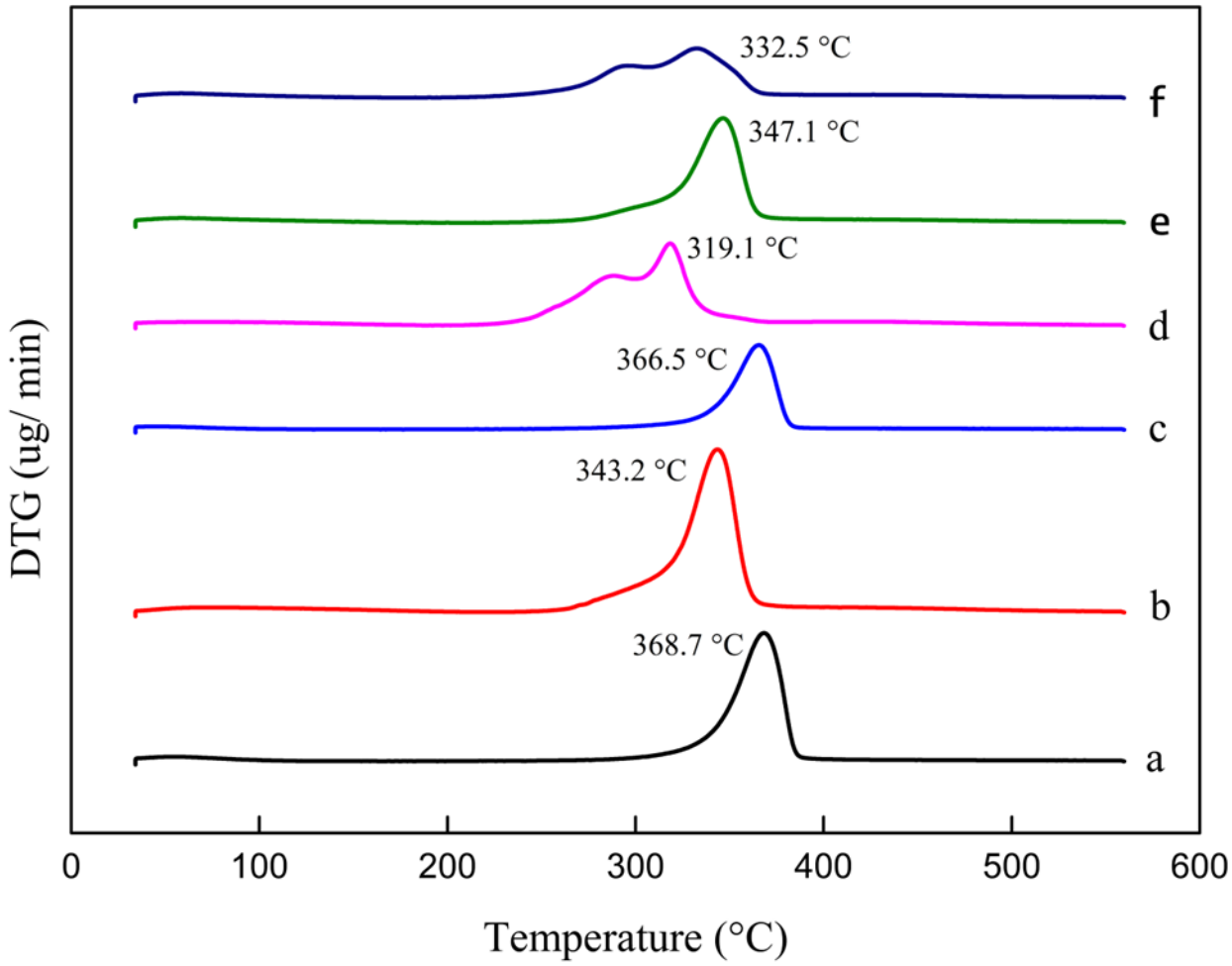


**Figure 7.10.** DTG thermograms of a) PHKP, (b) RPHKP-1 (c) RPHKP-2 (d) RPHKP-3 (e) RPHKP-4, and (f) RPHKP-5

## 7.4. Conclusions

A double salt ionic liquid of $[C_4mim](CH_3CO_2)_{0.6}Cl_{0.4}$ has been prepared and used for the dissolution of pre-hydrolyzed kraft pulp (PHKP). Anti-solvent for cellulose water was used for the coagulation of pulp from pulp-DSIL solution. The regenerated (R) PHKP was obtained from the precipitate. DSIL was recycled from filtrate by the evaporation of water. The recycled DSIL has been used for the dissolution of fresh PHKP. Consecutive five recycling and regeneration of PHKP have been carried out. After the fifth recycling of DSIL, 99.4 % DSIL was recovered and 96 % of RPHKP was obtained. The structure of DSIL and recycled DSIL was investigated by FTIR and $^1H$ NMR spectroscopy. The FTIR spectra reveal that the C-H stretching vibrations of the alkyl chain and of C(2)-H and C(4, 5) stretching vibrations for $[C_4mim]^+$ cation was found to be similar for DSIL and recycled DSIL were 2870, 2935, 2955, and 3046, 3147 $cm^{-1}$, respectively. To understand the structure of DSIL and, recycled DSIL, three important $\delta$ values for the proton of C(2)-H, C(4)-H, and C(5)-H in $[C_4mim]^+$ ion is crucial. The $\delta$ of C(2)-H, C(4)-H, and C(5)-H for DSIL was found to be 10.65, 7.56,7.31 and 10.51, 7.55,7.40 for fifth times recycled DSIL respectively. The thermal stability of DSIL and recycled DSILs was found to be 197.9 and 227.6 °C respectively. FTIR spectroscopy confirmed the structure of PHKP and RPHKP. The crystallinity and the thermal stability of RPHKP were decreased. The structure of PHKP converted from cellulose I to cellulose II. SEM images showed that the morphology of the RC fibers was fused into a relatively homogeneous macrostructure, and RC had lower thermal stability as observed by TGA analysis. It is true that for the high cost of ILs is a limitation in case of their large-scale industrial application. As ILs are much more expensive than conventional solvents involved in the cellulose dissolution and derivatization process, recovery operations of ILs must be highly efficient to make them economically viable and sustainable.

**References**


[1] Sun, N., Rahman, M., Qin, Y., Maxim, M. L., Rodríguez, H., and Rogers, R. D. (2009). Complete dissolution and partial delignification of wood in the ionic liquid 1-ethyl-3-methylimidazolium acetate. *Green Chemistry*, *11*(5), 646-655.

[2] Raut, D. G., Sundman, O., Su, W., Virtanen, P., Sugano, Y., Kordas, K., and Mikkola, J. P. (2015). A morpholinium ionic liquid for cellulose dissolution. *Carbohydrate Polymers*, *130*, 18-25.

[3] HUANG, K., Rui, W. U., Yan, C. A. O., Huiquan, L., and Jinshu, W. (2013). Recycling and reuse of ionic liquid in homogeneous cellulose acetylation. *Chinese Journal of Chemical Engineering*, *21*(5), 577-584.

[4] Xiong, D., Wang, H., Li, Z., and Wang, J. (2012). Recovery of Ionic Liquids with Aqueous Two-Phase Systems Induced by Carbon Dioxide. *ChemSusChem*, *5*(11), 2255-2261.

[5] Elsayed, S., Hellsten, S., Guizani, C., Witos, J., Rissanen, M., Rantamäki, A.H., Varis, P., Wiedmer, S.K., and Sixta, H. (2020). Recycling of superbase-based ionic liquid solvents for the production of textile-grade regenerated cellulose fibers in the lyocell process. *ACS Sustainable Chemistry and Engineering*, *8*(37), 14217-14227.

[6] Mai, N. L., Nguyen, N. T., Kim, J. I., Park, H. M., Lee, S. K., and Koo, Y. M. (2012). Recovery of ionic liquid and sugars from hydrolyzed biomass using ion exclusion simulated moving bed chromatography. *Journal of Chromatography A*, *1227*, 67-72.

[7] Lazko, J., Sénéchal, T., Bouchut, A., Paint, Y., Dangreau, L., Fradet, A., Tessier, M., Raquez, J.M., and Dubois, P. (2016). Acid-free extraction of cellulose type I nanocrystals using Brønsted acid-type ionic liquids. *Nanocomposites*, *2*(2), 65-75.

[7a] Fang, W., Lim, E. Y., Nieminen, K. L., and Sixta, H. (2023). Optimization of Dry-Jet Wet Spinning of Regenerated Cellulose Fibers Using [mTBDH][OAc] as a Solvent. *ACS Omega*.

[8] Troshenkova, S. V., Sashina, E. S., Novoselov, N. P., Arndt, K. F., and Jankowsky, S. (2010). Structure of ionic liquids on the basis of imidazole and their mixtures with water. *Russian Journal of General Chemistry*, *80*, 106-111.

[9] Persil Çetinkol, Ö., Dibble, D.C., Li, C., Sun, L., George, A., Cheng, A., Benke, P., Holmes, B.M., Singha, S., and Simmonsa, B.A. (2011). A facile method for the recovery of ionic liquid and lignin from biomass pretreatment. *Green Chemistry*, *13*(11), 3255-3264.

[10] Gutowski, K. E., Broker, G. A., Willauer, H. D., Huddleston, J. G., Swatloski, R. P., Holbrey, J. D., and Rogers, R. D. (2003). Controlling the aqueous miscibility of ionic liquids: aqueous biphasic systems of water-miscible ionic liquids and water-structuring salts for recycle, metathesis, and separations. *Journal of the American Chemical Society*, *125*(22), 6632-6633.Lan, W., Liu, C. F., and Sun, R. C. (2011). Fractionation of

[11] bagasse into cellulose, hemicelluloses, and lignin with ionic liquid treatment followed by alkaline extraction. *Journal of Agricultural and Food Chemistry*, *59*(16), 8691-8701.

[12] Li, D., Sevastyanova, O., and Ek, M. (2012). Pretreatment of softwood dissolving pulp with ionic liquids. *Holzforschung*, *66*(8), 935-943.

[13] Cha, S., Ao, M., Sung, W., Moon, B., Ahlström, B., Johansson, P., and Kim, D. (2014). Structures of ionic liquid–water mixtures investigated by IR and NMR spectroscopy. *Physical Chemistry Chemical Physics*, *16*(20), 9591-9601.

[14] Haron, G. A. S., Mahmood, H., Noh, M. H., Alam, M. Z., and Moniruzzaman, M. (2021). Ionic liquids as a sustainable platform for nanocellulose processing from bioresources: Overview and current status. *ACS Sustainable Chemistry and Engineering*, *9*(3), 1008-1034.

[15] Miao, J., Yu, Y., Jiang, Z., Zhang, L. One-pot preparation of hydrophobic cellulose nanocrystals in an ionic liquid, *Cellulose*, 2016, 23 (2), 1209−1219.

[16] Tan, X. Y., Abd Hamid, S. B., Lai, C. W. Preparation of high crystallinity cellulose nanocrystals (CNCs) by ionic liquid solvolysis, *Biomass Bioenergy* 2015, 81, 584−591.

[17] Becker, E. D. (1999). High resolution NMR: theory and chemical applications. Elsevier.

[18] Li, B., Asikkala, J., Filpponen, I., and Argyropoulos, D. S. (2010). Factors affecting wood dissolution and regeneration of ionic liquids. *Industrial and Engineering Chemistry Research*, *49*(5), 2477-2484.

[19] Man, Z., Muhammad, N., Sarwono, A., Bustam, M. A., Vignesh Kumar, M., and Rafiq, S. (2011). Preparation of cellulose nanocrystals using an ionic liquid. *Journal of Polymers and the Environment*, *19*, 726-731

[20] Nelson, M. L., and O'Connor, R. T. (1964). Relation of certain infrared bands to cellulose crystallinity and crystal lattice type. Part II. A new infrared ratio for estimation of crystallinity in celluloses I and II. *Journal of Applied Polymer Science*, *8*(3), 1325-1341.

[21] Carrillo, F., Colom, X., Sunol, J. J., and Saurina, J. (2004). Structural FTIR analysis and thermal characterisation of lyocell and viscose-type fibres. *European Polymer Journal*, *40*(9), 2229-2234.

[22] Široký, J., Blackburn, R. S., Bechtold, T., Taylor, J., and White, P. (2010). Attenuated total reflectance Fourier-transform Infrared spectroscopy analysis of crystallinity changes in lyocell following continuous treatment with sodium hydroxide. *Cellulose*, *17*, 103-115.

[23] Dadi, A. P., Varanasi, S., and Schall, C. A. (2006). Enhancement of cellulose saccharification kinetics using an ionic liquid pretreatment step. *Biotechnology and Bioengineering*, *95*(5), 904-910.

[24] Swatloski, R. P., Spear, S. K., Holbrey, J. D., and Rogers, R. D. (2002). Dissolution of cellose with ionic liquids. *Journal of the American Chemical Society*, *124*(18), 4974-4975.

[25] Liu, Z., Wang, H., Li, Z., Lu, X., Zhang, X., Zhang, S., and Zhou, K. (2011). Characterization of the regenerated cellulose films in ionic liquids and rheological properties of the solutions. *Materials Chemistry and Physics*, *128*(1-2), 220-227.

# CHAPTER 8

## Functionalization of Jute-Based Cellulose in Double Salts Ionic Liquids


### Abstract

A novel process has been developed to produce cellulose acetated (CA) from pre-hydrolyzed kraft pulp (PHKP) from jute using double salts ionic liquids (DSILs), which include more than two different types of ions. Each DSIL is distinct in terms of the combination of ion types, ion ratios, and their attributes. The features of each combination are distinct from those of two ion ILs because each combination of ion types forms a unique DSIL. Ionic liquids (ILs) have found extensive applications across several industries owing to their ability to modify their properties by manipulating their ionic constituents. ILs, a type of salts, exhibit a relatively low melting point, typically at or below 100 ℃. A DSIL of $[C_4mim](CH_3CO_2)_{0.6}Cl_{0.4}$, was prepared from 1-butyl-3-methylimidazolium chloride ($[C_4mim]Cl$), and 1-butyl-3-methylimidazolium acetate ($[C_4mim]CH_3CO_2$). The structure of DSIL was characterized by FTIR and NMR spectroscopy. $^1H$ NMR spectroscopy confirmed the complete structure of cellulose acetate. The maximum degree of substitution (DS) of the synthesized CA was found to be 2.85. The synthesized CA samples were characterized by FTIR, $^1H$ NMR, XRD, TGA-DSC, and SEM. A strong band for stretching vibration of –OH of cellulose was absent and a strong band for carbonyl (C=O) group was observed suggesting successful esterification of PHKP. The crystallinity index of PHKP was determined to be 51.1%, which decreased upon acetylation. All these results indicate that the esterification of cellulose is successful. The exothermic and endothermic peaks on DSC thermograms provides insight into the thermal change that is taking place.



**Keywords**: PHKP, Cellulose acetate, Acetylation, Degree of substitution, $^1H$ NMR spectroscopy

## 8.1. Introduction

Cellulose derivatives, particularly those prepared through various chemical modifications using ionic liquids (ILs), have gained significant interest owing to their potential for application in a wide range of industries. So far, ILs have proved to be promising material for various industrial applications such as food, pharmaceutics, cosmetic, green energy storage materials, and polymer-based nanocomposites for sensor, energy storage, biomedicine, etc. [1-10]. There are several methods of modification i.e., esterification, etherification, nitration, and oxidation etc. that could be done in IL medium. Among these modifications, cellulose esterification is indeed one of the most important and widely studied processes as esters of cellulose are of significant importance due to its extensive applications in different fields and industries i.e., plastics, textiles, films, fibers, cigarette industries etc. [11-13]. Hence, the production of cellulose esters plays an important role in both socio-economic and environmental aspects as it is produced and utilized in large scale. Esters of cellulose are generally produced chemically in either heterogeneously or homogeneously. Although both processes have been widely utilized in different industries and fields, their quality of product and the efficiency of the process is quite different. Industrially, the heterogeneous process is widely employed however, the efficiency of the process and the quality of the product is poor compared to the homogeneous process [14, 15]. In heterogeneous process, the cellulose raw material is kept in solid form undissolved and the esterification is carried out on this solid form. Esterification reaction targets the –OH groups of the cellulose which are underexposed in heterogeneous process due to cellulose being a complex network of polymer chains. Thus, the esterification is inefficient in this method. In contrast, homogeneous reaction enables the cellulose chains to open up consequently –OH groups are exposed for effective esterification [16, 17]. As a result, homogeneous esterification of cellulose is highly efficient compared to heterogeneous esterification of cellulose. The limitation of homogeneous process lies in the dissolution of cellulose.

Cellulose is very challenging to dissolve due to its rigid nature and close chain packing caused by multiple inter and intramolecular H-bonding. Appropriate cellulose solvents that can dissolve cellulose and create an environment that is conducive to the homogenous reaction are urgently required. Only a few solvent systems, such as DMAc/LiCl, DMF/$N_2O_4$, NMNO, and DMSO/TBAF, as well as some hydrates of molten salt, including $LiClO_4*3H_2O$ and $LiSCN*2H_2O$, have been discovered so far. It has also been reported esterification, etherification,

and other homogeneous derivatization processes, can produce new compounds in these solvents [18–21]. Moreover, these methods sometimes create serious environmental problems for unable to recycle and reuse [22, 23]. Recent years have seen a lot of interest in ILs as the "green" reaction medium for homogeneous cellulose derivations. According to Zhang and his coworkers, cellulose could be homogeneously acetylated in AMIMCl with varying without degrees of substitution (DS) the need for any catalysts [24]. ILs provide a much better system to dissolve cellulose for further derivatization due to it being extremely polar, chemically inert, and thermally stable. Several studies have been conducted in dissolving cellulose using different ILs [23, 25–28]. However, there are limitations in terms of dissolution percentage in ILs. In addition to that, catalysts are required during the derivatization process which increases the system complexity and after the reaction the catalyst need to be removed from the system that is also a major limitation [29]. Many research studies have taken these limitations into consideration and proposed a different solution to these problems. One of the approaches is to create binary solvent systems with the ILs and other organic solvent to enhance its dissolution efficiency. Barthel and coworkers carried out homogeneous acetylation and carbonylation of cellulose with the aprotic ILs of [$C_4$mim]Cl, [$C_2$mim]Cl, 1-butyl-2,3-dimethylimidazolium bromide ([$C_4$dmim]Cl and 1-allyl-2,3-dimethylimidazolium bromide ([Admim]Br) for 2 h at 80 ℃ under mild conditions, small excess reagent, and short reaction time. They found that DS of CA in the range from 2.5 to 3.0 [30]. Liu *et al.* prepared cellulose acetoacetate (CAA) with the reaction of *tert*-butyl acetoacetate and AmimCl. CAA was utilized to prepare self-healing polysaccharide hydrogel incorporating with chitosan aqueous solution through a Schiff-base reaction. The DS of CAA is dependent on the molar ratio of *tert*-butyl acetoacetate and AmimCl and the reaction time [31].

One of the novel approaches of the IL mixture that is yet to be explored with in-depth analysis, is the mixture of two different ILs with common cation or anion or completely different ions pairs. These are termed as double salt ionic liquids (DSILs) which contains components of two different ILs. Interestingly, the properties of the DSILs are quite different not only from their components but also from their different mole fractions [32]. This unique change of properties depending on different mole fractions of ILs present in DSILs provide a promising way for tuning the properties of IL mixtures according to the requirements. Thus, the limitations of the ILs could be mitigated by preparing a suitable DSILs for the purpose of dissolving cellulose. Furthermore, derivatization of cellulose is easily obtained under mild reaction conditions.

This study explores the use of jute, a cost-effective textile fiber, as a potential source of cellulose for acetylation. Jute, historically known as the "Golden fiber of Bangladesh," has been widely used in packaging materials. It is a key export of Bangladesh, providing jobs to many. However, due to competition from synthetic materials, its traditional applications have declined, leading to reduced demand. This research aims to find new uses for jute to revitalize the jute industry. In this study, DSIL of $[C_4mim](CH_3CO_2)_{0.6}Cl_{0.4}$ was employed as solvent for the purpose of dissolving cellulose. The dissolved cellulose system was subjected to the acetylation for the preparation of CA.

## 8.2. Materials and Methods

The materials and methods that were followed to accomplish this work are discussed below.

### 8.2.1. Materials

The prehydrolysis kraft pulp (PHKP) were prepared from jute fiber in the laboratory by following the detailed conditions described elsewhere [32]. The pulping procedure was conducted utilizing a 5-liter capacity stainless-steel digester, which was electrically heated and rotated at a rate of 1 revolution per min (rpm). Prehydrolysis was carried out employing water at a temperature of 170 ℃ for a duration of 30 min. The material to liquor ratio was maintained at 1:5 (g/mL). Maximum temperature was reached after 40 min. Following the completion of the prehydrolysis phase, pressure was released through venting the valve, and subsequently, the liquid component was filtered to separate it from the solid mass. The material was then subjected to washing with water, disintegration, and reserved for the ensuing kraft pulping procedure, which was executed following the aforementioned protocol. ILs, $[C_4mim]Cl$ and $[C_4mim]CH_3CO_2$, were purchased from Sigma-Aldrich with purities of $\geq$98% and $\geq$95%, respectively. Acetone (Sigma-Aldrich, $\geq$99.5%) and distilled water (distilled by Laboratory Water Purification System, MRC) were used throughout the study. The standard cellulose acetate, average Mn ~ 30000 by GPC, assay 39.3-40.3%, were purchased from Sigma-Aldrich, CHEMIE Gmbh.

### 8.2.2. Preparation of DSIL

To prepare DSIL of $[C_4mim](CH_3CO_2)_{0.6}Cl_{0.4}$, 0.6 mole of $[C_4mim]CH_3CO_2$ and 0.4 mole of $[C_4mim]Cl$ were mixed together to prepare 6 g of DSIL. The detail procedure for the preparation of DSIL have been discussed in Chapter 2 (sub-section 2.2.2)

### 8.2.3. Synthesis of cellulose acetate using DSIL

Cellulose acetate (CA) was synthesized following the method mentioned in the reference with few modifications [33]. 5 wt% of PHKP was added with DSIL. It was the kept for 30 min for swelling. The cellulose-DSIL mixture was then heated at 80 ℃ with constant stirring in an oil bath. Cellulose samples used in this study were dried for 24 h under vacuum before use. The dissolution of cellulose was carried out in a closed system. All the experiments were carried out very carefully to keep the moisture at a negligible amount to avoid adsorption by cellulose samples for consequent interference with the dissolution process. The dissolution of cellulose was followed by an optical microscope (Oxion, Euromax, Holland) as well as by visual monitoring. After that,

2-3 mL of acetic anhydride was added with the cellulose solution. It was heated at 80-100 ℃ for 2-3 h for the acetylation of cellulose. Methanol was added for the regeneration of CA. It was the filtered with G-2 filter (Funnels, Buchner, with Sintered Disc, Glasscolabs) under vacuum. The precipitates were washed five times to remove unreacted chemical species from the product. The obtained CA was dried under vacuum for 24 h at 75 ℃ and 0.1 MPa.

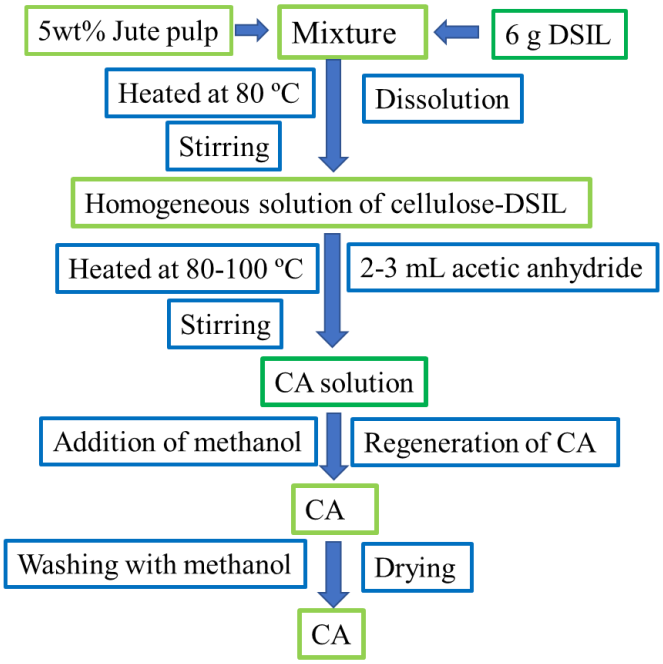


**Scheme 8.1.** A schematic diagram for the preparation of cellulose acetate (CA)

### 8.2.4. Characterizations

The structure of DSIL and CA were determined by spectroscopic techniques and crystallinity, morphology, and thermal properties of CA have been investigated by the following methods.

#### 8.2.4.1. Spectroscopic analysis

The structure DSIL and CA were characterized by using ATR-FTIR spectroscopy and $^{1}H$ NMR spectroscopy.

#### 8.2.4.1.1. ATR-FTIR spectroscopy

The structure DSIL and CA were characterized by using ATR-FTIR spectroscopy and $^{1}$H NMR spectroscopy. The details of the instrument and operating conditions have been described in Chapter 2 (Sub-section 2.2.3.1)

#### 8.2.4.1.2. $^{1}$H NMR spectroscopic analysis

The structure of DSIL and CA was characterized by using $^{1}$H NMR spectroscopy. The details of the instrument and operating conditions have been discussed in Chapter 2 (Sub-section 2.2.3.3)

### 8.2.4.2. X-ray diffraction (XRD) analysis

The crystallinity of CA was studied by an X-ray diffractometer. The details of the instrument and operating conditions have been described previously in Chapter 5 (Sub-section 5.2.4.2). The crystallinity index (*CI*) was calculated using the eq. 1 [34].

$$CI = \frac{A\ (\text{cryst.})}{A\ (\text{total})} \times\ 100 \qquad (1)$$

where, *A* (cryst.) is area of crystalline domain and *A* (total) is the area of crystalline and amorphous domain, respectively.

### 8.2.4.3. Scanning electron microscopic analysis

The morphology CA was studied by using scanning electron microscopy (SEM). The details of the instrument and operating conditions have been described in Chapter 5 (Sub-section 5.2.4.4).

### 8.2.4.4. Thermogravimetric analysis

The thermal properties CA have been studied by thermogravimetric analysis. The details of the instrument and operating conditions have been described in Chapter 5 (Sub-section 5.2.4.1)

### 8.2.4.5. Determination of degree of substitution (DS)

$^{1}$H-NMR were recorded on a 500 MHz Bruker AVIII spectrometer (Germany) at 25 °C using DMSO-$d_6$. The DS of the CA samples were determined using the integration peaks of $^{1}$H-

NMR spectra. From the spectra, the ratio of the 1/3 of the integration peak of acetyl group and 1/7 of anhydroglucose unit is calculated. Eq. 2 was used to calculate DS. [35]

$$\mathrm{DS} = \frac{7 \times \mathrm{I}(\mathrm{CH_3}, \mathrm{H})}{3 \times \mathrm{I}(\mathrm{AGU}, \mathrm{H})} \quad (2)$$

The variable I($CH_3$, H) represents the integration area of the peaks that correspond to the three methyl protons of the acetyl group, which are typically observed at a chemical shift range of approximately 1.6-2.3 ppm. On the other hand, I(AGU, H) refer to the integration of the peaks associated with the seven ring protons of the anhydroglucose unit, which are typically observed at a chemical shift range of approximately 2.8-5.5 ppm. It is important to note that the signal for residual water at a chemical shift of 3.3 ppm is excluded from this integration.

**8.2.4.6. Determination of %Yield**

The percent yield of the product was determined on the dry weight basis using the eq. 3 [36].

$$\text{Yield } (\%) = \frac{\text{Weight of dried CA}}{\text{Weight of dried cellulose}} \times 100 \quad (3)$$

## 8.3. Results and Discussion

As described above, the preparation of DSIL and synthesis of CA were attempted to be carried out. Here the results obtained from DSIL are described and then the initiatives taken for the synthesis of CA and related observations are systematically discussed.

### 8.3.1. Evaluation of structure of DSIL

The structure of prepared DSIL was determined by the ATR-FTIR and $^{1}$H NMR spectroscopic measurements.

#### 8.3.1.1. ATR-FTIR spectroscopic analysis

FTIR spectroscopy is a useful analytical technique that offers significant insights into the functional groups and molecular-level interactions present in DSIL. The deconvoluted ATR-FTIR spectra of synthesized DSILs of $[C_4mim](CH_3CO_2)_{0.9}Cl_{0.1}$ is presented in Fig. 8.1. The Fig. 8.1 (A) represents the C-H stretching vibration of imidazolium ion [37]. The C-H stretching vibrational bands, especially those associated with the aromatic ring of the cation, give a lot of structural information. Fig. 8.1 (B) presents absorption bands obtained in 1100-1650 $cm^{-1}$. The analysis of this spectrum revealed several prominent peaks that provide valuable information about the molecular structure of $[C_4mim]^+$, which is likely an DSILs. The identified bands at specific wavenumbers are indicative of different types of chemical bonds and molecular vibrations within the $[C_4mim]^+$ ion. The bands at 2875, 2936, and 2961 $cm^{-1}$ represent several C-H stretching vibrations of the alkyl group. These three peaks correspond to C-H stretching vibrations of the alkyl group within the $[C_4mim]^+$ ion. The presence of C-H stretches in this region suggests the presence of alkyl chains in the molecule, typically associated with the DSIL structure.

The peaks at 3025 and 3055 $cm^{-1}$ indicates C(2)-H and C(4,5)-H, stretching vibrations, respectively. These specific wavenumbers provide critical information about the nature and location of carbon-hydrogen bonds within the $[C_4mim]^+$ of DSILs. Similar observations regarding the FTIR spectral bands corresponding to C-H stretching vibrations of alkyl groups and specific C-H stretching vibrations at different positions have been made by many researchers. These findings provide valuable consistency and confirmation of the molecular structure and vibrational modes of the $[C_4mim]^+$ ion, particularly in the context of ILs. Umebayashi *et al*. [38] have found bands 2951, 2970, and 2992 $cm^{-1}$ for C-H stretching vibrations of alkyl group. They also found

C(2)-H and C(4, 5)-H stretching vibrations at 3124 and 3162 $cm^{-1}$, respectively. Cha *et al.* [39] found C(2)-H and C(4,5)-H stretching vibrations at 3114 and 3163 $cm^{-1}$, respectively. Bands at 2877, 2938, and 2965 $cm^{-1}$ are attributable to several C-H stretching vibrations of alkyl group. The bands at 1561 and 1571 $cm^{-1}$ indicates the presence of C=C and C=O in $[C_4mim](CH_3CO_2)_{0.6}Cl_{0.4}$.

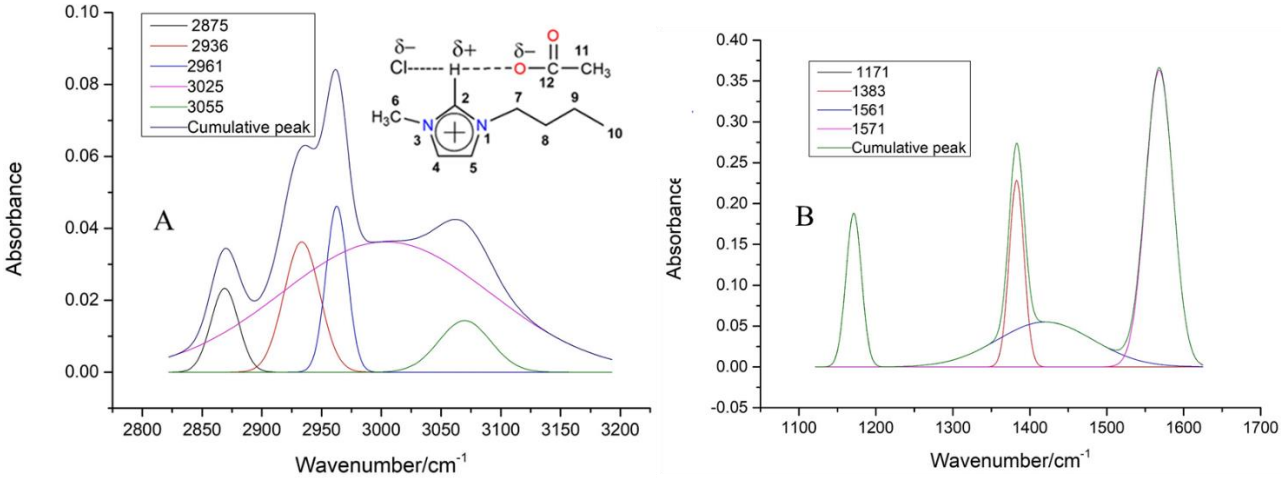


**Figure 8.1.** Deconvoluted ATR-FTIR spectra of $[C_4mim](CH_3CO_2)_{0.6}Cl_{0.4}$ : (A) C-H stretching region and (B) 1650-1100 $cm^{-1}$ region

### 8.3.1.2. $^1$H NMR spectroscopy

$^1$H NMR chemical shifts ($\delta$) pertaining to DSIL $[C_4mim](CH_3CO_2)_{0.6}Cl_{0.4}$ is illustrated in Fig. 8.2. These $\delta$ values exhibit distinct features influenced significantly by two key factors. Firstly, the protons in the system participate by H-bonding with the anion. Secondly, the presence of the anion exerts an effect on the chemical environment of the imidazolium ring. [40, 41]. The C(2)-H proton of the $[C_4mim]^+$ is located in close proximity to two nearby two electron-withdrawing N atom. The observed $\delta$ values undergo a significant downfield shift due to the spatial arrangement. The observed $\delta$ values can be attributed to the deshielding effect caused by nearby electron-withdrawing groups. This impact perturbs the immediate electronic environment of the proton, leading to the observed shift. To understand the structure of DSIL three important chemical shifts for the proton of C(2)-H, C(4)-H, and C(5)-H in $[C_4mim]^+$ ion is crucial. The $\delta$ values of C(2)-H, C(4)-H, and C(5)-H in $[C_4mim](CH_3CO_2)_{0.6}Cl_{0.4}$ are found to be 10.4, 7.6, and 7.4 ppm,

respectively. Zaoui *et al.* [42] reported that the 3-octyl-1-vinylimidazolium bromide imidazolium ring structure also had $\delta$ values at 7.32, 7.68, and 9.69 ppm, which corresponds to C(5)-H, C(4)-H, and C(2)-H, respectively. The $\delta$ values of C(2)-H protons of all mole fractions showed the highest value in the more downfield region. The anions of $Cl^-$ and $CH_3CO_2^-$ form H-bonding with the C(2)-H proton due to its acidic nature as its respective carbon is attached to two electron-withdrawing N atoms. The $\delta$ values of the other protons of $[C_4mim](CH_3CO_2)_{0.6}Cl_{0.4}$ are found to be 4.3, 4.0, 1.9, 1.8, 1.3, and 0.9 ppm for C(7)-H, C(6)-H, C(11)-H, C(8)-H, C(9)-H, and C(10)-H respectively. These $\delta$ values also provide information about the local electronic environment of these protons, which can be influenced by the nearby atoms and functional groups in the molecule. The $\delta$ values of C-11 protons of DSILs showed in the downfield region comparative to C(8)-H, C(9)-H, and C(10)-H protons due to the -C=O groups attached to it [43].

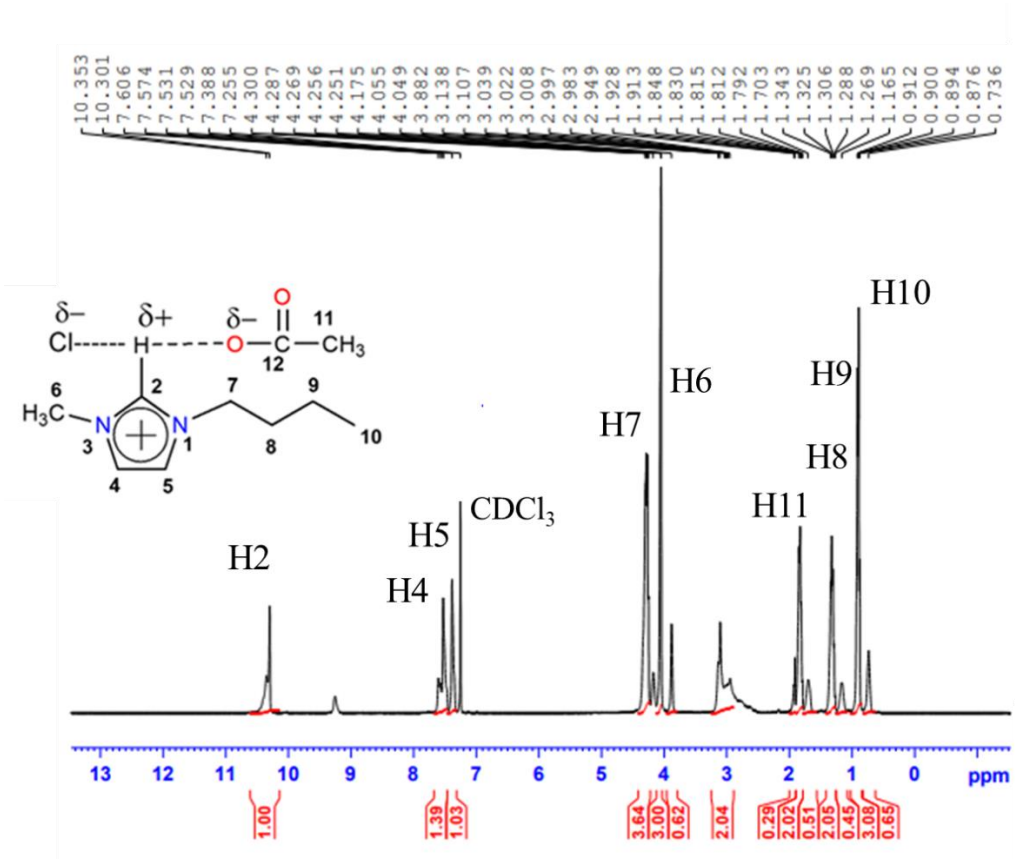


**Figure 8.2.** $^1$H NMR spectrum of DSIL

### 8.3.3. Synthesis of CA

The solubility, mechanical, chemical, physical, and thermal properties of CA depend on DS value. The DS value of prepared CA from PHKP was found to be 2.77, 2.70, 2.65 and 2.85 for CA1, CA2, CA3 and CA4, respectively, as summarized in Table 8.1. The maximum value of DS was found to be 2.85 for CA4 at 100 ℃ for 3 h reaction time. This happened due to possible increase in contact between cellulose and reactants. Consequently, the rate of reaction increased and as a result the DS value increases. The DS value increased to 2.85 from 2.77 with the increase in reaction time and temperature. Li *et al.* [44 has been suggested that during the initial stages of the reaction, the reaction system exhibited heterogeneity, whereby the –OH groups present on the surface of solid cellulose were selectively subjected to acetylation. Subsequently, as the acetylation process advanced, the acetylated cellulose gradually underwent dissolution within the reaction medium, leaving behind unreacted –OH groups. The –OH groups were replaced by larger acetate groups in case of CA samples with higher DS. Similar results are observed for carboxymethylcellulose preparation [36, 45]. The percent yield of the synthesized CA was found to be 145, 138, 125, 125 % for CA1, CA2, CA3, and CA4 respectively have been tabulated in Table 8.1. The solubility of CA were tested in di-methylsulfoxide (DMSO) and acetone. The solubility of the synthesized CA were found completely soluble in DMSO.

**Table 8.1.** The percent yield, DS and solubility of CA

| Sample name | Reaction time (h) | Reaction temperature (ºC) | Solubility in acetone | Solubility in DMSO | DS | Yield (%) |
|---|---|---|---|---|---|---|
| CA1 | 2 | 80 | × | ✓ | 2.77 | 145 |
| CA2 | 2 | 80 | × | ✓ | 2.70 | 138 |
| CA3 | 3 | 100 | × | ✓ | 2.65 | 125 |
| CA4 | 3 | 100 | × | ✓ | 2.85 | 152 |

✓: soluble; ×: insoluble

### 8.3.4. Identification of functional groups of CA synthesized

The FTIR spectra of PHKP, standard CA and synthesized CA have been presented in Fig. 8.3. The strong absorption bands at 3308 $cm^{-1}$ in PHKP are due to –OH stretching, which completely disappeared upon acetylation. All prepared CA exhibited a strong band of the carbonyl (C=O) group at 1735 $cm^{-1}$, confirming the effective chemical conversion to an ester. Shaikh *et al.* also observed the disappearance of –OH stretching and the formation of a prominent band of carbonyl (C=O) group [46]. Rodrigues Filho *et al.* [47] reported the presence of a strong band at 1746 $cm^{-1}$, corresponding to the stretching vibration of the C=O of CA, and a corresponding decrease in the intensity of the –OH stretching band at 3460 $cm^{-1}$. The bands at approximately 1050 $cm^{-1}$ for C–O–C in anhydroglucose units of cellulose were also clearly seen. As seen from Fig. 8.3, the intensity of this band was almost similar, which indicated that the esterification was happened only in –OH group [46]. The bands at 1364 $cm^{-1}$ and 1223 $cm^{-1}$ corresponds to C–H bending and C–O stretching vibrations of acetyl group, respectively. Das *et al.* [26] also observed increased band intensity for the carbon-hydrogen (C-H) bending vibration at 1369 $cm^{-1}$ and carbon-oxygen (C-O) stretching vibration at1220 $cm^{-1}$. The intensity of band absorption bands for amorphous region in CA at 896 $cm^{-1}$ was higher than the PHKP.

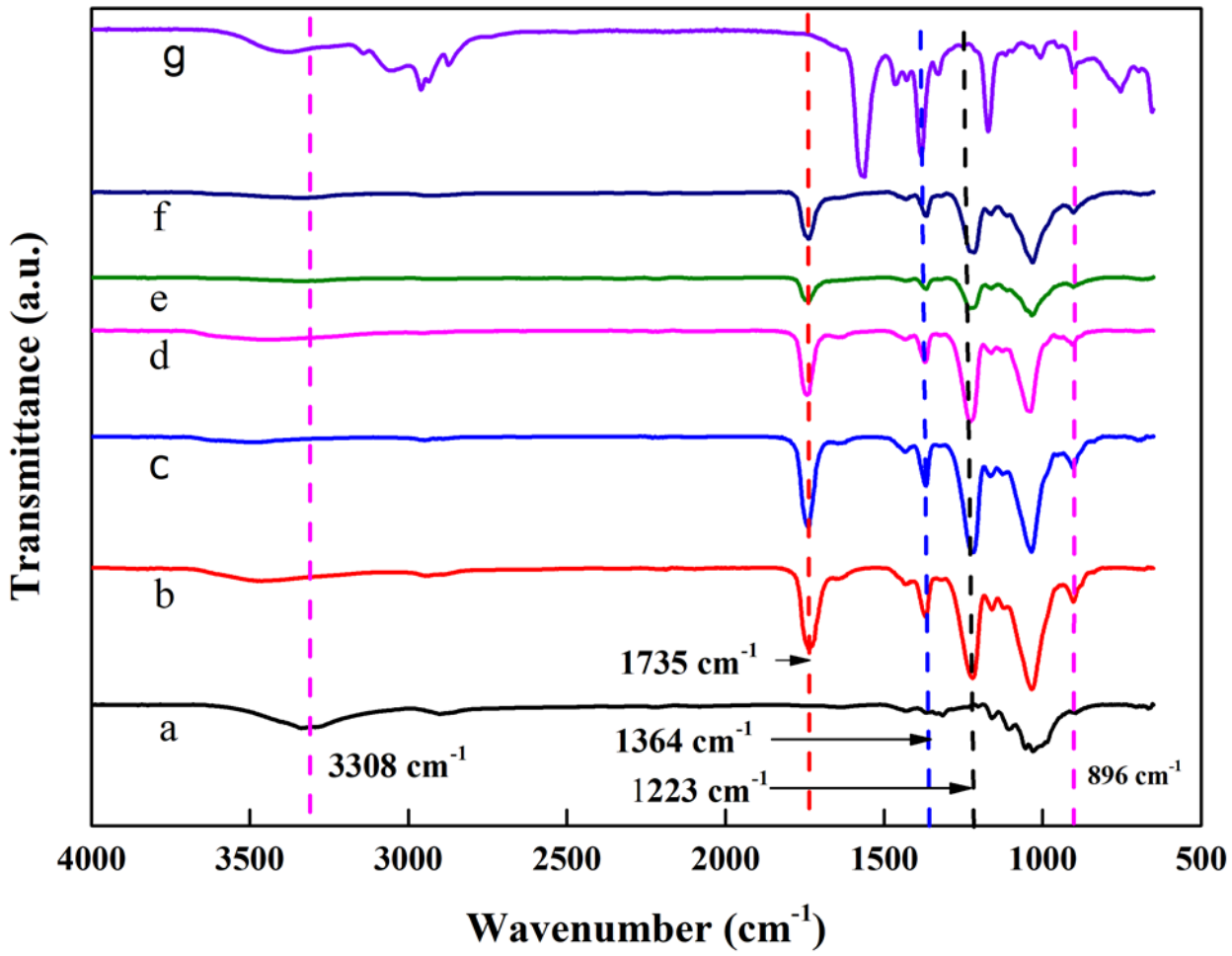


**Figure 8.3.** ATR-FTIR spectra of (a) PHKP, (b) standard CA, (c), CA1, (d) CA2 (e) CA3 and (f) CA4, and (g) $[C_4mim](CH_3CO_2)_{0.6}Cl_{0.4}$

### 8.3.5. $^1$H NMR spectroscopic analysis of prepared CA

Fig. 8.4 displays the $^1$H-NMR spectra of CA-1 dissolved in DMSO-$d_6$ recorded at 25 ℃ that has been produced with a DS of 2.77. The H atoms present in the methyl (–$CH_3$) of acetyl groups are corresponded to chemical shift of around 1.9 – 2.1 ppm. The resonance peak observed at a chemical shift of 1.9 ppm can be attributed to the H atom attached to the third carbon atom (C3) inside the framework of cellulose. Similarly, the resonance peak observed at a chemical shift of 2.1 ppm can be attributed to the proton attached to the sixth carbon atom (C6). The observed peaks within the chemical shift range of 5.20 – 2.80 ppm can be attributed to the seven ring protons of anhydroglucose unit (AGU). However, the large signal observed at ~3.3 ppm corresponds to the

residual water which is not part of the AGU. Similarly, peaks arising at $\delta$ value of 2.5 is attributable to the DMSO-$d_6$. The signals observed at $\delta$ of 4.7, 4.5, 5.1, 3.7, and 3.8 ppm were assigned to the carbon atoms C1, C2, C3, C4, and C5, respectively. Additionally, the signal at 4.3 and 4.1 ppm was attributed to the carbon atoms C6 and $C6_0$ of the AGU compound, as reported in reference [48]. The DS was determined by utilizing the integration of the $^1$H-NMR spectra [34]. The DS is thus calculated by taking the ratio of the 1/3 and 1/7 of the integrated peaks of acetyl group and AGU, respectively. The DS for the CA1 sample are at around 2.77.

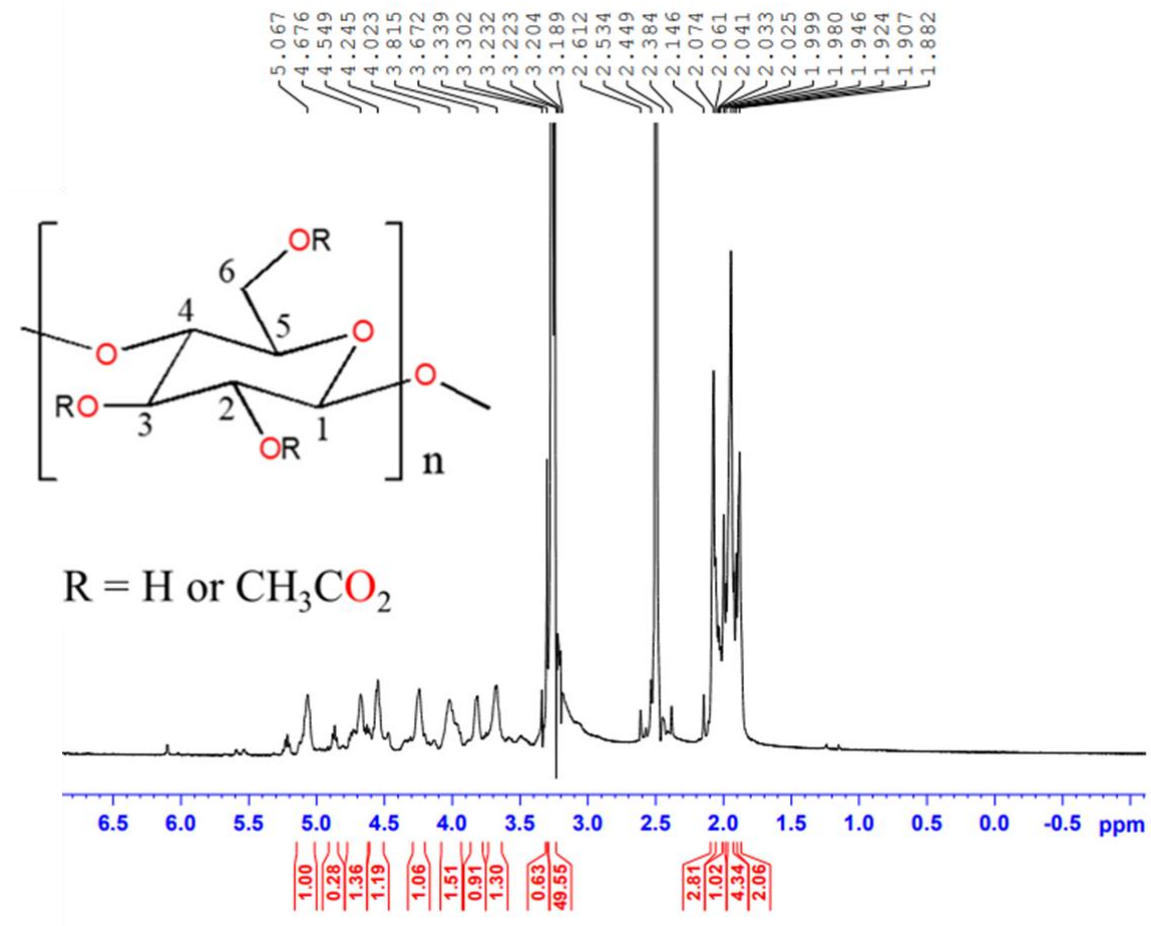


**Figure 8.4**. $^1$H NMR spectra of CA1

### 8.3.6. Crystallinity of the prepared CAs

Fig. 8.5 represents XRD pattern of PHKP and CA obtained from acetylation reactions at different conditions. The main peak for PHKP was observed at 2θ = 23.0º and 15.4º for crystalline and amorphous phase respectively, which attributed to crystalline cellulose, corresponds to the (200)

plane [49]. A prominent peak at around 2θ of 15.4° is observed, corresponding to the overlapping of crystallographic planes characterized by Miller indices (1–10) and (110). The XRD patterns of CA exhibited the absence of these peaks, indicating the successful esterification of cellulose. The crystallinity index of PHKP was 51.5%, which was completely changed on acetylation. Other studies also showed disappearance of these peaks on esterification [50]. During the process of substituting –OH groups with acetyl groups, the inter- and intra-molecular hydrogen bonds of cellulose were entirely disrupted. A low intensity semi-crystalline CAs diffraction peaks showed at 2θ of 8.7°, 10.5° and 11.5°, while the diffraction peak for amorphous material is found at the 2θ of 17.5° [51]. Chen *et al.* [52] also observed similar XRD pattern of CA.

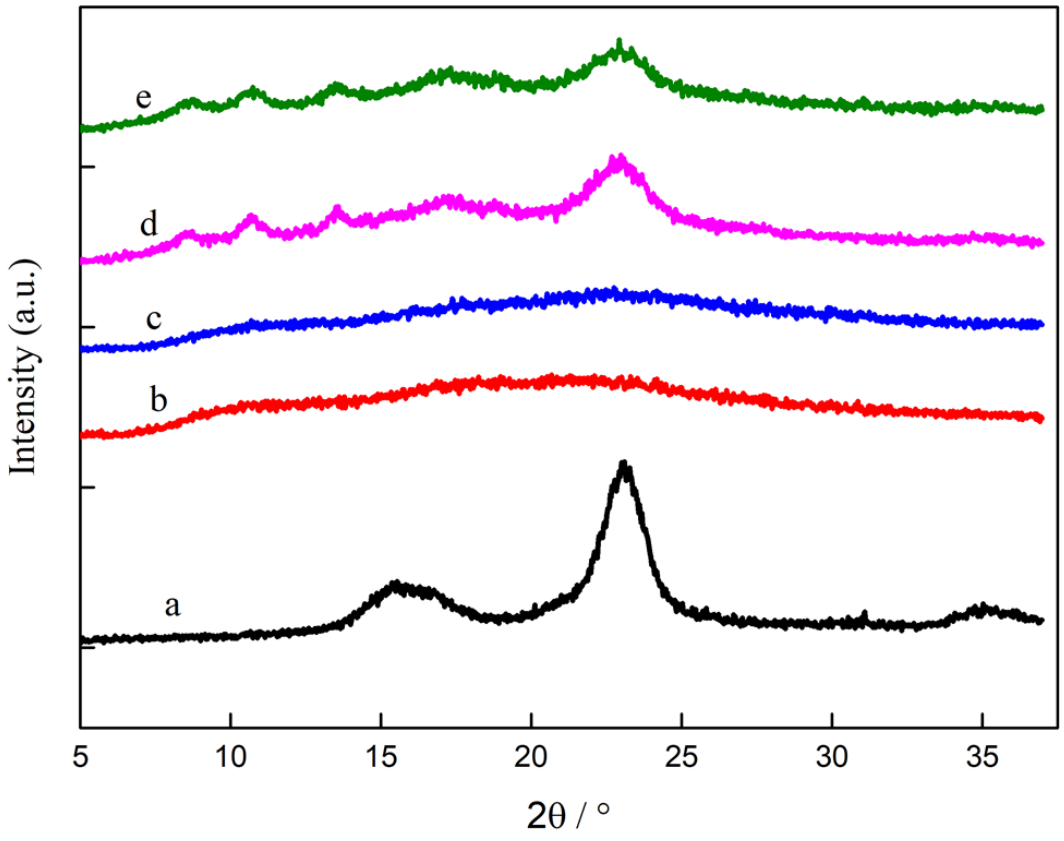


**Figure 8.5.** XRD patterns of (a) PHKP, (b) CA1, (c) CA2, (d) CA3, and (e) CA4

### 8.3.7. Thermal properties of CA

The TGA thermograms have been presented in Fig. 8.6 for the precursor PHKP and prepared cellulose acetate samples. The thermograms could be segregated into three regions. The first region ranging from 25 to 100 ℃ exhibits a slight loss of mass for the both the cellulose and acetate

samples. This region depicts mass loss because of the desorption of water from the surface of the sample. This mass loss is more prominent in case of cellulose sample than the acetylated samples. This observation leads to the fact that cellulose acetate is hydrophobic in nature compared to the cellulose sample. Second region of the thermogram varies depending on the cellulose acetate sample. In case of CA-1 and CA-2, onset and end thermal degradation temperature is at 295 and 373 ℃. On the other hand, CA-3, CA-4, and PHKP showed similar onset and end degradation temperature at around ~340 and ~390 ℃, respectively. CA-3 has slightly greater thermal stability compared to CA-4 and all of the cellulose acetate samples exhibit better thermal stability compared to their precursor PHKP. This region with the highest loss of mass indicates the decomposition of polymer chains of cellulose and cellulose acetate samples [53, 54]. The degradation of the crystalline region of the CA and cellulose samples and disintegration of polymer chains occur simultaneously in this temperature range. Consequently, the crystalline cellulose and cellulose acetate transformed into amorphous structure and the degree of polymerization (DP) decreased. Finally, at around 400-550 ℃, crystalline region of the samples has been degraded completely and the cellulose is converted into D-glucopyranose monomer. This D-glucopyranose could be further degraded into free radicals [53]. On the other hand, thermogram curve of DSIL $[C_4mim](CH_3CO_2)_{0.6}Cl_{0.4}$ could be divided into two part change of mass. The two onset degradation temperature at 219 and 271 ℃ are observed attributable to the decomposition of the $[C_4mim](CH_3CO_2)$ and $[C_4mim]Cl$ component of the DSIL, respectively. Thermogram of the DSIL exhibit that the degradation is initiated prior to the decomposition of PHKP and CA samples. Moreover, the complete removal of DSIL is confirmed from the absence of initial loss of mass at around 219 and 271 ℃ for CA samples.

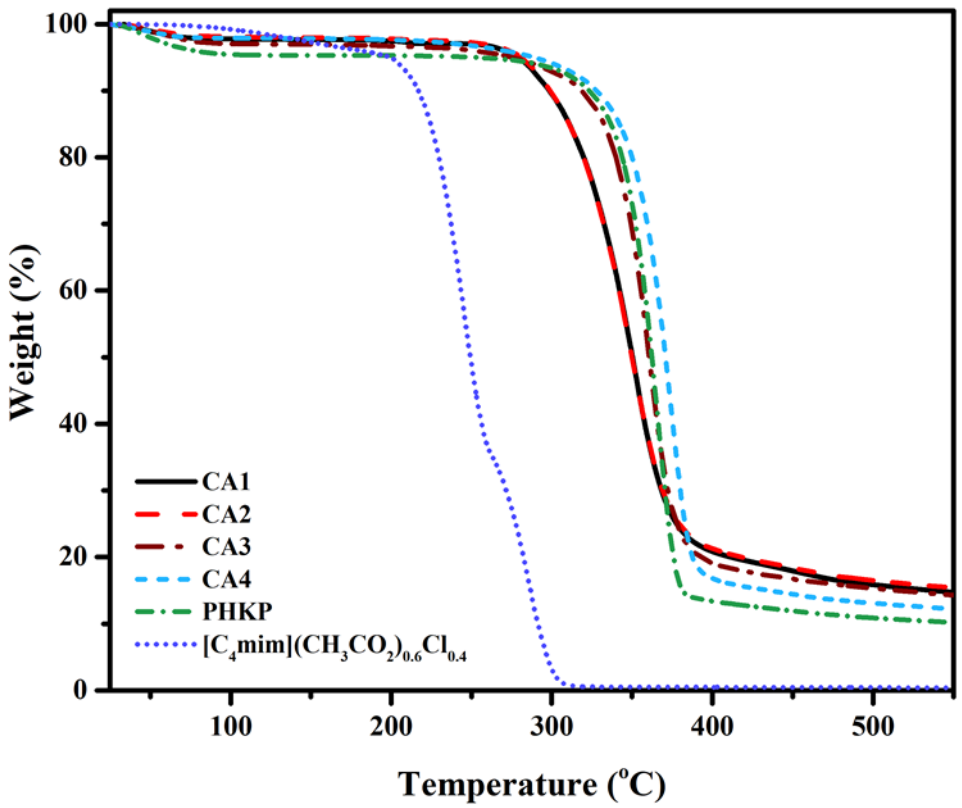


**Figure 8.6.** TGA thermograms of PHKP, prepared CA samples and $[C_4mim](CH_3CO_2)_{0.6}Cl_{0.4}$

DSC plays a crucial role in understanding the changes in material with respect to heat treatment. The typical DSC thermogram could provide valuable information about the thermal processes occurring in specific temperature regions. Moreover, DSC provides clear picture about the nature specific process by categorizing it on the basis of heat released or absorbed. The phases of materials change with the heat treatment and different processes takes place during this phase changes. Consequently, the exothermic or endothermic changes could give insight into the thermal change that is taking place. For instance, crystallization temperature, glass transition temperature, melting point, etc. could be identified based on the nature of the thermal change. Fig. 8.7 illustrates the DSC thermogram of cellulose acetate samples CA1 to CA4. Peaks and valleys in this thermogram indicate exothermic and endothermic changes, respectively. Initially an endothermic change is observed at temperature around 95 °C. This change corresponds to the dehydration of the materials. In case of CA4, large endothermic change is observed at around 244 °C indicating the melting of the cellulose acetate which is consistent with the literature [55]. On the other hand, CA1 exhibit broad endothermic change associated with melting of the cellulose acetate. CA1 and CA2 depicts

almost similar changes along the thermogram. First at 300 ℃, both samples show endotherm of fusion suggesting their semi-crystalline nature [56]. Second, an exotherm located at 345 ℃ for both samples which is attributable to the decomposition of the polymer and also due to the disintegration of the intra molecular hydrogen bond of the cellulose acetate samples [1]. CA4 displays lower melting point compared to the CA1 and CA2 which is due to the more non-uniform acetylation leading to formation of more heterogeneous structure [57].

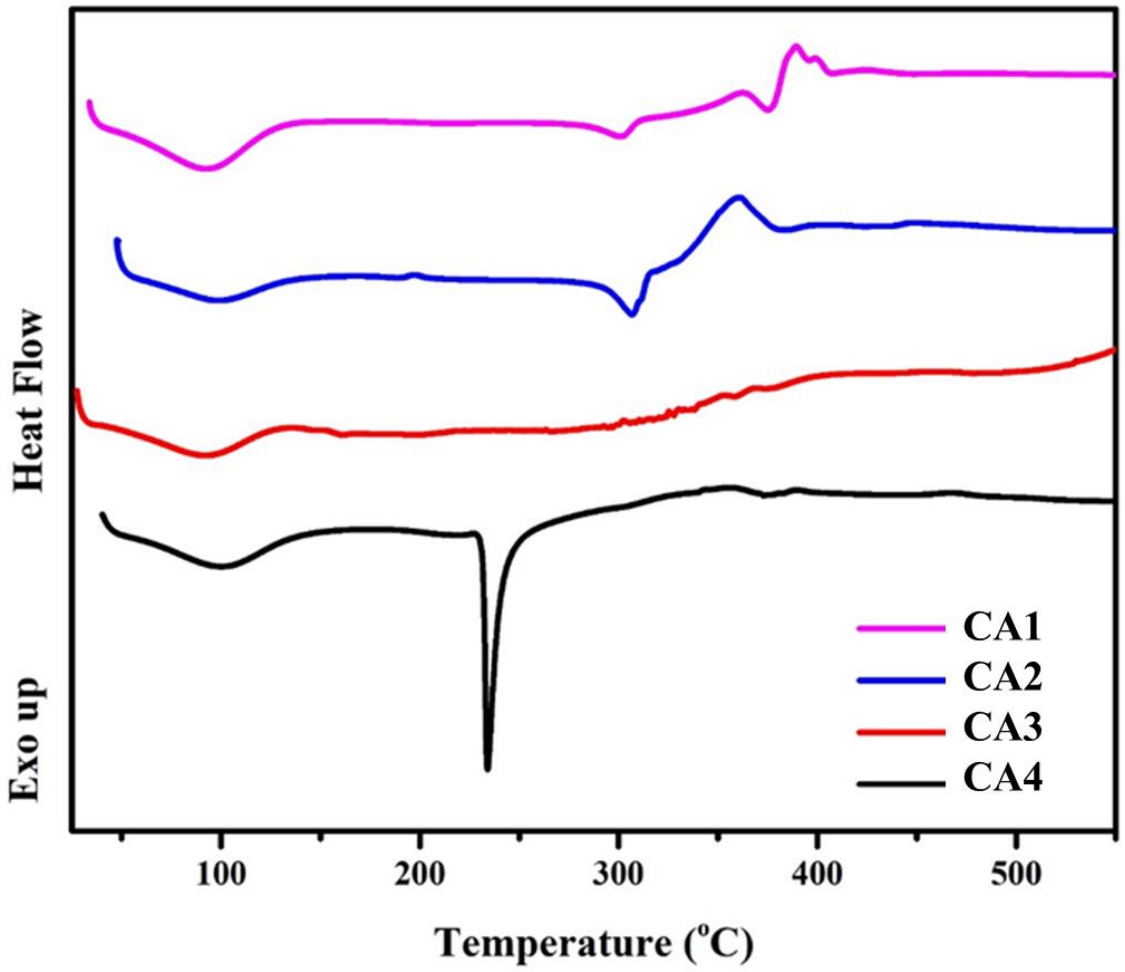


**Figure 8.7.** DSC thermograms of the prepared CAs

### 8.3.8. Morphology of CA

The morphology of the PHKP and CA monitored by SEM is typically depicted, in Fig. 8.8. The surface of PHKP is fibrous. The CA produced from PHKP had a surface that displayed a collapsed morphology. The presence of a porous structure in the CA fibers was readily apparent, indicating

its likely formation during the process of regeneration. Cao *et al.* [58] showed that CA with DS 2.84 was rich in pores and almost all the cellulose structure was destroyed.

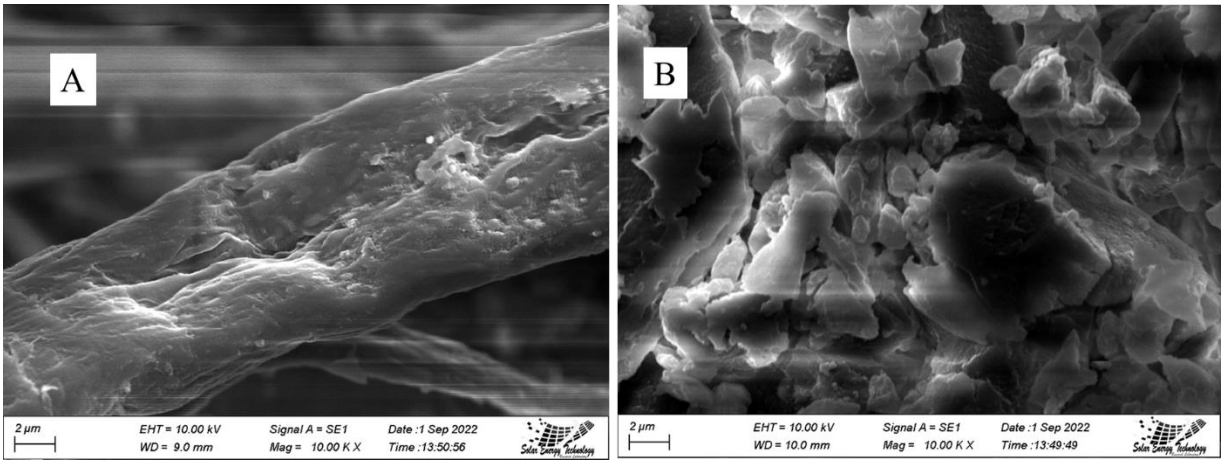


**Figure 8.8.** SEM images of (A) PHKP, (B) CA1

## 8.4 Conclusions

The present investigation showed that the cellulose acetate (CA) could be produced from PHKP by using double salts ionic liquid (DSIL). The prepared DSIL was characterized by FTIR and $^{1}H$ NMR spectroscopy. These two important bands which is associated with the structure of DSIL correspond to C-H stretching vibrations of imidazolium cation $[C_4mim]^+$ were found to be at 3025 and 3055 $cm^{-1}$ indicating C(2)-H and C(4,5)-H, stretching vibrations, respectively. The $^{1}H$ NMR spectroscopy proved the chemical shifts ($\delta$) values of C(2)-H, C(4)-H, and C(5)-H in $[C_4mim](CH_3CO_2)_{0.6}Cl_{0.4}$ are found to be 10.4, 7.6, and 7.4 ppm, respectively. The synthesized CA was characterized by FTIR and $^{1}H$ NMR spectroscopy. The strong absorption bands at 3308 $cm^{-1}$ in PHKP are due to –OH stretching, which completely disappeared upon acetylation. All prepared CA exhibited a strong band of the carbonyl (C=O) group at 1735 $cm^{-1}$, confirming the effective chemical conversion to an ester. The absence of C(2)-H stretching absorption bands in the region of 3200-2800 $cm^{-1}$ indicate the complete removal of $[C_4mim](CH_3CO_2)_{0.6}Cl_{0.4}$ from CA samples.The protons present in the methyl ($–CH_3$) of acetyl groups are corresponded to chemical shift of around 1.9-2.1 ppm. Similarly, the resonance peak observed at a chemical shift of 2.1 ppm can be attributed to the hydrogen atom attached to the sixth carbon atom (C6). The observed peaks within the chemical shift range of 5.20 - 2.80 ppm can be attributed to the presence of the seven ring protons of anhydroglucose unit (AGU). The crystallinity index of PHKP was 51.1%, which has been decreased on acetylation, demonstrating the successful esterification of cellulose. The exothermic and endothermic peaks on DSC thermograms provides insight into the thermal change that is taking place.

**References**


[1] de Souza Mesquita, L. M., Murador, D. C., and de Rosso, V. V. (2023). Application of ionic liquid solvents in the food industry. In Encyclopedia of Ionic Liquids. *Springer Nature Singapore*, 72-87.

[2] Zhuang, W., Hachem, K., Bokov, D., Ansari, M. J., and Nakhjiri, A. T. (2022). Ionic liquids in pharmaceutical industry: A systematic review on applications and future perspectives. *Journal of Molecular Liquids*, *349*, 118145.

[3] Toledo Hijo, A.A., Meirelles, A.A., Maximo, G.J., Cunha, R.L., Cristianini, M., Leite, T.S., Pereira, J.F., and Meirelles, A.J. (2022). Synergetic Application of Ionic Liquids as New Naturally based Antimicrobial Preservatives and Emulsifiers. *ACS Sustainable Chemistry and Engineering*, *10*(46), 15017-15024.

[4] Vilas-Boas, S. M., Coelho, A. Z., Martins, M. A., Coutinho, J. A., Ferreira, O., and Pinho, S. P. (2023). Evaluation of Ionic Liquids for the Sustainable Fractionation of Essential Oils. *Industrial and Engineering Chemistry Research*, *62*(17), 6749-6758.

[5] Marfavi, Y., AliAkbari, R., Kowsari, E., Sadeghi, B., and Ramakrishna, S. (2022). Application of ionic liquids in green energy-storage materials. In Ionic Liquid-Based Technologies for Environmental Sustainability. *Elsevier*, 155-166.

[6] Mishra, K., Devi, N., Siwal, S. S., Zhang, Q., Alsanie, W. F., Scarpa, F., and Thakur, V. K. (2022). Ionic Liquid-Based Polymer Nanocomposites for Sensors, Energy, Biomedicine, and Environmental Applications: Roadmap to the Future. *Advanced Science*, *9*(26), 2202187.

[7] Zhao, D., Wu, M., Kou, Y., and Min, E. (2002). Ionic liquids: applications in catalysis. *Catalysis Today*, *74*(1-2), 157-189.

[8] MacFarlane, D. R., Tachikawa, N., Forsyth, M., Pringle, J. M., Howlett, P. C., Elliott, G. D., Davis Jr., J. H., Watanabe, M., Simon, P. and Angell, C. A. (2014). Energy applications of ionic liquids. *Energy and Environmental Science*, *7*(1), 232-250.

[9] Liang, L., Gan, Q., and Nancarrow, P. (2014). Composite ionic liquid and polymer membranes for gas separation at elevated temperatures. *Journal of Membrane Sience*, *450*, 407-417.

[10] Seddon, K. (2002). Ionic liquids: designer solvents for green synthesis. *Chemical Engineer*, 730, 33-35.

[11] Edgar, K. J. (2007). Cellulose esters in drug delivery. *Cellulose*, *14*, 49-64.

[12] El Seoud, O. A., and Heinze, T. (2005). Organic esters of cellulose: new perspectives for old polymers. *Polysaccharides I: Structure, Characterization and Use*, 103-149.

[13] Fischer, S., Thümmler, K., Volkert, B., Hettrich, K., Schmidt, I., and Fischer, K. (2008, January). Properties and applications of cellulose acetate. In Macromolecular Symposia. *Weinheim: WILEY-VCH Verlag*, 262(1), 89-96.

[14] Heinze, T., Dicke, R., Koschella, A., Kull, A. H., Klohr, E. A., and Koch, W. (2000). Effective preparation of cellulose derivatives in a new simple cellulose solvent. *Macromolecular Chemistry and Physics*, *201*(6), 627-631.

[15] Heinze, T., Schwikal, K., and Barthel, S. (2005). Ionic liquids as reaction medium in cellulose functionalization. *Macromolecular Bioscience*, *5*(6), 520-525.

[16] Yan, C. A. O., Zhang, J., Jiasong, H. E., Huiquan, L. I., and Zhang, Y. (2010). Homogeneous acetylation of cellulose at relatively high concentrations in an ionic liquid. *Chinese Journal of Chemical Engineering*, *18*(3), 515-522.

[17] Wu, J., Zhang, J., Zhang, H., He, J., Ren, Q., and Guo, M. (2004). Homogeneous acetylation of cellulose in a new ionic liquid. *Biomacromolecules*, *5*(2), 266-268.

[18] Edgar, K. J., Buchanan, C. M., Debenham, J. S., Rundquist, P. A., Seiler, B. D., Shelton, M. C., and Tindall, D. (2001). Advances in cellulose ester performance and application. *Progress in Polymer Science*, *26*(9), 1605-1688.

[19] Liebert, T. F., and Heinze, T. J. (2001). Exploitation of reactivity and selectivity in cellulose functionalization using unconventional media for the design of products showing new superstructures. *Biomacromolecules*, *2*(4), 1124-1132.

[20] Edgar, K. J., Arnold, K. M., Blount, W. W., Lawniczak, J. E., and Lowman, D. W. (1995). Synthesis and properties of cellulose acetoacetates. *Macromolecules*, *28*(12), 4122-4128.

[21] Fischer, S., Voigt, W., and Fischer, K. (1999). The behaviour of cellulose in hydrated melts of the composition LiX·n $H_2O$ (X= $I^-$, $NO_3^-$, $CH_3COO^-$, $ClO_4^-$). *Cellulose*, *6*, 213-219.

[22] Zhang, H., Wu, J., Zhang, J., and He, J. (2005). 1-Allyl-3-methylimidazolium chloride room temperature ionic liquid: a new and powerful nonderivatizing solvent for cellulose. *Macromolecules*, *38*(20), 8272-8277.

[23] Clough, M. T., Geyer, K., Hunt, P. A., Son, S., Vagt, U., and Welton, T. (2015). Ionic liquids: not always innocent solvents for cellulose. *Green Chemistry*, *17*(1), 231-243.

[24] Turner, M. B., Spear, S. K., Holbrey, J. D., and Rogers, R. D. (2004). Production of bioactive cellulose films reconstituted from ionic liquids. *Biomacromolecules*, *5*(4), 1379-1384.

[25] Li, Y., Wang, J., Liu, X., and Zhang, S. (2018). Towards a molecular understanding of cellulose dissolution in ionic liquids: Anion/cation effect, synergistic mechanism and physicochemical aspects. *Chemical Science*, *9*(17), 4027-4043.

[26] Xu, A., Wang, J., and Wang, H. (2010). Effects of anionic structure and lithium salts addition on the dissolution of cellulose in 1-butyl-3-methylimidazolium-based ionic liquid solvent systems. *Green Chemistry*, 12(2), 268-275.

[27] de Oliveira, H. F. N., and Rinaldi, R. (2015). Understanding cellulose dissolution: energetics of interactions of ionic liquids and cellobiose revealed by solution microcalorimetry. *ChemSusChem*, *8*(9), 1577-1584.

[28] Zavrel, M., Bross, D., Funke, M., Büchs, J., and Spiess, A. C. (2009). High-throughput screening for ionic liquids dissolving (ligno-) cellulose. *Bioresource Technology*, *100*(9), 2580-2587.

[29] Luan, Y., Zhang, J., Zhan, M., Wu, J., Zhang, J., and He, J. (2013). Highly efficient propionylation and butyralation of cellulose in an ionic liquid catalyzed by 4-dimethylminopyridine. *Carbohydrate Polymers*, 92(1), 307-311.

[30] Barthel, S., and Heinze, T. (2006). Acylation and carbanilation of cellulose in ionic liquids. *Green Chemistry*, *8*(3), 301-306.

[31] Liu, H., Sui, X., Xu, H., Zhang, L., Zhong, Y., and Mao, Z. (2016). Self-healing polysaccharide hydrogel based on dynamic covalent enamine bonds. *Macromolecular Materials and Engineering*, *301*(6), 725-732.

[32] Jahan, M. S., Chowdhury, D. N., and Islam, M. K. (2007). Atmospheric formic acid pulping and TCF bleaching of dhaincha (Sesbania aculeata), kash (Saccharum spontaneum) and banana stem (Musa Cavendish). *Industrial Crops and Products*, *26*(3), 324-331.

[33] Heinze, T., Schwikal, K., and Barthel, S. (2005). Ionic liquids as reaction medium in cellulose functionalization. *Macromolecular Bioscience*, *5*(6), 520-525.

[34] de Freitas, R. R., Senna, A. M., and Botaro, V. R. (2017). Influence of degree of substitution on thermal dynamic mechanical and physicochemical properties of cellulose acetate. *Industrial Crops and Products*, *109*, 452-458.

[35] Chen, J., Xu, J., Wang, K., Cao, X., and Sun, R. (2016). Cellulose acetate fibers prepared from different raw materials with rapid synthesis method. *Carbohydrate Polymers*, *137*, 685-692.

[36] M.M. Rahman, M. Alam, M.M. Rahman, M.A.B.H Susan, M.A.A. Shaikh, J. Nayeem and M.S. Jahan, A novel approach in increasing carboxymethylation reaction of cellulose. *Carbohydrate Polymer Technology and Application, 4* (2022) 100236.

[37] Zheng, Y. Z., Zhou, Y., Deng, G., Guo, R., and Chen, D. F. (2020). The structure and interaction properties of two task-specific ionic liquids and acetonitrile mixtures: A combined FTIR and DFT study. *Spectrochimica Acta Part A: Molecular and Biomolecular Spectroscopy*, *226*, 117641.

[38] Umebayashi, Y., Jiang, J.C., Shan, Y.L., Lin, K.H., Fujii, K., Seki, S., Ishiguro, S.I., Lin, S.H., and Chang, H.C. (2009). Structural change of ionic association in ionic liquid/water mixtures: A high-pressure infrared spectroscopic study. *The Journal of Chemical Physics*, *130*(12), 124503.

[39] Cha, S., Ao, M., Sung, W., Moon, B., Ahlström, B., Johansson, P., Ouchi, Y., and Kim, D. (2014). Structures of ionic liquid–water mixtures investigated by IR and NMR spectroscopy. *Physical Chemistry Chemical Physics*, *16*(20), 9591-9601.

[40] Damodaran, K. (2016). Recent NMR studies of ionic liquids. *Annual Reports on NMR Spectroscopy*, *88*, 215-244.

[41] Pauric, A. D., Halalay, I. C., and Goward, G. R. (2016). Combined NMR and molecular dynamics modeling study of transport properties in sulfonamide based deep eutectic lithium electrolytes: LiTFSI based binary systems. *Physical Chemistry Chemical Physics*, *18*(9), 6657-6667.

[42] Zaoui, A., Cherifi, Z., and Belbachir, M. (2019). Ultrasound-induced synthesis of an imidazolium based poly (ionic liquid) in an aqueous media: A structural, thermal and morphological study. *Ultrasonics Sonochemistry*, *55*, 149-156.

[43] Hesse-Ertelt, S., Heinze, T., Kosan, B., Schwikal, K., and Meister, F. (2010, August). Solvent effects on the NMR chemical shifts of imidazolium-based ionic liquids and

cellulose therein. In Macromolecular Symposia, *Weinheim: WILEY-VCH Verlag*, 294(2), 75-89.

[44] Li, J., Zhang, L. P., Peng, F., Bian, J., Yuan, T. Q., Xu, F., and Sun, R. C. (2009). Microwave-assisted solvent-free acetylation of cellulose with acetic anhydride in the presence of iodine as a catalyst. *Molecules*, 14(9), 3551-3566.

[45] Mondal, M. I. H., Yeasmin, M. S., and Rahman, M. S. (2015). Preparation of food grade carboxymethyl cellulose from corn husk agrowaste. *International Journal of Biological Macromolecules*, 79, 144-150.

[46] Shaikh, H. M., Anis, A., Poulose, A. M., Al-Zahrani, S. M., Madhar, N. A., Alhamidi, A., and Alsubaie, F. S. (2022). Synthesis and characterization of cellulose triacetate obtained from date palm (Phoenix dactylifera L.) trunk mesh-derived cellulose. *Molecules*, 27(4), 1434.

[47] Rodrigues Filho, G., Monteiro, D. S., da Silva Meireles, C., de Assunção, R. M. N., Cerqueira, D. A., Barud, H. S., and Messadeq, Y. (2008). Synthesis and characterization of cellulose acetate produced from recycled newspaper. *Carbohydrate Polymers*, 73(1), 74-82.

[48] Kono, H., Hashimoto, H., and Shimizu, Y. (2015). NMR characterization of cellulose acetate: chemical shift assignments, substituent effects, and chemical shift additivity. *Carbohydrate Polymers*, *118*, 91-100.

[49] Pereira, P. H. F., Ornaghi Júnior, H. L., Coutinho, L. V., Duchemin, B., and Cioffi, M. O. H. (2020). Obtaining cellulose nanocrystals from pineapple crown fibers by free-chlorite hydrolysis with sulfuric acid: physical, chemical and structural characterization. *Cellulose*, 27, 5745-5756.

[50] Soto-Salcido, L. A., Anugwom, I., Ballinas-Casarrubias, L., Mänttäri, M., and Kallioinen, M. (2020). NADES-based fractionation of biomass to produce raw material for the preparation of cellulose acetates. *Cellulose*, 27, 6831-6848.

[51] Sun, X., Lu, C., Zhang, W., Tian, D., and Zhang, X. (2013). Acetone-soluble cellulose acetate extracted from waste blended fabrics via ionic liquid catalyzed acetylation. *Carbohydrate Polymers*, 98(1), 405-411.

[52] Chen, J., Xu, J., Wang, K., Cao, X., and Sun, R. (2016). Cellulose acetate fibers prepared from different raw materials with rapid synthesis method. *Carbohydrate Polymers*, 137, 685-692.

[53] Das, A. M., Ali, A. A., and Hazarika, M. P. (2014). Synthesis and characterization of cellulose acetate from rice husk: Eco-friendly condition. *Carbohydrate Polymers*, *112*, 342-349.

[54] Ebrahim, S., Morsy, A., Kenawy, E., Abdel-Fattah, T., and Kandil, S. (2016). Reverse osmosis membranes for water desalination based on cellulose acetate extracted from Egyptian rice straw. *Desalination and Water Treatment*, *57*(44), 20738-20748.

[55] Cardea, S., and De Marco, I. (2020). Cellulose acetate and supercritical carbon dioxide: Membranes, nanoparticles, microparticles and nanostructured filaments. *Polymers*, *12*(1), 162.

[56] Cerqueira, D. A., Rodrigues Filho, G., and Assunção, R. M. (2006). A new value for the heat of fusion of a perfect crystal of cellulose acetate. *Polymer Bulletin*, *56*, 475-484.

[57] Barud, H. S., de Araújo Júnior, A. M., Santos, D. B., de Assunção, R. M., Meireles, C. S., Cerqueira, D. A., Filho, G. R., Ribeiro, C. A., Messaddeq, Y., and Ribeiro, S. J. (2008). Thermal behavior of cellulose acetate produced from homogeneous acetylation of bacterial cellulose. *Thermochimica Acta*, *471*(1-2), 61-69.

[58] Cao, L., Luo, G., Tsang, D. C., Chen, H., Zhang, S., and Chen, J. (2018). A novel process for obtaining high quality cellulose acetate from green landscaping waste. *Journal of Cleaner Production*, 176, 338-347.

# Chapter 9

## Correlation of the Physicochemical Properties of Imidazolium-Based Ionic Liquids and Their Double Salts with the Dissolution of Cellulose


### Abstract

The physicochemical properties of imidazolium-based ionic liquids (ILs) and their double salts (DSILs) play a crucial role in their ability to dissolve cellulose. 1-butyl-3-methylimidazolium chloride ([$C_4$mim]Cl ) and1-butyl-3-methylimidazolium acetate ([$C_4$mim]$CH_3CO_2$) were used to prepared for DSILs over the whole mole fraction range. The structure of DSILs was investigated by using FTIR and NMR spectroscopy. The physicochemical properties such as density, viscosity and conductivity were measured. The measured density, viscosity and conductivity of ILs and DSILs were correlated with the dissolution of cellulose. Higher densities and viscosities in ILs and DSILs can hinder cellulose dissolution. This is because a more viscous solvent may have reduced mobility, making it less effective in penetrating and disrupting the cellulose structure. On the other hand, moderate viscosity can be beneficial, providing a balance between penetration and solubility. ILs and DSILs with higher electrical conductivities typically facilitate cellulose dissolution more efficiently. Enhanced conductivity signifies greater ion mobility, which aids in breaking down the cellulose structure by disrupting hydrogen bonds. Cellulose was regenerated from cellulose-ILs solution by using anti-solvent water. The crystallinity and thermal stability of cellulose and regenerated cellulose were studied. The thermal stability was decreased in the course of regenerated cellulose.



**Keywords:** Corelation, Ionic Liquids, DSILs, Density, Viscosity, and Conductivity


### 9.1. Introduction

Properties of ionic liquids (ILs) and double salt ionic liquids (DSILs) such as density [1], viscosity [2], conductivity [3], and entropy of activation [4] are interlinked with each other. Their trends in changes can be easily correlated with each other [1-4]. In this work, [$C_4$mim]$CH_3CO_2$ and [$C_4$mim]Cl ILs were used. These were mixed in different composition to obtain DSILs. The total number of prepared DSILs were nine. All of these along with the ILs were characterized with several physical techniques. Some important properties namely density, viscosity, conductivity,

and entropy of activation were determined and the corresponding values are presented in Table 2. All the experiments were conducted at 70 °C. In all of the cases, densities, viscosities, conductivities, and energies of activation increases in general. However, there are some exceptions in between. As we increase the proportion of $[C_4mim]Cl$ with $[C_4mim]CH_3CO_2$ then the number of available ions increases which lead to increased ionic conductivities. Again, as the overall number or population of ions in the DSILs increases. This also facilitates the overall electrical conductivity [5, 6]. Furthermore, density as well as viscosity increases due to the increased number of ions such as $[C_4mim]^+$, $Cl^-$, and $CH_3CO_2^-$. The $[C_4mim]^+$ ion now can form H-bonds with both $Cl^-$ and $CH_3CO_2^-$. This enhanced concentration and amount of H-bond networks restrict the ionic motion of the constituent ions increasing the density and viscosity of the DSILs [7, 8]. All these changes are induced due to the mixing of the ILs. The increase of entropy of activation indicates the facile mixing of $[C_4mim]CH_3CO_2$ and $[C_4mim]Cl$ to give the DSILs [4].

These parameters have a pronounced impact on the dissolution of cellulose. They dictate the percentage of dissolution of cellulose [9, 10]. Highest dissolution was achieved using the DSIL $[C_4mim](CH_3CO_2)_{0.6}Cl_{0.4}$. 26.2 and 32.8% cellulose were dissolved in this DSIL at 80 and 100 °C temperatures, respectively. The unprecedented outcomes can be explained with the help of density, viscosity and conductivity. At this particular $[C_4mim]CH_3CO_2$ : $[C_4mim]Cl$ = 6 : 4 composition, all of these properties are so well adjusted that the aid the most in cellulose dissolution. The tri-ionic system of $[C_4mim]^+$, $Cl^-$, and $CH_3CO_2^-$ forms many supramolecular bonds such as H-bonds, and electrostatic bonds with the -OH functional groups of cellulose [11]. These types of bonds pull the threads or fibers of cellulose apart from each other destroying the prevailing H-bonds among them [9, 10]. This causes the efficient dissolution of cellulose in the $[C_4mim](CH_3CO_2)_{0.6}Cl_{0.4}$ system. In the rest of the systems, the ions are not in correct harmony with each other to act upon the cellulose fibers together, hence they are less efficient for cellulose dissolution.

## 9.2. Materials and Methods

### 9.2.1. Materials

Commercial cellulose powder and cellulose obtained from jute fiber have used in this chapter for the correlation of dissolution of cellulose with different physicochemical properties such as density, viscosity, and conductivity of ILs and DSILs. The $^{1}$H NMR spectroscopic properties of ILs and DSILs have also been correlated with the dissolution of cellulose. The details of cellulose and ILs and DSILs have been discussed in Chapter 5 in materials and methods section.

### 9.2.2. Methods

The methods used for the measurement of density, viscosity, and conductivity have been discussed in materials and methods section of chapter 3. $^{1}$H NMR spectroscopic method has been discussed in Chapter 2 (sub-section 2.2.3.2). X-ray diffraction technique has been discussed in chapter 5 (sub-section 5.2.5)

## 9.3. Results and Discussion

The correlation of the physicochemical properties of ILs and DSILs and their spectroscopic properties with the dissolution of cellulose have been discussed in the following sections

### 9.3.1. Correlation of density of ILs and DSILs with the dissolution of cellulose

The density of ILs and DSILs can have a significant impact on their ability to dissolve cellulose. While a direct linear correlation between ILs density and cellulose dissolution does not exist however, several factors come into play that influence the dissolution process. The measured density of ILs and DSILs at 70 °C have been presented in Table 9.1. The variation of the dissolution of cellulose with the density of DSILs have been presented in Fig. 9.1. The density of DSILs are found to be 1.02874, 1.03411, 1.0359, 1.04096, 1.0436, 1.04635, 1.04989, 1.05304, 1.05684, 1.06001 g/cm for $[C_4mim](CH_3CO_2)_{0.9}Cl_{0.1,}$ $[C_4mim](CH_3CO_2)_{0.8}Cl_{0.2,}$ $[C_4mim](CH_3CO_2)_{0.7}Cl_{0.3,}$ $[C_4mim](CH_3CO_2)_{0.6}Cl_{0.4,}$ $[C_4mim](CH_3CO_2)_{0.5}Cl_{0.5,}$ $[C_4mim](CH_3CO_2)_{0.4}Cl_{0.6,}$ $[C_4mim](CH_3CO_2)_{0.3}Cl_{0.7,}$ $[C_4mim](CH_3CO_2)_{0.2}Cl_{0.8,}$ $[C_4mim](CH_3CO_2)_{0.1}Cl_{0.9}$, respectively. It can be seen that the density of DSILs lies in between the component ILs of $[C_4mim]Cl$ and $[C_4mim]CH_3CO_2$. The dissolution of cellulose increased up to $[C_4mim](CH_3CO_2)_{0.6}Cl_{0.4,}$ where the solubility of cellulose was found 26.2 wt% after that it is decreased. The density of an IL is closely linked to its molecular structure and composition. ILs with higher densities often have more closely packed ions, which can lead to stronger interactions between the solvent and cellulose. These stronger interactions can facilitate the dissolution process by breaking the hydrogen bonds between cellulose chains. Hanabusa *et al.* [12] investigated correlation of the physicochemical properties of protic ILs (PILs) with the dissolution of cellulose. They investigated the variation of density of 1,8-diazabicyclo[5.4.0]-undec-7-ene (DBU) with the change in anions. They found that as the density of PILs increases the dissolution of cellulose increased.

**Table 9.1.** Correlation between density, viscosity and conductivity with solubility of cellulose

| ILs and DSILs | Density ($g/cm^3$) at 70 °C | Viscosity (mPa.s) at 70 °C | Conductivity (mS/cm) at 70 °C | Solubility of cellulose (wt %) 80 °C |
|---|---|---|---|---|
| $[C_4mim]CH_3CO_2$ | 1.02506 | 30.74 | 8.77794 | 11.2 |
| $[C_4mim](CH_3CO_2)_{0.9}Cl_{0.1}$ | 1.02874 | 33.45 | 8.52143 | 13.5 |
| $[C_4mim](CH_3CO_2)_{0.8}Cl_{0.2}$ | 1.03411 | 31.7 | 9.96012 | 14.9 |
| $[C_4mim](CH_3CO_2)_{0.7}Cl_{0.3}$ | 1.0359 | 36.05 | 8.78506 | 14.5 |
| $[C_4mim](CH_3CO_2)_{0.6}Cl_{0.4}$ | 1.04096 | 34.38 | 11.07548 | 26.2 |
| $[C_4mim](CH_3CO_2)_{0.5}Cl_{0.5}$ | 1.0436 | 35.7 | 11.97649 | 24.1 |
| $[C_4mim](CH_3CO_2)_{0.4}Cl_{0.6}$ | 1.04635 | 44.05 | 11.98813 | 22.6 |
| $[C_4mim](CH_3CO_2)_{0.3}Cl_{0.7}$ | 1.04989 | 43.92 | 11.8125 | 12.2 |
| $[C_4mim](CH_3CO_2)_{0.2}Cl_{0.8}$ | 1.05304 | 53.96 | 9.14211 | 10.5 |
| $[C_4mim](CH_3CO_2)_{0.1}Cl_{0.9}$ | 1.05684 | 40.32 | 15.62249 | 12.4 |
| $[C_4mim]Cl$ | 1.06001 | 38.09 | - | 9.3 |

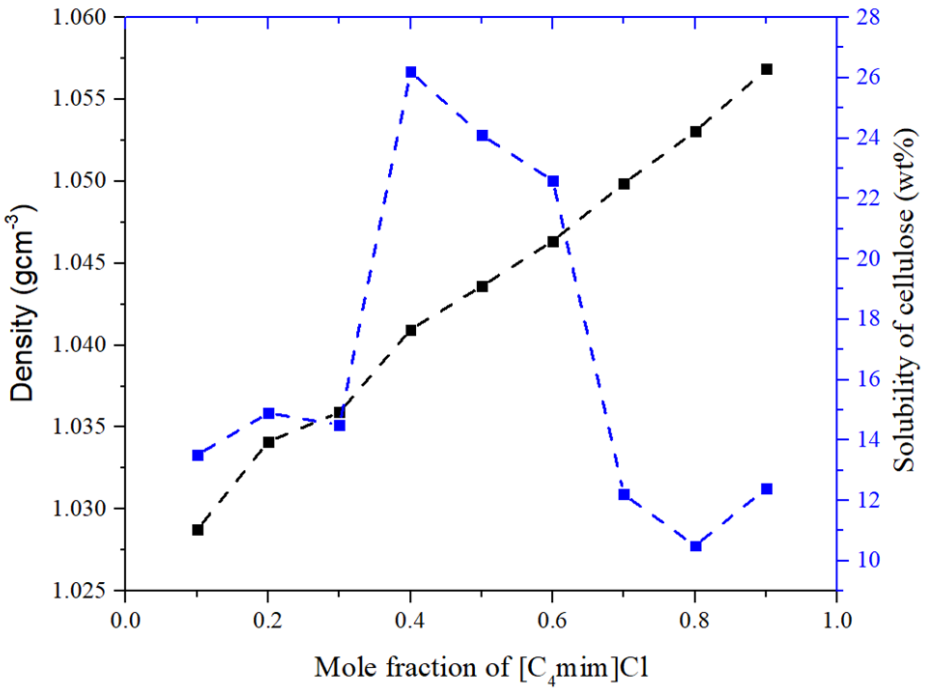


**Figure 9.1.** The correlation of the density of DSILs with the solubility of cellulose

### 9.3.2. Correlation of viscosity of ILs and DSILs with the dissolution of cellulose

The viscosity of ILs can have a significant impact on the dissolution of cellulose. Lower viscosity ILs are generally preferred for efficient cellulose dissolution, as they promote better interaction between the solvent and cellulose chains, leading to improved solubility and processing efficiency. In general, there is an inverse relationship between the viscosity of ILs and its ability to dissolve cellulose [13-15]. The viscosity of ILs and DSILs have been tabulated in Table 9.1. The correlation of variation of viscosity of DSILs at 70 ℃ with the dissolution of cellulose have been shown in Fig. 9.2. In Fig. 9.2 can be seen that the dissolution of cellulose is increases as the viscosity of DSILs increased with the addition of $[C_4mim]Cl$. The increase in the dissolution of cellulose continued up to $[C_4mim](CH_3CO_2)_{0.6}Cl_{0.4.}$ where the maximum solubility of cellulose found 26.2 wt%. From Table 9.1, it can be seen that the viscosity of ILs and DSILs are 30.74, 33.45, 31.7, 36.05, **34.38,** 35.7, 44.05, 43.92, 53.96, 40.32, 53.96, 40.32, and 38.09 mPa.s for $[C_4mim]CH_3CO_2$, $[C_4mim](CH_3CO_2)_{0.9}Cl_{0.1,}$ $[C_4mim](CH_3CO_2)_{0.8}Cl_{0.2,}$ $[C_4mim](CH_3CO_2)_{0.7}Cl_{0.3,}$ $[C_4mim](CH_3CO_2)_{0.6}Cl_{0.4,}$ $[C_4mim](CH_3CO_2)_{0.5}Cl_{0.5,}$ $[C_4mim](CH_3CO_2)_{0.4}Cl_{0.6,}$ $[C_4mim](CH_3CO_2)_{0.3}Cl_{0.7,}$ $[C_4mim](CH_3CO_2)_{0.2}Cl_{0.8,}$ $[C_4mim](CH_3CO_2)_{0.1}Cl_{0.9,}$ and $[C_4mim]Cl$ at 80 ℃, respectively. Their corresponding dissolution of cellulose were found to be 11.2, 13.5,14.9,14.5,26.2,24.1,22.6,12.2,10.5,12.4,9.3 wt % at 80 ℃. The higher dissolution of cellulose was found in the composition of $[C_4mim](CH_3CO_2)_{0.6}Cl_{0.4,}$ $[C_4mim](CH_3CO_2)_{0.5}Cl_{0.5,}$ $[C_4mim](CH_3CO_2)_{0.4}Cl_{0.6}$ whose viscosity were **34.38,** 35.7, 44.05 mPa.s, respectively, that are greater than $[C_4mim]CH_3CO_2$ and $[C_4mim]Cl$. The higher dissolution of cellulose in this composition can be explain as viscosity increases due to the increased number of ions of $[C_4mim]^+$, $Cl^-$, and $CH_3CO_2^-$. These ions can penetrate into cellulose structure, allowing for better interaction between the solvent and cellulose chains, and destroy the supramolecular structure of cellulose which facilitates dissolution [16, 17].

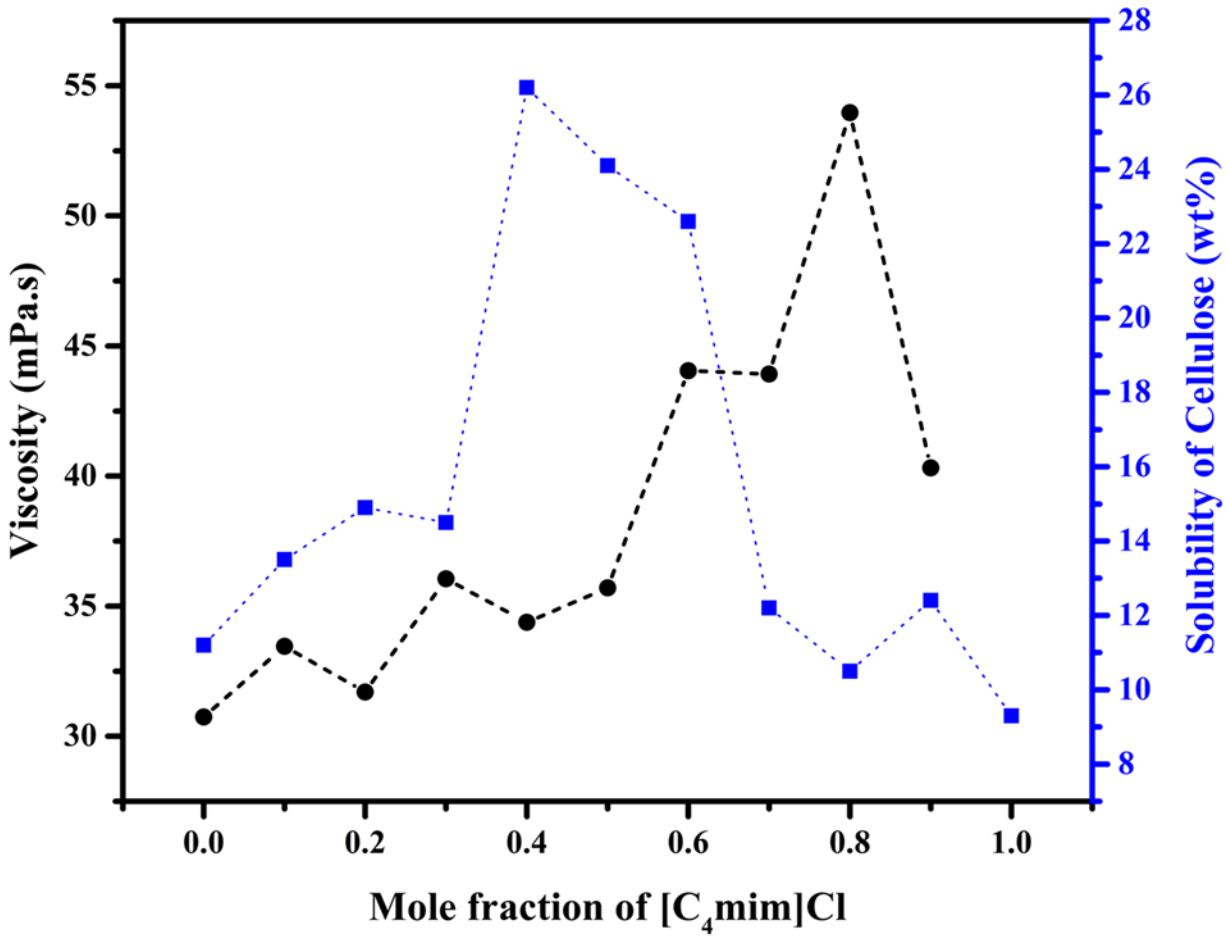


**Figure 9.2**. Correlation of viscosity of DSILs and the solubility of cellulose with the mole fraction of [$C_4$mim]Cl

### 9.3.3. Correlation of conductivity of ILs and DSILs with the dissolution of cellulose

The correlation between the electrical conductivity of ILs and the dissolution of cellulose is of significant academic interest due to its relevance in green chemistry and sustainable materials. ILs, being non-aqueous electrolytes, exhibit varying levels of electrical conductivity, which can influence their ability to dissolve more amount of cellulose [18-21]. The experimental ionic conductivities of ILs and DSILs and their corresponding amount of the dissolution of cellulose have been tabulated in Table 9.1. The variation of conductivities of ILs and DSILs and their corresponding amount of dissolve cellulose with the mole fraction of [$C_4$mim]Cl have been presented in Fig. 9.3. The conductivities of [$C_4$mim]$CH_3CO_2$, [$C_4$mim]$(CH_3CO_2)_{0.9}Cl_{0.1}$, [$C_4$mim]$(CH_3CO_2)_{0.8}Cl_{0.2}$, [$C_4$mim]$(CH_3CO_2)_{0.7}Cl_{0.3}$, [$C_4$mim]$(CH_3CO_2)_{0.6}Cl_{0.4}$,

$[C_4mim](CH_3CO_2)_{0.5}Cl_{0.5}$, $[C_4mim](CH_3CO_2)_{0.4}Cl_{0.6}$, $[C_4mim](CH_3CO_2)_{0.3}Cl_{0.7}$, $[C_4mim](CH_3CO_2)_{0.2}Cl_{0.8}$, $[C_4mim](CH_3CO_2)_{0.1}Cl_{0.9}$, and $[C_4mim]Cl$ at 70 ℃ are 8.77794, 8.52143, 9.96012, 8.78506, 11.07548, 11.97649, 11.98813, 11.8125, 9.14211, 15.62249, respectively. Their respective amount of the dissolution of cellulose are found to be 11.2, 13.5, 14.9,14.5, 26.2,24.1,22.6,12.2,10.5,12.4 wt% at 80 ℃. Similar to the density, viscosity highest conductivity was found at $[C_4mim](CH_3CO_2)_{0.6}Cl_{0.4}$ in which the maximum amount of the dissolution of cellulose obtained is 26.2 wt%. This is due to the mobility of $[C_4mim]^+$, $Cl^-$, and $CH_3CO_2^-$ ions are maximum which enhanced the dissolution of cellulose [22, 23].

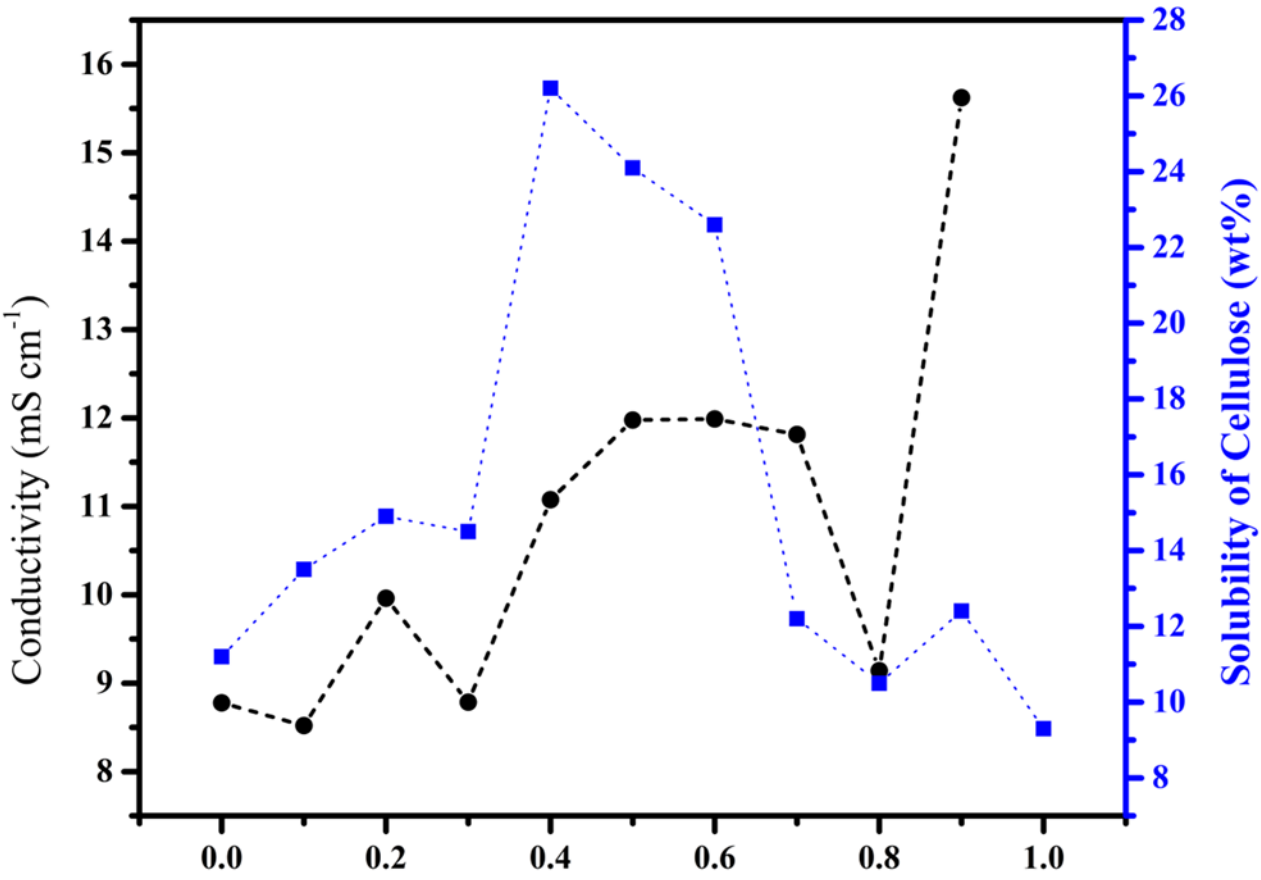


**Figure 9.3**. Correlation of conductivity of ILs and DSILs with the solubility of cellulose with the mole fraction of $[C_4mim]Cl$

### 9.3.4. Correlation of C(2)-H, $^{1}$H NMR chemical shifts of ILs and DSILS with the dissolution of commercial cellulose (wt%) at 80 ℃

The chemical shift of the C(2)-H proton in the imidazolium cation, as observed in $^{1}$H NMR spectroscopy, reflects the hydrogen bonding ability of the anion in ILs and DSILs. A downfield shift indicates strong anion-C(2)-H hydrogen bonds, while an upfield shift suggests weaker or fewer hydrogen bonds. Cellulose dissolution in ILs or DSILs relies on disrupting cellulose's hydrogen bonds. ILs with anions forming strong hydrogen bonds with the C(2)-H proton penetrate cellulose effectively, breaking its hydrogen bonds. A more downfield C(2)-H proton shift correlates with higher cellulose solubility, indicating ILs with such anions are better cellulose solvents [24-26]. The C(2)-H chemical shifts of $[C_4mim]CH_3CO_2$, $[C_4mim](CH_3CO_2)_{0.9}Cl_{0.1}$, $[C_4mim](CH_3CO_2)_{0.8}Cl_{0.2}$, $[C_4mim](CH_3CO_2)_{0.7}Cl_{0.3}$, $[C_4mim](CH_3CO_2)_{0.6}Cl_{0.4}$, $[C_4mim](CH_3CO_2)_{0.5}Cl_{0.5}$, $[C_4mim](CH_3CO_2)_{0.4}Cl_{0.6}$, $[C_4mim](CH_3CO_2)_{0.3}Cl_{0.7}$, $[C_4mim](CH_3CO_2)_{0.2}Cl_{0.8}$, $[C_4mim](CH_3CO_2)_{0.1}Cl_{0.9}$, and $[C_4mim]Cl$ are 10.60, 10.87, 10.46, 10.74, 10.65, 10.64, 10.61, 10.63, 10.23, 10.30, and 10.24, respectively. Their respective amount of the dissolution of cellulose are found to be 11.2, 13.5, 14.9,14.5, 26.2,24.1,22.6,12.2,10.5,12.4 wt % at 80 ℃ that have tabulated in Table 9.2 and C(2)-H chemical shifts, dissolution of cellulose with the mole fraction of $[C_4mim]Cl$ have been presented in Fig. 9.4. It can be seen that the down field shifts of the C(2)-H of $[C_4mim](CH_3CO_2)_{0.6}Cl_{0.4}$, $[C_4mim](CH_3CO_2)_{0.5}Cl_{0.5}$, $[C_4mim](CH_3CO_2)_{0.4}Cl_{0.6}$, shows higher amount of the dissolution of cellulose. In this composition, the anions of DSILs form strong H-bonds with the C(2)-H proton in $[C_4mim]^+$ that have been participated in the disruption of H-bonds in the supramolecular structure of cellulose, results more amount of the dissolution of cellulose.

**Table 9.2.** Relationship between C(2)-H chemical shifts of ILs and DSILS with the dissolution of commercial cellulose (wt%) at 80 ℃

| ILs and DSILs | Chemical shift (ppm) C(2)-H | Solubility of cellulose (wt %) 80 ℃ |
|---|---|---|
| $[C_4mim]CH_3CO_2$ | 10.60 | 11.2 |
| $[C_4mim](CH_3CO_2)_{0.9}Cl_{0.1}$ | 10.87 | 13.5 |
| $[C_4mim](CH_3CO_2)_{0.8}Cl_{0.2}$ | 10.46 | 14.9 |
| $[C_4mim](CH_3CO_2)_{0.7}Cl_{0.3}$ | 10.74 | 14.5 |
| $[C_4mim](CH_3CO_2)_{0.6}Cl_{0.4}$ | 10.65 | 26.2 |
| $[C_4mim](CH_3CO_2)_{0.5}Cl_{0.5}$ | 10.64 | 24.1 |
| $[C_4mim](CH_3CO_2)_{0.4}Cl_{0.6}$ | 10.61 | 22.6 |
| $[C_4mim](CH_3CO_2)_{0.3}Cl_{0.7}$ | 10.63 | 12.2 |
| $[C_4mim](CH_3CO_2)_{0.2}Cl_{0.8}$ | 10.23 | 10.5 |
| $[C_4mim](CH_3CO_2)_{0.1}Cl_{0.9}$ | 10.30 | 12.4 |
| $[C_4mim]Cl$ | 10.24 | 9.3 |

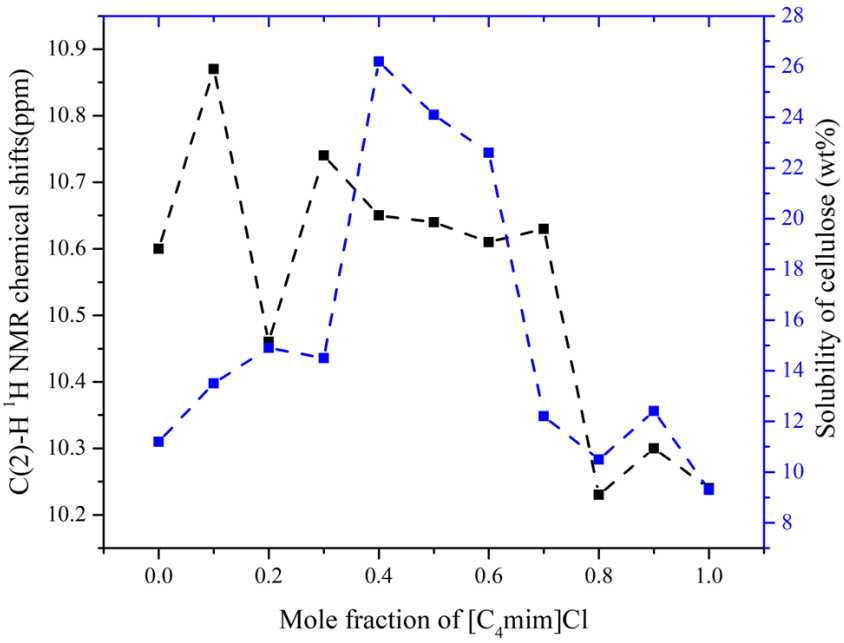


**Figure 9.4**. Correlation of C(2)-H chemical shifts of ILs and DSILs with the solubility of cellulose with the mole fraction of $[C_4mim]Cl$

### 9.3.5. Correlation between crystallinity of cellulose and the degradation temperature

Cellulose exists in two main forms: crystalline and amorphous. Crystalline cellulose has a highly ordered structure, with cellulose chains arranged in a regular pattern. Amorphous cellulose lacks these regular orderly arrangements. The more crystalline cellulose is, the higher its degradation temperature tends to be. This is because the well-ordered crystalline structure requires more energy to break the intermolecular bonds during degradation. This correlation between crystallinity and degradation temperature is crucial in various industrial applications. For example, in the paper and textile industries, where cellulose fibers are prevalent, high crystallinity is desirable to ensure thermal stability during processing. On the other hand, in applications like pharmaceuticals and food products, where cellulose derivatives with lower crystallinity are used, lower thermal stability may be acceptable or even advantageous. Table 9.3 and Fig. 9.5 show the correlation between degradation temperature of different native cellulose and regenerated cellulose and their crystallinity index (CrI). It is clearly observed that degradation temperature is linearly correlated with CrI. The correlation coefficient ($R^2$) is 0.974. Yang *et al.* [27] showed that the crystalline regions of cellulose improved the thermal stability. The highest crystalline index and higher crystallite size of cellulose also increased thermal stability [28]. Authors also showed that a higher amount of hydrogen bonds between neighboring cellulose increased crystallinity and thermal stability. H-bonds was disrupted in ILs causing dissolution of cellulose, consequently, CrI of regenerated cellulose was lower and ultimately degradation temperature was lower.

**Table 9.3.** Correlation between crystallinity and thermal decomposition temperature of cellulose

| Sample | Crystallinity (%) | $T_d$ / ℃ |
|---|---|---|
| KP | 48.5 | 337 |
| PHKP | 55.1 | 340 |
| ReKP from[$C_4$mim]$CH_3CO_2$ | 25.2 | 245 |
| RePHKP from [$C_4$mim]$CH_3CO_2$ | 28.8 | 260 |

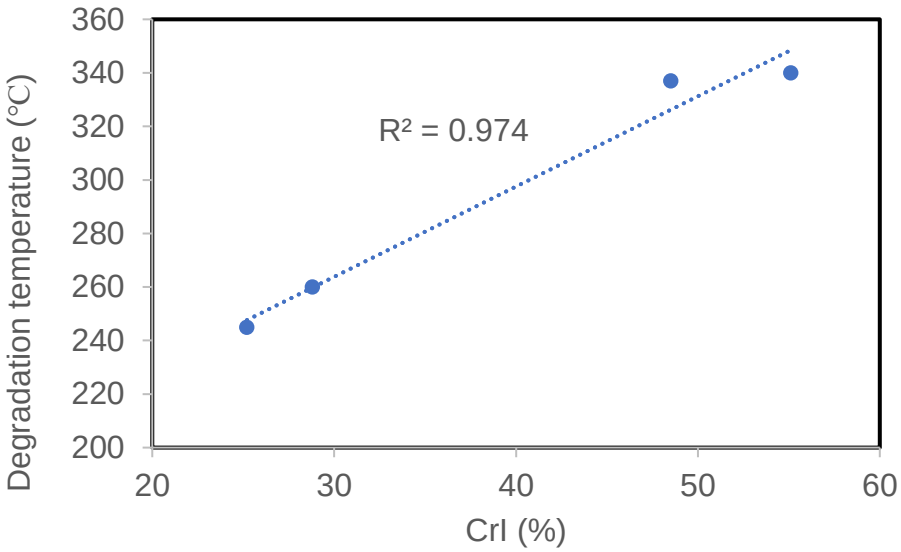


**Figure 9.5.** Correlation of the degradation temperature and crystallinity of cellulose

## 9.4. Conclusions

The physicochemical properties of imidazolium-based ionic liquids and their double salts are pivotal determinants of their effectiveness in cellulose dissolution. This study utilized 1-butyl-3-methylimidazolium chloride ([$C_4$mim]Cl) and 1-butyl-3-methylimidazolium acetate ([$C_4$mim]$CH_3CO_2$) to synthesize DSILs across the entire mole fraction range. The structural characteristics of DSILs were investigated through FTIR and NMR spectroscopy**.** The study demonstrated that certain physicochemical properties, including density, viscosity, and conductivity, significantly influence cellulose dissolution. Higher densities and viscosities in ILs and DSILs can hinder cellulose dissolution by reducing solvent mobility, limiting its ability to penetrate and disrupt the cellulose structure. Conversely, moderate viscosity can strike a balance between penetration and solubility.

## References


[1] Mantz, R. A., and Trulove, P. C. (2008). Viscosity and density of ionic liquids. *Ionic Liquids in Synthesis*, *2*, 72-88.

[2] Jacquemin, J., Husson, P., Padua, A. A., and Majer, V. (2006). Density and viscosity of several pure and water-saturated ionic liquids. *Green Chemistry*, *8*(2), 172-180.

[3] Jarosik, A., Krajewski, S. R., Lewandowski, A., and Radzimski, P. (2006). Conductivity of ionic liquids in mixtures. *Journal of Molecular Liquids*, *123*(1), 43-50.

[4] Yau, H. M., Croft, A. K., and Harper, J. B. (2012). Investigating the origin of entropy-derived rate accelerations in ionic liquids. *Faraday Discussions*, *154*, 365-371.

[5] Stacy, E. W., Gainaru, C. P., Gobet, M., Wojnarowska, Z., Bocharova, V., Greenbaum, S. G., and Sokolov, A. P. (2018). Fundamental limitations of ionic conductivity in polymerized ionic liquids. *Macromolecules*, *51*(21), 8637-8645.

[6] Ueno, K., Tokuda, H., and Watanabe, M. (2010). Ionicity in ionic liquids: correlation with ionic structure and physicochemical properties. *Physical Chemistry Chemical Physics*, *12*(8), 1649-1658.

[7] Mokhtarani, B., Sharifi, A., Mortaheb, H. R., Mirzaei, M., Mafi, M., and Sadeghian, F. (2009). Density and viscosity of pyridinium-based ionic liquids and their binary mixtures with water at several temperatures. *The Journal of Chemical Thermodynamics*, *41*(3), 323-329.

[8] Song, D., and Chen, J. (2014). Densities and viscosities for ionic liquids mixtures containing [eOHmim][BF4],[bmim][BF4] and [bpy][BF4]. *The Journal of Chemical Thermodynamics*, *77*, 137-143.

[9] Zhu, S., Wu, Y., Chen, Q., Yu, Z., Wang, C., Jin, S., Ding, Y., and Wu, G. (2006). Dissolution of cellulose with ionic liquids and its application: a mini-review. *Green Chemistry*, *8*(4), 325-327.

[10] Kosan, B., Michels, C., and Meister, F. (2008). Dissolution and forming of cellulose with ionic liquids. *Cellulose*, *15*, 59-66.

[11] Verma, C., Mishra, A., Chauhan, S., Verma, P., Srivastava, V., Quraishi, M. A., and Ebenso, E. E. (2019). Dissolution of cellulose in ionic liquids and their mixed cosolvents: A review. *Sustainable Chemistry and Pharmacy*, *13*, 100162.

[12] Hanabusa, H., Takeoka, Y., Rikukawa, M., and Yoshizawa-Fujita, M. (2018). Effect of alkyl chain length in anions on the physicochemical properties of cellulose-dissolving protic ionic liquids. *Australian Journal of Chemistry*, *72*(2), 55-60.

[13] Pinkert, A., Marsh, K. N., Pang, S., and Staiger, M. P. (2009). Ionic liquids and their interaction with cellulose. *Chemical Reviews*, *109*(12), 6712-6728.

[14] Mai, N. L., and Koo, Y. M. (2016). Computer-aided design of ionic liquids for high cellulose dissolution. *ACS Sustainable Chemistry and Engineering*, *4*(2), 541-547.

[15] Yuan, X., and Cheng, G. (2015). From cellulose fibrils to single chains: understanding cellulose dissolution in ionic liquids. *Physical Chemistry Chemical Physics*, *17*(47), 31592-31607.

[16] Medronho, B., and Lindman, B. (2015). Brief overview on cellulose dissolution/regeneration interactions and mechanisms. *Advances in Colloid and Interface Science*, *222*, 502-508.

[17] Ghasemi, M., Tsianou, M., and Alexandridis, P. (2017). Assessment of solvents for cellulose dissolution. *Bioresource Technology*, *228*, 330-338.

[18] Vekariya, R. L. (2017). A review of ionic liquids: Applications towards catalytic organic transformations. *Journal of Molecular Liquids*, 227, 44-60.

[19] Smiglak, M., Pringle, J.M., Lu, X., Han, L., Zhang, S., Gao, H., Macfarlane, D.R., and Rogers, R.D. (2014). Ionic liquids for energy, materials, and medicine. *Chemical Communications*, 50(66), 9228-9250.

[20] Berga, L., Bruce, I., Nicol, T.W., Holding, A.J., Isobe, N., Shimizu, S., Walker, A.J., and Reid, J.E. (2020). Cellulose dissolution and regeneration using a non-aqueous, non-stoichiometric protic ionic liquid system. *Cellulose*, 27(16), 9593-9603.

[21] Medronho, B., and Lindman, B. (2015). Brief overview on cellulose dissolution/regeneration interactions and mechanisms. *Advances in Colloid and Interface Science*, 222, 502-508.

[22] Huang, Y. B., Xin, P. P., Li, J. X., Shao, Y. Y., Huang, C. B., and Pan, H. (2016). Room-temperature dissolution and mechanistic investigation of cellulose in a tetra-butylammonium acetate/dimethyl sulfoxide system. *ACS Sustainable Chemistry and Engineering*, 4(4), 2286-2294.

[23] Halder, P., Kundu, S., Patel, S., Ramezani, M., Parthasarathy, R., and Shah, K. (2019). A comparison of ionic liquids and organic solvents on the separation of cellulose-rich material from river red gum. *BioEnergy Research*, 12, 275-291.

[24] Lungwitz, R., and Spange, S. (2008). A hydrogen bond accepting (HBA) scale for anions, including room temperature ionic liquids. *New Journal of Chemistry*, 32(3), 392-394.

[25] Fukaya, Y., Sugimoto, A., and Ohno, H. (2006). Superior solubility of polysaccharides in low viscosity, polar, and halogen-free 1, 3-dialkylimidazolium formates. *Biomacromolecules*, 7(12), 3295-3297.

[26] Fukaya, Y., Hayashi, K., Wada, M., and Ohno, H. (2008). Cellulose dissolution with polar ionic liquids under mild conditions: required factors for anions. *Green Chemistry*, 10(1), 44-46.

[27] Yang, H., Yan, R., Chen, H., Zheng, C., Lee, D. H., and Liang, D. T. (2006). In-depth investigation of biomass pyrolysis based on three major components: hemicellulose, cellulose and lignin. *Energy and Fuels*, 20(1), 388-393.

[28] Poletto, M., Ornaghi Junior, H. L., and Zattera, A. J. (2014). Native cellulose: structure, characterization and thermal properties. *Materials*, 7(9), 6105-6119.

# Chapter 10

# General Conclusions and Future Prospects

## 10.1. General Conclusions

Double salts ionic liquids could be prepared by the homogeneous mixing of 1-butyl-3-methyl imidazolium chloride ([$C_4$mim]Cl) and 1-butyl-3-methyl imidazolium acetate ([$C_4$mim]$CH_3CO_2$) over the whole mole fraction range and the structure of the prepared DSILs could be determined at a molecular level. ATR-FTIR spectroscopy reveals the insights of interactions and functional groups present in DSILs. The most vulnerable C(2)-H stretching absorption bands for DSILs in FTIR spectra have been strongly influenced by the mixing of [$C_4$mim]Cl and [$C_4$mim]$CH_3CO_2$ with different mole fractions. These sharp blue shifts for the addition [$C_4$mim]Cl in [$C_4$mim]$CH_3CO_2$ indicated the synergistic participation of $Cl^-$ and $CH_3CO_2^-$ ions in the formation of hydrogen bonds with the C(2)-H protons in DSILs which weakens the C(2)-H bond. NMR spectroscopy is imperative in elucidating the intricate molecular structure of DSILs. The chemical shifts value of C(2)-H showed more downfield region. The physicochemical properties of ILs and DSILs were investigated by the measurement of density, viscosity, refractive index, and conductivity. The excess properties were evaluated which gave the insights into the DSILs. The negative values of excess molar volume also indicated that strong intermolecular interactions between $[C_4mim]^+$, $CH_3CO_2^-$ and $Cl^-$ are present in DSILs. Viscosity data were used to evaluate thermodynamic properties of DSILs. $\Delta G$ for [$C_4$mim]$CH_3CO_2$ and DSILs was positive and decreased with temperature, signifying efficient mixing and DSIL formation. Positive $\Delta S$ values suggest increasing disorder with rising temperature, particularly at higher temperatures, indicating higher entropy. $\Delta H$ decreases with temperature, signifying increased activation energy due to higher $Cl^-$ ion concentration in DSILs, consistent with the hole theory for solvent flow. DSILs exhibit superior ionic conductivity compared to ILs due to the presence of triple ions $[C_4mim]^+$, $Cl^-$, and $CH_3CO_2^-$. These ions disrupt existing inter-ionic interactions and hydrogen bonds, enhancing ion mobility. The Walden plot illustrates that by increasing temperature and [$C_4$mim]Cl concentration, DSILs show improved ionic conductivity, behaving similarly to good ILs. In this work, the optical and the thermal analysis of single ILs and DSILs have been carried out to investigate the optical and thermal behavior of the subjected materials. The optical properties of

ILs and DSILs were investigated using fluorescence spectroscopy. The blue shift towards shorter wavelengths with increasing [$C_4$mim]Cl concentration suggests potential tuning of UV-shielding properties, while the role of anions highlights the importance of molecular structure in determining their UV-absorbing behavior. ILs and DSILs exhibit good thermal stability around 220-250 ℃. Mixtures of ILs demonstrate higher thermal decomposition temperatures ($T_d$) than ILs, which is advantageous for industrial applications. DSC analysis determined glass transition temperatures ($T_g$) and heat capacity ($C_p$). The $T_g$ of DSILs, while similar to ILs, slightly decreased. $C_p$ in DSILs increased with temperature and with a higher $CH_3CO_2$ species content, showing the significant influence of anions and composition on $C_p$. These properties expand the potential applications of ILs and DSILs in cellulose dissolution, efficient reactions, optoelectronics, photoelectrochemical processes, sustainable fuel cells, and more. The dissolution of commercial cellulose and jute cellulose were carried in ILs and DSILs. The highest dissolution of cellulose was obtained in [$C_4$mim]$(CH_3CO_2)_{0.6}Cl_{0.4}$ at 100 ℃ was 32.8 wt% and 30.5 wt% for pre-hydrolysed kraft pulp (PHKP). The higher amount cellulose was dissolved in this composition due to the synergistic participation of both anions of $CH_3CO_2^-$ and $Cl^-$ ions. Kraft pulping process showed a significant impact on the dissolution of cellulose. The dissolution of PHKP in ILs and DSILs was higher due to the purity of cellulose. The cellulose was regenerated from the solution using anti-solvent water. From the point of view of economic and sustainability, [$C_4$mim]$(CH_3CO_2)_{0.6}Cl_{0.4}$ was recycled successfully and reused for five times without alteration of the chemical structure. Cellulose was efficiently functionalized with the use of DSILs and formed cellulose acetate (CA). The successful acetylation was confirmed by FTIR and NMR spectroscopy. A strong band for stretching vibration of –OH of cellulose was absent and a strong band for carbonyl (C=O) group was observed in FTIR spectra suggested successful esterification of PHKP. All cellulose and regenerated cellulose (RC) samples were characterized by the state of art instrument FTIR, XRD, TGA, and SEM. The XRD analysis of cellulose confirmed the conversion of crystalline cellulose I to amorphous cellulose II structure. TGA studies confirmed that thermal stability of RC decreased on regeneration. A smooth and rough surface was observed for RC. Finally, the results obtained from the correlation of the physicochemical properties of ILs and DSILs with the dissolution of cellulose established the optimized density, viscosity, and conductivity of ILs and DSILs for enhanced the dissolution of cellulose.

## 10.2 Future Prospects

The future prospects of DSILs hold significant promise across various industrial applications. DSILs are engineered by fine-tuning the physicochemical and spectroscopic properties of ionic liquids , resulting in novel properties that offer substantial benefits in diverse fields, including food, pharmaceuticals, cosmetics, textiles, and fuel cell devices. One particularly exciting avenue for DSILs is their potential in the realm of biomass fractionation and functionalization. Their enhanced properties, such as improved cellulose dissolution capabilities, can significantly reduce the quantity of ILs needed for specific applications. This not only enhances cost-effectiveness but also contributes to sustainability in industrial processes. Moreover, ability of DSILs to dissolve substantial amounts of cellulose opens up new possibilities for synthesizing cellulose-based derivatives with unique properties, expanding their utility in various industries. DSILs are also poised to make ILs more economically viable for industrial applications. ILs are known to be relatively expensive, but DSILs offer a potential solution to this cost challenge while maintaining sustainability. Furthermore, DSILs can play a pivotal role in reducing environmental pollution. Unlike conventional volatile solvents, ILs, including DSILs, are non-volatile. This property can lead to a reduction in environmental pollution associated with the use of volatile solvents, making processes more environmentally friendly. In conclusion, the future prospects of DSILs are bright and multifaceted. Their potential applications in cellulose dissolution and derivatization represent just one facet of the vast opportunities they offer. DSILs hold the potential to revolutionize industrial processes, making them more efficient, cost-effective, and environmentally sustainable. Their adoption in various sectors is likely to spark new avenues for academic research and innovation.

# List of Publications

1. **M. Mahbubur Rahman**, M. Mostafizur Rahman, Md. Abu Bin Hasan Susan, and M. Sarwar Jahan, "Production of Nanomaterials from Forest Resources." Applications of Emerging Nanomaterials and Nanotechnology. Eds. N.B. Singh, Md. Abu Bin Hasan Susan and Ratiram Gomaji Chaudhary. *Materials Research Foundations*, 148, 200-228, 2023.

2. **M. Mahbubur Rahman**, M. Sarwar Jahan, Md. Mominul Islam, Md. Abu Bin Hasan Susan, "Enhanced dissolution of cellulose in imidazolium-based double salt ionic liquids." *International Journal of Biological Macromolecules*, Elsevier, under review.